SIMULATION, DEVELOPMENT AND PERFORMANCE EVALUATION OF A SOLAR/GAS HYBRID POWERED ABSORPTION AIR – CONDITIONING SYSTEM

BY

Talib Onimisi AHMADU*B.Eng. (A.B.U., 2003), M.Sc. (A. B. U., 2008)*

P16EGME9053

A THESIS SUBMITTED TO THE
SCHOOL OF POSTGRADUATE STUDIES
AHMADU BELLO UNIVERSITY, ZARIA,
NIGERIA

IN PARTIAL FULFILLMENT OF THE REQUIREMENTS FOR THE AWARD OF THE
DOCTOR OF PHILOSOPHY IN
MECHANICAL ENGINEERING

DEPARTMENT OF MECHANICAL ENGINEERING,
AHMADU BELLO UNIVERSITY,
ZARIA, NIGERIA

MAY, 2018

DECLARATION

I declare that the work in this thesis entitled 'Simulation, Development and Performance Evaluation of a Solar/ Gas Hybrid Powered Absorption Air – Conditioning System' has been performed by me in the Department of Mechanical Engineering under the supervision of Prof. C. O. Folayan, Prof. D. S. Yawas and Dr. F. O. Anafi.

The information derived from the literature has been duly acknowledged in the text and a list of references provided. No part of this thesis was previously presented for another degree or diploma at this or any other institution.

Talib OnimisiAHMADU _____ _____

Signature Date

CERTIFICATION

This thesis entitled **SIMULATION, DEVELOPMENT AND PERFORMANCE EVALUATION OF A SOLAR/ GAS HYBRID POWERED ABSORPTION AIR – CONDITIONING SYSTEM**meets the regulation governing the award of the degree of Doctor of philosophy in the **Department of Mechanical Engineering,** of **Ahmadu Bello University, Zaria** and it is approved for its contribution to knowledge and literary presentation.

Prof. C. O. Folayan Chairman, Supervisory Committee	_____ Signature	_____ Date
Prof. D. S. Yawas Member, Supervisory Committee	_____ Signature	_____ Date
Dr. F. O. Anafi Member, Supervisory Committee	_____ Signature	_____ Date
Dr. F. O. Anafi Head of Department	_____ Signature	_____ Date
Prof. S. Z. Abubakar Dean, School of Post Graduate Studies	_____ Signature	_____ Date

DEDICATION

I give all Praise and Glory to Allah (S.W.A), the Lord of the worlds, Whose Will and Power made the completion of my entire PhD programme a reality.

ACKNOWLEDGEMENTS

I would like to express my most sincere appreciation to the chairman of the supervisory committee of this work, Prof. C. O. Folayan for the patience, direction and wealth of experience that was committed throughout the period of this work that has led to the successful completion.

My very special thanks goes to other members of the supervisory committee of this work; Prof. D. S.Yawas and Dr. F. O. Anafi. Theirconstructive criticisms, highly valued contributions and motivations especially at the concluding stage of the work has ensured it came out successful.

To my caringmum; Hajiya A. Ahmadu, I thank her for the prayers, encouragement and words of wisdom throughout the period of this work.

To my lovely wife, Pharm (Mrs) K. Ahmadu, thanks for understanding and the support offered to ensure this work was successfully completed.

To my children, I say thanks for understanding and being there for me.

I would like to express my gratitude to my siblings for all the support rendered to me throughout the period of this work.

I would like to say a very big thank you to Mr. S. Anthony, chief technician and proprietor of Safari Air Conditioning and Refrigeration, Kaduna. The efforts and expertise which was put into the construction made the system construction a reality. Many thanks also to other staff of Safari Air Conditioning and Refrigeration, Kaduna and indeed all staff of the workshop, Department of Mechanical Engineering, A. B. U. Zaria.

I would like to express my appreciation to all my colleagues at the Department of Mechanical Engineering, A.B.U. Zaria, and friends who have made contributions to this work.

I extend my appreciation to Dr. S. A. Oke of the Department of Mechanical Engineering, University of Lagos, for his concern and contributions to ensure this work turns out successful.

ABSTRACT

In this study, a gas assisted solar powered absorption air – conditioning system was designed, constructed and tested under Zaria weather conditions in Nigeria. A technical and economic viability study of the system was first carried out by developing and simulating a TRNSYS model of the system to cool an office block with an average space cooling demand of 151.8kWh/m^2 per annum, under Zaria weather conditions. System components were sized and optimized to give maximum coefficient of performance (COP), solar coefficient of performance (SCOP) and solar fraction (SF). Design of the optimised system components was done through a programming based design, optimisation and performance evaluation method using MATLAB. A reduced size version of the system, which includes a 4 kW absorption chiller prototype was constructed. Experimental tests were conducted on the constructed system. The experiments were carried out on a test room in the months of April and June 2017. The experimental days were classified as: hot clear sky days, fairly clear sky days, cloudy days and rainy days. Results indicated that the system is capable of operating in any of the days as classified. However, the cloudy days recorded the highest gas consumption of 0.95kg, as the system relied more on the gas boiler heating mode. The hot clear sky days recorded the least gas consumption of 0.48 kg as the system operated more on the solar power heating mode. Room temperatures were cooled to between 24^oC and 27^oC, from initial temperatures ranging from 29^oC to 33^oC. Maximum cooling power of 2.7 kW was achieved by the absorption chiller. Maximum daily average COP of 0.438 was attained. Solar fraction of 0.55 was achieved in the experimental day of April, while 0.27 was attained for June. Results from life cycle cost savings simulation showed energy savings of ₦2, 172,558 with 35m^2 collector area for a period of 20 years. Life cycle cost savings analysis of the constructed system showed the system is economically viable in the Nigerian climate studied, with a savings of ₦39,991.93 achievedwith a collector area of 1.7 m^2over a 20 year period. Environmental impact assessment showed CO_2 emission reduction in the range of 2.7% to 58.4%. It was concluded that the system operates satisfactorily in the Nigerian climate studied and it is economically viable. Recommendations for further improvements were made.

TABLE OF CONTENTS

DECLARATION ……ii

CERTIFICATION ……...iii

DEDICATION ……iv

ACKNOWLEDGEMENTS ……v

ABSTRACT ……vi

TABLE OF CONTENTS ……vii

LIST OF FIGURES ……xii

LIST OF TABLES ……...xxii

LIST OF APPENDICES ……xxiii

NOMENCLATURE ……xxiv

CHAPTERS

1. INTRODUCTION……..1

1.1 Background to the Study……...1

1.2 Statement of the Problem…….3

1.3 The Present Research……...4

1.4 Aim and Objectives…….....4

1.5 Justification for the Research……...5

1.6 Scope of and limitations of the Research…….5

2. LITERATURE REVIEW……...6

2.1 Refrigeration and Air-conditioning……..……6

2.2 History of Air conditioning…….....……6

2.3 Applications of Air-conditioning…….....……7

2.3.1Industrial air conditioning…….7

2.3.2Comfort Air-Conditioning…….....8
2.4 Conventional Air Conditioning Systems…….....9
2.5 Solar Cooling Systems…….....10

2.5.1 Solar electrical air conditioning……...11

2.5.2 Solar thermal air conditioning……....11

2.5.3 The adsorption system……....13

2.5.4 The absorption system…….....14

2.6 The Absorption Chiller……...14

2.7 Software Tools for Design, Modelling and Simulation of Solar Thermal Air conditioning Systems……15

2.7.1 TRNSYS software…… 15

2.7.2 Microsoft excel……16

2.7.3 Matrix laboratory…….16

2.7.4 Energy plus……..17

2.7.5 Engineering equation solver……17

2.8 Review of Past Works in the Area…….18

2.8.1 Studies on simulation of solar absorption air conditioning systems done for different climates……18

2.8.2 Experimental studies on pre-installed solar absorption air conditioning plant done in different climates……24

2.8.3 Studies on design construction and test of small andmicro scale capacity absorption chiller prototypes……....28

2.8.4 Mathematical modelling and theoretical studies on absorption cooling cycle……..32

2.9 Conclusion from Literature Review and Research Gap……...33

3. MATERIALS AND METHODS……...35

3.1 Description and Working Principle of the Proposed Solar/ Gas Hybrid Powered Absorption Air Conditioning System……...35

3.2 Materials……..37

3.2.1 Software tools ……..37

3.2.2 Materials for the construction……...37

3.2.3 Materials for the experiment……..38

3.3Cooling Energy Demand Simulation using TRNSYS……..38

3.3.1 Mathematical description of type 56…….....39

3.4 TRNSYS Modelling and Simulation of the Solar/ Gas Hybrid PoweredAbsorption Air conditioning System……47

3.4.1 TRNSYS components (types) used in the system model with mathematical descriptions……....48

3.4.2 The control system……..55

3.4.3 Sizing of the absorptioncooling system components in TRNSYS……57

3.4.4 TRNSYS modelling and Simulation procedure…….....61

3.5 Design Theories, Optimization, Programming and Calculations…….62

3.5.1 Design considerations……....63

3.5.2 Materials selection…… ……64

3.5.3 Flat plate collector design……..65

3.5.4 Flat plate collector design optimization and design parameters calculation……71

3.5.5 Absorption chiller design……..71

3.5.6 Absorption chiller components optimization and performance simulation ……91

3.5.7 Wet cooling tower design……....103

3.5.8 Design of hot water storage tank…….....108

3.5.9 Fan coil unit sizing and selecting……110

3.6 Construction of the Solar/ Gas Hybrid Powered Absorption Air conditioning System……..112

3.6.1 Construction of the absorption chiller……..112

3.6.2 Construction of the flat plate collector. …….....116

3.6.3 Construction of the of storage tank……...117

3.6.4 Construction of the cooling tower…….....118

3.7 Experiment……...119

3.7.1 Experimental apparatus…….....119

3.7.2 Experimental procedure…….....120

3.7.3 Performance measurement……122

3.8 Economic Analysis……...124

3.8.1 Economic viability simulation and optimization of the solar/ gas hybrid absorption air conditioning system……..124

3.8.2 Economic assessment of the constructed system……..126

3.9 Environmental Impact Assessment (CO_2 emission reduction & global warming potential)……129

4. RESULTS & DISCUSSION…….....130

4.1 Results from Building Cooling Energy Demand Simulation……130

4.2 Results from Modelling Simulation and Optimization of theSolar/ Gas Hybrid Powered Absorption System in TRNSYS……131

4.2.1 Results from optimization of the absorption air conditioning system components…….132

4.2.2: Results from building cooling simulation using optimized absorption air conditioning system components……..144

4.3 Results from system Components Designand Optimization……...157

4.3.1 Results from flat plate collector design and optimization……157

4.3.2 Results from design calculations of absorption chiller ……...161

4.3.3 Results from optimization of absorption chiller design ……...161

4.3.4 Results from performance simulation of the

absorption chiller……..169

4.3.5 Results from cooling tower design……172

4.3.6 Results from fan coil unit sizing…….....173

4.4 Results from Experiments Conducted……...173

4.4.1 Results from experiment……....173

4.4.2 Performance parameters from experiments conducted ……211

4.5 Results from Economic Analysis……..215

4.5.1 Results from economic viability simulation……...215

4.5.2. Economic assessment of the constructed system……....217

4.6 Comparison of Performance Parameters……..221

4.6.1 Comparison of coefficient of performance……221

4.6.2 Comparison of solar fraction…….222

4.6.3 Comparison of average space cooling temperatures…….222

4.6.4 Comparison of power consumption……..222

4.6.5 Comparison of cost per kWh of cooling……...223

4.7 Results from Environmental Impact Assessment (CO2 emission reduction and global warming potential)…….224

5. CONCLUSION &RECOMMENDATIONS……226

5.1 Conclusion……...226

5.2 Recommendations……...227

5.3 Contribution to Knowledge……227

REFERENCES……..229

LIST OF FIGURES

Figure 2.1: Vapour compression refrigeration system……...9

Figure 2.2: Solar cooling paths……...10

Figure 2.3: Basic scheme of an open cycle system……12

Figure 2.4: Basic scheme of a closed cycle system……13

Figure 3.1 Schematic of the solar/ gas hybrid absorption cooling system…….36

Figure 3.2 Plan view of the building……..38

Figure 3.3 Convective heat balance on the air node……...39

Figure 3.4 Radiative energy flows considering one wall
with its surface temperature node…….....40

Figure 3.5 Surface heat fluxes and temperatures……41

Figure 3.6 Black box model of wall……...42

Figure 3.7: Two-node window model used in TYPE 56 energy balance equation……44

Figure 3.8 TRNSYS model for the cooling load simulation……..45

Figure 3.9 Model of the solar/ gas hybrid powered absorption cooling system in TRNSYS
studio ……48

Figure 3.10: Segmented layers of stratified storage tank……...53

Figure 3.11: Schematic of pump arrangement……...56

Figure 3.12 Geometric configuration of the absorber plate- tube……..……69

Figure 3.13 Schematic of absorption chiller components……..……72

Figure 3.14 Idealized hexagonal grid boundary imposed over bundle
cross section to identify local void fraction per tube……..85

Figure 3.15 Idealized local saturated liquid film surrounding circumference of tube……...85

Figure 3.16 Generator flow diagram……..94

Figure 3.17 Evaporator flow diagram……97

Figure 3.18 Condenser flow diagram……99

Figure. 3.19 Absorber flow diagram…….101

Figure 3.20: Algorithm block diagram for absorption chiller design optimization and simulation……...103

Figure 3.21: Approximating the curve for H_s with a straight line……106

Figure 3.22: Schematic of the experimental set up……120

Figure 4.1: Peak cooling energy demand for the months……..130

Figure 4.2 Hourly cooling load for the 21st of April……..131

Figure4.3: Year round temperature variation within the zones without cooling……..132

Figure 4.4: Variation of COP with collector area and hot water storage tank volume for January……133

Figure 4.5: Variation of SCOP with collector area and hot water storage tank volume for January……...133

Figure 4.6: Variation of COP with collector area and hot water storage tank volume for February……...133

Figure 4.7: Variation of SCOP with collector area and hot water storage tank volume for February……..134

Figure 4.8: Variation of COP with collector area and hot water storage tank volume for March……..134

Figure 4.9: Variation of SCOP with collector area and hot water storage tank volume for March……134

Figure 4.10: Variation of COP with collector area and hot water storage tank volume for April……..135

Figure 4.11: Variation of SCOP with collector area and hot water storage tank volume for April……..135

Figure 4.12: Variation of COP with collector area and hot water storage tank volume for May……...135

Figure 4.13: Variation of SCOP with collector area and hot water storage tank volume for May……..136

Figure 4.14: Variation of COP with collector area and hot water storage tank volume for June……...136

Figure 4.15: Variation of SCOP with collector area and hot water storage tank volume for June……..136

Figure 4.16: Variation of COP with collector area and hot

water storage tank volume for July…….137

Figure 4.17: Variation of SCOP with collector area and hot water storage tank volume for July…….....137

Figure 4.18: Variation of COP with collector area and hot water storage tank volume for August……..137

Figure 4.19: Variation of SCOP with collector area and hot water storage tank volume for August……..138

Figure 4.20: Variation of COP with collector area and hot water storage tank volume for September……138

Figure 4.21: Variation of SCOP with collector area and hot water storage tank volume for September……138

Figure 4.22: Variation of COP with collector area and hot water storage tank volume for October……139

Figure 4.23: Variation of SCOP with collector area and hot water storage tank volume for October……139

Figure 4.24: Variation of COP with collector area and hot water storage tank volume for November……139

Figure 4.25: Variation of SCOP with collector area and hot water storage tank volume for November……....140

Figure 4.26: Variation of COP with collector area and hot water storage tank volume for December……140

Figure 4.27: Variation of SCOP with collector area and hot waterstorage tank volume for December……140

Figure 4.28: Variation of solar fraction with collector area for the months of January to April……...142

Figure 4.29: Variation of solar fraction with collector area for the months of May to August……..143

Figure 4.30: Variation of solar fraction with collector area for the months of September to December…….....143

Figure. 4.31: Year round temperature variation within the zones with cooling from the optimized system……144

Figure 4.32: Relative humidity variation within zones, January (no cooling)…….145

Figure 4.33: Relative humidity variation within zones, January (with cooling)……..145

Figure 4.34: Relative humidity variation within zones, February (no cooling)…….146

Figure 4.35: Relative humidity variation within zones, February (with cooling)……..146

Figure 4.36: Relative humidity variation within zones, March (no cooling)…….147

Figure 4.37: Relative humidity variation within zones, March (with cooling)……..147

Figure 4.38: Relative humidity variation within zones, April (no cooling)……...148

Figure 4.39: Relative humidity variation within zones, April (with cooling)……148

Figure 4.40: Relative humidity variation within zones, May (no cooling)……149

Figure 4.41: Relative humidity variation within zones, May (with cooling)…….149

Figure 4.42: Relative humidity variation within zones, June (no cooling)……150

Figure 4.43: Relative humidity variation within zones, June (with cooling)…….150

Figure 4.44: Relative humidity variation within zones, July (no cooling)…….151

Figure 4.45: Relative humidity variation within zones, July (with cooling)……..151

Figure 4.46: Relative humidity variation within zones, August (no cooling)……152

Figure 4.47: Relative humidity variation within zones, August (with cooling)…….152

Figure 4.48: Relative humidity variation within zones, September (no cooling)……..153

Figure 4.49: Relative humidity variation within zones, September (with cooling)……...153

Figure 4.50: Relative humidity variation within zones, October (no cooling)……..154

Figure 4.51: Relative humidity variation within zones, October (with cooling)……...154

Figure 4.52: Relative humidity variation within zones, November (no cooling)……..155

Figure 4.53: Relative humidity variation within zones, November (with cooling)……...155

Figure 4.54: Relative humidity variation within zones, December (no cooling)……..156

Figure 4.55: Relative humidity variation within zones, December (with cooling)……...156

Figure 4.56: Variation of heat removal factor with absorber plate thickness at different tube diameters…….157

Figure 4.57: Variation of heat removal factor with tube spacing at different tube diameters……..158

Figure 4.58: Variation of heat removal factor with back insulation thickness at different tube diameters……..159

Figure 4.59: Variation of heat removal factor with Edge insulation thickness at different tube diameters…….159

Figure 4.60: Variation of COP with heat transfer area for generator……161

Figure 4.61: Variation COP with number of tubes for generator……...161

Figure 4.62: Variation of COP with shell diameter for generator……..162

Figure 4.63: Variation COP with baffle spacing for generator……..162

Figure 4.64: Variation of COP with tube diameter for generator……..162

Figure 4.65: Variation COP with tube layout for generator……..162

Figure 4.66: Variation of COP with heat transfer area for evaporator……..163

Figure 4.67: Variation COP with number of tubes for evaporator……163

Figure 4.68: Variation of COP with shell diameter for evaporator……...164

Figure 4.69: Variation COP with baffle spacing for evaporator……...164

Figure 4.70: Variation of COP with tube diameter for evaporator……...164

Figure 4.71: Variation COP with tube layout for evaporator……...164

Figure4.72: Variation of COP with heat transfer area for condenser……..165

Figure 4.73: Variation COP with number of tubes for condenser……165

Figure 4.74: Variation of COP with shell diameter for condenser……...166

Figure 4.75: Variation COP with baffle spacing for condenser……..166

Figure 4.76: Variation of COP with tube diameter for condenser……..166

Figure. 4.77: Variation COP with tube layout for condenser……...166

Figure 4.78: Variation of COP with heat transfer area for absorber……167

Figure 4.79: Variation COP with number of tubes for absorber……..167

Figure 4.80: Variation of COP with shell diameter for absorber…….167

Figure 4.81: Variation COP with baffle spacing for absorber…….167

Figure 4.82: Variation of COP with tube diameter for absorber……168

Figure 4.83: Variation COP with tube layout for absorber……168

Figure 4.84: Variation of COP with hot water inlet temperature to generator…….. ……....170

Figure 4.85: Variation of COP with cooling water inlet temperature……170

Figure 4.86: Variation of evaporator cooling power with hot water inlet temperature……..170

Figure 4.87: Variation of evaporator cooling power with cooling water inlet temperature...170

Figure 4.88. Variation of solar radiation with time for April 22, 2017……..174

Figure 4.89. Variation of collector temperatures and gas consumption with time for April 22, 2017……....174

Figure 4.90: Variation of system temperatures with time for April 22, 2017……174

Figure 4.91: Variation of ambient and room temperatures with time for April 22……175

Figure 4.92: Variation of system power with time for April 22, 2017……..175

Figure 4.93: Variation of COP and SCOP with time for April 22, 2017……...175

Figure 4.94: Variation of cooling tower temperatures with time for April 22, 2017…….176

Figure 4.95: Variation of collector efficiency with time for April 22, 2017……..176

Figure 4.96. Variation of relative humidity with time for April 22, 2017…….176

Figure 4.97: Variation of solar radiation with time for June 3, 2017……179

Figure 4.98: Variation of collector temperatures and gas consumption with time for June 3, 2017……...179

Figure 4.99: Variation of system temperatures with time for June 3, 2017……...179

Figure 4.100: Variation of ambient and room temperatures with time For June 3, 2017……180

Figure 4.101: Variation of system power with time for June3, 2017……180

Figure 4.102: Variation of COP and SCOP with time for June 3, 2017……180

Figure 4.103: Variation of cooling tower temperatures with time for June 3, 2017……..181

Figure 4.104: Variation of collector efficiency with time for June 3, 2017……...181

Figure 4.105: Variation of solar radiation with time for June 6, 2017……...183

Figure 4.106 Variation of collector temperatures and
gas consumption with time for June 6, 2017……....183

Figure 4.107: Variation of system temperatures with time for June 6, 2017……183

Figure 4.108: Variation of ambient and room temperatures with time
For June 6, 2017……..184

Figure 4.109: Variation of system power with time for June 6, 2017……....184

Figure 4.110: Variation of COP with time for June 6, 2017……..184

Figure 4.111: Variation of cooling tower temperatures with time for June 6, 2017……..185

Figure 4.112: Variation of collector efficiency with time for June 6, 2017……...185

Figure 4.113: Variation of solar radiation with time for June 7, 2017……...186

Figure 4.114: Variation of collector temperatures and
gas consumption with time for June 7, 2017……...187

Figure 4.115: Variation of system temperatures with time for June 7, 2017……187

Figure 4.116: Variation of ambient and room temperatures with time for June 7, 2017…...187

Figure 4.117: Variation of system power with time for June 7, 2017……....188

Figure 4.118: Variation of COP with time for June 7, 2017……..188

Figure 4.119: Variation of collector efficiency with time for June 7, 2017……...188

Figure 4.120: Variation of solar radiation with time for June 8, 2017……...190

Figure 4.121: Variation of collector temperatures and
gas consumption with time for June 8, 2017……...190

Figure 4.122: Variation of system temperatures with time for June 8, 2017……191

Figure 4.123: Variation of ambient and room temperatures with time for June 8, 2017…...191

Figure 4.124: Variation of system power with time for June 8, 2017……191

Figure 4.125: Variation of COP and SCOP with time for June 8, 2017……192

Figure 4.126: Variation of cooling tower temperatures with time for June 8, 2017……..192

Figure 4.127: Variation of collector efficiency with time for June 8, 2017……...192

Figure 4.128: Variation of solar radiation with time for June 12, 2017……194

Figure 4.129: Variation of collector temperatures and
gas consumption with time for June 12, 2017……194

Figure 4.130 Variation of system temperatures with time for June 12, 2017……194

Figure 4.131 Variation of ambient and room temperatures with time for June 12, 2017…..195

Figure 4.132 Variation of system power with time for June 12, 2017……...195

Figure 4.133: Variation of COP with time for June 12, 2017……195

Figure 4.134: Variation of cooling tower temperatures with time for June 12, 2017……196

Figure 4.135: Variation of solar radiation with time for June 13, 2017…….197

Figure 4.136: Variation of collector temperatures and
gas consumption with time for June 13, 2017……197

Figure 4.137: Variation of system temperatures with time for June 13, 2017……...198

Figure 4.138: Variation of ambient and room temperatures with time for June 13, 2017….198

Figure 4.139: Variation of system power with time for June 13, 2017……..198

Figure 4.140: Variation of COP with time for June 13, 2017……199

Figure 4.141: Variation of cooling tower temperatures with time for June 13, 2017……199

Figure 4.142: Variation of solar radiation with time for June 17, 2017…….200

Figure 4.143: Variation of collector temperatures and
gas consumption with time for June 17, 2017……..201

Figure 4.144 Variation of system temperatures with time for June 17, 2017……201

Figure 4.145: Variation of ambient and room temperatures with time for June 17, 2017….201

Figure 4.146: Variation of system power with time for June 17, 2017……..202

Figure 4.147 Variation of COP with time for June 17, 2017……..202

Figure 4.148: Variation of cooling tower temperatures with time for June 17, 2017……202

Figure 4.149: Variation of relative humidity with time for June 17, 2017……203

Figure 4.150: Variation of solar radiation with time for June 18, 2017……204

Figure 4.151: Variation of collector temperatures and
gas consumption with time for June 18, 2017……205

Figure 4.152: Variation of system temperatures with time for June 18, 2017……...205

Figure 4.153: Variation of ambient and room temperatures with time for June 18, 2017….205

Figure 4.154: Variation of system power with time for June 18, 2017……..206

Figure 4.155: Variation of COP with time for June 18, 2017……206

Figure 4.156: Variation of cooling tower temperature with time for June 18, 2017…….206

Figure 4.157: Variation of relative humidity with time for June 18, 2017……207

Figure 4.158: Variation of solar radiation with time for June 19, 2017……208

Figure 4.159: Variation of collector temperatures and gas consumption with time for June 19, 2017…….208

Figure 4.160: Variation of system temperatures with time for June 19, 2017……...209

Figure 4.161: Variation of ambient and room temperatures with time for June 19, 2017….209

Figure 4.162: Variation of system power with time for June 19, 2017……..209

Figure 4.163: Variation of COP with time for June 19, 2017……210

Figure4.164: Variation of cooling tower temperatures with time for June 19, 2017……210

Figure 4.165: Variation of relative humidity with time for June 19, 2017……210

Figure 4.166: Solar fraction of the experimental days……...212

Figure 4.167: Daily gas consumption of the experimental days……213

Figure 4.168: Average daily COP of the experimental days…….214

Figure 4.169: Variation of total cost of cooling system, cost of cooling load covered by solar power and cost of auxiliary energy with collector area…...215

Figure 4.170: Variation of life cycle savings with collector area……...216

Figure 4.171: Variation of daily energy cost for the experimental days……218

Figure 4.172: Variation of cost per kWh of cooling for the experimental days……..219

Figure 4.173: Variation of COP of constructed absorption chillers……221

Figure 4.174: Comparison of power consumption of constructed chiller with conventional chiller of varying EER……..223

Figure 4.175: Comparison of cost per kWh of coolingof constructed chiller

with conventional chiller of varying EER……223

Figure 4.176: Comparison of CO_2 emitted to the atmosphere from constructed chiller with conventional of varying EER……224

Figure 4.177: Comparison of GWP of refrigerant in constructed chiller (water) with GWP of common refrigerant in conventional chillers…….225

LIST OF TABLES

Table 3.1: Inputs to Type 56…….46

Table 3.2: Monthly energy ratio from TRNSYS simulation……58

Table 3.3: Temperatures of state points……....74

Table 3.4: Components full scale size and constructed size……112

Table 3.5: Construction process of the absorption chiller……113

Table 3.6: Construction process of the flat plate solar collector……...116

Table 3.7: Construction process of the storage tank……117

Table 3.8: Construction process of the cooling tower……...118

Table 3.9: Component prices……126

Table 3.10: Cost analysis of the constructed system……126

Table 3.11: Energy efficiency standards for different countries……...128

Table 3.12: Global Warming Potential (GWP) values of commonly used HCFC refrigerants……....129

Table 4.1: Outputs from flat plate collector design program……....160

Table 4.2: Optimized system components for the absorption chiller……...169

Table 4.3: Output from cooling tower design calculation program……172

Table 4.4: Outputs from cooling coil design program……173

LIST OF APPENDICES

APPENDIX A1: TRNSYS input file for building cooling load simulation……241

APPENDIX A2: TRNSYS input file for solar absorption cooling system model and simulation……..251

APPENDIX B: MATLAB Program for flat plate solar collector design……273

APPENDIX C: MATLAB Program for generator design……275

APPENDIX D: MATLAB Program for condenser design……279

APPENDIX E: MATLAB Program for evaporator design……283

APPENDIX F: MATLAB Program for absorber design……...287

APPENDIX G: MATLAB Program for solution heat exchanger design……..291

APPENDIX H: MATLAB Program for performance simulation of absorption chiller…...295

APPENDIX I: MATLAB Program for cooling tower design……....298

APPENDIX J: MATLAB Program for fan coil sizing……..300

APPENDIX K1: Outputs from generator design programme……...301

APPENDIX K2: Outputs from condenser design programme……..303

APPENDIX K3: Outputs from evaporator design programme…….305

APPENDIX K4: Outputs from absorber design programme……....307

APPENDIX K5: Outputs from SHX design programme…….....309

APPENDIX L: Measured values for experimental days…….....311

APPENDIX M: Plates……...321

APPENDIX N: Working drawings……...327

NOMENCLATURE

Roman

c_p	Specific heat capacity	(kJ/kgK)
d	Diameter	(m)
f	Friction coefficient	
g	Acceleration due to gravity	(m/sec^2)
h	Enthalpy, Heat transfer coefficient	(kJ/kg, W/m^{2}K)
k	Thermal conductivity	(W/m^{o}C)
$\dot{m}$	Mas flow rate	(kg/sec)
p	Pitch	(m)
q	Heat flux	(W/m^2)
t	Time	(sec)
v	Velocity	(m/sec)
As	Surface area	(m^2)
Ax	Cross sectional area	(m^2)
D	Diameter	(m)
E	Energy	(J)
F	LMTD correction factor	
G	Mass velocity	(kg/m^{2}sec)
I	Solar irradiation	(W/m^2)
L	length	(m)
N	Number	
P	Pressure	(N/m^2)
Q	Heat load	(W)
$\dot{Q}$	Energy flow rate	(kJ/sec)
T	Temperature	(^{o}C)
V	Volume	(m^3)
$\dot{V}$	Volume flow rate	(m^3/sec)
X	Concentration	(%)

Subscript

1, 2, 3……17	State points
a	Absorber
aux	Auxiliary
c	Condenser
cb	Convective boiling
cf	Cross flow
cfl	Circumferential flow
chw	Chilled water
ct	Cooling tower
cw	Cooling water
e	Evaporator, Equivalent
f	Fluid
g	Generator
h	Hot fluid
hc	Heater capacity
hex	Hexagon
hw	Hot water
i	Inlet, inner
in	Inlet
l	Liquid
max	Maximum
nb	Nucleate boiling
o	Outlet, outer
out	Outlet
p	Plate
ph	Horizontal pitch
pr	Provisional
pv	Vertical pitch
ref	Refrigerant

s	Shell side
sat	Saturation
set	Set point
SHX	Solution Heat Exchanger
sol	Solution
$surf$	Surface
t	Tube
T	Total, Tank
ss	Strong solution
v	Vapour
w	Wall, Water
ws	Weak solution

Greek

η	Efficiency	
τ	Transmittance	
α	Absorptance	
φ	Condensation heat transfer coefficient	(W/m^2K)
μ	Dynamic viscosity	(kg/ms)
ρ	Density	(kg/m^3)
δ	Liquid film thickness	(m)
Γ	Falling film flow rate	(kg/ms)
U	Overall heat transfer coefficient	(kW/m^2k)
Δ	Change	
λ	Latent heat	(kJ/kg)

Acronyms

Bo	Boiling number
COP	Coefficient of performance
EES	Engineering equation solver
H_2O	Water
HVAC	Heating ventilation and air conditioning

LiBr	Lithium bromide
LMTD	Logarithmic mean temperature difference
$LMTD_c$	Corrected logarithmic mean temperature difference
MATLAB	Matrix Laboratory
Nu	Nusselt number
Pr	Prandtl number
Re	Reynolds number
SHX	Solution heat exchanger
TR	Tonnes of refrigeration
TRNSYS	Transient systems simulation software

CHAPTER ONE

INTRODUCTION

1.1 Background to the Study

Energy is an essential need of all human beings in the world. The technological advancement and economic growth of any country rests on the availability of utilisable form of energy in that country (Sarbu and Sebarchievici, 2015). So far, fossil fuels are considered and utilised as the prominent source of generating utilisable form of energy (Choudhury *et al.* 2013). It is estimated that 80% of the energy currently used on earth is generated from fossil fuel sources (Sarbu and Sebarchievici, 2015). However, concerns are growing on a daily basis over the negative effects on the environment that are caused by burning fossil fuels that include global warming and ozone layer depletion (Said *et al.*, 2015).

The energy demand for air conditioning is increasing continuously, due to growing thermal loads, changing building architectural modes and especially due to increasing occupants indoor comfort demands resulting in higher electricity demand notably during peak periods (Kalkan *et al.*, 2012).Vapour compression based refrigerating systems are generally employed in refrigeration and air conditioning units. These units operate with synthetic refrigerants such as chlorofluorocarbons (CFCs) and hydro – chlorofluorocarbons (HCFCs), which when released into the atmosphere deplete the ozone layer and contribute to the global warming (Sarbu and Sebarchievici, 2015). Also, usual vapour compression based cycles are electrically powered, consuming large amounts of high quality energy. According to the International Institute of Refrigeration in Paris, the amount of electricity consumption from different types of refrigeration and air conditioning processes is approximately 15% of the electricity produced worldwide (Kalkan *et al.*, 2012). Also, electricity consumption for air conditioning systems has been

estimated around 45% of electricity consumption in residential and commercial buildings (Kalkan *et al.,* 2012).

Renewable energy sources are being sought as alternative sources of energy for refrigeration and air conditioning. Amongst the many renewable energy sources, solar energy stands out as a very attractive alternative. The main reason being in its cleanliness and natural availability (Anand *et al.,* 2015). Also, the cooling load usually reaches its peak value when solar energy is mostly available. This synchronism between solar irradiance and building cooling load gives an advantage (Li and Sumathy, 2000).

Solar electrical and solar thermal powered refrigeration systems can be used to produce cooling. The first is photovoltaic based in which solar energy is converted directly to electricity then utilised for producing cooling, similar to conventional methods. The second utilises solar thermal energy to power the generator of an absorption refrigeration system (Otanicar *et al.,* 2012).Solar thermal cooling systems have the advantage of using absolutely harmless working fluids such as water, or solutions of certain salts as refrigerants. They are energy efficient and environmentally safe. Due to the advantages of solar thermal cooling systems over solar photovoltaic cooling systems, over the years, more research has been carried out in the field of solar thermal cooling (Otanicar *et al.,* 2012).However, despite the increased level of research in the field of solar thermal cooling over the years and the seeming advantage it can potentially have, the absorption air conditioning system still lacks the ability to compete favourably with its vapour compression counterpart in the market.This is due most especially to the initial high cost of the absorption air conditioning systems and the relatively low coefficient of performance (COP).

At present absorption chillers are mainly established for capacities in the range of tens of kilowatts to hundreds of kilowatts. Research works are presently ongoing to establish absorption chillers in the smallest of capacities, improve Coefficient of Performance and also to reduce the initial cost.

Research works are also being carried out to design Solar Absorption Cooling systems that will yield high Solar Fractions (SF) and be economically viable.

1.2 Statement of the Problem

The following are some of the problems that have necessitated the present research work.

i. Cost of electricity generated from fossil fuels is high.

ii. The vapour compression units consume high power which ultimately increases electricity bills.

iii. Most vapour compression systems commonly use chlorofluorocarbons (CFCs) and hydro – chlorofluorocarbons (HCFCs) refrigerants, which cause depletion in the ozone layer. The replacements, which are hydrofluorocarbons (HFCs) have zero ozone depleting potential (ODP), but high global warming potential (GWP) (Benhadid – Dib, 2012). To safeguard the environment, harmless refrigerants must be used as agreed in the "Kyoto Protocol" (Pachauri and Reisinger, 2007).

iv. In Nigeria, as a developing nation, the cooling load increases daily as a result of better comfort demands. This causes more load on the grid, especially during peak periods, which leads to total collapse in some areas. In addition to this, electricity tariff has been on the increase. As at October 2017, electricity tariff stands at ₦26.37 per kilowatt hour (residential),₦37.88 per kilowatt hour (commercial) and ₦44.22 per kilowatt hour (industrial) with increase still expected over the years (MYTO 2.1 report, 2015).The need for an alternative source of power cannot be overemphasized.

v. In the department of mechanical engineering, A.B.U. Zaria, the central vapour compression air conditioning unit for the office block has broken down beyond repair. There is need to design and simulate a solar absorption air conditioning system as a possible replacement.

vi. Solar absorption cooling is a very promising technology, however there is the need for more research work to improve COP to make it even more favourable.

1.3 The Present Research

The present research work is intended to develop a solar absorption air conditioning system. The system will comprise of an absorption chiller which will operate on the lithium bromide/ water pair. An array of solar collector to generate the required thermal energy. A storage tank to store the resulting hot water. An auxiliary heater powered by liquefied natural gas is to be incorporated to complement the solar power during periods of low solar radiation. A cooling tower for heat rejection. An indoor fan coil unit. This will be achieved by carrying out an initial simulation using TRNSYS to optimally size system components required to give monthly maximum COP and SF for an office block under Zaria weather conditions. The design of the system components will be done using program based design and calculation in MATLAB, where each of the system components will have design parameters optimized to give overall optimum COP. The system will be constructed using locally available materials and expertise. The constructed system will be tested on a test room to evaluate the performance. An economic evaluation of the system using life cycle cost savings analysis method will be carried out. An environmental impact assessment of the system to determine the carbon dioxide (CO_2) emission reduction will be carried out.

1.4 Aim and Objectives

The aim of this research is to simulate the performance of a TRNSYS model of agas assisted solar absorption air conditioning system under Zaria weather conditions, design, construct and test the system.

Specific objectives are:

i. To developa model to obtain optimum sizes of absorption chiller, collector area, storage tank volume required to achieve monthly maximum COP and SF for an office block under Zaria weather conditions using TRNSYS.

ii. To carry out the design and optimisation of the system components using MATLAB.

iii. To construct the optimised system design.

iv. To carry out experimental tests on the constructed system.

v. To carry out an economic analysis of the system.

vi. To carry out an environmental impact assessment of the system.

1.5 Justification for the Research

i. Synchronism between building cooling load and solar irradiance can lead to a successful operation of a solar absorption cooling system.

ii. Nigeria is a country with a vast availability of solar energy. A modest estimate of the technical potential of solar energy in Nigeria with 5% device efficiency is put at $15x10^{14}$kJ of useful energy annually (Onyebuchi, 1989). This translates to about $4.2x10^{5}$ GWh of electricity production annually (Oyedepo, 2012). Successful implementation of solar cooling technology in Nigeria could lead to significant reduction in power consumption.

iii. The refrigerant to be used (water) will have no global warming potential on the environment.

1.6 Scope and limitations of the Research

The scope of the present research is limited to:

i. Initial simulation of a solar absorption cooling system under Zaria weather conditions as a feasibility study and to optimally size system components.

ii. Design of the system components using programme based design and optimisation.

iii. Construct the optimised system.

iv. Test the performance of the system.

Limitations to the research work:

i. Due to the high cost required to construct the system as sized and limited funds available, reduced size version of the system was constructed within the limits of available resources.

ii. Due to the reduced size version constructed, system was tested using a test room rather than the office block.

CHAPTER TWO

LITERATURE REVIEW

2.1 Refrigeration and Air-Conditioning

The subject of refrigeration and air conditioning has evolved out of human need for food preservation and comfort, and its history dates back to centuries. Refrigeration may be defined as the process of achieving and maintaining a temperature below that of the surroundings, the aim being to cool some product or space to the required temperature (Arora, 2000). Air conditioning refers to the treatment of air so as to simultaneously control its temperature, moisture content, cleanliness, odour and circulation, as required by occupants, a process, or products in the space (Arora, 2000).

2.2 History of Air Conditioning

The widespread development of air conditioning is attributed to the American scientist and industrialist Willis Carrier. In 1902, Carrier discovered the relationship between temperature and humidity and how to control them (Wang, 2001). In 1904, he designed a central air conditioning plant using air washer. The first air conditioned office was the Larkin administration building, designed by Frank L. Wright in 1906 (Wang, 2001). The air conditioning plant distributed $10^{o}C$ chilled water to air cooling coils in air handling systems. Due to the pioneering efforts of Carrier and also due to simultaneous development of different components and controls, air conditioning

quickly became very popular, especially after 1923. The first fully air conditioned office building was the Milan building in San Antonio, Texas, which was designed by George Willis in 1928 (Wang, 2001). This air conditioned system consisted of one centralised plant to serve the lower floors and many small units to serve the top office floors. In 1937, Carrier developed the conduit induction system for multi-room buildings. The variable air volume systems which reduce the volume flow rate of supply air at reduced loads instead of varying the supply air temperature as in constant volume systems were introduced in early 1950s (Wang, 2001). These systems gained wide acceptance after the energy crises of 1973 as a result of their lower energy consumption in comparison with constant volume systems.Solar energy based refrigeration systems have also not been left out. Attempts have been made to run vapour absorption systems using solar energy with concentrating and flat plate solar collectors. Several small solar absorption refrigeration systems have been made around 1950s in several countries (Arora, 2000). Serious consideration to solar refrigeration systems was given since 1965, due to the scarcity of fossil fuel based energy sources. LiBr-water based systems have been developed for air conditioning purposes. The first solar air conditioning system was installed in an experimental solar house in University of Queensland, Australia in 1966 (Trott and Welch 2000). After this, several systems based on solar energy were built in many parts of the world. In 1976, there were about 500 solar absorption systems in USA alone. Almost all these were based on LiBr-water as these systems do not require very high heating temperatures. These LiBr-water systems were mainly used for space air conditioning (Trottand Welch, 2000). At present comfort air conditioning is widely used in residences, offices, commercial buildings, air ports, hospitals and in mobile applications such as rail coaches, automobiles, aircrafts etc. Industrial air conditioning is largely responsible for the growth of modern electronic, pharmaceutical, chemical industries etc (Wang, 2001).

2.3 Applications of Air-Conditioning

Air conditioning applications can be divided into two categories, namely industrial and comfort air conditioning.

2.3.1Industrial air conditioning

Industrial air conditioning applications include (Arora, 2000):

i. Laboratories: for precision measurement to performance testing of materials, equipment and processes at controlled temperature and relative humidity.

ii. Manufacture of precision parts: metal parts maintained at uniform temperature during manufacturing process will neither expand nor shrink, thus maintaining close tolerances.

iii. Pharmaceutical industries: To obtain sterile atmosphere, airborne bacteria and dust are removed in the air conditioning system by filters.

iv. Power plant control rooms: Most modern power plants are microprocessor controlled. Unlike the earlier designs which had very large control rooms and provided with natural ventilation, the modern designs are very compact, hence require air conditioning for persons and microprocessors.

v. Computer rooms: To protect computers, printers etc., rooms have to be kept free of dust by using micro filters in the air conditioning system.

vi. Textile industry: The yarn in the textile industry is spun and it moves over spools at very high speeds in modern machines. It is very sensitive to humidity, thus requires air conditioning.

vii. Printing: Improper humidity may cause static electricity, curling and buckling of paper. Air conditioning is required to control temperature and humidity.

2.3.2Comfort air-conditioning

Energy of food is converted into chemical energy for functioning of body organs and this energy is ultimately rejected to the surroundings. Regulatory mechanisms of human body maintain this

temperature by rejecting appropriate amount of heat. Human beings do not feel comfortable if some extra effort is required by the body to reject this energy.

The air temperature, humidity and velocity at which the human body does not have to take any extra action, is called comfort condition. Comfort condition is also referred to as neutral condition. The residences, offices, shopping centres, stores, large buildings, theatres, hospitals, auditorium, vehicles etc. all have different designs and comfort condition requirements which must be met by air conditioning.

2.4Conventional Air Conditioning Systems

An air conditioning equipment consists of components arranged in sequential order to heat or cool, humidify or dehumidify, clean and purify, transport the conditioned outdoor air and recirculate air to the conditioned space so as to maintain an indoor or enclosed environment at optimum energy use (Gugulothu *et al*, 2015).Most of the present day air conditioning systems are vapour compression based systems. However, due to the problems which are associated with the vapour compression systems, solar thermal air conditioning systems are beginning to see more usage recently. The vapour compression system is the most widely used method of air conditioning in modern applications. The vapours of the refrigerant are compressed in the compressor of the refrigerating system to develop the cooling effect. Most of the compressors are electric motor driven, thus the system consumes a large amount of electricity. These units operate with synthetic refrigerants such as chlorofluorocarbons (CFCs) and hydro – chlorofluorocarbons (HCFCs), which when released into the atmosphere deplete the ozone layer and contribute to global warming , (Sarbu and Sebarchievici, 2015). Figure 2.1 shows the basic components of a vapour compression refrigeration system. The basic system consists of an evaporator, compressor, condenser and an expansion valve.

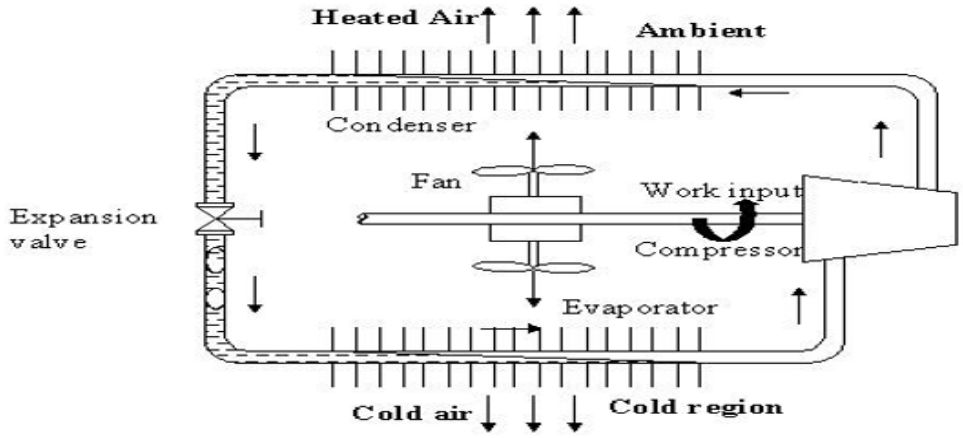


Figure 2.1 Vapour compression refrigeration system (Source: Trott and Welch, 2000).

2.5 Solar Cooling Systems

The solar cooling system is generally comprised of three sub-systems: the solar energy conversion system, refrigeration system, and the cooling load. The appropriate cycle in each application depends on cooling demand, power, and the temperature levels of the refrigerated object, as well as the environment.Solar air conditioning can be produced through two main paths:

i. Solar electrical (photovoltaic collectors to electricity)

ii. Solar thermal (thermal collectors to heat)

Figure 2.2 shows the available paths through which cooling can be attained from solar energy. Different collector types are used to attain the required input temperatures as shown in figure 2.2.

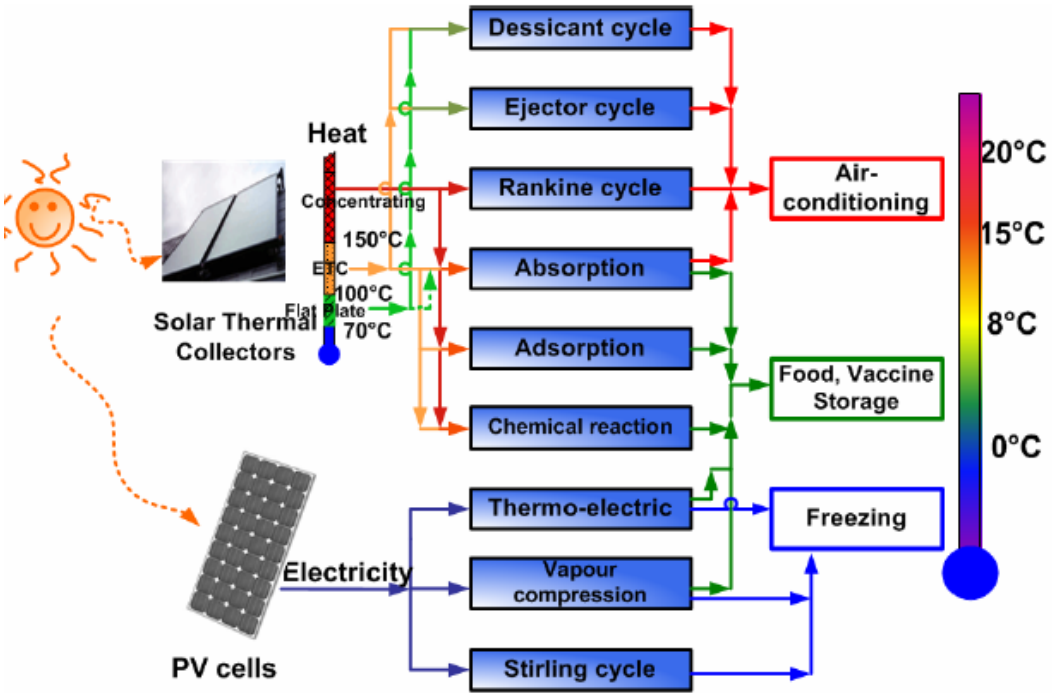


Figure 2.2: Solar cooling paths (Source: Pridasawas, 2006)

2.5.1 Solar electrical air conditioning

This system is photovoltaic based. Solar energy is converted directly to electricity using solar photovoltaic collectors. The electricity is then used to produce cooling using conventional methods (Otanicar *et al.*, 2012). During the past decade, because the efficiency of solar photovoltaic collectors increased only slightly (10 – 15) %, contrary to that of solar thermal collectors, and because the electrically driven systems are characterised by the limited useful power that can be achieved by solar means, more attention has been paid to solar thermal driven refrigeration technologies (Sarbu and Sebarchievici, 2015).

2.5.2 Solar thermal air conditioning

In solar thermal air conditioning systems, solar thermal collectors along with auxiliary heating unit (backup boiler in case of scarce or no solar radiation and during night time) are used to deliver heat to thermally driven cooling machines for producing chilled water used for air conditioning of the buildings (Ghafoor and Munir, 2015). Thermally driven technologies can be classified into two main categories: (a) Open cycles (direct treatment of air for temperature and humidity control) and (b) Closed cycles (chilled water systems) (Ghafoor and Munir, 2015).

2.5.2.1Open cycles

The open cycle process, also referred to as desiccant evaporative cooling (DEC) system, uses water as refrigerant and a desiccant (a hygroscopic material; moisture absorbing material) as the sorbent for producing conditioned air directly in ventilation systems (Ghafoor and Munir, 2015). Depending on their working principle, open cycle process can further be classified as: (i) Solid sorption: desiccant wheel, coated heat exchanger, silica gel or lithium chloride (LiCl) matrix. (ii) Liquid sorption: packed bed, plate heat exchanger (Mugnier and Jakob, 2012). The basic scheme of an open cycle system is shown in figure 2.3.

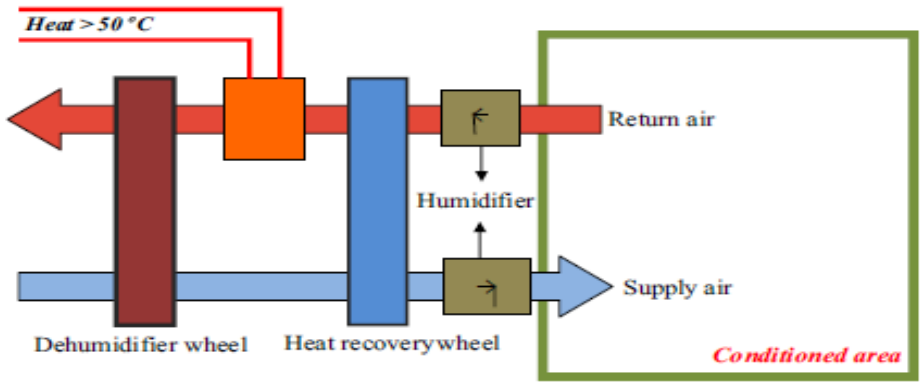


Figure 2.3: Basic scheme of an open cycle system (source: Ghafoor and Munir, 2015).

2.5.2.2 Closed cycles

In closed cycles, thermally driven sorption chillers produce chilled water being used for air conditioning of buildings using different types of conditioning equipment such as fan coils, air handling units, chilled beams, and chilled ceilings. Two types of sorption machines are commonly used: absorption and adsorption chillers (Ghafoor and Munir, 2015). Depending on their working principle, closed cycle process can further be classified as: (i) Liquid sorption: (absorption system), (ii) Solid sorption (adsorption system) (iii) ejector system (Mugnier and Jakob, 2012). The main advantage of solar absorption cooling technology is that their COP is higher than that of other thermally operated cycles (Hassan and Mohamad, 2012). The basic scheme of a closed cycle system is shown in figure 2.4.

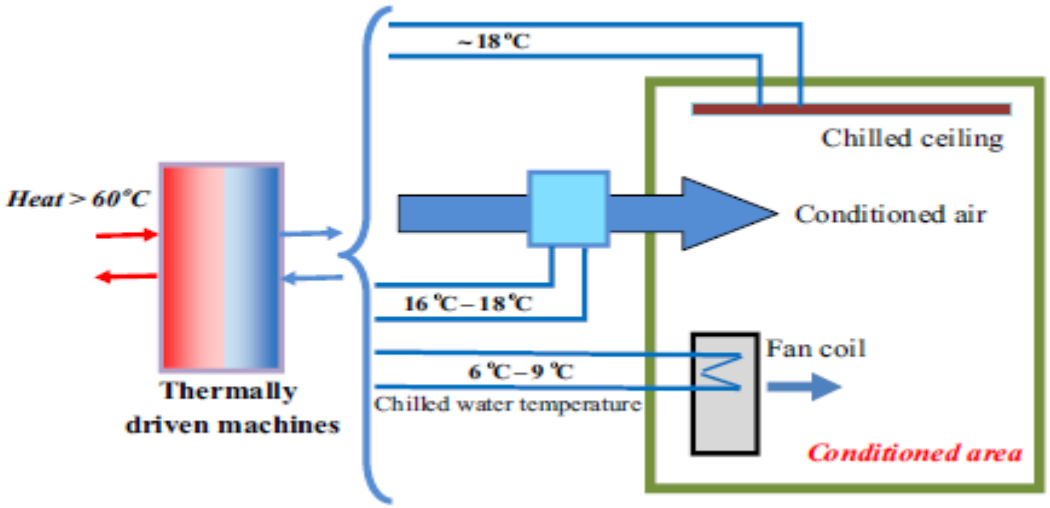


Figure 2.4: Basic scheme of a closed cycle system (source: Ghafoor and Munir, 2015).

2.5.3The adsorption system

Adsorption is a sorption process in which a solid sorbent attracts refrigerant molecules onto its surface by physical or chemical force and does not change its form in the process. Physical adsorption occurs when the molecules of the refrigerant (adsorbate) fix themselves to the surface of a porous solid element (adsorbent) and the molecules are adsorbed onto the surface. By applying heat, the refrigerant molecules can be released (desorption), whereby, this is a reversible

process (Hassan and Mohammad, 2012). Chemical adsorption results from the ionic or covalent bonds formed between the refrigerant molecules and the solid substance. The bonding forces are much greater than those of physical adsorption and thus more heat is released, however, the process cannot be easily reversed (Femandes *et al.,* 2014). The most commonly used adsorbents/ refrigerant working pairs are activated carbon/ methanol, activated carbon/ ammonia, zeolite/ water and silica gel/ water (Femandes *et al.,* 2014). For the same capacity, adsorption systems are larger than absorption systems due to the low specific cooling power of the adsorbent (Sarbu and Sebarchievici, 2015).

2.5.4The absorption system

Absorption refers to a sorption process where a liquid sorbent absorbs refrigerant molecules into its interior and changes physically and/ or chemically in the process. The absorbent has the ability to absorb large quantities of refrigerant vapour when cold and give it up when heated.These two states create a strong attraction to make a strong solution or mixture (Sarbu and Sebarchievici, 2015). The most commonly used refrigerant/ absorbent working pairs in absorption systems are water/lithium – bromide and ammonia/ water. A typical absorption refrigeration system is heat driven, it can thus operate on low grade energy such as waste heat from industrial plants, solar energy, etc. It requires a small fraction of electricity to power the auxiliary components. The main components in an absorption refrigeration system are: generator, condenser, absorber and evaporator. The absorber, generator and pump in the absorption refrigeration system replace the compressor of a vapour compression system. Based on the thermodynamic cycle of operation and solution regeneration, the absorption system can be divided into three categories: single effect, half effect and multi effect (double effect and triple effect) absorption cycles. The single effect and

half effect chillers require relatively lower hot water temperatures with respect to multi effect systems (Ullah *et al.,* 2013).

2.6The Absorption Chiller

The most commonly used absorption chiller is that which operates on the lithium bromide/ water pair (Henning, 2007). The heat source temperature is usually within 70 – 100^{o}C, they therefore have the advantage of being powered by renewable or waste heat. Although great developments have been achieved in absorption air conditioning systems, with absorption chillers available in commercial stage in small capacity (10 to 40 kW), medium (50 to 250 kW) and large scale (up to tens of MW), the micro scale (3 to 10 kW) which is most suitable for residential and office applications is substantially unexplored (Franchini *et al.,* 2015). Major drawbacks in micro scale capacity applications is in the high fabrication cost as well as in the low coefficient of performance (COP) of the absorption chillers as compared to much higher COP obtained in electrically powered compression chillers of similar capacity (Du *et al.,* 2012).

The major components in absorption chillers are the generator, condenser, evaporator and absorber, which are all heat exchangers. The absorber can be said to be the most important component of absorption machines as in general, its performance impacts directly in the size and energy supply of all absorption devices. The absorber is therefore the ultimate component in optimizing the COP of the device (Ibarra – Bahena and Romero, 2014). Falling film absorbers which are generally employed in absorption chillers have a wettability problem which diminishes absorption process (Ibarra – Bahena and Romero, 2014). In this regard, over the years, a number of researchers have developed small capacity absorption chiller prototypes, with improvements in absorber design aimed at improving the COP.

2.7 Software Tools for Design, Modelling and Simulation of Solar Thermal Air Conditioning Systems

Below are software tools used for design, modelling and simulation of solar thermal air conditioning systems.

2.7.1 TRNSYS software

Transient Systems Simulation (TRNSYS) software is a complete and extensible modelling and simulation environment for the transient simulation of systems, including multi-zone buildings. It is used by engineers and researchers around the world to validate new energy concepts, from simple domestic hot water systems to the design and simulation of buildings and their equipment, including control strategies, occupant behaviour, alternative energy systems (wind, solar, photovoltaic, hydrogen systems) etc. TRNSYS can be easily connected to many other applications, for pre- or post- processing or through interactive calls during simulation (e.g. Microsoft excel, Matlab, COMIS, etc) (Klein *et al.,* 2006).

TRNSYS application includes:

i. Solar systems (solar thermal and solar photovoltaic (PV)).

ii. Low energy buildings,heating ventilation and air conditioning (HVAC) systems with advanced design features (natural ventilation, heating/cooling, etc).

iii. Renewable energy systems

iv. Cogeneration, fuel cells (Klein *et al.,* 2006).

TRNSYS components are often referred to as Types (The multi-zone building model is known as Type 56, type 1 is the solar collector, etc). Each type of component is designed by a mathematical model in the TRNSYS simulation engine and has a set of matching proforma's in the simulation studio. The proforma ties a black-box description of a component: inputs, outputs, parameters, etc. The simulation engine is programmed in FORTRAN. The engine is compiled into a windows dynamic link library (DLL), TRNDII.

The TRNSYS kernel reads all the information on the simulation (which components are used and how they are connected) in the TRNSYS input file, known as the deck file (*.dck). The simulation

engine is called by an executable programme, TRNExe.exe, which also implements the online plotter, a very useful tool that allows you to view dozens of output variables during a simulation (Klein *et al.*, 2006).

2.7.2 Microsoft excel

Microsoft excel is a spread sheet programme that allows you to create mathematical formulas and execute functions. It provides a grid interface to organise data manipulations like arithmetic operations. It has a store of supplied functions to answer statistical, engineering and financial needs. It can display information as line graphs, histograms and charts.

2.7.3Matrix laboratory (MATLAB)

Matrix Laboratory (MATLAB) is a high performance language for technical computing. It is both an environment and a programming language. It integrates computation, visualisation and programming in an easy to use environment where problems and solutions are expressed in familiar mathematical notation. MATLAB allows you to build your own reusable tools. You can create your own special functions and programmes known as M-files in MATLAB code. Typical uses include:

i. Math and computation,

ii. Algorithm development,

iii. Data acquisition,

iv. Modelling, simulation and prototyping,

v. Data analysis, exploration and visualisation.

2.7.4 Energy plus

Energy plus is a whole building energy simulation programme used by engineers to model energy consumption for cooling, heating, ventilation, lighting as well as water use in buildings. It includes many innovative simulation capabilities such as modular systems and plant integrated with heat balance based zone simulation, multi-zone air flow and photovoltaic systems.

Typical uses include:

i. Building energy simulation

ii. Photovoltaic systems simulation

2.7.5 Engineering equation solver (EES)

Engineering equation solver is a general equation solving programme that can numerically solve thousands of coupled non-linear algebraic and differential equations. The programme can be used to do optimisation, provide uncertainty analysis, and perform linear and non-linear regressions. It has high accuracy thermodynamic and transport property data base that is provided for hundreds of substances in a manner that allows it to be used with the equation solving capability.

2.8 Review of Past Works in the Area

This section contains the review of past works in the area of solar absorption cooling. It is divided into sub sections that highlight the works done in the area.

2.8.1Studies on simulation of solar absorption air conditioning systems done for different climates

Agrouaz *et al.* (2017) carried out a simulation study to evaluate the performance of a solar absorption cooling system under the Moroccan climate. Six reference cities were used in the study, each representing a climatic zone. The cooled building has a floor area of 200m^2. The solar absorption cooling system comprised of a 10 kW absorption chiller, 25m^2 collector area, cooling tower, hot and cold water storage tanks as well as an auxiliary heater. Results showed that the system operating under the city of Agadir had the highest average COP of 0.26, while the system operating under the weather conditions of Ifrane had the lowest COP of 0.19. The best average solar fraction of 0.3 was recorded for the system operating in the city of Errachidia.

Asim *et al.* (2016) presented a TRNSYS model and simulation of a solar absorption air conditioning system to provide cooling for a typical family house in Pakistan. The system is powered by hot water from an array of evacuated tube collectors. Results indicate that a collector area of $12m^2$ is sufficient to maintain the temperature of the house at or below 26^oC during the hot season.

Ahmed *et al.* (2016) conducted a simulation study of a single effect solar absorption cooling system for four Egyptian cities with different climates (Al Arish, Cairo, Assuit and Aswan) using the TRNSYS software. The system consisted of parabolic trough solar collectors, stratified storage tank, single effect absorption chiller, cooling tower. Results showed the best performance was obtained in the city of Aswan with a COP ranging from 0.54 to 0.57.

Kanan *et al.* (2015) simulated the performance of an absorption chiller driven by a salinity gradient solar pond, to provide cooling for a residential building. A coupled simulation between MATLAB and TRNSYS was used. The building was cooled under the weather conditions of Bagdad, Iraq. It was found that a solar pond area of $400m^2$ was required to provide satisfactory cooling for a residential building with a floor area of $125m^2$.

Abdullah *et al.* (2015) carried out a study to examine the option of running an absorption chiller by solely relying on solar heat energy for both heating and cooling of a typical Australian six star home. The TRNSYS software was used in modelling and simulation, while GenOpt software was used to carry out the optimisation. Results showed that the investment cost was higher and payback period longer with this system than one that does not rely solely on solar heat energy. However, this system consumes 50% less power than the one that does not rely solely on solar heat energy.

Shirazi *et al.* (2015) studied the performance of solar powered lithium bromide – water absorption chillers: single effect coupled with evacuated tube collectors, double and triple effects coupled with parabolic trough collectors. A simulation model was developed for each configuration using

TRNSYS software. A parametric study was conducted by varying the fraction of direct normal irradiance under three global horizontal irradiance categories: (low, medium and high). Simulation results reveal that there is no advantage in using multi effect absorption chillers over single effect chillers when the direct normal irradiance fraction is less than 60% of the total global irradiance. However a significant decrease in size of solar field for both double and triple effect chillers can be achieved in climates where direct normal irradiance fraction is above 60%.

Akhtar *et al.* (2015) carried out a feasibility study and basic design of a solar integrated absorption refrigeration system for a packaging industry in Lahore, Pakistan. The design calculations upon which the feasibility study was carried out include the solar collector area and type, cooling capacity, cooling area. The absorption chiller is to be water cooled and working on the ammonia / water (NH_3/H_2O) pair. Results from simulations conducted showed that a solar fraction of 69% can be achieved for the given location. The payback period is about four years.

He *et al.* (2015) carried out a TRNSYS model and optimization of a 50 tonnes of refrigeration capacity absorption air conditioning system to cool an office block under China weather conditions. Solar energy was supplied by evacuated tube collectors. Results showed the average annual efficiency of the collector was 37.6%, with a solar cooling fraction of 0.76. Simulation results also showed that 66% primary energy consumption can be reduced.

Mendoza *et al.* (2013) carried out TRNSYS modelling and simulation of a solar absorption cooling system under the weather condition of Guayaquil, Ecuador in order to partially satisfy the thermal demand of an office building with maximum hourly thermal load of 153kW. The model utilizes evacuated tube collectors and single effect LiBr-H_2O chiller, storage tank and external boiler. Results showed optimized system could achieve yearly solar fraction of 0.6.

Ssembatya *et al.* (2013) carried out the performance analysis of a 10tonnes of refrigeration capacity solar absorption cooling system using TRNSYS simulation. The simulation was done

under the weather conditions of the UAE. Simulation results showed that the solar absorption cooling system operates with a COP in the range 0.6 – 0.8 for the given location.

Tamasauskas *et al.* (2013) carried out the analysis of three innovative solar heating and cooling systems integrated into a high performance building. The analysis was done using TRNSYS simulation under the weather conditions of Quebec, Canada. The systems include solar driven absorption chiller and heat pump designs. The highest solar fractions were obtained for a solar driven absorption heat pump with the system achieving an annual solar fraction of 0.31.

Eicker *et al.* (2013) carried out a systematic system design study of solar thermal cooling systems. For each technology investigated, system models including an energy optimised control strategy was developed which maximises the primary energy efficiency. The models were implemented in the simulation environment INSEL, using weather data of the climates: Cologne, Stuttgart, Barcelona, Madrid, Jakarta, and Riyadh. Results indicate that for a given machine nominal power, solar fractions increase with collector surface area until saturation is reached. Single effect absorption cooling systems easily reach 80% solar cooling fractions for all but very humid climates. Results from economic performance show that solar thermal cooling is more viable in hot climates than in moderate European climates.

Calise (2012) developed a dynamic model of an innovative solar heating and cooling system based on the coupling of parabolic trough collectors with a double effect lithium - bromide/ water (LiBr – H_2O) absorption chiller. The auxiliary energy for both heating and cooling is supplied by a biomass fired heater. The system layout includes additional components such as cooling tower, pumps, and heat exchangers. Both the solar heating and cooling system and the building were dynamically simulated in TRNSYS. The simulation was done to provide space heating and cooling as well as domestic hot water for a small university hall all year round. The analysis of the system performance was carried out for seven Mediterranean cities in Italy, Spain, Egypt, France, Greece and Turkey. A parametric analysis was performed in order to evaluate the sensitivity of the

results when varying some of the main design and operating parameters. Results showed that in all cases investigated, primary energy savings higher than 80% were achieved. However, the economic profitability is higher for the hottest climates.

Al – Alili *et al.* (2012) studied the performance, economic and environmental benefits of a 10kW NH_3/H_20 absorption chiller under Abu Dhabi's weather conditions. The solar air conditioning system comprised of a specific collector area of $6m^2/kW$, specific tank volume of $0.1m^3/kW$. The complete solar absorption system was modelled using the TRNSYS software. The system was found to consume 47% less electrical energy than a vapour compression system of the same cooling capacity. The proposed system is found to reduce 12 metric tonnes/ year of carbon – dioxide (CO_2) emission.

Gebreslassie *et al.* (2012) developed a model for the multi-objective optimization of solar powered absorption cooling system for reducing greenhouse gas emissions. The design of the system was formulated in mathematical terms as a multi-objective non-linear programing problem that seeks to optimise simultaneously the economic and environmental performance of the cooling system. A case study of NH_3/H_2O single effect cooling system of a 100 kW capacity for Barcelona weather conditions was done. Results showed that with the current prices, reducing contribution to global warming is technically viable but economically not appealing.

Ayadi (2011) carried out design, experimental evaluation and optimisation of a novel absorption cooling system that allows a higher temperature lift for the Mediterranean region. The simulation software TRNSYS was used. Results were experimentally validated. Results showed that 44% improvement of the primary energy savings of the system has been achieved by applying the optimisation procedure.

Praene *et al.* (2011), carried out a simulation and experimental investigation of a solar absorption air conditioning system. The TRNSYS software was used in the simulation. The building to be air conditioned is a block of 4 class rooms that cover $54m^2$ each located in Saint Pierre, France. The

final configuration used in the simulation which was done for one year are: evacuated tube solar collectors ($60m^2$), absorption chiller (35kW), storage tank ($1m^3$). A comfort level of 25^oC was chosen for the temperature inside the class rooms. Simulation results showed that the system achieved an average temperature of 27^oC inside the class rooms.

Falahatkar and Assadi (2011) carried out the analysis of a solar single effect lithium bromide – water absorption cooling system in a typical office building in Tehran, covering a total floor area of $280m^2$ with a peak cooling load of 35.17kW. The solar energy is absorbed by heat pipes and stored in an insulated storage tank. Results showed the optimised system to compose of 16 collectors each with 30 tubes with a total absorber area of 45 m^2. The optimised system is capable of saving up to $2400m^3$/ year of natural gas.

Calise *et al.* (2010) developed a transient simulation model of a solar heating and cooling system, in which three different configurations were considered. The simulation model was developed using the TRNSYS software. In all configurations the solar heating and cooling system was based on the coupling of evacuated tube solar collectors with a single stage LiBr/ H_2O absorption chiller and a gas fired boiler included for auxiliary heating only during the winter season. The system was used to air condition a building with a maximum cooling load of 157kW, using typical weather conditions of south Italy. An economic model was developed to assess the operating and capital cost of the system. The results were analysed on a monthly and weekly basis. They concluded that the results were encouraging as for the potential of energy savings, with primary energy savings of between 36.7% and 48% achieved. However the solar heating and cooling systems appear still far from economic profitability.

Tsoutsos *et al.* (2010) carried out the performance and economic evaluation of a solar heating and cooling system for a hospital in Crete, Greece covering a total floor area of $1,250m^2$. A complete system comprising a solar collector, a hot water storage tank, back up heat source, cooling tower and LiBr/ H_2O absorption chiller was simulated and optimised using the TRNSYS software.

Results showed the optimised system consists of 500m^2 of solar collector area, 70 kW absorption chiller, 15m^3 hot water storage tank and an 87 kW pre heater. The optimised system was able to attain a solar fraction cooling of 74.23% and solar fraction heating of 70.78%.

Prasartkaew and Kumar (2010) presented a solar biomass hybrid absorption cooling system which was suitable for residential applications. It consisted of a solar water heating with storage tank, biomass fired hot water boiler and a single effect absorption chiller. Based upon the Bangkok meteorological data, the C.O.P. of the chiller and the overall system efficiency was found to be 0.7 and 0.55 respectively. The biomass (charcoal) consumption for 24 hour operation was 24.44kg/day. The system showed great potential for the residential building comfort and reduction of Green House Gas emissions.

Mazloumi *et al.* (2008) developed a thermodynamic model to simulate the performance of a single effect LiBr/ H_2O absorption cooling system. The system was designed to air condition a typical house with a peak cooling load of 17.5 kW in the city of Ahwaz, Iran. The minimum required parabolic trough collector area was about 57.6 m^2, which could supply the cooling loads for the sunshine hours of the design day for July. The system attained a COP of between 0.67 and 0.76.

Assilzadeh *et al.* (2005) presented the simulation and optimization of a LiBr/ H_2O absorption air conditioning system for Malaysia. The system used evacuated tube collectors. TRNSYS software was used in the modelling and simulation of the system. The optimized system for Malaysian climate for a 3.5kW system consists of 35m^2 evacuated tube collectors sloped at 20^o, with 0.8m^3 hot water storage tank.

Atmaca and Yigit (2003) simulated a solar cooling system based on a 10.5kW constant cooling load. A modular computer programme was developed for the absorption system to simulate various cycle configurations and solar energy parameters for Antalya, Turkey. It was shown that

the solar collector area of 50m^2 and 3750kg storage tank mass was sufficient to cover the cooling energy demand.

Florides *et al.* (2002) presented a TRNSYS model that allows the parametric optimisation of a LiBr-H_2O solar assisted absorption cooling system for an office building in the city of Nicosia, Cyprus. The final optimised system consists of a 0.6m^3 tank and a hot water set point of 87^{o}C, an array of parabolic collector 30^o tilted and an optimal area of 15m^2 which was obtained through economic analysis.

2.8.2Experimental studies on pre-installed solar absorption air conditioning plants done in different climates

Sun *et al.* (2015) carried out an experimental work on a solar and gas fired absorption system for cooling and heating. The system consists of a hybrid absorption chiller capable of solar cooling in single effect and gas fired cooling in double effect, horizontal pipe evacuated tube solar collectors and gravity assisted heat pipe evacuated tube solar collectors together covering an area of 1,020m^2, hot and cold water storage tanks, cooling tower. The system was tested in a five star hotel located in Changle, Shandong in China, covering a total floor area of 24,332m^2. The year round experiment showed a solar collector efficiency of 40 – 45%, absorption chiller COP of 0.75, Solar Coefficient of Performance of 0.28 – 0.34 for the given location. The gas consumption of the hybrid energy system had a 49.7% energy savings ratio compared with conventional gas fired system.

Zhai *et al.* (2015) conducted an experimental study on a mini type solar absorption cooling system of 8 kW capacity installed at the Shanghai Jiao Tong University in China. The system had a 96 m^2 collector array, and was used to cool a test room of 50 m^2. Chilled water was delivered either into fan coils or into radiant cooling panels. Cooling output reached 3.62 kW in the fan coil mode and 4.47 kW in the radiant cooling panel mode. Average COP of 0.32 was achieved.

Winston *et al.* (2014) in the United States carried out an experimental work on a solar thermal cooling system. The system consists of a novel non tracking external compound parabolic concentrators of 53.3m^2 which were used to power a 23 kW double effect LiBr/ H_2O absorption chiller. Its performance for providing power for space cooling was analysed. Results showed the solar collector array had an average daily efficiency of 36.7%, thermal COP of the system averaged at 0.99, daily solar COP of the entire system averaged at 0.363.

Schwerdt and Ali (2013) carried out performance test on a solar cooling facility installed in Assiut, Egypt. The system was used for cooling a heat lab of floor space area of 90m^2. The installed system consists of a hot water fired adsorption chiller of 7.5kW capacity, vacuum tube collectors of 40m^2 area, hot and cold storage tanks, cooling tower. Results indicate that over the summer cooling period the overall solar system COP of the installation ranged from 0.25 to 0.3.

Ketjoy *et al.* (2013) experimentally evaluated the performance of a 35kW lithium bromide – water absorption chiller for providing cooling under the weather conditions of Thailand. The chiller is driven by a 72m^2 heat pipe evacuated tube solar collector with a gas backup system. The results showed that the actual average COP of the system was 0.33, while the maximum and minimum values were 0.5 and 0.17 respectively. A solar fraction of 0.55 was obtained.

Darkwa *et al.* (2012) evaluated the overall performance of an integrated solar absorption cooling system installed at the University of Nottingham, Ningbo China for building cooling. The system consists of an array of evacuated tube solar collectors with an area of 220m^2, stratified hot water storage tanks, lithium – bromide /water absorption chiller of 55kW capacity. Results showed a practical collector efficiency of 61% as against a theoretical efficiency of 69%. The absorption chiller achieved a COP of 0.69. They concluded that supplementary heat source such as gas or biomass fired system would have to be incorporated to maintain appropriate hot water temperature level during period of low solar radiation.

Yin *et al.* (2012) presented results from the experimental investigation of a mini type solar absorption cooling system installed at the Shanghai Jiao Tong University in China. The system which was used to cool a test room consists of $96m^2$ solar collector array, an absorption chiller of 8kW capacity, hot water storage tank of $3m^3$ capacity, cooling tower. The chilled water was delivered either into fan coils or into radiant cooling panels. Results showed an average COP of 0.31 was achieved. In the fan coil mode the cooling output reached 4.27kW, while it increased by 23.5% in the radiant cooling mode.

Balghouthi *et al.* (2012) carried out an experimental investigation on a solar absorption cooling installation located at the Centre of Researches and Energy Technologies, in Bordj – Cedria, Tunisia. The system comprised of parabolic trough solar collectors, a 16kW double effect $LiBr/H_2O$ absorption chiller, a cooling tower, back up heater, cold and hot water storage tanks. Experimental results indicate that the COP ranged between 0.8 and 0.9, while the solar coefficient of performance was between 0.1 and 0.43. The maximum output of the absorption chiller was about 12kW. Solar fraction of 0.54 was achieved. The avoided CO_2 emission during the cooling season was estimated at 3000kg, corresponding to an equivalent energy saving of 1154 litres of gas oil.

Rosiek and Batlles (2012), experimentally investigated the performance of a 70kW absorption chiller operating under two modes of heat rejection from the absorber and condenser. The system was installed and tested in southern Spain. A conventional cooling tower was utilized in the first mode while a shallow geothermal system with 20m deep heat exchangers was utilized in the second mode. The two operating modes were compared in terms of energy consumption, water consumption and CO_2 savings. It was found that using the shallow geothermal system reduced the electricity consumption by 31%, reduced water consumption by $116m^3$ and led to a CO_2 savings of 833Kg CO_2.

Bujedo *et al.* (2011), experimentally studied different control strategies of a solar powered LiBr/H_2O absorption cooling cycle. A 77.5 m^2 collector area (40m^2 evacuated tube collector + 37.5m^2 flat plate collector) was used to drive a 35kW absorption chiller, with 2m^3 hot storage tank and 1m^3 cold storage tank. It was used to air condition an office block covering a total floor area of 200m^2 under Spain weather conditions. Overall system efficiency in the range of 44 – 48% was achieved.

Mammoli *et al.* (2011) carried out an experimental study on an existing solar absorption air conditioning facility of 70 kW capacity installed at the University of New Mexico. The system was driven by combined flat plate collectors and evacuated tube collectors totalling 232 m^2 surface area and a hot water storage tank of 34 m^3. Results showed that the collector field had a daily average efficiency of 0.58, while the chiller had an average COP of 0.63. Solar fraction of 0.14 was recorded.

Qu *et al.* (2010) evaluated the performance of a solar thermal heating and cooling system at Carnegie Mellon University, Pittsburgh, U.S.A. The building studied was the intelligence work space, which is a single floor building of 245m^2 of net floor area and 3.1m of average height. The solar cooling and heating system incorporates 52m^2 of linear parabolic trough collectors, a 16kW double effect LiBr – H_2O absorption chiller, heat recovery heat exchanger, circulation pumps, and control valves. Performance of the system was tested and measured data were used to verify system performance models developed in TRNSYS. It was found that the system could potentially supply 39% of heating and 20% of cooling for the building space.

Ali *et al.* (2008) carried out the performance assessment of an integrated cooling plant having both free cooling system and solar powered single effect LiBr/ H_2O absorption chiller in Oberhausen, Germany. The plant is to air condition a floor space of 270m^2. The plant consists of a 35.17kW absorption chiller, vacuum tube collectors of total area 108m^2, hot and cold storage tanks of 6.8m^3 and 1.5m^3 capacity respectively and 134kW cooling tower. Results showed that free cooling in

some months could be up to 70%. An average solar fraction of 60% was obtained over the five years of assessment. Absorption chiller COP varied from 0.37 to 0.81.

Pongtorukulpanich *et al.* (2008) experimented a solar driven 10 – tonne $LiBr/H_2O$ single effect absorption cooling system. It was shown that under Thailand weather conditions, the $72m^2$ evacuated tube solar collector delivered a yearly average 81% of the thermal energy required by the chiller with the remaining 19% generated by LPG fired back up heating unit.

Hidalgo *et al.* (2008) experimentally investigated the performance of a single effect lithium bromide – water absorption air conditioning system of 12 kW capacity installed in Spain. The system was driven by flat plate solar collectors of $50m^2$ area and natural gas auxiliary boiler. It was used to cool a building with floor area of 90 m^2. Results indicate the system used 56% solar energy and 44% natural gas. Cooling power of 6 – 10 kW was produced. The energy cost savings and CO_2 emission savings were found to be 62% and 36% respectively.

2.8.3Studies on design, construction and test of small and micro scale capacity absorption chiller prototypes

Said *et al.* (2016) designed, constructed and tested a solar powered NH3 – H_2O absorption cooling system in Saudi Arabia. The absorption chiller of 10kW capacity was developed and built at the University of Stuttgart, Germany. The demonstration plant was built and tested at the King Fahad University of Petroleum and Minerals, Saudi Arabia, to cool a hall with 10kW cooling load. The collector array was $42m^2$, an ice storage as well as cold water storage were integrated into the system. A COP ranging from 0.42 to 0.71 was achieved.

Franchini *et al.* (2015) carried out a modelling, design and construction study of a 5kW capacity absorption chiller prototype. A computer code was developed to carry out the design. The absorber was a falling film finned tube spiral absorber. The chiller was installed and tested in Bergamo University, Italy. Preliminary results showed a cooling capacity of 3.25kW

corresponding to a COP of 0.358 was achieved. Space cooling temperatures between 24 – 26 ^{o}C were achieved.

Said *et al.* (2015) carried out the design, manufacturing, installation, test and analysis of a solar powered absorption refrigeration system for air conditioning applications. The system is a modified system to increase the COP. The modifications include: the recovery of waste heat from a dephlegmator and utilization of a refrigerant storage unit. The 10kW capacity absorption chiller was installed and tested in Saudi Arabia. The results showed: an increase of 10% in COP due to dephlegmator heat recovery, an increase of 8% in COP due to refrigerant storage unit, an increase of 18% in COP due to combined effect of modifications.

Bolocan *et al.* (2015) developed a small capacity prototype cooling plant of 5 kW capacity for air conditioning in Brasov, Romania. The system operates using the NH_3/H_2O pair. The generator, absorber and evaporator are plate heat exchangers with mini channels. The condenser is cooled by a fan. Data acquisition system was used to monitor the operation of the prototype plant. The best COP obtained was 0.43.

Albers (2014) carried out an experimental work on a solar assisted cooling system using a developed absorption chiller at the federal environmental agency, in Dessau Germany. A new control strategy was developed which controls hot and cooling water temperatures simultaneously. Results showed that the seasonal energy efficiency ratio was above 0.75, electric efficiency was 35% higher and water consumption was reduced by 70%.

Prasartkaew (2014) experimentally investigated the performance of a small sized absorption chiller which was developed from an old out of order commercial absorption chiller. The objective was to gain experience on how to build an absorption chiller. The performance of the chiller was investigated under the local weather conditions of Thailand. Results showed that the cooling capacity obtained satisfied the cooling load of the air conditioned room.

Also, to obtain high COP, the chiller should be operated at 85^{o}C hot water temperature supply to the generator.

Balamurugan and Mani (2013) carried out experimental work to compare the performance of compact and tubular generators for Tetrafluoroethane R134a – Dimethyl formamide DMF based vapour absorption refrigeration system. The system which was built to a rated cooling capacity of 1 kW is made up of brazed plate heat exchangers for the condenser, evaporator, absorber and solution heat exchanger. The system has two generators, one made of plate heat exchanger and the other concentric steel tubes. By use of a valve, one of the generators could be activated at a time. Experimental tests were performed for different operating conditions. The authors concluded that for the same operating conditions, the compact generator performed better than the tubular generator.

Yin *et al.* (2013) designed and constructed a mini type solar absorption cooling system with a cooling capacity of 8 kW. Lithium bromide – water was used as the working pair. Solar collector of 96 m^2 area was installed, with a hot water storage tank of 3 m^3 included. The experimental set up was used to air condition a test space of 50m^2 area in Shanghai, China. The experimental results showed that space cooling temperatures between 24 – 27 ^{o}C was achieved and the average value of PMV (Predicted Mean Vote) and PPD (Predicted Percentage of Dissatisfaction) of the test room were 0.22 and 5.89 respectively.

Izquierdo *et al.* (2012) carried out an experimental study on a double effect LiBr/ H_2O air cooled absorption cooling prototype directly powered by fossil fuel. The test was carried out in Madrid, Spain. The prototype which was designed to supply 7 kW of cooling power was able to chill water up to 7 to 18^{o}C under extreme outdoor temperatures. A new flat sheet adiabatic absorber was used allowing it to operate at outdoor temperatures about 45^{o}C without any sign of crystallization. A mean daily COP of about 1.05 was obtained.

Du *et al.* (2012) carried out an experimental investigation on an air cooled two stage $NH_3 – H_2O$ solar absorption air conditioning prototype, proposed for small scale residential application. The prototype of 2kW capacity was built and experimented in Shanghai Jiao Tong University, Shanghai, China. A spray type absorber was adopted. Results indicate that the system operated smoothly and steadily and yielded a COP of 0.21 and electrical efficacy of 5.1 with feeding hot water of 85^oC, ambient air temperature of 29^oC and evaporating temperature of 8^oC. In summer the COP stabilizes between the range of 0.18 – 0.25, and the electrical efficacy varies between 3.6 and 5.1 when the prototype is driven by hot water from 76 to 88^oC.

Lostec *et al.* (2012) carried out an experimental study on a test bench of the performance of a single effect NH3 – H_2O absorption chiller of 10 kW capacity which was cooled with a water – ethylene glycol solution. Hot water of between 75^oC and 85^oC was used. Different operating conditions were imposed by varying the temperatures and flow rates of the secondary circuits and the flow rates of the rich solution. The results showed a COP of 0.6 for chilled ceiling applications.

Boudehenn *et al.* (2012) developed and experimentally tested a 5 kW capacity absorption chiller prototype working on the ammonia – water pair for solar cooling applications. Compact plate heat exchangers were used. Experimental tests were performed at the French National Institute for Solar Energy. Test results showed a cooling power of 4.2 kW was achieved and a COP of 0.65 was achieved.

Gonzalez – Gil *et al.* (2011) carried out an experimental evaluation of a direct air cooled single effect LiBr – H_2O absorption cooling prototype. The 4.5 kW prototype presents an adiabatic absorber using flat fan sheets, an air cooling system that directly cools both the absorber and condenser. The prototype was tested in Madrid, Spain. Results showed COP values around 0.6, cooling power varied from 2 to 3.8 kW, which represented about 85% of the prototype's nominal capacity. Space cooling temperatures ranged between 23 – 25 ^oC.

Agyenim *et al.* (2010), designed a solar thermal absorption cooling system with cold storage. A 4.5 kW, chiller unit utilising LiBr/H_2O, was driven by vacuum tube collectors of $12m^2$ area. The solar collector fluid was based on ethylene glycol. The system was experimentally tested in Cardiff, U.K. The chiller was activated at a minimum temperature of 80^oC. It was able to produce chilled water in the range of 7 – 16^oC. The daily average thermal and electrical COPs of the system were 0.58 and 3.6 respectively in the given location.

2.8.4Mathematical modelling and theoretical studies on absorption cooling cycle

Ketfi *et al.* (2015) developed a thermodynamic model to study the performance of a single effect absorption refrigeration system working on the LiBr/ H_2O pair. The absorption chiller modelled was a 70 kW Yazaki chiller. MATLAB software was used in the simulation. Results showed that COP of the cycle increased with increasing generator and evaporator temperatures, while it decreases with increasing condenser and absorber temperatures. Maximum COP of 0.77 was achieved in the simulation, which compared closely with 0.81 reported by the manufacturer.

Shaikh and Morabiya (2013) modelled a LiBr-water based absorption cycle using the software EES. It showed that increasing the generator temperature increases COP of the system, this continues to an optimum generator temperature, beyond which COP starts to decline.

Evola *et al.* (2013) developed a general mathematical model for the dynamic simulation of a single effect LiBr/ H_2O absorption chiller. The model is based on mass and energy balances applied to the internal components of the machine and it accounts for non-steady behaviour due to thermal and mass storage in the components. The validation of the mathematical model is performed through experimental data collected on a commercial small capacity water cooled unit. The model showed good agreement with experimental data, since the difference between the instantaneous simulated and experimental values of cooling power and COP never exceeded 5%.

Chiriac *et al.* (2013) did a theoretical investigation of an absorption chiller with cooling power 5-20 kW operating with the NH_3-H_2O pair driven by renewable energy sources. The economizer,

generator and evaporator are plate heat exchangers, the absorber and condenser are circular micro-channel heat exchangers with fins which are air cooled. Deviations of theoretical results from experimental fall within 5-10%. The concept offer possibility of low refrigerant charges as well as high heat transfer and compact design.

Lizarte *et al.* (2012)developed a mathematical model to evaluate performance of a directly cooled single effect LiBr/H_2O absorption chiller which utilized an innovative adiabatic flat fan sheets absorber. The model predicted the flat fan sheet configuration to exhibit a one order of magnitude higher mass transfer coefficient than the falling film or spray type absorbers.

Ahmed *et al.* (2011) developed a steady state thermodynamic model to predict the performance of a double effect steam fired absorption chiller working on the LiBr/ H_2O pair. Simulation results showed the cooling capacity is increased as the heat input to the generator increases. The simulation results were compared with actual data and the trend replicated with 1.12% deviation.

Hasenohrl (2011) developed a model to evaluate cycle and heat exchanger concepts for a 4 kW LiBr-H_2O absorption chiller based on compact plate heat exchangers. He concluded that recirculation provides enough solution to permit good wetting of the absorber, while an additional pump will be required at the generator for recirculation. He suggested pair-wise integration of heat exchangers result in a low overall heat exchanger increase.

2.9 Conclusion from Literature Review and Research Gap

From the forgoing we conclude that the technology of solar absorption cooling is very promising with research works being carried out in different aspects of the area globally, ultimately aimed at improving COP and having an economically viable system.

The following are the research gaps from the literature review.

i. There has not been any cognate research work in solar absorption air – conditioning targeted at the Nigerian climate, either via simulation or practical set up, despite the vast solar resource.

ii. In the area of prototype design to improve chiller COP, “double tube configuration” for tube wetting has not been explored.

The present study is intended to bridge this gap

CHAPTER THREE

MATERIALS AND METHODS

This study comprises of an initial feasibility/ performance study of the proposed solar and gas absorption cooling system as well as optimal sizing of the system components, done via simulation. Programme based design of the system components, construction of the system,experimental test of the constructed system, economic evaluation and environmental impact assessment.

3.1 Descriptionand Working Principle of the Proposed Solar/ Gas Hybrid Powered Absorption Air - Conditioning System

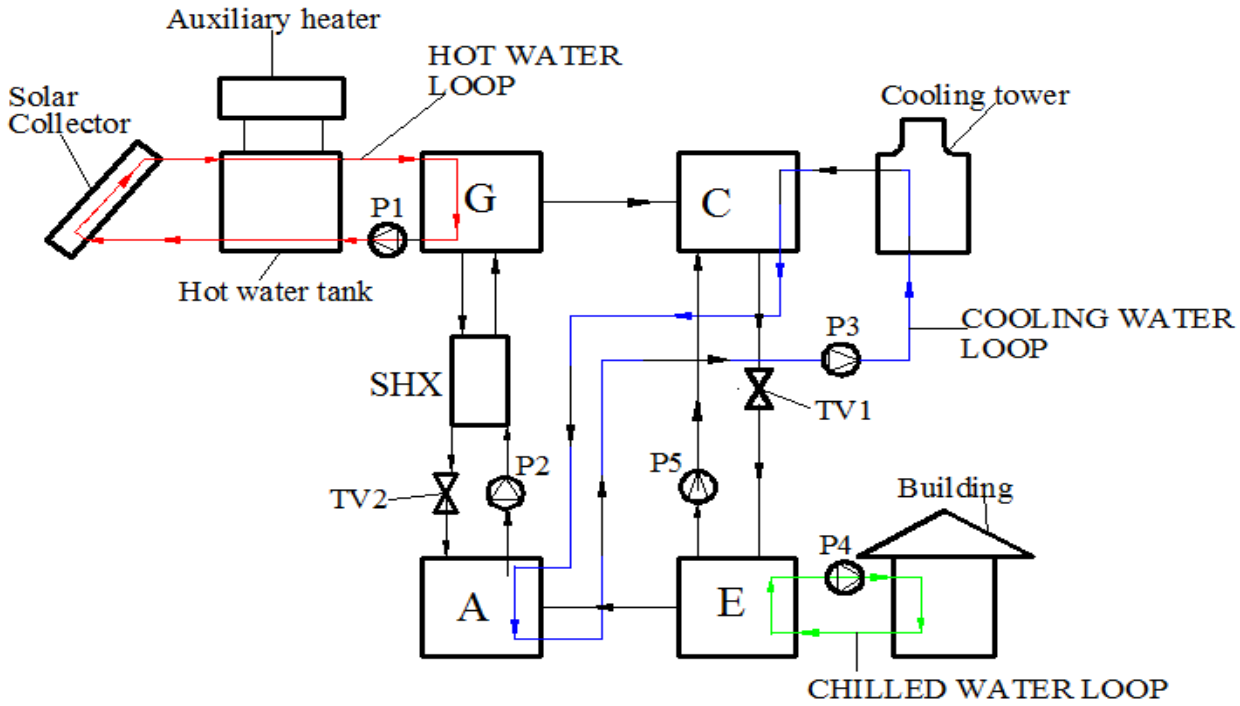
The proposed system consists of three main flow loops, the hot water loop, the cooling water loop and the chilled water loop, as shown in the system schematic in figure 3.1. In the hot water loop, solar radiation provides thermal energy to the collector fluid which is stored in the hot water tank.From the tank, the hot water is pumped by the hot water pump (P1) to the generator of the absorption chiller where desorption of Lithium bromide – water solution takes place. The resulting refrigerant vapour from the generator flows to the condenser, where it condenses. This results in a liquid refrigerant (water), which is then throttled via throttle valve 1 (TV1), reducing the pressure to evaporator pressure on entry to the evaporator. The resulting strong solution of lithium bromide from the generator flows down to the solution heat exchanger (SHX) where it loses heat to the weak solution of lithium bromide being pumped by the solution pump (P2) from the absorber to the generator.

From the SHX, the strong solution of lithium bromide is throttled via throttle valve 2 (TV2), reducing the pressure to absorber pressure on entry to the absorber. At the absorber, the strong solution of lithium bromide absorbs water vapour from the evaporator, causing it to become a weak solution before being pumped to the generator again. The hot water is then pumped back into the storage tank and then to the collector array where it again accumulates thermal energy and

the cycle repeats.An auxiliary heater which is a Liquefied Petroleum Gas (LPG) boiler is attached to heat the water in the hot water storage tank during periods of low solar radiation.

In the cooling water loop, cooling water from a cooling tower is pumped by the cooling water pump (P3) first to the condenser and then to the absorber, (both in the absorption chiller) to take away the heats of condensation and absorption respectively before returning to the cooling tower. In the cooling tower, the water is cooled and the process repeats.

In the chilled water loop, chilled water is produced at the evaporator of the absorption chiller as a result of evaporation at low pressure.The chilled water is pumped by the chilled water pump (P4) to the building, where it circulates round the building through cooling coils and takes away the cooling load. The water rises in temperature and is then returned to the absorption chiller where it is again chilled at the evaporator and the process repeats. A refrigerant pump (P5) circulates liquid refrigerant (water) between the evaporator and condenser.



G= Generator, C= Condenser, A= Absorber, E= Evaporator, SHX= Solution Heat Exchanger

Figure 3.1: Schematic of the solar/ gas hybrid absorption cooling system

3.2Materials

The materials used for the entire work consist of software tools for the simulation and design, equipment for the construction as well as measuring instruments for the experiment.

3.2.1 Software tools

i. Transient systems simulation (TRNSYS)

For this work, TRNSYS was used to:

- Simulate the cooling energy demand of an office block.
- Determine the hourly, daily and monthly cooling loads for the office block.
- Model, simulate and optimise system components sizes of the solar/ gas hybrid absorption Cooling system for the office block.

ii. Microsoft excel

For this work, Microsoft excel was used to:

- Process data from TRNSYS output file:

  Hourly output data from TRNSYS were exported to excel, where these data were averaged to daily data and then averaged to monthly data for all months of the year.
- Plot resulting averaged data for analysis

iii. Matrix laboratory (MATLAB)

For this work, MATLAB was used to:

- Develop MATLAB codes for the design of components in solar/gas hybrid absorption cooling system, using mathematical equations for the component design.
- Run the MATLAB codes to obtain design values used in the construction. This was done throughiterations and mathematical computing.
- Develop MATLAB codes to simulate the absorption chiller performance.

3.2.2 Materials for the construction

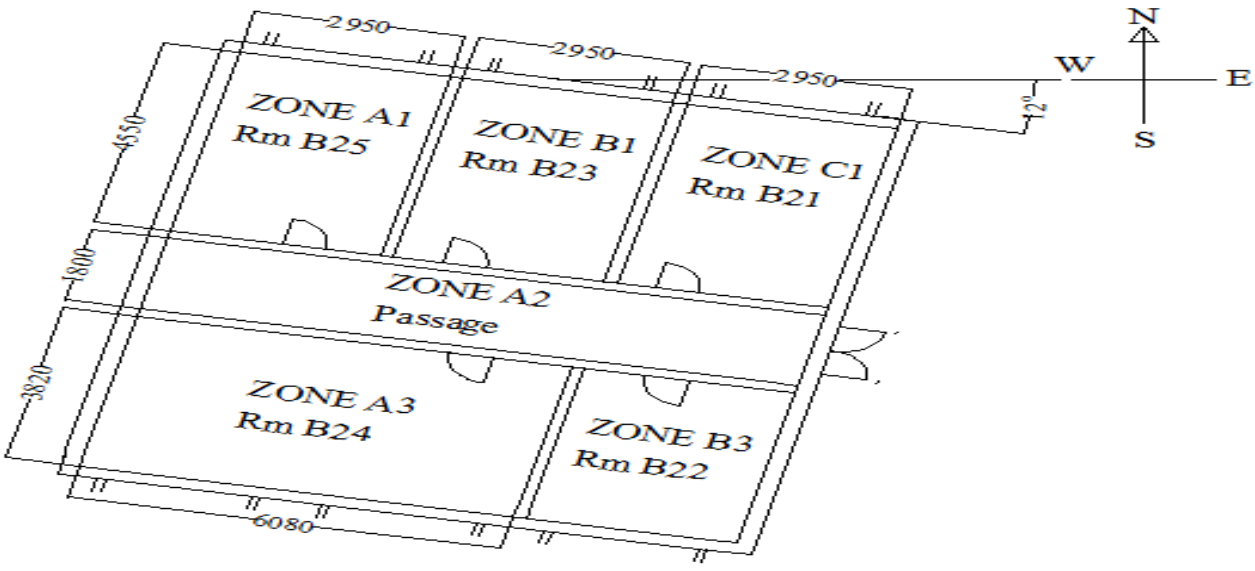
Locally available materials and equipment (stated in detail under system construction)

3.2.3 Materials for the experiment

System constructed components and measuring instruments (stated in detail under experiment)

3.3Cooling Energy Demand Simulation Using TRNSYS

In this section the hourly cooling energy demand of the office block was determined. This was done by simulation, using a TRNSYS sub programme TRNbuild.Details of the office block, including indoor design conditions were input into the TRNbuild component: Type 56. These inputs include: location, orientation, size, construction materials, cooling set point temperature, occupancy, activity of occupants, schedules which define the heat gain from occupants and equipment. The building is occupied throughout the working hours of 8am to 6pm, Mondays to Fridays.The office block to be cooled consists of 5 office rooms and a passage covering a total floor area of 90 m^2. The building is 3 metres in height. The building was subdivided into six thermal zones as shown in figure 3.2. This comprises the five offices and the single passage. The orientation of the building, the dimensions of the zones and the room numberings corresponding to each zone are shown. The internal walls serve as the boundary that separates one thermal zone from another. All zones were simulated to obtain hourly temperature changes, hourly relative humidity changes and hourly cooling loads for the whole year. Maximum cooling load for each of the zones were obtained.



All dimensions in mm
Figure 3.2: Plan view of the building

3.3.1 Mathematical description of type 56

Type 56 models the thermal behaviour of a building divided into different thermal zones. In order to use this type, a separate pre-processing programme (TRNBuild) must first be executed. The TRNBuild programme reads in and processes a file containing the building description (*BUI file) and generates two files, a file containing all information about the building excluding the wall construction (*.BLD) and another file that contains the ASHRAE transfer functions for the walls (*.TRN) that will be used by the TYPE 56 component during a TRNSYS simulation (Klein *et al.*, 2006).The mathematical equations used by Type 56 to model the building thermal behaviour are presented in this section.

3.3.1.1 Thermal zone /air-node

The building model in TYPE 56 is an energy balance model. The system boundary for this energy balance includes the inside surface node of all surfaces of the zone. This balance deals with radiative and convective heat flow into and out of the air-node (Klein *et al.*, 2006). Figure 3.3 shows the possible convective heat fluxes to the air node.

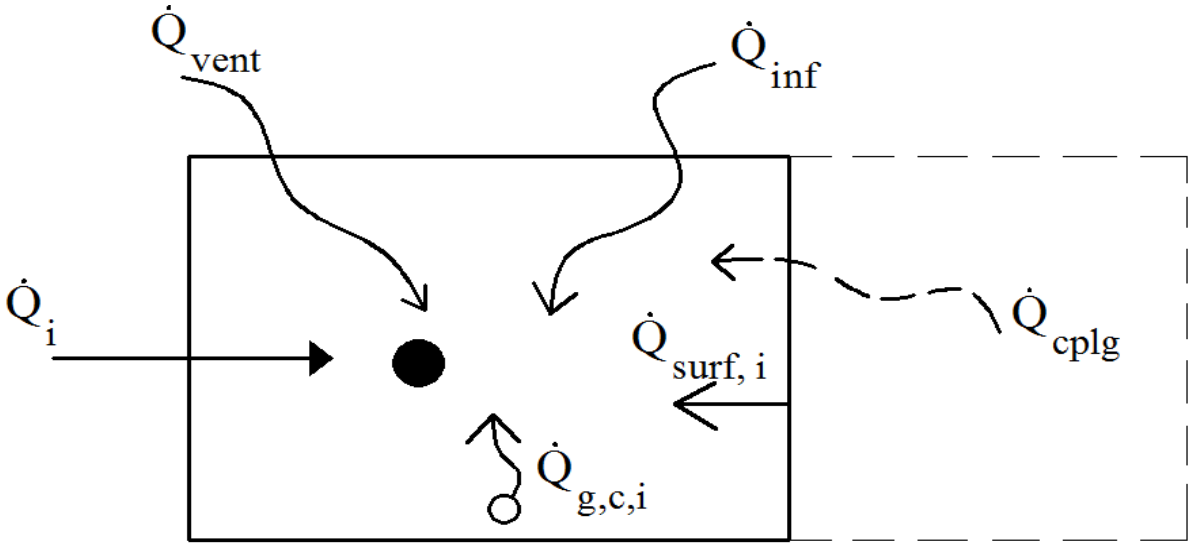


Figure 3.3: Convective Heat balance on the air node (source: Klein *et al.*, 2006)

The convective heat balance was determined by equation 3.1 (Klein *et al.*, 2006):

$$\dot{Q}_i = \dot{Q}_{surf,i} + \dot{Q}_{inf} + \dot{Q}_{vent} + \dot{Q}_{g,c,i} + \dot{Q}_{cplg} \quad (3.1)$$

where:

$\dot{Q}_{inf}$ = the infiltration gains (air flow from outside only), given by equation 3.2 as:

$$\dot{Q}_{inf} = \dot{V}.\rho.C_p(T_{outside} - T_{air}) \quad (3.2)$$

$\dot{Q}_{vent}$ = the ventilation gains (air flow from a user-defined source, like a heating ventilation and air conditioning(HVAC) System), determined by equation 3.3 as:

$$\dot{Q}_{vent} = \dot{V}.\rho.C_p(T_{ventilation,i} - T_{air}) \quad (3.3)$$

$\dot{Q}_{cplg}$ = the gain due to (convective) air flow from adjacent zone or boundary condition, determined by equation 3.4 as:

$$\dot{Q}_{cplg} = \dot{V}.\rho.C_p(T_{zone,i} - T_{air}) \quad (3.4)$$

$\dot{Q}_{surf,i}$= the convective heat gain from inner surface of zone (because of temperature difference between air- node temperature and surface temperature).

$\dot{Q}_{g,c,i}$= the internal convective gain (by people, equipment, illumination, radiators, etc.)

3.3.1.2 Radiative heat flows (only) to the walls and windows

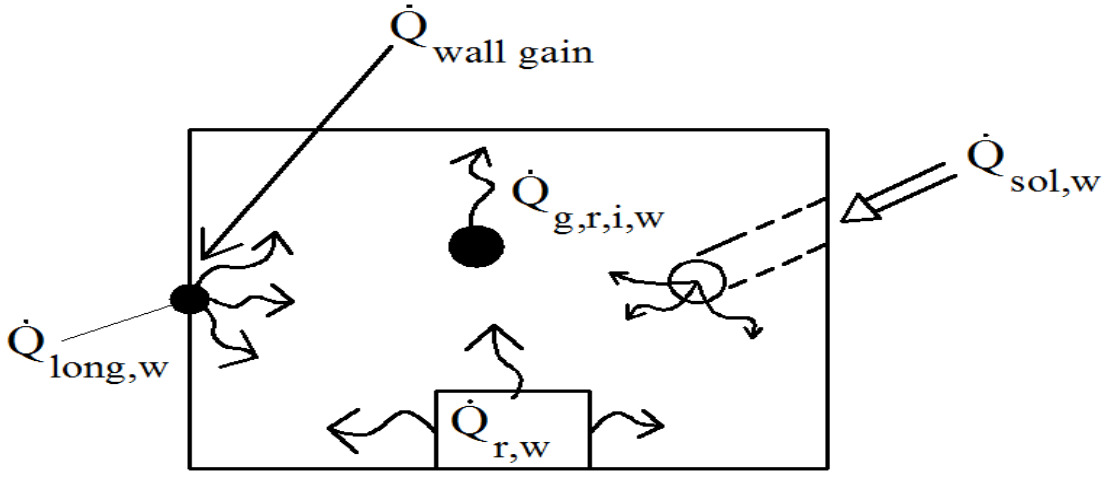


Figure 3.4 Radiative energy flows considering one wall with its surface temperature node (source: Klein *et al.*, 2006)

Figure 3.4 shows the radiative heat fluxes to the air-node. This balance was determined by equation 3.5 (Klein *et al.*, 2006):

$$\dot{Q}_{r,w} = \dot{Q}_{g,r,i,w} + \dot{Q}_{sol,w} + \dot{Q}_{long\ ,w} + \dot{Q}_{wall\ \ gain} \quad (3.5)$$

Where:

$\dot{Q}_{r,w}$ = the radiative gains for the wall surface temperature node,

$\dot{Q}_{g,r,i,w}$ = the radiative air-node internal gains received by wall,

$\dot{Q}_{sol,w}$ = the solar gain through zone windows received by wall,

$\dot{Q}_{long\ ,w}$ = the long-wave radiation exchange between this wall and all other walls and windows (ε=1) where ε is the emissivity of the glass, considered as a black body

$\dot{Q}_{wall\ \ gain}$ = the user-specified heat flow to the wall or window surface.

3.3.1.3 Integration of walls and windows

Figure 3.5 shows the heat fluxes and the temperatures that characterise the thermal behaviour of any wall or window, figure 3.6 shows the black box model of the wall.

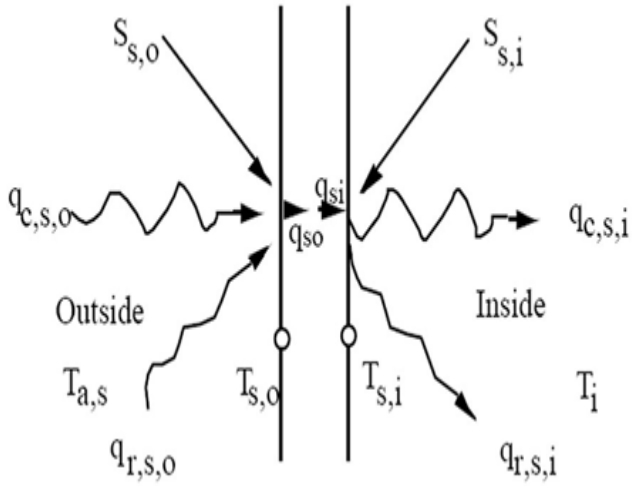


Figure 3.5 Surface heat fluxes and temperatures (Source: Klein *et al.*, 2006)

The nomenclature used in figure 3.5 is defined as follows:

$S_{s,i}$ =Radiation heat flux absorbed at the inside surface (solar and radiative gains)

$S_{s,o}$ =Radiation heat flux absorbed at the outside surface (solar gains)

$\dot{q}_{r,s,i}$= net radiative heat transfer with all other surfaces within the zone

$\dot{q}_{r,s,o}$= net radiative heat transfer with all surfaces in view of the outside surfce

$T_{a,s}$= outside surface air temperature

$\dot{q}_{s,i}$= conduction heat flux from the wall at the inside surface

$\dot{q}_{s,o}$= conduction heat flux into the wall at the outside surface

$\dot{q}_{c,s,i}$= convection heat flux from the inside surface to the zone air

$\dot{q}_{c,s,o}$= convection heat flux to the outside surface from the boundary/ambient

$T_{s,i}$ = inside surface temperature

$T_{s,o}$ = outside surface temperature

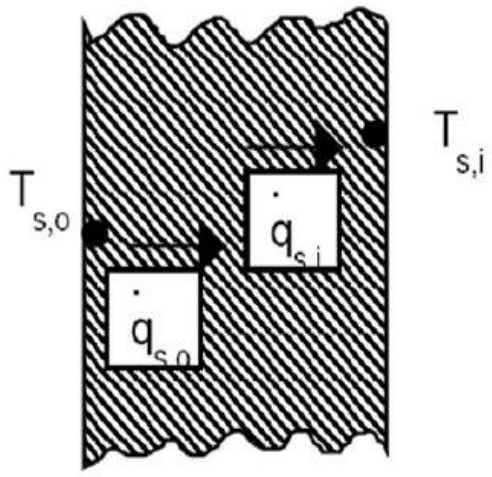


Figure 3.6 Black box model of wall (Source: Klein *et al.,* 2006)

The walls were modelled according to the transfer function relationships ofMitalas and Arseneault (Klein *et al.*,2006) and Stephenson and Mitalas (Klein *et al.,* 2006) defined from surface to surface. The walls for each zone were defined in TRNBuild from the outer to the inner surface using layers. TRNBuild has a library of wall construction materials (layers) form which the user specifies the materials used in the wall construction alongside their thickness. The thermal conductivities of these materials are also inbuilt in the programme from which heat transfer coefficients are calculated by the programme (from outer to inner surface). The black box representation of the wall is as shown in Figure 3.6. For any wall, the heat conduction at the surfaces are given by equations 3.6 and 3.7 (Klein *et al.,* 2006):

$$\dot{q}_{s,i} = \sum_{k=0}^{n_{b_s}} b_s^k T_{s,o}^k - \sum_{k=0}^{n_{c_s}} c_s^k T_{s,i}^k - \sum_{k=1}^{n_{d_s}} d_s^k \dot{q}_{s,i}^k \quad (3.6)$$

$$\dot{q}_{s,0} = \sum_{k=0}^{n_{a_s}} a_s^k T_{s,o}^k - \sum_{k=0}^{n_{b_s}} b_s^k T_{s,i}^k - \sum_{k=1}^{n_{d_s}} d_s^k \dot{q}_{s,0}^k \quad (3.7)$$

These time series equations in terms of surface temperatures and heat fluxes are evaluated at equal time intervals. The superscript ***k*** refers to the term in the time series, and it is specified by the user within the TRNBUILD description.The coefficients of the time series (**a's, b's, c's,** and **d's**) are determined within the TRNBUILD program using the **z** transfer function routines of Mitalas and Arseneault (Klein *et al.*,2006).Using the transfer function method, the TRNBUILD-program calculates the transfer function coefficients, listed above for the wall. In addition to the transfer function coefficients, the program calculates the heat conduction value of the wall construction and the total heat transfer coefficient U, considering a constant combined (convective and radiative) heat transfer (αi, αo) for the inside and outside surface.A window is thermally considered as an external wall with no thermal mass, partially transparent to solar, but opaque to long-wave internal gains.

In the energy balance calculation of the TYPE 56, the window is described as a 2-node model (Klein *et al.,* 2006) shown in Figure 3.7. Equations 3.6 and 3.7are valid for a window with the expressions given in equations 3.8 and 3.9 as (Klein *et al.*, 2006):

$$a_s^0 = b_s^0 = c_s^0 = d_s^0 = U_{g,s} \quad (3.8)$$

$$a_s^k = b_s^k = c_s^k = d_s^k = 0 \ \ for\ k > 0 \quad (3.9)$$

Where the coefficients of the time series (**a's, b's, c's,** and **d's**) are determined within the TRNBUILD program using the **z** transfer function routines of Mitalas and Arseneault (Klein *et al.*, 2006).

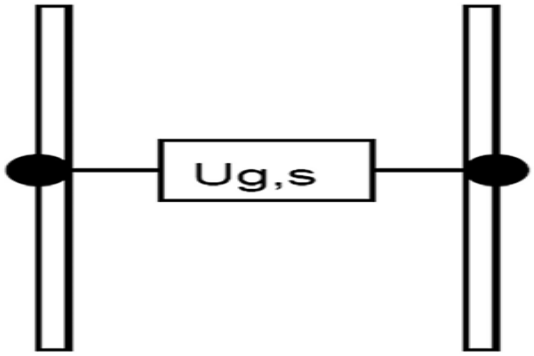


Figure 3.7: Two-node window model used in TYPE 56 energy balance equation (Source: Klein *et al.*, 2006).

The relative humidity in TRNBuild is calculated using the effective capacitance humidity model. (Klein *et al.*, 2006). The buffer effect of adsorptive and desorptive materials is considered by an effective moisture capacitance which is defined as the product of the zone air mass and moisture capacitance ratio as given in equation 3.10 (Klein *et al.*, 2006):

$$M_{eff,i} = Ratio \times M_{air,i} \quad (3.10)$$

Where: $M_{eff,i}$ = effective moisture capacitance of the zone

$M_{air,i}$ = mass of air in the zone

$Ratio$ = multiplication factor generally in the range of 1 to 10

A moisture balance for any zone results in the differential equation given in equation 3.11 (Klein *et al.*, 2006)

$$M_{eff,i}\frac{d\omega_i}{dt} = \dot{m}_{inf,i}(\omega_a - \omega_i) + \sum_{k}^{mvent} m_{v,k,i}(\omega_{v,k,i} - \omega_i) + W_{g,i} + \sum_{1}^{\substack{surfaces \\ i-j}} m_{cp,lg,s}(\omega_j - w_i) \quad (3.11)$$

Where:

$M_{eff,i}$ = effective moisture capacitance of the zone

ω_i = humidity ratio of the zone

ω_a = ambient humidity ratio

$\omega_{v,k,i}$= humidity ratio of the ventilation air from ventilation type k

$W_{g,i}$ =internal moisture gains

ω_j = humidity ratio of an adjacent zone j

$\dot{m}_{inf,i}$ = mass flow rate of infiltration air to the zone

$m_{v,k,i}$ = mass flow rate of ventilation air from ventilation type k

Subroutine DIFFEQ is used to independently solve for the final and average values of humidity ratio over each time step for each zone. If the average humidity ratio of the zone falls below or rises above a set point for humidification or dehumidification, then latent energy is added or removed to maintain the humidity ratio at the set point.

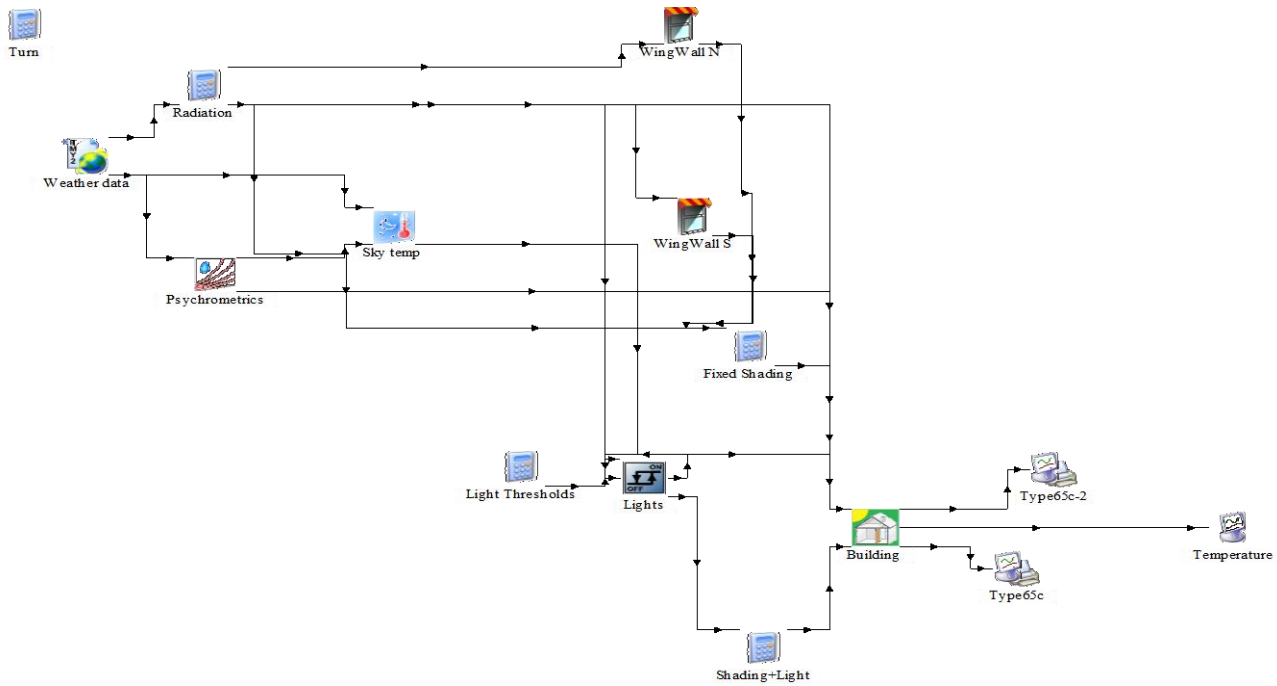


Figure 3.8 TRNSYS model for the cooling load simulation

In addition to type 56, the cooling load simulation model has some other components attached. Figure 3.8 is the TRNSYS model for the cooling energy demand simulation. It shows how the TRNSYS components together with Type 56 were connected in the simulation studio to simulate

the building cooling demand. Here, type 56 (building) has been connected with other components (types) used in the simulation, they are:

Type 109: weather data reader: This was used to read a meteorological data in a Typical Meteorological Year (TMY) format for the selected city, in this case, Zaria.

Type 33: psychrometrics, Type 69: sky temperature, Type 65: online plotter:

The direction of arrows shows the flow of variables which are outputs from one component and form inputs to the next component. Hourly simulation for the temperatures, relative humidity and cooling loads of the thermal zones were done. Table 3.1 shows the inputs made to Type 56.

Table 3.1: Inputs to Type 56

	ZONES					
INPUTS	**A1**	**B1**	**C1**	**A2**	**A3**	**B3**
Floor Area (m^2)	13.42	13.42	13.42	15.93	22.5	11.26
Height (m)	3	3	3	2.04	3	3
Volume (m^3)	40.26	40.26	40.26	32.49	67.5	33.78
Window area (m^2)	5.25	5.25	5.25		10.5	5.25
Window orientation	North	North	North		South	South
Window material	Glass	Glass	Glass		Glass	Glass
Door Area (m^2)	1.65	1.65	1.65	2.82	1.65	1.65
Door orientation	Internal	Internal	Internal	External/East	Internal	Internal
Door material	Metal	Metal	Metal	Metal	Metal	Metal
Wall material	Cement plaster - Hollow Block - cement plaster					
Floor material	Concrete all zones					
Roof material	Concrete	Concrete	Concrete	Concrete/Plastic	Concrete	Concrete
Occupancy period	8am - 6pm, (Mondays - Fridays) all zones					
No. of Occupants	1	1	2	0	2	2
Visitors	1	1	1	1	1	1
Computer/ Monitor	1	1	2		2	2
Printer	1	1	1		1	1
Lighting (W)	85	85	85	60	85	85
Density of air	1.204kg/m^3 at 25^{o}C all zones					
Specific heat of air	1.02kJ/kg at 25^{o}C all zones					
Heat of vapourisation of water	2454kJ/kg at 25^{o}C all zones					

Details of results obtained from the cooling load simulation are presented in Chapter 4: (Results and Discussion). Appendix A1 shows the TRNSYS input file for the building cooling energy demand simulation.

3.4 TRNSYS Modelling and Simulation of the Solar/ Gas Hybrid Powered Absorption Air Conditioning System

In this section modelling and simulation of the solar and gas hybrid poweredabsorption cooling system in the TRNSYS studio is presented. The objective is to model a system that will cover the cooling load demand of the office block as well as optimally size system components.Appropriate sizing and configuration of the system components was done. The system was integrated with the TRNSYS model of the cooling energy demand simulation done in Section 3.3. Simulation and optimization of the solar collector array size, storage tank volume,was done until the year round cooling load was met.

The system modelled in TRNSYS consists of a number of system components (types), linked together, with the output from one being the input to the next.Solar absorption cooling systems usually require a fraction of electricity to operate. This is required to power the auxiliaries (absorption chiller pumps, collector loop pump, cooling tower fan). This fractional power requirement could be obtained from the conventional electric power source, a solar power source, or any other form of alternative power.Figure 3.9 shows the model of the solar/ gas hybrid powered absorption cooling system in the TRNSYS studio.

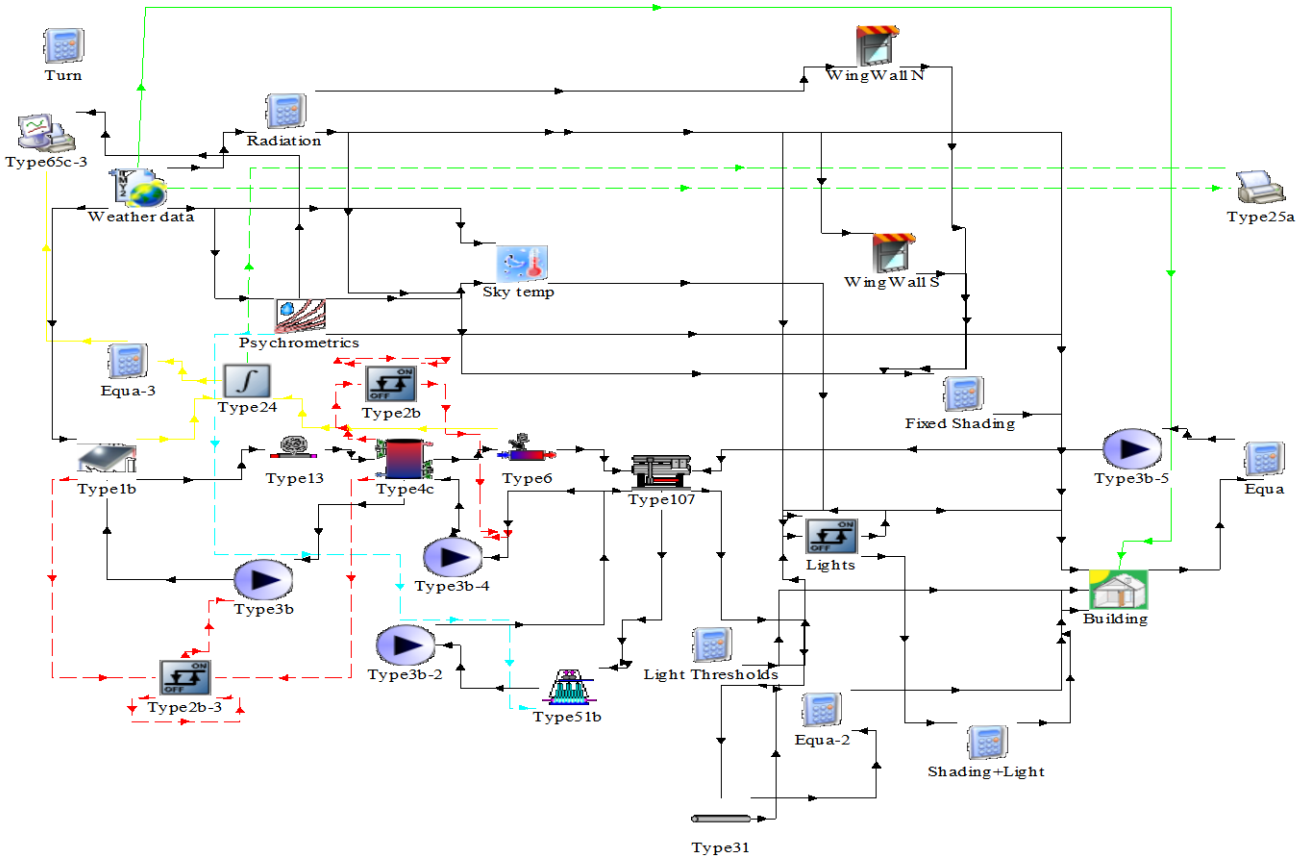


Figure 3.9 Model of the solar/ gas hybrid poweredabsorption cooling system in TRNSYS studio

3.4.1TRNSYS components (types) used in the system model with mathematical descriptions

The TRNSYS model as seen in the Graphical User Interface (GUI) presented in figure 3.9 consists of the components (types) that make up the system. These components were connected by links, with the output from one being the input to the next.The TRNSYS components have inbuilt models which have been programmed in FORTRAN.A description of the components and their mathematical models is here presented.

3.4.1.1 Absorption chiller (Type 107)

Type 107 was used to model the single effect hot water fired lithium bromide/ water absorption chiller. Type 107 is based on ordinary calculation and on external data (performance data) which supply the required values: normalized fraction of full load capacity and fraction of design energy Input. It also supplies values that are independent on fraction of design load: chilled water set point temperature (ºC), entering cooling water temperature (ºC),and hot water temperature (ºC)

(Klein et al., 2006).Type107 first determines the fraction of design load at which it must operate first by calculating the amount of energy that must be removed from the chilled water stream ($\dot{Q}_{remove}$)in order to bring it from its entering temperature to the set point temperature using equation 3.12 (Klein *et al.*, 2006).

$$\dot{Q}_{remove} = \dot{m}_{chw} c_{p,chw} (T_{chw,in} - T_{chw,set}) \quad (3.12)$$

where:

$\dot{m}_{chw}$ = mass flow rate of chilled water

$c_{p,chw}$ = specific heat capacity of chilled water

$T_{chw,in}$ = temperature of chilled water at inlet to the chiller

$T_{chw,set}$ = set point temperature of chilled water

The required energy removal is then divided by the machine's capacity to determine the fraction of design load at which the machine is required to operate using equation 3.13 (Klein *et al.*, 2006).

$$f_{Design\ load} = \frac{Q_{remove}}{Capacity_{\ rated}} \quad (3.13)$$

where:

$f_{Design\ load}$ = fraction of design load

$Capacity_{rated}$ = rated capacity of the chiller

Then Type 107 calls the dynamic data subroutine with the user specified chilled water set point temperature, entering cooling water temperature, inlet hot water temperature, and fraction of design load and return fraction of design energy input ($f_{Design\ Energy\ Input}$)for the specific values in the external data file at current work condition.

Afterward, type 107 calculates the machine capacity at the given time (Klein *et al.*, 2006).

When dynamic data returns the fraction of design energy input, then Type 107 calculates the energy delivered to the chiller by the hot water stream ($\dot{Q}_{hw}$) using equation 3.14

$$\dot{Q}_{hw} = \frac{Capacity_{\ rated}}{COP_{rated}} \times f_{Design\ Energy\ Input} \quad (3.14)$$

It then calculates the hot water stream outlet temperature ($T_{hw,out}$) according to equation 3.15 (Klein *et al.*, 2006):

$$T_{hw,out} = T_{hw,in} - \frac{\dot{Q}_{hw}}{\dot{m}_{hw} c_{p,hw}} \quad (3.15)$$

where:

$T_{hw,in}$ = temperature of hot water at inlet to chiller

$\dot{m}_{hw}$ = mass flow rate of hot water

$c_{p,hw}$ = specific heat capacity of hot water

The chilled water outlet temperature ($T_{chw,out}$), which should be the set point temperature but may be greater if the machine is capacity limited, is then calculated according to equation 3.16 (Klein *et al.*, 2006)

$$T_{chw,out} = T_{chw,in} - \frac{\dot{Q}_{remove}}{\dot{m}_{chw} C_{p,chw}} \quad (3.16)$$

Now Type 107 can balance the energy in the machine by calculating the energy rejection to the cooling water ($\dot{Q}_{cw}$) which is calculated by equation 3.17

$$\dot{Q}_{cw} = \dot{Q}_{chw} + \dot{Q}_{hw} + \dot{Q}_{aux} \quad (3.17)$$

where $\dot{Q}_{chw}$ = energy supplied to the chilling water stream

Here term $\dot{Q}_{aux}$ is counting for the energy needed by the auxiliary components on the entire system and it is used regardless if the machine works in a full capacity or not.

The temperature of the exiting cooling water stream ($T_{cw,out}$) is calculated using equation3.18 (Klein *et al.*, 2006)

$$T_{cw,out} = T_{cw,in} + \frac{\dot{Q}_{cw}}{\dot{m}_{cw} C_{p,cw}} \quad (3.18)$$

where:

$T_{cw,in}$ = temperature of the cooling water at inlet to the chiller

$\dot{m}_{cw}$ = mass flow rate of cooling water

$C_{p,cw}$ = specific heat capacity of cooling water

The performance indices are computed as follows:

(a) The machine COP is calculated according to equation 3.19 (Klein *et al.,* 2006):

$$COP = \frac{\dot{Q}_{chw}}{\dot{Q}_{hw} + \dot{Q}_{aux}} \quad (3.19)$$

(b) Solar Coefficient of Performance (SCOP)

The Solar Coefficient of Performance (SCOP) is the ratio of the total cooling energy produced to the total incident solar radiation energy. This value can be thought of as the overall system efficiency of a solar cooling facility (Klein *et al.,* 2006). This is calculated using equation 3.20.

$$SCOP = \frac{Q_e}{Q_r} \quad (3.20)$$

where:

Q_e = cooling energy produced at evaporator

Q_r = total incident solar radiation energy

For a Solar absorption cooling system with thermal energy storage, Q_r is calculated according to equation (Klein *et al.,* 2006) 3.21:

$$Q_r = Q_u + Q_{l,col} + Q_{hst} + Q_{l,hst} + Q_{l,p} \quad (3.21)$$

Where:

Q_u = useful energy gained at the collector

$Q_{l,col}$ = energy loss at the collector

Q_{hst} = energy gained at the hot storage tank

$Q_{l,hst}$ =energy loss at the hot storage tank

$Q_{l,p}$ = energy loss at the piping between collector and hot storage tank and between hot storage tank and absorption chiller

(c) Solar Fraction (SF)

The solar fraction is calculated as a ratio of the energy absorbed by the hot water stream from the solar collector array to the total energy absorbed by the hot water stream, where the total energy absorbed by the hot water stream is a summation of the energy delivered by the solar collector array and the energy delivered by the auxiliary heater.

It denotes the fraction of the cooling load that is met by solar energy. The solar fraction is calculated using equation 3.22 (Klein *et al.,* 2006).

$$SF = \frac{Q_{coll}}{Q_{coll} + Q_{aux\ heat}} \tag{3.22}$$

Where:

Q_{coll} = energy delivered to the hot water stream by the collector array

$Q_{aux\ heat}$ = energy delivered to the hot water stream by the auxiliary heater

3.4.1.2 Flat Plate Collector (type 1)

Type 1 was used to model the flat plate solar collector array. The TRNSYS flat plate collector model (type 1) assumes the efficiency versus ratio of fluid temperature minus ambient temperature to radiation ($^{\Delta T}/_{I_T}$)curve can be modelled as a quadratic equation (Klein *et al.,* 2006).

A general equation for solar thermal collector efficiency can be obtained from the Hottel-Whillier equation (Duffie and Beckman, 2013) this is as stated in equations 3.23 to 3.25

$$\eta = {}^{Q_u}/_{AI_T} \tag{3.23}$$

$$\eta = \frac{\dot{m} c_{pf} (T_o - T_i)}{AI_T} \tag{3.24}$$

$$\eta = F_R(\tau\alpha)_n - F_R \cup_{L/T} \frac{(T_i - T_a)}{I_T} - F_R \cup_{L/T} \frac{(T_i - T_a)^2}{I_T} \tag{3.25}$$

Equation 3.25 can be rewritten as:

$$\eta = a_o - a_1 \frac{(\Delta T)}{I_T} - a_2 \frac{(\Delta T)^2}{I_T} \tag{3.26}$$

Equation 3.26 is the general collector thermal efficiency equation used in type 1. The thermal efficiency is defined by three parameters: $a_o, a_1, and\ a_2$. These three parameters are available for collectors tested according to ASHRAE standards (Duffie and Beckman, 2013).

3.4.1.3 Storage tank (type 4)

Type 4 was used to model the hot water storage tank. Type 4 models the thermal performance of a fluid-filled sensible energy storage tank, subject to thermal stratification by assuming the tank consists of N ($N \leq 15$) fully mixed equal segments. The degree of stratification is determined by the value of N. If N is equal to 1, the tank is modelled as a fully mixed tank and no stratification effects are possible (Klein *et al.,* 2006). The model optionally includes two electrical resistance heating elements, subject to temperature and/or time control.

An assumption employed in the model is to assume that the fluid streams flowing up and down from each node are fully mixed before they enter each segment, as shown in figure 3.10.

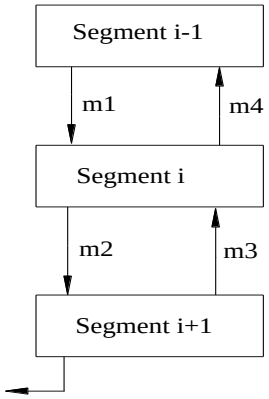


Figure 3.10: Segmented layers of stratified storage tank (Klein *et al.,* 2006)

This implies that $\dot{m}_1$ is added to $\dot{m}_4$and $\dot{m}_2$ is added to $\dot{m}_3$ and the resultant flow either up or down is determined. An energy balance on the segment neglecting losses is thencalculated according to equations 3.27 and 3.28 (Klein *et al.,* 2006):

$$M_i c_{pf} \frac{dT_i}{dT} = \{(\dot{m}_1 - \dot{m}_3) c_{pf} (T_{i-1} - T_i)\} \dot{m}_1 \geq \dot{m}_3 \qquad (3.27)$$

$$M_i c_{pf} \frac{dT_i}{dT} = \{(\dot{m}_3 - \dot{m}_1) c_{pf} (T_{i-1} - T_i)\} \dot{m}_1 < \dot{m}_3 \qquad (3.28)$$

3.4.1.4 Weather Data (type 109)

Type 109 reads weather data at regular time intervals from a data file. This file contains Total Meteorological Year (TMY) data of several cities worldwide. It converts this data to desired system of units and processes solar data radiation to obtain tilted surface radiation and angle of incidence for an arbitrary number of surfaces. Type 109 was used to provide weather data for Zaria.

3.4.1.5 Online Plotter (type 65c)

Type 65c is an online graphic plotter. It was used to display selected system variables while the simulation is progressing.

3.4.1.6 Psychrometrics (type 33)

Type 33 takes in dry bulb temperature and relative humidity of moist air for processing. It was used in calculating psychrometric conditions at a given time.

3.4.1.7 Sky Temperature (type 69)

Type 69 was used to calculate the long wave radiation exchange between arbitrary external surface and the atmosphere.

3.4.1.8 Integrator (type 24)

Type 24 is used to integrate a series of quantities over a period of time. It was used to integrate temperatures, solar radiation values over specified time intervals.

3.4.1.9 Pressure Relief Valve (type 13)

Type 13 models a pressure relief valve. This was used in the model at the collector and hot water storage tank to discard vapour in case of boiling.

3.4.1.10 Auxiliary Heater (type 6)

Type 6 models an auxiliary heater used to elevate the temperature of a flowing stream. It is designed to add heat to the flowing stream at a user designated rate $(\dot{Q}_{max})$ whenever the flowing

stream temperature falls below a certain pre-set value(T_{set}). For this work type 6 was modelled as an auxiliary gas boiler.

3.4.1.11 Differential Controller (type 2b)

Type 2b models a differential controller which generates a control function that can have a value of 0 or 1 to represent ON or OFF. Type 2b was used in the control strategy for the pumps.

3.4.1.12 Pump (type 3b)

Type 3b models a variable speed pump. This was used to model the various pumps in the system.

3.4.1.13 Cooling Tower (type 51b)

Type 51b models a multiple cell counter flow wet cooling tower. This was used to model the cooling tower of the system.

3.4.1.14 Pipe (type 31)

Type 31 models the thermal behaviour of fluid flow in a pipe or duct using variable size segment of fluid. This was used in modelling the piping connections of the system.

3.4.1.15 Printer (type 25)

Type 25 was used to output and print selected system variables at specified intervals of time.

3.4.1.16 Equation editors

The equation editors are used to input and compute user defined functions and equations that work with a TRNSYS model. Equation editors were used to input and compute the equations for the control as well as averaging of data for plotting.

3.4.2 The control system

A cooling set point temperature of 24^{o}C was used in the control system. A hot water maximum set point temperature of 90^{o}C for the chiller was used. The control was designed to allow the chiller operate between 80^{o}C and 90^{o}C, which is the hot water temperature range for cooling to be achieved. The control was implemented in the TRNSYS model by the use of type 2b and the equation editor. The type 2b acts like a sensor operating between upper and lower temperature

bands, thus actuating the pumps. Also whenever cooling is taking place, the control system monitors the relative humidity within the zones. The relative humidity was set to a range of 30 – 55 %. When the relative humidity falls below 30%, cooling and humidification takes place. When it rises above 55%, cooling and dehumidification takes place. Equation editors were used to input user defined equations. A schematic of the pump arrangement is as shown in figure 3.11

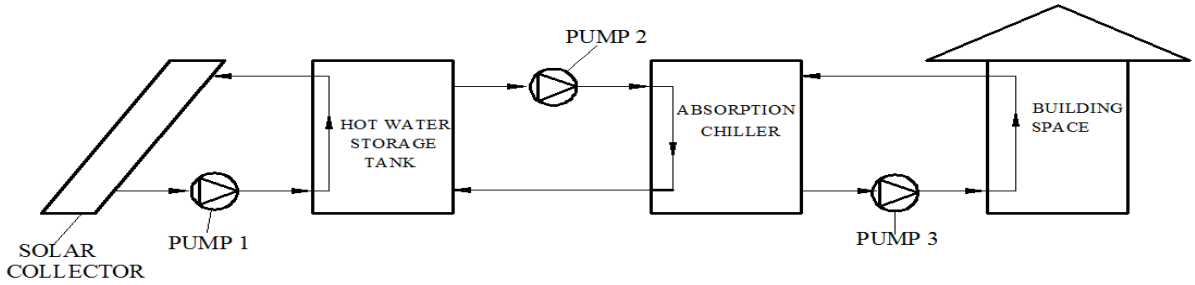


Figure 3.11: Schematic of pump arrangement

The control logic used is as follows:

<u>When there's a cooling demand (when temperature in the building is > 24°C)</u>

(a) If temperature in hot storage tank is $\geq 90^0C$

Pump 1 is OFF, auxiliary heater is OFF, and pumps 2 and 3 are ON

(b) If temperature in hot water storage tank is < 89°C but > 80°C and temperature from collector is $\geq 90^0C$

Pumps 1, 2 and 3 are ON, auxiliary heater is OFF

(c) If temperature in hot water storage tank is <87°C but >80°C and temperature from collector is <90°C

Pump 1 is OFF, auxiliary heater is ON, and pumps 2 and 3 are ON

(d) If temperature in the hot water storage tank is < 80°C and temperature from collector is

$\geq 90^0C$

Pump 1is ON, auxiliary heater is OFF, pumps 2 and 3 are OFF

(e) If temperature in hot water storage tank is < 80^{o}C and temperature from collector is < 90^{o}C

Pump 1 is OFF, auxiliary heater is ON, and pumps 2 and 3 are OFF

When there's no cooling demand (When temperature in the building is < 24^{o}C)

(a) If temperature in hot water storage tank is $\geq 90^{0}C$

Auxiliary heater, pumps 1, 2 and 3 are OFF

(b) If temperature in the hot water storage tank is < 88^{o}C and temperature from collector is

$$\geq 90^{0}C$$

Pump 1 is ON, pumps 2 and 3 are OFF, and auxiliary heater is OFF

(c) If temperature in hot water storage tank is < 87^{o}C and temperature from collector is < 90^{o}C

Auxiliary heater is OFF, pumps 1, 2 and 3 are OFF.

3.4.3 Sizing of the absorption cooling system components in TRNSYS

In this section, components sizing was done using the peak cooling load demand of 11.04 kW obtained from section 3.3. Initial sizing of components was done to obtain a baseline over which simulation was then carried out in TRNSYS to obtain optimized component sizes.

3.4.3.1 Determining the design months

Results from the cooling energy demand simulation carried out in section 3.3 is presented in Chapter Four (Results). However, for use in subsequent sections before the results the following is stated:

The month of April had the highest solar radiation on a flat surface and also the highest cooling load requirements for the year. It had the maximum cooling load of 11.04 kW which is a summation of the cooling loads in all the zones occurring on the 21st of April between 2 and 3pm. For this reason, the month of April was chosen as the design month to size the absorption chiller.

To determine the design month to size the flat plate solar collector, the energy ratio was used. The design month to size the solar collector is defined as the month with the least value of the energy ratioR_e. The energy ratio is the ratio of monthly average daily solar radiation on the collector surface to the monthly average daily system load, expressed in equation 3.29 as:

$$R_e = \frac{H_T}{Q_L} \tag{3.29}$$

where:

H_T = monthly average daily solar radiation on the tilted collector surface $(J/m^2 day)$

Q_L = monthly average daily cooling load (J/day)

The monthly average daily output values from the TRNSYS simulation used to calculate the energy ratio are shown in table 3.2.

Table 3.2: Monthly energy ratio from TRNSYS simulation

Month	H_T (J/m^2. day)	Q_L (J/day)	$Re=H_T/Q_L$
January	22749485	6934915	3.28
February	25523307	8090740	3.11
March	27941928	14101004	1.98
April	28677235	15603570	1.84
May	26141247	13638676	1.92
June	20249819	12136110	1.67
July	17243517	11558210	1.49
August	**15117665**	**10402380**	**1.45**
September	23020388	12714020	1.81
October	24669264	13291930	1.86
November	23968778	9246563	2.59
December	23473544	7281666	3.22

From table 3.2, the month of August is seen to have the least energy ratio (1.45). The month of August was therefore used as the design month to size the solar collector.

3.4.3.2 Absorption chillercapacity

The cooling energy demand simulation carried out in section 3.3 showed a peak cooling demand of 11.04 kW for the office block (details presented in chapter 4: Results). For this peak cooling demand, a 5% safety margin was applied. This safety margin was based on recommended safety

margin for chiller design according to Hanson *et al.* (2011).Rounding up resulted in an absorption chiller of 12 kW capacity to serve the cooling energy requirements. An absorption chiller of 12 kW capacity was therefore used in the TRNSYS model of the absorption cooling system.

3.4.3.3 Collector array area

The solar collector was sized based on the minimum monthly solar radiation obtainable at the given location (Zaria). As mentioned earlier, the month of August had the lowest solar radiation, it was therefore used in sizing the collector area.

The collector area was obtained using equation 3.29 (Duffie and Beckman, 2013)

$$A_{coll} = \frac{Q_{tot}}{G_{\perp}\eta_{coll}\, COP_{chiller}} \quad (3.30)$$

where:

$A_{coll} = collector\ area$

$Q_{tot} = Nominal\ cooling\ capacity\ of\ chiller\ (kW)$

$G_{\perp} = Average\ solar\ normal\ radiation\ incident\ on\ collector = 0.65\ kW/m^2$ (For Zaria in August). (Source: TRNSYS simulation)

η_{coll} = collector efficiency = 0.6. This value was used based on the efficiency of standard flat plate collectors tested according to ASHRAE standards, as reported in Duffie and Beckman(2013).

$COP_{chiller} = Coefficient\ of\ performance\ of\ chiller\ (\ rated)$

Here a desired coefficient of performance of 0.8 was used. This is based on available data on obtainable COP of single effect absorption chillers (Zheng, 2016), (Hanson *et al.*, 2011).

From which the collector area was obtained in equation 3.30 as:

$$A_{coll} = \frac{12.0}{0.65\times0.6\times0.8} = 38.46\ m^2$$

3.4.3.4 Wet cooling tower capacity

The heat rejected at the condenser and absorber of the absorption chiller is transferred to the environment by the cooling tower. This thermal waste is generated at the generator and rejected to

the cooling water stream at the condenser and absorber. The cooling tower capacity (Q_{ct}) is calculated according to equation 3.31(Williamson, 2008).

$$Q_{ct} = Q_g = \frac{Q_e}{COP_{desired}} \quad (3.31)$$

where:

Q_e = the heat duty at the evaporator which is equal to the peak cooling capacity of the chiller,

$$Q_e = 12.0\ kW$$

The generator heat load (Q_g) is calculated according to equation 3.32 (Arora, 2000)

$$Q_g = \frac{Q_e}{COP_{desired}} = \frac{12.0}{0.8} = 15\ kW \quad (3.32)$$

From which the cooling tower capacity is obtained as in equation 3.33

$$Q_{ct} = Q_g = 15\ kW \quad (3.33)$$

3.4.3.5 Hot water storage tank volume

The absorption chiller is to operate within a temperature range of 80^{o}C and 90^{o}C. The hot water storage tank was modelled to store hot water within the temperature range of 85^{o}C and 95^{o}C and supply to the absorption chiller. The water in the tank was heated by heat from the solar collector array or by an auxiliary gas heater when the heat from the collector array was not sufficient to meet the desired temperature. The control was modelled such that when there's a 1^{o}C drop in supply water temperature to the chiller from the tank below 80^{o}C, heating is activated. Also, when there's a 1^{o}C rise in supply water temperature to the chiller from the tank above 90^{o}C, heating is deactivated.

The volume of hot water storage tank ($V_{hw,T}$) was calculated using equation 3.34 according to Qu et al. (2010) as:

$$V_{hw,T} = \frac{Q_{peak} \times t}{COP_{rated} \times \rho \times C_p \times \Delta T} \quad (3.34)$$

$t = time(seconds)$ In which it is desired that the storage tank retains the water within the operating temperature range when the solar radiation is down, without heat supply by the auxiliary heater. In this case the time was 3600 seconds. ΔT= temperature difference, in this case = 11^{o}C

From which;

$$V_{hw,T} = \frac{11.04 \times 3600}{0.8 \times 1000 \times 4.2 \times 11} = 1.075\ m^3$$

3.4.3.6 Auxiliary heater capacity

The auxiliary heater was modelled as a liquefied petroleum gas heater, required to raise the temperature of water in the tank by 1^{o}C in 180 seconds, when the temperature of hot water in the storage tank falls below the set point temperature and there is no heating from the solar collector array. The auxiliary heater capacity ($Q_{aux,hc}$)was calculated using equation 3.35(Qu et al., 2010).

$$Q_{aux,hc} = \frac{m_{hw} C_p \Delta T}{t} \qquad (3.35)$$

During the simulation, Eq. (3.35) was used to calculate the auxiliary heater capacity and it varied as the volume of the hot water tank varied.

3.4.4TRNSYS modelling and simulation procedure

The initial capacity/ sizes obtained formed the base line in which the TRNSYS types were configured and the TRNSYS model developed. It also formed the basis for the range in which component sizes were varied during simulation. The process of simulation and optimization was carried out in the TRNSYS studio using the TRNSYS model of the absorption cooling system shown in figure 3.9. Based on the values obtained from initial sizing of system components, system components sizes were varied to obtain a system that will give the desired set point temperature within all zones for the whole year.

The effect of varying system components sizes on performance indices (COP, SCOP and SF) for all the months of the year was studied. The absorption chiller capacity was kept constant at 12 kW,

the collector area was varied from 5 to 60m^2, the hot water storage tank volume was varied from 0.3 to 1.8m^3, cooling tower capacity was kept constant at 15 kW, and capacity of the auxiliary heater was adjusted as the volume of storage tank varied. For maximum annual solar energy availability, a surface slope equal to latitude is best (Duffie and Beckman 2013). Therefore the collector was sloped at an angle of 11.08^o(which is the latitude for the location, Zaria) facing south.

Each time a parameter was varied, simulation was done using an hourly time step to see the effect on the zone temperatures. This was done until the cooling demand in the building block was met for the year round. The cooling demand was considered to be met when the temperatures within the zones fell below the cooling set point of 24^{o}C for the year round. Each time a simulation was done, TRNSYS displays graphically the temperature variation within each zone for the whole year. In addition, TRNSYS generates an output file where hourly values of performance indices (COP, SCOP and SF) are stored. To study the effect of varying component sizes on performance indices, Microsoft excel package was used.The output data file generated from simulations where the hourly values of COP, SCOP and SF. These were stored and exported from TRNSYS to Microsoft excel. For each of the three parameters, daily hourly data for each day were averaged to obtain daily average data. The daily average data for each month were then averaged to obtain monthly average data.

These monthly averaged data were then used to obtain graphs of COP vs collector area, SCOP vs collector area, Solar Fraction vs collector area, for each month of the year. The set of system component sizes that maximised COP, SCOP and SF as well as achieved the desired set point temperature within all the zones for the whole year was considered the optimised system. Results

arepresented in chapter four. Appendix A2 shows the TRNSYS input file for the solar/ gas hybrid powered absorption cooling system modelling and simulation.

3.5Design Theories, Optimisation, Programming and Calculations

In this section, design of the optimum sized gas assisted solar absorption air conditioning system components is presented. Optimum sizes/ capacities of system components required to cover the cooling energy demand of the building block for the whole year were determined in the previous section, the results are presented in chapter four. However, for use in this section, the optimum system components are: Solar collector array area: 40m^2, Absorption chiller capacity: 12kW, Cooling tower capacity: 15kW, Storage tank volume: 0.9m^3.

3.5.1 Design considerations

The design considerations for each of the system components is presented below:

3.5.1.1 Design considerations for the solar collector

i. The peak cooling load of the office block

ii. Solar radiation for the design month: From the TRNSYS simulations for optimum components sizing (presented in Chapter Four), the month with the lowest solar radiation was August. This makes it the design month for the solar collector.

iii. Average ambient temperature for Zaria

iv. Capacity of absorption chiller to be used

v. Number of glass covers to be used

vi. Diameter of the fluid tubes to be used

3.5.1.2 Design considerations for the Absorption Chiller

i. Peak cooling load of the office block

ii. Weather conditions of the location (Zaria)

iii. Required temperature within the office block

iv. Source by which the absorption chiller will be fired (Hot water)

v. Refrigerant/ absorbent pair (water/ LiBr)

vi. Heat sink (Cold water)

vii. Building chilling fluid (Chilled water)

viii. Inlet and exit hot water temperatures

ix. Inlet and exit cooling water temperatures

x. Inlet and exit chilled water temperatures

xi. Concentration of Water/ LiBr solution

xii. Crystallisation limit of Water/ LiBr solution

xiii. High and low pressure limits for the absorption chiller

xiv. Heat exchanger type (Shell and tube)

xv. Auxiliary heating source (Liquefied Petroleum Gas)

xvi. Source of power for auxiliary components: (conventional electric power)

3.5.1.3 Design considerations for the cooling tower

i. Capacity of the absorption chiller

ii. Average ambient dry bulb and wet bulb temperatures for the location (Zaria)

iii. Absorption chiller cooling water inlet and outlet temperatures

iv. Flow rate of cooling water

3.5.1.4 Design considerations for the Hot water storage tank

i. Type of storage fluid (Hot water)

ii. Required storage temperature range

iii. Duration of storage

iv. Storage volume

v. Mode of circulation of fluid

vi. Geometry of tank

3.5.2 Materials selection

Selection of materials for each of the components in the absorption air conditioning system was done based on:

i. Durability

ii. Availability

iii. Cost

3.5.2.1 Solar collector materials

i. Heat transfer fluid tubes: Copper (Strength, high heat transfer coefficient)

ii. Absorber plate: Zinc sheet (Strength, high heat transfer coefficient, economical)

iii. Glazing: Tempered glass (Durable)

iv. Frame: Wood (Durable, available, economical)

v. Insulation: Fibre glass (available)

3.5.2.2 Absorption chiller materials

i. Heat exchanger tubes: Copper (Strength, high heat transfer coefficient)

ii. Heat exchanger shell: Stainless steel (Strength, corrosion resistant)

iii. Suction pipe: Copper (Durable)

iv. Interconnecting pipes: PVC pipes (Durable, flexible)

v. Frame: Mild steel (Strength, economical)

3.5.2.3 Cooling tower materials

i. Body: Galvanised steel (Durable, economical)

ii. Piping: PVC pipes, pressure pipes (Strength, durable)

iii. Spray tray: Galvanized sheet (Durable, economical)

3.5.2.4 Storage tank materials

i. Tank body: Galvanised steel (Durable, economical)

ii. Insulator: Fibre glass: (Durable, available)

3.5.3 Flat plate collector design

The flat plate collector design is presented here. The optimised solar collector array area is 40m^2 (from simulation results). It is desired to have the collector in modules of 1.5m^2 each, therefore about 27 modules are required. The design of a single module is presented here.

3.5.3.1 Flat plate collector design specifications

i. Length of single collector module: 1.5m

ii. Width of single collector module: 1m

iii. Mean plate temperature: 373K

iv. Number of glass covers (glazing): 1

ix. Chiller capacity: 12000W

3.5.3.2 Useful energy gain by collector

In steady state, the performance of a flat-plate solar collector can be described by the useful gain from the collector, Q_u, this is calculated from the heat balance in the collector by the Hottel - Whilller – Bliss equation (Duffie and Beckman, 2013) as shown in equation 3.36:

$$Q_u = A_c F_R [G(\tau\alpha) - U_L(T_i - T_{amb})] \quad (3.36)$$

The useful energy gain per unit of collector area is as given in equation 3.37:

$$q_u = \frac{Q_u}{A_c} = F_R [G(\tau\alpha) - U_L(T_i - T_{amb})] \quad (3.37)$$

Where:

A_c= Area of collector

F_R= collector heat removal factor

G = solar radiation

U_L= overall heat loss coefficient

τ= transmittance of cover

α = absorptance of absorber plate

T_i = inlet fluid temperature

T_{amb} = ambient temperature

where $U_L = U_t + U_b + U_e$ (3.38)

where:

U_t= top loss coefficient

U_b= back loss coefficient

U_e= edge loss coefficient

3.5.3.3 Top loss heat coefficient

The top heat loss is made up of heat loss by radiation and heat loss by convection.

An empirical equation used to computeU_t as reported in Duffie and Beckman (2013) is as given in equation 3.39:

$$U_t = \left[\frac{N}{\frac{c}{T_{pm}}\left[\frac{(T_{pm}-T_{amb})}{(N+f)}\right]^e} + \frac{1}{h_w}\right]^{-1} + \frac{\sigma(T_{pm}+T_{amb})(T_{pm}^2+T_{amb}^2)}{\frac{1}{\varepsilon_p+0.00591Nh_w} + \frac{2N+f-1+0.133\varepsilon_p}{\varepsilon_g} - N} \quad (3.39)$$

where:

$$f = (1 + 0.089h_w - 0.1766h_w\varepsilon_p)(1 + 0.07866N) \quad (3.40)$$

$$c = 520(1 - 0.000051\beta^2)\ for\ 0^o < \beta < 70^0 \quad (3.41)$$

$$e = 0.430\left(1 - \frac{100}{T_{pm}}\right) \quad (3.42)$$

where N = number of glass covers

β= collector tilt angle

ε_g = emittance of glass

ε_p = emittance of plate

T_{amb} = ambient temperature

T_{pm} = mean plate temperature

$$\sigma = 5.67 \times 10^{-8}$$

The wind heat transfer coefficient h_w as given by McAdams(1954) is used in equation 3.43:

$$h_w = 5.7 + 3.8v \quad (3.43)$$

where v is the wind velocity

3.5.3.4 Back loss heat coefficient

The back loss coefficient U_b is calculated using equation 3.44 (Duffie and Beckman, 2013)

$$U_b = \frac{k_i}{l_i} \quad (3.44)$$

where

k_i= insulation thermal conductivity

l_i = insulation thickness

3.5.3.5 Edge loss heat coefficient

The edge loss coefficient U_e is calculated using equation 3.45 (Duffie and Beckman, 2013)

$$U_e = \frac{k_e}{x_e}\left[\frac{2(L+W)H}{LW}\right] \quad (3.45)$$

k_e= edge insulation conductivity W/mK

x_e = edge insulation thickness (m)

L = collector length (m)

W = collector width (m)

H = collector height (m)

3.5.3.6 Absorbed radiation by absorber plate

The absorbed radiation by the absorber plate, using the isotropic sky model of Hottel and Woertz (1942), as cited by Duffie and Beckman (2013)was evaluated as shown in equation 3.46:

$$S = I_b R_b(\tau\alpha)_b + I_d(\tau\alpha)_d\left(\frac{1+\cos\beta}{2}\right) + (I_b + I_d)(\tau\alpha)_g\,\rho_g\left(\frac{1+\cos\beta}{2}\right) \quad (3.46)$$

Subscripts *b, d* and *g* represent beam, diffuse and ground reflected radiation respectively.

I = intensity of radiation on a horizontal surface

$(\tau\alpha)$ is the transmittance – absorptance product

β = collector slope

ρ_g = diffuse reflectance of ground

R_b = ratio of beam radiation on the tilted surface to that on horizontal surface

3.5.3.7 Useful energy gain transferred to water in the tubes

The absorber plate – tube configuration of the collector is as shown in figure 3.12:

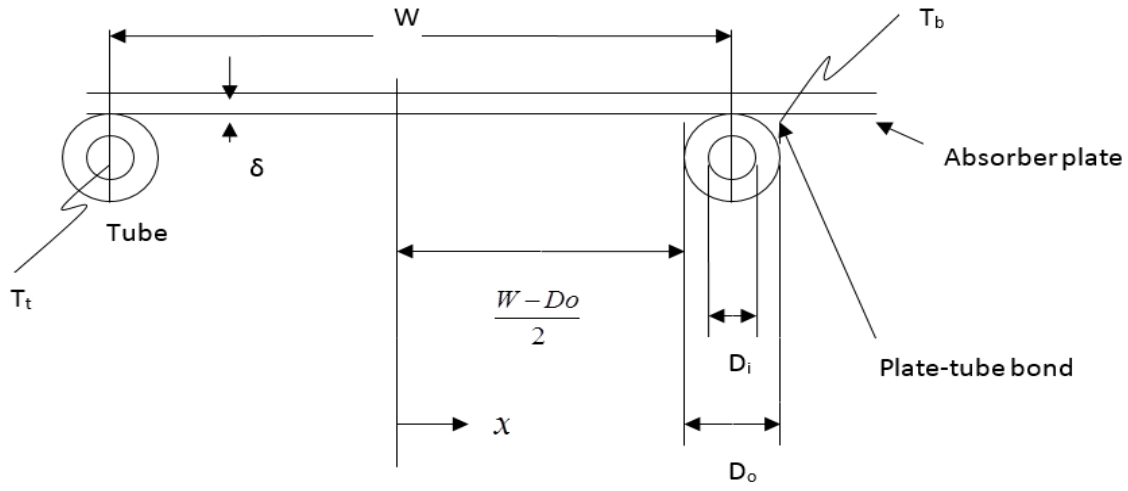


Figure 3.12 Geometric configuration of the absorber plate- tube

From the plate- tube arrangement shown in figure 3.12, if we take the bond to be at some local base temperature T_b , the region between the centre line separating the tubes and the tube base can then be considered as a classical fin problem.

The useful energy gain transferred to the water in the tube as given by Duffie and Beckman (2013) is as shown in equation 3.47:

$$q_u^{'} = WF^{'}\left[G(\tau\alpha) - U_L\left(T_f - T_{amb}\right)\right] \quad (3.47)$$

Where F^1 is the collector efficiency factor, which represents the temperature distribution along the absorber plate between tubes calculated using equation 3.48:

$$F^{'} = \frac{\frac{1}{U_L}}{W\left[\frac{1}{U_L(D_o+(W-D_o)F)}+\frac{1}{C_b}+\frac{1}{\pi D_i h_{fi}}\right]} \quad (3.48)$$

where:

W = tube spacing

D_o = outer diameter of tube

D_i = inner diameter of tube

h_{fi}= heat transfer coefficient between fluid and wall tube, calculated using the Sieder Tate equation (Welty *et al.*, 2014) as shown in equation 3.49:

$$h_{fi} = \frac{k_f}{D_i}\left(1.86Re^{\frac{1}{3}}Pr^{\frac{1}{3}}\left(\frac{D_i}{L}\right)^{\frac{1}{3}}\left(\frac{\mu_b}{\mu_w}\right)^{0.14}\right) \quad (3.49)$$

where:

C_b= bond conductance

$$C_b = {k_b b}/{\gamma} \quad (3.50)$$

k_b= bond thermal conductivity

γ = average bond thickness

b = bond width

F is standard fin efficiency for straight fin with rectangular profile calculated using equation 3.51 (Duffie and Beckman, 2013)

$$F = \frac{tanh\left(\frac{m(W-D_o)}{2}\right)}{\frac{m(W-D_o)}{2}} \quad (3.51)$$

where:

$$m = \sqrt{\frac{U_L}{k_p \delta}} \quad (3.52)$$

δ = collector sheet thickness

k_p= thermal conductivity of the plate

3.5.3.8 Collector heat removal factor

The collector heat removal factor F_R which relates the actual useful energy gain of collector to the useful gain if the whole collector surface were at the fluid inlet temperature was calculated using equation 3.53 according to Duffie and Beckman(2013)

$$F_R = \frac{\dot{m}C_p}{A_c U_L}\left[1 - exp\left(-\frac{A_c U_L F'}{\dot{m}C_p}\right)\right] \quad (3.53)$$

According to Duffie and Beckman (2013), the collector flow factor F'' can be defined as a ratio of collector heat removal factor F_R to collector efficiency factorF', as shown in equation 3.54:

$$F'' = \frac{F_R}{F'} = \frac{\dot{m}C_p}{A_c U_L F'}\left[1 - exp\left(-\frac{A_c U_L F'}{\dot{m}C_p}\right)\right] \quad (3.54)$$

3.5.4 Flat plate collector design optimisation and design parameters calculation

Adequate sizing of system components is necessary to achieve optimum performance of the system. An optimisation process was done alongside calculation of design parameters. The entire set of equations from 3.36 to 3.54 were programmed and solved in MATLAB. The programme has as inputs, the design specifications as stated in 3.5.3.1 (details of other inputs in form of constants can be seen in Appendix B: the MATLAB programme).

It starts with an optimisation process in which the collector design variables were optimised by studying the effect of varying these design variables on a performance indicator (the heat removal factor). The design variables that were varied are: heat transfer tube diameter, tube spacing, absorber plate thickness, back insulation thickness and edge insulation thickness. One variable was varied at a time while others were kept constant. This was achieved using equation 3.53 in the MATLAB programme.

The value of a particular design variable which maximises the performance indicator was taken as the optimised value of the design variable. The optimised values of the variables then served as inputs to the programme and all other design parameters were calculated. For a given chiller cooling capacity, the programme calculates outputs which include: useful energy gain by the collector, number of fluid pipes required, heat loss coefficients.The outputs from the programme are presented in Chapter Four (Results).

3.5.5Absorption chiller design

The design of a 12kW capacity absorption chiller is presented here. The design done in this work is based on the single effect absorption refrigeration cycle. The absorption chiller major components: (Generator, Condenser, Evaporator, Absorber and SHX) are heat exchangers. These major components were designed as shell and tube heat exchangers.The LMTD method and existing correlations for heat transfer coefficients obtained from literature were employed in the design. Figure 3.13 shows a schematic of the arrangement of the components (heat exchangers) and flow of working fluids in the absorption chiller. The point numberings as shown was used in the design theories.

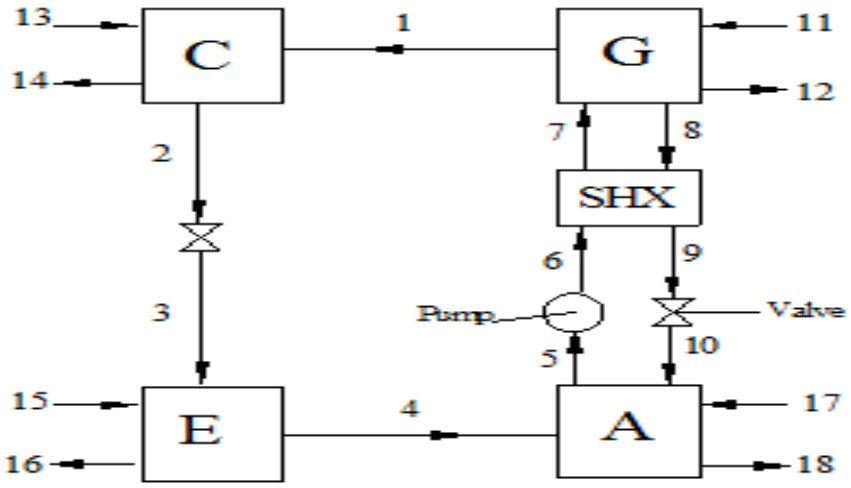


Figure 3.13 Schematic of absorption chiller components

The system description presented here is done using the state points as seen in figure 3.13. Hot water flows from external heat source (11/12) to the generator, where vaporisation of refrigerant takes place. The vapour streams to the condenser (1) where cooling water (13/14) aids condensation under condenser temperature and pressure. The resulting weak solution from generator flows to the absorber through the SHX and valve (8, 9, 10). The condensate (water) flows through the valve (2, 3)to the evaporator, where it takes away heat from the chilling water (15/16) and evaporates again under evaporator temperature and pressure. The refrigerant vapour streams to the absorber (4) where it is absorbed by the strong solution of lithium bromide. The

resulting weak solution, is then pumped via the solution pump, through the solution heat exchanger, back to the generator (5, 6, 7) and the cycle repeats again.

3.5.5.1 Absorption chiller design specifications

i. Temperatures and concentrations

It is desired to have the chiller operate with low hot water temperatures obtainable from flat plate collectors, also, care is taken to avoid risk of chiller operating in the crystallization range. When the hot water temperature starts to exceed 95^{o}C, solution becomes over concentrated and crystallization sets in. For these reasons, the operating temperatures at inlet and outlet to the generator were set at 90^{o}C and 80^{o}C respectively. The vapour leaving the generator into the condenser is considered as pure water vapour at generator pressure and temperature of 90^{o}C.

Based on an available cooling water temperature of 29^{o}C and the operating temperatures at the generator, a design condenser temperature of 40^{o}C and absorber temperature of 40^{o}C were used. With cooling water outlet temperatures of 35^{o}C and 37^{o}C set at the condenser and absorber respectively.

The lowest operating refrigerant temperature attainable for lithium bromide water pair, in which water is used as refrigerant is about 7^{o}C (Duffie and Beckman, 2013). This is due to the freezing point of water. For this reason, the design inlet and outlet refrigerant temperatures to the evaporator were set at 6^{o}C and 8^{o}C respectively.

The design chilled water inlet and outlet temperatures to the evaporator were set at 15^{o}C and 10^{o}C respectively. This is a typical range for absorption air conditioning purposes using lithium bromide water pair (Duffie and Beckman, 2013).

Starting with a condenser and evaporator temperature of 40^{o}C and 8^{o}C respectively, we obtained from table of water vapour pressures (Mayhew and Rogers, 1972) the condenser pressure (P_{cond})and evaporator pressure (P_{evap}) corresponding to the respective temperatures:

$P_{cond} = 7.34KPa, \qquad P_{evap} = 1.072KPa$

The condenser pressure equals the generator pressure (P_{gen})and the evaporator pressureequals the absorber pressure(P_{ab}):

$P_{cond} = P_{gen} = 7.34KPa \; and \; P_{evap} = P_{ab} = 1.072KPa$

With these pressures and temperatures, using the Equilibrium chart for aqueous lithium bromide solution (Arora, 2000), the design strong solution and weak solution concentrations were obtained as $(X_{ss}) = 0.63$ and $(X_{ws}) = 0.55$ respectively. The remaining design temperatures were obtained as well. The design temperatures corresponding to each state point (fig. 3.13) are shown in table 3.3.

Table 3.3: Temperatures of state points

Point	1	2	3	4	5	6	7	8	9	10	11	12	13	14	15	16	17	18
Design Temp. (	90	40	6	8	40	40	74	81	55	55	90	80	29	35	15	10	29	37

ii. Tube diameter:

For a start, a standard tube diameter of 3/8 inch (12.25mm outer diameter and 10.53mm inner diameter) was chosen for all the heat exchangers.

iii. Tube length:

A constant tube length of 0.5m was chosen for all the heat exchangers.

iv. Number of tube passes:

For simplicity, the number of tube passes was chosen as 1.

v. Desired C.O.P.:

A design C.O.P of 0.8 was used

3.5.5.2 Calculation of heat exchanger loads

Energy flows are described using the point numberings as shown in fig. 3.13.

i. Generator heat load

The Generator heat load was calculated using equation 3.55:

$$Q_g = \frac{Q_e}{COP} \quad (3.55)$$

where Q_e is the cooling capacity.

ii. The condenser load was calculated using equation 3.56 (Arora, 2000)

$$Q_c = \frac{D}{60}(h_1 - h_2) \quad (3.56)$$

Where:

$$D = \frac{Q_e \times 60}{q_o} \quad (3.57)$$

$$q_o = h_4 - h_3 \quad (3.58)$$

q_o= refrigerating effect

h_4= enthalpy of chilled water exit from evaporator

h_3=enthalpy of refrigerant at inlet to evaporator

Where the enthalpies were calculated using the relations shown in equations 3.59 to 3.61 according to Lienhard and Lienhard (2005).

$$h_3 = 4.18 \times T_3 \quad (3.59)$$

$$h_4 = 2501 + 1.88(T_4) \quad (3.60)$$

$$h_1 = 2501 + 1.88(T_1) \quad (3.61)$$

where h_1 = Enthalpy of refrigerant at inlet to condenser

$$h_2 = h_3 \quad (3.62)$$

where h_2 = Enthalpy of refrigerant at exit from condenser

T_3 = temperature of the refrigerant vapour at inlet to evaporator

T_4 = temperature of refrigerant vapour at exit from evaporator

T_1= temperature of refrigerant vapour at inlet to condenser

iii. Absorber load

The absorber load was calculated using equation 3.63 (Arora, 2000):

$$Q_a = Q_g + Q_e - Q_c \quad (3.63)$$

iv. Solution Heat Exchanger Load

From fig. 3.13 solution heat exchanger load was calculated using equation 3.64

$$Q_{SHX} = \dot{m}_{ws}(h_7 - h_6) \quad (3.64)$$

where h_7 and h_6 are the enthalpies of the weak solution from the SHX to the generator and from the absorber to the SHX respectively, calculatedusing equations 3.65 and 3.66 according to Lansing (1984):

$$h_7 = \left[4.19[(42.81 - 425.92X_{ws} + 404.67X_{ws}^2) + (1.01 - 1.23X_{ws} + 0.48X_{ws}^2)(T_7)]\right] \quad (3.65)$$

$$h_6 = \left[4.19[(42.81 - 425.92X_{ws} + 404.67X_{ws}^2) + (1.01 - 1.23X_{ws} + 0.48X_{ws}^2)(T_6)]\right] \quad (3.66)$$

3.5.5.3 Calculation of flow rates

The flow rates were calculated using point numberings in fig. 3.13.

The relationsin equations 3.67 to 3.73 according to Arora (2000) were employed:

i. Mass flow rate of hot water at generator

$$\dot{m}_{g,hw} = \frac{Q_g}{C_{p,g}(T_{11} - T_{12})} \quad (3.67)$$

ii. Mass flow rate of chilled water at evaporator

$$\dot{m}_{e,chw} = \frac{Q_e}{C_{p,e}(T_{15} - T_{16})} \quad (3.68)$$

iii. Mass flow rate of cooling water at condenser

$$\dot{m}_{c,cw} = \frac{Q_c}{C_{p,c}(T_{14} - T_{13})} \quad (3.69)$$

iv. Mass flow rate of cooling water at absorber

$$\dot{m}_{a,cw} = \frac{Q_a}{C_{p,a}(T_{18} - T_{17})} \quad (3.70)$$

v. Mass flow rate of refrigerant

$$\dot{m}_{ref} = \frac{Q_e}{h_4 - h_3} \quad (3.71)$$

vi. Mass flow rate of weak solution

$$\dot{m}_{ws} = \dot{m}_{ref} \left(\frac{X_{ss}}{X_{ss} - X_{ws}}\right) \quad (3.72)$$

vi. Mass flow rate of strong solution

$$\dot{m}_{ss} = \dot{m}_{ws} - \dot{m}_{ref} \quad (3.73)$$

3.5.5.4 Calculation of Logarithmic Mean Temperature Difference (LMTD)

The Logarithmic Mean Temperature Difference was calculated using equation 3.74 according to Lienhard and Lienhard(2005):

$$LMTD = \frac{\theta_1 - \theta_2}{ln\left[\frac{\theta_1}{\theta_2}\right]} \quad (3.74)$$

where:

Generator: $\theta_1 = (T_{11} - T_8)$ and θ_2=$(T_{12} - T_7)$

Condenser: Considering the condensing part only (Lienhard and Lienhard, 2005)

$\theta_1 = (T_2 - T_{13})$ and θ_2=$(T_2 - T_{14})$

Evaporator: $\theta_1 = (T_{15} - T_4)$ and θ_2=$(T_{16} - T_3)$

Absorber: $\theta_1 = (T_{10} - T_{18})$ and θ_2=$(T_5 - T_{17})$

SHX: $\theta_1 = (T_8 - T_7)$ and θ_2=$(T_9 - T_6)$

3.5.5.5 Calculation of LMTD correction factors

Using heat exchanger charts (Lienhard and Lienhard, 2005) for cross flow single pass with one fluid mixed and the other unmixed the following correction factors were obtained:

Generator (F_g) = 0.93

Absorber (F_a) = 0.98

Condenser (F_c) = 0.99

Evaporator (F_e) = 0.96

SHX (F_{SHX}) = 0.97

3.5.5.6 Calculation of corrected LMTD

The corrected LMTD was obtained using equation 3.75 (Lienhard and Lienhard, 2005):

$$LMTD_{c,X} = LMTD \times F_x \quad (3.75)$$

Where: $LMTD_c$ is the corrected LMTD

x represents the generator, absorber, condenser, evaporator, SHX

3.5.5.7 Calculation of flow cross sectional area per tube

The flow cross sectional area per tube (Ax) was calculated using equation 3.76 (Butterworth, 1996):

$$Ax = \frac{\pi d_i^2}{4} \quad (3.76)$$

3.5.5.8 Calculation of surface area of tube

Surface area of tube (As)was calculated using equation3.77 (Butterworth, 1996):

$$As = \pi d_o L_t \quad (3.77)$$

3.5.5.9 Calculation of provisional total heat transfer Area ($A_{pr,T}$)

A provisional total heat transfer area was calculated based on an assumed overall heat transfer coefficient (U_{assume}) for each of the heat exchangers. This was used to initiate the iteration process at the end of which a final overall heat transfer coefficient was calculated. The provisional heat transfer area was calculated using equation 3.78 (Butterworth, 1996):

$$A_{pr,T,x} = \frac{Q_x}{U_{assume}\ LMTD_{c,x}} \quad (3.78)$$

x represents the generator, absorber, condenser, evaporator, SHX

3.5.5.10 Calculation of number of tubes (N_t)

The tubes were designed as single pass and housed inside the shell. The generator tubes convey hot water, cooling water flows through the condenser and absorber tubes, chilled water flows through the evaporator tubes, weak solution of LiBr flows through the SHX tubes.

The number of tubes in each of the heat exchangers was calculated using equation 3.79 (Butterworth, 1996):

$$N_t = \frac{A_{pr,T}}{\pi d_o L_t} \tag{3.79}$$

3.5.5.11 Calculation of number of tubes per pass

The number of tubes per pass ($N_{t/p}$) for each of the heat exchangers was calculated using equation 3.80 (Butterworth, 1996):

$$N_{t/p} = \frac{N_t}{N_p} \tag{3.80}$$

3.5.5.12 Calculation of tube pitch

According to (Butterworth, 1996) the tube pitch was calculated using equation 3.81:

$$p_t = 1.25 d_o \tag{3.81}$$

3.5.5.13 Calculation of shell diameter (D_s)

The shell encloses the tube bundles and contains the shell side fluids.

The shell diameter(D_s) for each of the heat exchangers was calculated according toButterworth (1996) using equation 3.82:

$$D_s = 0.659 \sqrt{\frac{CL}{CTP}} \left[\pi \left(\frac{p_t}{d_o} \right)^2 d_o^2 N_t \right]^{\frac{1}{2}} \tag{3.82}$$

where CTP is the tube count constant which accounts for the incomplete coverage of the shell diameter by the tubes due to necessary clearances between the shell and outer tube circle (Butterworth, 1996)

CTP = 0.93 for 1 tube pass, 0.9 for 2 tube pass, 0.85 for 3 tube pass

CL is the tube layout constant

CL= 1.0 for 90^o and 45^o square pitch, 0.87 for 30^o and 60^o equilateral pitch (Butterworth, 1996)

3.5.5.14 Calculation of volume of tube bundle section (V_{tb})

The volume of tube bundle section was calculated using equation 3.83:

$$V_{tb} = \frac{\pi D_s^2}{4} L_t \quad (3.83)$$

3.5.5.15 Calculation of volume of header (V_h)

The volume of header, for convenience, was taken as 10 percent of the tube bundle section volume, this was calculated using equation 3.84

$$V_h = 0.1 V_{tb} \quad (3.84)$$

3.5.5.16 Calculation of length of header (L_h)

The length of header was calculated using equation 3.85:

$$L_h = \frac{4V_h}{\pi D_s^2} \quad (3.85)$$

3.5.5.17 Calculation of total shell length (L_s)

The total shell length is the sum of the tube bundle length and the length of header at the two ends of the tube bundle. This was calculated using equation 3.86

$$L_s = L_t + (2L_h) \quad (3.86)$$

3.5.5.18 Calculation of total shell volume (V_s)

The total shell volume was calculated using equation 3.87

$$V_s = \frac{\pi D_s^2}{4} L_s \quad (3.87)$$

3.5.5.19 Calculation of tube bundle cross flow area (A_{cf})

The tube bundle cross flow area (A_{cf}) for each of the heat exchangers was calculated according to Incropera et al (2004) using equation 3.88:

$$A_{cf} = \frac{(p_t - d_o) D_s B}{p_t} \quad (3.88)$$

where B is the baffle spacing

For heat exchanger without baffles, the equation becomes:

$$A_{cf} = \frac{(p_t - d_o) D_s L_t}{p_t} \quad (3.89)$$

3.5.5.20 Calculation of shell side mass velocity (G_s)

The shell side mass velocity (G_s) for each of the heat exchangers was calculated according to Incropera *et al.*, (2004)using equation 3.90:

$$G_s = \frac{\dot{m}_s}{A_{cf}} \quad (3.90)$$

3.5.5.21 Calculation of shell equivalent diameter ($D_{s,e}$)

The shell equivalent diameter for each of the heat exchangers was calculated according to Butterworth(1996) using equations 3.91 and 3.92:

$$D_{s,e} = \frac{1.27}{d_o}(p_t^2 - 0.785 d_o^2) \quad (3.91)$$

For a square pitch

and

$$D_{s,e} = \frac{1.1}{d_o}(p_t^2 - 0.917 d_o^2) \quad (3.92)$$

For an equilateral triangular pitch

3.5.5.22 Calculation of shell side Reynolds number (Re_s)

The shell side Reynolds number for each of the heat exchangers was calculated using equation 3.93:

$$Re_s = \frac{G_s D_{s,e}}{\mu} \quad (3.93)$$

Where the dynamic viscosities of the aqueous lithium bromide solutions at the generator and absorber $\mu_{g,sol}$ and$\mu_{a,sol}$respectively were calculated using the following empirical relations of Jeter(1990) shown in equations 3.94 to 3.103.

$$\mu_{g,sol} = {}^{e^{B1}}/_{1000} \quad (3.94)$$

$$\mu_{a,sol} = {}^{e^{B2}}/_{1000} \quad (3.95)$$

Where:

$$B1 = A1 + \left(\frac{A2}{T_8}\right) + A3ln(T_8) \quad (3.96)$$

$$B2 = A4 + \left(\frac{A5}{T_5}\right) + A5ln(T_5) \quad (3.97)$$

where:

$$A1 = -494.122 + 16.396X_{ss} - 0.145X_{ss}^2 \quad (3.98)$$

$$A2 = 28606.4 - 934.568X_{ss} + 8.527X_{ss}^2 \quad (3.99)$$

$$A3 = 70.384 - 2.350X_{ss} + 0.02X_{ss}^2 \quad (3.100)$$

$$A4 = -494.122 + 16.396X_{ws} - 0.1451X_{ws}^2 \quad (3.101)$$

$$A5 = 28606.4 - 934.568X_{ws} + 8.527X_{ws}^2 \quad (3.102)$$

$$A6 = 70.384 - 2.350X_{ws} + 0.02X_{ws}^2 \quad (3.103)$$

Where X_{ss} and X_{ws} are the concentrations of the strong solution of lithium bromide and weak solution of lithium bromide respectively.

The dynamic viscosity of water was obtained from tables (Mayhew and Rogers, 1972) using the mean temperatures at inlet and outlet to each of the heat exchangers.

3.5.5.23 Calculation of Prandtl number (Pr)

The shell side and tube side Prandtl number for each of the heat exchangers were calculated using equation 3.104:

$$Pr = \frac{\mu C_p}{k_l} \quad (3.104)$$

3.5.5.24 Calculation of tube side velocities

The tube side mass velocity (G_t) for each of the heat exchangers was calculated using equation 3.105 (Incropera *et al*., 2004) :

$$G_t = \frac{\dot{m}_t}{N_{t/p}\left(\pi\frac{d_i^2}{4}\right)} \quad (3.105)$$

The tube side velocity, (v_t) for each of the heat exchangers was calculated using equation 3.106 (Incropera *et al*., 2004) :

$$v_t = \frac{G_t}{\rho} \quad (3.106)$$

where ρ is the density of the fluids in the tubes of the generator, condenser, absorber, evaporator and SHX. The densities of the strong lithium bromide solution at the generator $(\rho_{g,sol})$and weak lithium bromide solution at the absorber $(\rho_{a,sol})$were calculated according to the empirical relations of Lansing(1984) as shown in equations 3.107 and 3.108

$$\rho_{g,sol} = 1145.36 + 470.48X_{ss} + 1374.79X_{ss}^2 - (0.333 + 0.5717X_{ss})(273 + T_8) \quad (3.107)$$

$$\rho_{a,sol} = 1145.36 + 470.48X_{ws} + 1374.79X_{ws}^2 - (0.333 + 0.5717X_{ws})(273 + T_5) \quad (3.108)$$

3.5.5.25 Calculation of tube side Reynolds number (Re_t)

The tube side Reynolds number for each of the heat exchangers was calculated using equation 3.109:

$$Re_t = \frac{\rho v_t d_i}{\mu} \quad (3.109)$$

3.5.5.26 Calculation of tube side heat transfer coefficients

Heat transfer coefficients were computed using empirical correlations obtained from literature.

For the generator, absorber, condenser and evaporator, water flows inside the tubes without phase change. Also, for the SHX, aqueous LiBr solution flows inside the tubes without phase change. The tube side heat transfer coefficients was thus calculated using the Petukhov – Popov relation according to Incropera *et al.*,(2004) as shown in equation 3.110:

$$Nu_{D,x} = \frac{\left(\frac{f_x}{8}\right) Re_{D,x} Pr_x}{K_1 + K_2\left(\frac{f}{8}\right)^{\frac{1}{2}}\left(Pr_x^{\frac{2}{3}} - 1\right)} \quad (3.110)$$

where:

Nu_D = Nusselt number

$$f_x = (1.82 log Re_x - 1.64)^{-2} \quad (3.111)$$

$$K_1 = 1 + 3.4f_x \quad (3.112)$$

$$K_2 = 11.7 + \left(\frac{1.8}{Pr_x^{\frac{1}{3}}}\right) \quad (3.113)$$

From which $h_{i,x} = \frac{Nu_{D,x}K}{d_i}$ (3.114)

f is the friction factor, h_i is the heat transfer coefficient inside the tubes, x represents generator, absorber, evaporator, condenser, SHX.

3.5.5.27 Calculation of shell side heat transfer coefficients

i. Condenser:

In the condenser, water vapour from the generator condenses over the horizontal tubes, the condensate drains down to the bottom of the condenser shell.

For the condensation on the surface of horizontal tube bundles, the Nusselt integral correlation according to Incropera *et al.*(2004) was used. The mean condensation heat transfer coefficient (α) for an entire array of tubes is as given in equation 3.115:

$$\frac{\varphi}{\varphi(N=1)} = N_t^{-\frac{1}{4}} \quad (3.115)$$

where: N_t = number of tubes

$\varphi(N = 1)$ = the condensation heat transfer coefficient for a single tube, given by:

$$\varphi(N = 1) = 0.725\left[\frac{g\rho_l(\rho_l-\rho_v)h_{fg}k_l^3}{\mu_l(T_v-T_w)D_o}\right]^{0.25} \quad (3.116)$$

where h_{fg} = enthalpy of vaporization

ii. Evaporator:

The condensate from the condenser flows down by gravity through a suction pipe and expansion valve to the evaporator, the pressure drops from condenser pressure to evaporator pressure.

The evaporator was designed as a falling film evaporator. In addition, a "double tube" configuration was employed for the vertical falling film of refrigerant. This was done by providing an outer tube which directs the falling film refrigerant over the inner tube in which chilled water

flows. The empirical correlation of Thome and Robinson (2006) for predicting bundle boiling heat transfer coefficient on the surface of plain tube bundles was used. This is shown in equation 3.117:

$$h_b = (h_{nb}^2 + h_{cb}^2)^{\frac{1}{2}} \quad (3.117)$$

where:

h_b = the bundle boiling heat transfer coefficient

h_{nb} = nucleate boiling heat transfer coefficient, given by Rohsenow's correlation for nucleate boiling according to Incropera *el al.*(2004) shown in equation 3.118:

$$\frac{C_p(T_w - T_{sat})}{h_{fg} Pr^c} = 0.013 \left[\frac{h_{nb}}{\mu h_{fg}} \sqrt{\frac{\sigma}{g(\rho_l - \rho_v)}}\right]^{0.33} \quad (3.118)$$

h_{cb} = convective boiling heat transfer coefficient calculated using equation 3.119 as given by Thome and Robinson(2006):

$$h_{cb} = 4.032 Re_\delta^{0.236} Pr^{0.4} \left(\frac{k_l}{\delta}\right) \quad (3.119)$$

The required diameter of the outer tube was determined by first calculating the liquid film thickness around the inner tube. The liquid film thickness was determined by fitting a hexagonal grid to the tube layout with one tube at the centre of each hexagon. Applying the void fraction to this geometry and its cross sectional flow area, (the area of the hexagon minus that of the cross sectional area of the tube, the fraction of the area occupied by the liquid phase is calculated and this area is applied to the perimeter of the tube to find the mean liquid film thickness as shown in figures. 3.14 and 3.15.

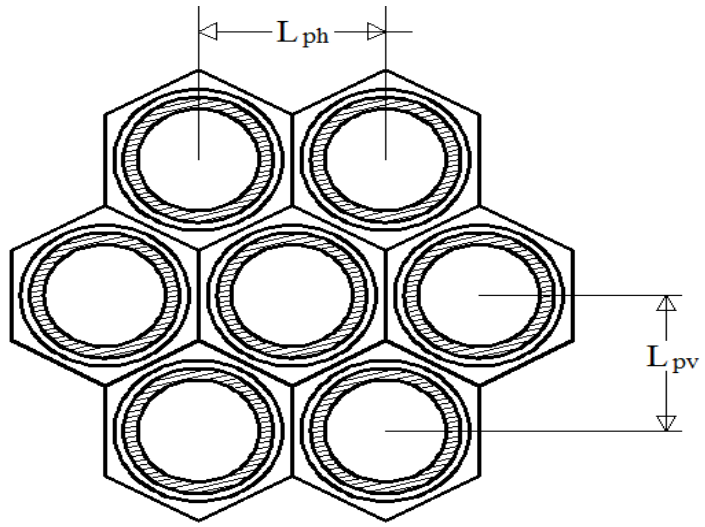


Figure 3.14 Idealised hexagonal grid boundary imposed over bundle cross section to identify Local void fraction per tube (Thome and Robinson (2006)).

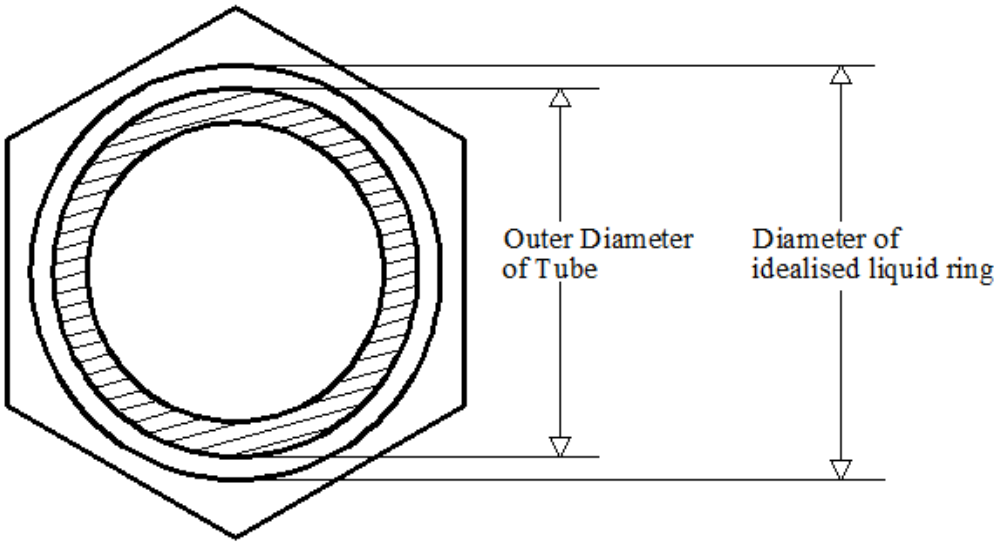


Figure 3.15 Idealised local saturated liquid film surrounding circumference of tube.(Thome and Robinson, 2006).

Area encompassed by the hexagon A_{hex} was calculated using equation 3.120 (Thome and Robinson, 2006):

$$A_{hex} = 6\left(\frac{L_{ph}}{3}\right)\left(\frac{L_{pv}}{2}\right) \quad (3.120)$$

The circumferential flow area A_{cfl} to which the void fraction is applicable was calculated using equation 3.121 (Thome and Robinson, 2006).

$$A_{cfl} = A_{hex} - \frac{\pi d_o}{4} \quad (3.121)$$

The diameter of the idealized liquid ring D_δ created by the liquid film around the inner tube which forms the required outer tube diameter was calculated according to equation 3.122 (Thome and Robinson, 2006):

$$D_t = \sqrt{\frac{4A_{cf\,l}}{\pi} + d_o^2} \tag{3.122}$$

The liquid film thickness δ was then calculated using equation 3.123:

$$\delta = \frac{D_\delta - d_o}{2} \tag{3.123}$$

iii. Generator

In the generator, hot water flowing through the tubes heats up aqueous LiBr solution in the shell, as a result, refrigerant (water) vapourises at generator pressure and the vapour flows to the condenser.

The generator was designed as a pool generator. The Rohsenow correlation for nucleate boiling according to Incropera *et al.*,(2004) was used to calculate the heat transfer coefficient as shown in equation 3.124:

$$\frac{C_p\,(T_w - T_{sat}\,)}{h_{fg}\,Pr^{\,c}} = C_{sf}\left[\frac{h_{nb}}{\mu h_{fg}}\sqrt{\frac{\sigma}{g(\rho_l - \rho_v)}}\right]^{0.33} \tag{3.124}$$

iv. Absorber

In the absorber, strong solution of LiBr flowing in the shell absorbs water vapour flowing from the evaporator.The absorber was designed as a vertical falling film shell and tube heat exchanger with falling film of aqueous lithium bromide at the shell side and cooling water in the tube bundles. The “double tube” configuration was also employed in the absorber, in which an outer tube directs aqueous lithium bromide solution over the inner tube in which cooling water flows. The required outer tube diameter was calculated using equations 3.120 to 3.123. The correlation of Wilke according to Thome (2016) was used in calculating the heat transfer coefficient of absorption. This is shown in equation 3.125:

$$h = \frac{k_{sol}}{\delta}(0.029Re^{0.53}Pr^{0.344}) \tag{3.125}$$

where$\delta = \left(\frac{3\mu\Gamma}{\rho^2 g}\right)^{\frac{1}{3}}$ (3.126)

h= heat transfer coefficient of absorption

δ = film thickness

$\Gamma = \frac{\dot{m}_{a,sol}}{L_t}$ (3.127)

Γ = falling film of lithium bromide solution flow rate

3.5.5.28 Calculation of Overall Heat Transfer Coefficients

The overall heat transfer coefficient for each of the heat exchangers was calculated according to Butterwort (1996) using equation 3.128:

$$U = \frac{N_t}{A_{pr,T}\left[\frac{1}{h_i A_i} + \frac{1}{2\pi k_t L} ln\frac{d_o}{d_i} + \frac{1}{h_o A_o}\right]} \quad (3.128)$$

Where:

$A_{pr,T}$= provisional total heat transfer area as calculated in equation 3.78.

h_i = heat transfer coefficient at tube side

h_o = heat transfer coefficient at shell side

A_i = interior surface area of one tube

A_o = exterior surface area of one tube

3.5.5.29 Pipeline Design (Suction line sizing)

The flow of condensed refrigerant from the condenser to the evaporator is by gravity through a suction pipe line. In the same manner, flow of strong solution from the generator to the absorber is by gravity through a suction pipe line. The generator and condenser are at the same pressure (7340Pa), while the evaporator and absorber are at the same pressure (1072Pa).The pressure drop between the condenser and the evaporator is equal to the pressure drop between the generator and absorber. This was used to determine the length of pipe required using standard pipe diameters.

From the Darcy equation (White, 2006) the pressure drop (ΔP) in a pipe flow was calculated as shown in equation 3.129:

$$\Delta P = f\frac{L}{D}\frac{\rho V_{avg}^2}{2} \quad (3.129)$$

where ΔP is expressed in N/m^2

From which the required length was obtained using equation 3.130:

$$L = \frac{2(\Delta P)D}{f_D \rho V_{avg}^2} \quad (3.130)$$

where:

V_{avg} = the average fluid velocity which was obtained using equation 3.131:

$$V_{avg} = \frac{\dot{V}}{A_{cf}} \quad (3.131)$$

where:

$\dot{V}$= volume flow rate of fluid

A_{cf} = area of cross flow of pipe

f = friction coefficient, calculated using equation 3.132:

$$f = 0.11\left(\frac{\varepsilon}{D} + \frac{68}{Re}\right)^{\frac{1}{4}} \quad (3.132)$$

3.5.5.30 Volume of aqueous Lithium bromide solution to be charged into the generator

According to Butterworth (1996), for proper wetting of tubes in pool generator, volume of fluid in the shell should be at least 0.75 volume of shell. Therefore, volume of aqueous lithium bromide solution ($V_{LiBr,aq}$) was calculated using equation 3.133:

$$V_{LiBr,aq} = 0.8\pi\frac{D_s^2}{4}L_t \quad (3.133)$$

3.5.5.31 Volume of absorber sump

It is desired to have a sump at the absorber, into which the weak solution from the absorber will flow by gravity. From here the weak solution is pumped back to the generator.

The volume of the sump V_{sump} was taken as one tenth the volume of the absorber shell. Therefore volume of sump was calculated using equation 3.134:

$$V_{sump} = 0.1V_{abs\ shell} \quad (3.134)$$

3.5.5.32 Rate of Evaporation of Water

The heat transfer rate per unit area of tube surface($q_s^{'}$)was calculated according to Incropera *et al.*,(2004) as shown in equation 3.135:

$$q_s^{'} = \mu_l h_{fg} \left[\frac{g(\rho_l - \rho_v)}{\sigma}\right]^{\frac{1}{2}} \left[\frac{C_p \Delta T}{0.013\, h_{fg} Pr}\right]^3 \quad (3.135)$$

where, $\Delta T = T_{surf} - T_{sat}$ (3.136)

T_{sat} = saturation temperature corresponding to pressure at the generator or evaporator

T_{surf} = temperature at the tube surface

The boiling heat transfer rate (q_s) was calculated according to Incropera *et al.*,(2004) as shown in equation 3.137:

$$q_s = q_s^{'} \times \left(\frac{\pi d_o^2}{4} \times L_t \times N_t\right) \quad (3.137)$$

In steady state conditions, all heat addition to the tubes will result in evaporation of water at the tube surface, hence, the heat transfer rate was then calculated using equation 3.138:

$$q_s = \dot{m}_b h_{fg} \quad (3.138)$$

Therefore;

$$\dot{m}_b = \frac{q_s}{h_{fg}} \quad (3.139)$$

where $\dot{m}_b$ = rate at which water evaporates from the surface

3.5.5.33 Rate of condensation of steam

The rate of condensation of steam for a single tube ($\dot{m}_1$) on an array of square pitched tubes with N number of tubes per column and R number of columns in the array was calculatedaccording to Incropera *et al.*(2004) as given in equation 3.140:

$$\dot{m}_1 = \frac{h_{c,N} \pi d_o (T_{sat} - T_w)}{h_{fg}^{'}} \quad (3.140)$$

where, $h_{c,N}$ is the condensation heat transfer coefficient for a column of *N* tubes given as:

$$h_{c,N} = 0.729\left[\frac{g\rho_l(\rho_l-\rho_v)K_l^3 h_{fg}^{'}}{N\mu_l(T_{sat}-T_w)d_o}\right]^{\frac{1}{4}} \quad (3.141)$$

For the complete array the condensation rate per unit length was calculated using equation 3.142:

$$\dot{m} = N \times R \times \dot{m}_1 \quad (3.142)$$

3.5.5.34 Pump selection

The flow pumps were selected based on the required flow rate calculated and the head required to be met by the pump. The electric power taken from the electricity supply by each pump was calculated based on the maximum head and flow requirements using equation 3.143 (White, 2006):

$$P_{elec} = \frac{\dot{Q}\Delta P}{(36\eta_{pump}\ \eta_{trans}\ \eta_{motor}\ )} \quad (3.143)$$

where:

$\dot{Q}$ is the flow rate in m^3/hr

$$\Delta P = (P_{td} - P_{ts}) + (H_d - H_s)\rho g + \sum H_L \quad (3.144)$$

where:

$(H_d - H_s)$ is the vertical difference in height called the geodetic or static head

P_{td} is the pressure at the discharge side

P_{ts} is the pressure at the suction side

$\sum H_L$ is the total head loss given as:

$$H_L = \frac{f\,Lv^2}{2Dg} \quad (3.145)$$

where:

$$v = \frac{4\dot{Q}}{\pi d^2} \quad (3.146)$$

f = the pipe friction factor, L = the length of the pipe, D= the pipe inner diameter and $\dot{Q}$ is in m^3/s

The entire set of equations from equation 3.55 to 3.146 were programmed and solved in MATLAB according to the design sequence calculations using an iterative procedure for each of the heat exchangers. The programme has as inputs, the design specifications as stated in section 3.5.5.1 (details of other inputs in form of constants can be seen in Appendices C to G: the MATLAB program).The overall heat transfer coefficient U as calculated in equation 3.128 is compared with the assumed overall heat transfer coefficient U_{assume} and the iteration continues until convergence is achieved. The program is flexible as it can be used to design for any required cooling capacity. For this work, the required cooling capacity is 12kW and this was used in the programming. The MATLAB codes are as shown in appendices:

C: MATLAB programme for generator

D: MATLAB programme for condenser

E: MATLAB programme for evaporator

F: MATLAB programme for absorber

G: MATLAB programme for SHX

The outputs from each of the programmes is presented in Chapter Four (Results).

3.5.6Absorption chiller components optimisation and performance simulation

In this section, a mathematical model was developed and programmed in MATLAB to optimize the absorption chiller components. The model was also used to carry out performance simulation of the absorption chiller. It operates as an extension to the program used to solve the design equations. An energy balance equation and heat transfer equation were developed for each of the heat exchangers. The program uses as input the values for the overall heat transfer coefficient (U) and the heat transfer surface area (A) of the heat exchangers obtained from the design calculations to evaluate the UA values. Other inputs to the program are the operating fluid stream inlet temperatures: hot water inlet temperature at generator, cooling water inlet temperature and chilled water inlet temperature at the evaporator, as well as the flow rates.

The program solves the pair of equations for each of the heat exchangers simultaneously to determine the unknown quantities: hot water outlet temperature, cooling water outlet temperature, chilled water outlet temperature and COP. For the optimization, a set of decision variables: (tube diameter, baffle spacing, tube layout, number of tubes, shell diameter, and heat transfer area) for each of the heat exchangers were varied over a range,the aim being to maximize the performance indicator (COP of the chiller). The tube diameter, baffle spacing and tube layout are design parameters that were programmed as inputs. The tube diameter was varied over standard tube sizes of (0.008m to 0.022m), the baffle spacing was varied from (0 to 0.5m), and the tube layout was varied over standard tube layout configurations of (30^o to 90^o).

The number of tubes, shell diameter and heat transfer area are design variables that were calculated via iteration process. These variables were varied over a range in which solution convergence occurred during the iteration. Each time a decision variable was varied, a new UA value was calculated and subsequently a new COP computed. The set of decision variables that maximized the COP was taken as the final design parameters. Performance simulation was done by varying inlet fluid stream temperatures and effect on COP studied.The point numberings as seen in figure 3.13, section 3.4.5 was used in the energy balance equations and heat transfer equations.

3.5.6.1 Model development

The assumptions made in the model development are:

i. Steady state conditions.
ii. Constant UA values for the heat exchangers.
iii. The pressure in the generator is equal to that in the condenser, while the pressure in the absorber is equal to that in the evaporator.

iv. Pressure changes occur only in the expansion valves and in the pump.

v. No heat losses to the environment.

vi. The refrigerant leaves the condenser and evaporator as saturated liquid and saturated vapour respectively.

vii. Steam leaving the generator is at superheated state.

viii. Weak solution leaving the absorber and strong solution leaving the generator are in saturated state.

The following relations were used in the equations development:

$\dot{m}_1 = \dot{m}_4 = \dot{m}_{ref}$ = Mass flow rate of refrigerant vapour.

The enthalpy of the refrigerant vapour was computed using equation 3.147 (Lienhard and Lienhard, 2005):

$(2501.3 + 1.87T)$ (3.147)

where T is the temperature of the hot fluid stream (in this case temperature of hot water inlet to the generator).

$\dot{m}_5 = \dot{m}_6 = \dot{m}_7 = \dot{m}_{ws}$ = Mass flow rate of weak solution.

$\dot{m}_{11} = \dot{m}_{12} = \dot{m}_g$ Mass flow rate of hot water at the generator

The enthalpy of the weak solution was computed using equation 3.148 (Lansing, 1984):

$\left[4.19[(42.81 - 425.92X_{ws} + 404.67X_{ws}^2) + (1.01 - 1.23X_{ws} + 0.48X_{ws}^2)(T_7)]\right]$ (3.148)

where:

X_{ws} = concentration of weak solution

T_7= temperature of weak solution at inlet to the generator

$\dot{m}_8 = \dot{m}_9 = \dot{m}_{10} = \dot{m}_{ss}$ = Mass flow rate of strong solution.

The enthalpy of the strong solution was computed using equation 3.149 (Lansing, 1984):

$\left[4.19[(42.81 - 425.92X_{ss} + 404.67X_{ss}^2) + (1.01 - 1.23X_{ss} + 0.48X_{ss}^2)(T_8)]\right]$ (3.149)

where:

X_{ss}= concentration of strong solution

T_8= temperature of strong solution at exit from the generator

3.5.6.2 Generator

i. Energy balance equation

Figure 3.16 is the generator flow diagram extracted from figure 3.13 in section 3.5.5

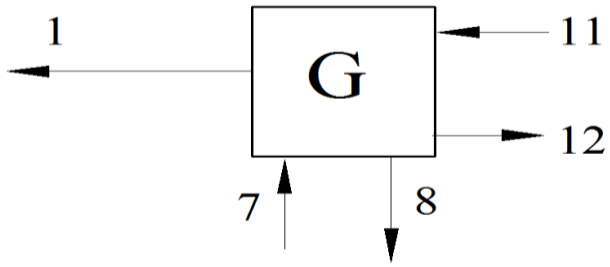


Figure 3.16 Generator flow diagram

Performing an energy balance on the generator gives equation 3.150:

$$\dot{m}_{11}h_{11} - \dot{m}_{12}h_{12} - \dot{m}_1 h_1 + \dot{m}_7 h_7 - \dot{m}_8 h_8 = 0 \quad (3.150)$$

On substituting from relations above yields equation 3.151:

$$\dot{m}_g(h_{11} - h_{12}) - \dot{m}_{ref}\left(2501.3 + 1.87T_g\right)$$
$$+\dot{m}_{ws}\left[4.19[(42.81 - 425.92X_{ws} + 404.67X_{ws}^2) + (1.01 - 1.23X_{ws} + 0.48X_{ws}^2)(T_7)]\right]$$
$$-\dot{m}_{ss}\left[4.19[(42.81 - 425.92X_{ss} + 404.67X_{ss}^2) + (1.01 - 1.23X_{ss} + 0.48X_{ss}^2)(T_8)]\right] = 0 \quad (3.151)$$

where $T_g = T_{11}$ = hot water inlet temperature to the generator

From equation 3.151, Let:

$$\dot{m}_{ref}\left(2501.3 + 1.87T_g\right) = A_1 \quad (3.152)$$

$$(42.81 - 425.92X_{ws} + 404.67X_{ws}^2) = A_2 \quad (3.153)$$

$$(1.01 - 1.23X_{ws} + 0.48X_{ws}^2) = A_3 \quad (3.154)$$

$$(42.81 - 425.92X_{ss} + 404.67X_{ss}^2) = A_4 \quad (3.155)$$

$$(1.01 - 1.23X_{ss} + 0.48X_{ss}^2) = A_5 \quad (3.156)$$

Then equation 3.151 becomes:

$$\dot{m}_g(h_{11} - h_{12}) - A_1 + \dot{m}_{ws}[4.19(A_2 + A_3.T_7)] - \dot{m}_{ss}\left[4.19\left(A_4 + A_5(T_8)\right)\right] = 0$$

(3.157)

Using $h = C_pT$, where C_p= 4.2, equation 3.157 becomes:

$$4.2\dot{m}_gT_{11} - 4.2\dot{m}_gT_{12} - A_1 + 4.19\dot{m}_{ws}.A_2 + 4.19\dot{m}_{ws}.A_3T_7 -$$

$$\dot{m}_{ss}\left[4.19\left(A_4 + A_5(T_8)\right)\right] = 0 \quad (3.158)$$

Which simplifies to:

$$-4.2\dot{m}_gT_{12} + 4.19\dot{m}_{ws}.A_3T_7 =$$

$$A_1 - 4.19\dot{m}_{ws}.A_2 - 4.2\dot{m}_gT_{11} + \dot{m}_{ss}\left[4.19\left(A_4 + A_5(T_8)\right)\right] \quad (3.159)$$

Which is the energy balance equation for the generator.

ii. Heat transfer equation

From the equation$Q_g = UA\Delta T$ (3.160)

where:

$Q_g = \dot{m}_g(h_{11} - h_{12})$

$U = U_g$= Overall heat transfer coefficient at generator

$A = A_{Tg}$= Total effective heat transfer surface area at generator

$\Delta T = \Delta T_{lm}$, expressed as: $\left[\left(\frac{T_{11}+T_{12}}{2}\right) - \left(\frac{T_7+T_8}{2}\right)\right]$ (3.161)

Substituting $h = C_pT$,

Thus the heat transfer equation is:

$$\dot{m}_gC_p(T_{11} - T_{12}) = U_g.A_{Tg}\left[\left(\frac{T_{11}+T_{12}}{2}\right) - \left(\frac{T_7+T_8}{2}\right)\right] \quad (3.162)$$

Simplifying, where$C_p = 4.2$ gives:

$$4.2\dot{m}_gT_{11} - 4.2\dot{m}_gT_{12} = U_g.A_{Tg}\left[\frac{T_{11}}{2} + \frac{T_{12}}{2} - \frac{T_7}{2} - \frac{T_8}{2}\right] \quad (3.163)$$

From equation 3.163, Let= $U_g.A_{Tg}$= Z (3.164),

then:

$$4.2\dot{m}_g T_{11} - 4.2\dot{m}_g T_{12} = Z\left[\frac{T_{11}}{2} + \frac{T_{12}}{2} - \frac{T_7}{2} - \frac{T_8}{2}\right] \quad (3.165)$$

$$4.2\dot{m}_g T_{11} - 4.2\dot{m}_g T_{12} = \frac{ZT_{11}}{2} + \frac{ZT_{12}}{2} - \frac{ZT_7}{2} - \frac{ZT_8}{2} \quad (3.166)$$

$$4.2\dot{m}_g T_{11} - \frac{ZT_{11}}{2} = 4.2\dot{m}_g T_{12} + \frac{ZT_{12}}{2} - \frac{ZT_7}{2} - \frac{ZT_8}{2} \quad (3.167)$$

Simplifying:

$$\left(4.2\dot{m}_g + \frac{Z}{2}\right)T_{12} - \frac{ZT_7}{2} - \frac{ZT_8}{2} = \left(4.2\dot{m}_g - \frac{Z}{2}\right)T_{11} \quad (3.168)$$

From which the heat transfer equation becomes:

$$(4.2\dot{m}_g + 0.5Z)T_{12} - 0.5ZT_7 = (4.2\dot{m}_g - 0.5Z)T_{11} + 0.5ZT_8 \quad (3.169)$$

The energy equation and the heat transfer equation (equations 3.159 and 3.169 respectively) were then solved simultaneously. The MATLAB programme which solves simultaneous equations in matrix form was used for this.

Rewriting the equations in matrix form gives equation 3.170:

$$\begin{pmatrix} (4.2\dot{m}_g + 0.5Z) & -(0.5Z) \\ -(4.2\dot{m}_g) & (4.19\dot{m}_{ws}A_3) \end{pmatrix}\begin{pmatrix} T_{12} \\ T_7 \end{pmatrix} =$$

$$\begin{pmatrix} (4.2\dot{m}_g - 0.5Z)T_{11} + 0.5ZT_8 \\ A_1 - 4.19\dot{m}_{ws}.A_2 - 4.2\dot{m}_g T_{11} + \dot{m}_{ss}\left[4.19\left(A_4 + A_5(T_8)\right)\right] \end{pmatrix} \quad (3.170)$$

Which was solved in the form:

$$AT = b$$

$$T = A^{-1}b$$

$$T = A\backslash b$$

Where:

$$A = \begin{pmatrix} (4.2\dot{m}_g + 0.5Z) & -(0.5Z) \\ -(4.2\dot{m}_g) & (4.19\dot{m}_{ws}A_3) \end{pmatrix} \quad (3.171)$$

$$T = \begin{pmatrix} T_{12} \\ T_7 \end{pmatrix} \quad (3.172)$$

$$b = \begin{pmatrix} (4.2\dot{m}_g - 0.5Z)T_{11} + 0.5ZT_8 \\ A_1 - 4.19\dot{m}_{ws}.A_2 - 4.2\dot{m}_g T_{11} + \dot{m}_{ss}\left[4.19\left(A_4 + A_5(T_8)\right)\right] \end{pmatrix} \quad (3.173)$$

Here we have three unknown temperature parameters:$T_7, T_8 and\ T_{12}$, which are the temperature of the weak solution at inlet to the generator, the temperature of the strong solution at exit from the generator and the temperature of the hot water at exit from the generator respectively. The only known temperature parameter is T_{11}: the temperature of hot water at inlet to the generator.An iterative procedure was employed to solve for the set of unknown parameters. First by assuming a value for T_8 then solving the set of equations up toequation 3.170 iteratively. The iteration process continues until convergence of the set of temperature valuesis obtained.

3.5.6.3 Evaporator

i. Energy balance equation

Figure 3.17 is the evaporator flow diagram extracted from figure 3.13 in section 3.5.5

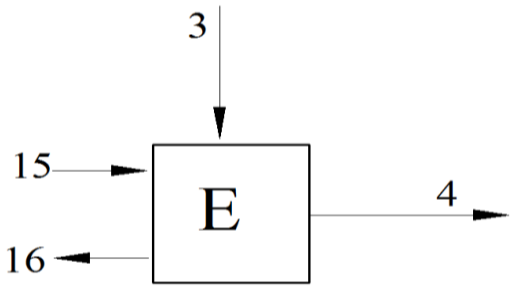


Figure 3.17 Evaporator flow diagram

Performing an energy balance on the evaporator gives equation 3.174:

$$\dot{m}_{ref}\, h_3 + \dot{m}_{chw}\, h_{15} - \dot{m}_{ref}\, h_4 - \dot{m}_{chw}\, h_{16} = 0 \quad (3.174)$$

Substituting $h = C_p T$,

$$\dot{m}_{ref}.4.19T_3 + \dot{m}_{chw}.4.19T_{15} - \dot{m}_{ref}\,(2501.3 + 1.87T_4) - \dot{m}_{chw}.4.19T_{16} = 0 \quad (3.175)$$

Simplifying gives:

$$-1.87\dot{m}_{ref}\,T_4 - \dot{m}_{chw}.4.19T_{16} = \dot{m}_{ref}.2501.3 - \dot{m}_{chw}.4.19T_{15} - \dot{m}_{ref}.4.19T_3 \quad (3.176)$$

From which the energy equation becomes:

$$-1.87\dot{m}_{ref}\,T_4 - \dot{m}_{chw}.4.19T_{16} = \dot{m}_{ref}\,(2501.3 - 4.19T_3) - \dot{m}_{chw}.4.19T_{15} \quad (3.177)$$

ii. Heat transfer equation

From the equation $Q_e = UA\Delta T$, where:

$Q_e = \dot{m}_e(h_{15} - h_{16})$

$U = U_e$= Overall heat transfer coefficient at the evaporator

$A = A_{Te}$= Total effective heat transfer area at the evaporator

$\Delta T = \Delta T_{lm,e}$, evaluated as: $\left[\left(\frac{T_{15}+T_{16}}{2}\right) - \left(\frac{T_3+T_4}{2}\right)\right]$ (3.178)

Substituting $h = C_p T$,

Thus the heat transfer equation is:

$$\dot{m}_e C_p (T_{15} - T_{16}) = U_e A_{Te} \left[\left(\frac{T_{15}+T_{16}}{2}\right) - \left(\frac{T_3+T_4}{2}\right)\right] \quad (3.179)$$

Simplifying we get:

$$4.2\dot{m}_e T_{15} - 4.2\dot{m}_e T_{16} = U_e A_{Te} \left(\frac{T_{15}}{2} + \frac{T_{16}}{2} - \frac{T_3}{2} - \frac{T_4}{2}\right) \quad (3.180)$$

which gives:

$$4.2\dot{m}_e T_{15} - 4.2\dot{m}_e T_{16} = 0.5U_e A_{Te}.(T_{15} + T_{16} - T_3 - T_4) \quad (3.181)$$

Let$0.5U_e A_{Te}$=Z_3,

Then equation 3.181 becomes:

$$4.2\dot{m}_e T_{15} - 4.2\dot{m}_e T_{16} = Z_3 T_{15} + Z_3 T_{16} - Z_3 T_3 - Z_3 T_4 \quad (3.182)$$

Simplifying gives the heat transfer equation as:

$$Z_3 T_4 - (4.2\dot{m}_e + Z_3) T_{16} = (Z_3 - 4.2\dot{m}_e) T_{15} - Z_3 T_3 \quad (3.183)$$

The energy equation and the heat transfer equation (equations 3.177 and 3.183 respectively) were then solved simultaneously. The MATLAB programme which solves simultaneous equations in matrix form was used for this.

Rewriting the equations in matrix form:

$$\begin{pmatrix} Z_3 & -(4.2\dot{m}_e + Z_3) \\ -1.87\dot{m}_{ref} & -(\dot{m}_{chw}.4.19) \end{pmatrix} \begin{pmatrix} T_4 \\ T_{16} \end{pmatrix} = \begin{pmatrix} (Z_3 - 4.2\dot{m}_e) T_{15} - Z_3 T_3 \\ \dot{m}_{ref}(2501.3 - 4.19T_3) - \dot{m}_{chw}.4.19T_{15} \end{pmatrix}$$

(3.184)

Which was solved in the form:

$Ei = l$

$i = E^{-1}l$

$i = E\backslash l$

where:

$$E = \begin{pmatrix} Z_3 & -(4.2\dot{m}_e + Z_3) \\ -1.87\dot{m}_{ref} & -(\dot{m}_{chw}.4.19) \end{pmatrix} \quad (3.185)$$

$$i = \begin{pmatrix} T_4 \\ T_{16} \end{pmatrix} \quad (3.186)$$

$$l = \begin{pmatrix} (Z_3 - 4.2\dot{m}_e)T_{15} - Z_3T_3 \\ \dot{m}_{ref}\,(2501.3 - 4.19T_3) - \dot{m}_{chw}.4.19T_{15} \end{pmatrix} \quad (3.187)$$

3.5.6.4 Condenser

i. Energy balance equation

Figure 3.18 is the condenser flow diagram extracted from figure 3.13 in section 3.5.5

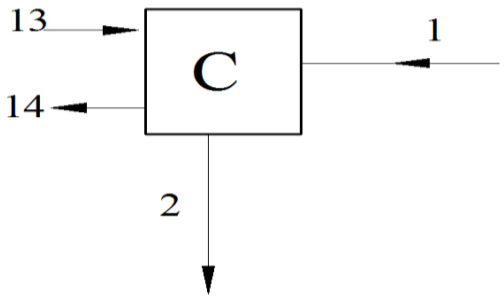


Figure 3.18 Condenser flow diagram

Performing an energy balance on the condenser gives equation 3.188:

$$\dot{m}_{ref}\,h_1 + \dot{m}_c h_{13} - \dot{m}_{ref}\,h_2 - \dot{m}_c h_{14} = 0 \quad (3.188)$$

Substituting $h = C_pT$, equation 3.188 becomes:

$$\dot{m}_{ref}\left(2501.3 + 1.87T_g\right) + 4.2\dot{m}_c T_{13} - 4.2\dot{m}_{ref}\,T_2 - 4.2\dot{m}_c T_{14} = 0 \quad (3.189)$$

From equation 3.189, Let$\dot{m}_{ref}\left(2501.3 + 1.87T_g\right) = A_6$

Then equation 3.189 becomes:

$$A_6 + 4.2\dot{m}_c T_{13} - 4.2\dot{m}_{ref} T_2 - 4.2\dot{m}_c T_{14} = 0 \quad (3.190)$$

From which the energy equation becomes:

$$4.2\dot{m}_c T_{14} + 4.2\dot{m}_{ref} T_2 = A_6 + 4.2\dot{m}_c T_{13} \quad (3.191)$$

ii. Heat transfer equation

From the equation $Q_c = UA\Delta T$, where:

$Q_c = \dot{m}_c(h_{14} - h_{13})$

$U = U_c$= Overall heat transfer coefficient at the condenser

$A = A_{Tc}$= Total effective heat transfer surface area at the condenser

Considering the refrigerant part only (Lienhard and Lienhard, 2005),

$\Delta T = \Delta T_{lm,c}$, is evaluated as: $\left[\left(\frac{T_2+T_2}{2}\right) - \left(\frac{T_{13}+T_{14}}{2}\right)\right]$ (3.192)

Substituting $h = C_p T$,

$$\dot{m}_c C_p (T_{14} - T_{13}) = U_c A_{Tc} \left[\left(\frac{T_2+T_2}{2}\right) - \left(\frac{T_{13}+T_{14}}{2}\right)\right] \quad (3.193)$$

which simplifies to:

$$4.2\dot{m}_c C_p T_{14} - 4.2\dot{m}_c C_p T_{13} = 0.5U_c A_{Tc}.(2T_2 - T_{13} - T_{14}) \quad (3.194)$$

From equation 3.194, Let $0.5U_c A_{Tc}$=Z_2,

Then equation 3.194 becomes:

$$4.2\dot{m}_c C_p T_{14} - 4.2\dot{m}_c C_p T_{13} = Z_2(2T_2 - T_{13} - T_{14}) \quad (3.195)$$

which simplifies to:

$$4.2\dot{m}_c C_p T_{14} - 4.2\dot{m}_c C_p T_{13} = 2Z_2 T_2 - Z_2 T_{13} - Z_2 T_{14} \quad (3.196)$$

From which the heat transfer equation is obtained as:

$$(4.2\dot{m}_c + Z_2)T_{14} - 2Z_2 T_2 = (4.2\dot{m}_c - Z_2)T_{13} \quad (3.197)$$

The energy equation and the heat transfer equation (equations 3.191 and 3.197 respectively) were then solved simultaneously. The MATLAB programme which solves simultaneous equations in matrix form was used for this.

Rewriting the equations in matrix form:

$$\begin{pmatrix} (4.2\dot{m}_c + Z_2) & -(2Z_2) \\ 4.2\dot{m}_c & 4.2\dot{m}_{ref} \end{pmatrix} \begin{pmatrix} T_{14} \\ T_2 \end{pmatrix} = \begin{pmatrix} (4.2\dot{m}_c - Z_2)T_{13} \\ (A_6 + 4.2\dot{m}_c T_{13}) \end{pmatrix} \quad (3.198)$$

which was solved in the form:

$$Bd = c$$

$$d = B^{-1}c$$

$$d = B\backslash c$$

where:

$$B = \begin{pmatrix} (4.2\dot{m}_c + Z_2) & -(2Z_2) \\ 4.2\dot{m}_c & 4.2\dot{m}_{ref} \end{pmatrix} \quad (3.199)$$

$$d = \begin{pmatrix} T_{14} \\ T_2 \end{pmatrix} \quad (3.200)$$

$$c = \begin{pmatrix} (4.2\dot{m}_c - Z_2)T_{13} \\ (A_6 + 4.2\dot{m}_c T_{13}) \end{pmatrix} \quad (3.201)$$

3.5.6.5 Absorber

i. Energy balance equation

Figure 3.19 is the absorber flow diagram extracted from figure 3.13 in section 3.5.5

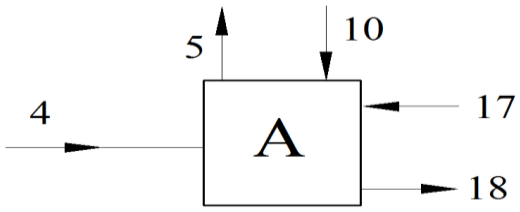


Figure. 3.19 Absorber flow diagram

Performing an energy balance on the absorber yields equation 3.202:

$$-\dot{m}_{18}h_{18} + \dot{m}_{17}h_{17} + \dot{m}_{10}h_{10} - \dot{m}_5 h_5 + \dot{m}_4 h_4 = 0 \quad (3.202)$$

On substituting yields:

$$-\dot{m}_a(h_{18} - h_{17})$$

$$+\dot{m}_{ss}\left[4.19[(42.81 - 425.92X_{ss} + 404.67X_{ss}^2) + (1.01 - 1.23X_{ss} + 0.48X_{ss}^2)(T_{10})]\right]$$

$$-\dot{m}_{ws}\left[4.19[(42.81 - 425.92X_{ws} + 404.67X_{ws}^2) + (1.01 - 1.23X_{ws} + 0.48X_{ws}^2)(T_5)]\right]$$

$$+\dot{m}_{ref}\,(2501.3 + 1.87T_4) = 0 \quad (3.203)$$

Substituting $h = C_pT$, the energy equation becomes:

$$-\dot{m}_a C_p (T_{18} - T_{17})$$

$$+\dot{m}_{ss}\left[4.19[(42.81 - 425.92X_{ss} + 404.67X_{ss}^2) + (1.01 - 1.23X_{ss} + 0.48X_{ss}^2)(T_{10})]\right] = 0$$

$$-\dot{m}_{ws}\left[4.19[(42.81 - 425.92X_{ws} + 404.67X_{ws}^2) + (1.01 - 1.23X_{ws} + 0.48X_{ws}^2)(T_5)]\right]$$

$$+\dot{m}_{ref}\,(2501.3 + 1.87T_e) = 0 \quad (3.204)$$

ii. Heat transfer equation

From the equation$Q_a = UA\Delta T$

where:

$Q_a = \dot{m}_a(h_{18} - h_{17})$

$U = U_a$

$A = A_{Ta}$

$\Delta T = \Delta T_{lm}$, evaluated as: $\left[\left(\frac{T_5+T_{10}}{2}\right) - \left(\frac{T_{17}+T_{18}}{2}\right)\right]$ (3.205)

Substituting $h = C_pT$,

Thus the heat transfer equation is:

$$\dot{m}_a C_p (T_{18} - T_{17}) = U_a.A_{Ta}\left[\left(\frac{T_5+T_{10}}{2}\right) - \left(\frac{T_{17}+T_{18}}{2}\right)\right] \quad (3.206)$$

Incorporating a solution heat exchanger between the generator and absorber, with an assumed efficiency of 0.8, the MATLAB programme uses the results of T_7 and T_8 obtained at the generator to calculate T_5 and T_{10}. With T_{17} known, the remaining unknowns at the absorber are T_4 and T_{18}, which the programme solves using the energy balance and heat transfer equation at the absorber.

The COP was calculated as:

$$COP = \frac{Q_e}{Q_g} \quad (3.207)$$

The MATLAB program for the model is shown in Appendix H.Results are presented in Chapter Four (Results).

Figure 3.20 shows the algorithm block diagram for the design calculation, optimization and performance simulation program.

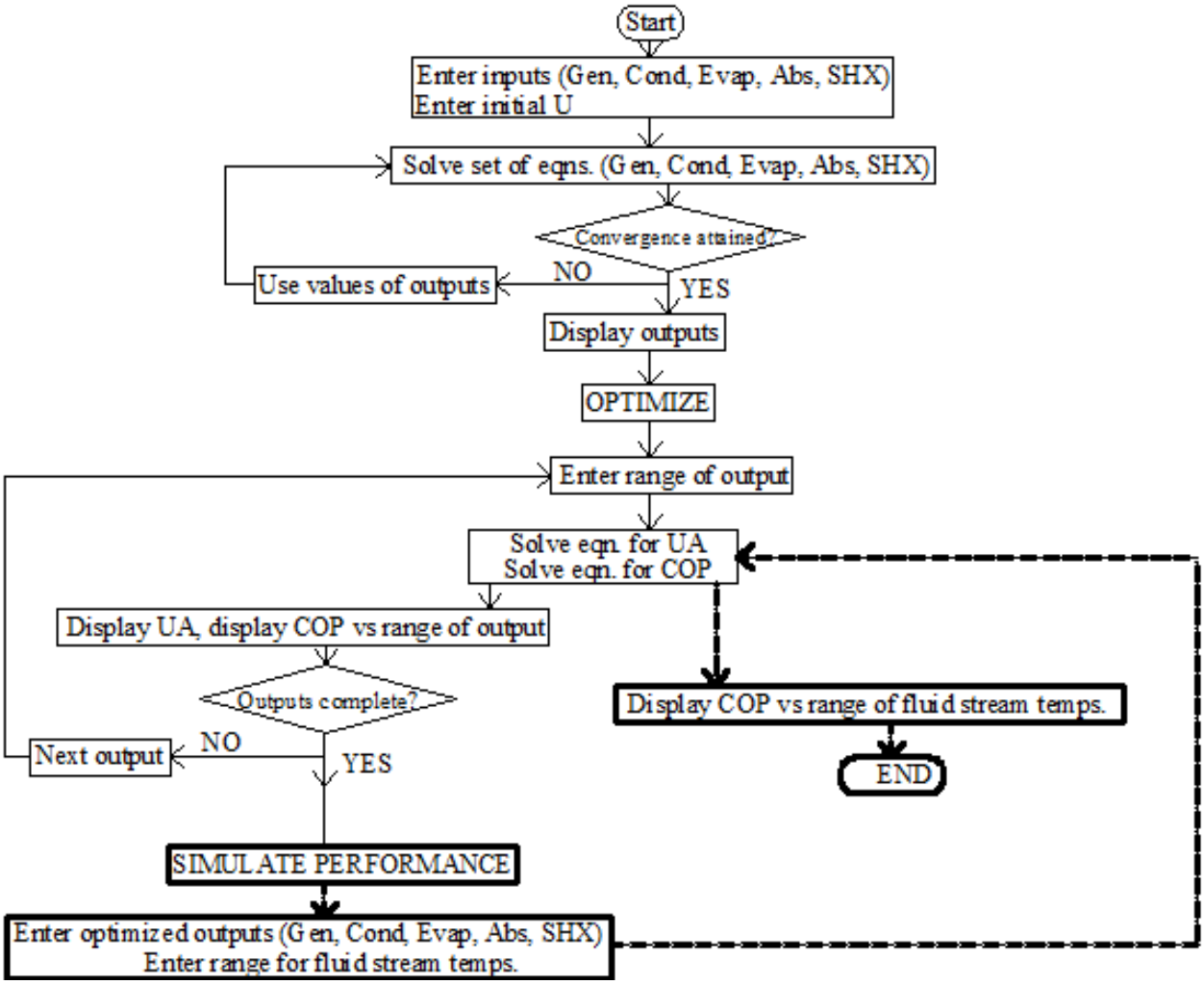


Fig. 3.20: Algorithm block diagram for absorption chiller design optimization and simulation

3.5.7 Wet cooling tower design

The design of a 15 kW capacity wet cooling tower is presented here. The cooling tower was designed as an induced draft counter flow cooling tower.

3.5.7.1 Cooling tower design specifications

i. Range:

The range is given as the difference between the inlet water temperature to the cooling tower and the outlet water temperature from the cooling tower (Hensley, 2009). The cooling tower was designed for an inlet water temperature of 40^{o}C and an outlet water temperature of 30^{o}C. This gives a range of 10^{o}C.

iii. Approach:

The approach is the difference between the outlet water temperature from the cooling tower and the wet bulb temperature(Hensley, 2009). Theoretically, a cooling tower will cool water to the entering wet bulb temperature. In practice however, water is cooled to a temperature higher than the wet bulb temperature because heat needs to be rejected from the cooling tower (Hensley, 2009). The design wet bulb temperature was taken as the average highest wet bulb temperature in Zaria during the summer months, taken as 26^{o}C (Eke, 2011). The design outlet water temperature is 30^{o}C, this gave anapproach of 4^{o}C.

iv. Water flow rate:

The water flow rate was calculated according to Hensley (2009) using equation 3.208:$\frac{Cooling\ \ tower\ \ capacity}{Range\ \times C_{p,w}}$

(3.208)

From which a water flow rate of 0.357 kg/sec was obtained.

3.5.7.2 Calculation of cooling tower parameters

The design of the cooling tower was done using the Merkel's method, which follows from the Merkel's equation given by equation 3.209 (Williamson,2008):

$$\frac{KaV}{\dot{m}} = C_{p,w} \int_{T_{w,o}}^{T_{w,i}} \frac{dt}{H_s - H_a} \qquad (3.209)$$

The factor $\frac{KaV}{\dot{m}}$is the tower characteristic

where:

K is the mass transfer coefficient

a is the surface area per unit volume of packing

V is the volume of the packing

$\dot{m}$is the mass flow rate of water

$T_{w,i}$ and $T_{w,o}$ are the inlet and outlet water temperatures to the cooling tower respectively

$C_{p,w}$ is the specific heat capacity of water

H_s is the enthalpy of saturated air at local water temperature

H_a is the enthalpy of the local air stream

The enthalpy of the inlet air (H_{a1}) was taken at the prevailing air wet bulb temperature, the heat balance equation was obtained using equation 3.210 according to Williamson (2008):

$$\dot{m}C_{p,w}\Delta T_w = \Delta H_a G \tag{3.210}$$

where G is the flow rate of air. From which ΔH_a was calculated using equation 3.211:

$$\Delta H_a = \frac{\dot{m}}{G} C_{p,w}\Delta T_w \tag{3.211}$$

The enthalpy of outlet air was then calculated using equation 3.212 (Williamson,2008):

$$H_{a2} = H_{a1} + \frac{\dot{m}}{G} C_{p,w} T_{w,i} - T_{w,o} \tag{3.212}$$

If the curve of $\frac{1}{H_s - H_a}$ is plotted against the local water temperature, the value of the tower characteristic can be obtained from the area under the curve. However, this method is tedious. Therefore a simplified method according to Fraas (1989) was used. In this method, the curve for H_s is approximated to a straight line as shown in figure 3.21.

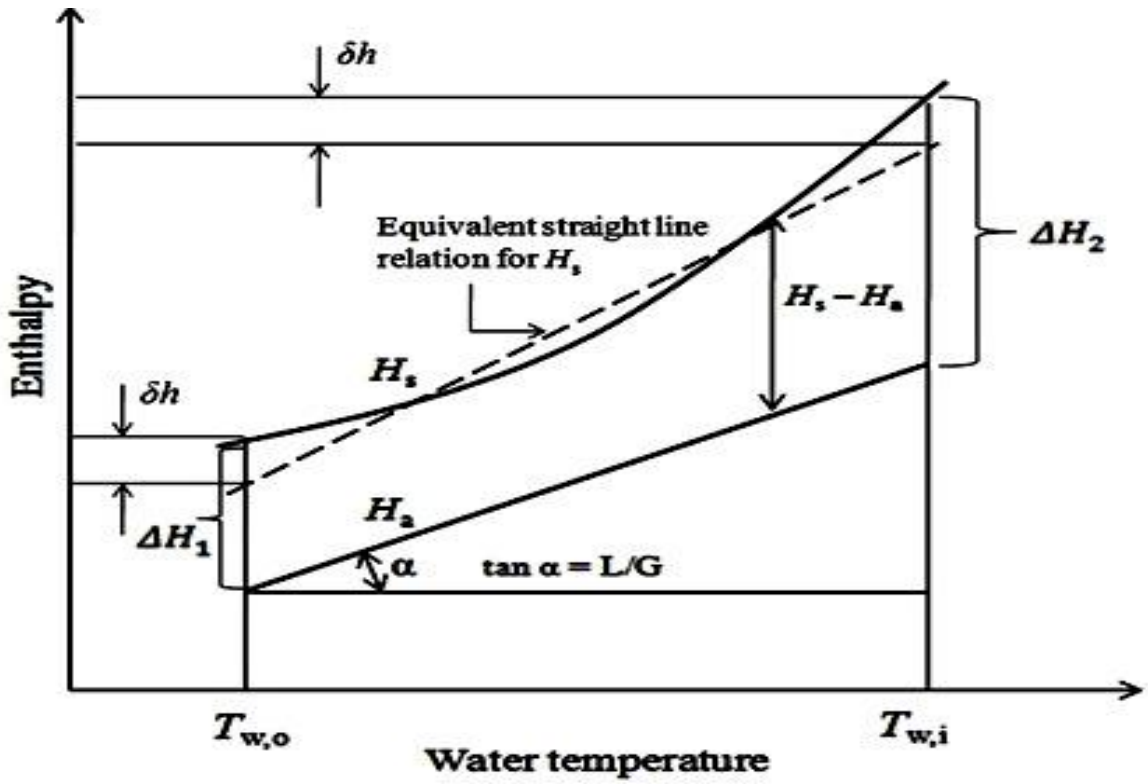


Fig. 3.21: Approximating the curve for H_s with a straight line (Source: Fraas, 1989)

The position of this line is defined by introducing a correction factorδh given by equation 3.213 (Fraas, 1989)

$$\delta h = \frac{H_{s1}+H_{s2}-2H_{sm}}{4} \quad (3.213)$$

H_{s1} and H_{s2} are the values of H_s at the inlet and outlet respectively, H_{sm} is the value of H_s at the mean water temperature.

The tower characteristic was then calculated using equation 3.214 (Fraas, 1989):

$$\frac{KaV}{\dot{m}} = C_{p,w}\frac{(T_{w,i}-T_{w,o})}{\Delta H_m}, \quad (3.214)$$

where ΔH_m is the log mean enthalpy difference calculated using equation 3.215:

$$\Delta H_m = \frac{\Delta H_2 - \Delta H_1}{2.3log\left(\frac{\Delta H_2-\delta h}{\Delta H_1-\delta h}\right)} \quad (3.215)$$

where $\Delta H_1$and ΔH_2 are inlet and outlet enthalpy differences between H_s and H_a

The enthalpy of the air stream increases linearly with the water temperature. The total increase of enthalpy ΔH was evaluated using the equation 3.216 (Fraas, 1989):

$$\Delta H = \left(\frac{\dot{m}}{G}\right)_{opt} C_{p,w} \Delta T_w \quad (3.216)$$

where the optimum ratio of flow rate of water to flow rate of air $\left(\frac{\dot{m}}{G}\right)_{opt}$ was evaluated according toWilliamson(2008), as shown in equation 3.217:

$$\left(\frac{\dot{m}}{G}\right)_{opt} = \frac{C_{p,a}}{C_{p,w}} + \frac{h_{fg} \times 0.622 \times e^{18.6 - \frac{5206.9}{T_w}} \times 5206.9 \times P}{C_{p,w} \times T_w^2 \times \left[P - e^{18.6 - \frac{5206.9}{T_w}}\right]^2} \quad (3.217)$$

where P is the atmospheric pressure

The cooling tower was designed to operate without packing. The volume of the spray area was therefore taken equal to$V$. A rectangular geometry was chosen for the cooling tower, from which an optimum height of the spray zone:h was determined from the solution to the Merkel equation as given in equation 3.218:

$$\frac{KaLW\,h}{4\dot{m}} = C_{p,w} \int_{T_{w,o}}^{T_{w,i}} \frac{dt}{H_s - H_a} \quad (3.218)$$

where *L* and *W* are the length and width of the cooling tower respectively.

3.5.7.3 Volume of water required

Evaporation loss (E_{loss}) of the cooling tower was calculated according to (Hensley, 2009)as shown in equation 3.219:

$$E_{loss} = 0.00153 \times Cooling\ range \times water\ flow\ rate \quad (3.219)$$

The operating time of the absorption air conditioning system is from 8am to 6pm, if the cooling tower operates throughout this period, it corresponds to 10hours operation daily.

The volume of water used daily (V_w) was calculated using equation 3.220 (Hensley, 2009):

$$V_w = E_{loss} \times Operation\ time \quad (3.220)$$

The equations 3.209 to 3.220 were programed and solved in MATLAB according to the sequence in which they follow. The design specifications formed inputs to the programme. The MATLAB code for the program is shown in appendix I.

3.5.8Design of hot water storage tank

The design of the storage tank was done for a storage capacity of 0.9 m^3. The design equations as well as the design calculations are presented here.

3.5.8.1 Storage tank design specifications

i. Storage temperature range: 85 – 95^oC

ii. Geometry: A cylindrical geometry was used for convenience

iii. Height: A convenient height of 1.3m was chosen.

3.5.8.2 Diameter of tank

The storage tank was designed to store hot water between 85^oC and 95^oC. It was designed to be cylindrical in geometry. Choosing a height of 1.3m for the tank, then the required diameter of the tank was computed using equation 3.221:

$$D_T = \sqrt{\frac{4V_T}{\pi H_T}} \tag{3.221}$$

where:

V_T= volume of tank (storage capacity)

H_T= height of tank

From which the diameter was obtained as:

$$D_T = \sqrt{\frac{4 \times 0.9}{\pi \times 1.3}} = 0.9386m$$

3.5.8.3 Stress Analysis on the Tank

The storage tank was constructed of galvanized steel material. Water inside the tank subjects the tank to internal pressure, this pressure is taken to be uniformly distributed over the internal surface of the tank. If the wall thickness is equal to or less than 1/20 of the internal diameter, the vessel is taken to be thin walled, otherwise it is taken to be a thick walled vessel (Bansal, 2009).

The following specification apply to the tank design

Material: Galvanized steel (A635)

Yield strength (σ): 250.2Mpa

Thickness (t) : 0.0015m

From the above, the thickness is less than 1/20 of the internal diameter, the vessel was then considered to be thin walled.

A bursting stress known as hoop stress (σ_h) will be set up on the walls of the storage tank caused by water pressure (Bansal, 2009). This was calculated using equation 3.222 (Bansal, 2009)

$$\sigma_h = \frac{P_T D_T}{2t} \quad (3.222)$$

From which:

$$\sigma_h = \frac{4732.34 \times 0.5}{2 \times 0.0015} = 788{,}723.3Pa = 0.788MPa$$

3.5.8.4 Tank insulation

The critical insulation radius is that insulation radius which maximizes heat transfer, that is, radius above which heat loss decreases with increasing vessel radius. This was calculated according to Incropera et al, (2004) as given in equation 3.223:

$$r_{cr} = \frac{K}{h} \quad (3.223)$$

where:

K= thermal conductivity of the insulating material (0.03W$/mK$ for free fibre glass)

h=convection coefficient (10W/m^2 for free convection in air)

From which

$$r_{cr} = \frac{0.03}{10} = 0.003m$$

Since $r_T = \frac{D_T}{2} = \frac{0.5}{2} = 0.25 > r_{cr}$ insulation thickness in excess of r_{cr} will prevent heat loss.

Fibre glass material was used in insulating the tank to prevent heat loss

3.5.9 Fan coil unit sizing and selecting

The chilled water produced at the evaporator is required to circulate through fan coil units to cool each of the zones in the building. Each zone requires a fan coil unit for this purpose which will depend on the maximum cooling load expected within the zone. The component was sized and selected off shelf based on the specifications of commercially available units.

3.5.9.1 Specification of commercially available fan coil unit

i. Tube outer diameter (d_o): 0.0134m

ii. Tube inner diameter (d_i): 0.0121m

iii. Longitudinal tube spacing (S_L): 0.0261m

iv. Transverse tube spacing (S_T): 0.0317m

v. Finned surface weighted efficiency(η_s): 0.85

vi. Number of tube rows(N_p): 6

vii. Air face velocity(V_{face}): 2.8m/s

viii. Exchanger compactness(β): 1060m^2/m^3

Source: (Manufacturers data of commercially available fan coil unit)

3.5.9.2 Design fluid temperatures

i. Chilled water inlet temperature(T_{w1}): 10^{o}C

ii. Chilled water outlet temperature(T_{w2}): 15^{o}C

The inlet air condition to the cooling coil (T_{a1}) was taken as the cooling set point temperature within the zones plus a safety margin (24^{o}C + 4^{o}C) = 29^{o}C dry bulb and 19^{o}C design indoor wet bulb. From the psychometric chart (Hensley, 2009),at inlet air conditions, the following inlet air properties were obtained:

Enthalpy of air at inlet $(h_{a1}) = 53.75KJ/kg$

Humidity ratio of air at inlet $(W_{a1}) = 0.0102kJ/kg$

The condition of the air leaving a chilled water coil is nearly saturated, therefore, the relative humidity of the outlet air from the coil (ϕ_2) can be assumed as 95%. (Arora, 2000).

From the inlet air properties and the outlet air relative humidity, using the psychometric chart, the following outlet properties were obtained:

The enthalpy of air at outlet $(h_{a2}) = 40.5KJ/Kg$

The temperature of air at outlet $(T_{a2}) = 16^{o}C$

The mass flow rate of air (m_a) was calculated using equation 3.224 (Arora, 2000):

$$m_a = \frac{Q_{cool}}{(h_{a1} - h_{a2})} \tag{3.224}$$

The mass flow rate of water (m_w) was calculated using equation 3.225 (Arora, 2000):

$$m_w = \frac{Q_{cool}}{C_{p,w}(T_{w2} - T_{w1})} \tag{3.225}$$

where Q_{cool} is the maximum cooling load per zone

The mean temperature difference was calculated using equation 3.226 (Wang, 2001):

$$\Delta T_{wmean} = \frac{[(T_{a1} - T_{w2}) - (T_{a2} - T_{w1})]}{ln\left[\frac{(T_{a1} - T_{w2})}{(T_{a2} - T_{w1})}\right]} \tag{3.226}$$

The number of coil tubes was calculated using equation 3.227 (Wang, 2001):

$$N_{c,t} = \frac{4N_p m_w}{\pi \rho_w d_i^2 V_{coil}} \tag{3.227}$$

The height of coil was calculated using equation 3.228 (Wang, 2001):

$$H_{coil} = S_t N_{c,t} \tag{3.228}$$

The depth of coil was calculated using equation 3.229 (Wang, 2001):

$$D_{coil} = N_{c,row} S_L \tag{3.229}$$

The set of equations from 3.224 to 3.229 were programmed and solved in MATLAB. The design specifications as stated in section 3.5.9.1 formed inputs to the program. The MATLAB code is seen in appendixJ. The maximum cooling load for each zone Q_{cool} was used in the programme to size the cooling coil for each zone respectively.

3.6 Construction of the Solar/ Gas Hybrid Powered Absorption Air Conditioning System

One of the specific objectives of this work is to construct the solar/ gas hybrid powered absorption air conditioning system using locally available materials and expertise. Due to the huge cost implications of constructing the system as sized (12 kW), a reduced size version of the system was constructed within the limits of available funds. Table 3.4 shows the full scale design sizes as well as the constructed sizes. Reduction was done basically considering cost and least sizes to achieve primary energy savings.

Table 3.4: Components full scale size and constructed size

Component	**Full scale size**	**Constructed size**
Absorption chiller	12 kW	4 kW
Cooling tower	20 kW	6 kW
Solar collector	40 m^2	1.7 m^2 (least area expected to give primary energy savings was used).
Hot water tank	0.9 m^3	0.05 m^3 (based on volume of hot water required to circulate round the system).

Construction of the absorption air conditioning system components was carried out at Safari air conditioning and refrigeration workshop, in Trikania, Kaduna, as well as in the workshop, Department of Mechanical Engineering, Ahmadu Bello University, Zaria. Details of the construction process are outlined below.

3.6.1 Construction of the absorption chiller

The absorption chiller was constructed as a 4.0 kW prototype. The generator, condenser, absorber, evaporator and SHX were shell and tube heat exchangers. The generator was constructed as a pool boiling generator, the evaporator and absorber were constructed to operate in falling film mode.

A unique feature in the 4 kW prototype is in the falling film evaporator and absorber. In order to enhance the falling film mode for better tube wetting, a “double tube” configuration was employed, in which an outer tube directs falling film onto the inner tube.This is to facilitate better wetting of tubes for effective evaporation and absorption in the evaporator and absorber respectively.

Here, for the evaporator, chilled water flows in the inner tubes, while refrigerant falling film is conveyed by the outer tubes over the inner tubes in counter flow mode. The outer tubes are shorter in length towards the sump to allow for refrigerant vapour, which flows into the shell and then out to the absorber. For the absorber, cooling water flows in the inner tubes, strong solution of lithium bromide falling filmis conveyed by the outer tubes over the inner tubes in counter flow mode. The outer tubes are much shorter towards the sump where the solution absorbs refrigerant vapour. See drawing number 13 in appendix M.The absorption chiller was constructed at Safar air conditioning and refrigeration, Trikania, Kaduna.The construction process is outlined in table 3.5.

Table 3.5: Construction process of the absorption chiller

S/n	Part/ process	Material	Construction process	Equipment
1	Heat exchanger tubes (for: generator, condenser, absorber, evaporator, SHX)	Copper	Standard rolls of copper tube of diameter 9.4mm were purchased. They were cut into the required tube length (1m) for each of the heat exchangers. The number of tubes for each heat exchanger are: Generator: 10, Condenser:8, Evaporator:11, Absorber:12, SHX: 1. See drawing nos. 8 and 14	Power saw was used in cutting out the tube lengths.
2	Heat exchanger shell (for generator, condenser, absorber, evaporator, SHX)	Stainless steel	Standard size stainless steel tubes of diameters closest to the calculated shell sizes for each heat exchanger were purchased and cut to the required lengths. The shell diameters are: Generator: 20mm, Condenser: 20mm, Evaporator: 20mm, Absorber: 20mm, SHX: 20mm. Holes were drilled on the shells at required positions to house the inlet and outlet ports for fluid flow. See drawing nos. 9, 10, 11, 12 and 15	Power saw was used in cutting out the shell lengths, drilling machine was used to drill the holes.
3	Baffles	Copper	Copper sheet of 3mm thickness was purchased. The baffles were cut into diameters to fit into the respective heat exchangers. Holes were constructed in the resulting circular sheets. The number of holes on each baffle corresponds to the number of tubes in each heat exchanger. Each of the heat exchangers have 5 baffles spaced at 20mm intervals.	Milling machine, drilling machine, hand file.

			See drawing nos. 1 to 4.	
4	Outer tubes for evaporator and absorber	copper	Standard rolls of copper tube of diameter 12.25mm were purchased. They were cut into the required tube length (0.8m) for each of the heat exchangers. See drawing no. 13.	Power saw was used in cutting out the tube lengths.
5	Sub assembly (Tubes & Baffles)	Copper	For each of the heat exchangers, (generator, condenser, evaporator absorber, SHX), the tubes were passed through the holes in the baffles. The baffles were spaced at the specified intervals and then welded onto the tubes using gas welding	Gas welding set
6	Sub assembly (tubes, baffles and shell).	Copper and stainless steel	For each of the heat exchangers, the tubes and baffles assembly obtained in (5) were placed into their respective shells, according to specifications. The tubes were then welded to the outer edge of their respective shell using argon gas welding. See drawing nos. 16 to 20.	Gas welding set, argon
7	Leakage test/ pressure (vacuum) test		For each of the heat exchangers, the shell and tubes assembly as obtained in (6) were subjected to leakage test, this was done using nitrogen gas. Vacuum test were then carried out on each of the heat exchangers by using a vacuum pump to remove air from the heat exchangers.	Nitrogen gas, vacuum pump.
8	Fluid distributors	Galvanized steel pipe	The fluid distributors were made of galvanized steel pipes and copper tubes cut to the specified length and diameter. The copper tubes were welded to the galvanized steel pipe using gas welding. See drawing nos. 6 and 7.	Hack saw, gas welding set
9	Frame	Mild steel	Angle iron rods were cut to the specified lengths and welded together according to specifications to house each of the heat exchangers and also provide space for mounting the pumps and pipes. See drawing no. 21.	Power saw, hack saw, arc welding set
10	Clamps	Mild steel	Clamps were constructed of mild steel to clamp the heat exchangers to the frame. They were cut to diameters of the heat exchangers with holes drilled for bolting. See drawing no. 5.	Hack saw, drilling machine

11	Sub assembly (heat exchangers and frame)	Copper, stainless steel, mild steel	The heat exchangers, after the leakage/ vacuum test done in (7) were then mounted onto the frame by clamping them onto specified positions.	Bolts and nuts, spanner.
12	Insulation	Fibre glass	The evaporator and absorber were insulated using fibre glass and glue.	Hand done: fibre glass, glue
13	Solution/ refrigerant pipes	Copper pipes	Copper pipes of specified diameter and length were cut out. The condenser was linked to a throttle valve and then to the evaporator using a copper pipe by welding. The generator was linked to the absorber using a copper pipe by welding.	Hack saw, Gas welding set
14	Control box	Mild steel	The control box was constructed of mild steel. The components for the electrical control as well as sensors were fixed at specific locations. These include switches, cables, relays, sensors. See drawing no. 22.	Hack saw, arc welding set, screw drivers, bolts and nuts
15	Mounting of pumps		The fluid pumps were fixed at their specified locations. They are: the hot water pump, the cooling water pump, the chilled water pump, the solution pump, the refrigerant pump.	Screw drivers. Spanner, bolts and nuts
16	Electric circuiting		The pumps were linked to the control box using electric cables, sensors were connected to specified remote areas	Pliers, screws, screw driver
17	External Piping/ complete assembly	PVC pipes	The heat exchangers were then linked together by the piping system. This included linking pipes from pumps to heat exchanger as well as from one heat exchanger to the other according to specifications. Flow valves and meters were placed in required locations	Screw drivers, bolts and nuts, clips, sealants.
18	Sealing of joints		All joints of pipes and tubes were sealed using araldite glue. The process was repeated after six hours and then the system was allowed to dry for 48 hours.	Araldite glue
19	Leakage test		Another round of leakage test was carried out on the complete assembly to ensure a leak free system.	Nitrogen gas
20	Vacuum test		The complete assembly was vacuumed using a vacuum pump to make the system air free	Vacuum pump
21	Complete assembly		The complete assembly was done by mounting and connecting the pumps to	Manual operation

			the heat exchanger and piping system. See drawing no. 33.	
22	Charging the lithium bromide solution		One litre of lithium molybdate (a corrosion inhibitor) was added to five litres of lithium bromide solution. The solution mixture was first charged into a vacuumed cylinder. The cylinder outlet pipe was welded to a charging port at the generator. The flow valve was opened and the solution streamed from the cylinder into the generator. The cylinder was thereafter removed.	Manual operation

3.6.2 Construction of the solar collector

The collector was constructed as a flat plate collector with single glazing, absorber plate, wooden base and fibre glass as insulation. Construction of the flat plate collector was carried out at the department of mechanical engineering workshop, Ahmadu Bello University, Zaria. The construction process is outlined in table 3.6.

Table 3.6: Construction process of the flat plate solar collector

S/n	Part/ process	Material	Construction process	Equipment
1	Header	Copper	Copper tube was cut out to the required length and holes drilled in positions to accommodate risers	Hand saw, Drilling machine
2	Inlet pipe	Copper	Copper tube was cut out to the required length and holes drilled in positions to accommodate risers	Hand saw, Drilling machine
3	Risers	Copper	The required number of risers (tubes) were cut to the required length	Hand saw
4	Sub-Assembly (Header, inlet pipe and risers)	Copper	The risers were placed with the ends of each tube fit to adjacent holes on the header and inlet pipe. The ends were then welded at the corresponding holes in the header and inlet pipe. See drawing no. 23.	Gas welding machine
5	Absorber plate	Aluminium	Aluminium plate of specified thickness was cut out to the area of a single module using specified length and width. See drawing no. 26.	Power saw
6	Wooden base	Ply wood	Ply wood of specified thickness was cut out to the area of a single module using specified length and width	Hack saw
7	Glazing	Tempered	Tempered glass of specified thickness	Hand saw

		glass	was cut out to the area of a single module using specified length and width. See drawing no. 25.	
8	Frame	Wood	Wood of required thickness was cut out to the required length and width (2 each) to form the frame. See drawing no. 24	Hack saw, plying machine
9	Assembly		Absorber plate was placed on the wooden base, the sub assembly in 4 was then placed on the absorber plate. The frame was then mounted round the assembled components. The glazing was then fixed to position at the top of the frame. See drawing no. 27.	Manually assembled

3.6.3 Construction of the storage tank

The storage tank was constructed as a cylindrical tank using galvanised steel. Fibre glass was used as insulation. The tank was constructed at Safari air conditioning and refrigeration, Trikania, Kaduna. The construction process is outlined in table 3.7.

Table 3.7: Construction process of the storage tank

S/n	Part/ process	Material	Construction process	Equipment
1	Tank inner surface	Galvanized steel sheet	Galvanized steel sheet of specified thickness was cut out to the required length, rolled into the required diameter and welded at the edges. Holes were drilled at the sides to accommodate the inlet and outlet water pipes. See drawing no. 32	Cutting machine, rolling machine, gas welding set drilling machine.
2	Tank outer surface	Galvanized steel sheet	Galvanized steel sheet of specified thickness was cut out to the required length, rolled into the required diameter and welded at the edges. Holes were drilled at the sides to accommodate the inlet and outlet water pipes. See drawing no. 32	Cutting machine, rolling machine, gas welding set, drilling machine.
3	Tank bottom	Galvanized steel sheet	Galvanized steel sheet was cut out to a circle equal in diameter to the outer surface diameter. See drawing no. 32.	Cutting machine
4	Tank top	Galvanized steel sheet	Galvanized steel sheet was cut out to a circle equal in diameter to the outer surface diameter. See drawing no 32.	Cutting machine
5	Insulation	Fibre glass	Fibre glass was cut out to the required insulation thickness, length and width.	Pair of scissors.

6	Assembly		The inner tank surface was placed concentrically inside the outer tank surface. The tank bottom was welded to the base of the concentric surfaces. The insulation was then used to fill the gap between the concentric surfaces. The tank top was then welded to the top of the concentric surfaces. See drawing no. 32.	Manually assembled, gas welding set.

3.6.4 Construction of the cooling tower

The cooling tower was constructed as an induced draft counter flow wet cooling tower, without packing. It was constructed at Safari air conditioning and refrigeration, Trikania, Kaduna. The construction detail is outlined in table 3.8.

Table 3.8: Construction process of the cooling tower

S/n	Part/ process	Material	Construction process	Equipment
1	Cooling tower body	Galvanized steel sheet	Galvanized steel sheet of required thickness was cut out to the required length and width, rolled out to the specified diameter and welded at the edges. Slants were cut out to specified sizes and at specified positions for air flow. Hole was drilled at the side to accommodate the water flow pipe. See drawing no. 28.	Cutting machine, rolling machine, gas welding set.
2	Cooling tower top	Galvanized steel sheet	Galvanized steel sheet of specified thickness was cut out into a circle equal in diameter to the cooling tower body. See drawing no. 28.	Cutting machine
3	Sump	Galvanized steel sheet	Galvanized steel sheet of specified thickness was cut out and welded into a cylinder, open at the top and equal in volume to the required sump volume	Cutting machine, gas welding machine
4	Water spraying tray	Galvanized steel sheet	Galvanized steel sheet of required thickness was cut out to a circle equal in diameter to the diameter of the cooling tower body. Holes were then drilled all around the circular plate. See drawing no. 30.	Cutting machine, drilling machine
5	Water pipes	PVC pipes	PVC pipes of specified diameter were cut out to specified lengths.	Hand saw.
6	Cooling tower stand	Ply wood	Ply wood of specified thickness was cut out to the required area. See drawing no. 29.	Hack saw

7	Assembly		The water spray tray was welded inside the cooling tower body at specified position. The cooling tower top was welded to the top of the cooling tower body. The bottom of the cooling tower body was welded to the open end of the cooling tower sump. The water pipes were fit to specified positions. The assembly was then bolted to the cooling tower base. The pump was bolted to the cooling tower base as well. See drawing no. 31.	Manually assembled, gas welding set, bolts and nuts, spanners, screw drivers.

Working drawings are shown in appendix N.

3.7 Experiment

On completion of the construction work, a process of instrumentation / bench test was done on the absorption chiller to ascertain its workability.

Experiments were conducted to test the performance of the constructed gasassisted solar absorption air conditioning system. The experiments were conducted on the 22nd of April 2017 and between the 3rd and 19th of June 2017. The experiment was done on a test room in the heat engine laboratory of the Department of Mechanical Engineering, Ahmadu Bello University, Zaria, with a floor area of9.21m^2.The cooling load profile for the test room was obtained using TRNSYS to determine the peak cooling demand for the months test was done.

The peak cooling energy demand for the test room in the month of April was 8352000J (2.32kWh). The peak cooling energy demand for the test room in the month of June was 7596000J (2.11 kWh). The annual cooling energy demand for the test room was 4,371kWh.

3.7.1 Experimental apparatus

In addition to the entire system components: collector, storage tank, absorption chiller, cooling tower, fan coil unit, the following were used to take readings:

i. Digital solar power meter: model no. DBTU 1300, measuring range: 0 – 2000 W/m^2, accuracy: $\pm$5%of reading

ii. Digital infrared thermometer: model no. PM6350D, measuring range: -50 – 800^{o}C, accuracy: $\pm$1.5^{o}C

iii. Digital thermocouple thermometer: model no. T407291, measuring range: -50 – 1300^{o}C, accuracy: $\pm$0.1^{o}C

iv. Thermocouple wires (copper – constantan)

v. Watt meter: model no. H3680W, measuring range: 0 – 3680W, accuracy class: 1.0

vi. Humidity meter: model no. TA318, measuring range: 25% RH – 98% RH, accuracy: $\pm$5% RH

vii. Digital weighing scale: model no. SF – 400, measuring range: 0 – 7000g, accuracy: $\pm 1g$

viii. Bourdon tube pressure guage: model no. ASME B40 – 100 measuring range: -1bar – 24bar, accuracy class: 2% in the first 75% of scale, 5% in the last 25% of scale.

ix. Wet and dry bulb hygrometer: model no. HX – D28, measuring range: -30 – 50^{o}C, accuracy: 5% RH.

A schematic diagram of the experimental set up is shown in figure 3.22. Pictures of the experimental facility are presented as plates in Appendix M.

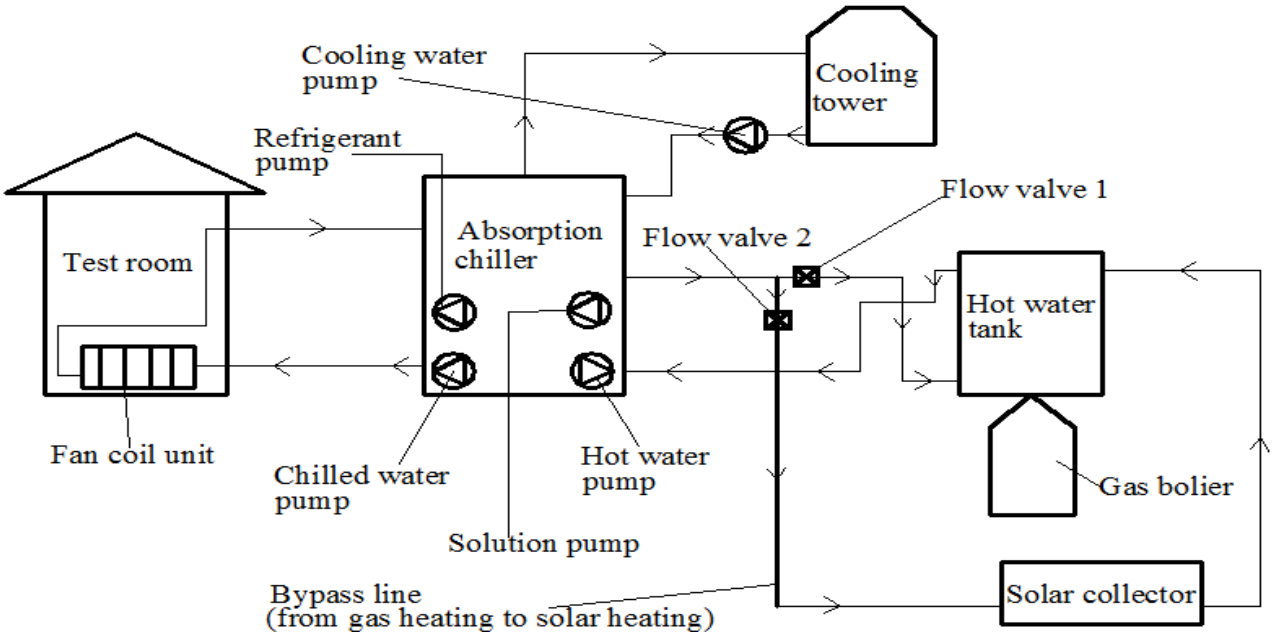


Fig. 3.22: Schematic of the experimental set up

3.7.2 Experimental procedure

The experiments reported here were conducted in the month of April 2017, which is a very hot month and in the month of June 2017 which is a rainy month. Each of the experimental days span from 8.30 am to 5.30 pm. Two heating modes were employed to provide the thermal energy required for the hot water: the solar power heating mode, provided via the solar collector and the gas boiler heating mode, provided by the liquefied petroleum gas burner. Switching between solar heating and gas heating modes was achieved via a bypass line activated by flow valves.

At the start-up of each experimental day,thermal energy was supplied to the water in the tank using the gas burner. This was because solar radiation is usually very low at the early hours of the day to attain heating to required water temperature. When the required temperature in the tank was attained (90^oC – 95^oC), the hot water pump was then turned on to circulate the hot water between the tank and the generator in the absorption chiller.An interval of 10 – 15mins was allowed for desorption of the solution in the generator to commence. The solution pump and the cooling tower pump were then turned on. At this stage, desorption of lithium bromide solution at the generator, condensation at the condenser and absorption at the absorber were in progress. The refrigerant pump and the chilled water pump were then turned on and the process of chilling commenced.

In situations where the temperature of the collector fluid increased to 80^oC and above, the gas boiler was disengaged and the system was switched to solar heating mode. This was achieved by activating flow valve 2, while flow valve 1 stays closed. When temperature of the collector fluid dropped below 70^oC, the system was switched back to gas boiler heating mode. Chilled water was produced at the evaporator and pumped to the fan coil unit in the test room. Reading of experimental variables were done every 30mins.

Temperature readings were done using digital thermocouple from thermocouple wires attached at the collector inlet and outlet (to measure collector fluid temperature), collector plate (to measure collector plate temperature), storage tank interior (top and bottom levels) (to measure storage tank fluid temperature), generator inlet and outlet (to measure hot water temperature), evaporator inlet and outlet (to measure chilled water temperature), cooling tower inlet and outlet (to measure cooling water temperature). The solar radiation on the collector was measured using a solar meter. The gas boiler was placed on a digital weighing scale and the reading on the scale recorded every 30mins. This way, the weight loss indicated the weight of gas consumed within a certain interval. The ambient temperature as well as the test room temperature were measured using an infra-red thermometer. The relative humidity (outdoor and indoor) were measured using a humidity meter as well as a wet – and dry – bulb hygrometer. A watt meter was used to measure the power consumption, while Bourdon tube pressure guage was used to monitor system pressures.

3.7.3 Performance measurement

The following performance parameters were calculated:

3.7.3.1 Evaporator cooling power(Q_e)

The evaporator cooling power was calculated using equation 3.230 (Arora, 2000):

$$Q_e = \dot{m}_e C_p (T_{e2} - T_{e1}) \quad (3.230)$$

Where $\dot{m}_e$ is the mass flow rate of chilled water at the evaporator $= 0.24\ Kg/s$

C_p is the specific heat capacity of the chilled water

T_{e2} and T_{e1} are the outlet and inlet chilled water temperatures to the evaporator respectively

3.7.3.2 Generator heat load(Q_g)

The generator heat load was calculated using equation 3.231 (Arora, 2000):

$$Q_g = \dot{m}_g C_p (T_{g1} - T_{g2}) \quad (3.231)$$

where $\dot{m}_g$ is the mass flow rate of hot water at the generator$= 0.223\ Kg/s$

C_p is the specific heat capacity of the hot water

T_{g1} and T_{g2} are the inlet and outlet hot water temperatures to the generator respectively

3.7.3.3 Collector efficiency (η_c)

The collector efficiency was calculated according to Duffie and Beckman (2013) using equation 3.232:

$$\eta_c = \frac{\dot{m}_c C_p \Delta T}{A_c G_T} \quad (3.232)$$

where $\dot{m}_c$ is the mass flow rate of fluid at the collector = 0.1kg/sec

ΔT is the fluid temperature difference between inlet and outlet to the collector

A_c is the area of the collector

G_T is the solar radiation on the collector surface

3.7.3.4 Cooling tower efficiency (η_{ct})

The cooling tower efficiency was calculated according to the equation 3.233 (Williamson,2008):$\eta_{ct} = \frac{T_{cw\,1} - T_{cw\,2}}{T_{cw\,1} - T_{wb}} \times 100$

(3.233)

where:

$T_{cw\,1}$= cooling tower inlet water temperature

$T_{cw\,2}$= cooling tower outlet water temperature

T_{wb} = wet bulb temperature

3.7.3.5 Solar power used (P_{solar})

The solar power used was calculated using equation 3.234 (Duffie and Beckman, 2013):

$$P_{solar} = A_c G_T \quad (3.234)$$

3.7.3.6 Gas consumption

The weight of gas consumed at an interval of time was determined using a digital weighing scale. The gas consumption in kW(P_{gas}) was computed using equation 3.235 (Demirel, 2012):

$$P_{gas} = \frac{m Cal_g}{t} \quad (3.235)$$

where:

m is the weight of the gas consumed in the time interval (kg)

Cal_g is the calorific value of liquefied petroleum gas taken as 46.1MJ/kg(Demirel, 2012)

t is the time interval in which the gas was used

3.7.3.7 Coefficient of performance (COP)

The COP was computed using equation 3.236:

$$COP = \frac{Q_e}{Q_g} \tag{3.236}$$

3.7.3.8 Solar coefficient of performance (SCOP)

The SCOP was calculated using equation 3.237 (Duffie and Beckman, 2013):

$$SCOP = \eta_c COP \tag{3.237}$$

3.7.3.9 Solar Fraction

A simplified approach was used to compute the solar fraction for the experimental days in which solar heating mode was used at a certain instance. This was done by simply dividing the number of hours in which the chiller was fired in the solar heating mode by the total number of hours of chiller operation for the experimental day.

3.8 Economic Analysis

An economic assessment of the solar/ gas hybrid powered absorption coolingsystem was carried out by simulation to ascertain the economic viability of the system in a Nigerian climate, also, an economic assessment of the constructed system was carried out.

3.8.1 Economic viability simulation and optimization of the solar/ gas hybrid powered absorption air conditioning system

Several methods of economic analysis of solar cooling systems are available in literature. For the purpose of this study, the Life cycle Cost Saving method (LCS) was used for the analysis. The life cycle saving of a solar absorption cooling system over a conventional system can be expressed as

the difference between a reduction in the fuel cost and an increase in expenses incurred as a result of the additional investment for the solar system. This is as given in equation 3.238(Duffie and Beckmann, 2013).

$$LCS = P_1 \times C_F \times L \times F - P_2 \times C_S \quad (3.238)$$

where:

C_F is the unit cost of delivered conventional energy for the first year of analysis.

L is the annual load (kWh)

F is the annual fraction of load supplied by solar energy

C_s is the total cost of installed solar energy equipment (Naira), given by equation 3.239:

$$C_S = C_A \times A_C + C_E \quad (3.239)$$

where:

C_A is the collector area dependent cost (Naira/m^2)

A_c is the collector area (m^2)

C_E is the collector area independent cost (Naira) which includes the cost of gas used and the cost of electricity consumed by the chiller.

P_1 is given by equation 3.240 (Duffie and Beckman, 2013):

$$P_1 = PWF(N_e, i, d) \quad (3.240)$$

where:

$PWF =$ Present worth factor, calculated using equation 3.241 (Duffie and Beckman, 2013)

$$PWF(N_e, i, d) = \frac{1}{(d-i)}\left[1 - \left(\frac{1+i}{1+d}\right)^{N_e}\right] \quad (3.241)$$

where:

$N_e =$ Number of years of economic analysis

$i =$ Inflation rate on cost of conventional fuel

$d =$ Discount rate

The factor P_2 accounts for investment related expenses which in the present study consists only of the investment, since the investment is made at once and is only expected in current naira. Therefore for the present study, P_2 = unity.

The building cooling energy demand simulation showed an annual total cooling energy demand of 13,663.14kWh for the building block. This corresponds to an average space cooling demand of 151.8kWh/m^2 – annum.

The present electricity tariff for residential (used in this work) under the Multi Year Tariff Order (MYTO) for Zaria in Nigeria is ₦26.37/kWh(MYTO 2.1 report, 2015).The inflation rate on electricity tariff under the MYTO is 3.1% (MYTO 2.1 report, 2015).The discount rate going by the CBN figures is 4.25%(World fact book 2016). Solar absorption cooling systems have a lifespan of about 20 years (Duffie and Beckmann, 2013).Therefore the number of years of the economic analysis for this study was set at 20 years. These figures were used in evaluation of equation 3.241.

Table 3.9 shows the prices of components used in evaluation of equations 3.238 and 3.239. The prices were obtained from a current market survey of components prices from manufacturers in China and Germany as at the time this study was done. The prices in Dollars were converted to Naira using the exchange rate of naira to the dollar as at the time this study was done (1 Dollar = 375 Naira).

Table 3.9: Component prices

Component	**Price (Naira)**
Solar Collector	28,170/m^2
Absorption chiller (12kW)	638,000
Cooling tower (20kW)	550,000
Hot water tank (1.0m^3)	95,700
Installation cost	20% of collector area
Miscellaneous cost	120,000

(Source: online market survey of manufacturer prices as at Dec. 2016)

The auxiliary heater was powered by liquefied natural gas. The cost of liquefied petroleum gas in Zaria, Nigeria as at the time the study was conducted (Dec. 2016) was 333.33 naira /kg. This was used in evaluating the cost of auxiliary energy, which contributes to C_E in equation 3.239.

3.8.2 Economic assessment of the constructed system

The running cost of the cooling plant was determined. The cost per kWh of cooling was also determined. Power consumption and cost per kWh of cooling of the cooling plant was compared to that of conventional air conditioner of the same capacity by employing the Energy Efficiency Ratio (EER) of conventional air conditioners.

3.8.2.1 Life cycle cost savings analysis of the constructed cooling plant

Table 3.10presents the cost analysis of the constructed system

Table 3.10: Cost analysis of the constructed system

ABSORPTION CHILLER				
S/N	**Item**	**Quantity**	**Unit price (Naira)**	**Total price (Naira)**
1	Copper tubes	6 Rolls	9,500	57,000
2	Stainless steel pipes	4(1m by 70mm dia.)	25,000	100,000
3	Angle iron	10 lengths	2,400	24,000
4	Set of throttle valve & nozzle	1 set		10,000
5	Water/ gas valves	14	1,800	25,200
6	PVC pipe	10mm dia. 42m length	200/m length	8,400
7	PVC pipe	20mm dia. 20m length	500/m length	10,000
8	Bolts, nuts, clips, washers			7,000
9	Hot water pump	1	18,000	18,000
10	Chilled water pump	1	18,000	18,000
11	Refrigerant pump	1	10,000	10,000
12	Solution pump	1	10,000	10,000
13	Control unit panel	1	7,000	7,000
14	Control unit cables	1 Roll	15,000/ roll	15,000
15	Control unit accessories	Relays, switches, terminals, sensors, lamps		10,000
16	Nitrogen gas	1 cylinder	20,000	20,000
17	Insulator	Fibre glass 1 sq. m, 20mm thick		10,000
18	PVC (pressure) pipe	4 lengths	2,200/ length	8,800
19	Lithium bromide	5kg	$35/kg $60 shipment	$235 (N91,650)
20	Distilled water	20 litres	200/litre	4,000
21	Workmanship	Metal arc welding, gas welding, plumbing, painting, others		100,000

SUB – TOTAL				**564,050**
COOLING TOWER				
1	Mild steel sheet	(3mm thick) 3 sheets	6,000/ sheet	18,000
2	Fan	1	3,000	3,000
3	Cooling tower pump			20,000
3	Workmanship	Welding, painting, others		10,000
SUB – TOTAL				**51,000**
SOLAR COLLECTOR				
1	Copper tubes	9mm dia. 1 Roll 15mm dia. 4m length	9,500 2,200/m length	9,500 8,800
2	Ply wood	1 sheet	12,000	12,000
3	Sq. wood			3,000
4	Glazing	$2.2m^2$		5,000
5	Insulator	Fibre glass (7mm thick) $2m^2$		6,500
6	Workmanship			5,000
SUB – TOTAL				**49,800**
HOT WATER TANK				
1	Mild steel sheet	(3mm thick) 2 sheets	6,000/ sheet	12,000
2	Galvanized steel pipe	2.5m length		5,000
3	Insulator	Fibre glass (5mm thick)$2m^2$		5,000
4	Workmanship	Welding, painting, others		5,000
SUB – TOTAL				**27,000**
FAN COIL UNIT				
Fan coil unit		1		**10,000**
GRAND TOTAL				**701,200**

(All cost were as at the time system construction was done (Jan. 2017))

From table 3.10, the entire system (experimental set up) was constructed at a total cost of seven hundred and one thousand two hundred naira only. This figure was used together with the set of equations already presented in section 3.8.1 to carry out the economic evaluation of the constructed system. Results are presented in Chapter Four.

3.8.2.2 Comparison of energy used by constructed chiller with energy used by conventional air conditioner

The energy efficiency ratio (EER) of an air conditioner is the ratio of the cooling output to the power consumed. The power consumed includes all inputs to the compressor, fan motor and controls. The higher the EER, the more efficient the air conditioner and the less power it consumes. Table 3.11shows the energy efficiency standards for manufactured air conditioners of different countries.

Table 3.11: Energy efficiency standards for different countries

Energy efficiency sandards for different countries

Country	Minimum energy efficiency ratio (EER)** allowed	Maximum EER available	Average EER
Australia	2.75	5.75	3.16
Brazil	2.92	4.04	3.19
Canada	2.14	4.33	3.6
China	2.9	6.14	3.23
EU	2.21	5.55	3.22
Japan	2.37	6.67	4.1
Korea	3.05	5.73	3.78
South Africa	2.28	5	2.91
USA	-	4.6	3.04
India	2.7	3.8	2.9

Source: Phadke *et al*., (2014)

Using table 3.11, the power consumption for conventional air conditioners of same rated capacity (4.0 kW) at varying EER were calculated. It was assumed a constant cooling power of 4 kWh will be produced by the conventional air - conditioner and the compressor will run for 75% of the daily time (daily time = 9hrs). Cost of energy is N26.37/ kWh.

3.9 Environmental Impact Assessment (Co_2 Emission Reduction & Global warming potential)

Environmental impact assessment was carried out regarding the CO_2emission to the atmosphere and global warming potential (GWP) of refrigerant. Comparison was made between the CO_2 emitted to the atmosphere from the constructed chiller with that emitted from conventional chillers of varying EER. This was done to cover the number of experimental days. Also comparison was made between the GWP of the refrigerant used (water) with those of commonly used refrigerants in conventional chillers. The following were employed:

680 kg of CO_2 are emitted into the atmosphere for every kWh of electricity produced by fossil fuel fired power plants (Balghouthi *et al.,* 2012). 0.2 kg of CO_2 are emitted into the atmosphere for every kg of LPG gas burned (Balghouthi *et al.,* 2012). The analysis was for a total of 10 experimental days of 9 hours each.

The table 3.12 shows the Global Warming potential for commonly used HCFC refrigerants.

Table 3.12: Global Warming Potential (GWP) values of commonly used HCFC refrigerants

Industrial designation or common name	Chemical formula	GWP values for 100-year time horizon		
		Second assessment report (SAR)	Fourth Assessment Report (AR4)	Fifth Assessment Report (AR5)
HCFC-21	$CHCl_2F$			148
HCFC-22	$CHCLF_2$	1,500	1,810	1,760
HCFC-123	$CHCl_2CF_3$	90	77	79
HCFC-124	$CHClFCF_3$	470	609	527
HCFC-141b	CH_3CCl_2F	600	725	782
HCFC-142b	CH_3CClF_2	1,800	2,310	1,980
HCFC-225ca	$CHCl_2CF_2CF_3$		122	127
HCFC-225cb	$CHClFCF_2CClF_2$		595	525

Source: Stocker *et al.*, 2014

CHAPTER FOUR

RESULTS & DISCUSSION

4.1 Results from Building Cooling Energy Demand Simulation

This section presents results obtained from section 3.3. The cooling energy demand simulation carried out in section 3.3 was done with the TRNSYS software to determine peak cooling energy demand for each month. A peak cooling load of 11.04 kW for the office block was obtained. This peak load occurred in the month of April, (precisely on the 21st of April). Figure 4.1 shows the monthly peak cooling energy demand for the whole year.

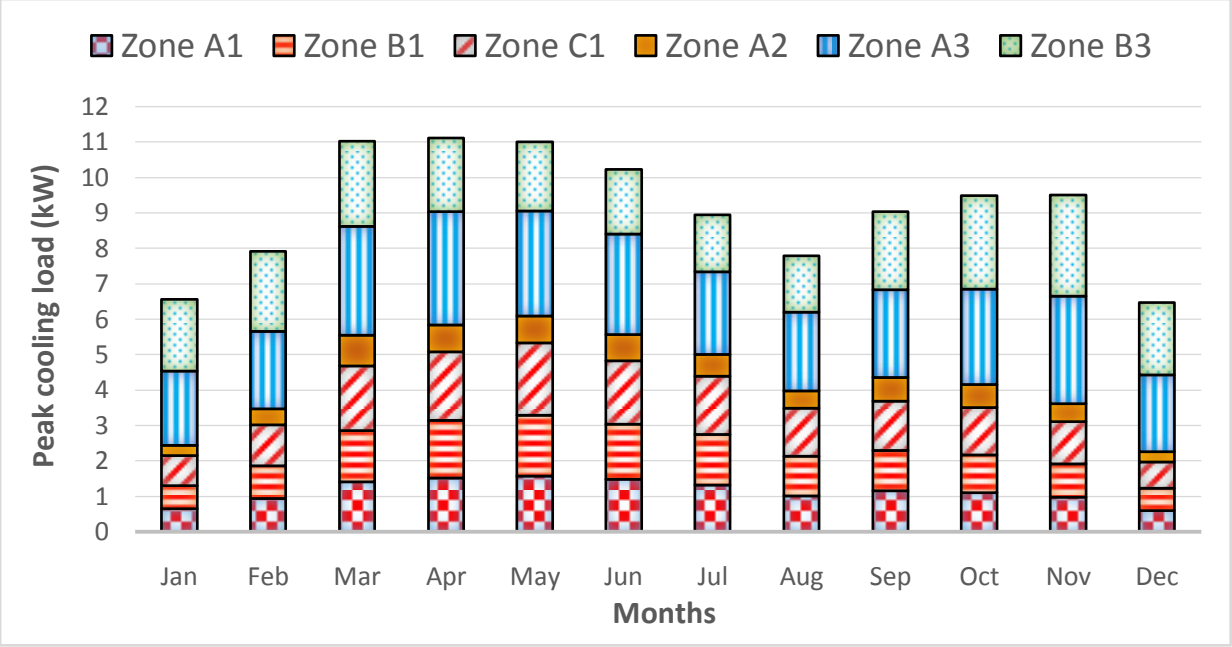


Fig. 4.1: Peak cooling energy demand for the months

From the figure 4.1 the cooling energy demand is seen to be highest in the months of March, April and May, with the peak of 11.04 kW recorded in April. Cooling energy demand are lowest in the months of January and December, which are very cold months. The month of August also has a relatively low cooling energy demand, due to the rainy nature of the month.Figure 4.2 shows the cooling load profile for April 21.

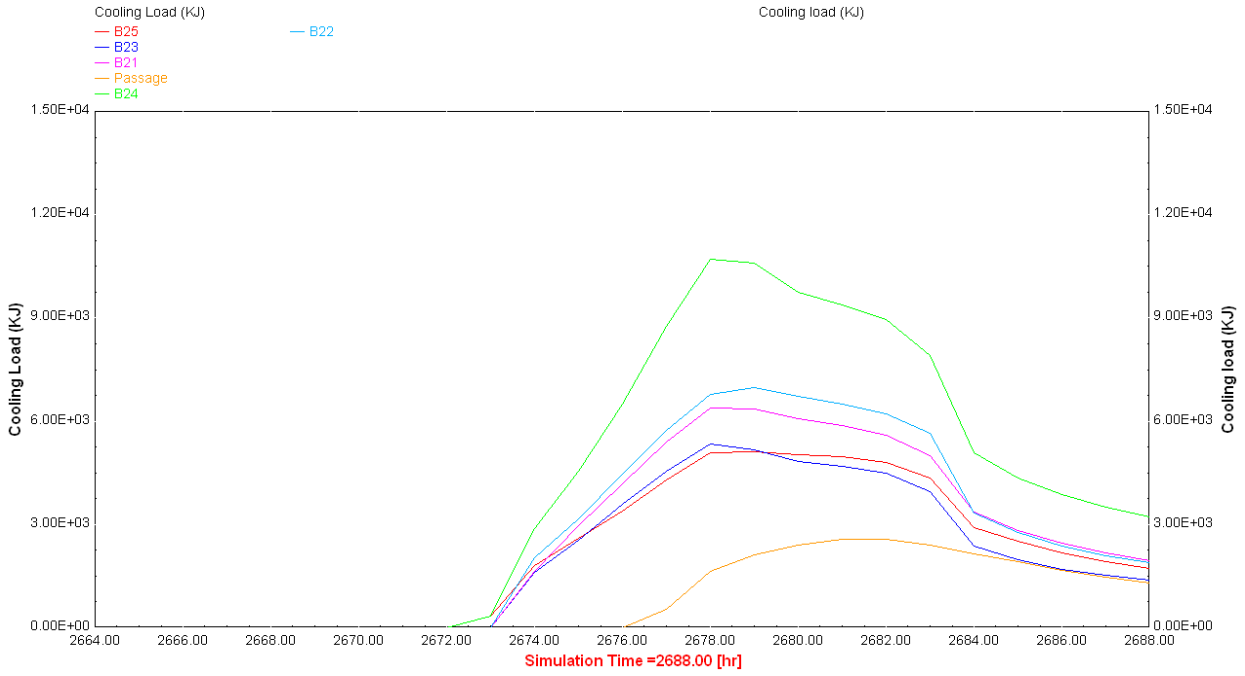


Fig. 4.2 Hourly cooling load for the 21st of April

From figure 4.2, the peak cooling load can be seen to have occured betweem 2678 and 2679hrs (2 – 3 pm). The zone cooling load requirements at this hour are: Room B25: 5,472kJ, Room B23: 5,868kJ, Room B21: 6,948kJ, Passage: 2,772kJ, Room B24: 11,484kJ, Room B22: 7,236kJ.

4.2 Results from Modelling Simulation and Optimization of the Solar/ Gas Hybrid Powered Absorption Air Conditioning System in TRNSYS

In this section results from TRNSYS modelling, simulation and optimization of the absorption cooling system done in section 3.4 are presented.

The peak cooling load of 11.04kW obtained from the building cooling load simulation done in section 3.3and presented in figure 4.1 was used in the modelling of the absorption air conditioning system. Initial sizing of system components was done, after which optimization and simulation of optimized system was done. Figure 4.3shows the temperature variation within the zones for the whole year without cooling applied to the building block.

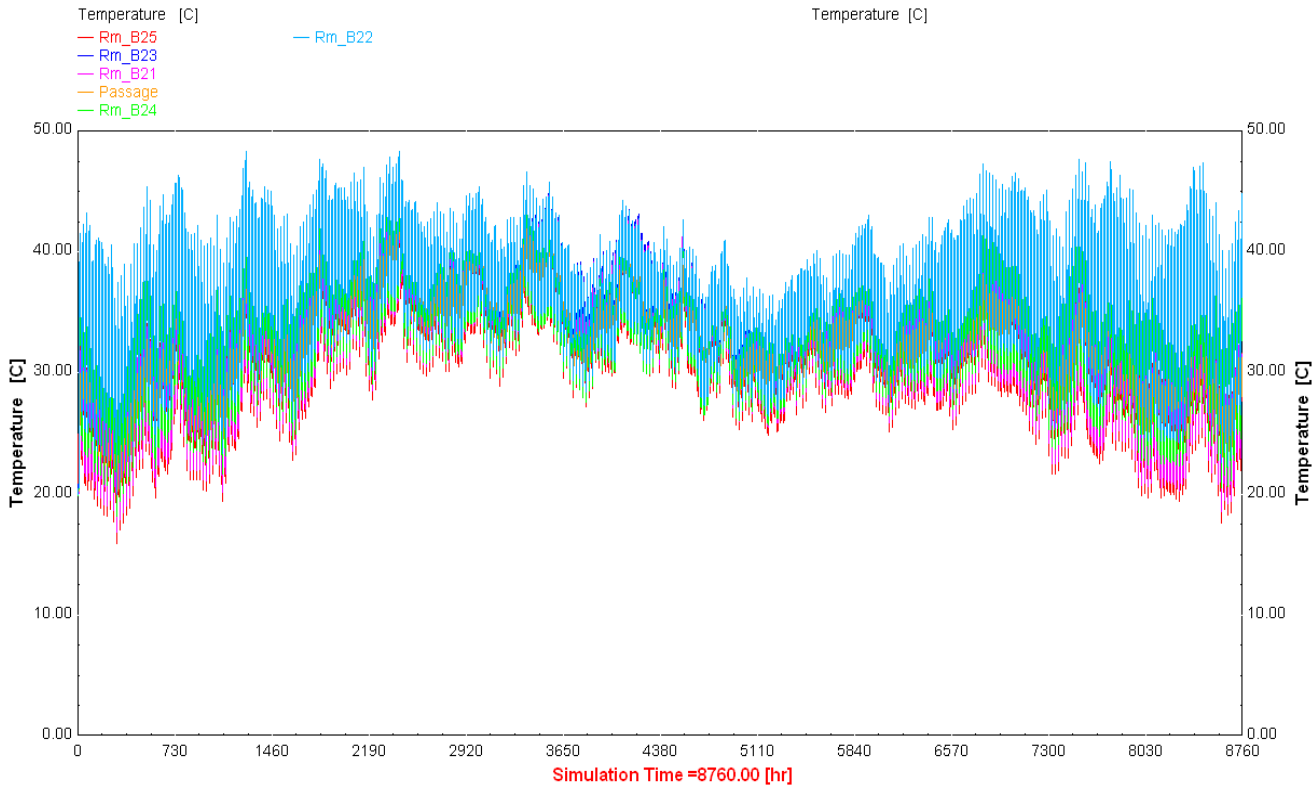


Fig. 4.3: Year round temperature variation within the zones without cooling

As seen from figure4.3, the temperature variation within the zones are well above the set point temperature of 24^{o}C, with temperatures rising above 40^{o}C in some instances. This is as a result of occupants activities within the zones as well as solar radiation reaching the zones.

4.2.1Results from optimization of the absorption air conditioning system components

This section presents the results from the optimization of the collector area and storage tank volume. This was done to maximize the COP, SCOP and SF at the same time achieve the desired set point temperature within the zones.

Figures 4.4 to 4.27 shows the graphs of COP vs collector area and SCOP vs collector area with varying hot water storage tank volumes.

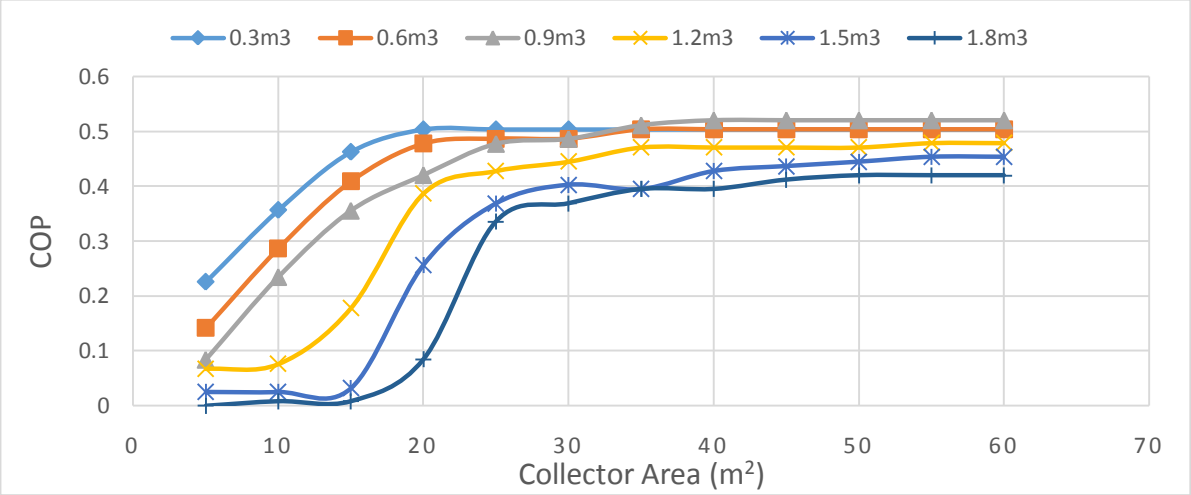


Fig. 4.4: Variation of COP with collector area and hot water storage tank volume for January

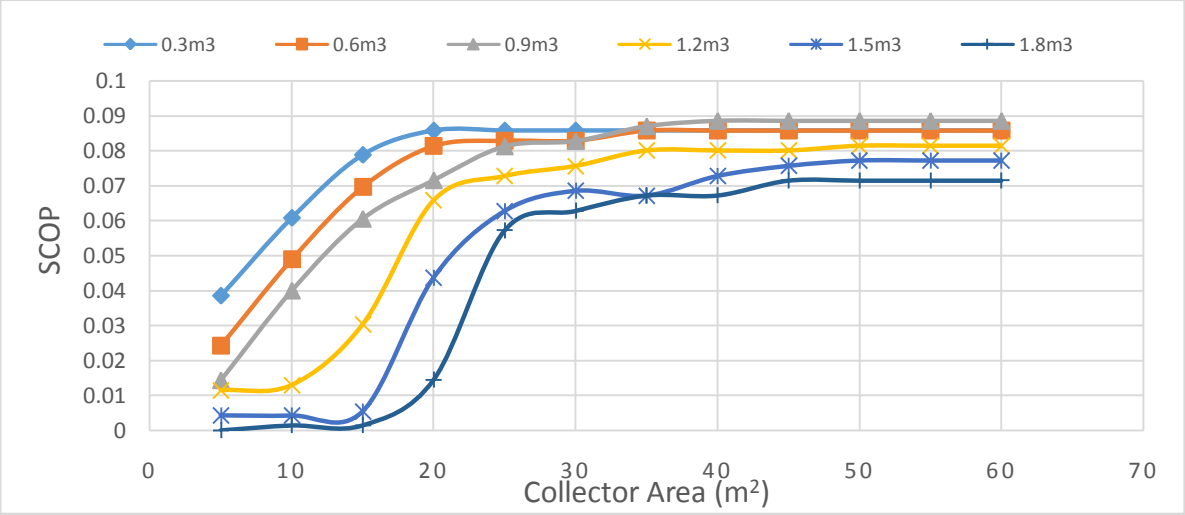


Fig. 4.5: Variation of SCOP with collector area and hot water storage tank volume for January

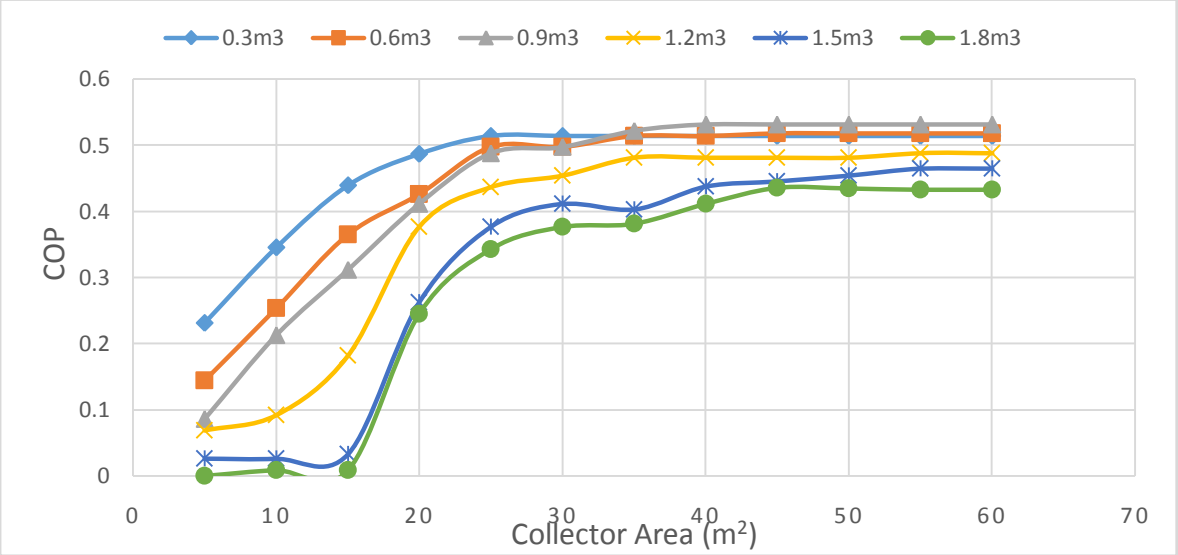


Fig. 4.6: Variation of COP with collector area and hot water storage tank volume for February

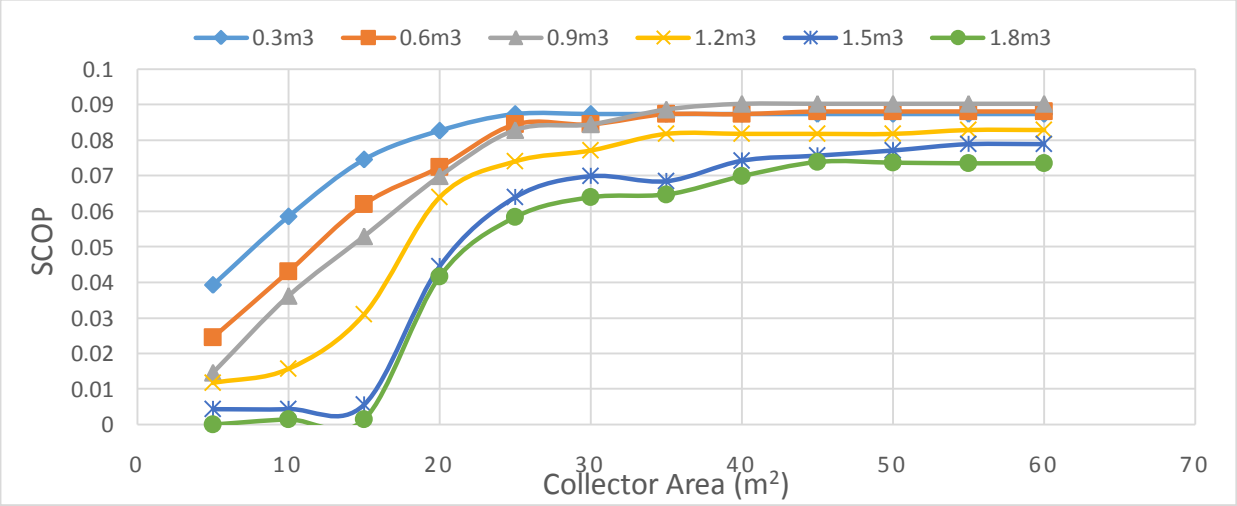


Fig. 4.7: Variation of SCOP with collector area and hot water storage tank volume for February

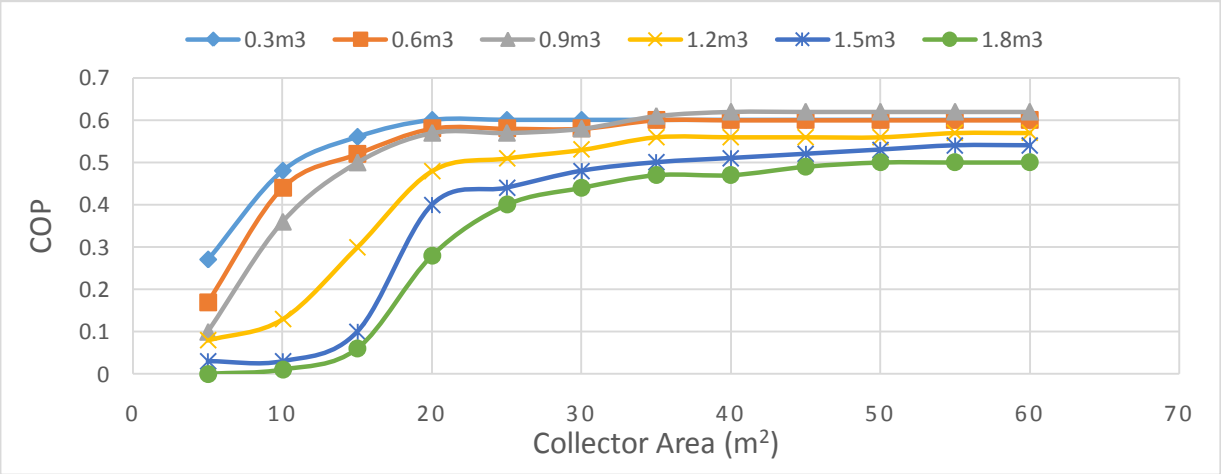


Fig. 4.8: Variation of COP with collector area and hot water storage tank volume March

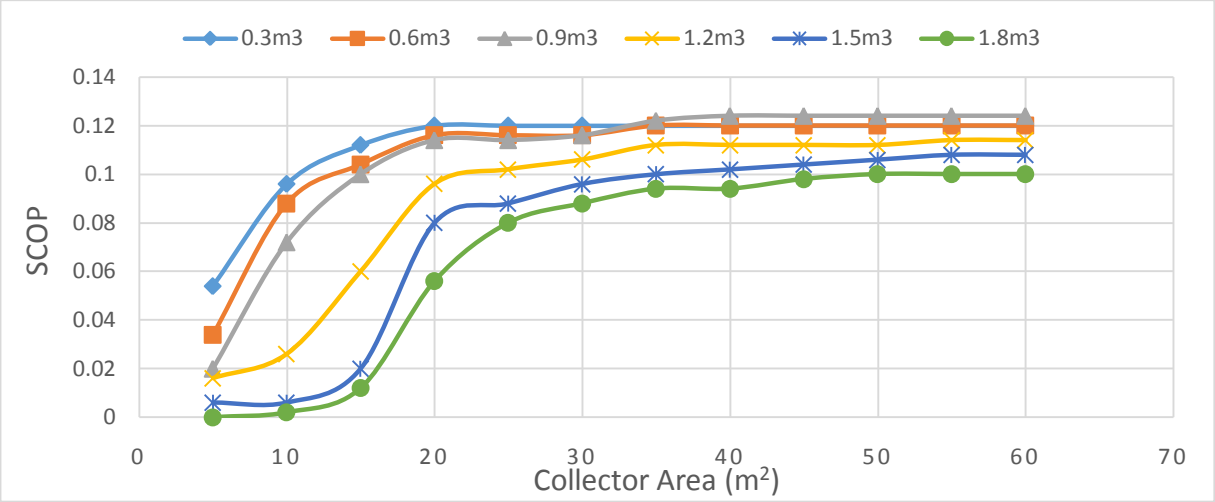


Fig. 4.9: Variation of SCOP with collector area and hot water storage tank volume for March

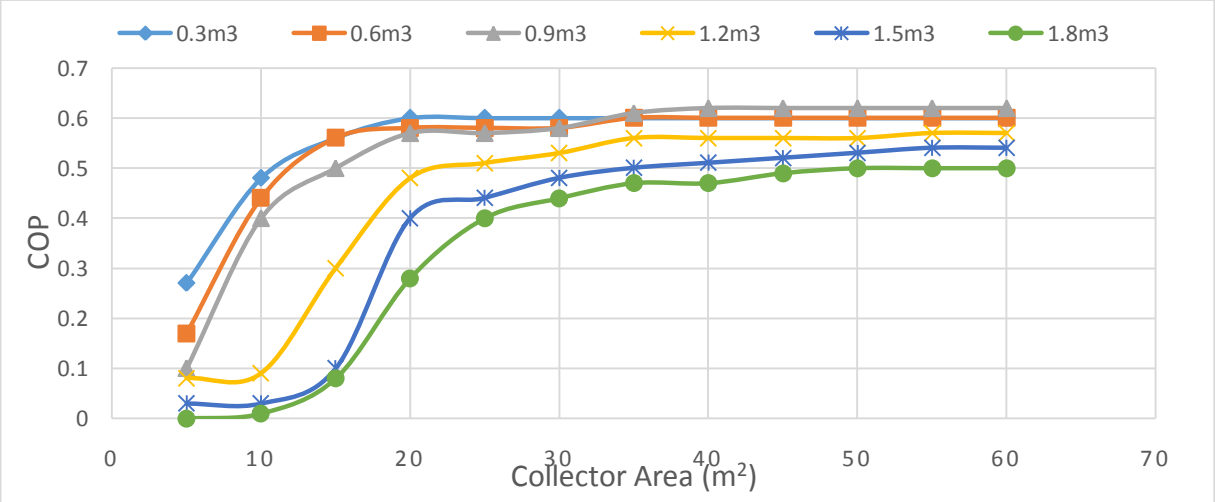


Fig. 4.10: Variation of COP with collector area and hot water storage tank volume for April

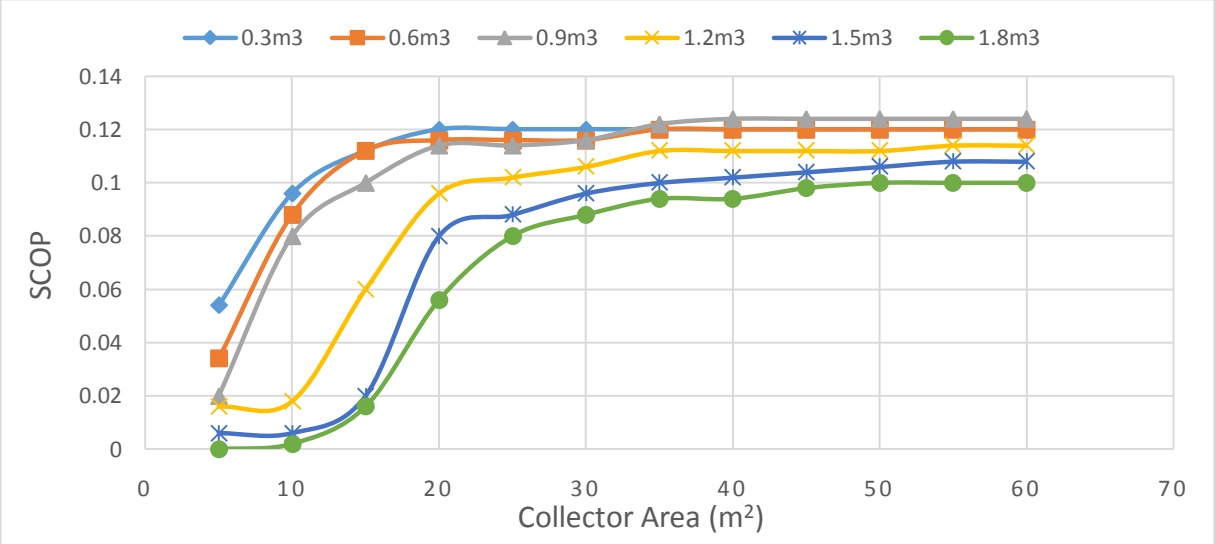


Fig. 4.11: Variation of SCOP with collector area and hot water storage tank volume for April

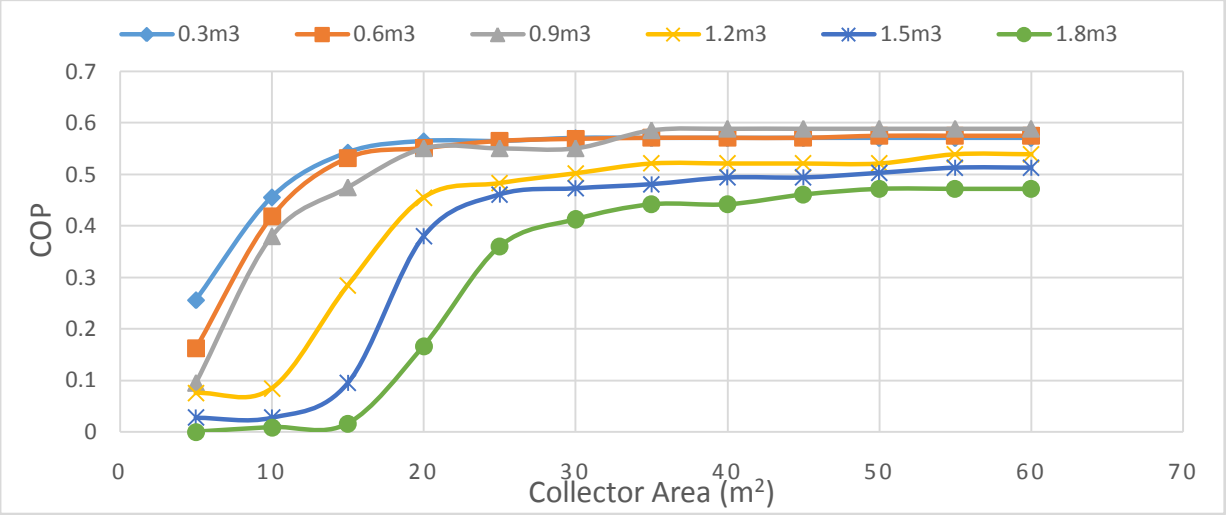


Fig. 4.12: Variation of COP with collector area and hot water storage tank volume for May

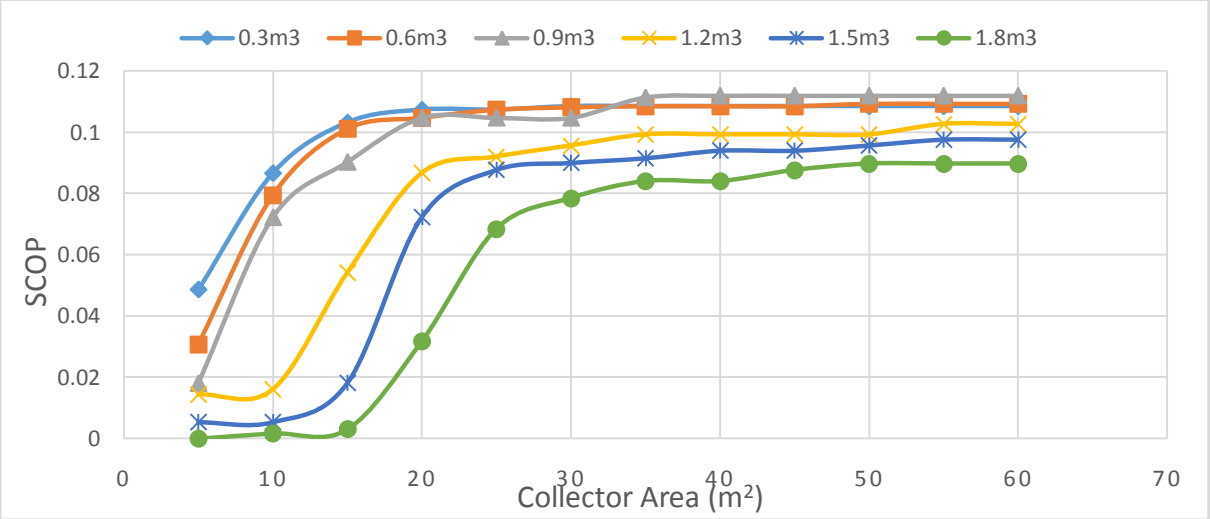


Fig. 4.13: Variation of SCOP with collector area and hot water storage tank volume for May

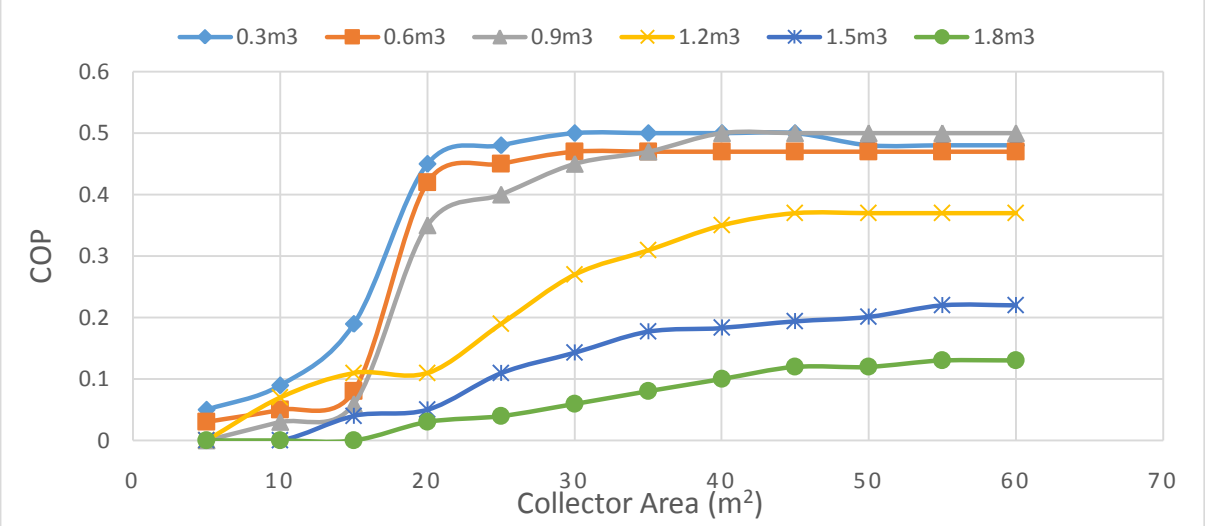


Fig. 4.14: Variation of COP with collector area and hot water storage tank volume for June

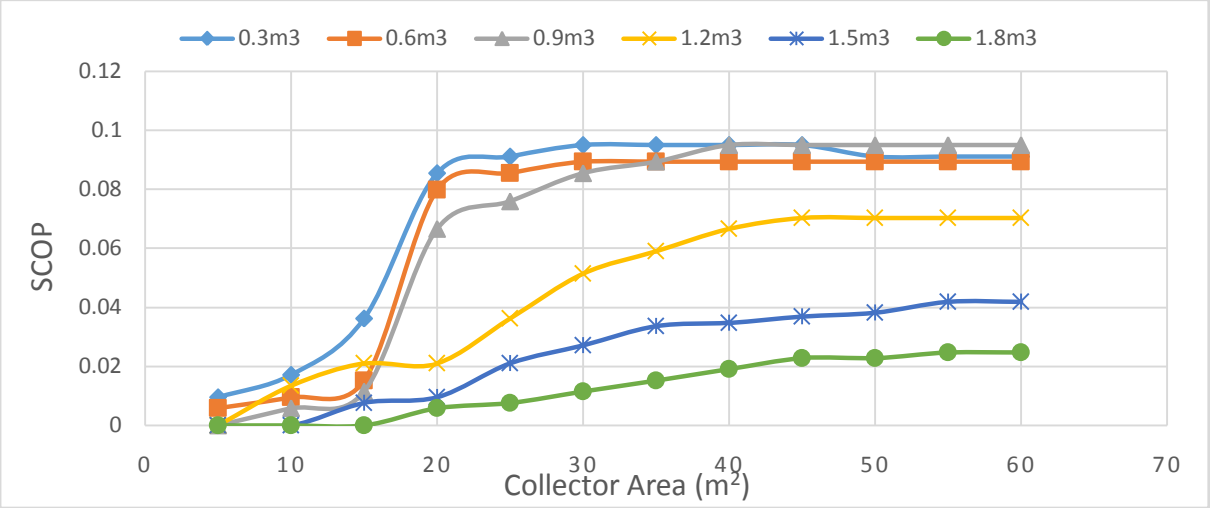


Fig. 4.15: Variation of SCOP with collector area and hot water storage tank volume for June

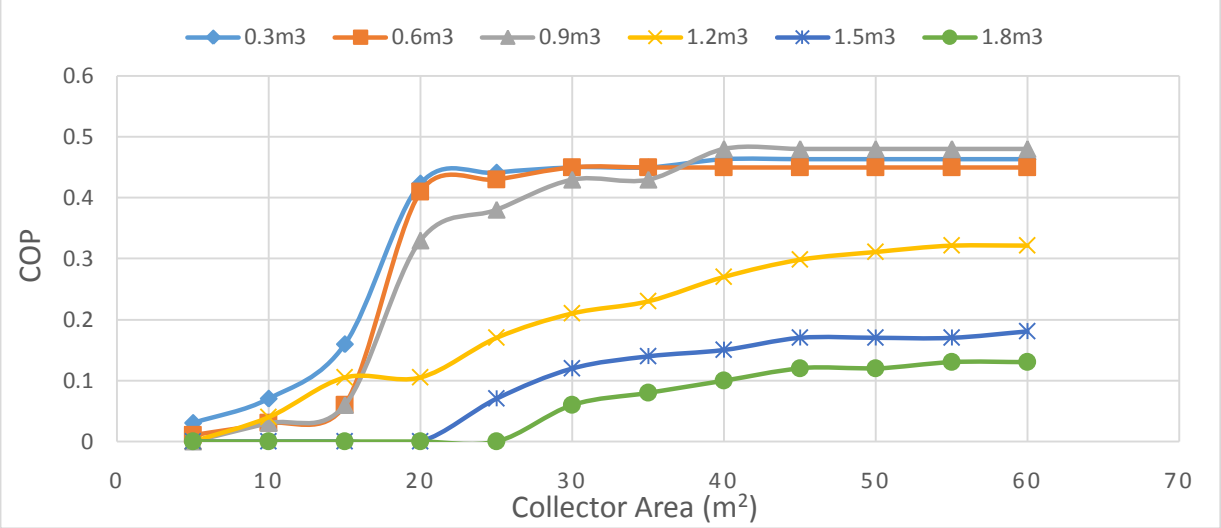


Fig. 4.16: Variation of COP with collector area and hot water storage tank volume for July

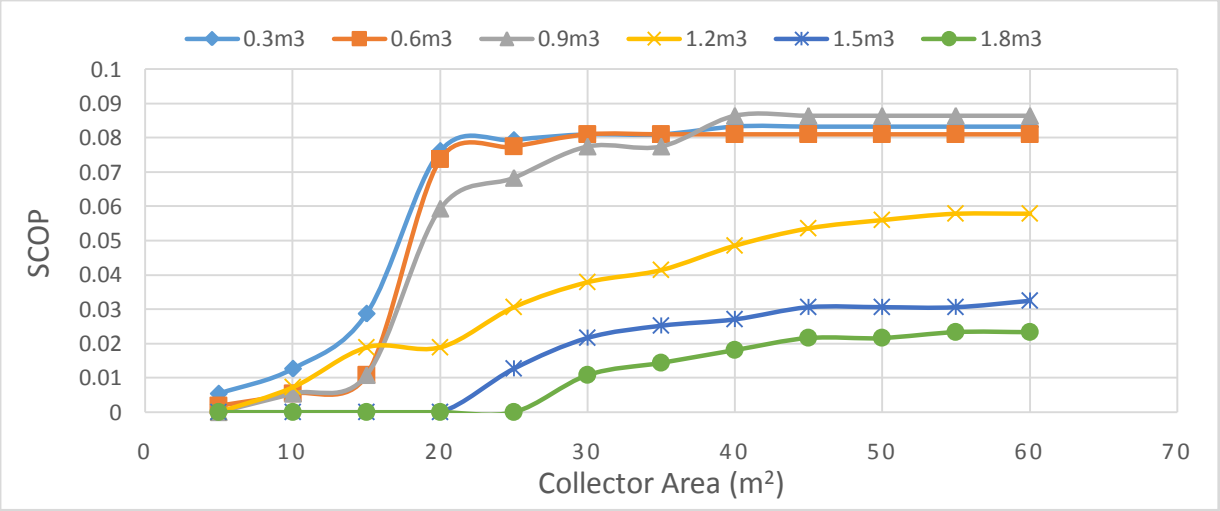


Fig. 4.17: Variation of SCOP with collector area and hot water storage tank volume for July

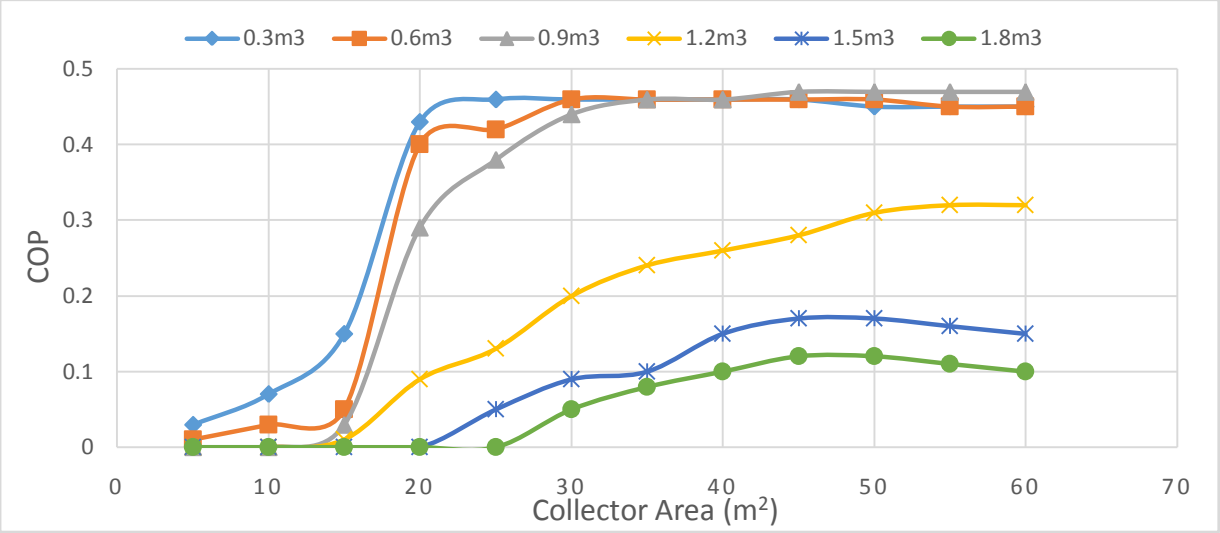


Fig. 4.18: Variation of COP with collector area and hot water storage tank volume for August

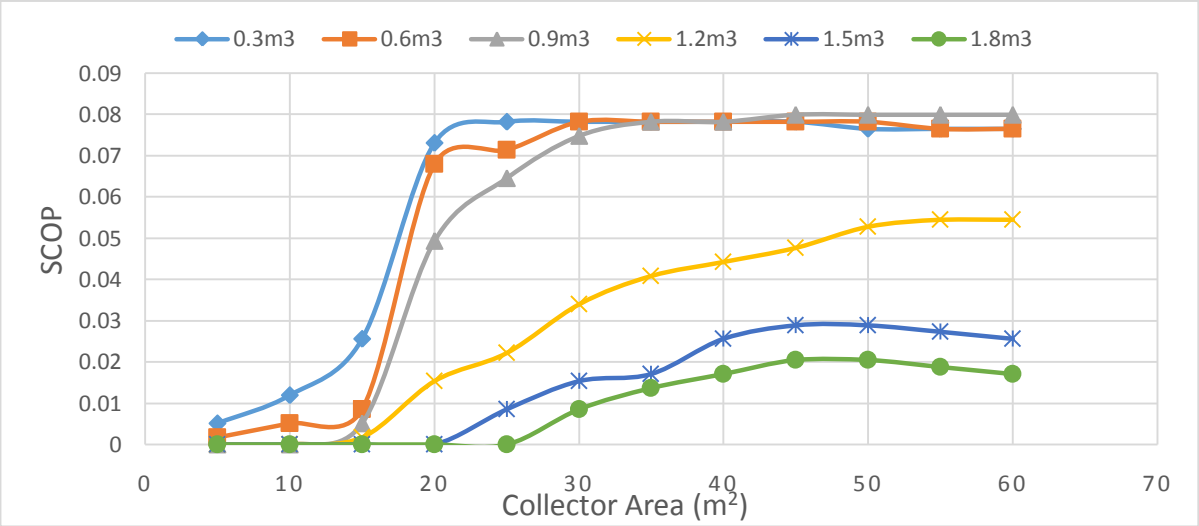


Fig. 4.19: Variation of SCOP with collector area and hot water storage tank volume for August

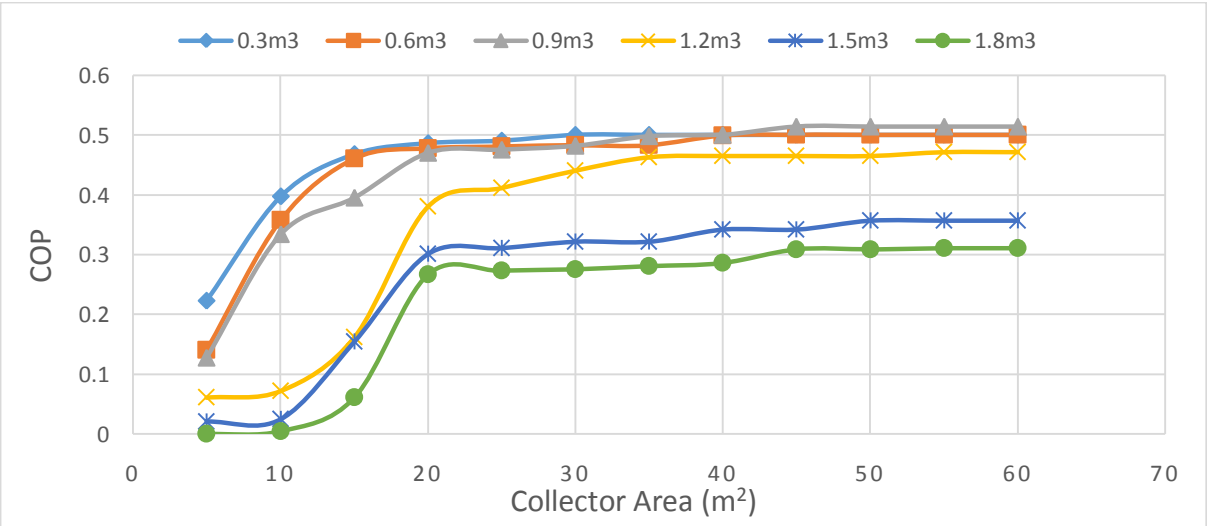


Fig. 4.20: Variation of COP with collector area and hot water storage tank volume for September

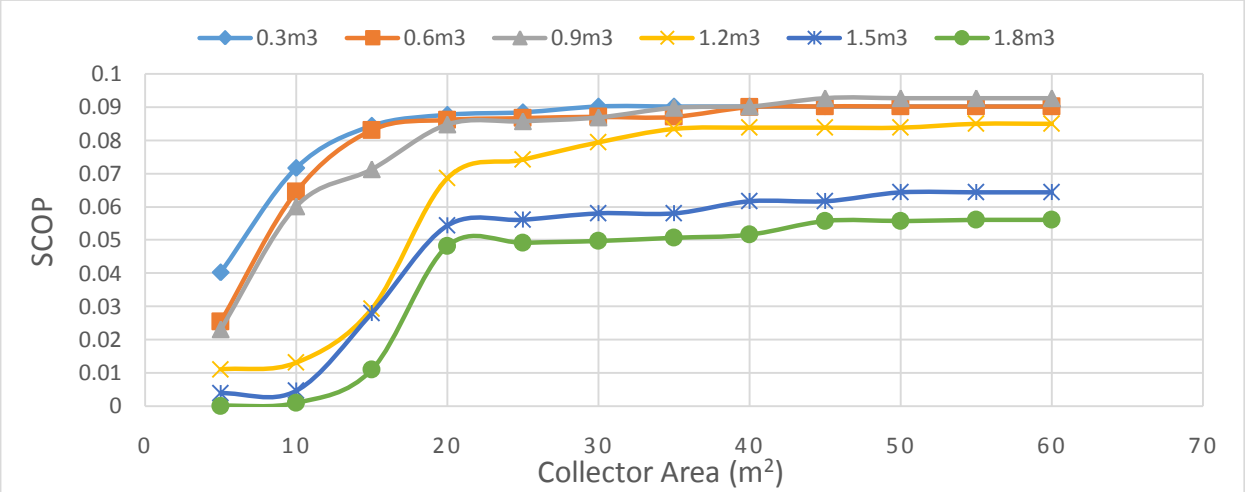


Fig. 4.21: Variation of SCOP with collector area and hot water storage tank volume for September

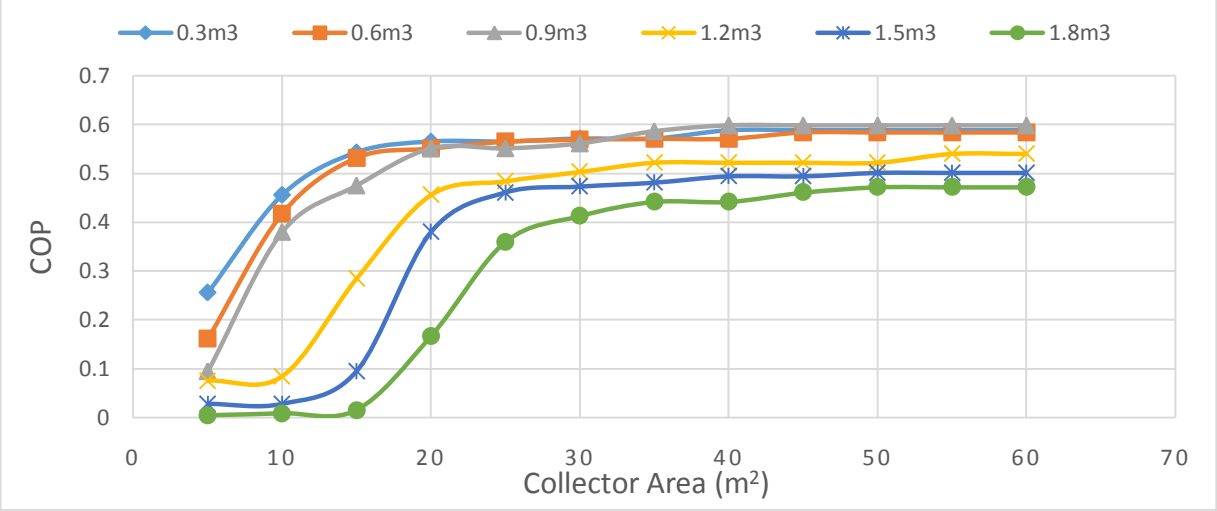


Fig. 4.22: Variation of COP with collector area and hot water storage tank volume for October

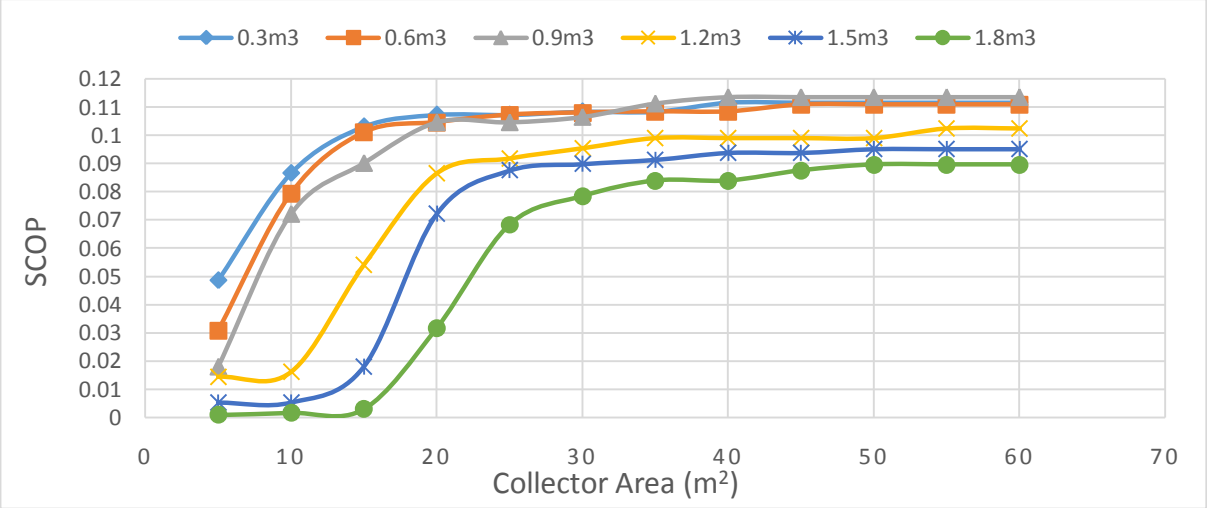


Fig. 4.23: Variation of SCOP with collector area and hot water storage tank volume for October

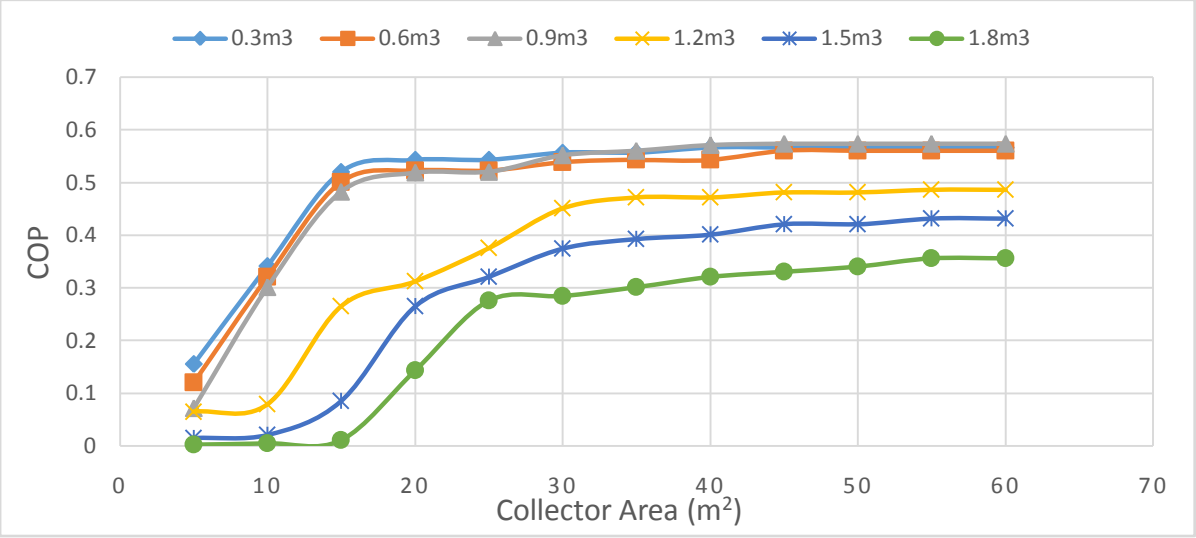


Fig. 4.24: Variation of COP with collector area and hot water storage tank volume for November

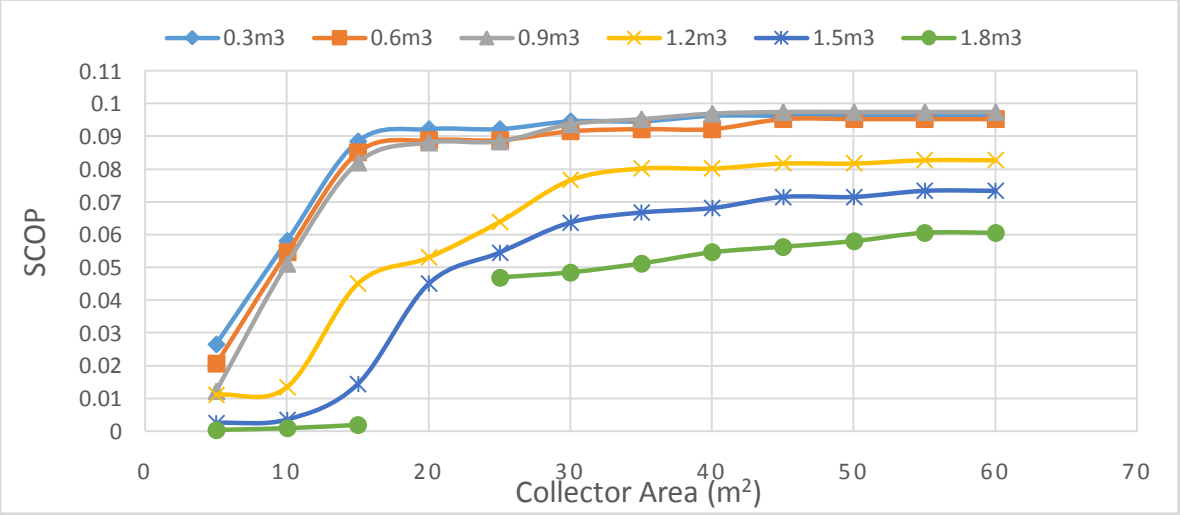


Fig. 4.25: Variation of SCOP with collector area and hot water storage tank volume for November

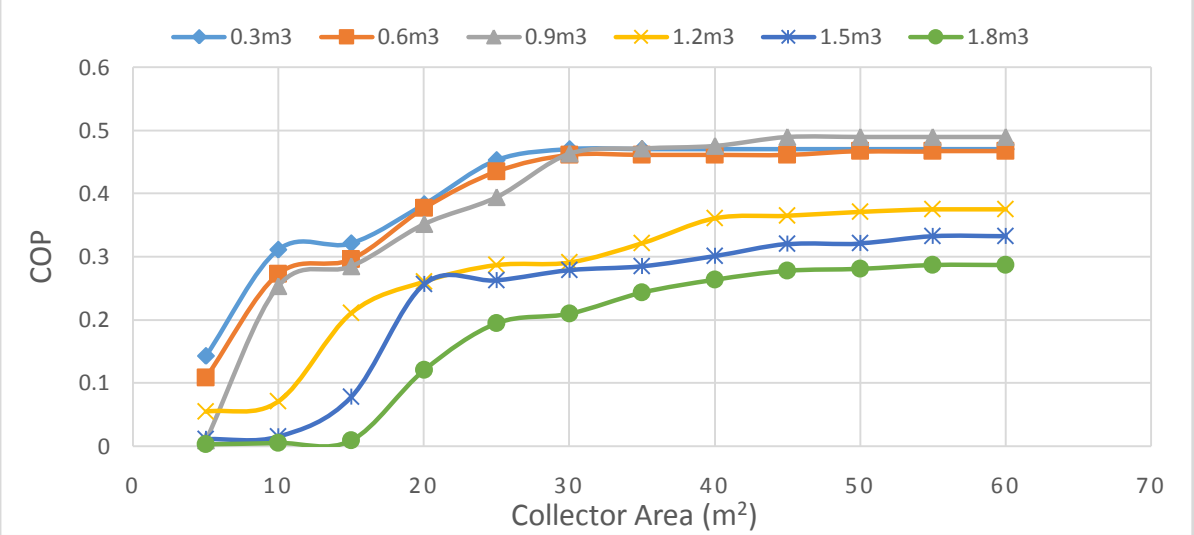


Fig. 4.26: Variation of COP with collector area and hot water storage tank volume for December

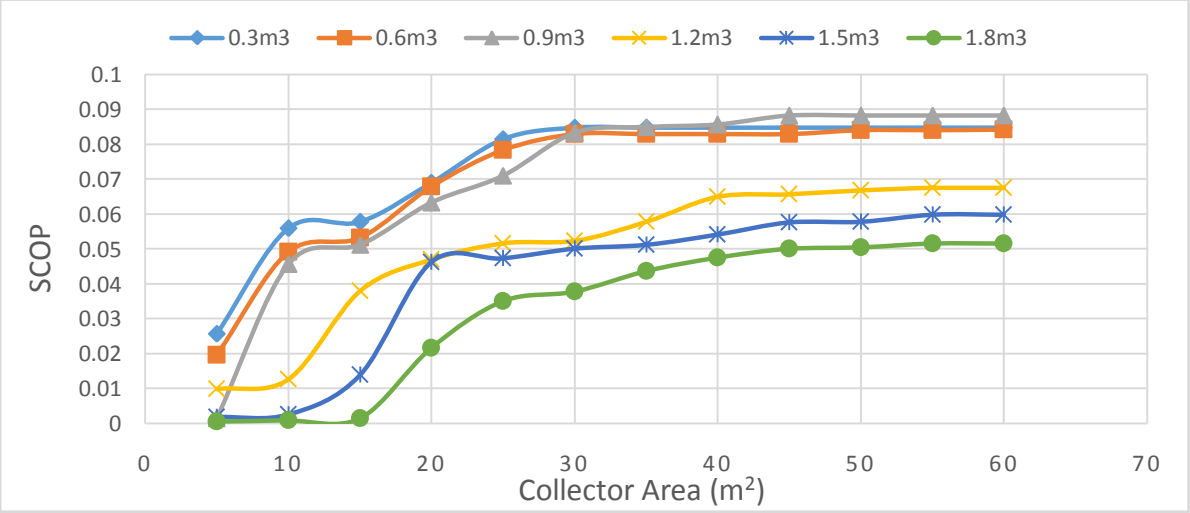


Fig. 4.27: Variation of SCOP with collector area and hot water storage tank volume for December

From figures. 4.4 to 4.27, it is seen that for all the months, the COP increases with increasing collector area, this is because a larger collector area harnesses more thermal energy, thus resulting to better performance. The COP however gets to a peak where increase in collector area doesn't translate to significant increase in COP, this starts at collector area between $30m^2$ to $40m^2$. This is because at this point, the chiller has almost attained its rated COP, increasing the collector area would not necessarily increase the COP beyond the rated limit.Also, the COP decreases with increasing storage tank volume, this is because more thermal energy is required to heat the fluid in the storage tank as the size increases.

However, as the collector area increases, the larger volume tanks begin to record increase in COP. This is because a larger collector area results in harnessing more thermal energy. The larger tanks now have sufficient thermal energy to raise the temperature of the water in the tank to the required set point to keep the system running even when solar radiation has dropped. There is a collector area that optimizes the storage tank volume. As seen from the figures, starting from a collector area of between $35m^2$ and $40m^2$, the $0.9m^3$ tank gives a higher COP than both the $0.3m^3$ and $0.6m^3$ tanks. Storage tank volume of $0.9m^3$ performs best for all months. The month of April has the highest COP,

while the month of August has the lowest COP. Maximum COP of 0.62 is attainable in the month of April with $40m^2$ collector area, while maximum COP of 0.47 is attainable with $40m^2$ collector area for the month of August.

From the monthly COP therefore, the optimum collector area is $40m^2$ and the optimum storage tank volume is $0.9m^3$. Similar trend of increasing COP with collector area, as well as decreasing COP with increasing hot water tank volume, leading to optimum sizes of collector and tank have been reported in simulation works: Al – Alili *et al.* (2012) reported an optimum collector area of 60 m^2 and 1 m^3 tank volume for a cooling load of 10 kW, resulting in a COP of 0.54 in Abu Dhabi.

For all the months, the SCOP increases with increasing collector area and decreases with increasing storage tank volume. It also gets to a point where increase in collector area does not translate to significant increase in SCOP.

The months of March and April have the highest SCOP of 0.12 with $40m^2$ collector area as seen in figures 4.9 and 4.11 respectively. This is the maximum attainable SCOP for the system. The month of August has the lowest SCOP of 0.08 with $40m^2$ collector area as seen in figure 4.19. This is the lowest SCOP for the system. All other months have a SCOP greater than 0.08 with $40m^2$ collector area. The relatively low solar performance of the system for the months of July and August, as compared to the other months is because the months of July and August are the peak of the rainy season with very cloudy days. From the system SCOP therefore, the optimized collector area is $40m^2$.

Figures 4.28 to 4.30shows graph of solar fraction vs collector area for all the months

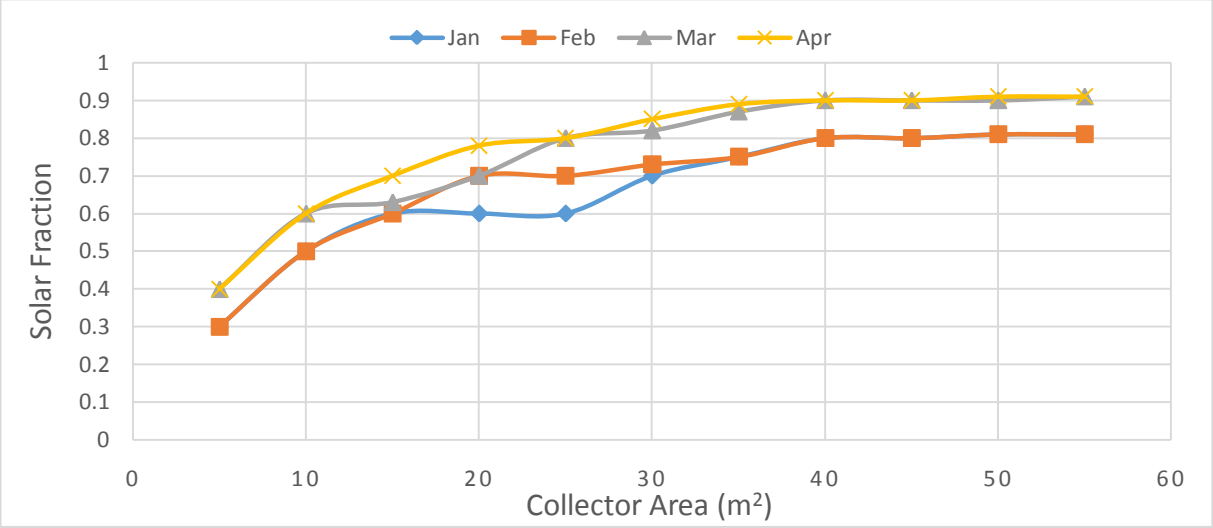


Fig. 4.28: Variation of solar fraction with collector area for the months of January to April.

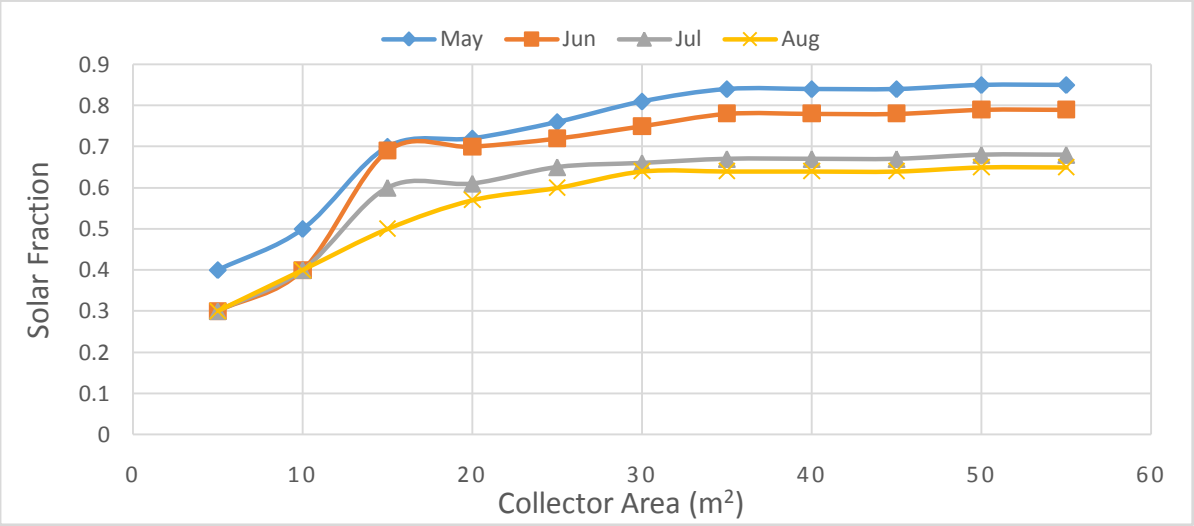


Fig. 4.29: Variation of solar fraction with collector area for the months of May to August.

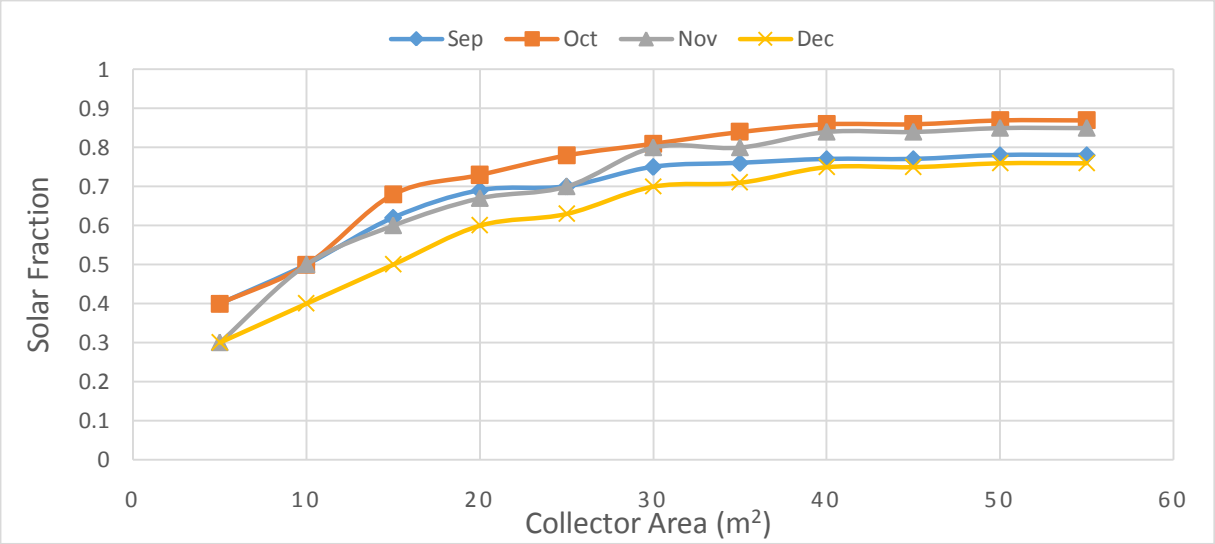


Fig. 4.30: Variation of solar fraction with collector area for the months of September toDecember.

From figures 4.28 to 4.30, the solar fraction is seen to increase with increasing collector area for all months. The months of April and March have the highest solar fraction of 0.9 with a collector area of $40m^2$. The month of August has the lowest solar fraction of 0.64 with a collector area of $35m^2$.

For all the months, solar fraction of 0.6 can be attained with $30m^2$ collector area. However, apart from the months of July and August, which record a solar fraction of 0.67 and 0.65 respectively with a collector area of $40m^2$, a solar fraction of at least 0.7 can be achieved for all the other months with $40m^2$ collector area. This is as a result of the lower solar radiation in the cloudy months of July and August, therefore, more auxiliary energy is used. Similar trend of increasing solar fraction with collector area have been reported in simulation works: Mendoza *et al.*, 2013, reported an optimum collector area of $600m^2$ and hot water tank volume of 16 m^3 for a cooling load of 153 kW, resulting in a solar fraction of 0.6 for Guayaquil, Ecuador. From the system solar fraction therefore, the optimum collector area is $40m^2$. The optimized system components therefore are: Absorption chiller: 12 kW, Cooling tower: 15 kW, Solar collector: $40m^2$, Hot water storage tank: $0.9m^3$.

4.2.2: Results from building cooling simulation using optimized absorption air conditioning system components

Figure 4.31 shows the hourly variation of temperatures within the zones with cooling from the optimized absorption air conditioning system for the whole year.

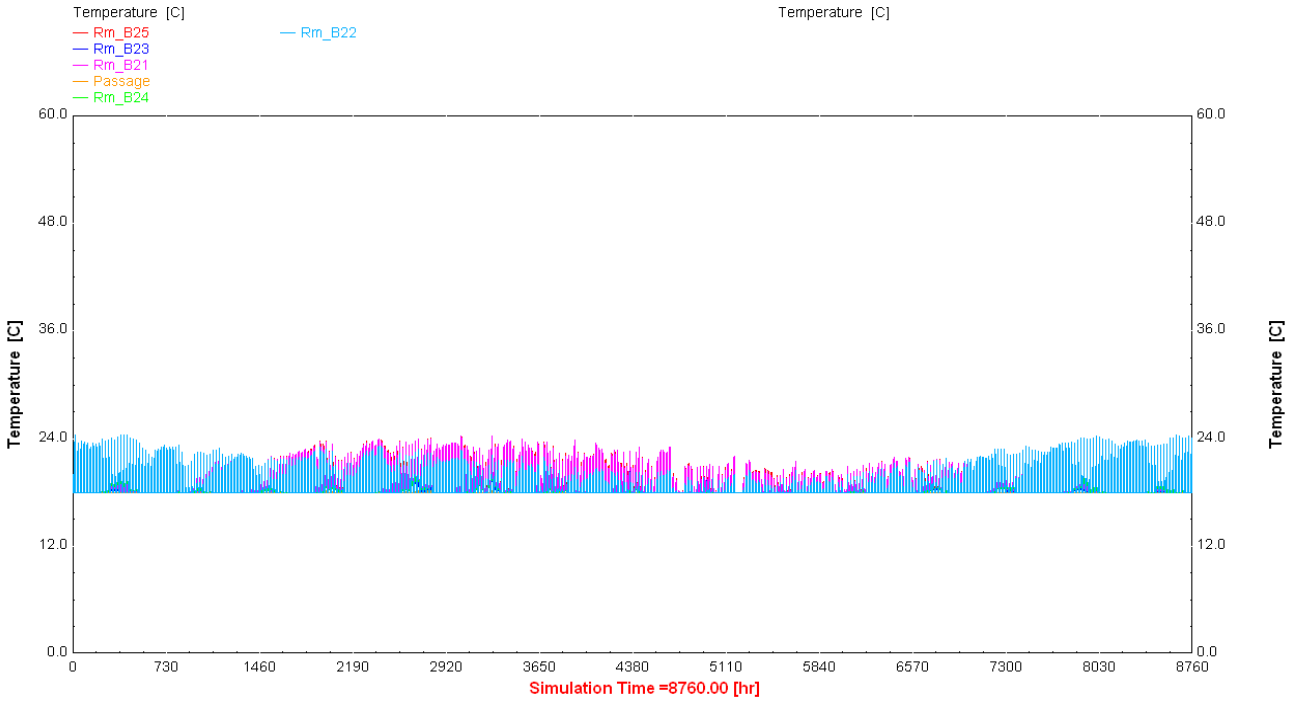


Fig. 4.31: Year round temperature variation within the zones with cooling from the optimized system

As seen from figure 4.31, the optimized gas assisted solar absorption cooling system was able to cool the thermal zones. Temperatures are seen to be at 24^{o}C and below throughout the year.

Figures 4.32 to 4.55 show the variation in relative humidity within the zones without cooling and with cooling from the optimized system on a monthly basis.

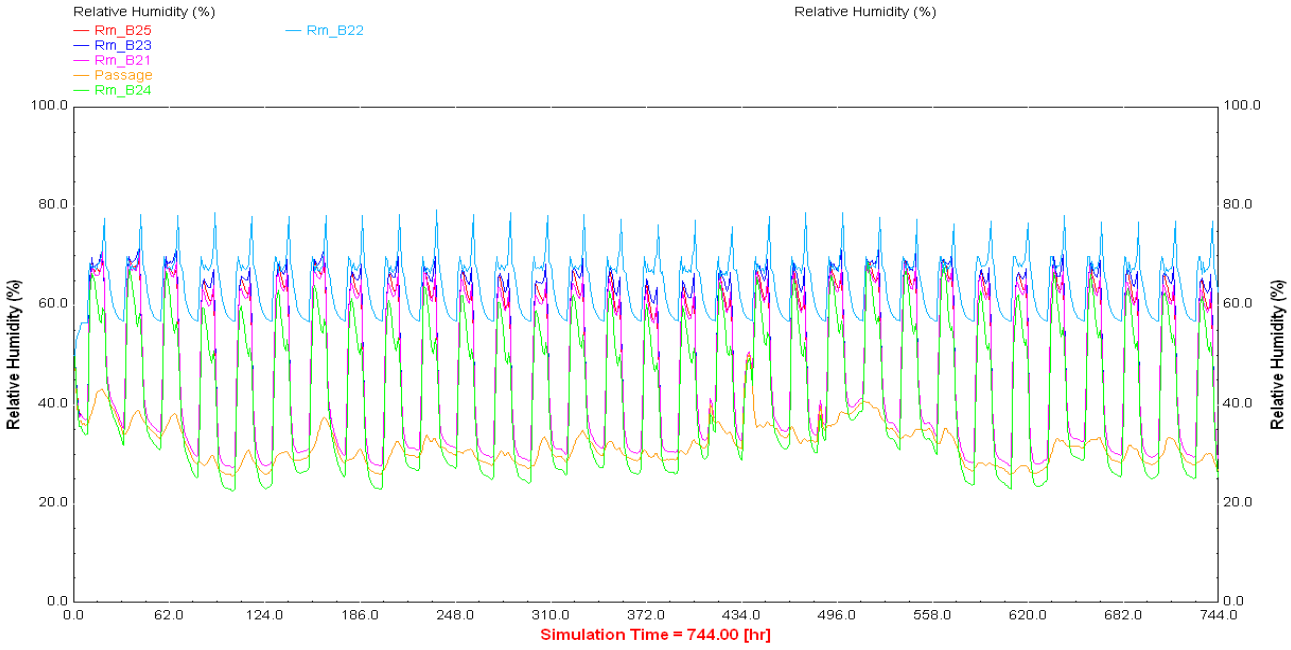


Fig. 4.32: Relative humidity variation within zones, January (no cooling)

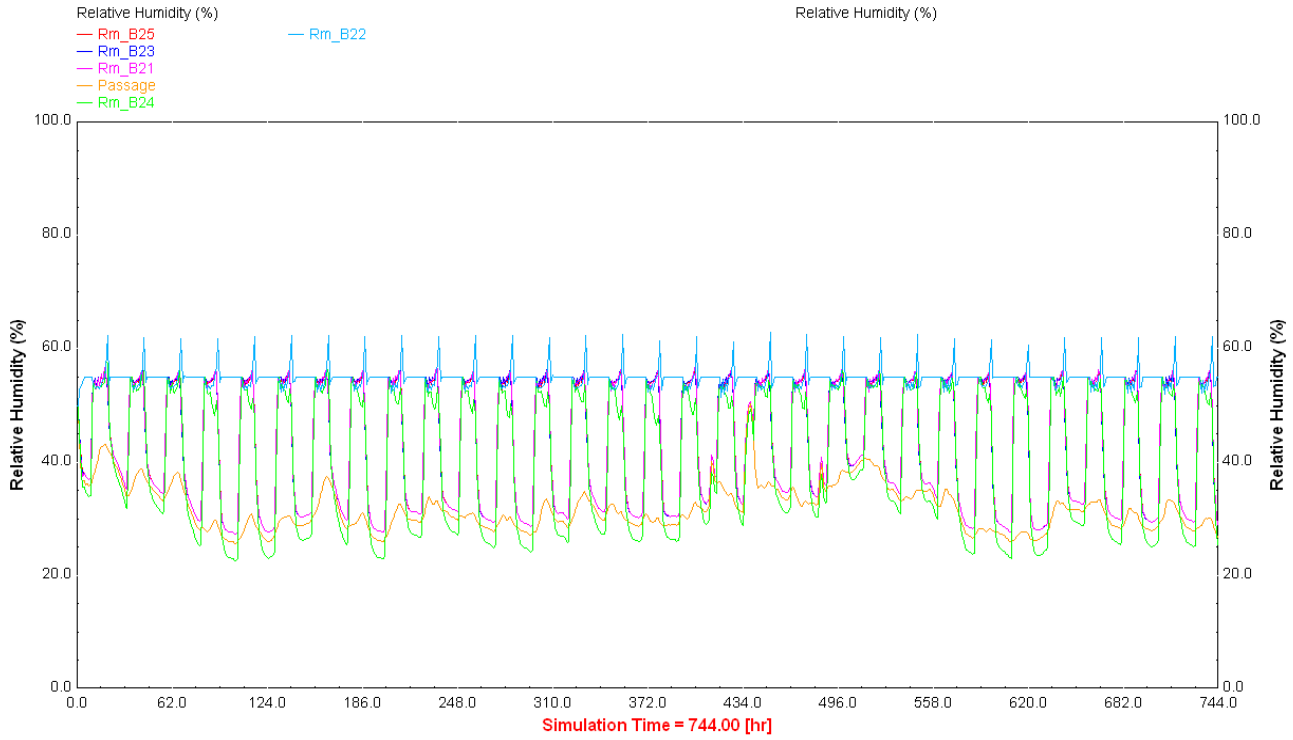


Fig. 4.33: Relative humidity variation within zones, January (with cooling)

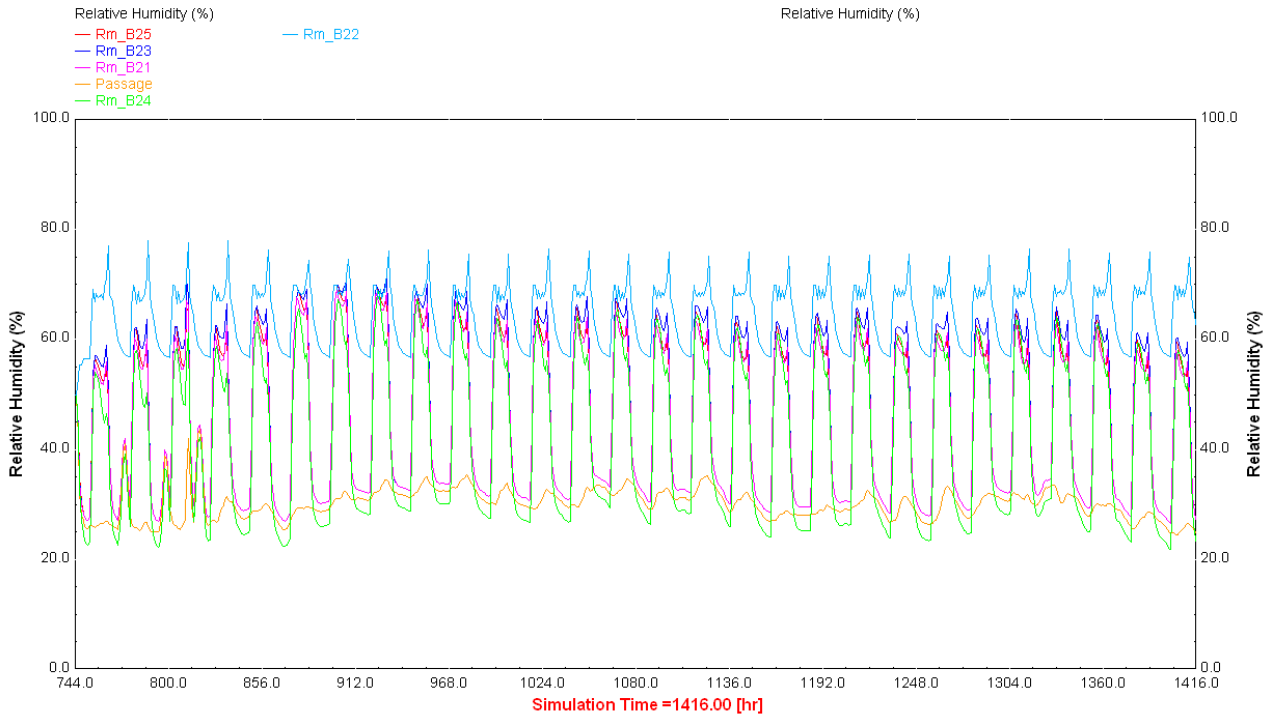


Fig. 4.34: Relative humidity variation within zones, February (no cooling)

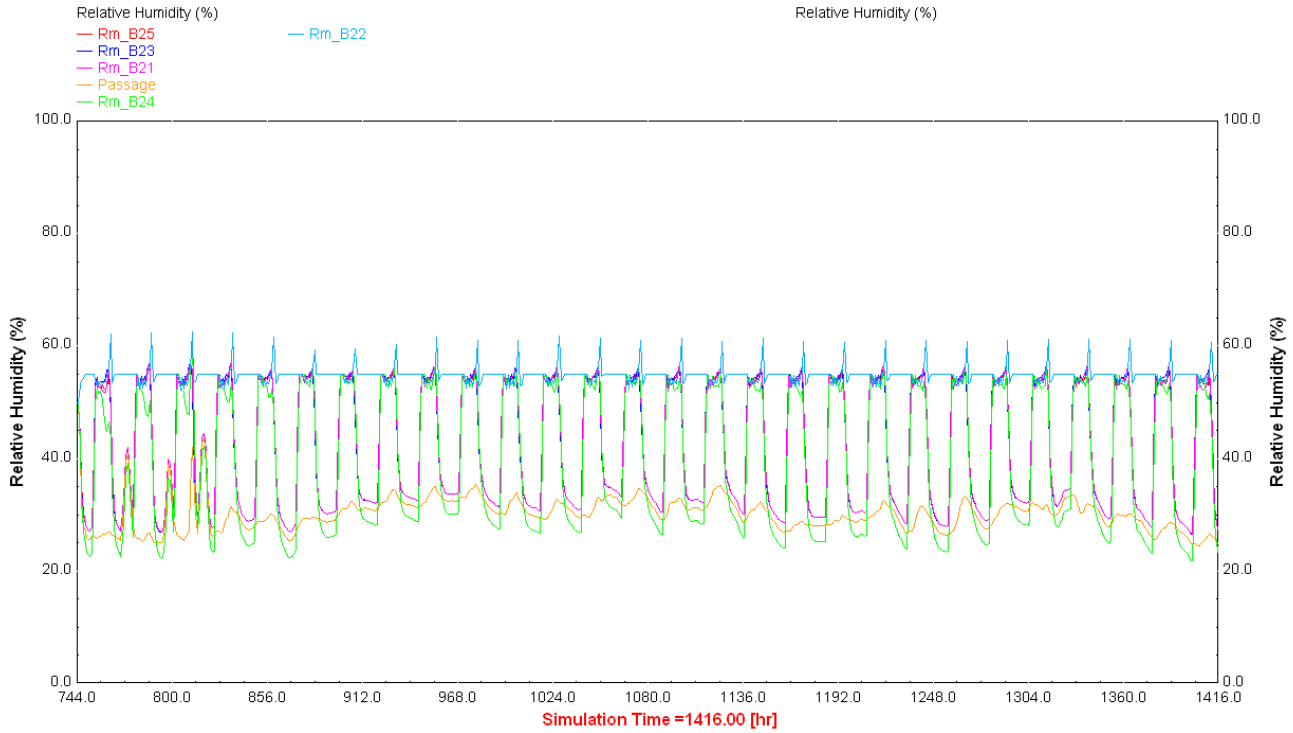


Fig. 4.35: Relative humidity variation within zones, February (with cooling)

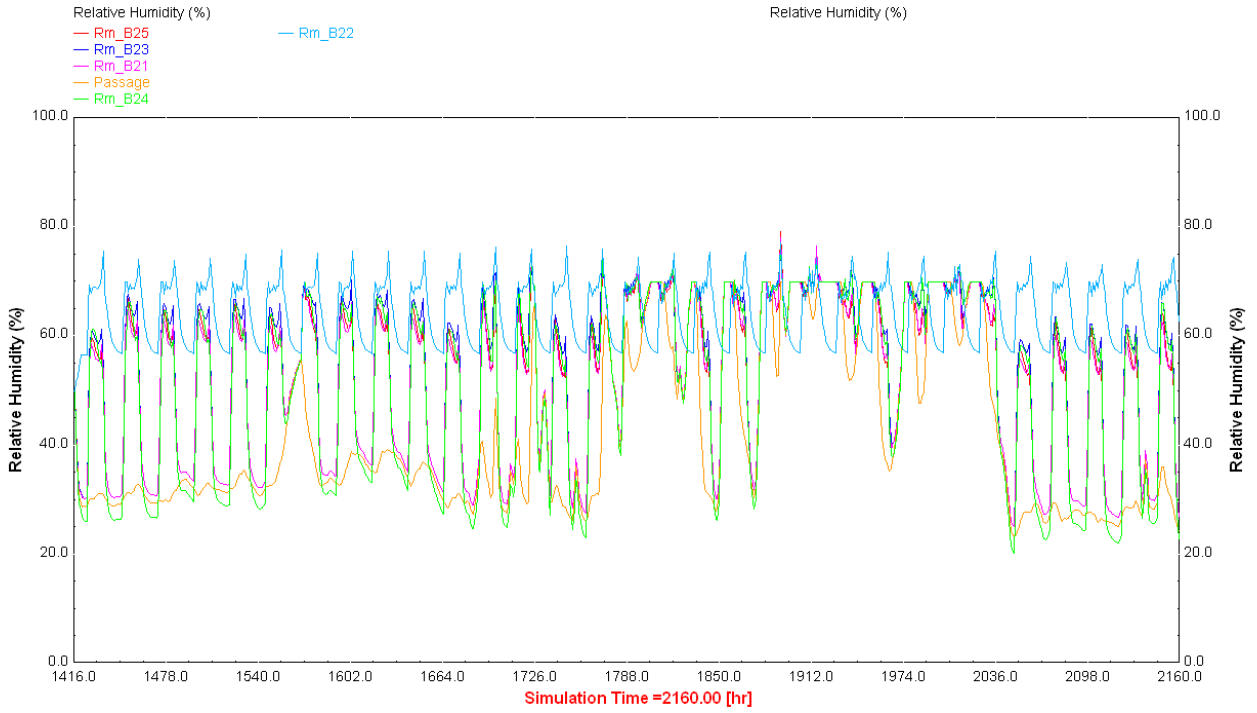


Fig. 4.36: Relative humidity variation within zones, March (no cooling)

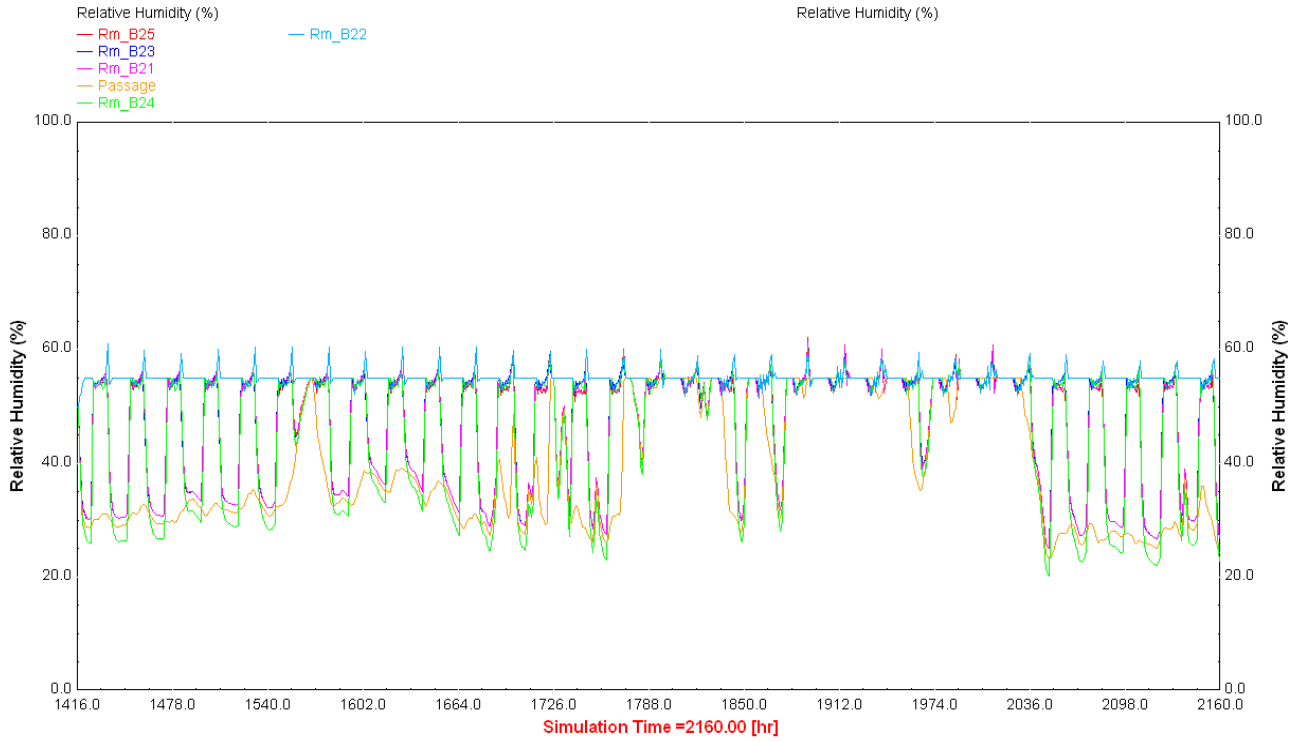


Fig. 4.37: Relative humidity variation within zones, March (with cooling)

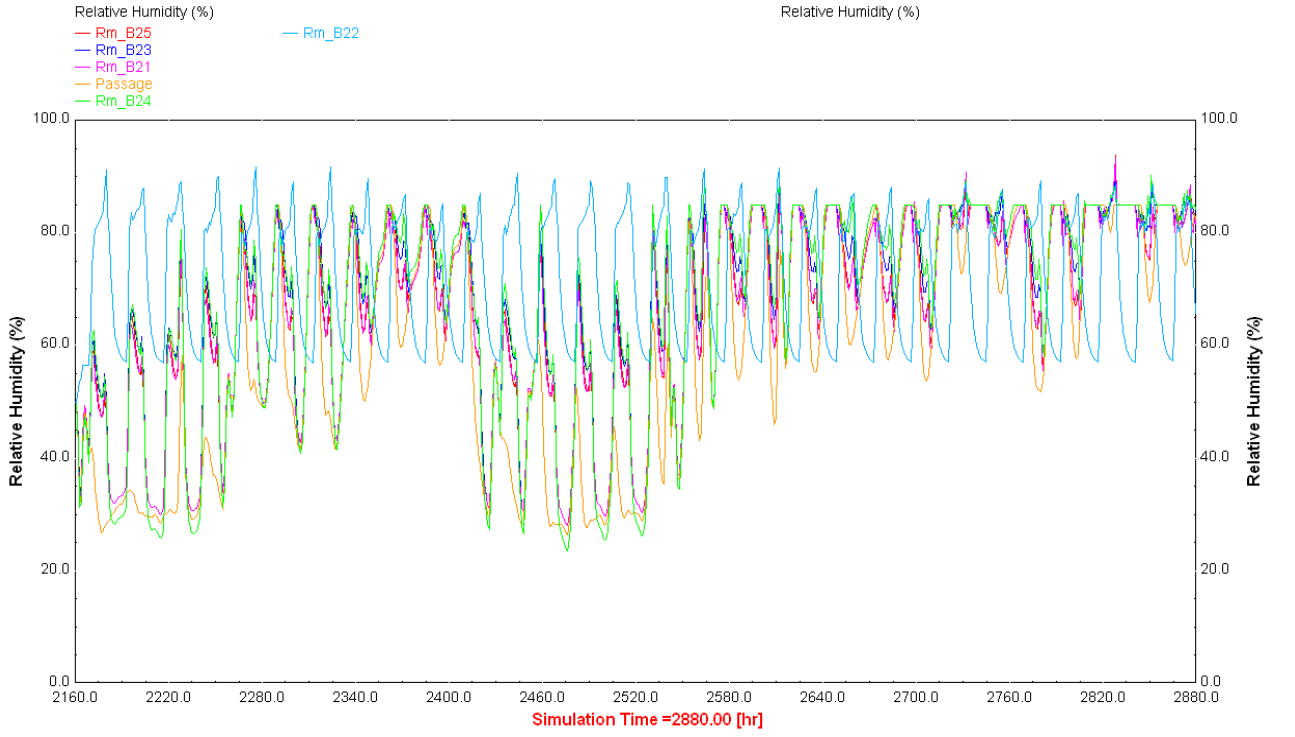


Fig. 4.38: Relative humidity variation within zones, April (no cooling)

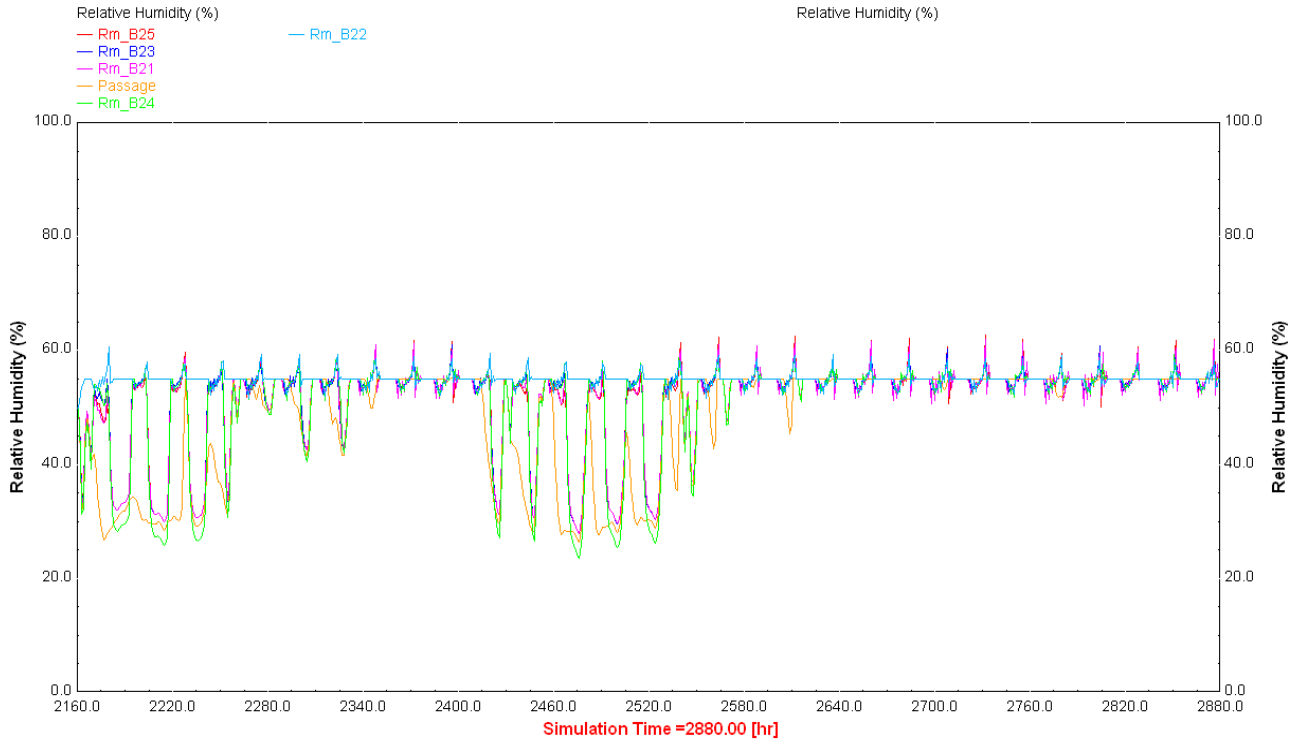


Fig. 4.39: Relative humidity variation within zones, April (with cooling)

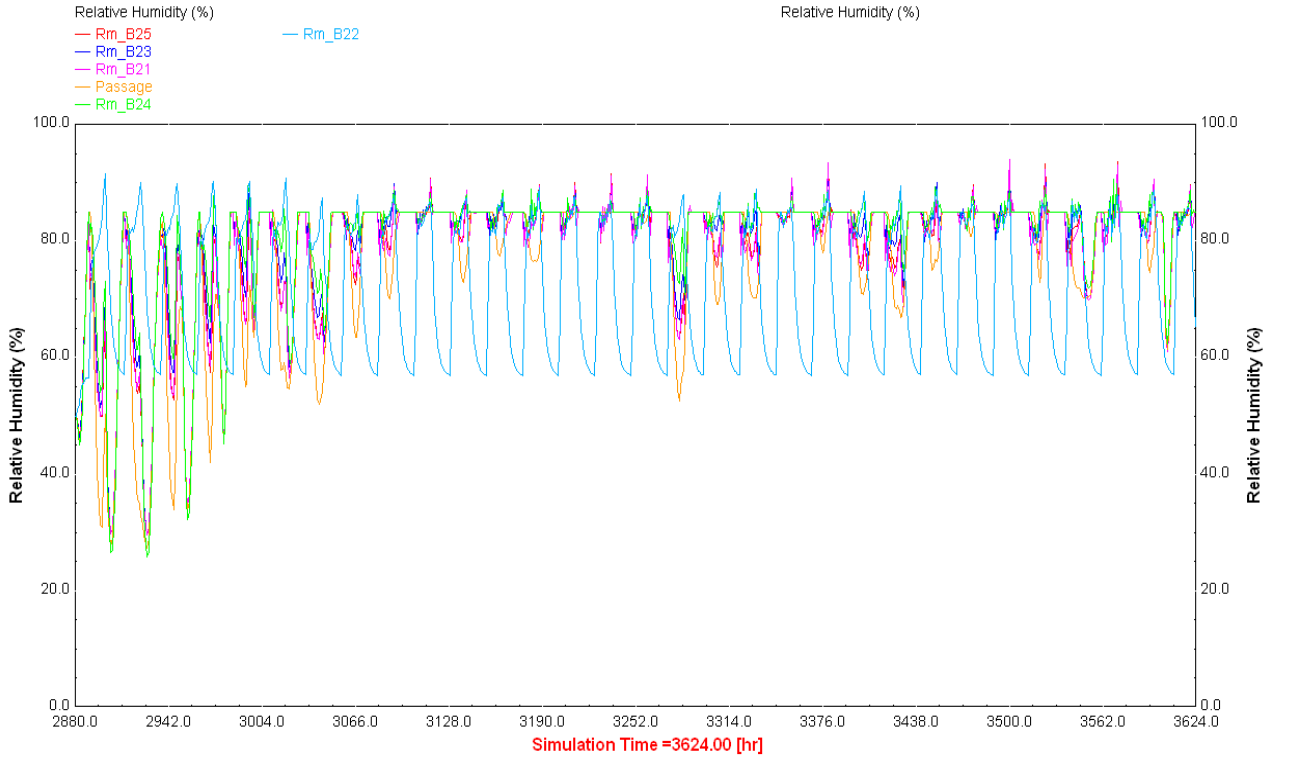


Fig. 4.40: Relative humidity variation within zones, May (no cooling)

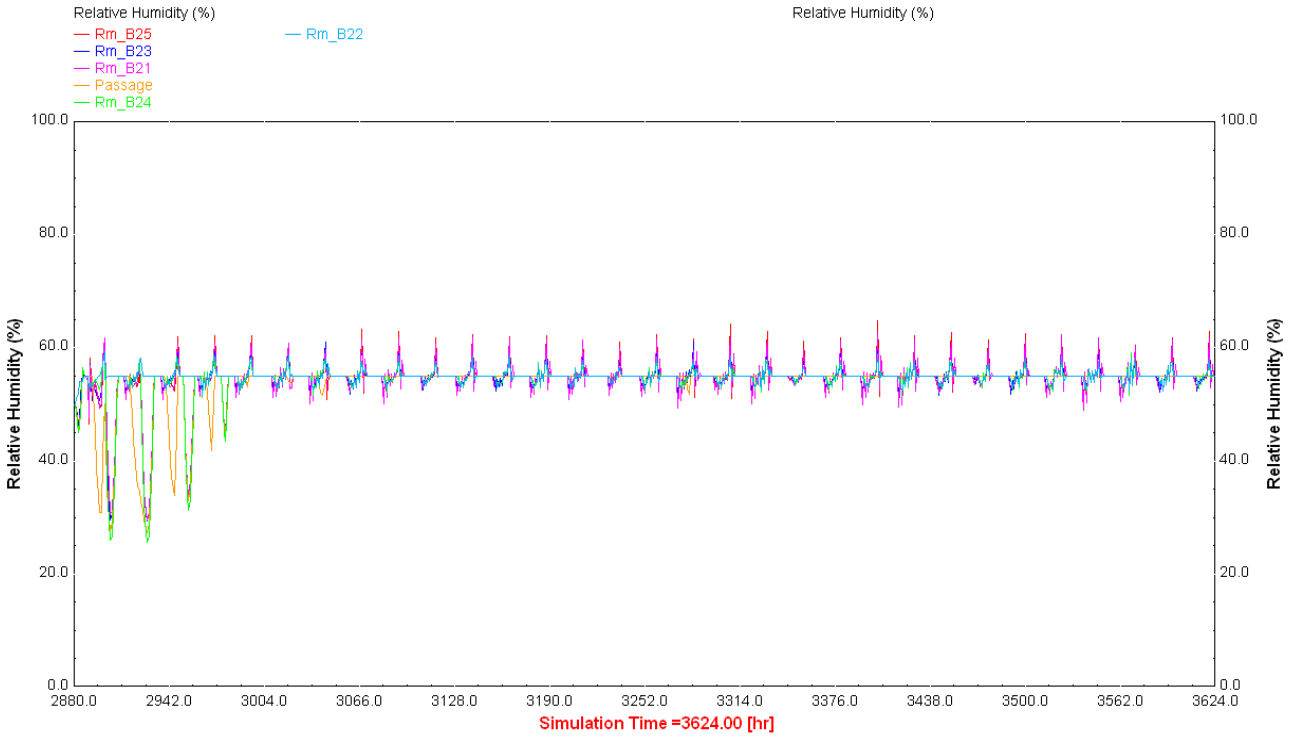


Fig. 4.41: Relative humidity variation within zones, May (with cooling)

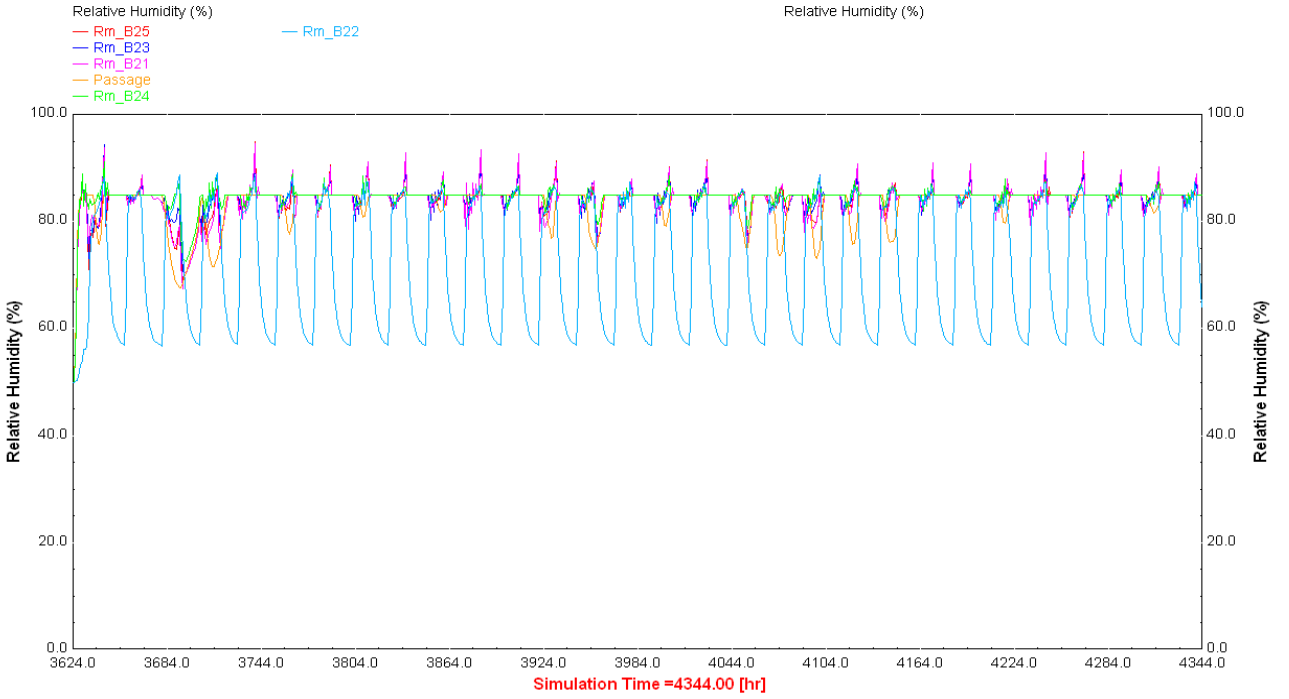


Fig. 4.42: Relative humidity variation within zones, June (no cooling)

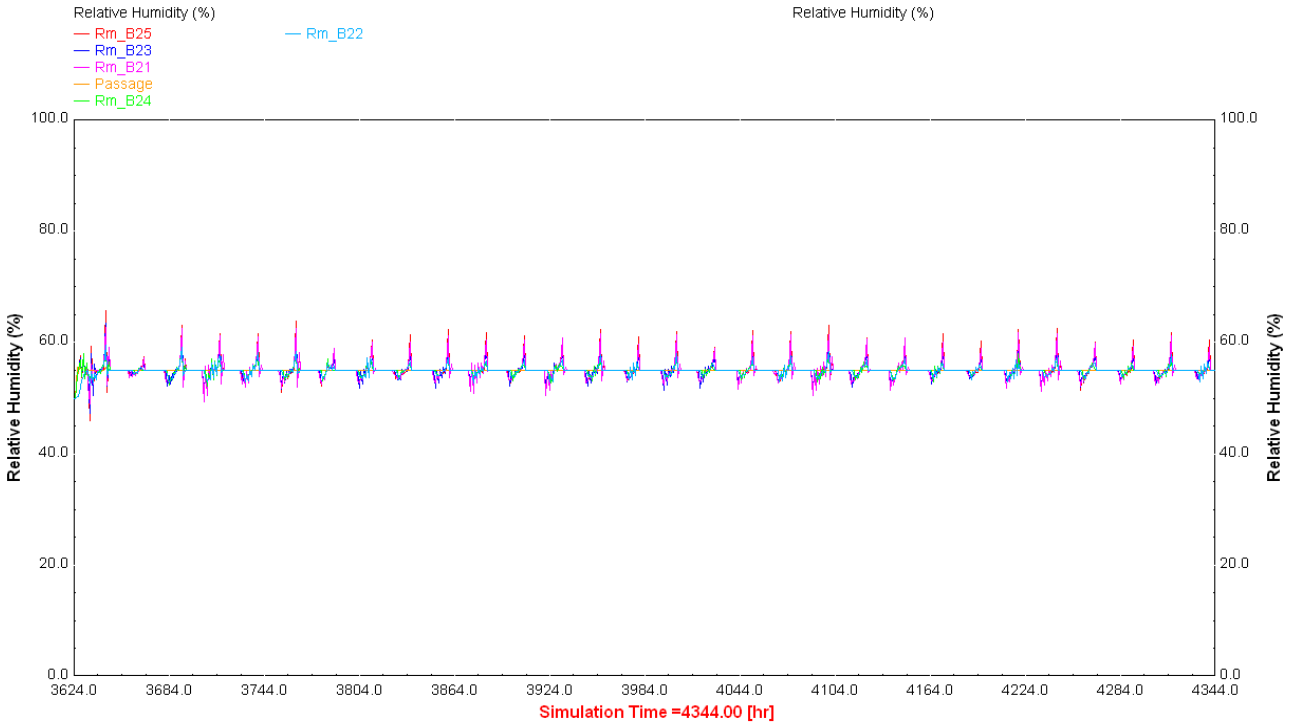


Fig. 4.43: Relative humidity variation within zones, June (with cooling)

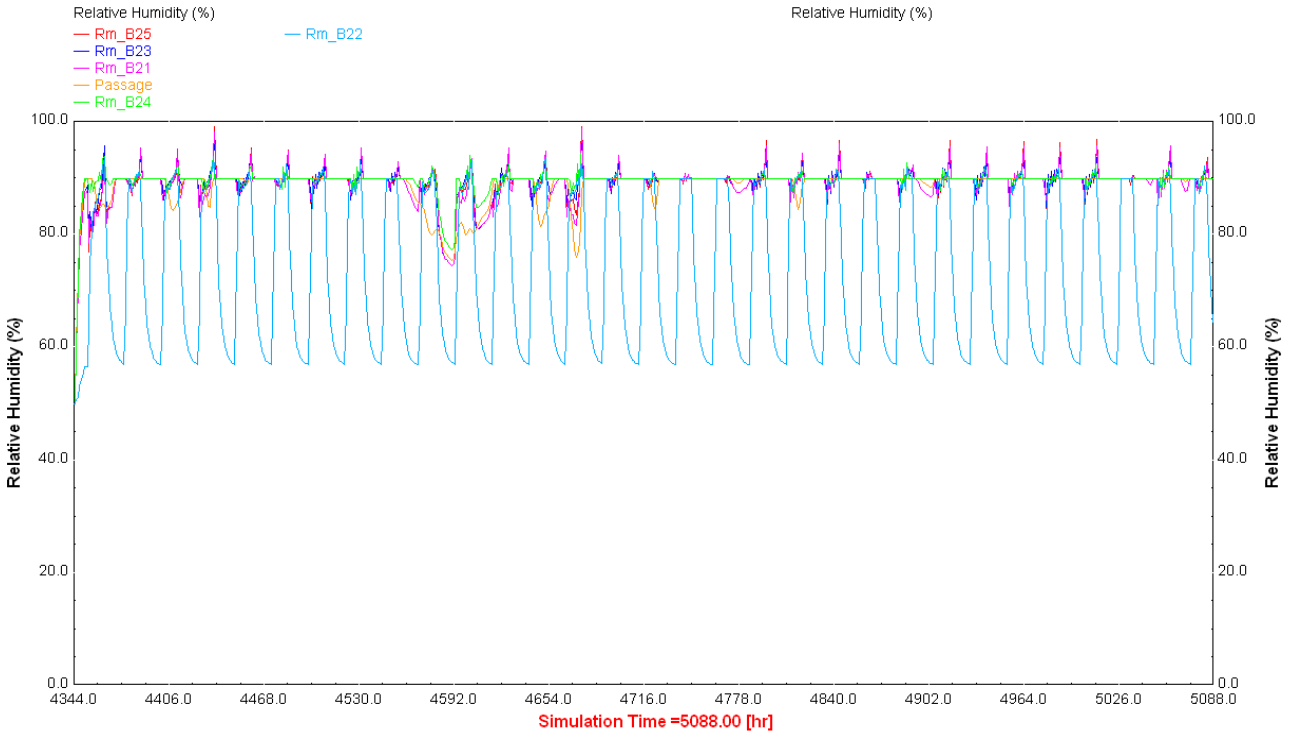


Fig. 4.44: Relative humidity variation within zones, July (no cooling)

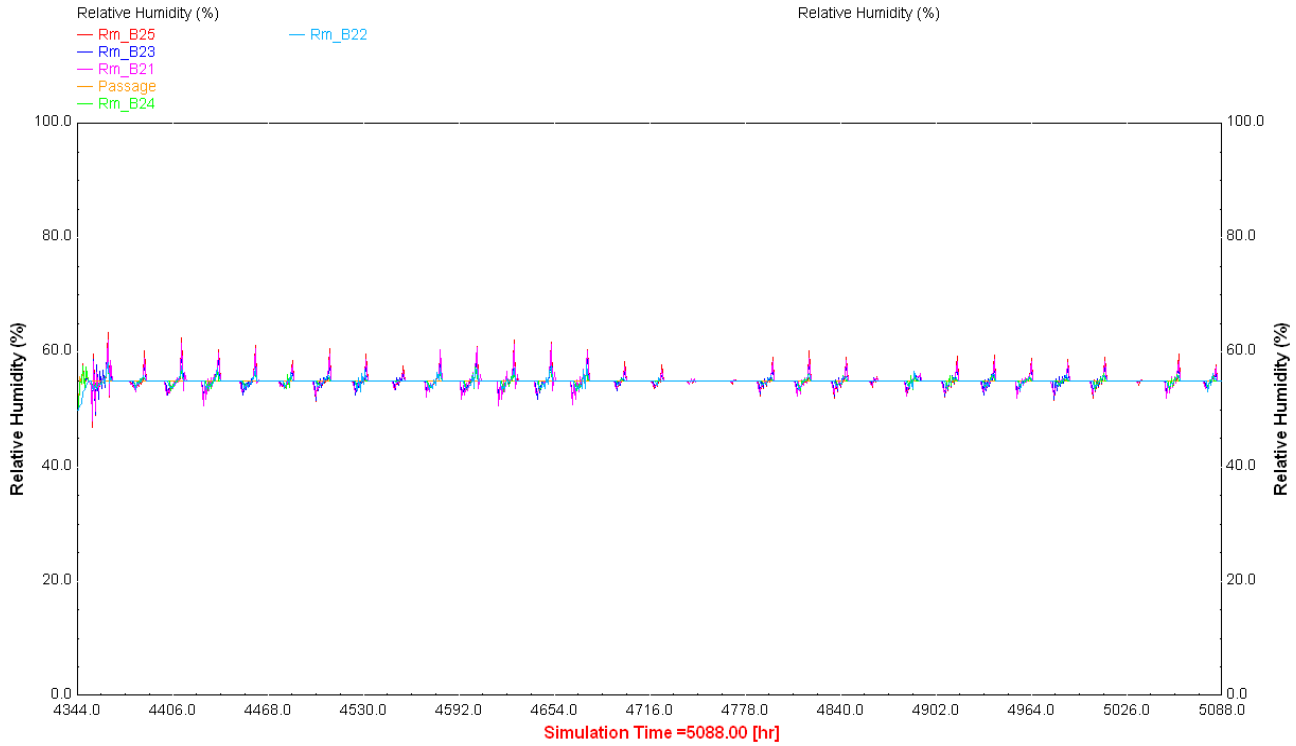


Fig. 4.45: Relative humidity variation within zones, July (with cooling)

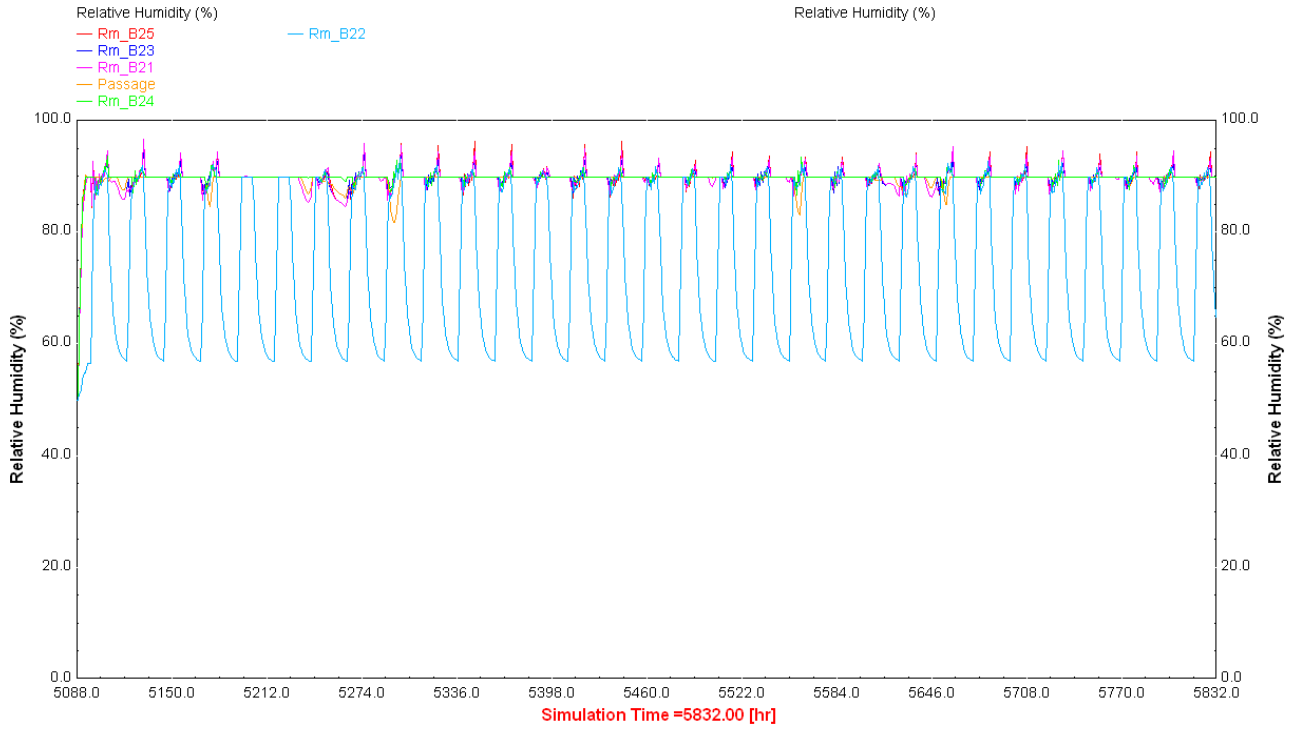


Fig. 4.46: Relative humidity variation within zones, August (no cooling)

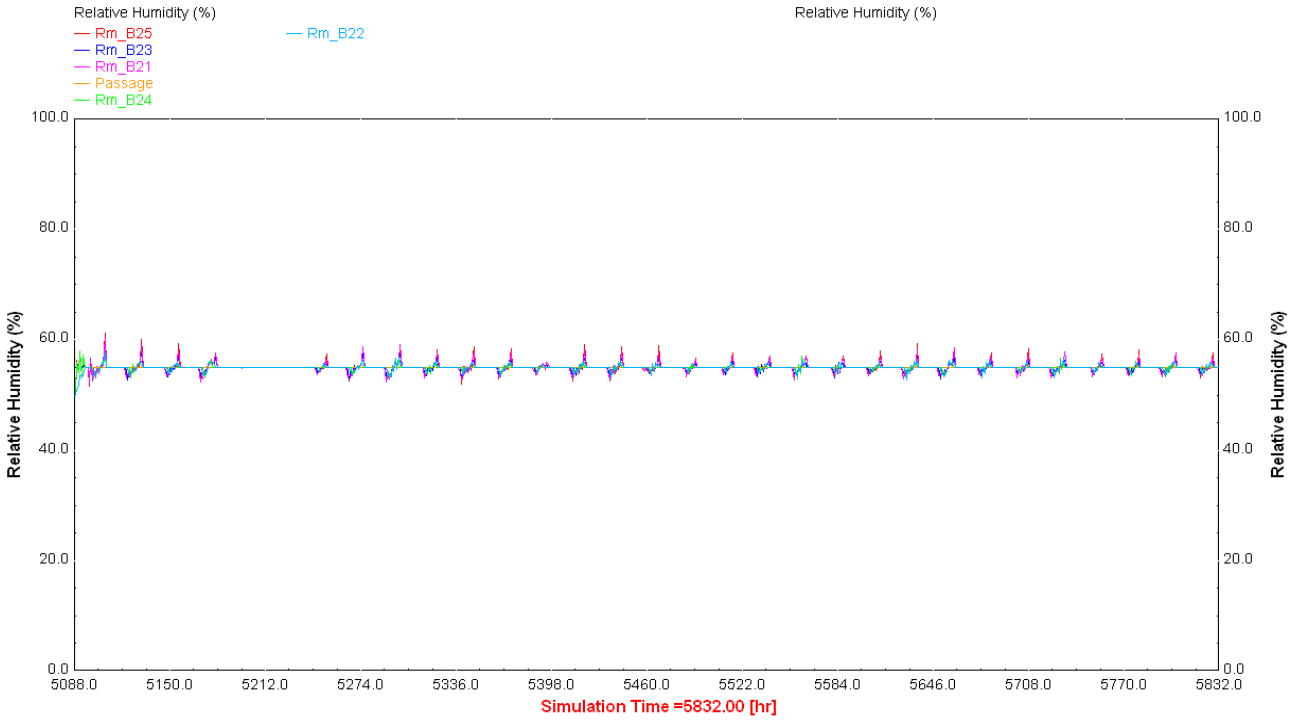


Fig. 4.47: Relative humidity variation within zones, August (with cooling)

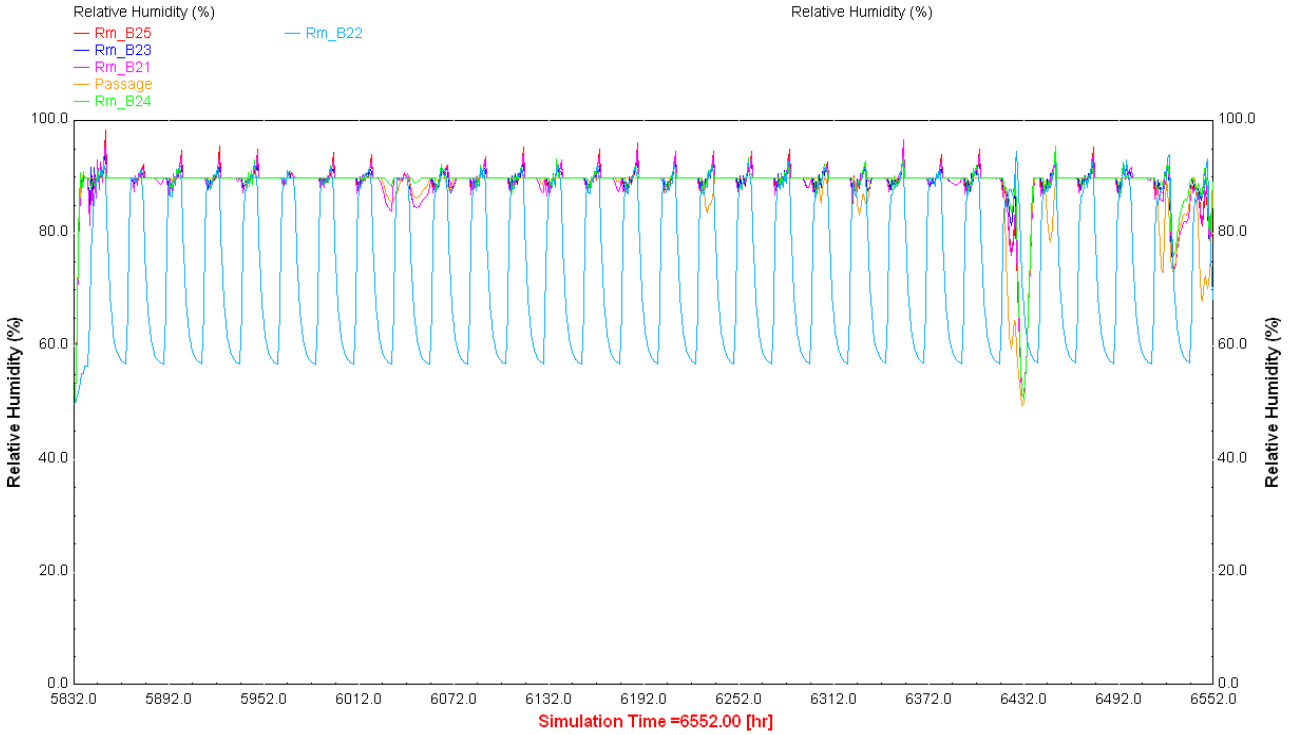


Fig. 4.48: Relative humidity variation within zones, September (no cooling)

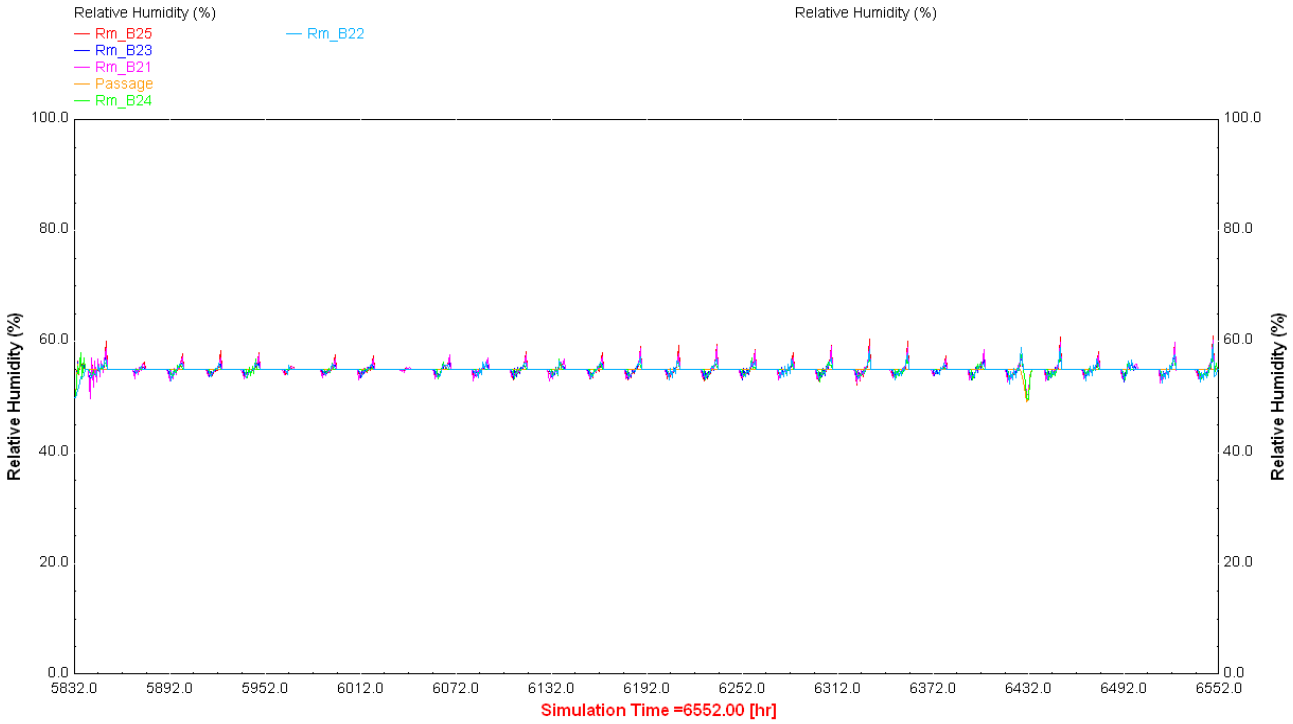


Fig. 4.49: Relative humidity variation within zones, September (with cooling)

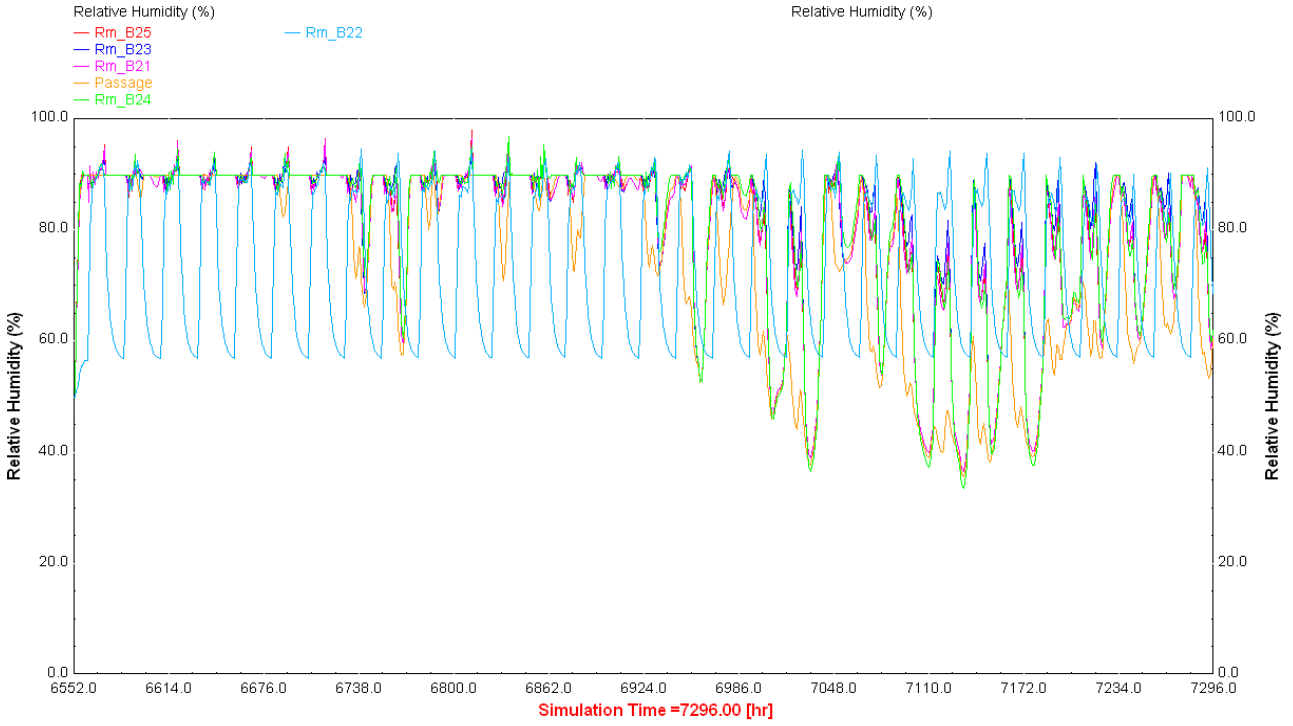


Fig. 4.50: Relative humidity variation within zones, October (no cooling)

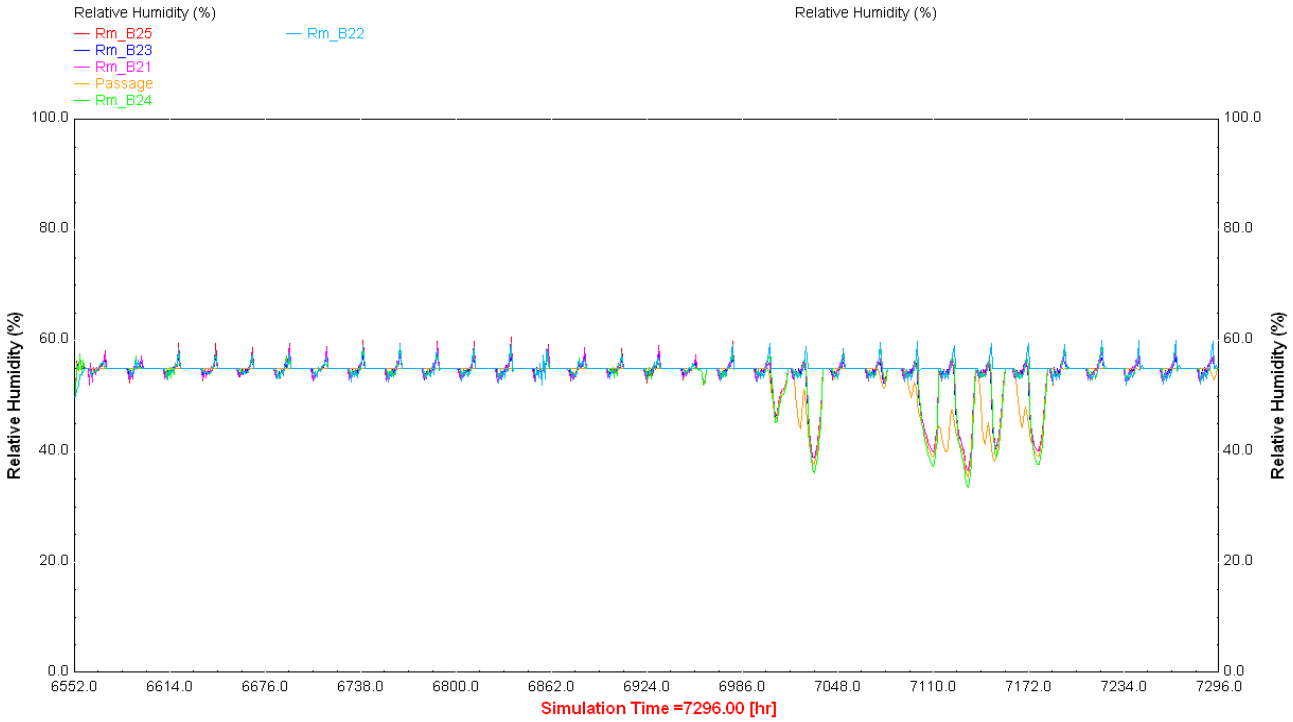


Figure 4.51: Relative humidity variation within zones, October (with cooling)

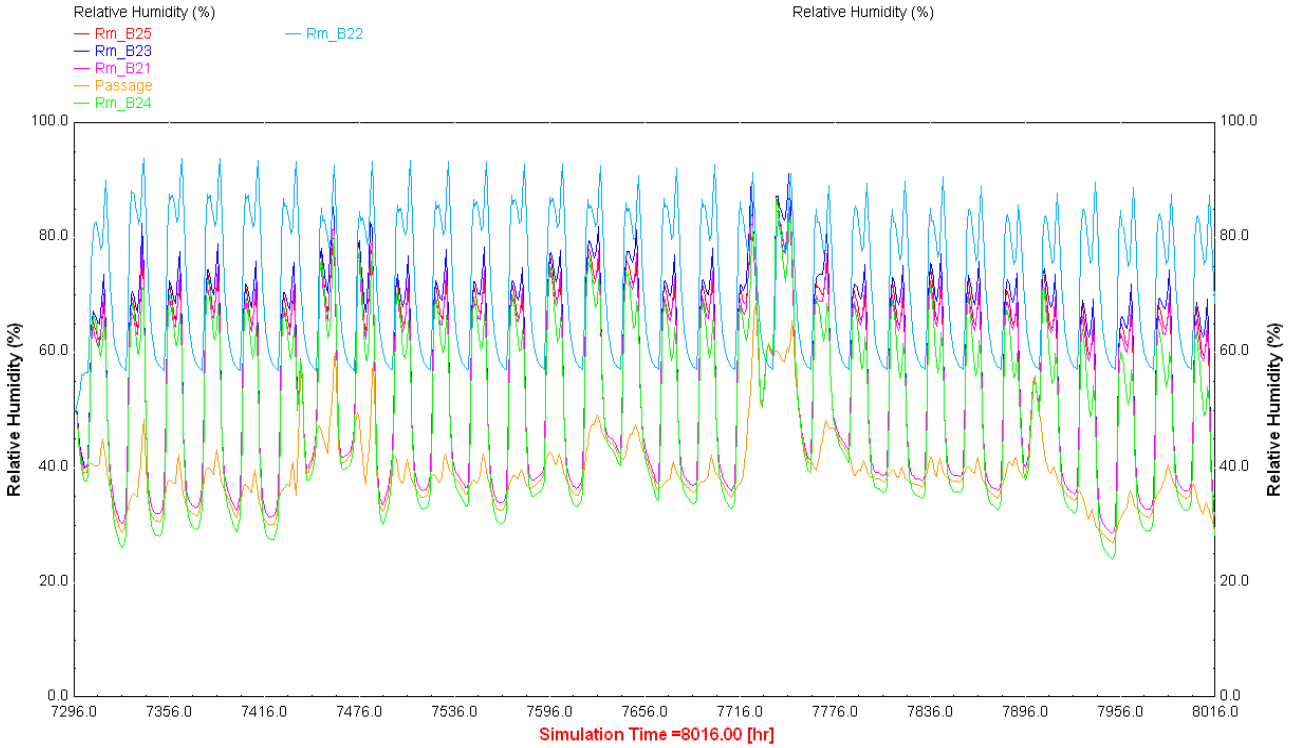


Fig. 4.52: Relative humidity variation within zones, November (no cooling)

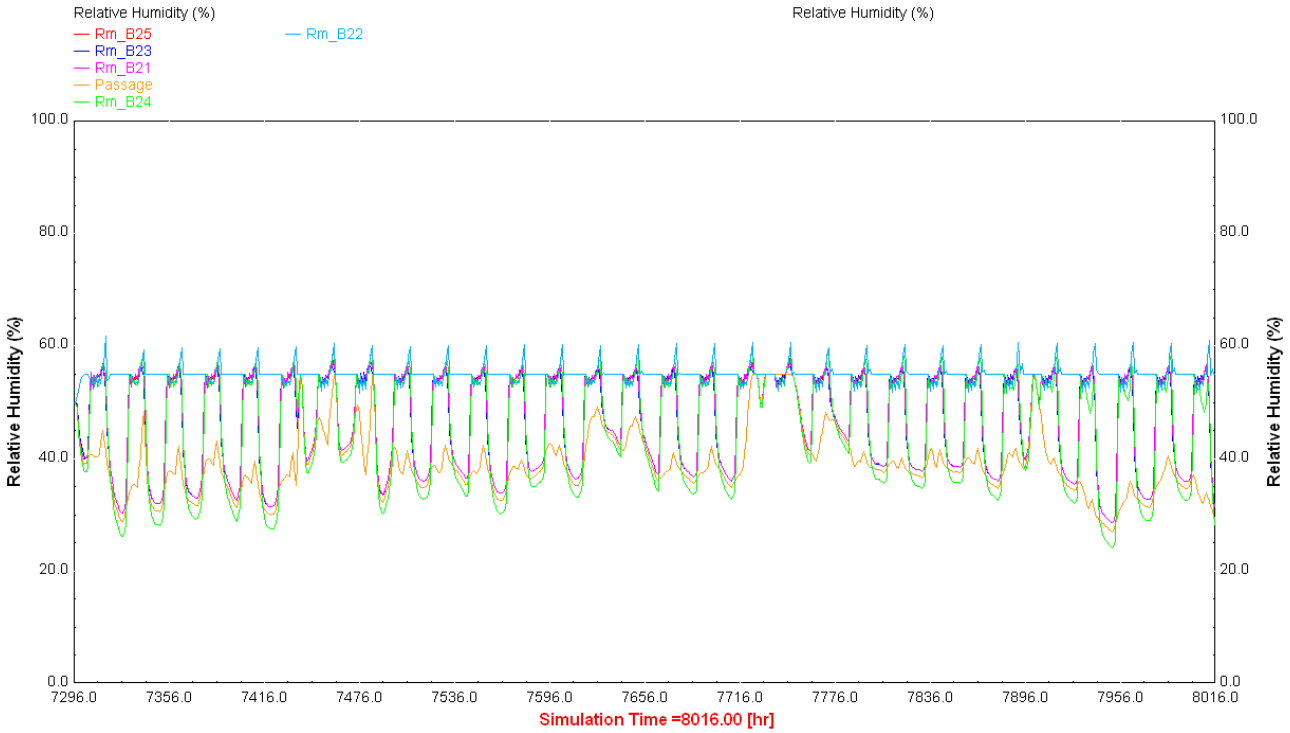


Fig. 4.53: Relative humidity variation within zones, November (with cooling)

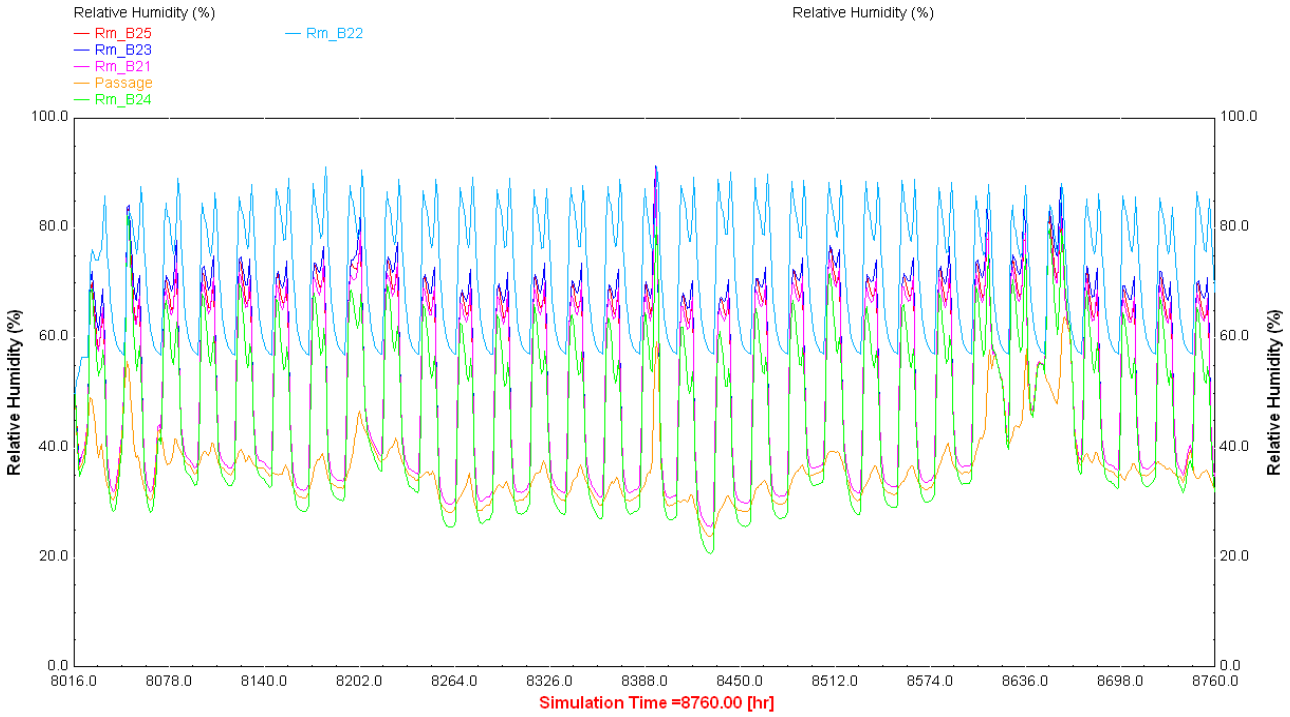


Fig. 4.54: Relative humidity variation within zones, December (no cooling)

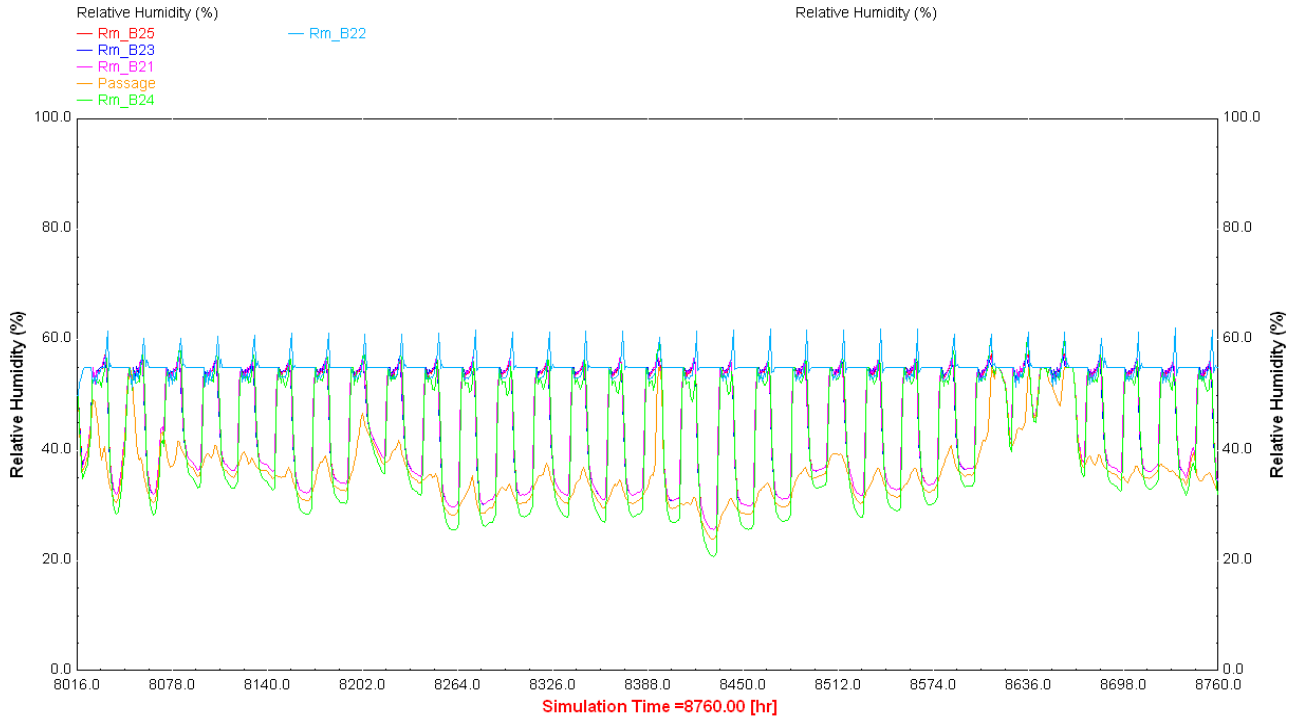


Fig. 4.55: Relative humidity variation within zones, December (with cooling)

From figures 4.32 to 4.55, comparing the graphs of relative humidity variations within zones without cooling for each of the months with the graphs of relative humidity variation within the zones when cooling is applied for the corresponding months, it can be seen that the relative humidity variations within the zones fall reasonably within the range of 30 – 55%. The results of the simulation show that the absorption cooling system as modelled in TRNSYS has been able to satisfy the cooling requirement of the building.

4.3 Results from System Components Designand Optimization

This section presents results of design of system components that were done through programming of design equations.

4.3.1 Results from flat plate collector design and optimization

The graphs shown in figures 4.56 to 4.59 show the results from the optimization of the flat plate solar collector.

4.3.1.1 Absorber plate thickness

The absorber plate thickness was varied from 0.001m to 0.035m, for a range of tube diameter from 0.01m to 0.05m, while other design variables were kept constant.

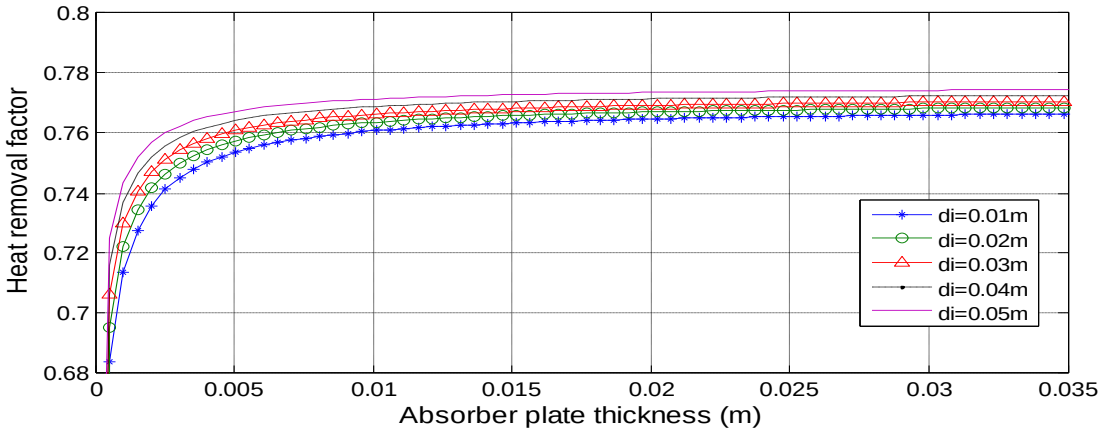


Fig. 4.56: Variation of heat removal factor with absorber plate thickness at different tube diameters

Figure 4.56 shows the variation of heat removal factor with absorber plate thickness. From the figure it is seen that for all the diameters, the heat removal factor increases as the absorber plate thickness increases up to a thickness of 0.01m. As the absorber plate thickness increases above 0.01m, there is no significant increase in the heat removal factor. Also, the heat removal factor is seen to be higher with increasing tube diameter. For these reasons, an absorber plate thickness of 0.01m was chosen and standard tube diameter of ½ inch (15.3mm outer diameter and 13.35mm inner diameter) was chosen.

4.3.1.2 Tube spacing

The tube spacing was varied from 0.01m to 1.5m for a range of tube diameter from 0.01m to 0.05m, while other design variables were kept constant.

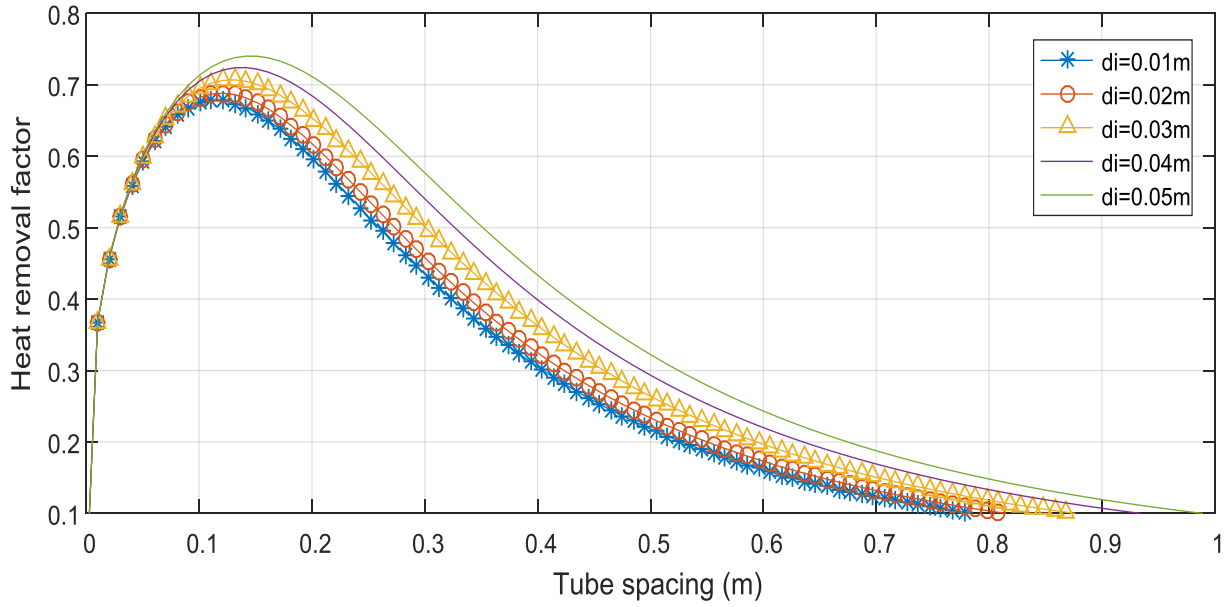


Fig. 4.57: Variation of heat removal factor with tube spacing at different tube diameters

Figure 4.57 shows the variation of heat removal factor with tube spacing. From the figure it is seen that for all the tube diameters, the heat removal factor increases with increasing tube spacing up toa tube spacing of about 0.12 m, from where heat removal factor now decreases with increasing tube spacing. For this reason, a tube spacing of 0.12 m was chosen. Also, at the point of optimum tube spacing (0.12 m), it is seen that the heat removal factor is slightly higher for increasing tube diameters. However, for economic purposes and also to maintain the chosen plate thickness and tube diameter as discussed from figure 4.56, then a standard tube diameter of ½ inch (15.3mm outer diameter and 13.35mm inner diameter) was chosen.

4.3.1.3 Back insulation thickness

The back insulation thickness was varied from 0 to 0.1m for a range of tube diameters from 0.01m to 0.05m, while other design variables were kept constant.

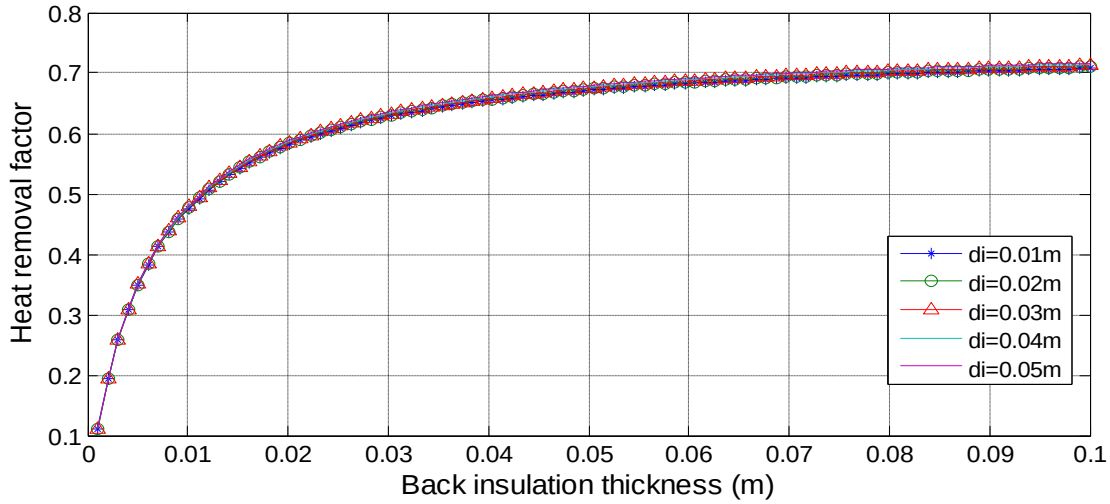


Fig. 4.58: Variation of heat removal factor with back insulation thickness at different tube diameters

Figure 4.58 shows the variation of heat removal factor with back insulation thickness. As seen from the figure, for all the tube diameters, the heat removal factor increases with increasing back insulation thickness up to a thickness of 0.07m. As the back insulation thickness increases above 0.07m, there is no more substantial increase in heat removal factor. Also, from the figure it is seen that the size of the tube diameter does not affect the variation of heat removal factor substantially with back insulation thickness. Therefore, a back insulation thickness of 0.07m was chosen.

4.3.1.4 Edge insulation thickness

The edge insulation thickness was varied from 0 to 0.1m for a range of tube diameter from 0.01m to 0.05m, while the other design variables were kept constant.

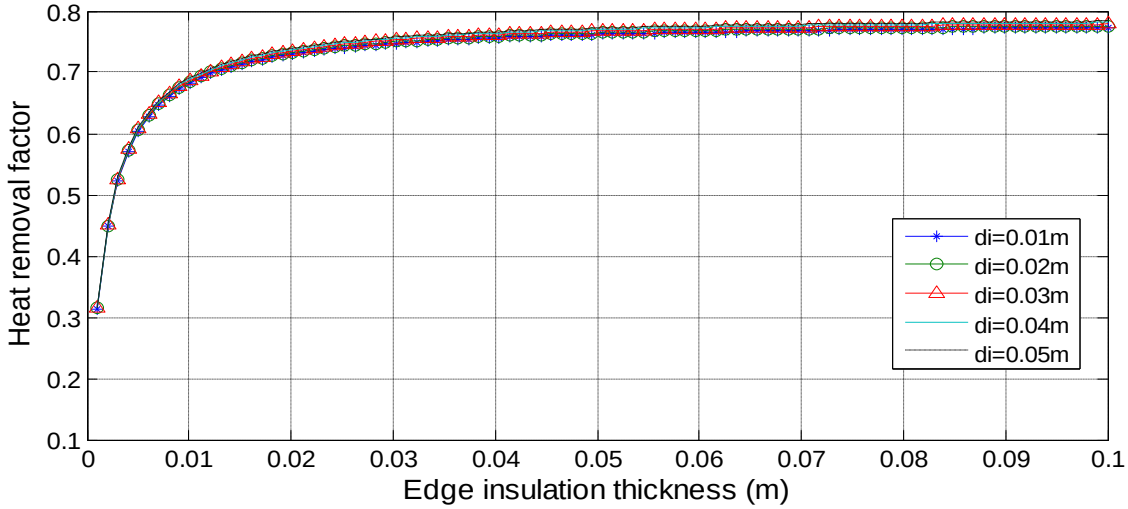


Fig. 4.59: Variation of heat removal factor with Edge insulation thickness at different tube diameters

Figure 4.59 shows the variation of heat removal factor with edge insulation thickness. As seen from the figure, for all the tube diameters, the heat removal factor increases with increasing edge insulation thickness up to a thickness of 0.03m. As the edge insulation thickness increases above 0.03m, there is no more significant increase in heat removal factor. Also, from the figure it is seen that the size of the tube diameter does not affect the variation of heat removal factor with edge insulation thickness. Therefore, an edge insulation thickness of 0.03m was chosen.

4.3.1.5 Outputs from flat plate collector design calculation and optimization

Table 4.1 shows the outputs from the flat plate collector design calculations and optimized parameters.

Table 4.1: Outputs from flat plate collector design program

Parameter	**Value**
Total area of collector array (m^2)	27.34
Area of single collector module (m^2)	1.5
Number of collector modules	18.23
Absorber plate thickness (m)	0.1
Back insulation thickness (m)	0.07
Edge insulation thickness (m)	0.03
Tube inner diameter (m)	0.01335
Tube outer diameter (m)	0.015
Number of tubes per module	12.01
Tube spacing (m)	0.1248
Mass flow rate through each collector module (Kg/sec)	0.0266
Useful energy gain by collector array (J)	8961.6
Top loss coefficient (W/m^2K)	6.99
Bottom loss coefficient (W/m^2K)	0.642
Edge loss coefficient (W/m^2K)	0.375
Total loss coefficient (W/m^2K)	6.991

4.3.2 Results from design calculations of absorption chiller

The design equations obtained in section 3.5.5 were programmed and solved in MATLAB through an iterative procedure. The number of iterations and the corresponding values of calculated design parameters for each of the heat exchangers are shown in Appendices K1 to K5.

4.3.3 Results from optimization of absorption chiller design

The absorption chiller design was optimized by varying some design parameters with the chiller COP as the performance indicator. Figures 4.60 to 4.83 show the variation of COP with absorption chiller design parameters.

4.3.3.1 Optimization of generator parameters

Figures 4.60 to 4.65 show the variation of the performance indicator (COP) with generator design variables. One parameter was varied at a time while the others were kept constant.

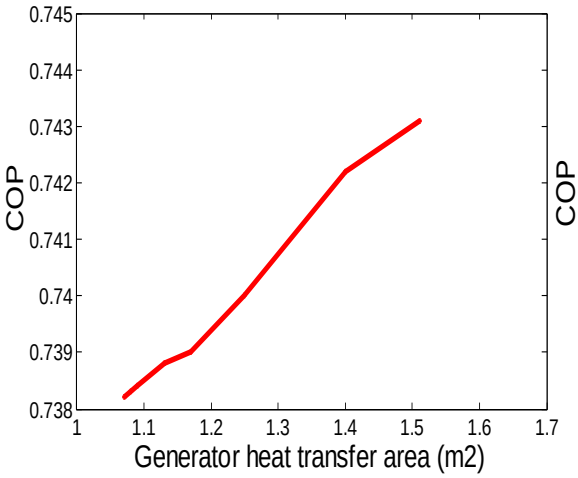


Fig. 4.60: Variation of COP with heat transfer area For generator

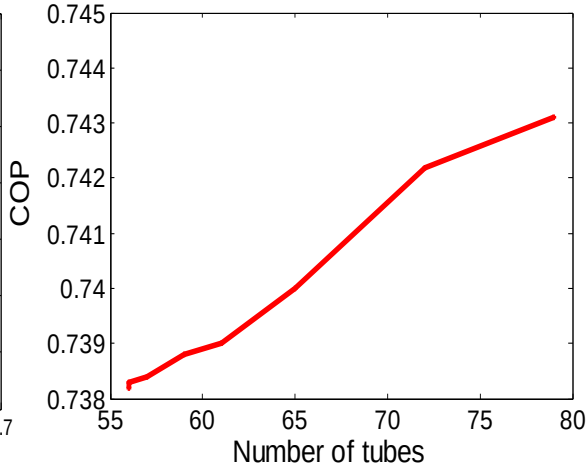


Fig. 4.61: Variation COP with number of tubes for generator

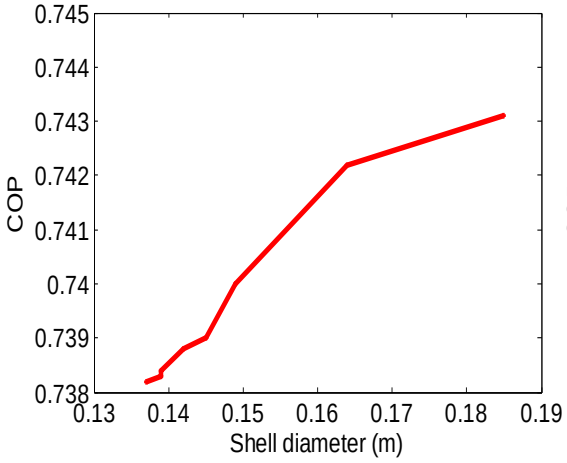


Fig. 4.62: Variation of COP with shell diameter For generator

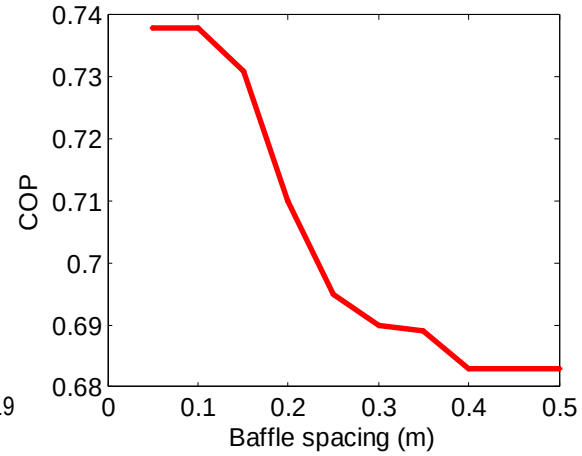


Fig. 4.63: Variation COP with baffle spacing for generator

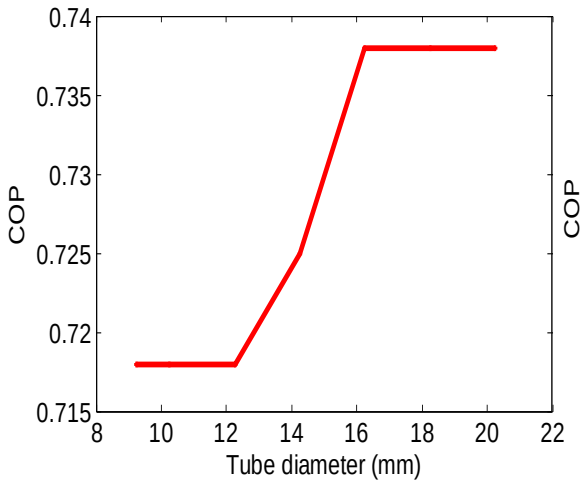


Fig. 4.64: Variation of COP with tube diameter For generator

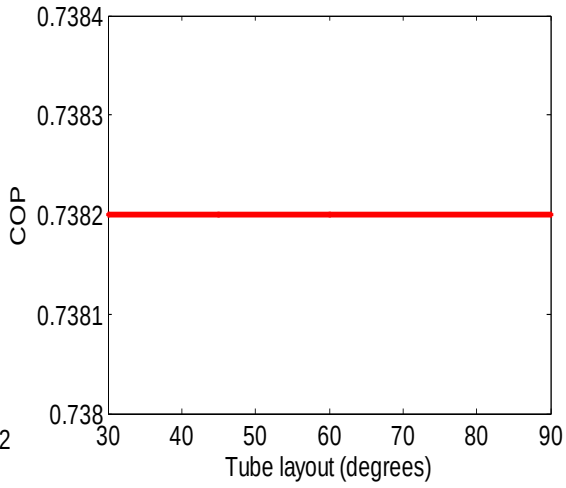


Fig. 4.65: Variation COP with tube layout for generator

From figure 4.61, increasing number of tubes increases the COP. This is so because increasing the number of tubes results in larger heat transfer area which leads to increase in COP as seen in figure 4.60. A larger heat transfer area increases the UA value which results in an increase in COP. However, as seen in figure 4.60, the increase in COP is marginal for heat transfer area in excess of 1.25m^2. Likewise, from figure 4.61 for number of tubes above 67, the increase in COP is marginal. Therefore the number of tubes was chosen as 67 and the corresponding heat transfer area of 1.293m^{2}taken. Figure 4.62 shows the COP increases marginally as shell diameter increases above 0.15. The shell diameter of 0.1513m corresponding to 67 tubes was taken. Figure 4.63

shows the COP decreases with increasing baffle spacing. This is so because baffles facilitate proper mixing of the shell fluid which enhances heat transfer. When the baffles become too few, there is less heat transfer leading to lower COP. A baffle spacing of 0.1m was taken. Figure 4.64 shows the COP increases with increasing tube diameter. This is so because the generator, which is a pool generator now has a higher heat transfer area at the tubes, resulting into better heat transfer and eventually higher COP. With tube diameter of 12 mm, COP of 0.719 is attained, while COP of 0.7359 is attained with tube diameter of 16 mm and above. However, for economic purposes, a standard tube diameter of 3/8 inch (0.5inch outer diameter and 0.43 inch inner diameter) was taken. Figure 4.65 shows the COP is not affected by the tube layout. Therefore a tube layout of 90^{o} was taken.

4.3.3.2 Optimization of evaporator parameters

Figures 4.66 to 4.71 show the variation of the performance indicator (COP) with evaporator design variables. One parameter was varied at a time while the others were kept constant.

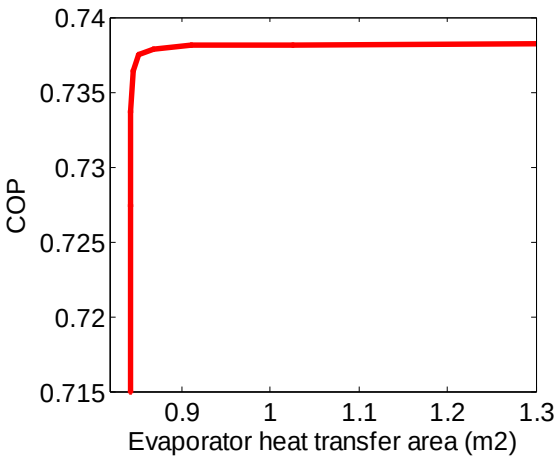


Fig. 4.66: Variation of COP with heat transfer area For evaporator

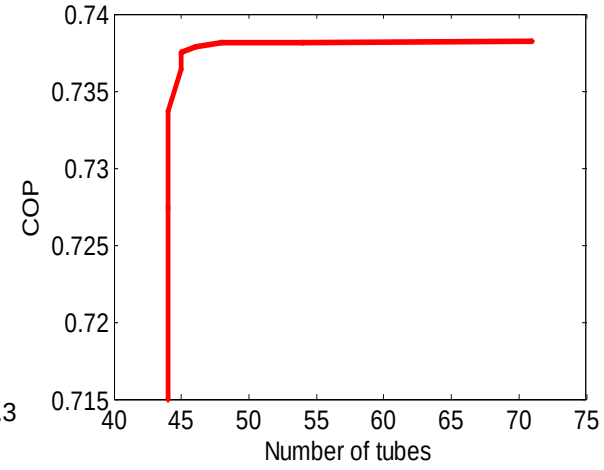


Fig. 4.67: Variation COP with number of tubes for evaporator

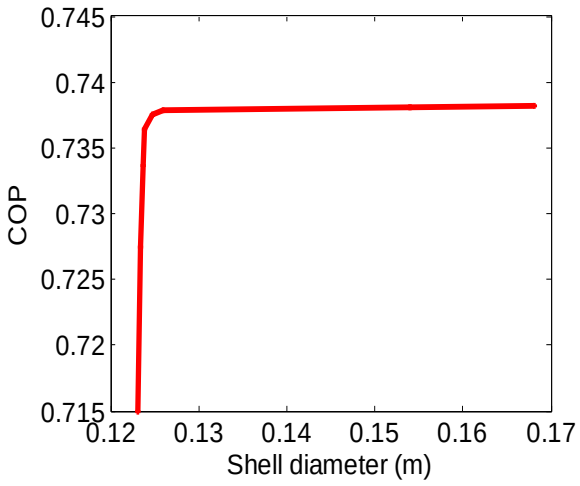


Fig. 4.68: Variation of COP with shell diameter For evaporator

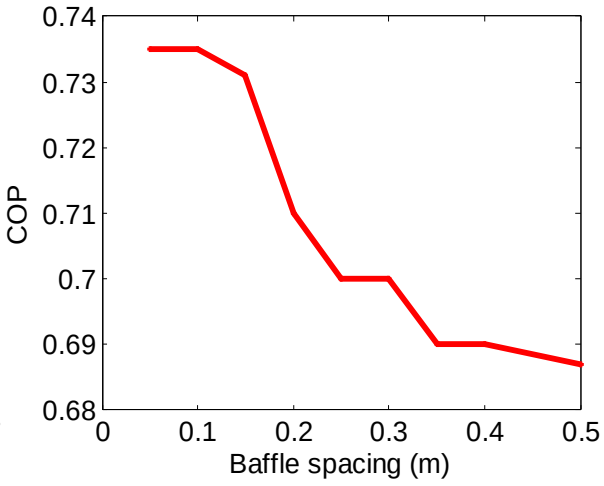


Fig. 4.69: Variation COP with baffle spacing for evaporator

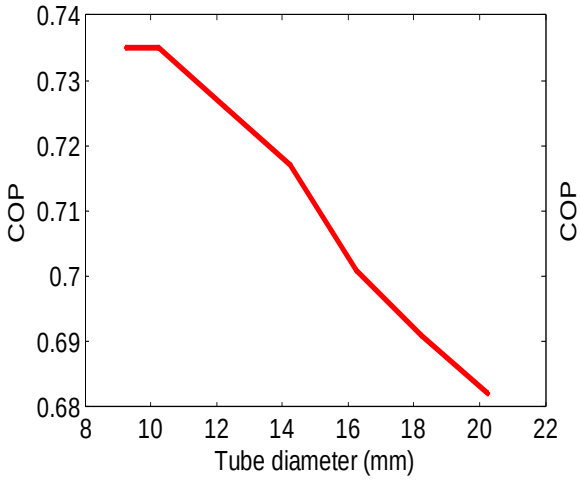


Fig. 4.70: Variation of COP with tube diameter For evaporator

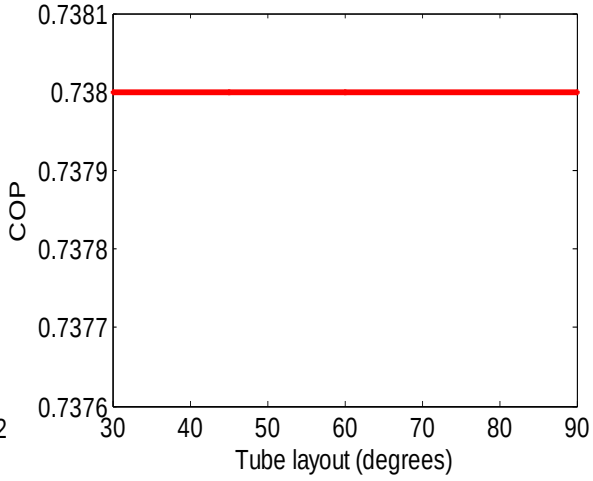


Fig. 4.71: Variation COP with tube layout for evaporator

Figures 4.66 to 4.71 show the variation of the performance indicator (COP) with evaporator design variables. From figure 4.67, 45 tubes maximizes the COP, the COP remains steady even with further increase in number of tubes. Also, from figure 4.66 the COP reaches a maximum at $0.9m^2$ heat transfer area and remains steady with increase in number of tubes. 45 tubes was therefore taken for the evaporator and a corresponding heat transfer area of $0.873m^2$ taken. A corresponding shell diameter of 0.125m was taken from figure 4.68. From figure 4.69, the COP is seen to decrease with increasing baffle spacing. This is so because fewer baffles results in less mixing of fluid and lower heat transfer, eventually reducing COP. A baffle spacing of 0.1m was

taken. From figure 4.70, the COP is seen to decrease with increasing tube diameter. This is due to the configuration of the evaporator which was designed as a vertical falling film evaporator. With larger tube diameter, total wetting of the tubes surface by the falling film refrigerant becomes difficult, resulting in more patches of dry tubes surfaces. This leads to weaker evaporation process thereby reducing the COP. A standard tube diameter of 3/8 inch (0.5inch outer diameter and 0.43 inch inner diameter) was therefore taken for the evaporator. Figure 4.71 shows the COP is not affected by the tube layout. A tube layout of 90^{o} was taken.

4.3.3.3 Optimization of condenser parameters

Figures 4.72 to 4.77 show the variation of the performance indicator (COP) with evaporator design variables. One parameter was varied at a time while the others were kept constant.

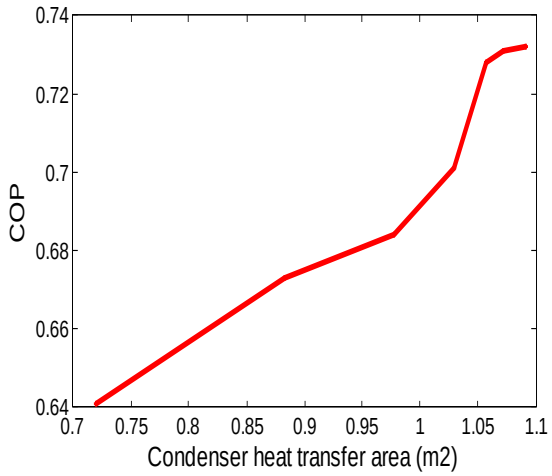


Fig.4.72: Variation of COP with heat transfer area For condenser

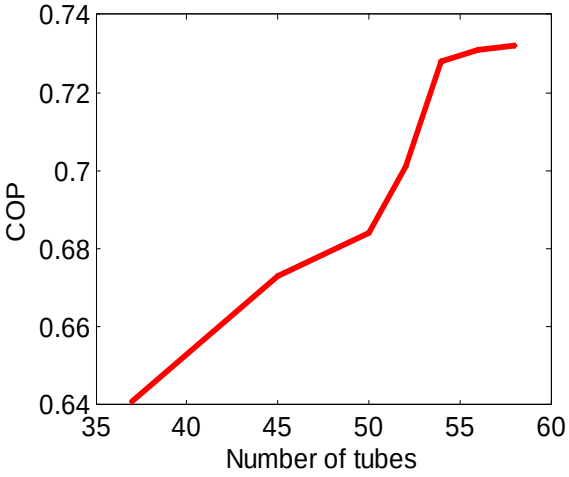


Fig. 4.73: Variation COP with number of tubes for condenser

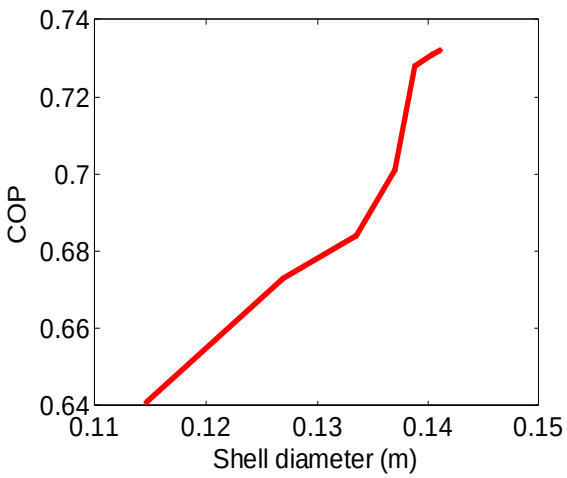


Fig. 4.74: Variation of COP with shell diameter For condenser

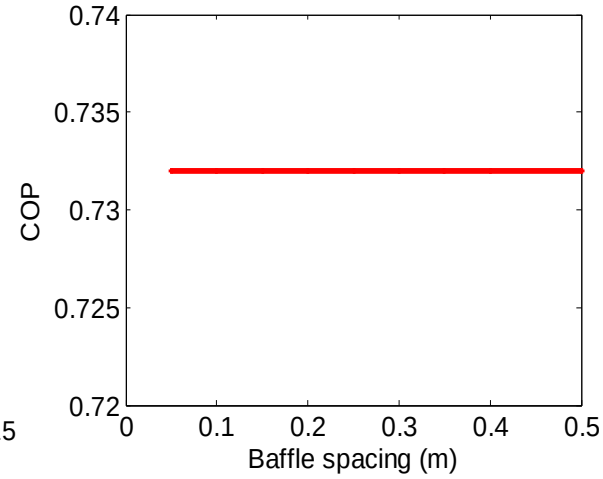


Fig. 4.75: Variation COP with baffle spacing for condenser

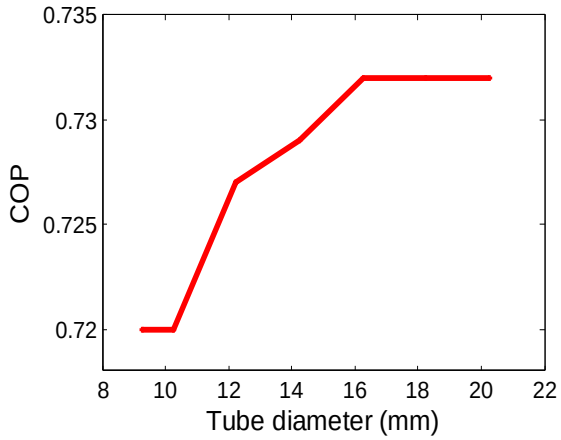


Fig. 4.76: Variation of COP with tube diameter For condenser

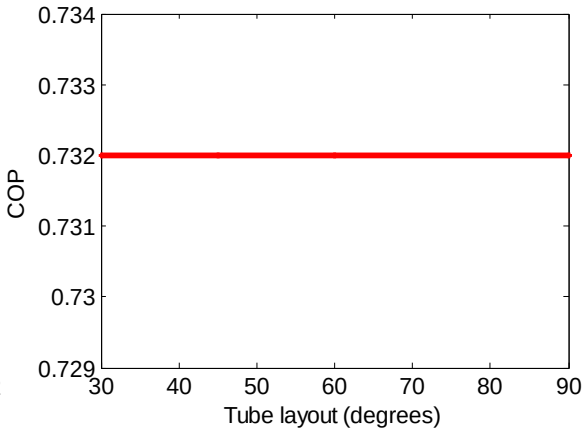


Fig. 4.77: Variation COP with tube layout for condenser

From figure 4.73, as from 55 number of condenser tubes, there is no significant increase in the COP with increase in number of tubes. Also, from figure 4.72, there is no significant increase in COP when the heat transfer area increases above 1.05m^2. Therefore 55 tubes was taken for the condenser and a corresponding heat transfer area of 1.083m^2 taken. A corresponding shell diameter of 0.1406m was taken from figure 4.74. From figure 4.75, it is seen that the COP is not affected by a variation in baffle spacing in the condenser. This is so because the baffles have no significant effect on the condensation of steam over cooled horizontal tubes which takes place in the condenser. However, to maintain uniformity and to ensure the condenser tubes are well

supported, a baffle spacing of 0.1m was taken. From figure 4.76, it is seen that the COP increases with increasing tube diameter. This is so because a larger tube diameter provides a larger cooled surface area for steam to condense. This aids the condensation process thereby improving COP. A standard tube diameter of ½ inch (0.625 inch outer diameter and 0.545 inner diameter) was taken. From figure 4.77, the COP is not affected by a variation in tube layout. Therefore a tube layout of 90^{o} was taken.

4.3.3.4 Optimization of absorber parameters

Figures 4.78 to 4.83 show the variation of the performance indicator (COP) with absorber design variables. One parameter was varied at a time while the others were kept constant.

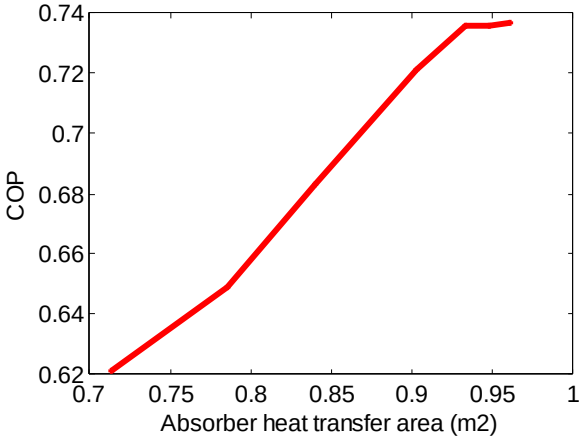


Fig.4.78: Variation of COP with heat transfer area For absorber

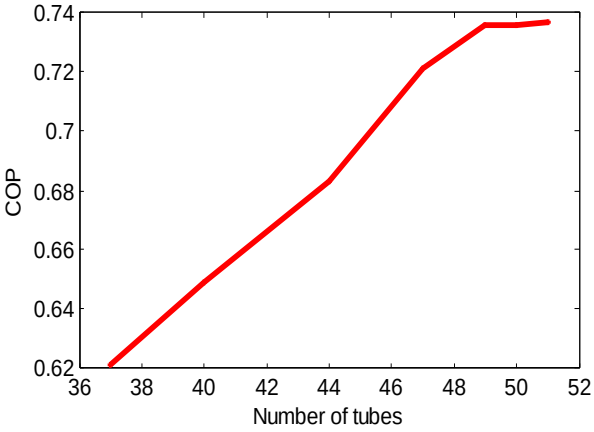


Fig. 4.79: Variation COP with number of tubes for absorber

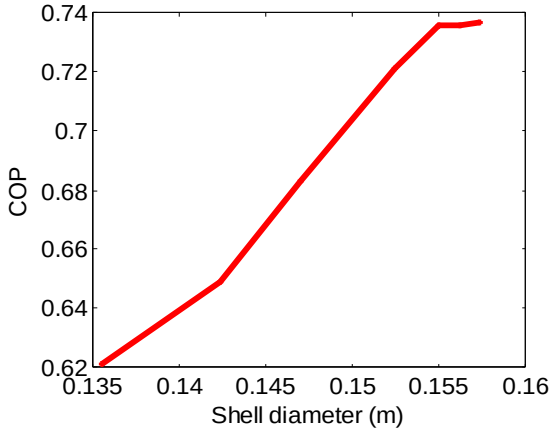


Fig. 4.80: Variation of COP with shell diameter For absorber

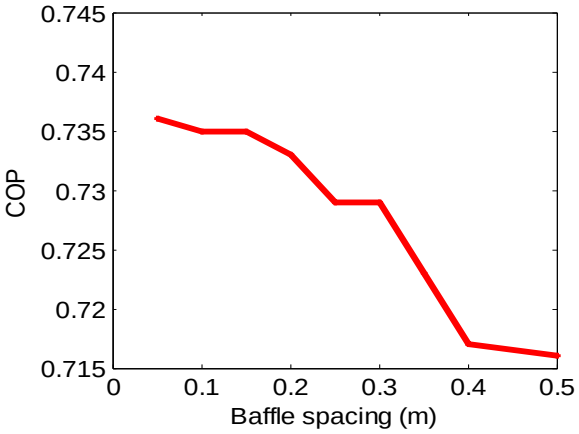


Fig. 4.81: Variation COP with baffle spacing for absorber

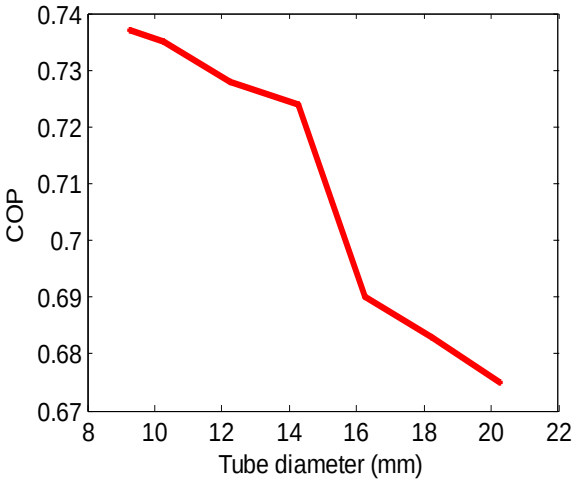


Fig. 4.82: Variation of COP with tube diameter For absorber

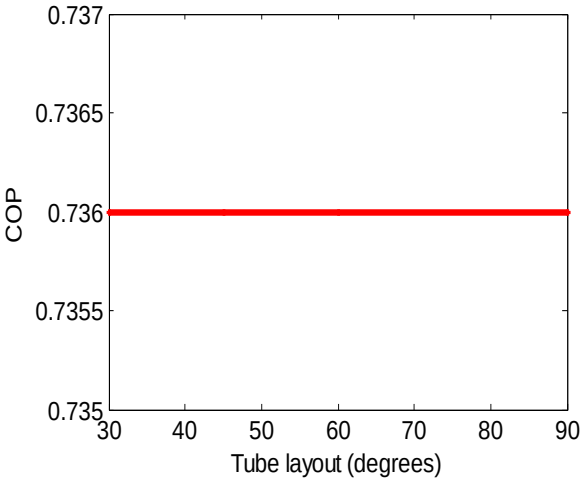


Fig. 4.83: Variation COP with tube layout for absorber

From figure 4.79, starting from an absorber tube number of 49 the COP is maximized. Increasing the number of tubes above this doesn't increase the COP further. Also, from figure 4.78, a heat transfer area starting from 0.93m^2 maximizes the COP. Therefore, 50 tubes was taken for the absorber, corresponding to a heat transfer area of 0.964m^2. This also corresponds to a shell diameter of 0.158 m, which was taken as seen in figure 4.80.

From figure 4.81, the COP is seen to decrease with increasing baffle spacing. This is so because fewer baffles results in less mixing of fluid and lower heat transfer, eventually reducing COP. A baffle spacing of 0.1m was taken. From figure 4.82, the COP is seen to decrease with increasing tube diameter. This is because, for the absorber which is a vertical falling film absorber, as the tube diameter increases, the ability of the falling film solution of lithium bromide to completely wet the tubes surfaces declines. This leads to patches of dry tube surface which reduces ability of the solution to absorb water vapour from the evaporator, thereby decreasing COP. Therefore, a standard tube diameter of 3/8 inch (0.5inch outer diameter and 0.43 inch inner diameter) was taken. From figure 4.83, it is seen that the COP is not affected by a variation in the tube layout. Therefore a tube layout of 90^o was taken.

Table 4.2 shows the values of the optimized system components for the absorption chiller design.

Table 4.2: Optimized system components for the absorption chiller

Parameter	**Generator**	**Evaporator**	**Condenser**	**Absorber**	**SHX**
No. of tubes	67	45	55	50	21
Tube length (m)	0.5	0.5	0.5	0.5	0.5
Tube outer dia. (m)	0.01225	0.01225	0.0153	0.01225	0.01225
Tube inner dia. (m)	0.01053	0.01053	0.01335	0.01053	0.01053
Shell dia. (m)	0.1513	0.125	0.1406	0.158	0.109
Baffle spacing (m)	0.1	0.1	0.1	0.1	0.1
Heat transfer area (m^2)	1.293	0.873	1.083	0.964	0.427
Tube layout (degrees)	90	90	90	90	90
Tube pitch (m)	0.0153	0.0153	0.0191	0.153	0.0153
Shell length (m)	0.6	0.6	0.6	0.6	0.6
Mass flow rate of strong solution (Kg/s)	0.0351				0.0351
Mass flow rate of weak solution (Kg/s)				0.0403	0.0403
Mass flow rate of refrigerant (Kg/s)		0.0051			
Mass flow rate of hot water (Kg/s)	0.4094				
Mass flow rate of cooling water (Kg/s)			0.7822	0.7822	
Mass flow rate of chilled water (Kg/s)		0.5732			

4.3.4Results from performance simulation of the absorption chiller

Performance simulation of the absorption chiller done in section 3.5.9 is presented here. The optimized design parameters of the absorption chiller were used in simulating its performance. The graphs below show variation of performance indices with system parameters. The set of conditions for which the simulation was carried out are: hot water inlet temperature ranging from 40^oC to 90^oC, cooling water inlet temperature ranging from 24^oC to 40^oC, evaporator temperature ranging from 9^oC to 13^oC.

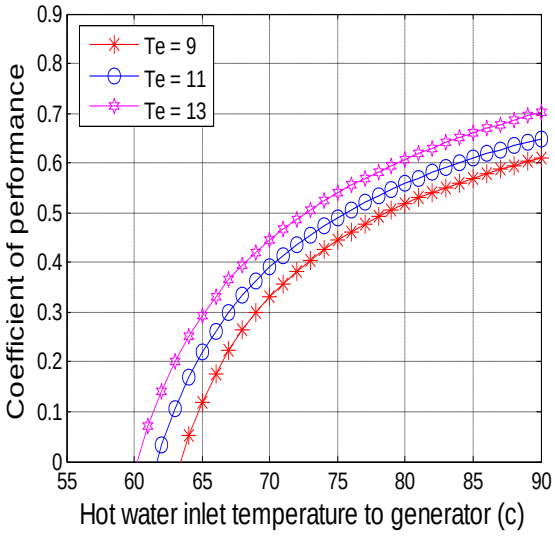


Fig. 4.84: Variation of COP with hot water inlet Temperature to generator

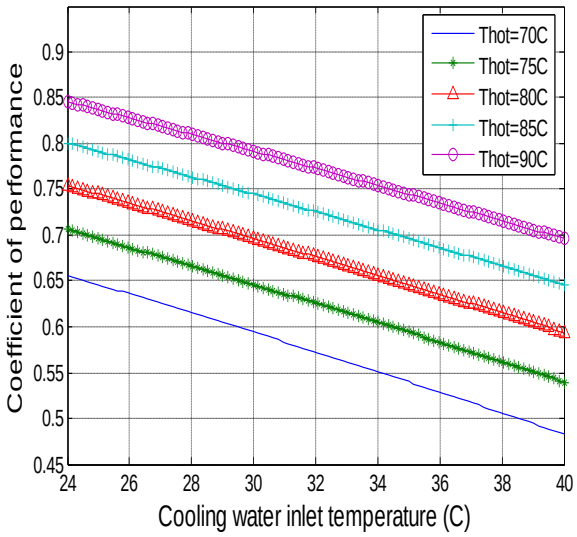
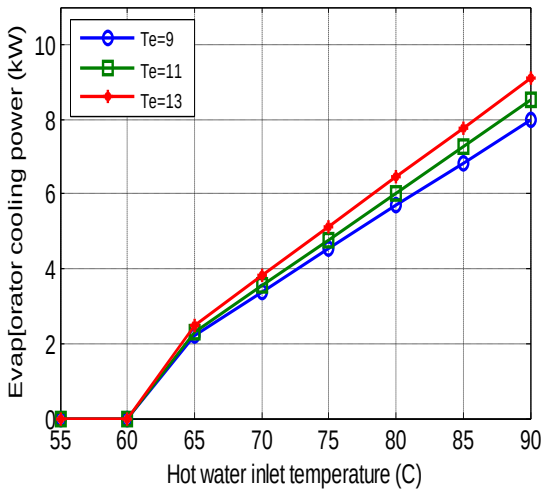


Fig. 4.85: Variation of COP with cooling water inlet temperature



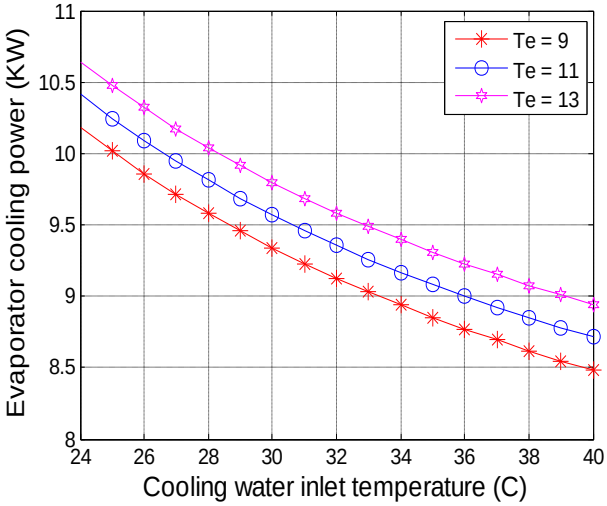


Fig. 4.86: Variation of evaporator cooling power with hot water inlet temp

Fig. 4.87: Variation of evaporator cooling power with cooling water inlet temperature

From figure 4.84, it is seen that the COP increases with increasing hot water inlet temperature to the generator, this is so because an increase in the hot water inlet temperature leads to higher vapourization rate of the refrigerant from the aqueous lithium bromide solution at the generator, which improves COP. Also from figure 4.84, the COP is seen to increase with increasing evaporator chilled water inlet temperature. A maximum COP of 0.7 was attained with 90^{o}C hot water inlet temperature and 13^{o}C chilled water inlet temperature to the evaporator. Similar

research works on absorption cooling cycle modelling and simulation have also reported increasing COP with increasing generator hot water temperature and evaporator chilled water temperature: Kefti *et al.*, (2015), reported a COP of 0.77 with 93^{o}C hot water temperature and 12^{o}C evaporator temperature, Eicker and Pietruschka, (2008), reported a COP of 0.71 with 85^{o}C hot water temperature and 12^{o}C evaporator temperature.

From figure 4.85, it is seen that the COP decreases with increasing cooling water inlet temperature. This is so because a low cooling water temperature facilitates better cooling of the absorber and condenser which ensures continuous absorption and condensation processes respectively, thereby improving COP. When the cooling water inlet temperature begins to rise, absorption and condensation process decline, thereby reducing COP. With an average cooling water inlet temperature of 33^{o}C, COP of about 0.75 is seen to be achieved at 90^{o}C hot water inlet temperature. The trend of decreasing COP with increasing cooling water inlet temperature is consistent with the works of Evola *et al.*, (2013) who reported a COP of 0.71 with 90^{o}C hot water temperature, 13.7^{o}C evaporator temperature and 31^{o}C cooling water temperature, Eicker and Pietruschka, (2008), who reported a COP of 0.71 with 85^{o}C hot water temperature, 12^{o}C evaporator temperature and 27^{o}C cooling water temperature.

From figure 4.86, the evaporator cooling power is seen to increase with increasing hot water inlet temperature to the generator. Increasing the hot water inlet temperature at the generator leads higher rate of vapourization of refrigerant. Continuous supply of liquid refrigerant from the condenser to the evaporator improves evaporation process thereby increasing the cooling power of the chiller. A maximum cooling power of 9 kW was attained with 13^{o}C chilled water temperature at the evaporator and 90^{o}C hot water temperature. The trend of increasing evaporator cooling

power with hot water inlet temperature to the generator is consistent with the works of Kefti *et al.*, (2015), Evola *et al.*, (2013), Eicker and Pietruschka, (2008) and Mittal *et al.*, (2006).

From figure 4.87, the evaporator cooling power is seen to decrease with increasing cooling water inlet temperature. As cooling water temperature increases, absorption and condensation process decline, thereby reducing the cooling ability of the chiller. With an average cooling water inlet temperature of 33^{o}C, a cooling power of about 9.5 kW was attained with 13^{o}C chilled water inlet temperature at the evaporator. The trend of decreasing evaporator cooling power with increasing cooling water inlet temperature is consistent with the works of Kefti *et al.*, (2015), Evola *et al.*, (2013) and Eicker and Pietruschka, (2008). Eicker and Pietruschka, (2008) reported a maximum cooling power of 12.3 kW with 27^{o}C cooling water inlet temperature, the design cooling power was 15 kW.

4.3.5 Results from cooling tower design

Table 4.3 shows the results from the cooling tower design calculation program.

Table 4.3: Output from cooling tower design calculation program

Parameter	**Value**
Diameter (m)	0.5
Mass flow rate of cooling water (kg/s)	1.0253
Optimum ratio of water to air flow rate	1.8497
Mass flow rate of air (kg/s)	0.5543
Outlet temp. of water (^{o}C)	32.8
Approach temp.	9.86
Saturated water vapour pressure (Pa)	3753.8
Enthalpy of water at inlet (kJ/kg)	167.47
Enthalpy of water at outlet (kJ/kg)	137.69
Cooling tower characteristic	0.219
Height of cooling tower spray zone (m)	3.17
Evaporation loss (Kg/s)	0.006
Volume of water used daily (litres)	217.4

4.3.6 Results from fan coil unit sizing

The fan coil unit was sized for each of the thermal zones. A program was developed for the sizing in section 3.5.5. The outputs from the program is presented in table 4.4.

Table 4.4: Outputs from Cooling coil design program

Zone	Peak Cooling Load (kW)	Mass flow rate of air (kg/s)	Mass flow rate of chilled water (kg/s)	Number of coil tubes	Height of coil (m)	Depth of coil (m)
A1	1.52	0.1147	0.0734	4	0.0281	0.1905
B1	1.63	0.123	0.0787	4	0.0301	0.1905
C1	1.93	0.1457	0.0932	5	0.0356	0.1905
A2	0.77	0.0581	0.0372	2	0.0142	0.1905
A3	3.19	0.2408	0.1541	7	0.0589	0.1905
B3	2	0.1509	0.0966	5	0.0369	0.1905

4.4 Results from Experiments Conducted

This section presents results from the experiments conducted on the complete gas assisted solar absorption air conditioning system installation.

4.4.1 Results from experiment

This section presents the results obtained on the experimental days. The days were classified as:

Hot clear sky day: days with very clear sky, hot weather with high ambient temperatures, no rain.

Fairly clear sky day: days with intermittently clear sky and partly cloudy sky, high ambient temperatures, no rain.

Cloudy sky day: days with very cloudy sky, average ambient temperatures, no rain.

Rainy day: days in which rain occurred within any interval of the experimental day.

Figures to 4.88 to 4.96 show the graphs that describe the variation in experimental parameters for the experimental day of April 22nd 2017, which was classified as a hot clear sky day.

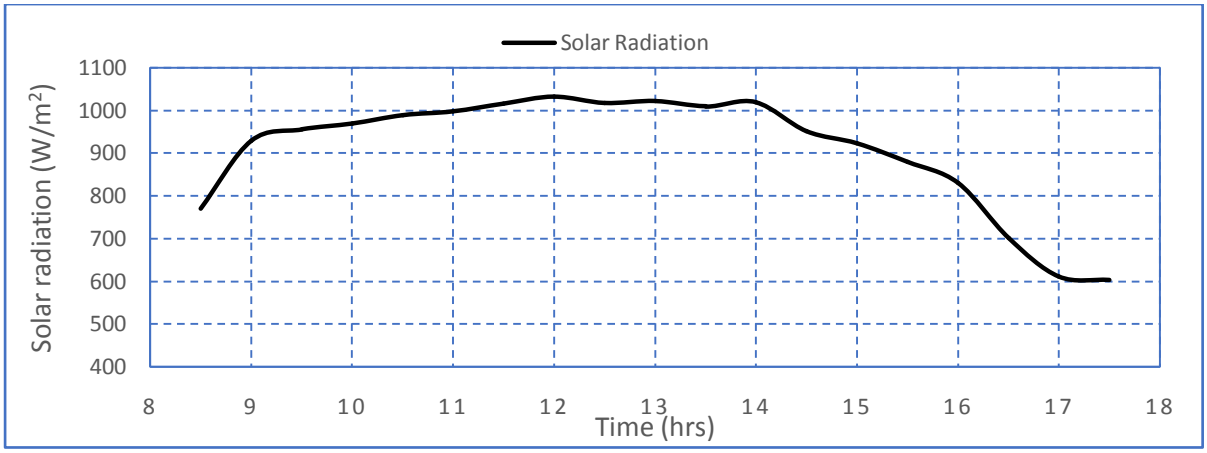


Fig. 4.88. Variation of solar radiation with time for April 22, 2017

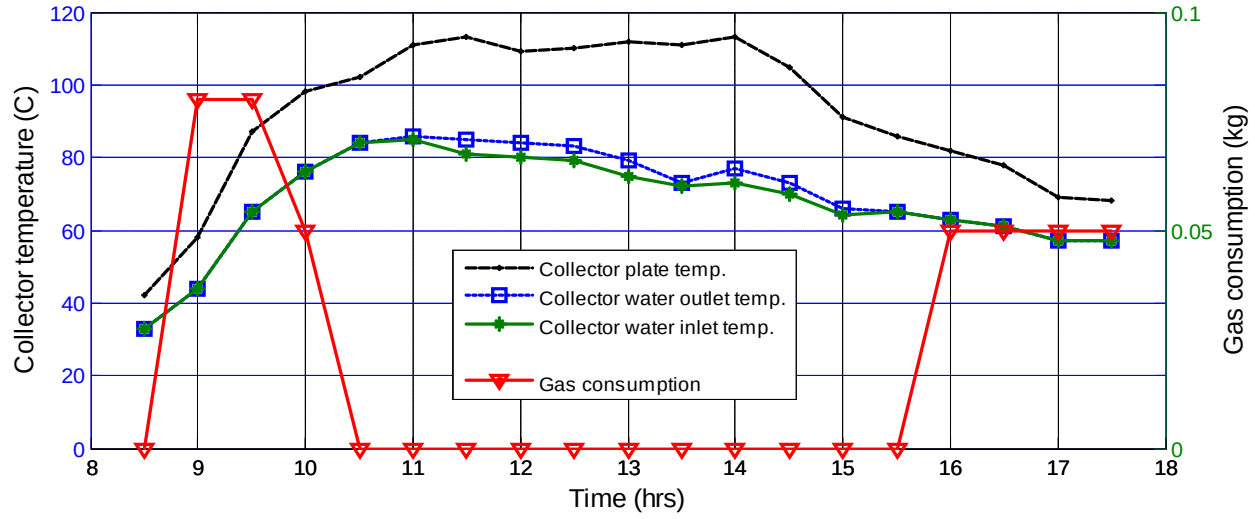


Fig. 4.89. Variation of collector temperatures and gas consumption with time for April 22, 2017

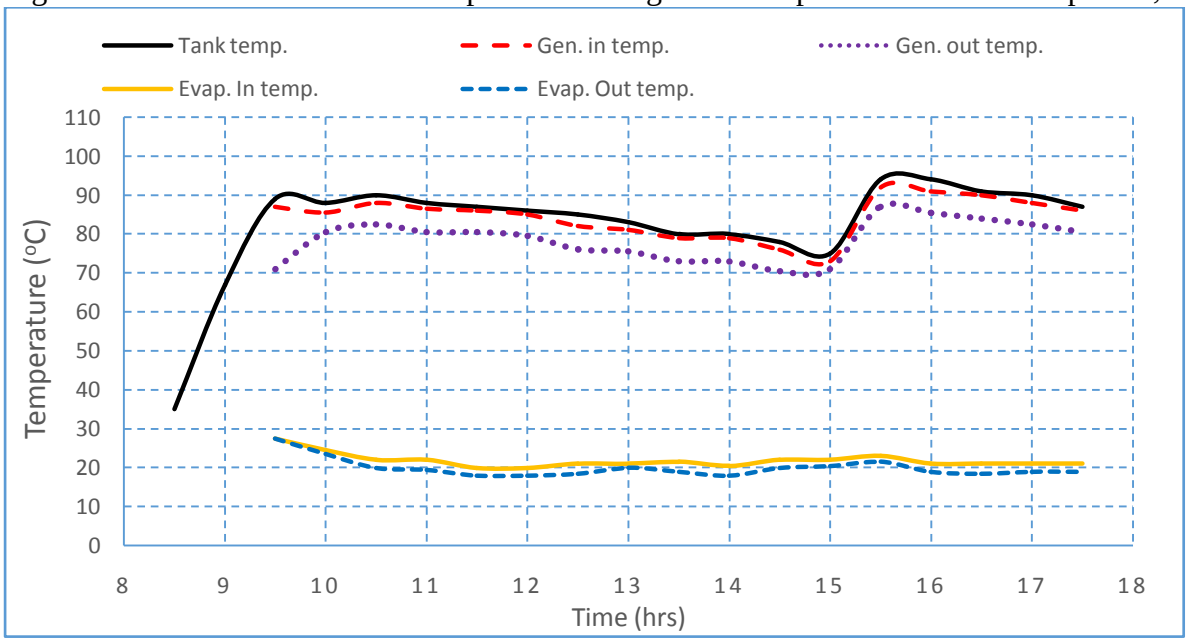


Fig. 4.90. Variation of system temperatures with time for April 22, 2017

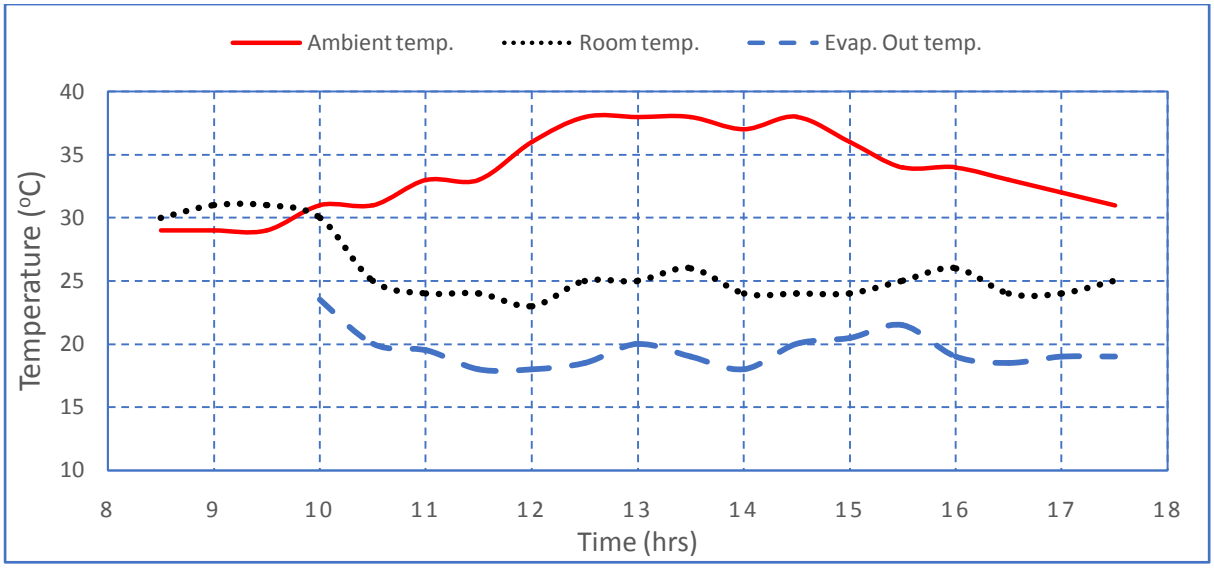


Fig. 4.91. Variation of ambient and room temperatures with time for April 22, 2017

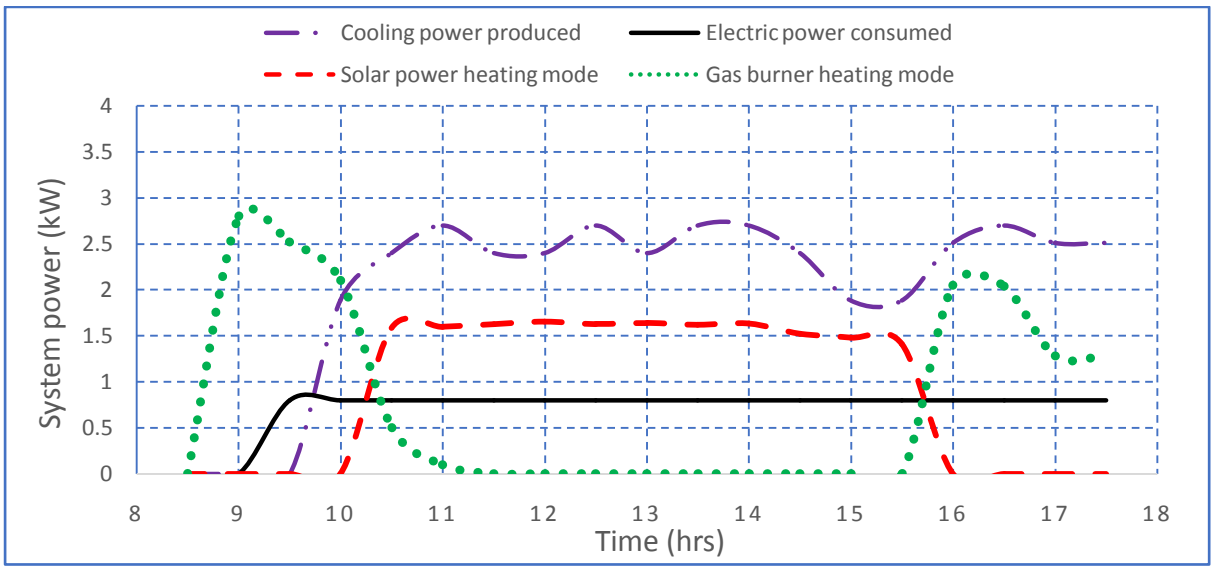


Fig. 4.92: Variation of system power with time for April 22, 2017

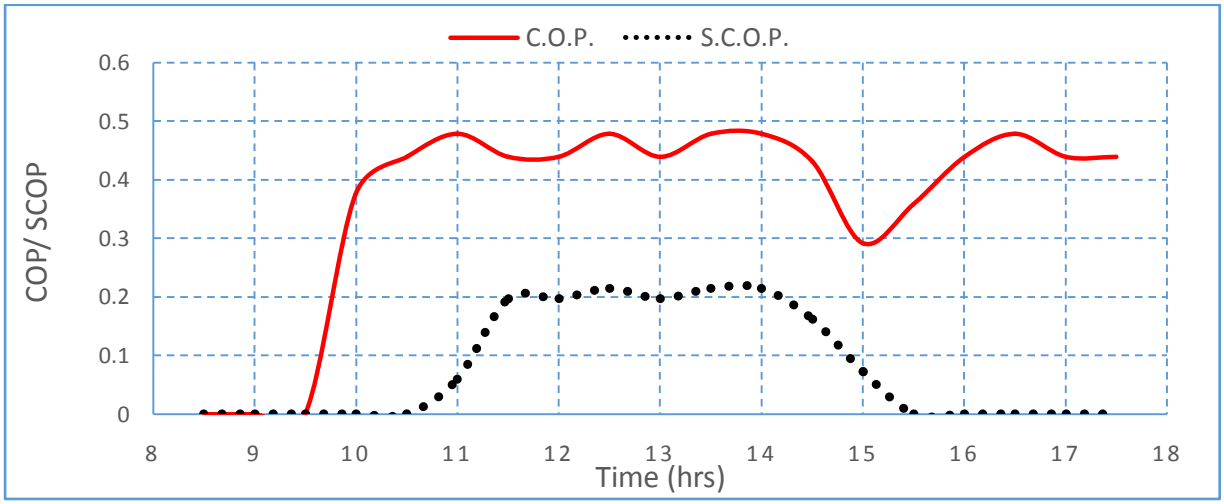


Fig. 4.93: Variation of COP and SCOP with time for April 22, 2017

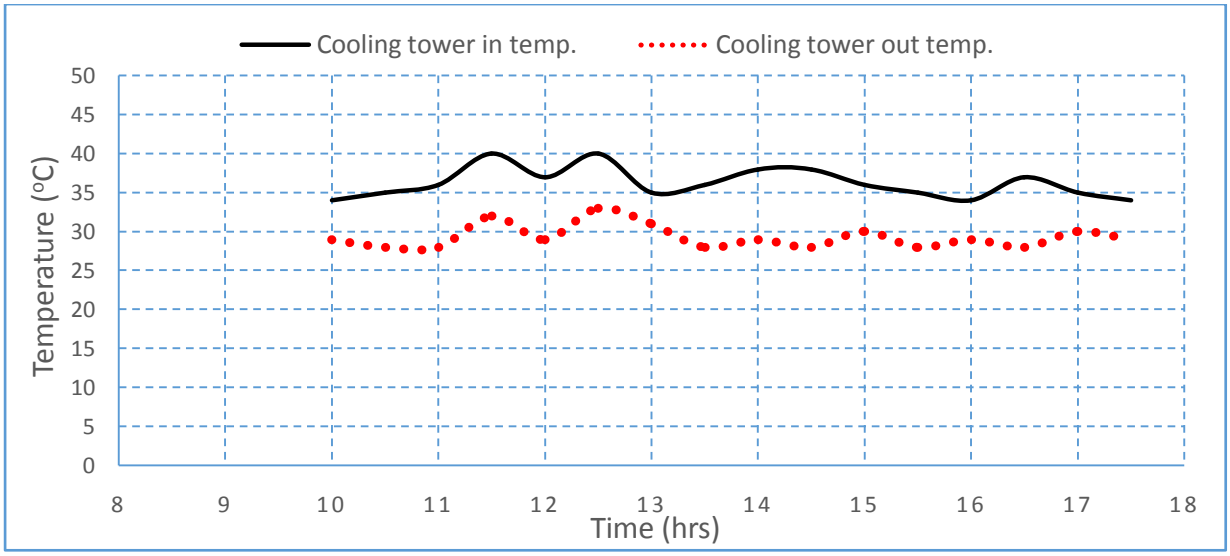


Fig. 4.94: Variation of cooling tower temperatures with time for April 22, 2017

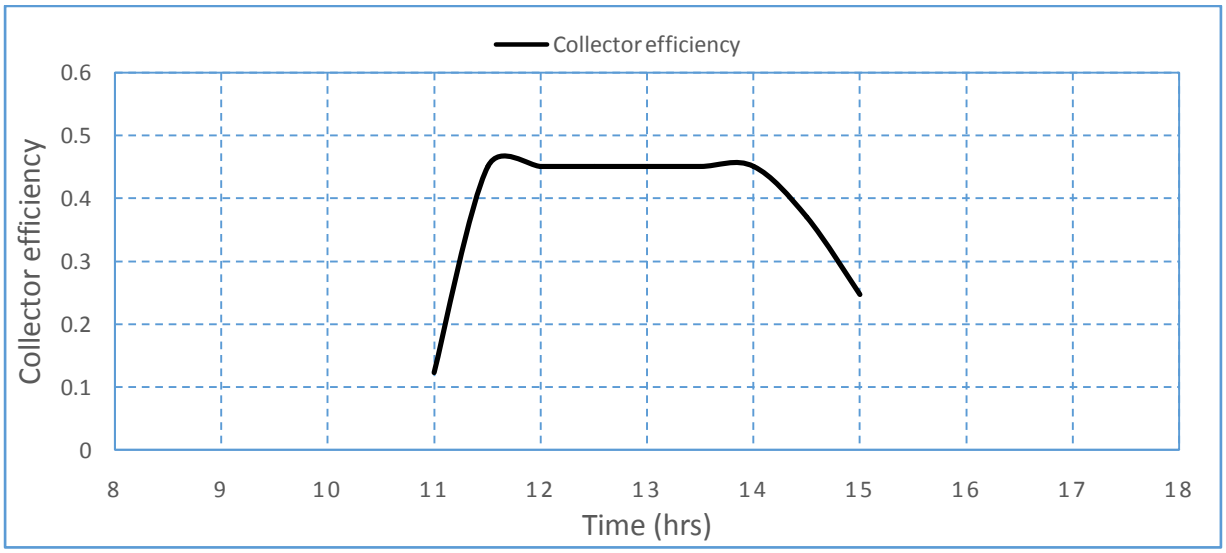


Fig. 4.95. Variation of collector efficiency with time for April 22, 2017

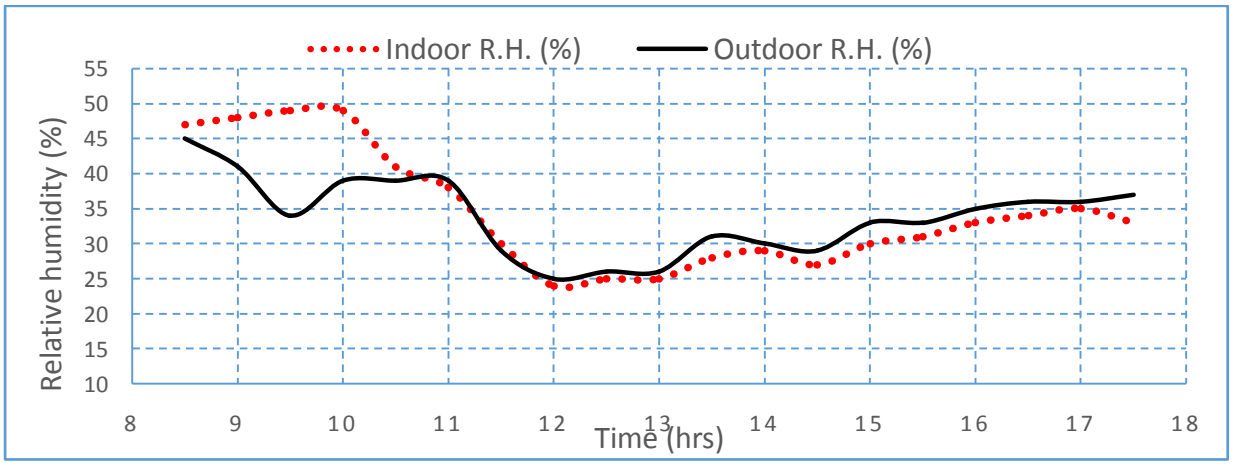


Fig. 4.96: Variation of relative humidity with time for April 22, 2017

From figure 4.88, high solar radiation can be seen on the experimental day. Solar radiation above 1000W/m^2 were recorded in the peak sunshine hours. From figure 4.89, gas consumption can be seen to be at the peak from the start of the experimental day to about 10 am, this is because the system was started in the gas burner heating mode due to the low solar radiation available at that time. However, at about 10 am, collector plate temperature starts to rise above 100^{o}C and collector fluid temperature attains a range of about 80^{o}C. As seen from the same figure, the gas boiler heating mode was disengaged at about 10.30 am and switched to solar heating mode. It can be seen that the collector fluid temperatures begin to decline until the temperatures fall well below 80^{o}C at about 4pm. This is because a few hours after midday, the solar radiation starts to decline. At this point the system was switched back to gas heating mode for the rest of the day.

From figure 4.90, it is seen that the tank and generator temperatures decline from above 80^{o}C at the commencement of solar power heating mode (10am) to below 80^{o}C at about 3pm. This is as a result of decline in solar radiation as the day progressed, which resulted in lower hot water temperatures. However, the temperatures rapidly return to 90^{o}C when the gas boiler heating mode was restored at about 3pm. Evaporator chilled water temperatures are seen to have dropped from 28^{o}C at the start of cooling to 23^{o}C and below. Chilled water outlet temperatures are seen to be below 20^{o}C in some instances.

From figure 4.91, test room temperature can be seen to be higher than the ambient temperature before the cooling commenced. When cooling commenced, room temperature can be seen to decline to as low as 24^{o}C, while ambient temperatures continue to rise to 38^{o}C. This is an indication that the chiller was able to achieve cooling. Room temperatures between 24^{o}C to 26^{o}C were recorded. From figure 4.92, maximum cooling power of 2.7 kW was recorded, while minimum cooling power of 1.8 kW was recorded. Gas burner heating mode was employed in the early hours of 8:30 to 10:30 am, as well as late in the evening hours of 4:00 to 5:30 pm. Also from the figure, solar power heating mode was used during more hours of the experimental day

compared to the gas boiler heating mode. This was as a result of high solar radiation recorded for most part of the experimental day.

From figure 4.93, the COP is seen to be stable above 0.4, until it dropped to 0.3 at about 3pm. This was because the system had been in solar power heating mode, solar radiation declined and subsequently collector, tank and generator temperatures declined until the lowest level at 3pm. At this point the generator hot water temperature was only a little over 70^{o}C, desorption of lithium bromide became weak and subsequently the performance declined. However, COP began to rise steadily as soon as the system was switched to gas burner heating mode. Also from figure 4.93, the SCOP is seen to be at about 0.2 for the period in which the solar heating mode was employed (11:00 to 15:00 hrs).

From figure 4.94, it is seen that the cooling tower was able to cool the cooling water from above 35^{o}C to well below 35^{o}C all through the experimental day. From figure 4.95, the collector efficiency can be seen to increase gradually from 0.11 at the start of the solar heating mode (11 am) and attained a peak of about 0.47 during the peak solar radiation hours (12 noon to 2 pm) and then declined to 0.25 at 3 pm. This indicates that the collector efficiency is directly related to the available solar radiation. Figure 4.96 shows the indoor relative humidity to be higher than the outdoor relative humidity before the commencement of cooling. However, when cooling commenced, the indoor relative humidity is seen to drop and eventually falls a little below the outdoor relative humidity which has also reduced in value. This indicates that there was no humidification of the room resulting from the chilled water passing through the fan coil unit.

Figures to 4.97 to 4.104 show the graphs that describe the variation in experimental parameters for the experimental day of June 3rd, 2017 which was classified as a fairly clear sky day.

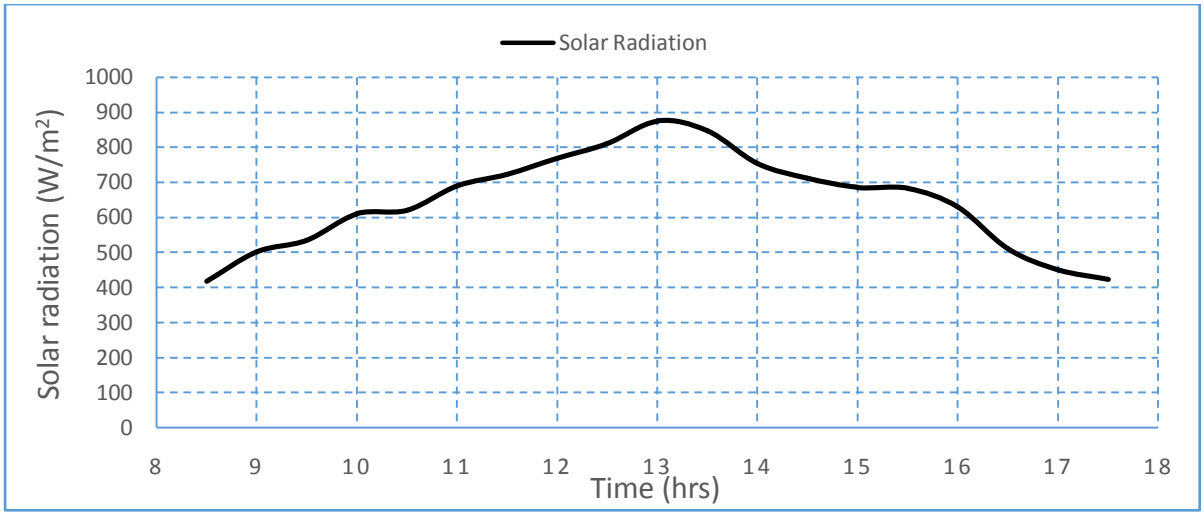


Fig. 4.97. Variation of solar radiation with time for June 3, 2017

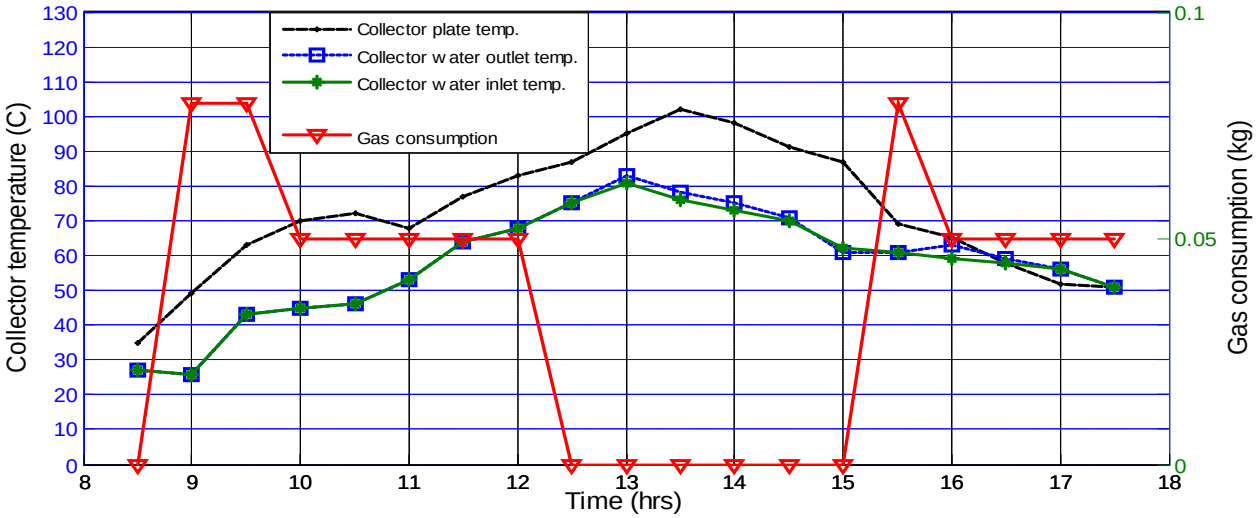


Fig. 4.98. Variation of collector temperatures and gas consumption with time for June 3, 2017

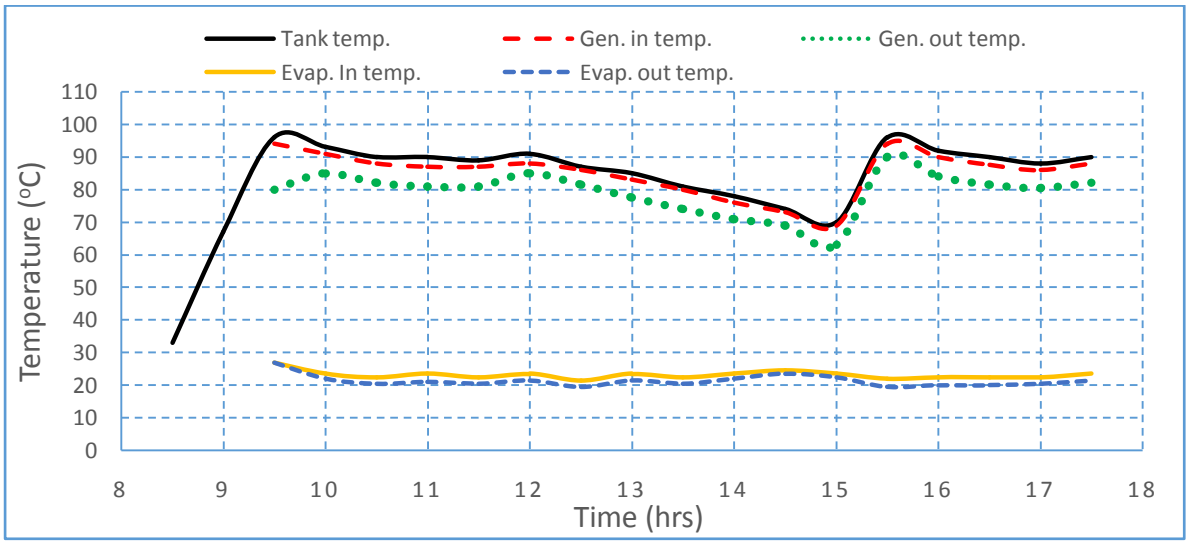


Fig. 4.99. Variation of system temperatures with time for June 3, 2017

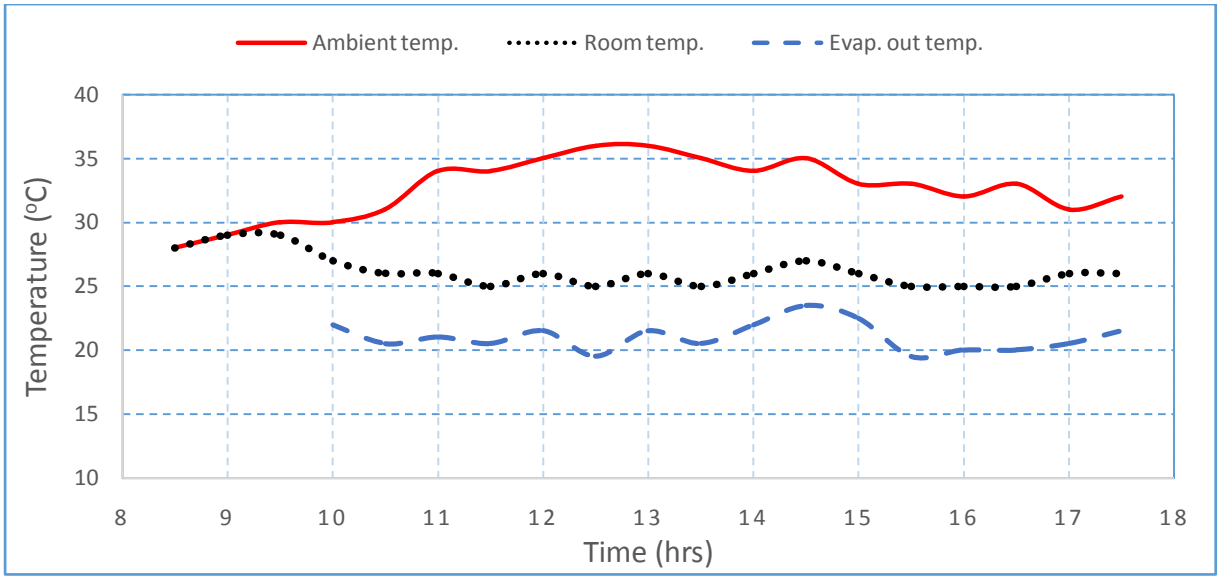


Fig. 4.100. Variation of ambient and room temperatures with time for June 3, 2017

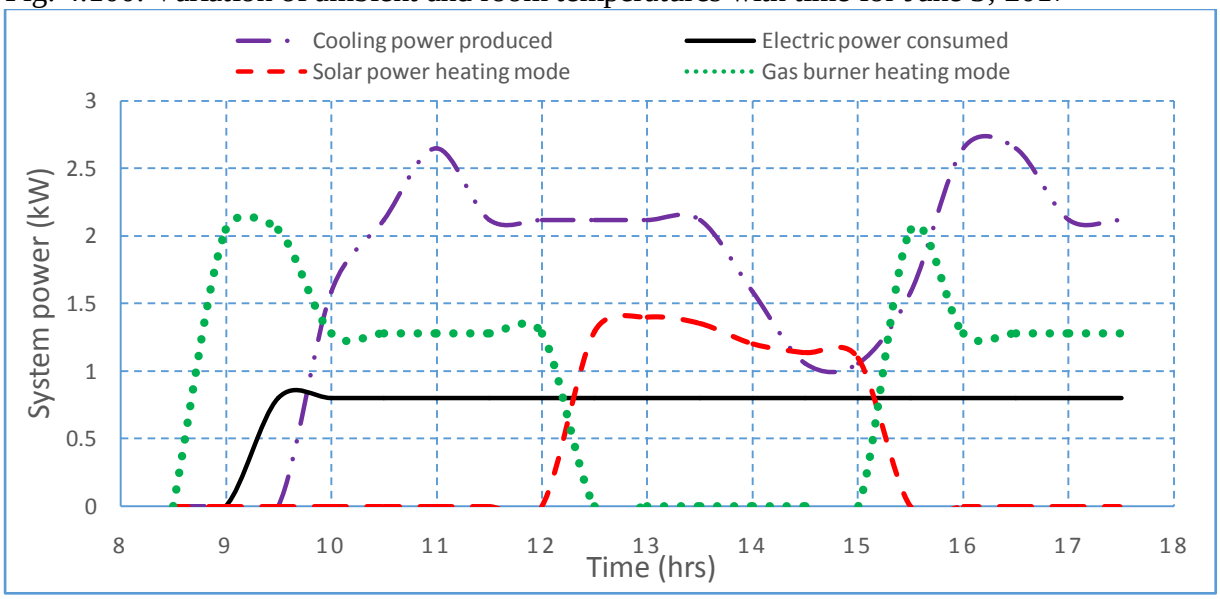


Fig. 4.101. Variation of system power with time for June 3, 2017

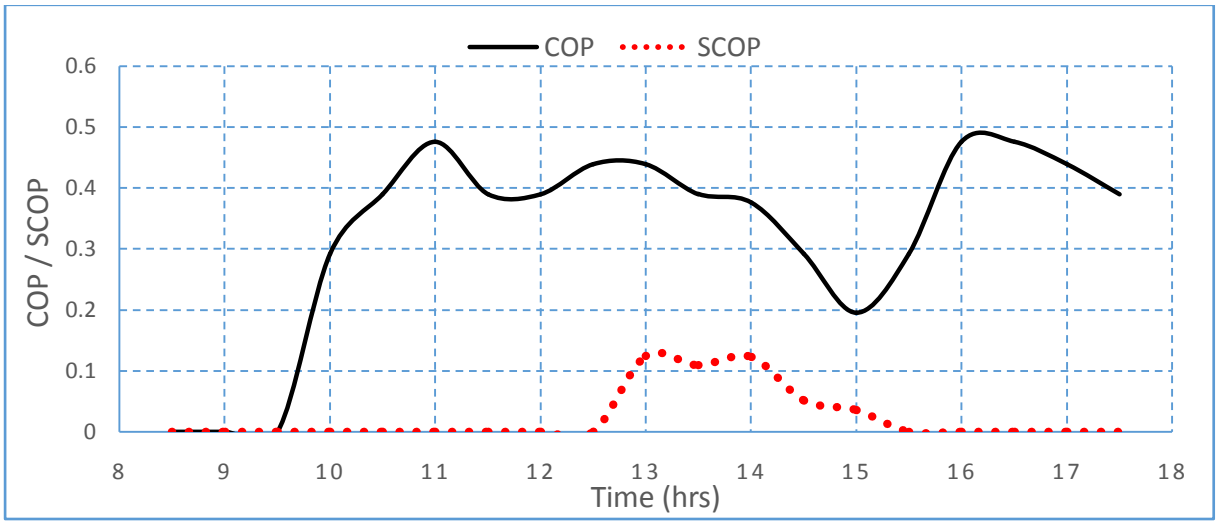


Fig. 4.102. Variation of COP and SCOP with time for June 3, 2017

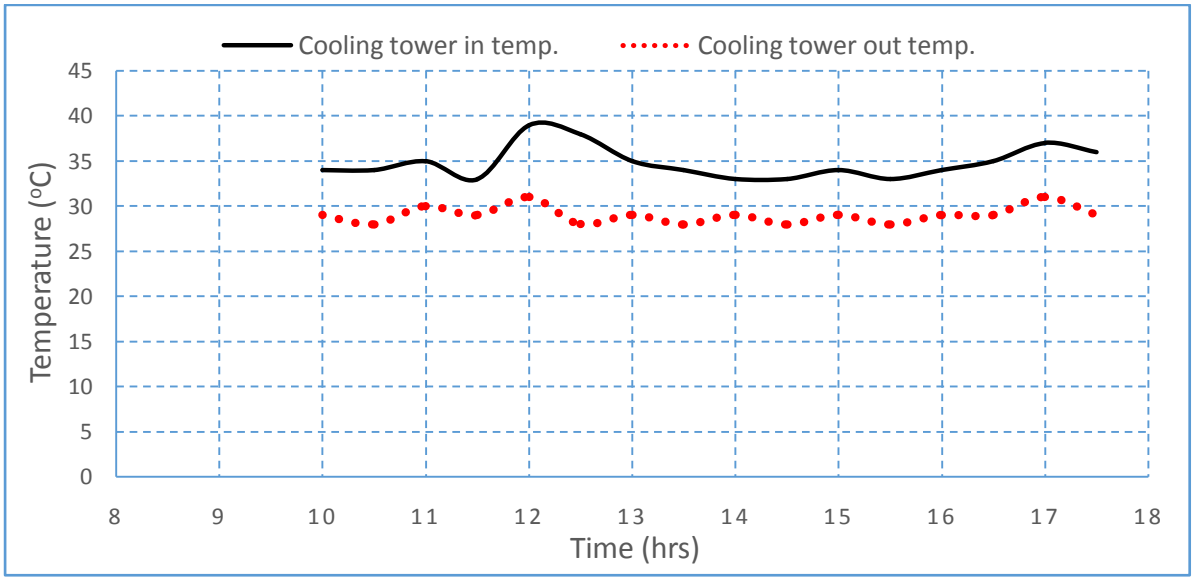


Fig. 4.103. Variation of cooling tower temperatures with time for June 3, 2017

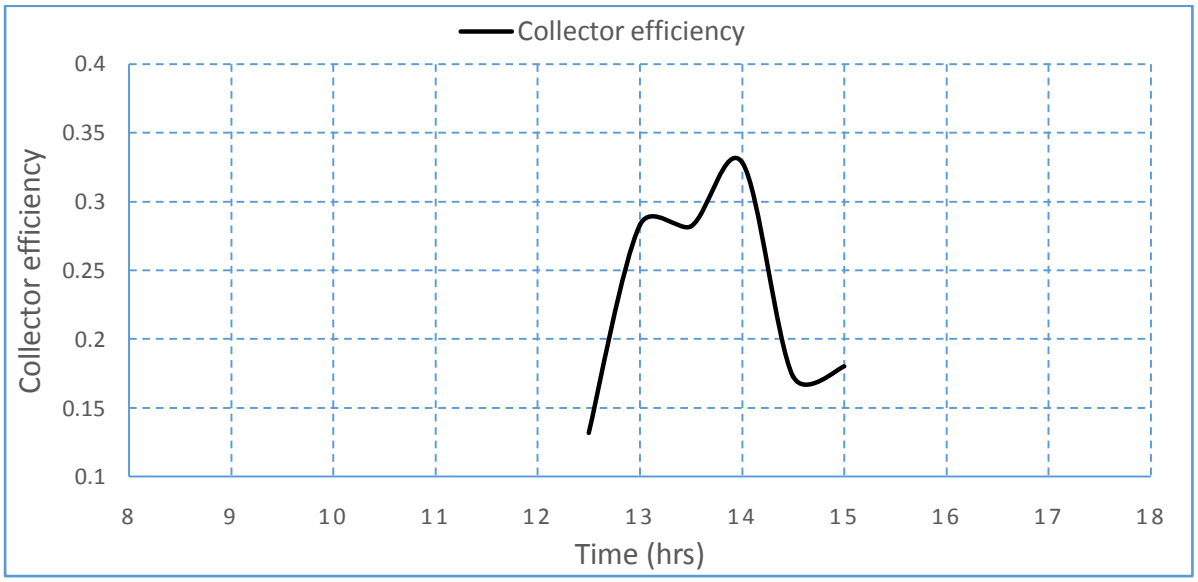


Fig. 4.104. Variation of collector efficiency with time for June 3, 2017

From figure 4.97, solar radiation is seen to increase gradually, eventually it peaks at above 800W/m^2 between 12 noon and 2 pm, after which it declines. From figure 4.98, gas consumption is seen to peak in the early hours of the experimental day (9 am to 10 am), after which the consumption drops and continues until the gas consumption is disengaged at past noon. At this stage the solar heating mode was switched on. From the figure, the decline in collector fluid temperatures between 1 pm and 3 pm is a result of decline in solar radiation. The system was then restored to gas boiler heating mode.

From figure 4.99, the decline in tank and generator temperatures as seen is as a result of decline in solar radiation while the system was in the solar heating mode within the same time interval (12:30 to 15:00 hrs). This can be seen to have resulted in a little rise in evaporator chilled water temperatures also in the same time interval (12:30 to 15:00 hrs). This is as a result of weak desorption at the generator.

From figure 4.100, room temperature is seen to decrease from the commencement of cooling. Room temperature falls well below the ambient temperature, an indication that cooling was achieved. Room temperatures between 24 and 26^{o}C were recorded. From figure 4.101, a cooling power produced can be seen to be between 1.1 and 2.6 kW. Cooling power produced was above 2 kW for most of the experimental day. The system was operated in the gas boiler heating mode for a greater part of the day.

From figure 4.102, the lowest recorded COP of 0.18 is seen to have occurred during the interval in which the system was in solar heating mode. This is an indication that the system performance declines as solar radiation drops. Also, highest SCOP of 0.12 was recorded for the experimental day. From figure 4.103, the cooling tower is seen to have been able to cool the cooling water by keeping the outlet cooling water at 30^{o}C and below. From figure 4.104, collector efficiency varied from 0.135 to 0.34.

Figures to 4.105 to 4.112 show the graphs that describe the variation in experimental parameters for the experimental day of June 6, which was classified as a hot clear sky day.

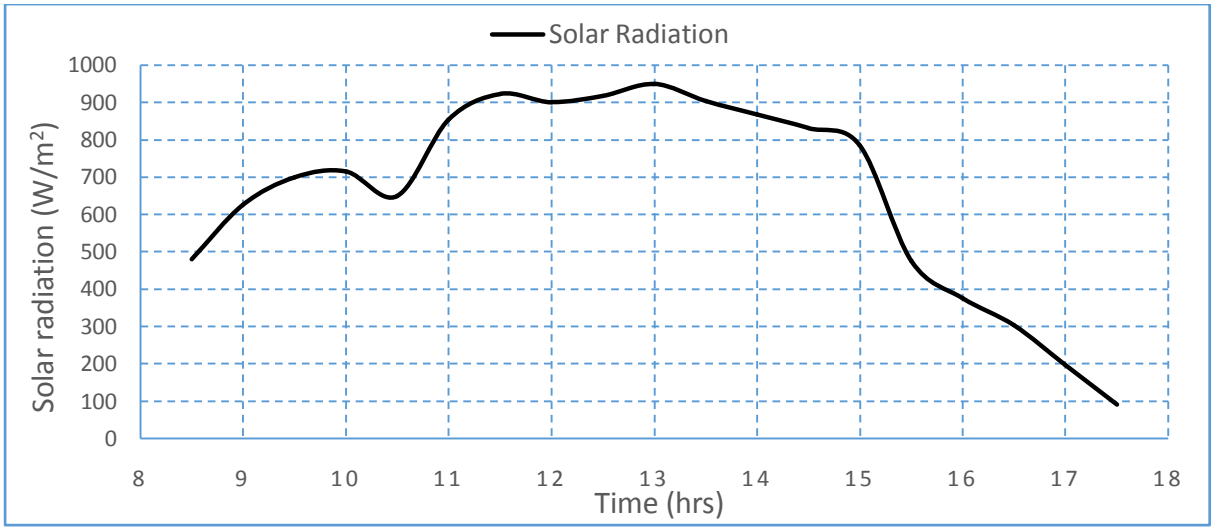


Fig. 4.105. Variation of solar radiation with time for June 6, 2017

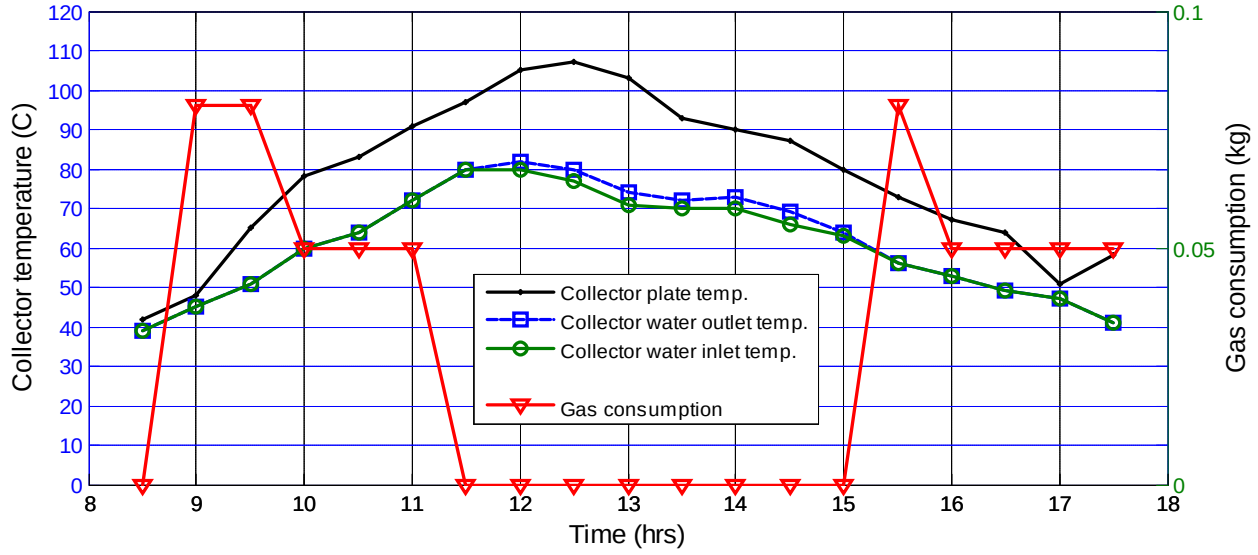


Fig. 4.106. Variation of collector temperatures and gas consumption with time for June 6, 2017

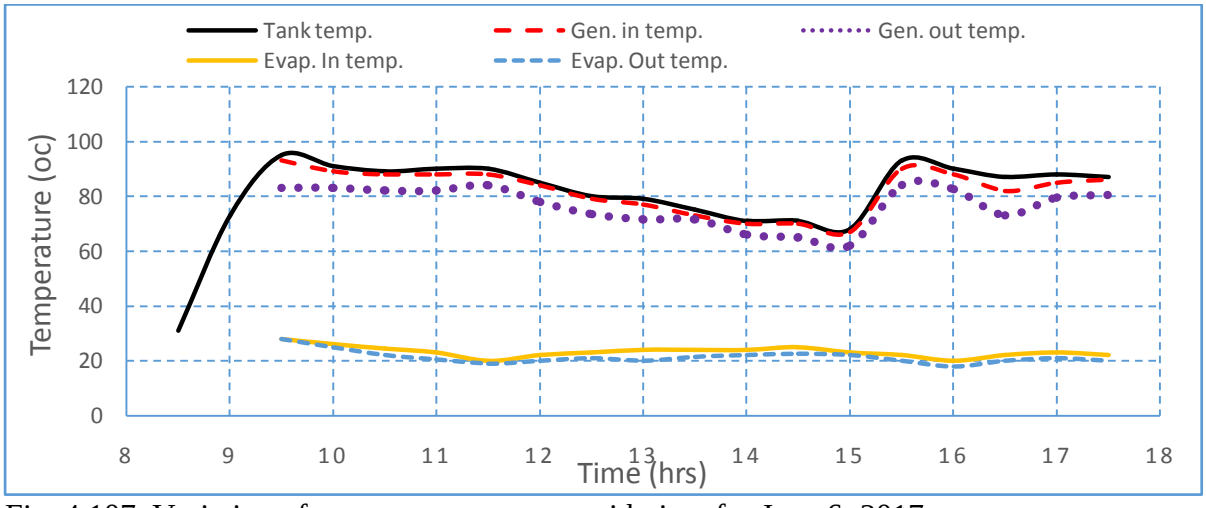


Fig. 4.107. Variation of system temperatures with time for June 6, 2017

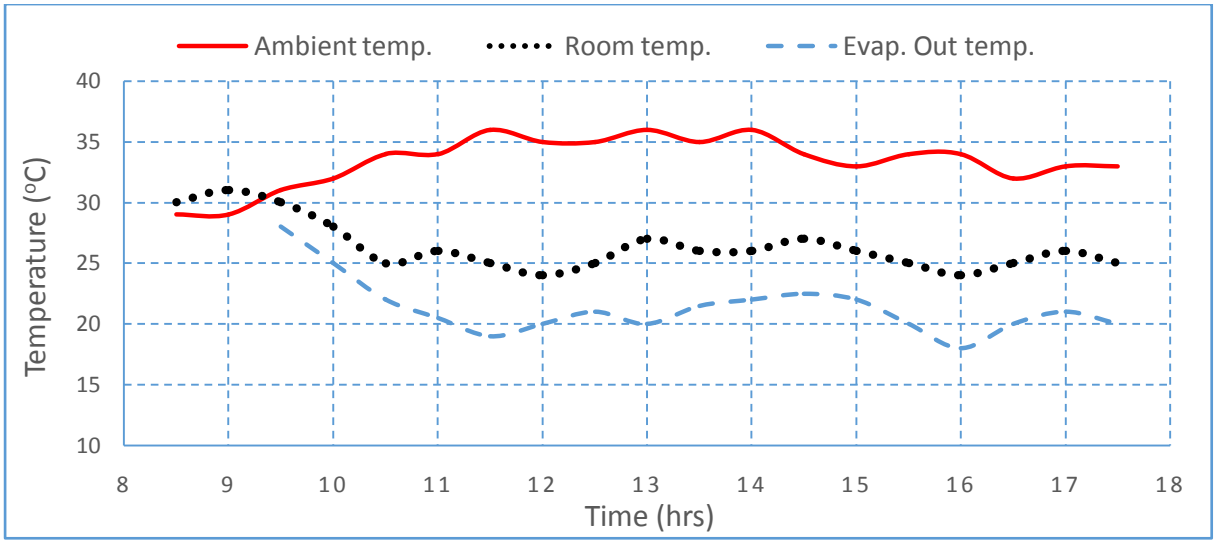


Fig. 4.108. Variation of ambient and room temperatures with time for June 6, 2017

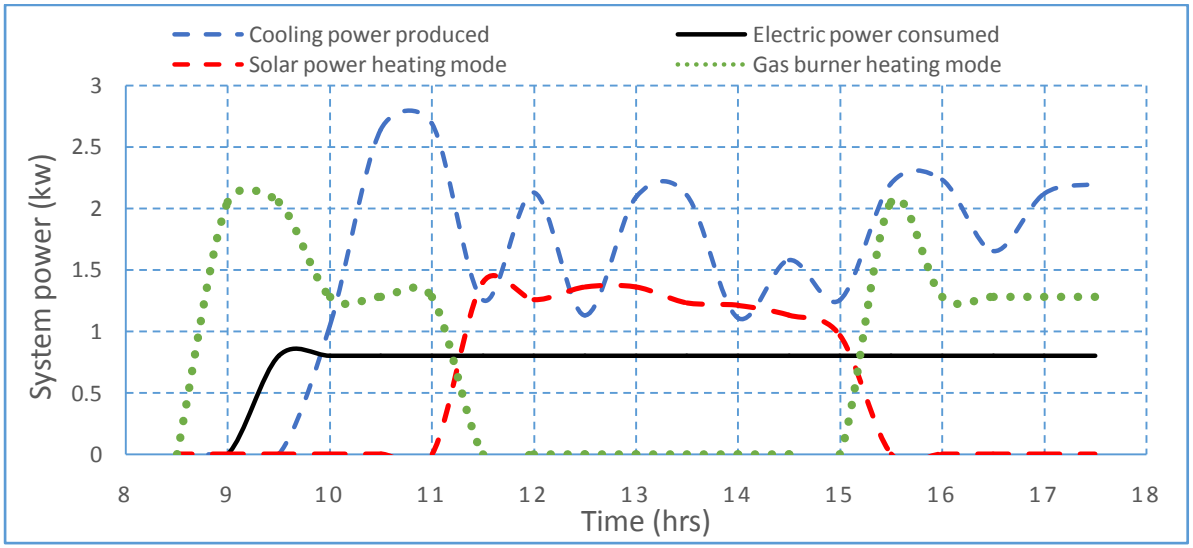


Fig. 4.109. Variation of system power with time for June 6, 2017

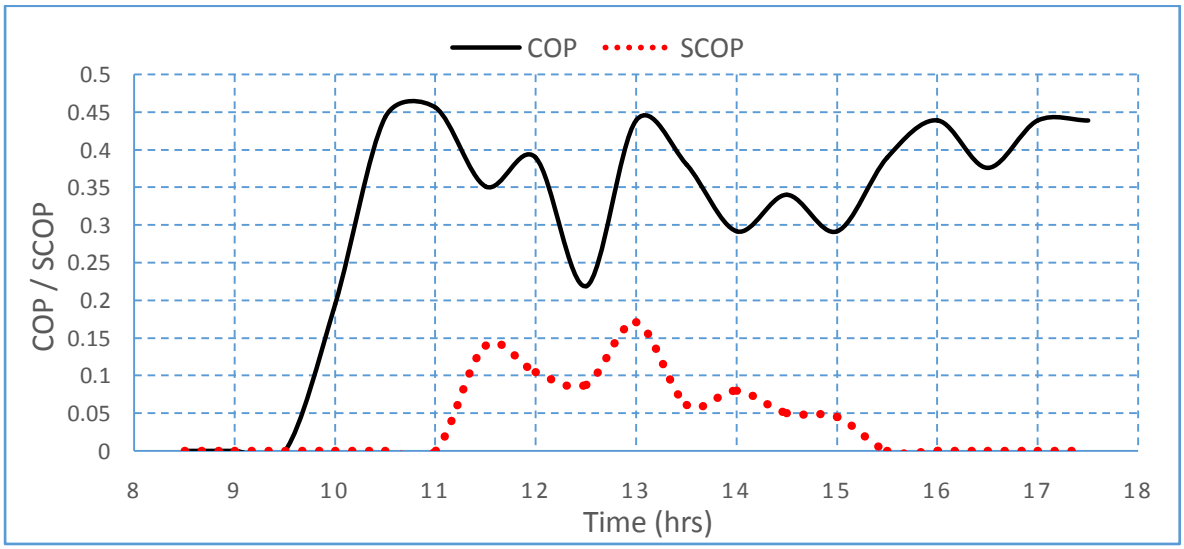


Fig. 4.110. Variation of COP with time for June 6, 2017

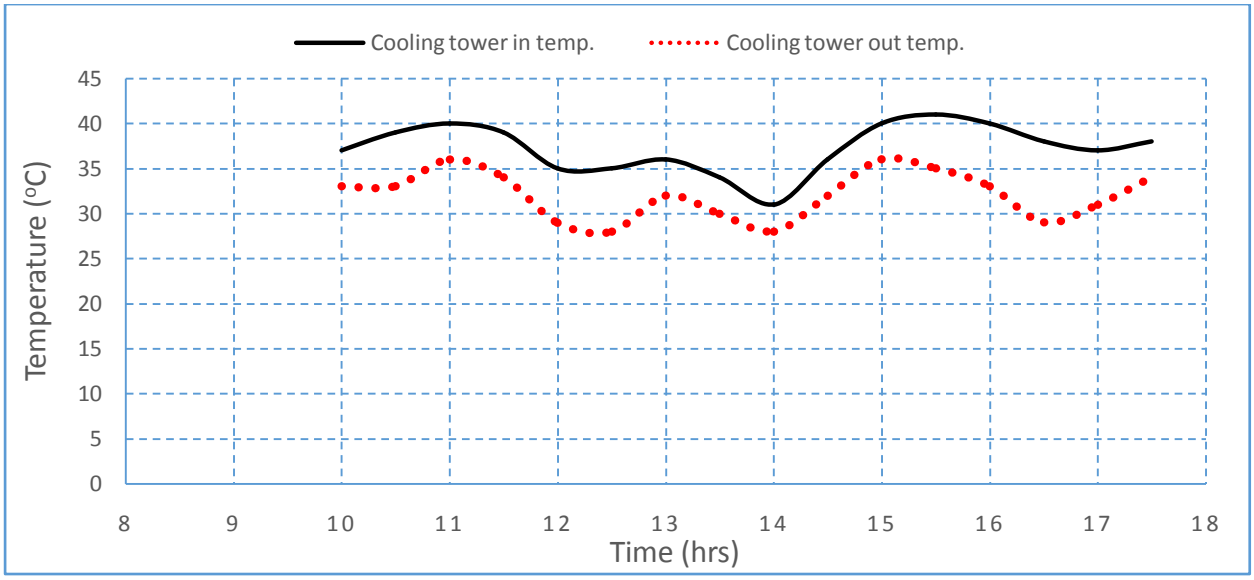


Fig. 4.111. Variation of cooling tower water temperatures with time for June 6, 2017

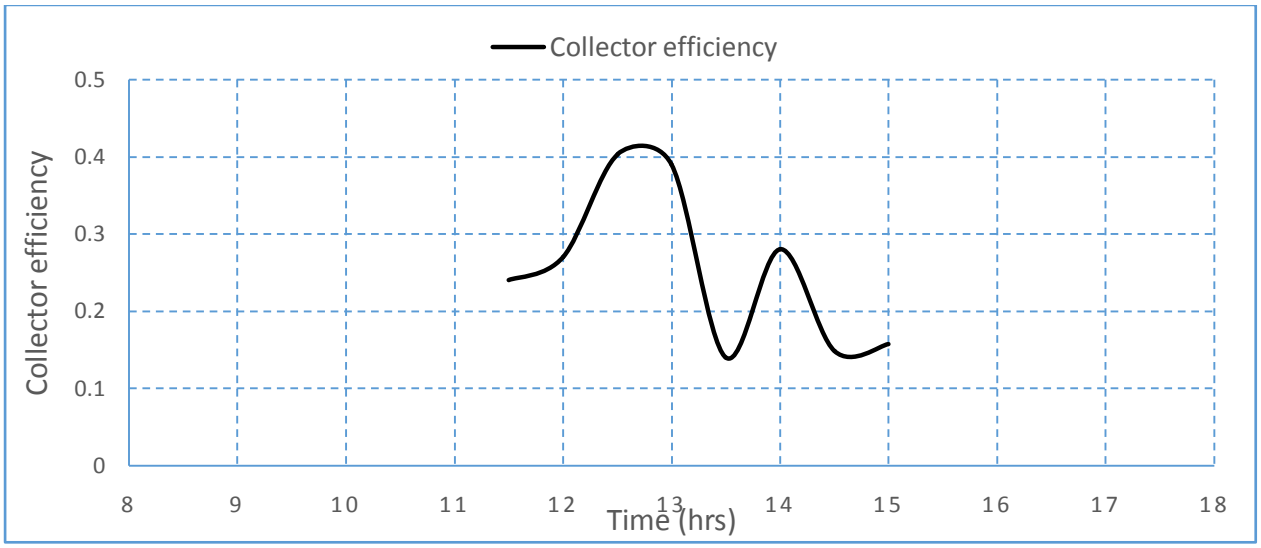


Fig. 4.112. Variation of collector efficiency with time for June 6

Figure 4.105 shows the experimental day to have solar radiation at levels above 900W/m^2 between 11 am and 2:30pm. From figure 4.106, there was no gas consumption between the hours of 11:30am and 3pm. During this period the system operated in solar heating mode. The collector temperatures declined from 80^{o}C to 60^{o}C within this period. This was as a result of fluctuating solar radiation. Eventually gas boiler heating mode had to be restored. From figure 4.107, the tank and collector temperatures are seen to have experienced a decline during the period of solar heating mode (11:30 am to 3:00pm). This was because the collector system temperatures have also dropped. This resulted in a slight increase in evaporator temperatures within the time interval.

From figure 4.108, the room temperature decreased from above 30^{o}C before the cooling commenced and stayed between 24 to 27^{o}C during cooling. Room temperature stayed well below the ambient temperature for the experimental day. From figure 4.109, peak cooling power of 2.7 kW is seen to have been produced in gas burner heating mode. The cooling power produced in the solar heating mode is seen to fluctuate between 1.1 and 2.2 kW. This is an indication of fluctuation in available solar radiation. From figure 4.110, the system recorded maximum SCOP of 0.16 in the solar heating mode and peak COP of 0.46 in the gas burner heating mode. Figure 4.111 shows the cooling tower was able to provide the required cooling of the cooling water. The cooling water temperature at outlet from the cooling tower were kept at 35^{o}C and below. Figure 4.112 shows the collector efficiency to be between 0.23 and 0.42.

Figures to 4.113 to 4.119 show the graphs that describe the variation in experimental parameters for the experimental day of June 7, which was classified as a rainy day.

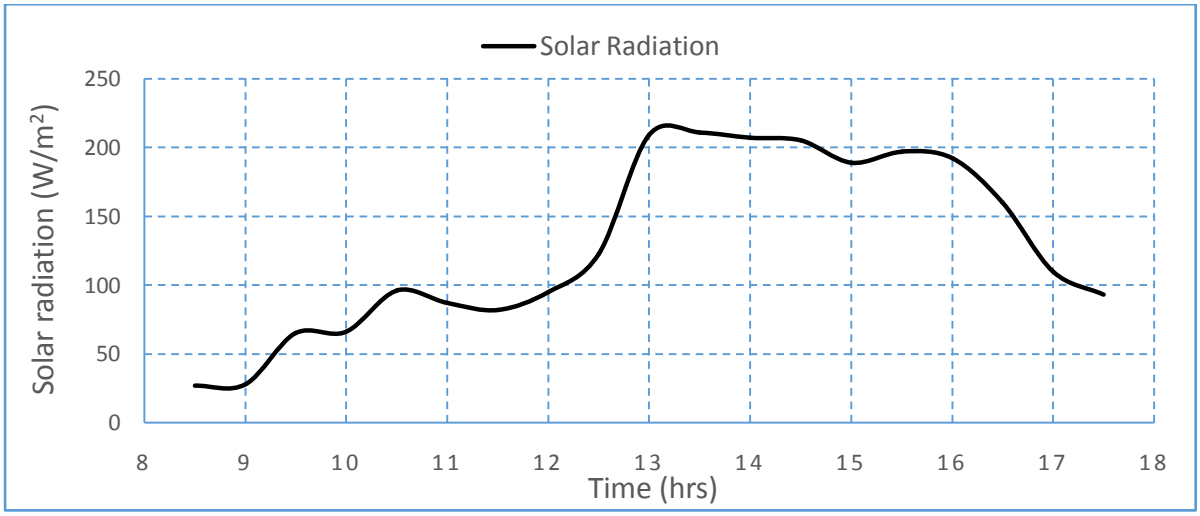


Fig. 4.113. Variation of solar radiation with time for June 7, 2017

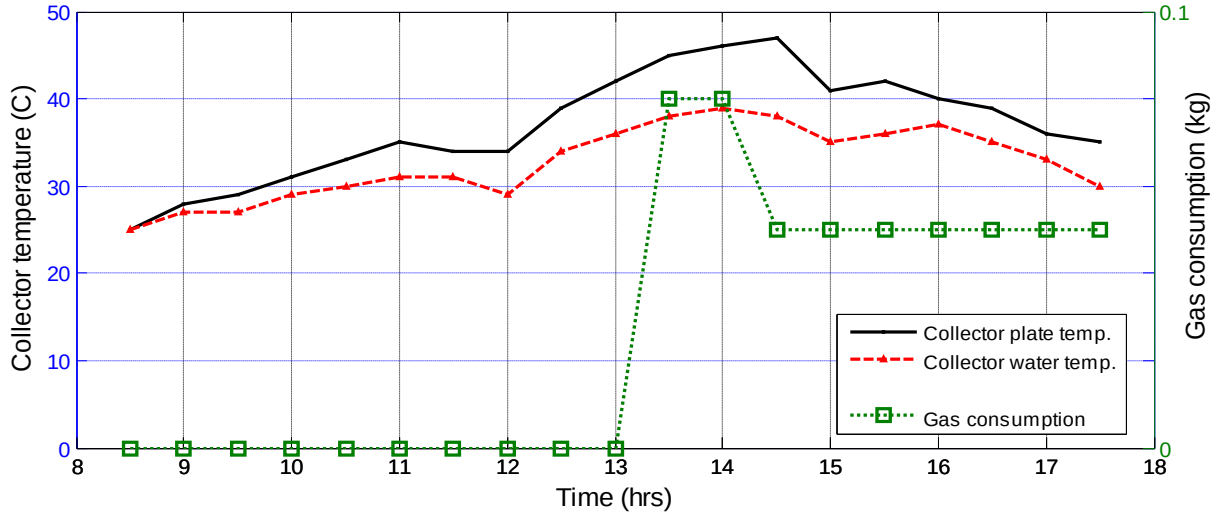


Fig. 4.114. Variation of collector temperatures and gas consumption with time for June 7, 2017

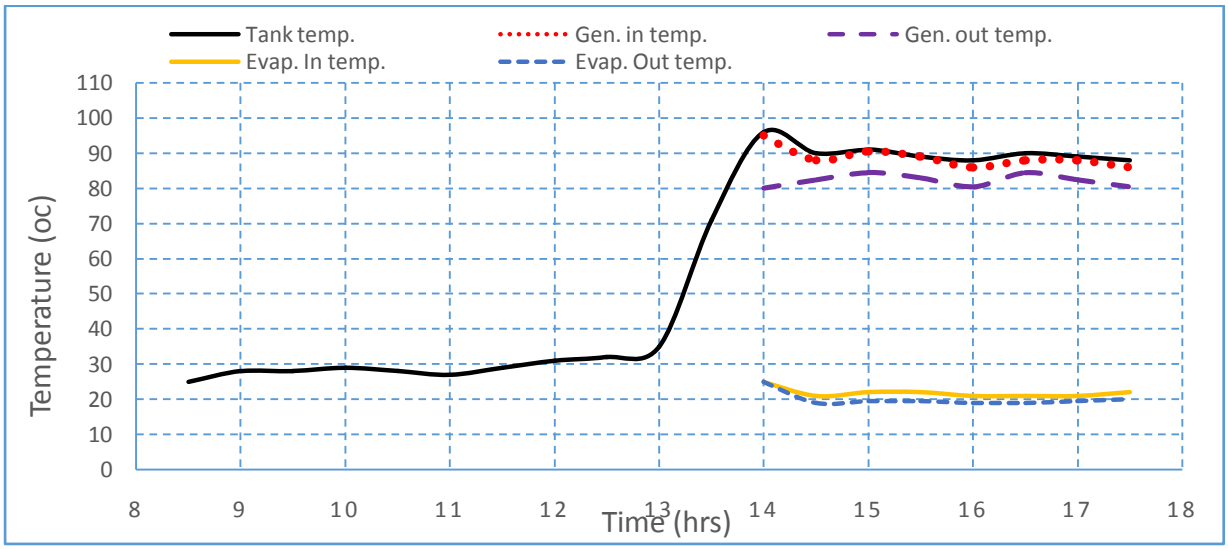


Fig. 4.115. Variation of system temperatures with time for June 7, 2017

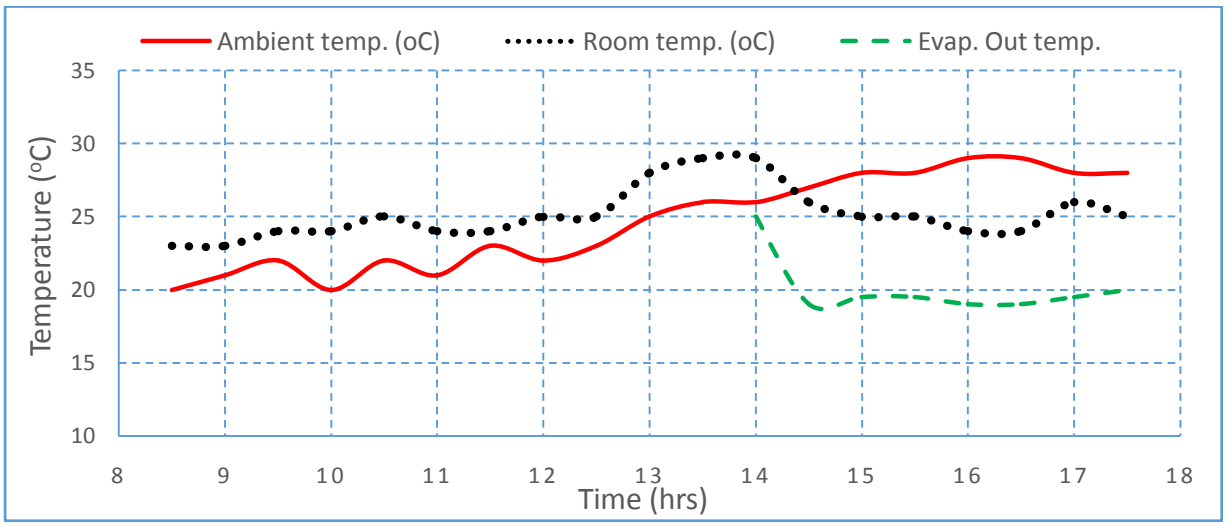


Fig. 4.116. Variation of ambient and room temperatures with time for June 7, 2017

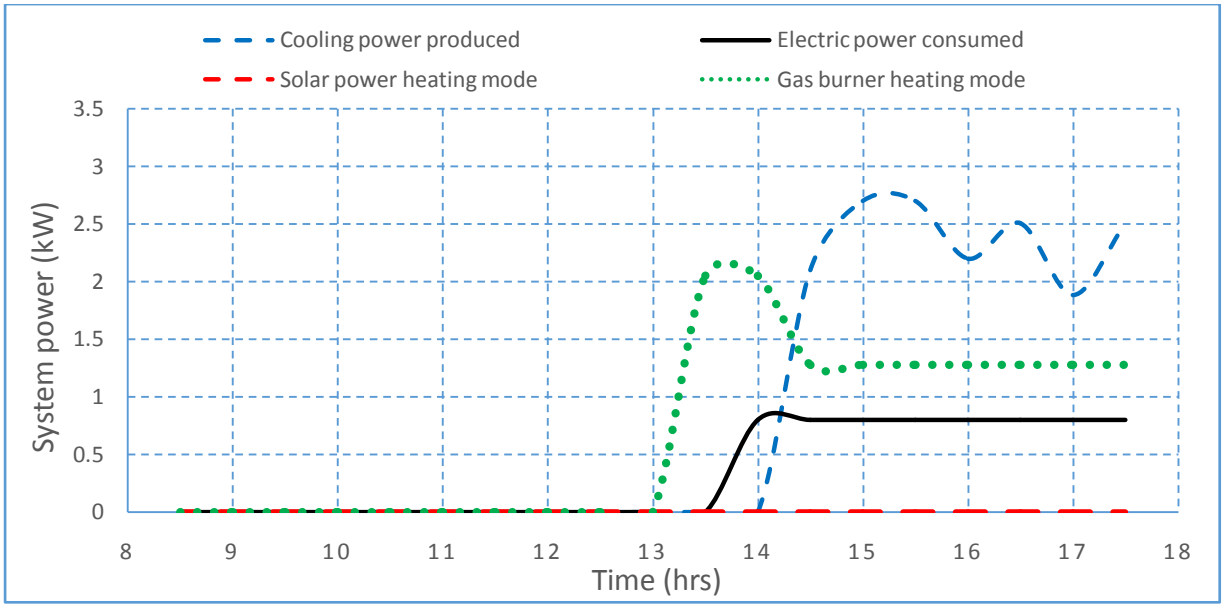


Fig. 4.117. Variation of system power with time for June 7, 2017

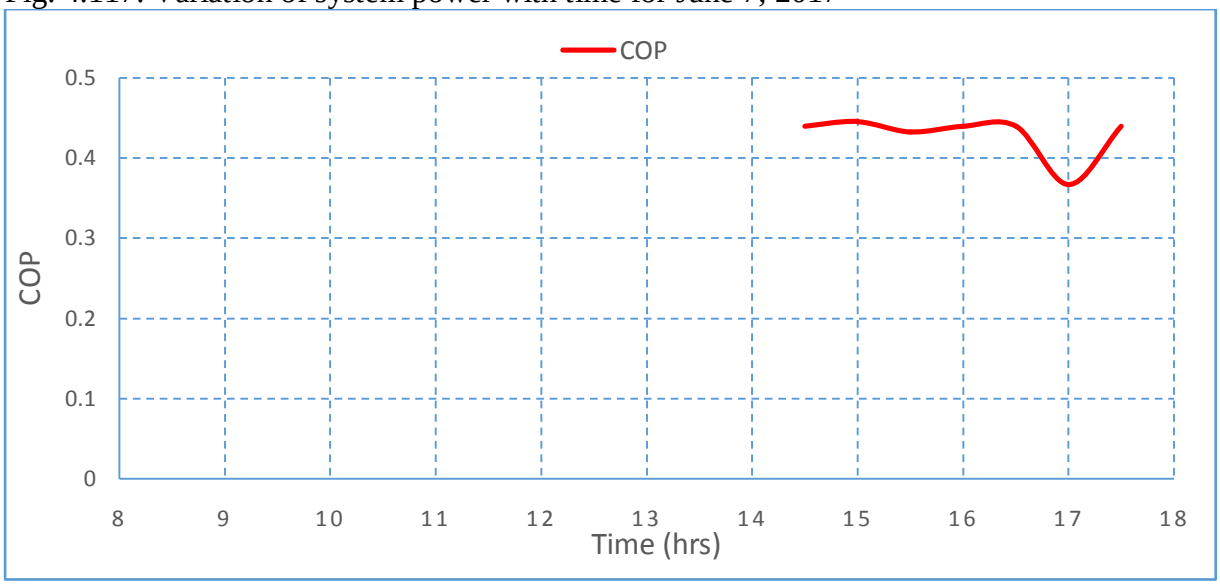


Fig. 4.118. Variation of COP with time for June 7, 2017

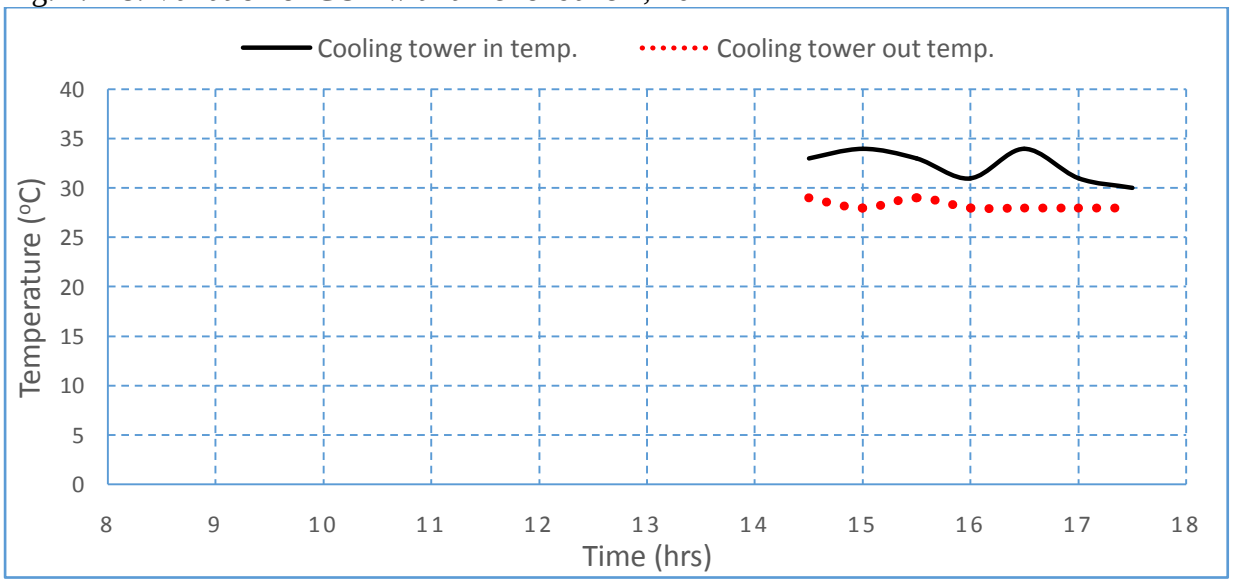


Fig. 4.119. Variation of cooling tower water temperatures with time for June 7, 2017

From figure 4.113, very low solar radiation can be seen to have been recorded on the experimental day. This was as a result of the rainy and cloudy nature of the day. Figure 4.114 shows very low collector temperatures for the day as a result of the very low solar radiation. There was no gas consumption from the start of the day up to 1pm, this was the period in which the rain lasted. The absorption chiller was not operated during this period as there was no cooling demand from the test room.

Figure 4.115 shows the process of cooling started at 1 pm, by heating the storage tank in gas boiler heating mode. Generator temperatures are seen to rise above 80^{o}C afterwards, chilled water outlet temperature is seen to drop from 27^{o}C at the start of cooling to 20^{o}C and below. From figure 4.116, room temperature and ambient temperature stayed well below 25^{o}C from 8: 30 up to noon, this was due to the rainy nature of the period. With the low room temperature, the absorption chiller was not operated within this interval. However after the rain, temperatures started to rise. Cooling of the room commenced at 1 pm and room temperature is seen to fall below the ambient temperature. Room temperatures below 25^{o}C were recorded.

From figure 4.117, cooling power between 1.8 and p222.7 kW was attained, while the gas burner heating mode was applied throughout the cooling interval. From figure 4.118, COP between 0.36 and 0.44 were recorded during the cooling period (14 to 17:30 hrs). From figure 4.119, cooling water outlet temperatures from the cooling tower stayed below 30^{o}C as required, this indicates the cooling tower was functional during the period cooling was applied.

Figures 4.120 to 4.127 show the graphs that describe the variation in experimental parameters for the experimental day of June 8, which was classified as a fairly clear sky day.

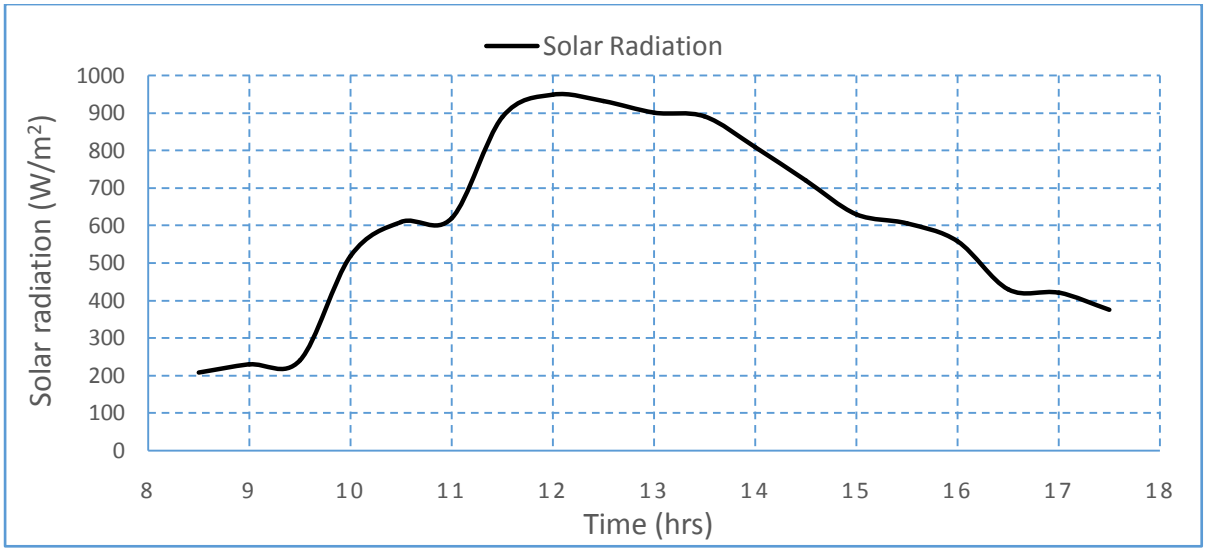


Fig. 4.120: Variation of solar radiation with time for June 8, 2017

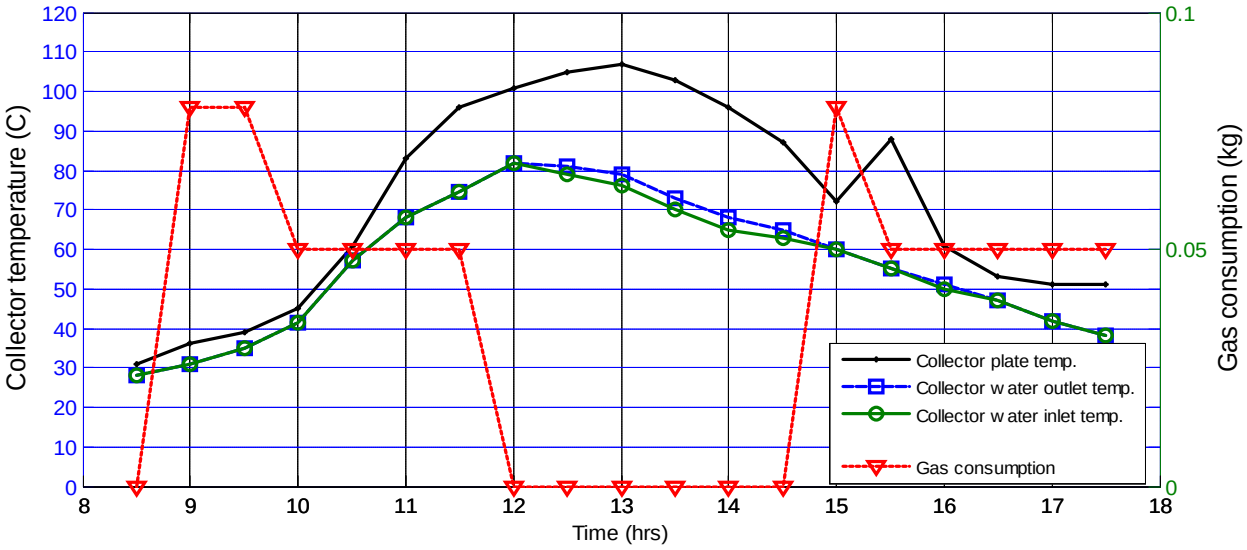


Fig. 4.121: Variation of collector temperatures and gas consumption with time for June 8, 2017

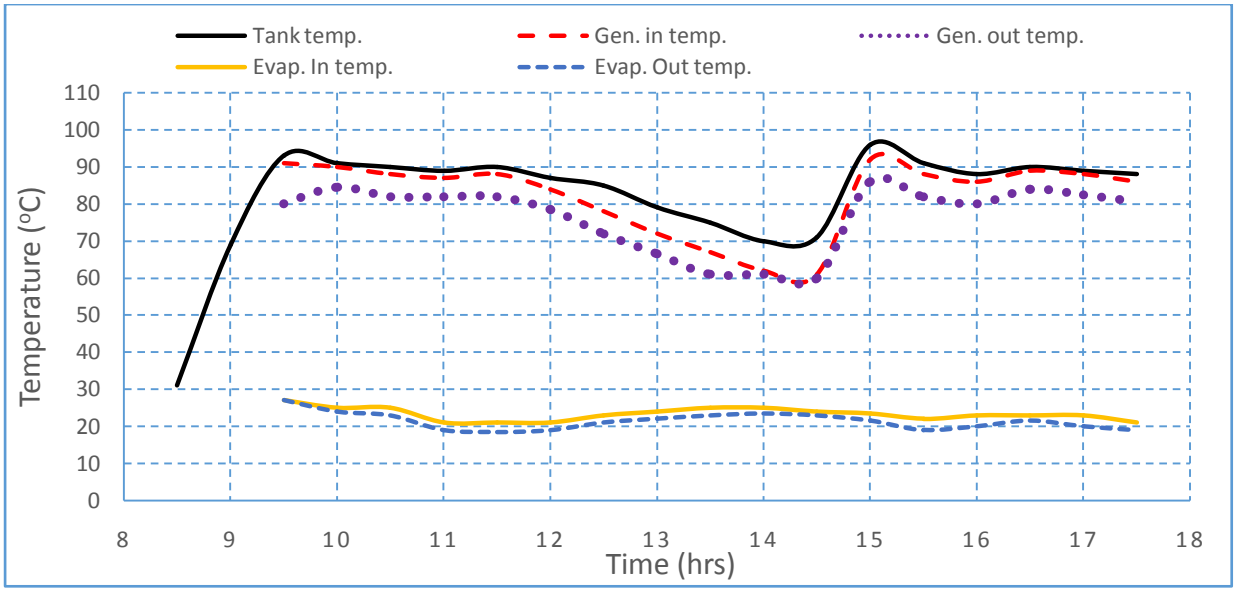


Fig. 4.122. Variation of system temperatures with time for June 8, 2017

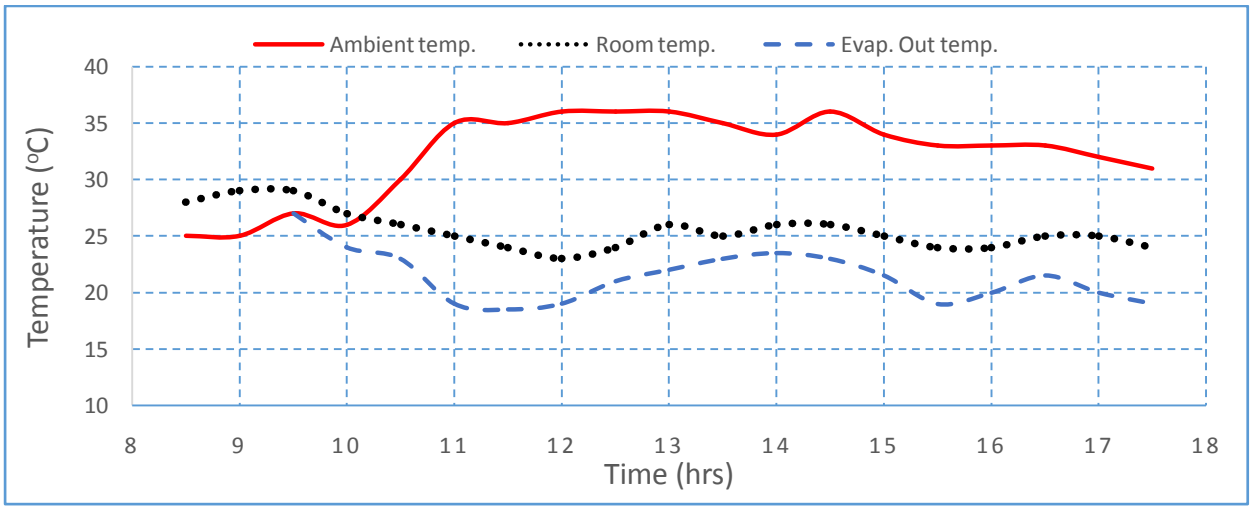


Fig. 4.123. Variation of ambient and room temperatures with time for June 8, 2017

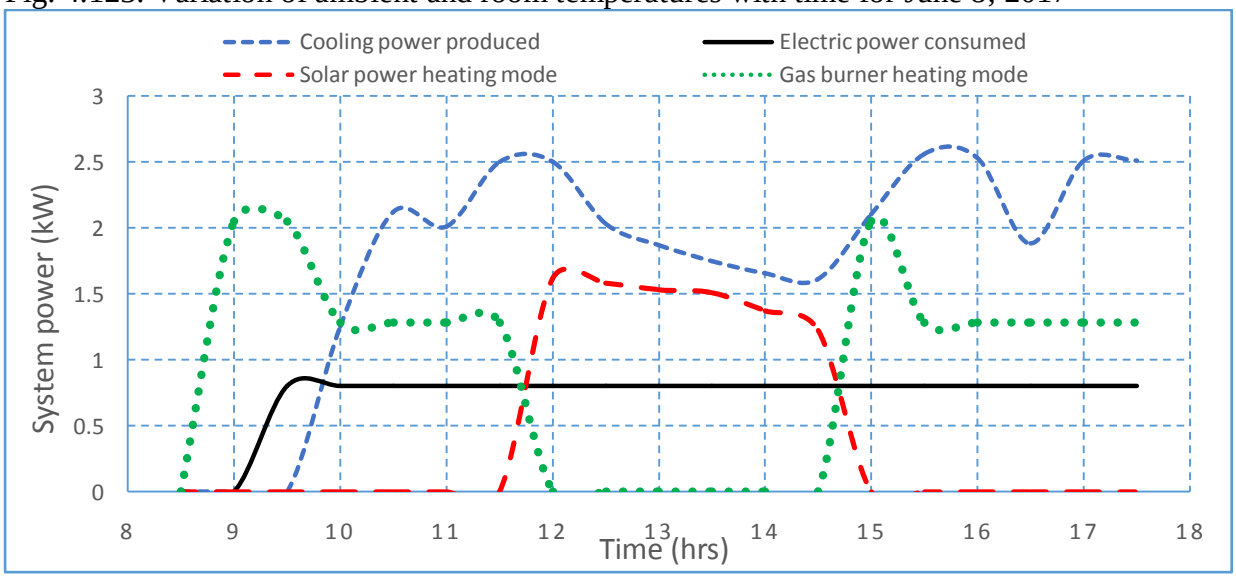


Fig. 4.124. Variation of system power with time for June 8, 2017

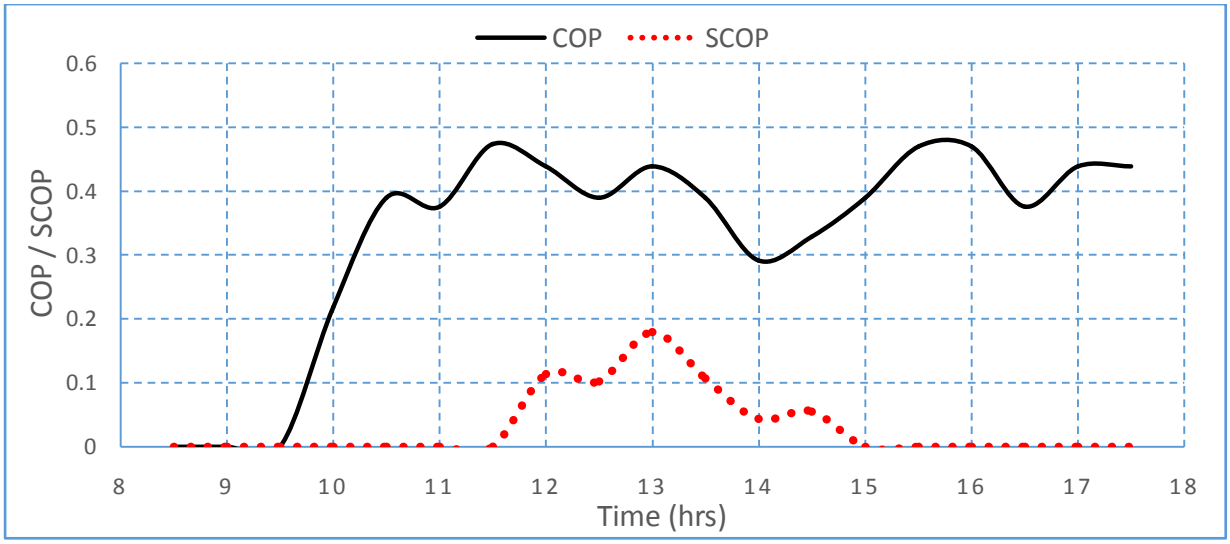


Fig. 4.125. Variation of COP and SCOP with time for June 8, 2017

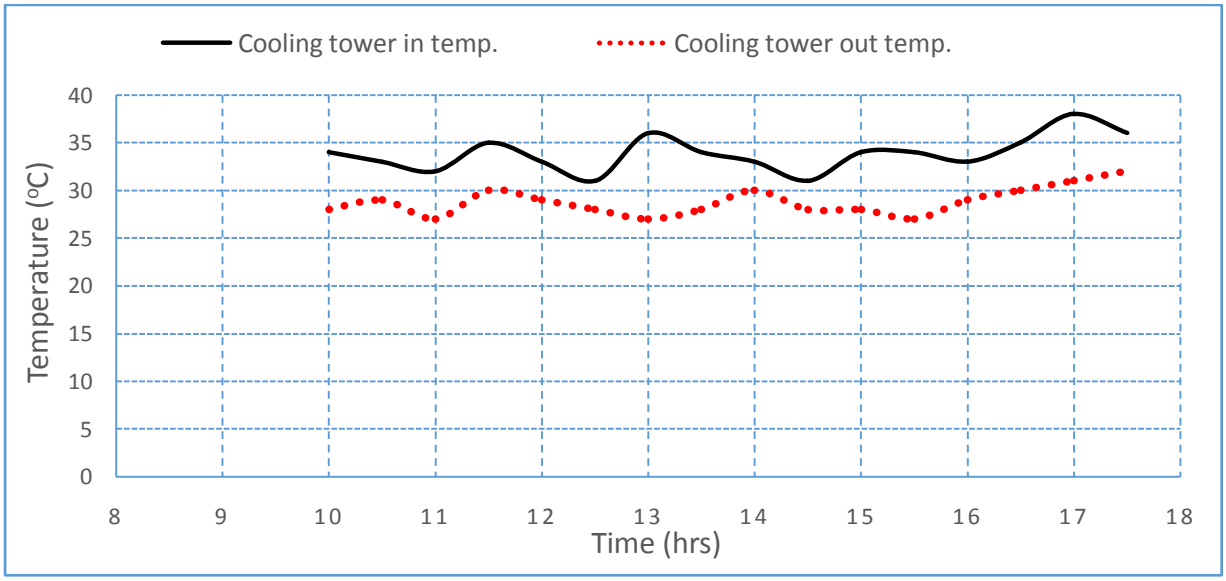


Fig. 4.126. Variation of cooling tower temperatures with time for June 8

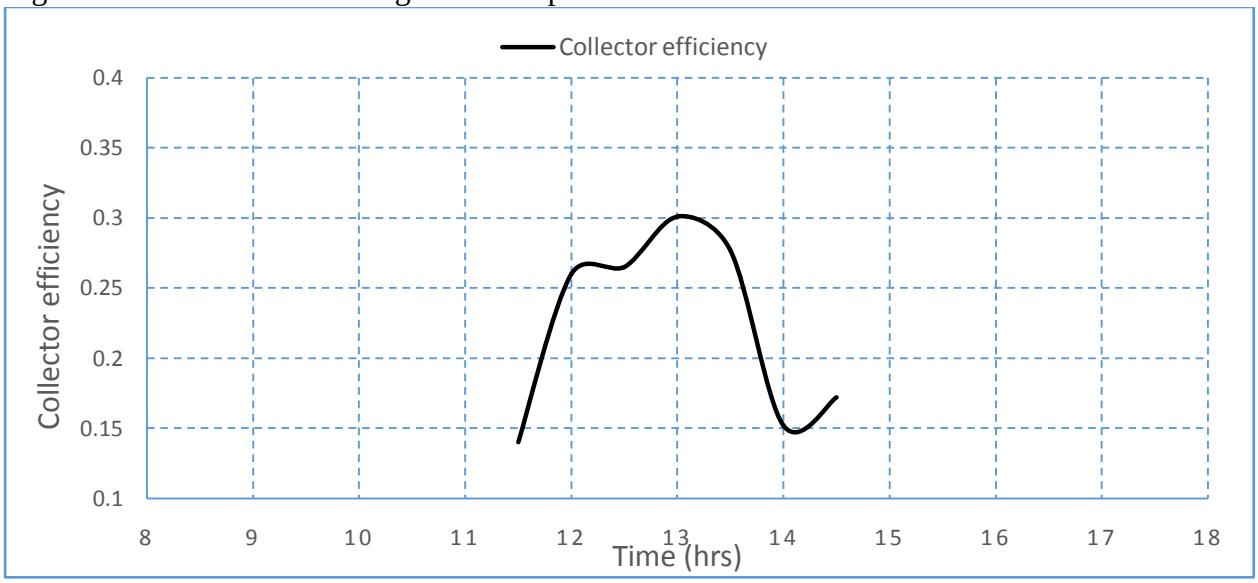


Fig. 4.127 Variation of collector efficiency with time for June 8, 2017

From figure 4.120, peak solar radiation of 930 W/m^2 was recorded at about midday, solar radiation values stayed much lower for the most part of the experimental day. This was due to the fairly clear nature of the sky.From figure 4.121, it is seen that there was no gas consumption between the hours of 12 noon and 2:30pm, the solar collector was operated during this period. The collector temperatures are seen to decline during this period. This was as a result of the declining solar radiation within the same period. As seen from figure 4.122, the generator temperatures declined within the period in which solar heating was applied (12 noon to 2:30 pm). Evaporator temperatures also increased slightly within this interval of solar heating. This was as a result of weak evaporation process resulting from low desorption at the generator. From figure 4.123, room temperatures dropped from 29^oC before cooling to between 23^oC and 27^oC. Room temperatures stayed well below the ambient temperature, the ambient temperatures were between 32 to 36^oC. This indicated cooling was achieved. From figure 4.124, maximum cooling power of 2.6 kW was achieved. Cooling power declined during the period of solar heating mode (12 noon to 2:30 pm), this was due to weak evaporation process as a result of low generator temperatures. From figure 4.125, maximum COP of 0.46 was achieved, while maximum SCOP of 0.17 was recorded. From figure 4.126, the cooling tower is seen to have maintained the cooling water outlet temperature below 32^oC. From figure 4.127, collector efficiency between 0.14 and 0.3 was achieved.

Figures to 4.128 to 4.134 show the graphs that describe the variation in experimental parameters for the experimental day of June 12, 2017, which was classified as a cloudy sky day.

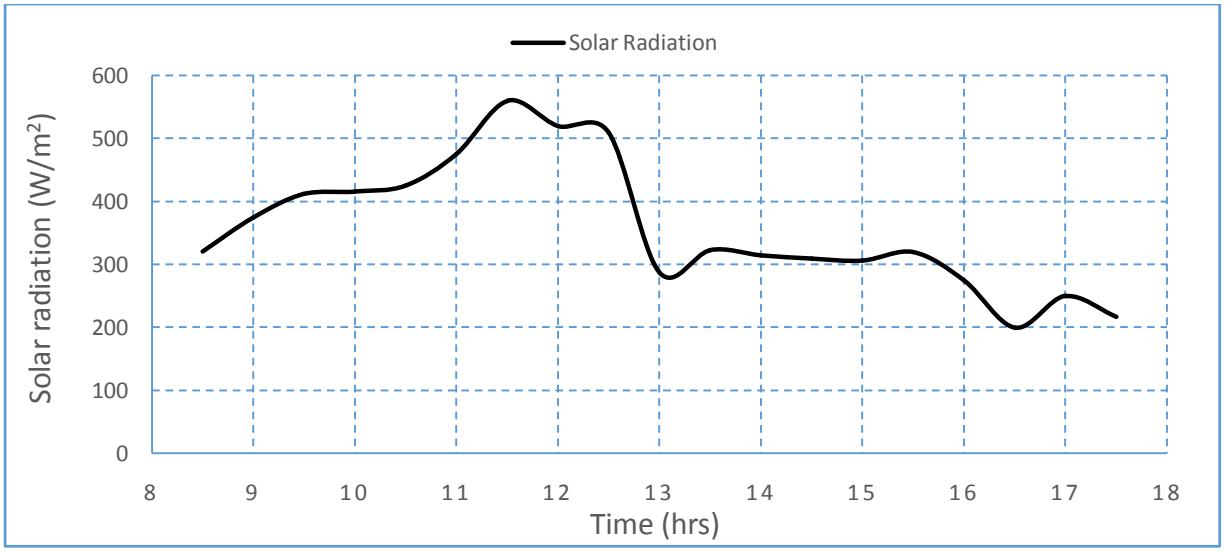


Fig. 4.128. Variation of solar radiation with time for June 12, 2017

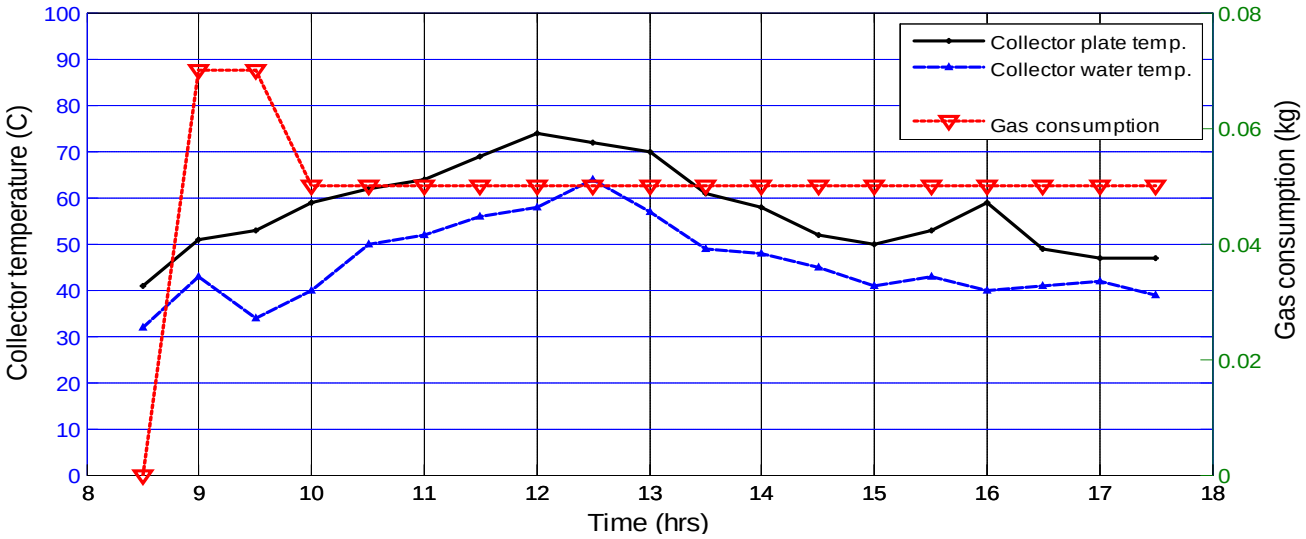


Fig. 4.129: Variation of collector temperatures and gas consumption with time for June 12, 2017

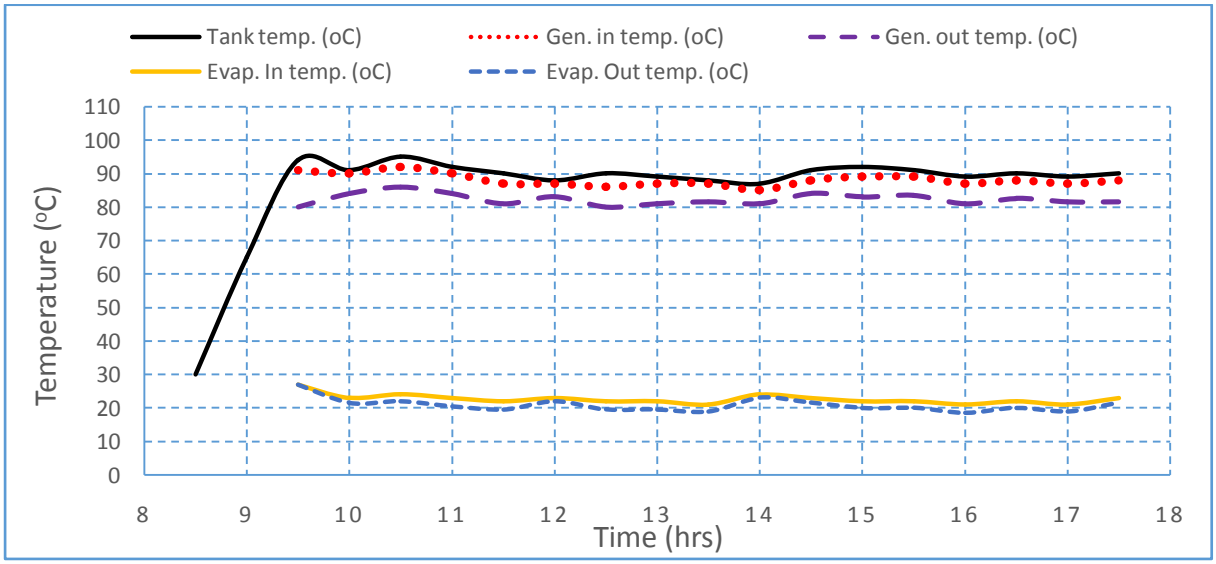


Fig. 4.130. Variation of system temperatures with time for June 12, 2017

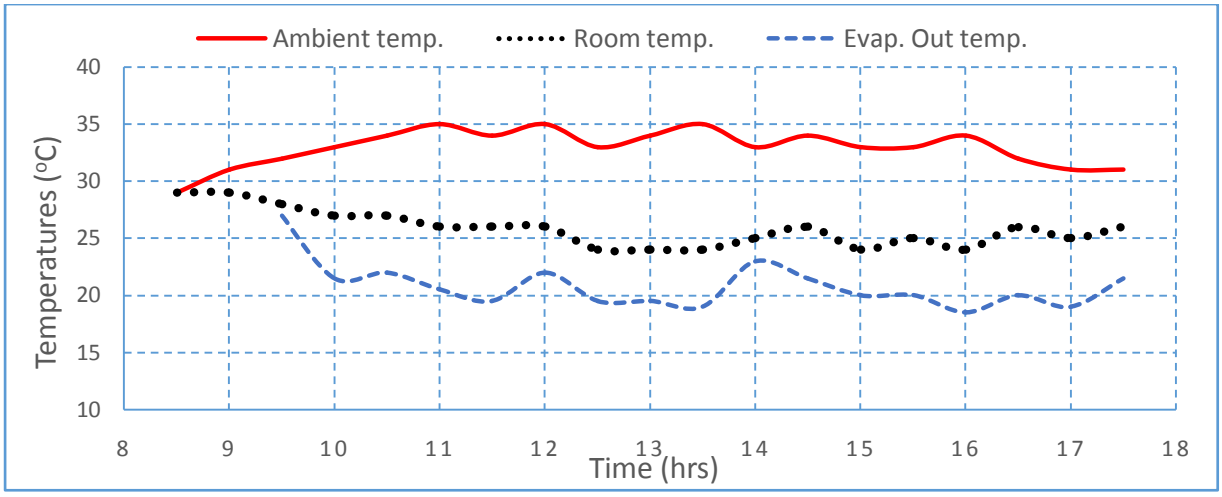


Fig. 4.131. Variation of ambient and room temperatures with time for June 12, 2017

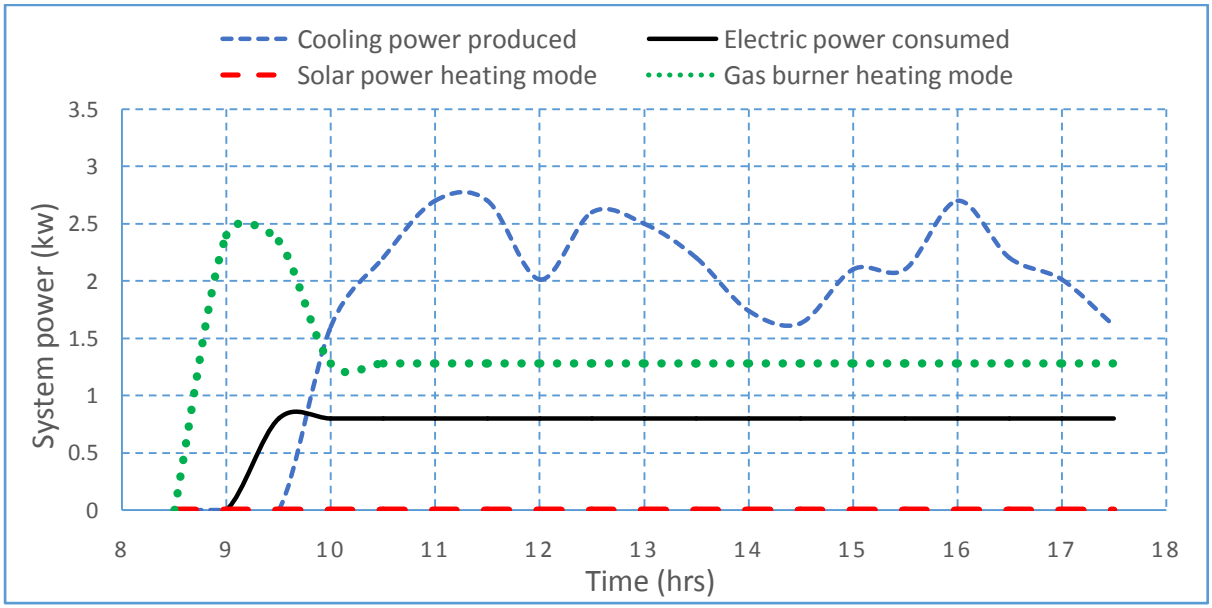


Fig. 4.132. Variation of system power with time for June 12, 2017

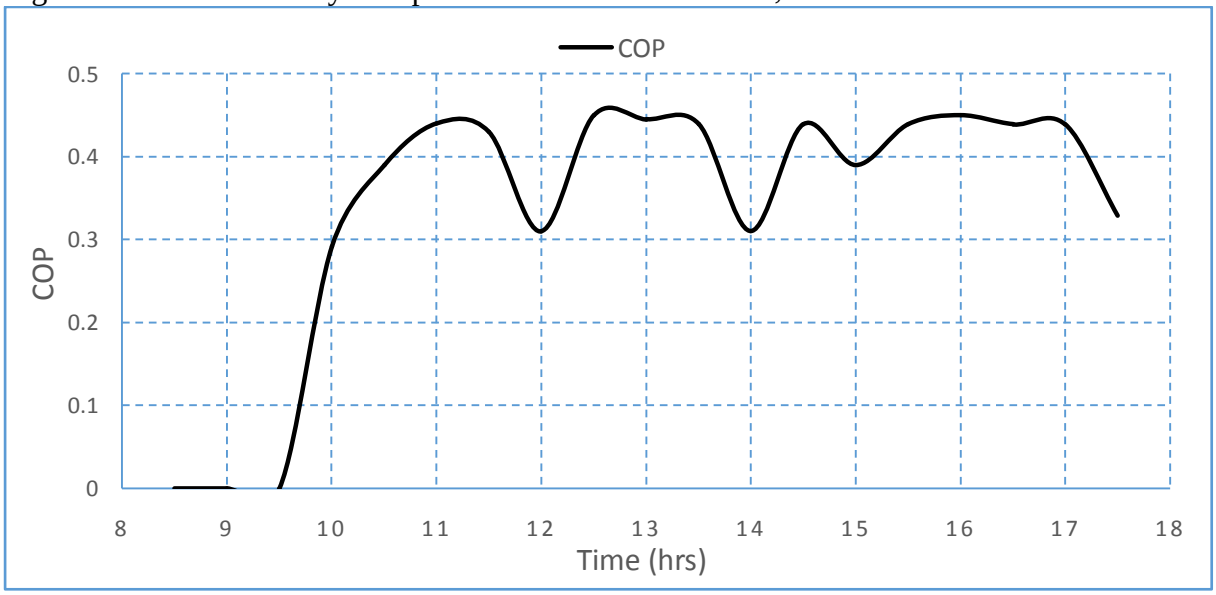


Fig. 4.133. Variation of COP with time for June 12, 2017

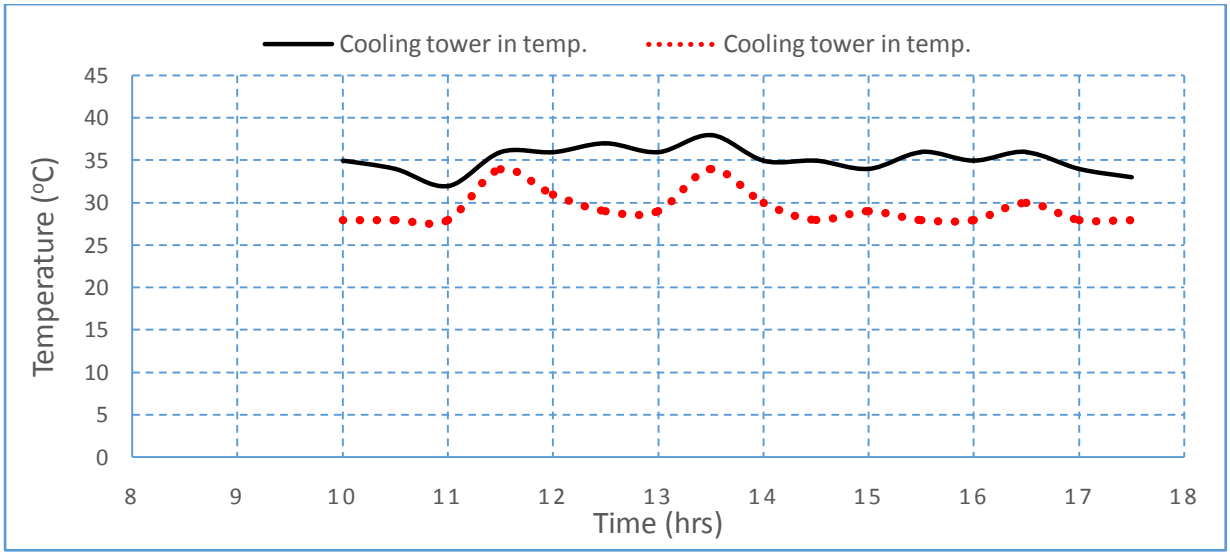


Fig. 4.134. Variation of cooling tower temperatures with time for June 12, 2017

From figure 4.128, solar radiation values stayed generally very low throughout the day. This was as a result of the very cloudy nature of the experimental day. From figure 4.129, it can be seen that the collector fluid temperatures stayed below 80^{o}C throughout the day, the temperatures were not adequate to fire the absorption chiller, and therefore gas had to be consumed throughout the day to fire the absorption chiller. From figure 4.130, the generator temperatures stayed generally above 80^{o}C throughout the day. An indication that the gas boiler heating mode was able to maintain constant heating of the hot water tank fluid. Also, from figure 4.130, evaporator chilled water outlet temperatures are seen to be between 18^{o}C and 21^{o}C, an indication that relatively constant desorption and evaporation was achieved. From figure 4.131, the system is seen to have achieved cooling of the test room. Room temperatures between 24^{o}C and 26^{o}C were recorded. From figure 4.132, the system was operated in the gas burner heating mode throughout the experimental day, this was as a result of very low solar radiation throughout the experimental day, and therefore solar heating mode could not be used. From figure 4.133, COP was relatively stable throughout the experimental day,staying above 0.3 from 10 am to the close of the experimental day. A maximum COP of about 0.45 was recorded. This is an indication of a relatively stable performance when the system is operated in the gas burner heating mode. From figure 4.134, the cooling tower was able to maintain the outlet cooling water temperature between 29 to 35^{o}C.

Figures to 4.135 to 4.141 show the graphs that describe the variation in experimental parameters for the experimental day of June 13, 2017, which was classified as a rainy day.

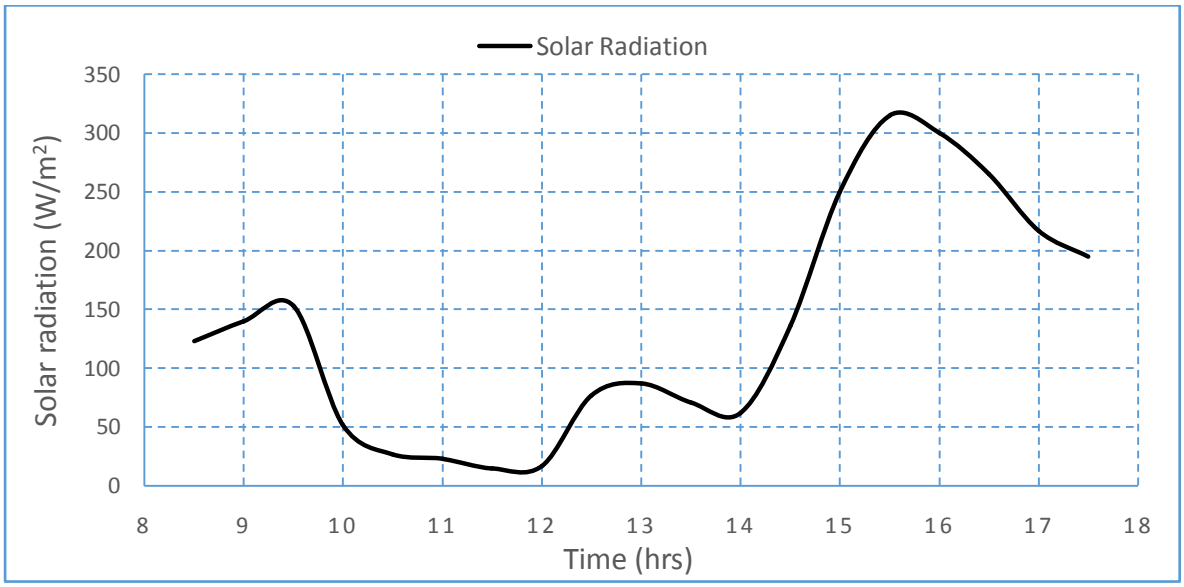


Fig. 4.135. Variation of solar radiation with time for June 13, 2017

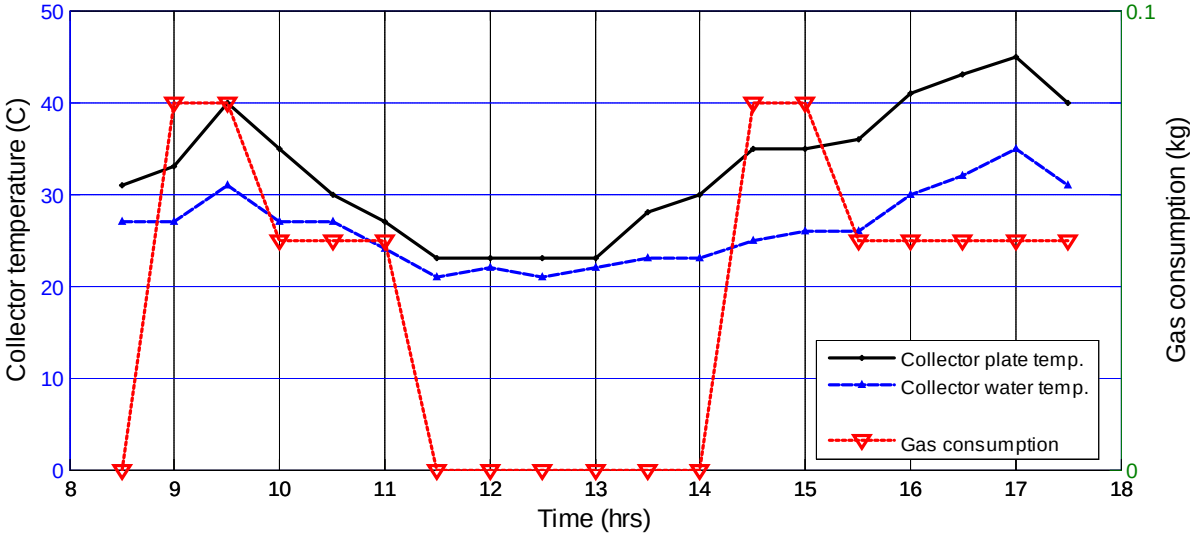


Fig. 4.136. Variation of collector temperatures and gas consumption with time for June 13, 2017

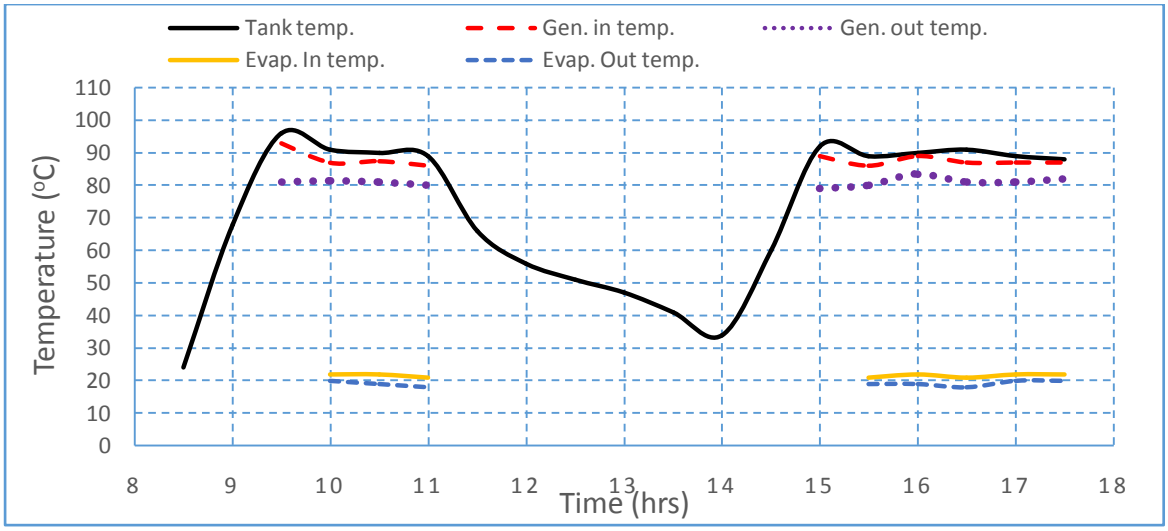


Fig. 4.137. Variation of system temperatures with time for June 13, 2017

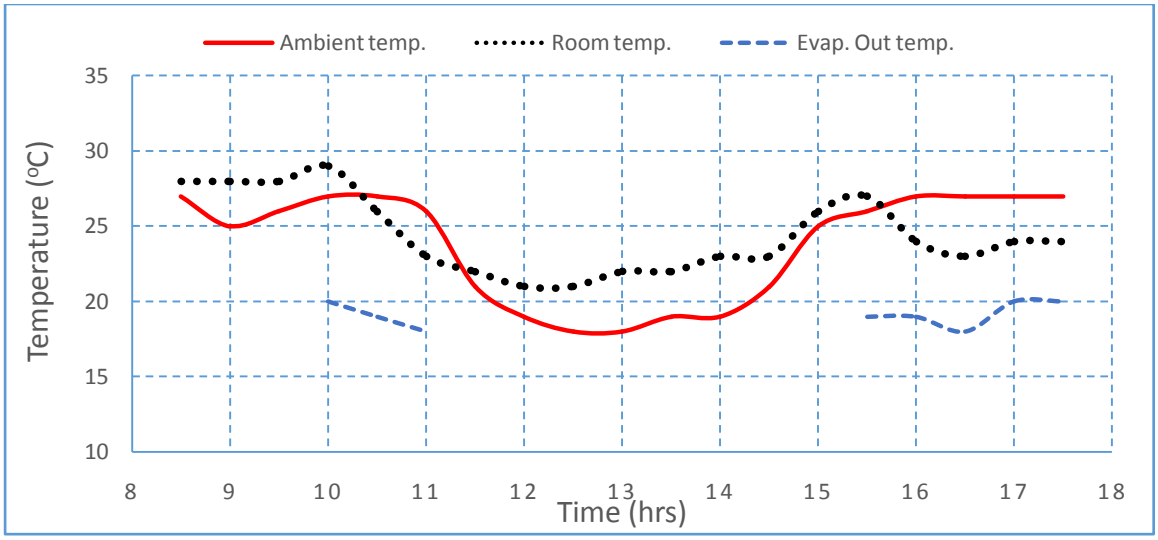


Fig. 4.138. Variation of ambient and room temperatures with time for June 13, 2017

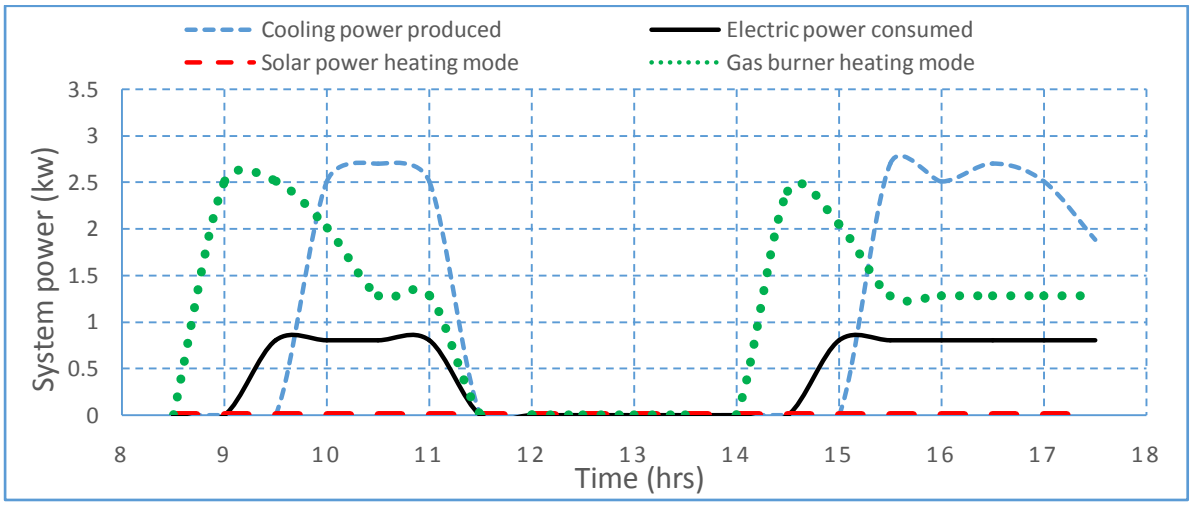


Fig. 4.139. Variation of system power with time for June 13, 2017

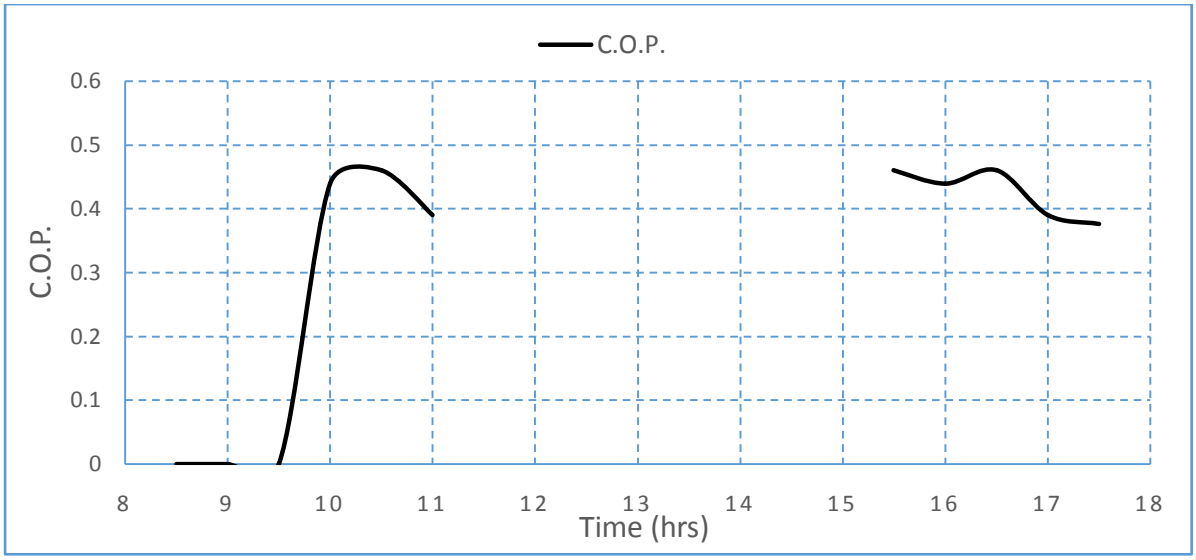


Fig. 4.140. Variation of COP with time for June 13, 2017

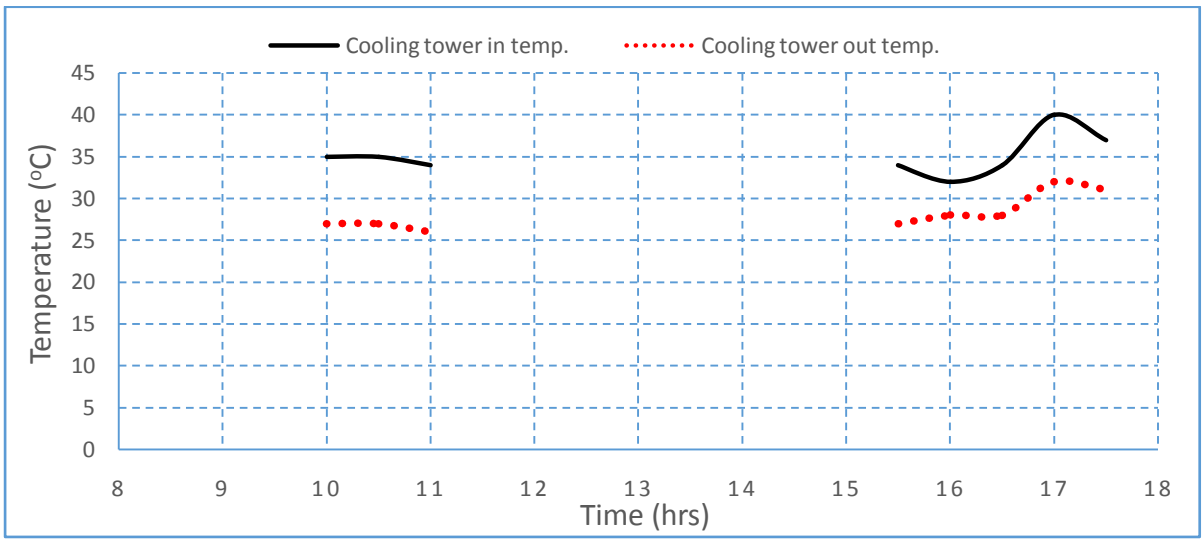


Fig. 4.141. Variation of cooling tower temperatures with time for June 13, 2017

From figure 4.135, very low solar radiation values can be seen. This was as a result of the rainy nature of the experimental day. From figure 4.136, gas consumption started at the beginning of the experimental day (8:30 am) up to 11.30 am. Between 11:30 am and 2 Pm, there was no gas consumption. This was because the absorption chiller was not operated in this period due to the rain recorded, which led to natural cooling. Gas consumption resumed afterwards when there was cooling requirement at 14:00 hours. Also from figure 4.136, the collector fluid temperatures were very low throughout the day, staying below 40^{o}C. From figure 4.137, between the hours of 11:30am and 2:30 pm, the absorption chiller was not operated. This was because there was no

cooling demand from the experimental room within the interval. From figure 4.138, between the hours of 9:30am and 11am in which cooling was applied, the room temperature is seen to have declined gradually to below the ambient temperature. Between 11:30am and 3pm, cooling was suspended. This was as a result of the rainy nature of the experimental day, which kept the room temperature naturally below a level that required cooling within the time interval. Cooling however resumed after the rain, the room temperatures can be seen to have been kept below the ambient temperature. From figure 4.139, maximum cooling power of 2.7kW was achieved. The gas boiler heating mode was employed to fire the absorption chiller throughout the period it operated for the experimental day. The solar power heating mode was not used throughout the day, as the required collector fluid temperature could not be attained. From figure 4.140, maximum COP of 0.45 was recorded by the chiller during the period of operation. From figure 4.141, the cooling tower is seen to have kept the cooling water outlet temperature below 35^{o}C.

Figures to 4.142 to 4.149 show the graphs that describe the variation in experimental parameters for the experimental day of June 17, 2017 which was classified as a rainy day.

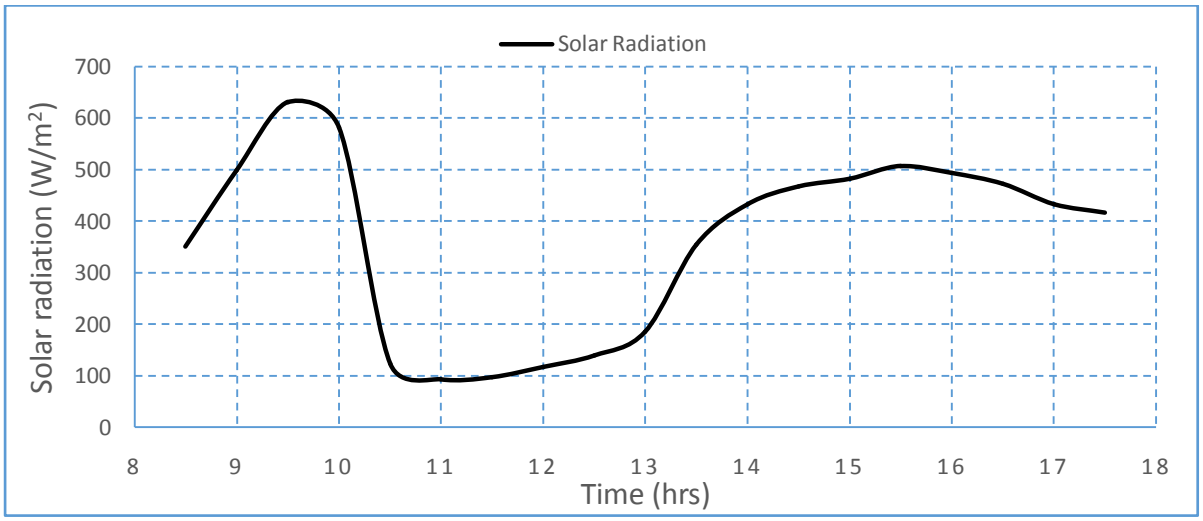


Fig. 4.142. Variation of solar radiation with time for June 17, 2017

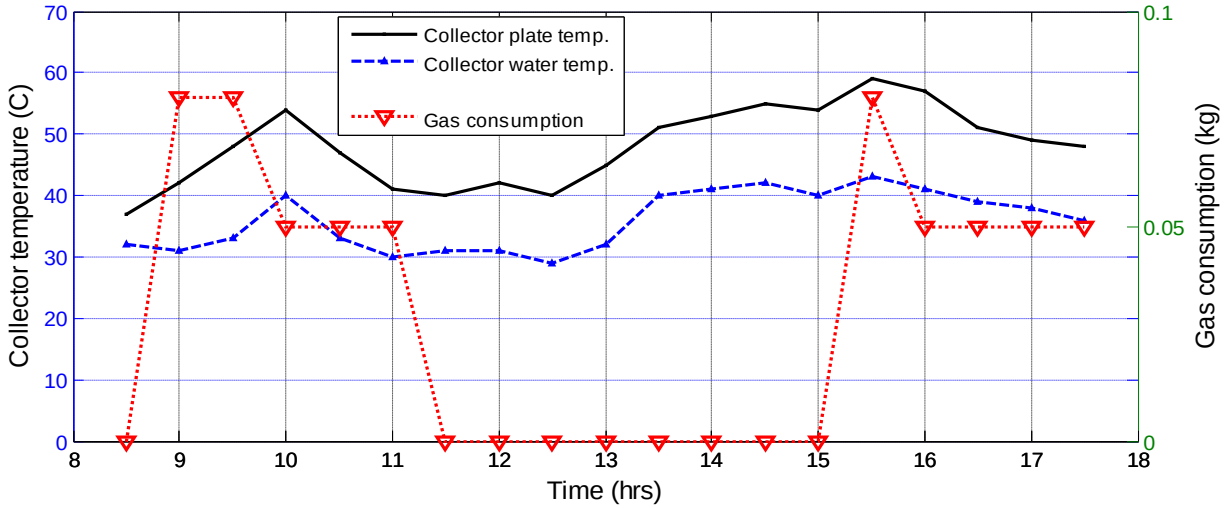


Fig. 4.143. Variation of collector temperatures and gas consumption with time for June 17, 2017

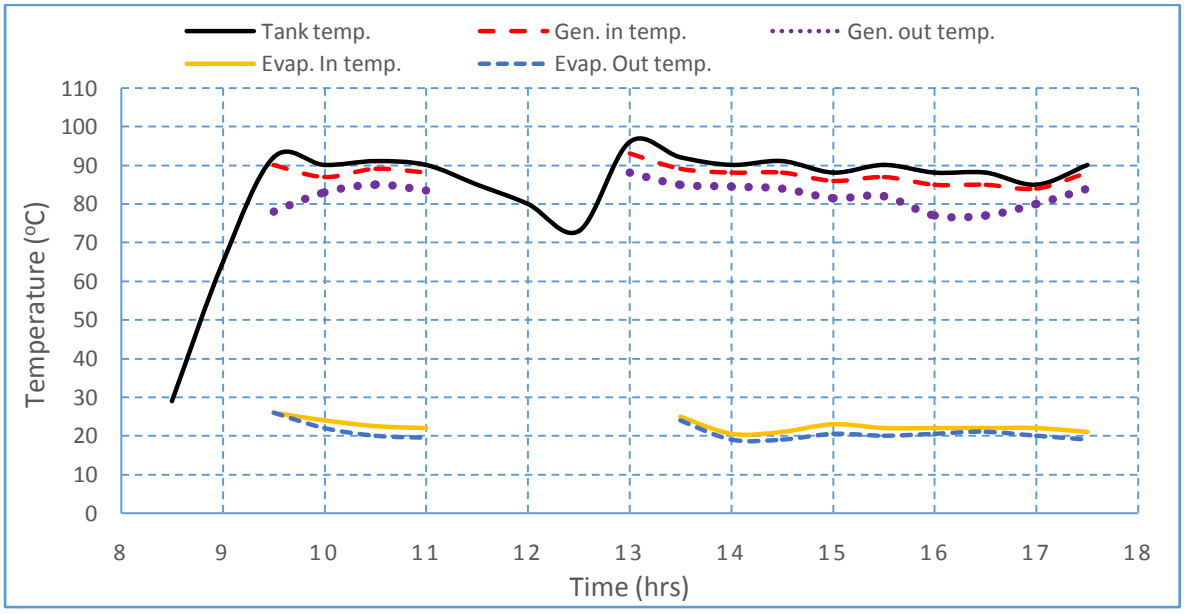


Fig. 4.144. Variation of system temperatures with time for June 17, 2017

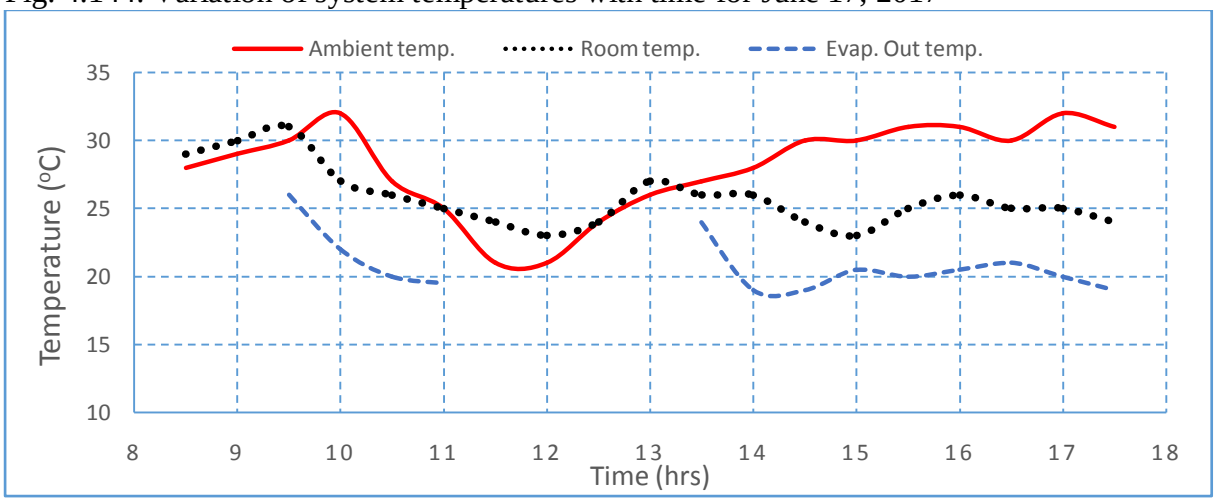


Fig. 4.145. Variation of ambient and room temperatures with time for June 17, 2017

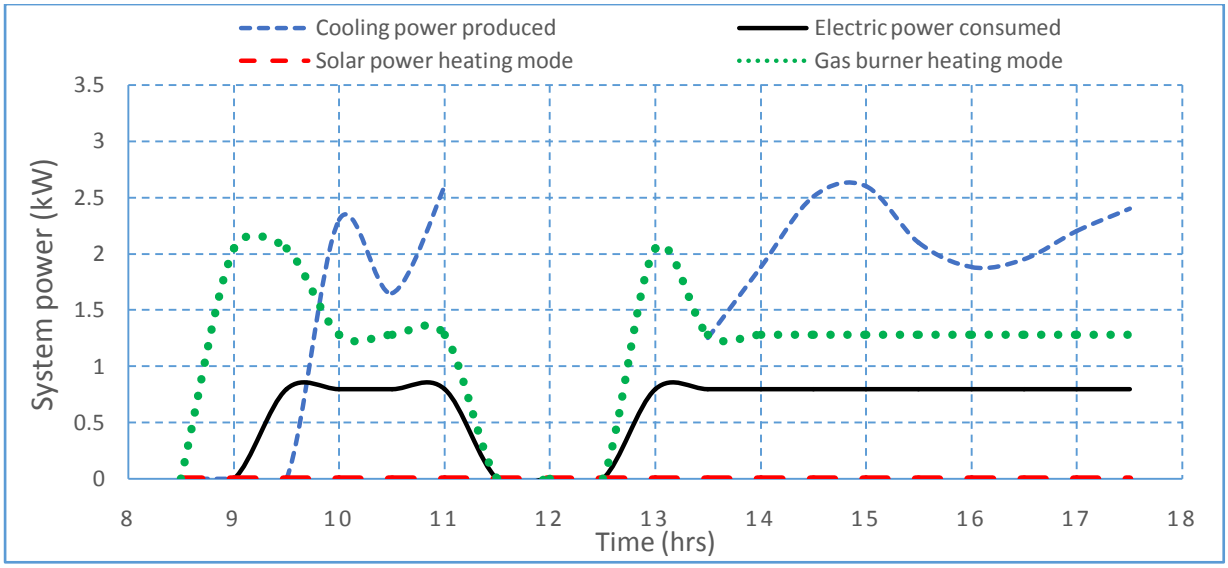


Fig. 4.146. Variation of system power with time for June 17, 2017

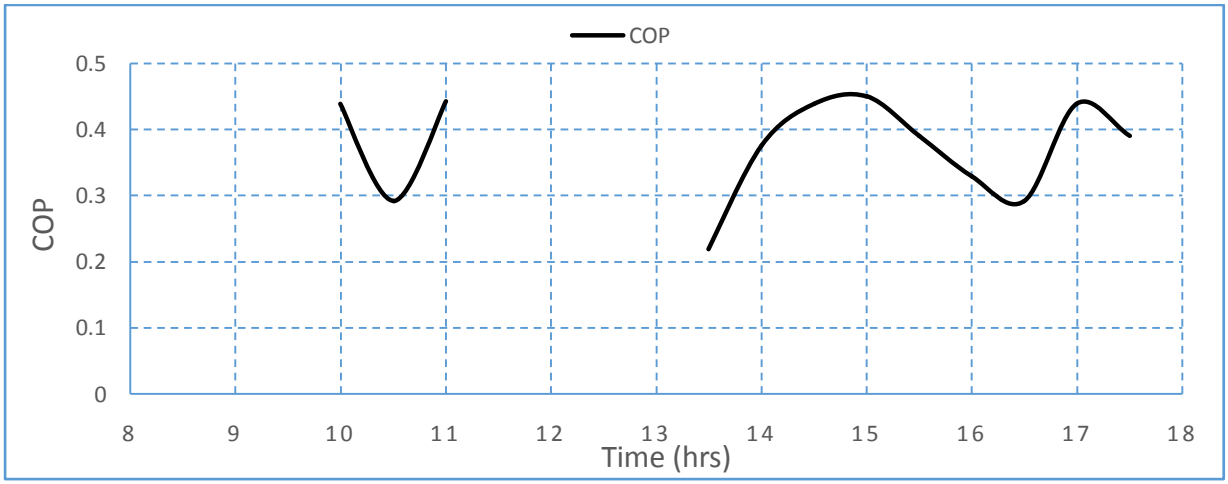


Fig. 4.147. Variation of COP with time for June 17, 2017

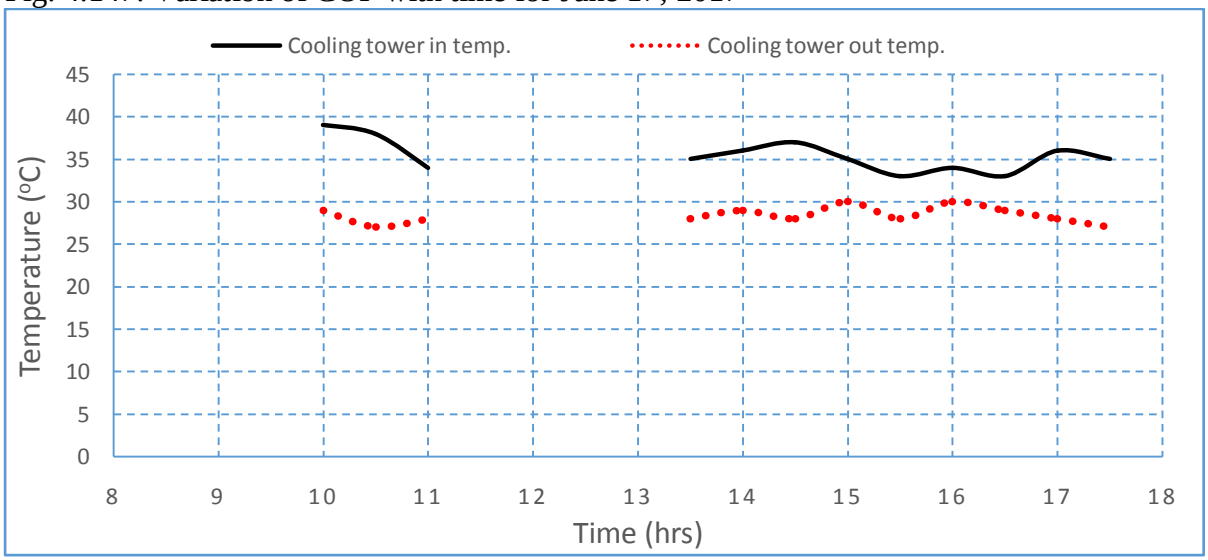


Fig. 4.148. Variation of cooling tower temperatures with time for June 17, 2017

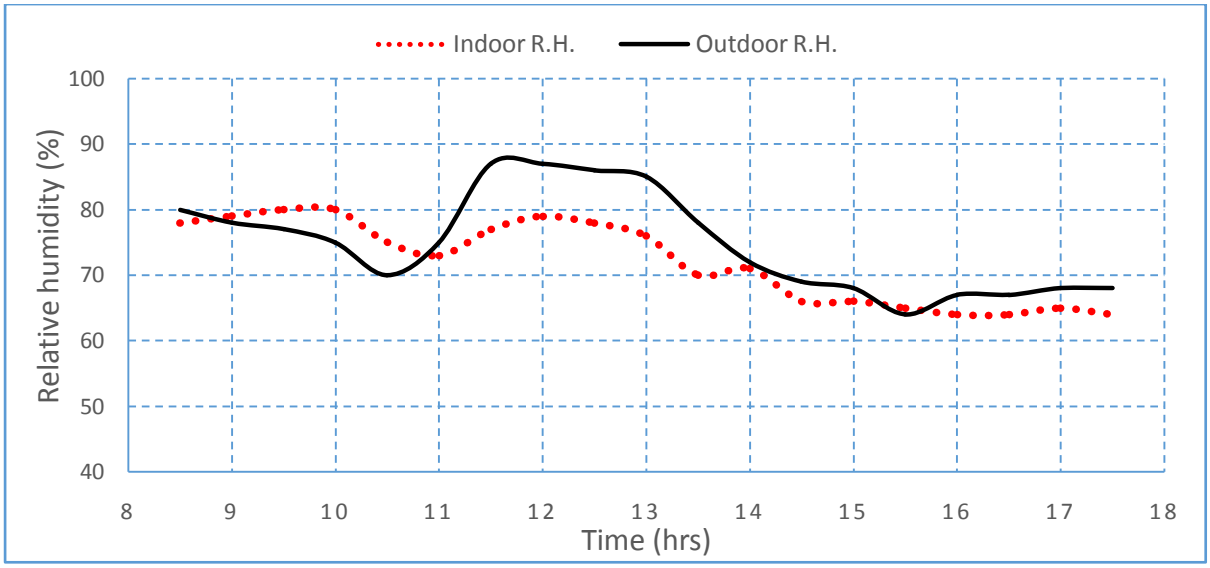


Fig. 4.149. Variation of relative humidity with time for June 17, 2017

From figure 4.142, solar radiation of 600W/m^{2}was recorded at 9:30 am. However, when it started to rain, solar radiation dropped below 200 W/m^2. After the rain, peak solar radiation of 500 W/m^2 was recorded at 15:30 hours. From figure 4.143, very low collector fluid temperatures were recorded throughout the experimental day. The temperatures were not sufficient to fire the absorption chiller using solar power. Gas was consumed throughout the experimental day. From figure 4.144, generator temperatures stayed relatively above 80^{o}C between 9:30 am and 11 am. Evaporator chilled water outlet temperatures between 19^{o}C and 21^{o}C were also recorded between 9:30 am and 11 am. Cooling from the absorption chiller was suspended between the hours of 11:30 and 1pm, as there was no cooling demand within the period the rain occurred. From figure 4.145, room temperature dropped from above 30^{o}C to about 25^{o}C between the hours of 9:30 and 11:00 am when cooling was applied. Cooling was suspended and room temperature continued to drop naturally to below 24^{o}C when it rained (11:00 am to 13:30 pm). When cooling resumed after the rain, room temperature can be seen to have been kept well below the ambient temperature for the rest of the experimental day (13:30 to 17:30 hours). From figure 4.146, peak cooling power of 2.6 kW was achieved. The absorption chiller was fired in the gas burner mode throughout the experimental day. The system could not be fired in the solar heating mode throughout the

experimental day due to insufficient solar radiation. From figure 4.147, COP between 0.23and 0.45 was attained for the experimental day. From figure 4.148, the cooling tower can be seen to have maintained cooling water outlet temperatures below 30^{o}C.From figure 4.149, the indoor relative humidity is seen to rise above the outdoor relative humidity before cooling commenced (8:30 am to 10:00 am). This was due to humidity introduced in the room as a result of activities in the test room. However, when cooling started, room relative humidity can be seen to decrease from 80% to 72% between 9:30 am and 10:30 am. This indicates a level of dehumidification by the system. At the onset of rain, cooling was suspended, both indoor and outdoor relative humidity are seen to rise (11:00 am to 14:00 am). This was as a result of additional humidity introduced by the rain. When cooling was resumed after the rain, indoor relative humidity can be seen to decrease from 70% to 65% between 14:00 hours and 17:30 hours. This indicates there is no additional humidity introduced to the test room as a result of the fan coil unit where air is blown over pipes with chilled water flowing through.

Figures 4.150 to 4.157 show the graphs that describe the variation in experimental parameters for the experimental day of June 18, 2017 which was classified as a cloudy sky day.

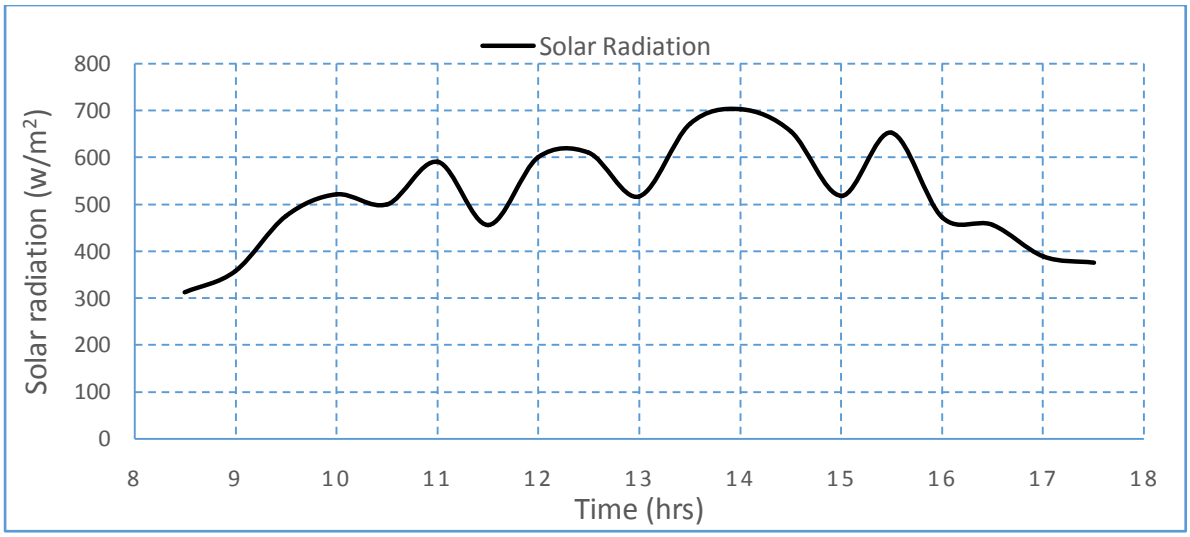


Fig. 4.150. Variation of solar radiation with time for June 18, 2017

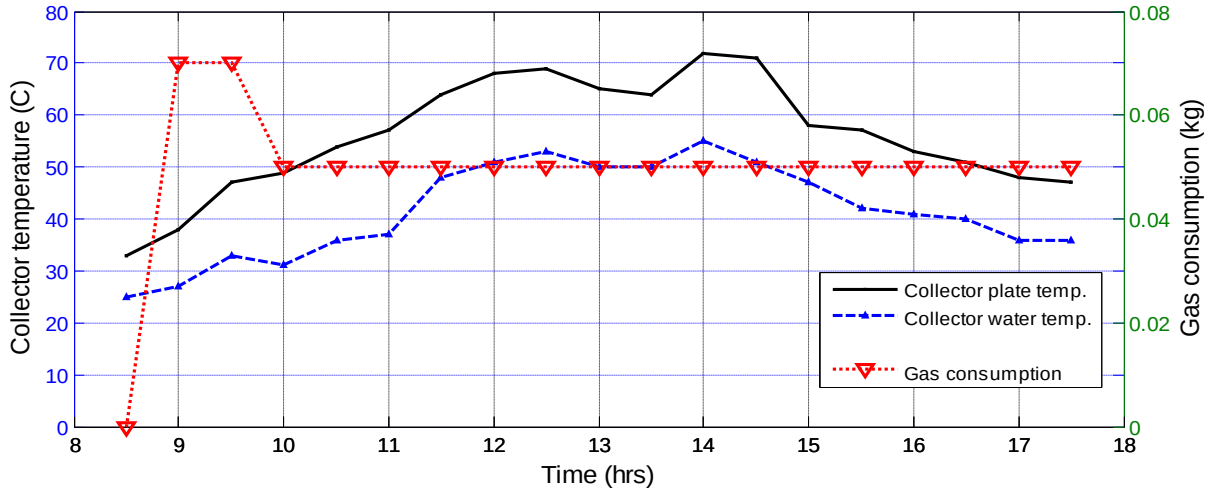


Fig. 4.151. Variation of collector temperatures and gas consumption with time for June 18, 2017

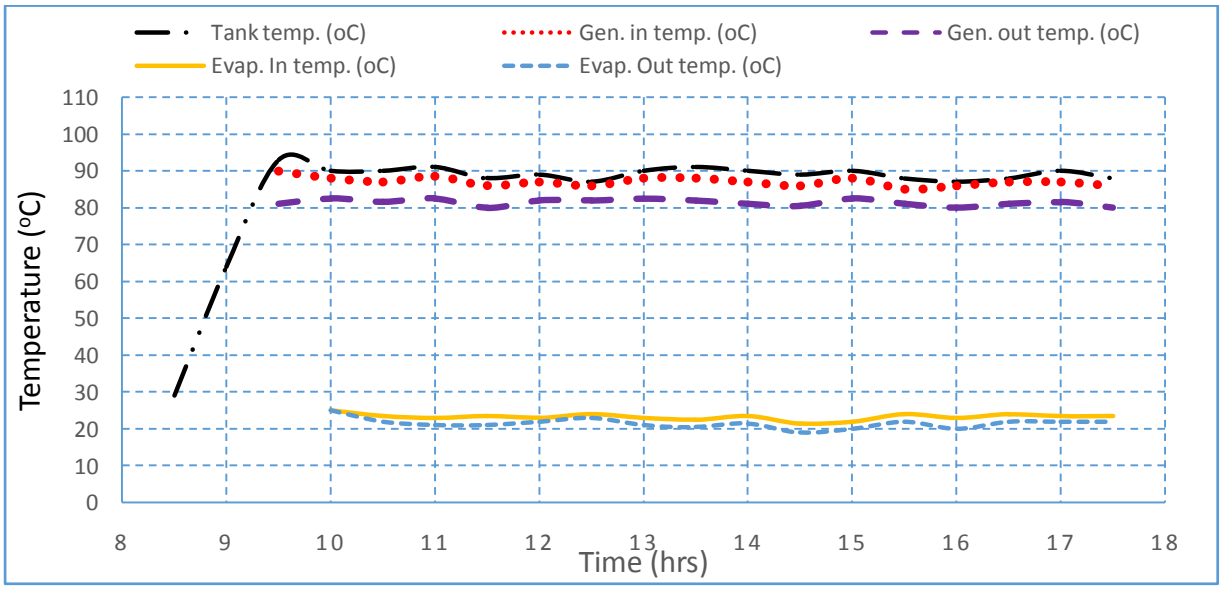


Fig. 4.152. Variation of system temperatures with time for June 18, 2017

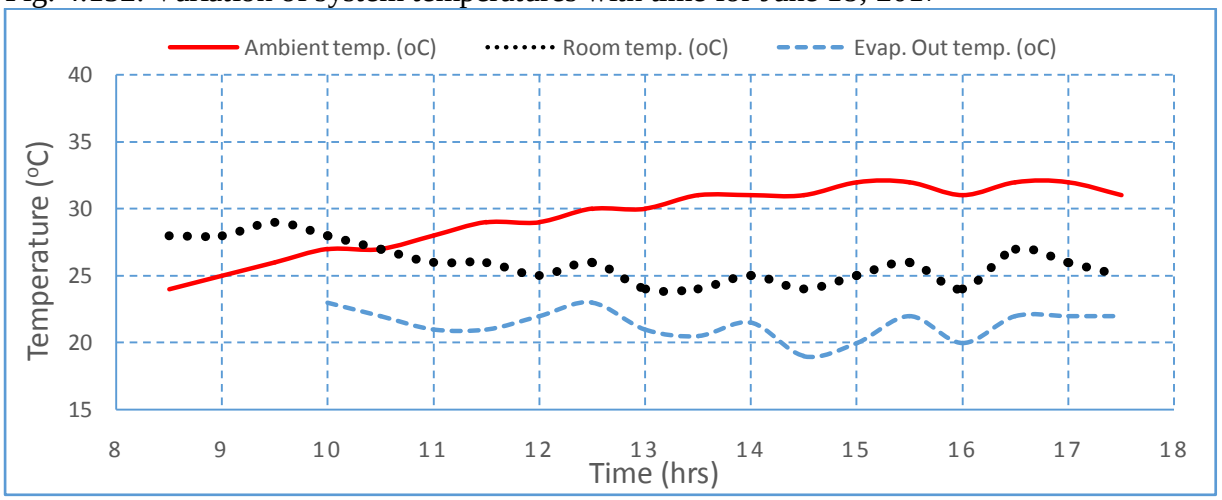


Fig. 4.153. Variation of ambient and room temperatures with time for June 18, 2017

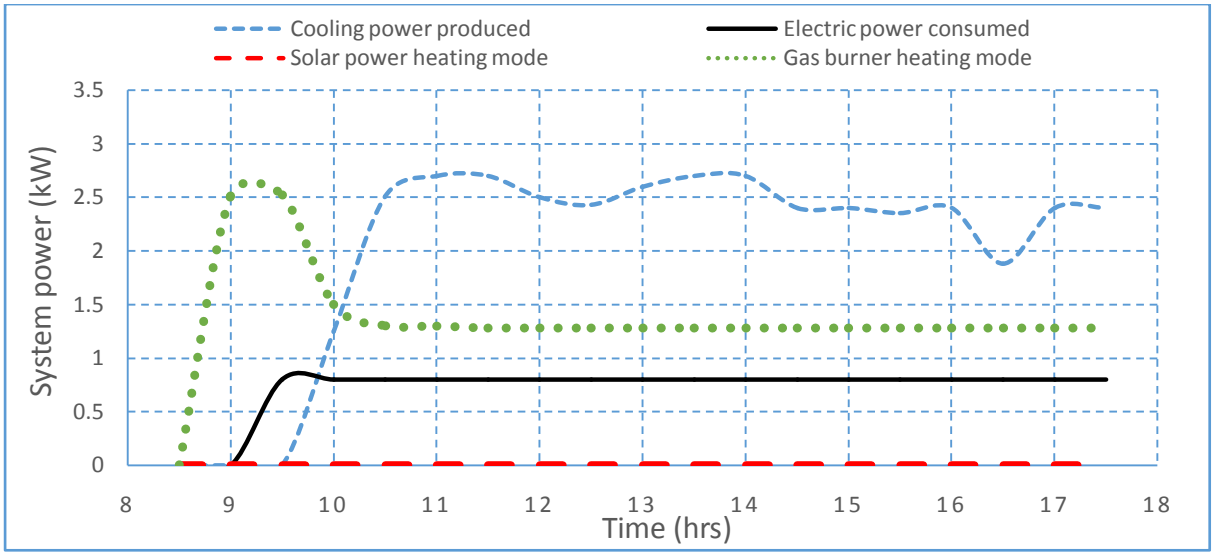


Fig. 4.154. Variation of system power with time for June 18, 2017

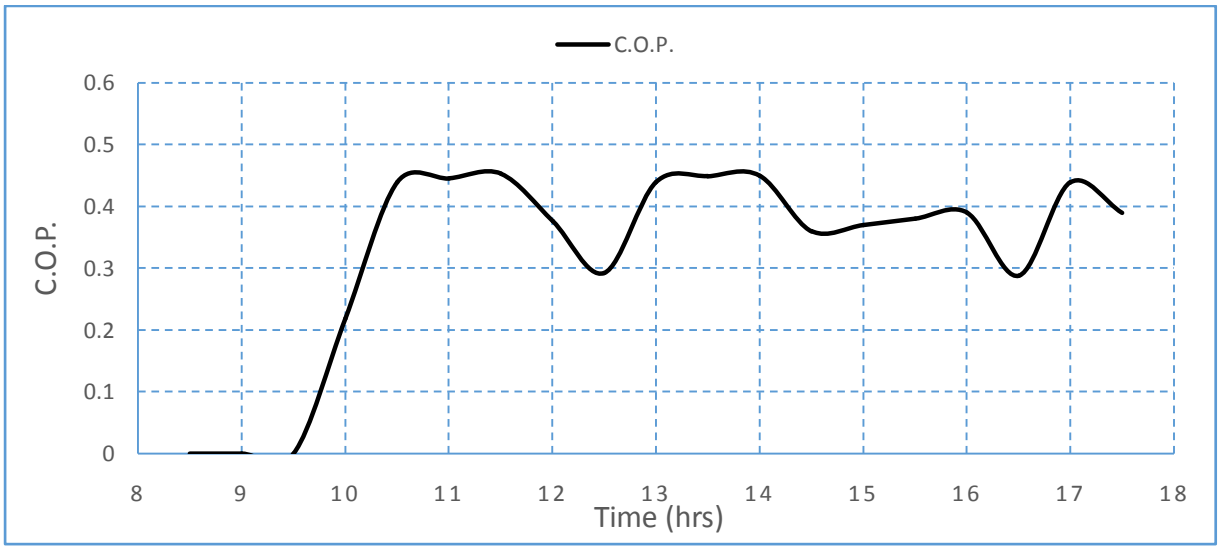


Fig. 4.155. Variation of COP with time for June 18, 2017

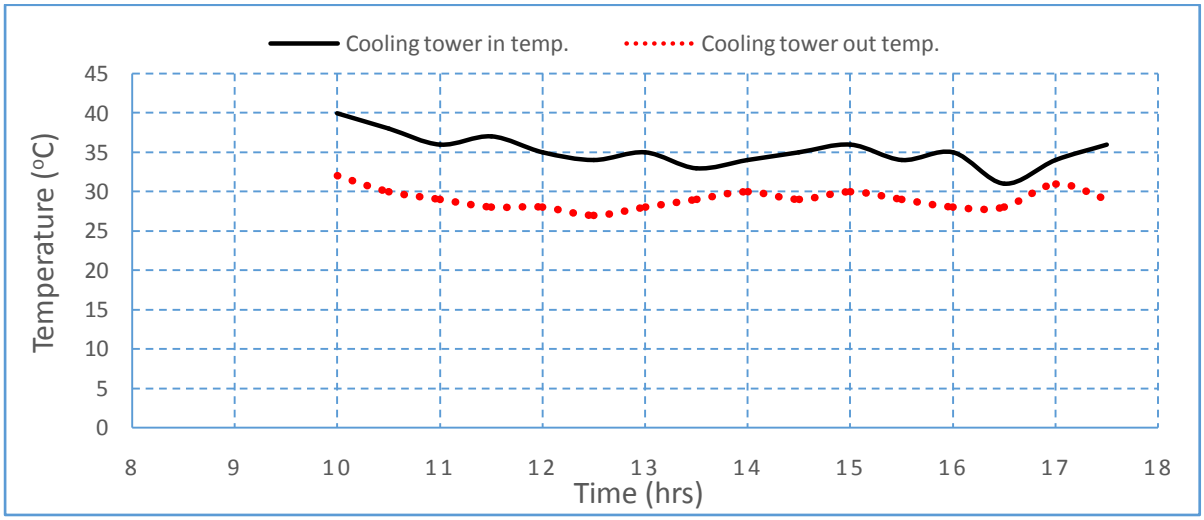


Fig. 4.156. Variation of cooling tower temperature with time for June 18, 2017

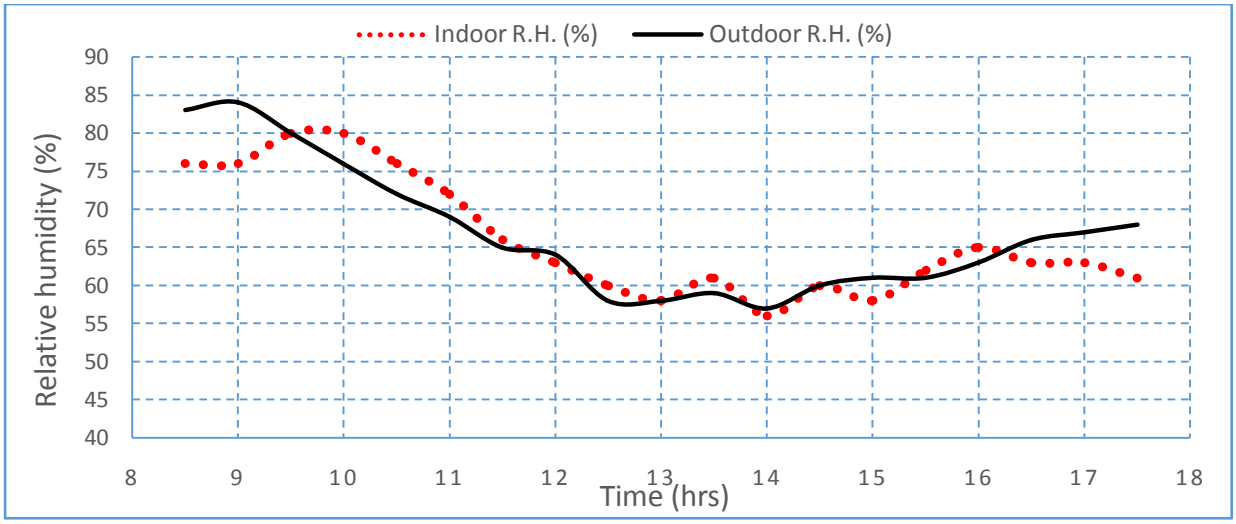


Fig. 4.157. Variation of relative humidity with time for June 18, 2017

From figure 4.150, solar radiation is seen to fluctuate throughout the day, attaining a maximum of 700 W/m^2 at 14:00 hours. This was as a result of the cloudy nature of the day. From figure 4.151, gas was consumed throughout the experimental day, as the collector fluid temperatures remained very low, insufficient for solar heating mode. From figure 4.152, generator temperatures styed generally above 80^{o}C throughout the experimental day, an indication of constant heat supply by the gas burner. Evaporator chilled water outlet temperature between 19 and 22^{o}C were achieved for the experimental day. From figure 4.153, room temperature can be seen to have dropped from above ambient temperature before cooling (8:30 am to 10:00 am) to well below ambient temperature during cooling (10:00 am to 17:30 pm). Room temperatures between 24^{o}C and 26^{o}C were recorded throughout the experimental day. From figure 4.154, peak cooling power of 2.7 kW was attained. Also, the absorption chiller was fired in the gas boiler heating mode throughout the experimental day. From figure 4.155, peak COP of 0.46 was recorded for the experimental day. From figure 4.156, the cooling tower was able to keep the cooling water outlet temperature below 32^{o}C for the entire experimental day. From figure 4.157, it can be seen that the indoor relative humidity increased above the outdoor relative humidity before cooling started (8:30 to 10:00 am). This was due to additional humidity introduced to the room as a result of activity within the test room. When cooling commenced (10:00 am), the indoor relative humidity is seen to decrease from

80% to 56% at 14:00 hours. From 14:00 hours to the close of the experimental day at 17:30 hours, indoor relative humidity is seen to increase from 56% to 60%, while outdoor relative humidity increases from 57% to 68%. This could be due to drop in ambient temperature at the time interval.

Figures 4.158 to 4.165 show the graphs that describe the variation in experimental parameters for the experimental day of June 19, 2017,which was classified as a cloudy sky day.

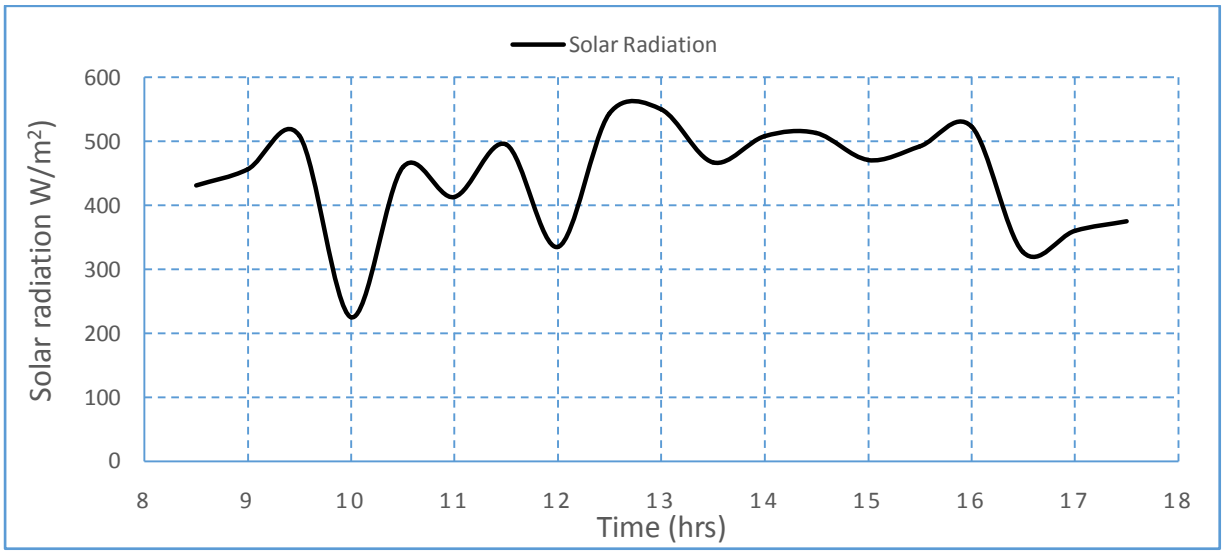


Fig. 4.158. Variation of solar radiation with time for June 19, 2017

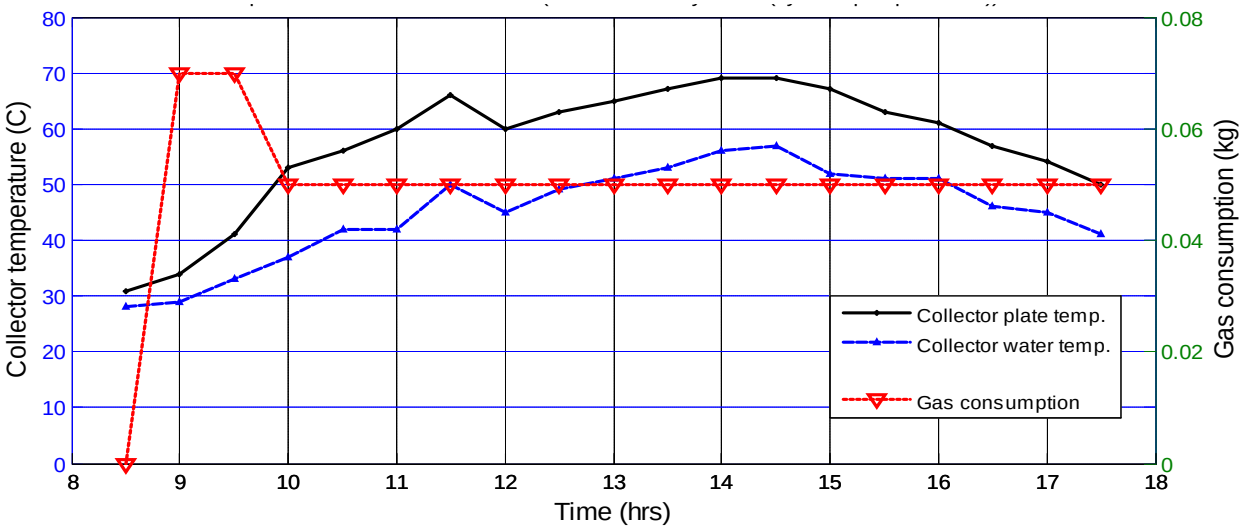


Fig. 4.159. Variation of collector temperatures and gas consumption with time for June 19, 2017

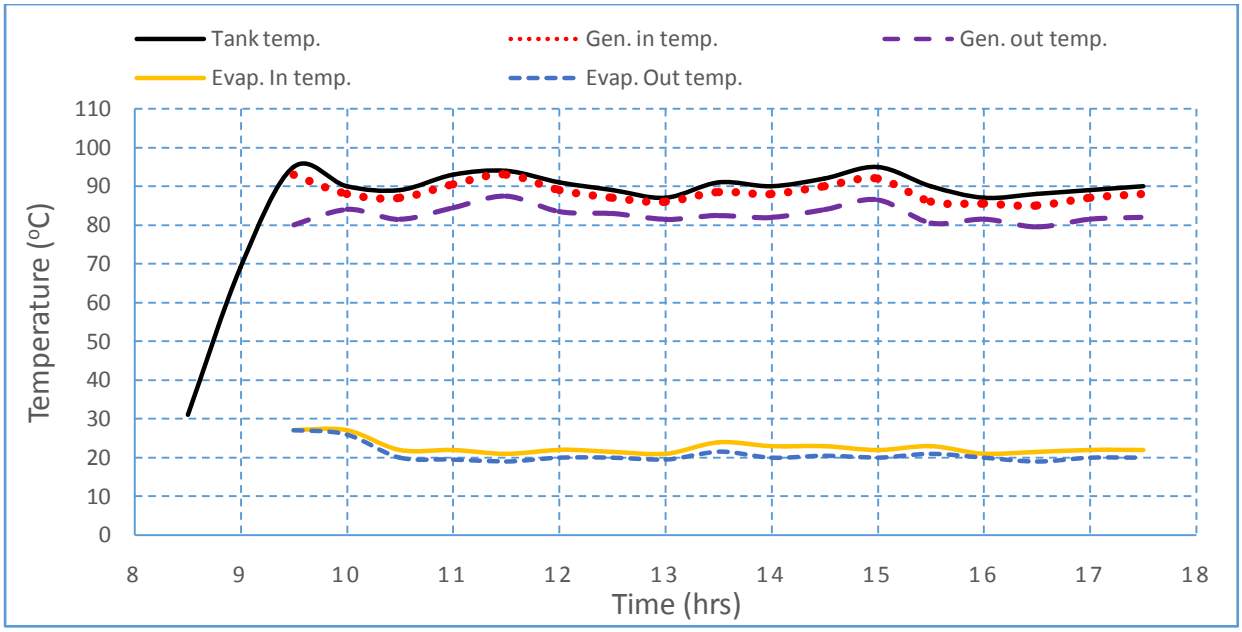


Fig. 4.160. Variation of system temperatures with time for June 19, 2017

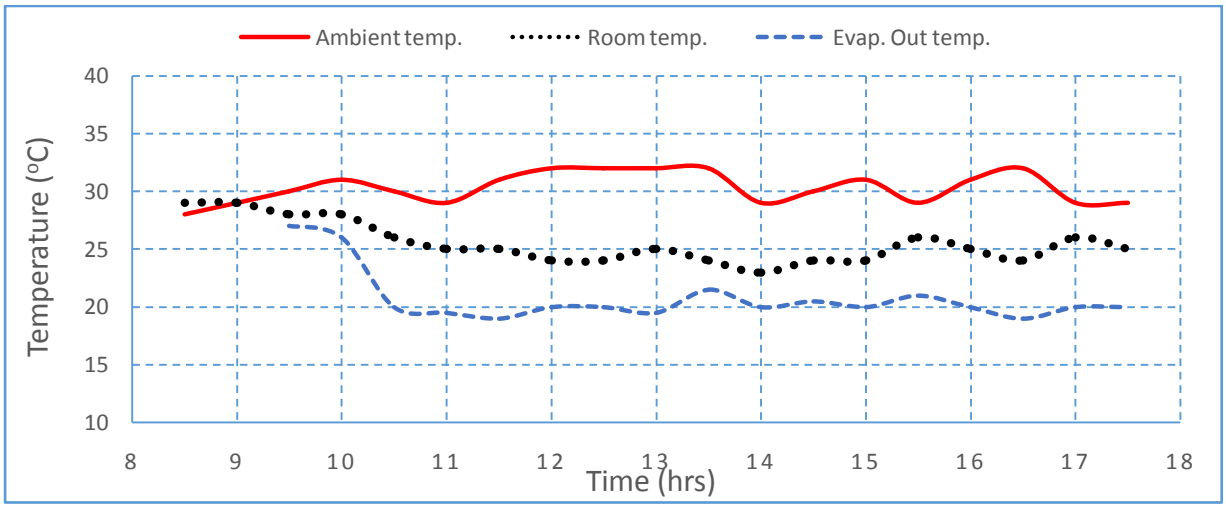


Fig. 4.161. Variation of ambient and room temperatures with time for June 19

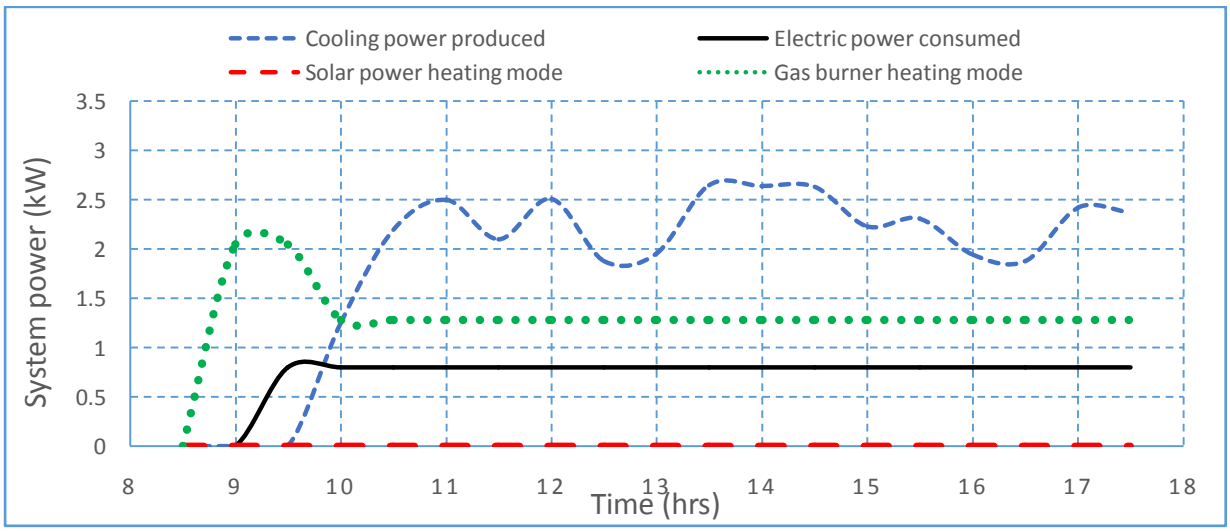


Fig. 4.162. Variation of system power with time for June 19, 2017

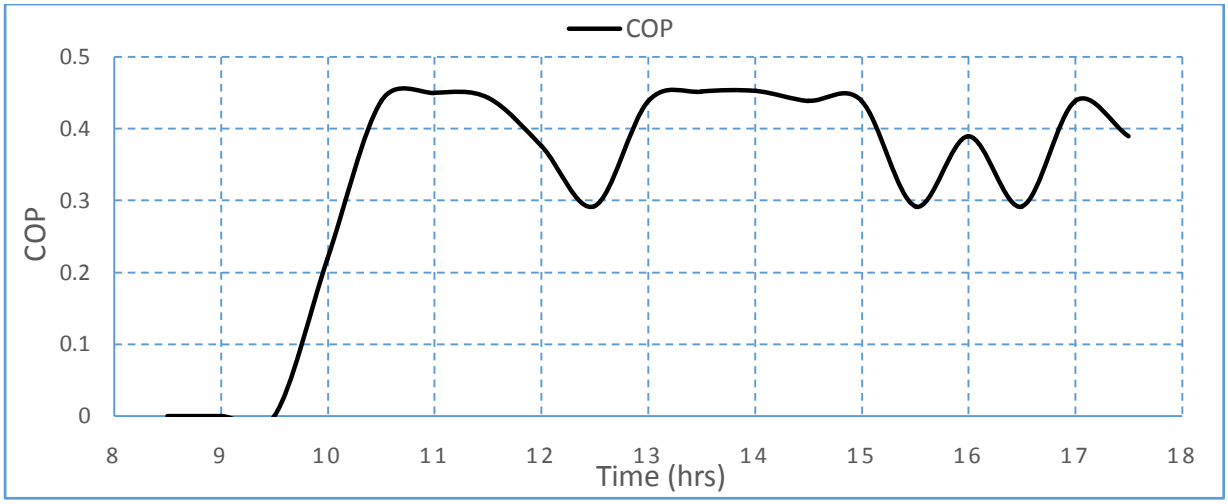


Fig. 4.163. Variation of COP with time for June 19, 2017

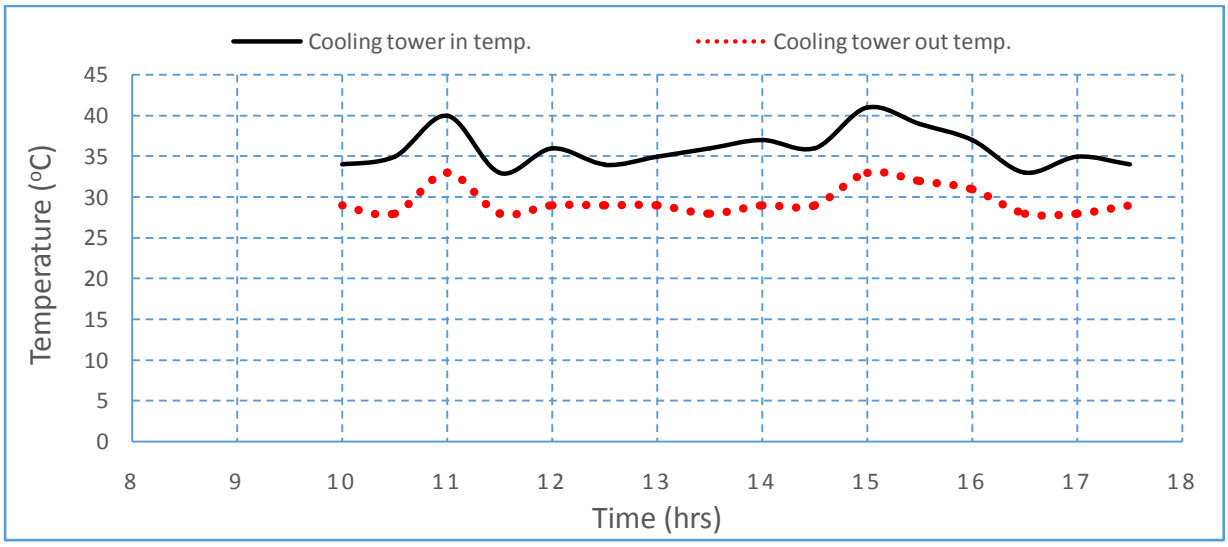


Fig. 4.164. Variation of cooling tower temperatures with time for June 19, 2017

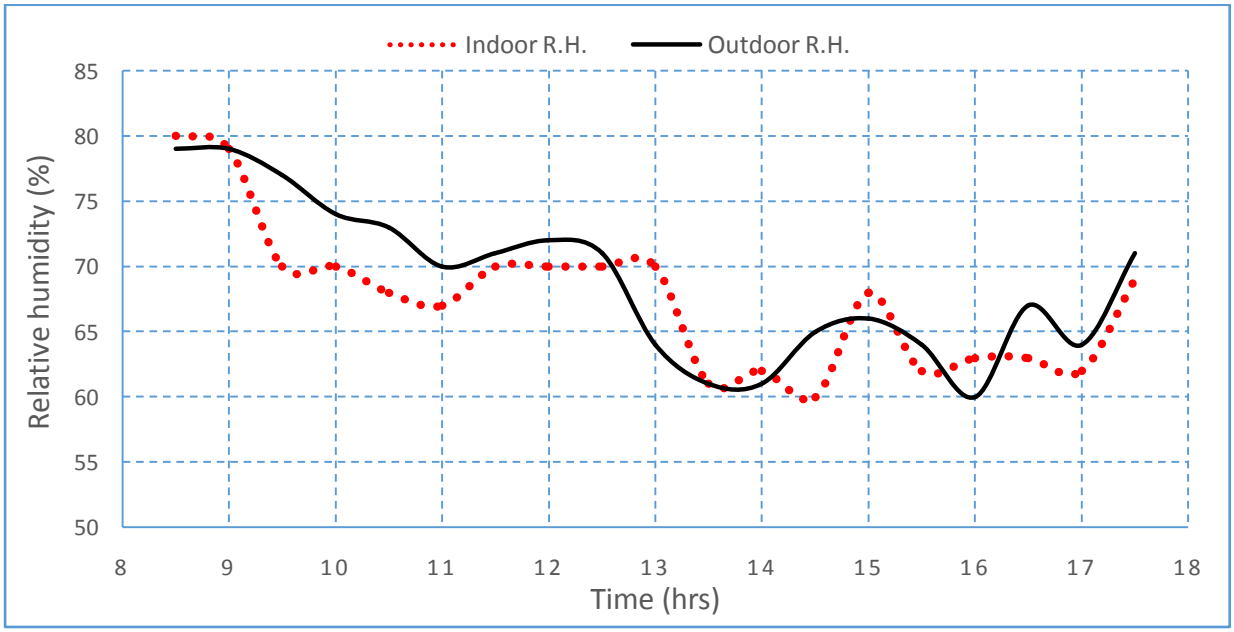


Fig. 4.165. Variation of relative humidity with time for June 19, 2017

From figure 4.158, solar radiation can be seen to be fluctuating and less than 600W/m^2 throughout the experimental day. This was as a result of the very cloudy nature of the experimental day. From figure 4.159, collector fluid temperatures were below 60^{o}C throughout the experimental day, insufficient for solar power heating mode. Gas was consumed throughout the experimental day to fire the absorption chiller. From figure 4.160, generator temperatures stayed generally above 80^{o}C throughout the experimental day, while evaporator chilled water outlet temperatures varied between 18^{o}C and 21^{o}C throughout the experimental day. An indication of stable heat supply to the generator. From figure 4.161, room temperatures between 24^{o}C and 26^{o}C were recorded throughout the experimental day. Room temperatures stayed well below the ambient temperatures, indicating cooling was achieved. From figure 4.162, peak cooling power of 2.6 kW was recorded for the experimental day. Also, gas burner heating mode was applied throughout the experimental day. From figure 4.163, peak COP of 0.46 was recorded for the experimental day. From figure 4.164, the cooling tower is seen to have kept the outlet cooling water temperatures between 28^{o}C and 33^{o}C.From figure 4.165, indoor relative humidity can be seen to be higher than outdoor relative humidity before cooling commenced (8:30 am to 9:00 am). When cooling commenced, indoor relative humidity dropped below the outdoor relative humidity between the hours of 9:00 am and 12:30 pm. From 12:30 pm to 17:30 hours, indoor relative humidity values fluctuated above and below the outdoor relative humidity.

4.4.2 Performance parameters from experiments conducted

The graphs that follow show the performance of the installed system in terms of daily solar fraction, daily gas consumption and daily coefficient of performance over the period of experiment.

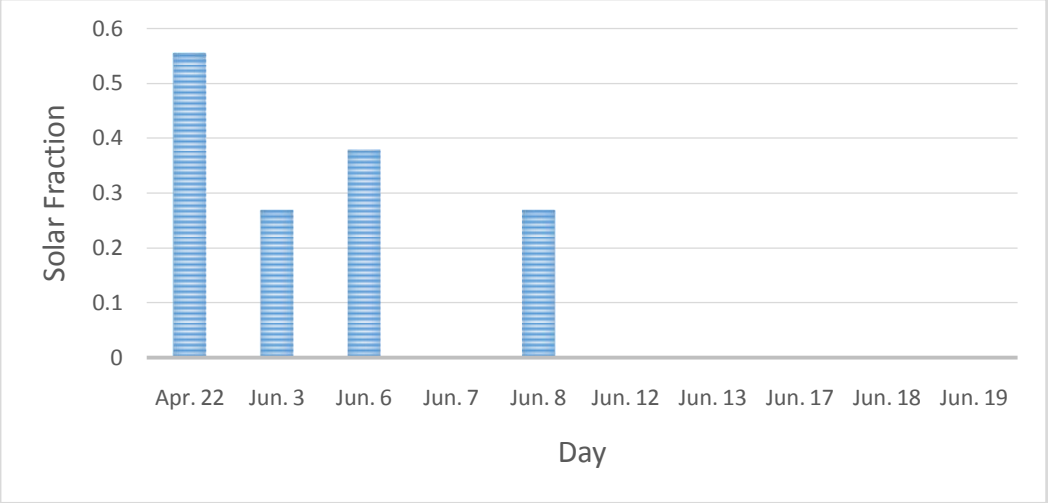


Fig. 4.166. Solar fraction of the experimental days

From figure 4.166, the experimental day of April 22 recorded the highest solar fraction of 0.55. This is expected due to the very high solar radiation recorded on the day, classified as a hot clear sky day. The available solar power was sufficient to fire the absorption chiller in the solar power heating mode for more hours in the experimental day, thereby reducing gas consumption. For the experiments in the month of June, the experimental day of June 6 had the highest solar fraction of 0.38. This is also expected, as the day (June 6), classified as a hot clear sky day also recorded high solar radiation.

The other experimental days in the month of June in which solar fraction was recorded: June 3 and June 8 had solar fractions of 0.27 each. Both days were classified as fairly clear sky days. Solar radiation was sufficient to fire the absorption chiller in solar power heating mode for a few hours in the experimental days. As seen from the figure, the remaining six experimental days in the month of June recorded zero solar fraction. This was because the days were either too cloudy and/ or rainy for sufficient solar radiation to fire the absorption chiller in solar power heating mode. The gas boiler heating mode was used throughout these experimental days. We can infer from this that for very cloudy and/ or rainy days, the system may only be able to function in the gas boiler heating mode.

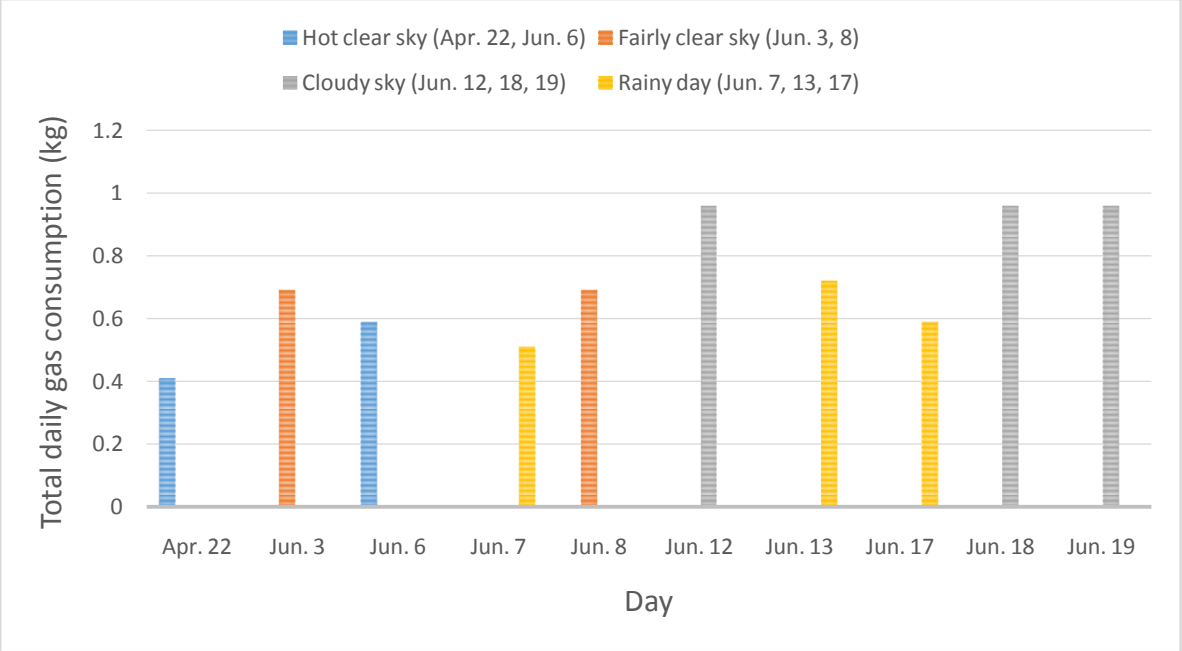


Fig. 4.167. Daily gas consumption of the experimental days

Figure 4.167 shows the daily gas consumption of the experimental days. It can be seen that the experimental day of April 22 had the least gas consumption of 0.41kg. This was as a result of the high solar fraction recorded on the day. The highest daily gas consumption of 0.96 kg occurred on the experimental days of June 12, 18 and 19, which were classified as cloudy sky days. Due to the very cloudy nature of the sky, at no point in time could the solar radiation be sufficient to get the collector temperatures up to the required levels for solar heating. Also, there was significant cooling demand from the test room, therefore the system had to be fired in gas boiler heating mode throughout the day. The rainy days of June 7, 13 and 17 recorded lower gas consumption as compared to the cloudy days and even the fairly clear sky days. This was because the rainy nature of the day resulted in a cool cloudy day with very low solar radiation, causing ambient and room temperatures to stay naturally low for a period of time the rain lasted. Therefore, there was naturally no cooling demand during this period and the gas that would have been used to fire the absorption chiller due to unavailable solar power was saved. From this we can infer that the system will consume least gas on hot clear sky days. The system is most likely to consume the most gas on very cloudy days. This is because, the cloudy nature of the sky will not give a chance

for solar power use, while also, room temperatures will still require cooling which must be met by gas boiler heating mode. The system is not likely to consume as much gas on rainy days as compared to cloudy days or fairly clear sky days. This is because there is a possibility for the room to be naturally cooled as a result of the rain, thereby reducing gas consumption.

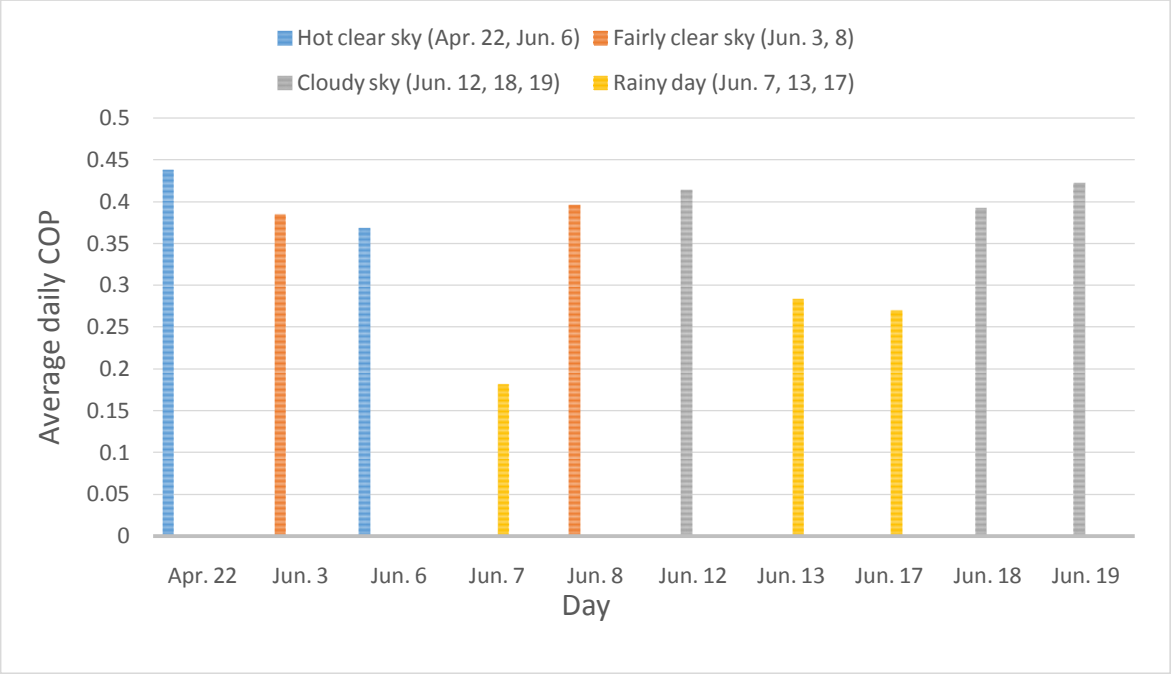


Fig. 4.168. Average daily COP of the experimental days

Figure 4.168 shows the average daily COP of the experimental days. The experimental day of April 22 had the highest COP of 0.438, indicating that the system performs best on hot clear sky days. This is because solar radiation values on this day are very high and can translate to high collector and generator temperatures to raise COP. The experimental days of June 12, 18 and 19 follow that of April 22 closely in terms of COP. These are classified as cloudy sky days, with June 12 and 19 having COP of above 0.4. The relatively good performance on these days as compared to the fairly clear sky days (June 3 and 8) is because the system was fired on gas burner heating mode throughout the days. The gas burner heating mode provided more constant heat supply to sustain generator temperatures high enough for better COP. For the fairly clear sky days, weaker generator temperatures result from lower solar radiation and switching from gas burner heating

mode to solar power heating mode and vice versa. The rainy days of June 7, 13 and 17 recorded the lowest COP.

4.5 Results from Economic Analysis

This section presents results from economic viability simulation as well as the economic assessment of the constructed system.

4.5.1 Results from economic viability simulation

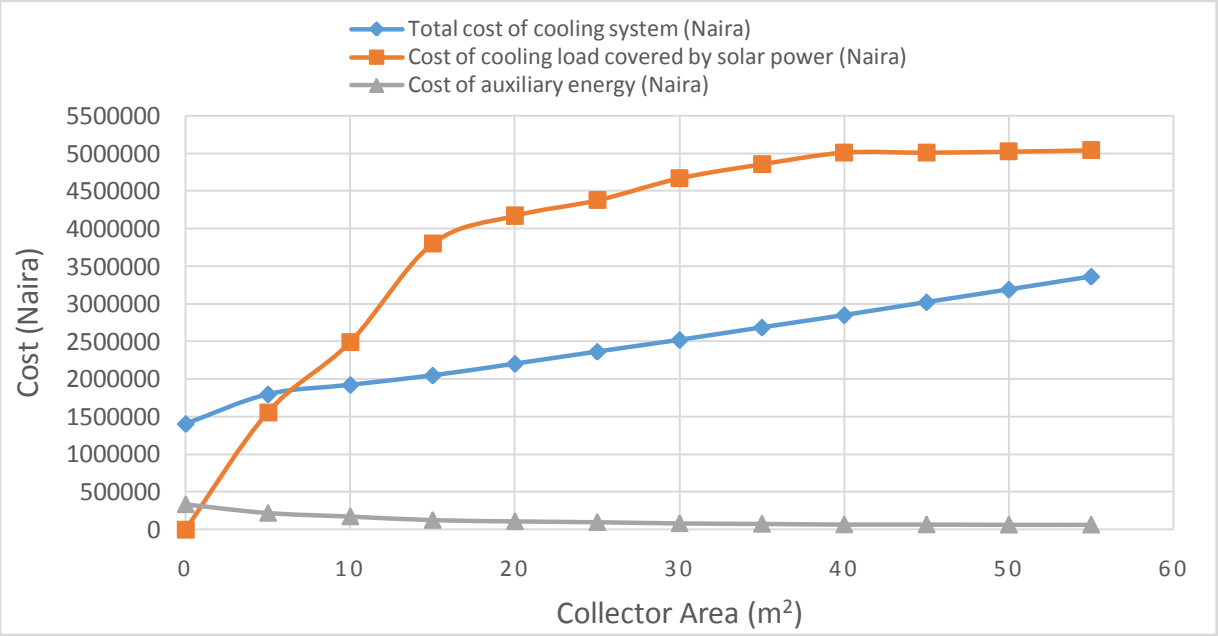


Fig. 4.169: Variation of total cost of cooling system, cost of cooling load covered by solar power and cost of auxiliary energy with collector area.

Fig. 4.169 shows the variation of total cost of cooling system, cost of cooling load covered by solar power and cost of auxiliary energy used by cooling system as a function of collector area. The total cost of the cooling system comprises the total components cost, installation cost, maintenance cost and running cost. The cost of cooling load covered by the solar power is the fraction of electricity cost for cooling the building over the life cycle of the system (20 years) that is met by solar energy. The cost of auxiliary energy is the cost spent on auxiliary energy during the life time of the system as well as cost of electricity consumed by the chiller.

As seen from the graph, the total cost of the cooling system increases linearly with collector area. This is so as other system components remain constant and increasing collector area also results in an increase in installation cost. The cost of cooling load covered by the solar power is seen to increase with increasing collector area. This is so as increasing collector area increases solar fraction, thereby the system is able to meet increasing percentage of the cooling energy demand running on solar energy. However, as from 40m^2 collector area, the cost of cooling load covered by solar power is seen to remain almost constant with increasing collector area. This is attributed to the fact that the solar fraction also remains fairly constant as from 40m^2 collector area.

Comparing the curves of total cost of cooling system with cost of cooling load covered by solar power, it is seen that the curve of cost of cooling load covered by solar power begins to peak above that of total cost of cooling system as from 10m^2 collector area. This indicates the point from which savings become achievable over the life cycle of the system.

Also, the cost of auxiliary energy is seen to decrease as the collector area increases. This again is because the solar fraction increases with increasing collector area, thus the system depends more on solar energy and less on the auxiliary energy.

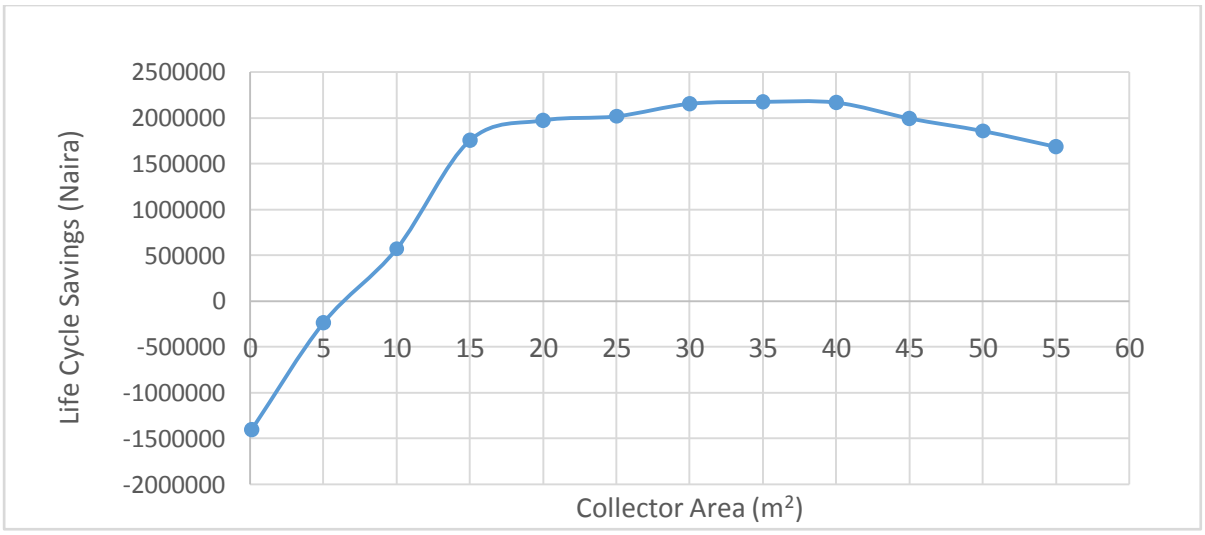


Fig. 4.170: Variation of life cycle cost savings with collector area

Figure 4.170 shows the variation of life cycle cost savings with collector area. As seen from the graph, negative savings are incurred from 0 to $7m^2$ collector area, from where the savings start to become positive. As from $10m^2$ collector area, savings start to become significant and continues to increase up to $30m^2$ collector area. Maximum life cycle savings are achieved between $30m^2$ and $40m^2$ collector area, with the peak life cycle savings of ₦2, 172,558.00 achieved with $35m^2$ collector area. With $40m^2$ collector area, the life cycle savings is reduced very marginally to ₦2, 164,401.00. On increasing the collector area above $40m^2$, then the life cycle savings start to decline rapidly with increasing collector area. This is so because as seen earlier, the solar fraction reaches the peak and becomes constant as from $40m^2$ collector area. Increasing the collector area above $40m^2$ results in additional cost of the system without a corresponding offset in the cost of electricity. Therefore for maximum savings, collector area of $35m^2$ should be adopted. However, in order to maintain maximum possible COP then a collector area of $40m^2$ can be adopted. This though will lead to a marginal decrease in savings.

From the forgoing, the techno – economic optimized system parameters are: Absorption chiller capacity: 12kW, Cooling tower capacity: 15kW, Solar Collector area: $35m^2$ - $40m^2$, Storage tank volume: $0.9m^3$. The economic viability simulation of the gas assisted solar absorption air – conditioning system shows that the system is economically viable in the given Nigerian climate (Zaria). Economic viability have been reported in similar works in different climates: Abdulateef *et al.*, (2009) recorded a LCS of $4,292 for a 7 kW solar absorption cooling system over conventional power system in Malaysia.

4.5.2. Economic assessment of the constructed system

In this section an economic assessment of the constructed system is presented. Daily running cost for the experimental days are presented, a Life cycle Cost Savings analysis is presented as well.

4.5.2.1 Daily running cost

Figure 4.171 shows the daily energy cost for the experimental days, while figure 4.172shows the cost per kWh of cooling for the experimental days.

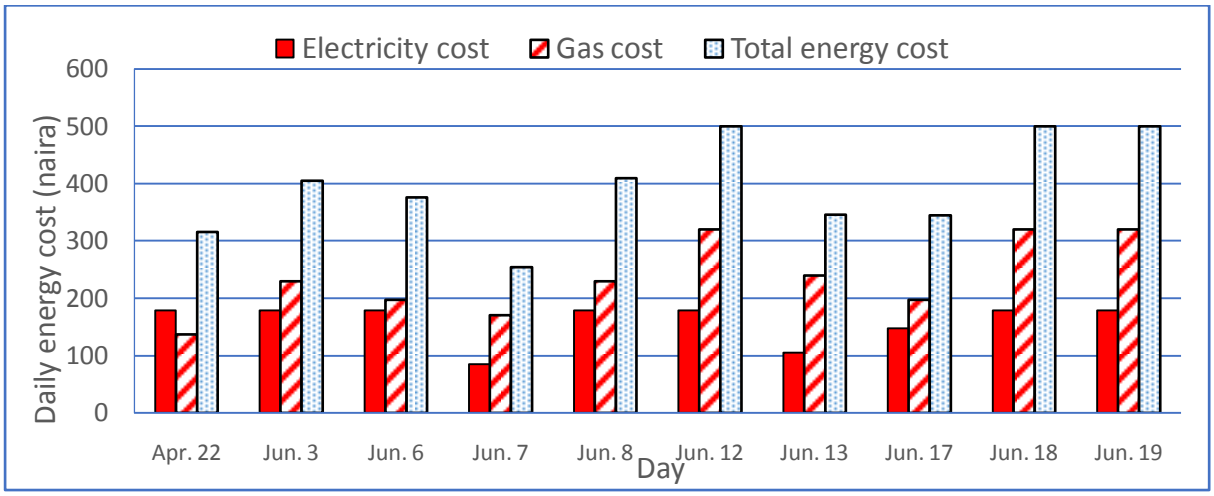


Fig. 4.171: Variation of daily energy cost for the experimental days

From figure 4.171, the experimental day of April 22, 2017 had the least cost of gas consumption, an indication that more solar power was used on the day. The highest cost of gas consumption occurred on the days of June 12, 18 and 19, 2017, which were all very cloudy days. This was because solar power could not be used at all on these days. The electricity cost for all the experimental days were the same, except for the days of June 7, 13 and 17, 2017, which were rainy days. This was because for the rainy days there were intervals in which free cooling was employed, thus the pumps were shut down within this interval.

The total cost is a summation of the electricity cost and gas cost for each day. As seen from the figure, it was most expensive to run the system on cloudy sky days as indicated by the experimental days of June 12, 18 and 19, 2017, with the cost at about 500 naira per day. This was due to the large amount of gas consumed on these days to provide thermal energy for the chiller. The total running cost was much less on clear sky days, with the experimental days of April 22 and June 6, 2017 requiring 315 naira/ day and 375 naira/ day respectively. This was because less gas was used on these days. It cost about 400 naira/ day for the fairly clear sky days. The rainy days are seen to be the least expensive for the system to run. This was because there were periods

with negligible cooling load due to natural cooling on these days. We can infer from this that for the rainy months, though solar radiation will be low, there may be no need to run the system throughout the day on gas burner heating mode as there may be negligible cooling demand at intervals, due to natural cooling occasioned by the rain. Therefore, system performance (solar mode) may be low in these months, but running cost is equally low.

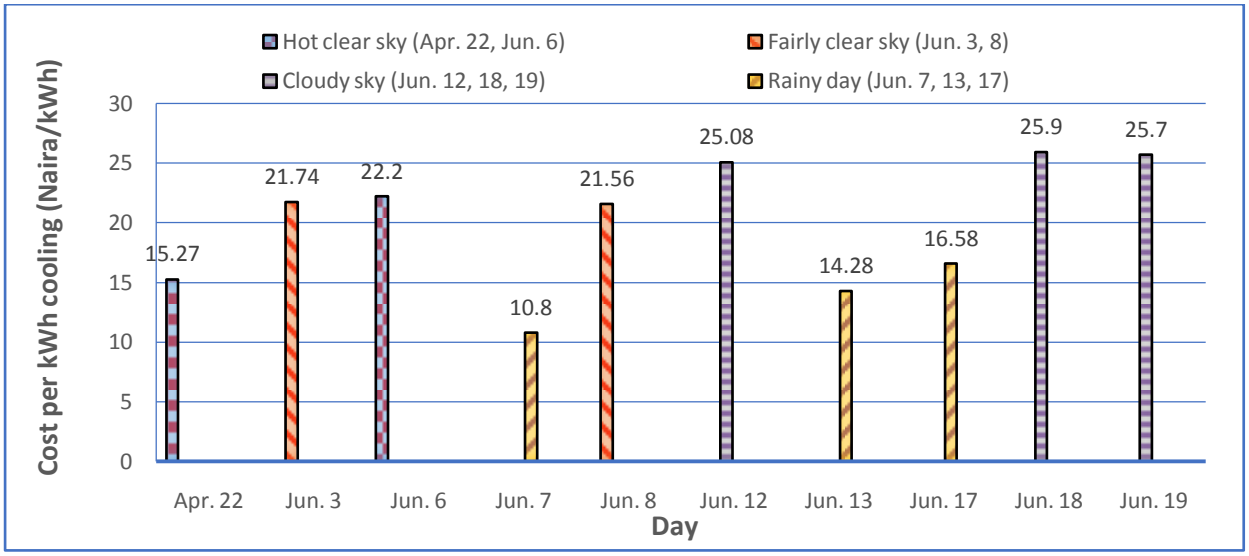


Fig. 4.172: Variation of cost per kWh of cooling for the experimental days

Fig. 4.172 shows the variation in cost per kWh of cooling recorded for the experimental days. The lowest costs were incurred on April 22 and June 7, 2017. On April 22, there was high solar radiation, thus, less gas was consumed. On June 7, there was rain which lasted for hours, the room was cooled naturally and less gas was consumed. The cloudy sky days of June 12, 18 and 19 are seen to have the highest cost /kWh cooling, due to high gas consumption.

The other experimental days also recorded varying degrees of cost per kWh of cooling, depending on the weather conditions.

The forgoing shows the system is capable of operating under varying weather conditions but at varying cost per kWh.

4.5.2.2 Life cycle savings analysis of the constructed system

The economic analysis was done using the life cycle cost savings method as illustrated in section 3.7.1. The equations presented in the section were used. The followings were used in evaluating the equations.

The total annual cooling load for the test room = 4,371kWh

Average solar fraction was taken as the average solar fraction for the experimental days. Solar fraction = 0.431

Cost of installed experimental system = ₦701, 200

Cost of energy = ₦26.37/kWh

Heating value of LPG = 4610000 J/kg

Fraction of the annual cooling load covered by solar power heating mode =

$Total\ annual\ cooling\ load \times solar\ fraction =$

$$= 4{,}371 \times 0.431 = 1{,}883.17kWh$$

Fraction of the annual cooling load covered by gas boiler heating mode =

$$Total\ annual\ cooling\ load - fraction\ of\ annual\ cooling\ load\ covered\ by\ solar\ power =$$

$$= 4{,}371 - 1{,}883.17 = 2{,}487.82kWh = 895615200J$$

The annual mass of gas consumed using the heating value of LPG as stated earlier is =

$$\frac{fraction\ of\ annual\ cooling\ load\ covered\ by\ gas\ heating\ mode}{heating\ vlue\ of\ LPG} =$$

$$= \frac{895615200}{4610000} = 194.27kg$$

The annual cost of gas @ ₦333.33/ kg is

$$= 194.27 \times 333.33 = ₦64{,}758.2$$

The annual cost of electricity consumed by the pumps and fan, using 261 annual working days, 8 hours daily running of pumps and fan, 0.8kW maximum power consumption of system and ₦26.37/ kWh electricity cost amounts to:

$$= 261 \times 8 \times 0.8 \times 26.37 = ₦44{,}048.45$$

From the equation for Life cycle Cost Savings as presented in equation 3.238, section 3.8.1

$$LCS = P_1 \times C_F \times L \times F - P_2 \times C_S$$

P_1 evaluated using the indices in section 3.8.1 gives: 17.11

$C_F, L\ and\ F$ are the cost of energy, total annual cooling load and solar fraction, which were computed using the values as stated above.

P_2 is unity, as stated in section 3.8.1 and C_S is the cost of installed system and running cost, which in this case is:

$$C_s = cost\ of\ system + annual\ cost\ of\ gas + annual\ cost\ of\ electricity$$

$C_s = 701{,}200 + 64{,}758.2 + 44{,}048.45 = N810{,}006.65$

Using these values in the equation for life cycle savings gives:

$LCS = (17.11 \times 26.37 \times 4{,}371 \times 0.431) - 810{,}006.65 = \text{₦}39{,}991.93$

Therefore, the constructed experimental system is capable of achieving a life cycle savings of thirty nine thousand, nine hundred and ninety one naira, ninety three kobo.

We can infer from the economic analysis that the solar/ gas hybrid powered absorption cooling system is economically viable in a Nigerian climate. This has been shown in both the economic viability simulation of the system as well as the economic analysis of the constructed system.

4.6 Comparison of Performance Parameters

4.6.1Comparison of coefficient of performance (COP)

Figure 4.173 compares the average COP of the constructed chiller with those of other constructed chillers of similar capacity.

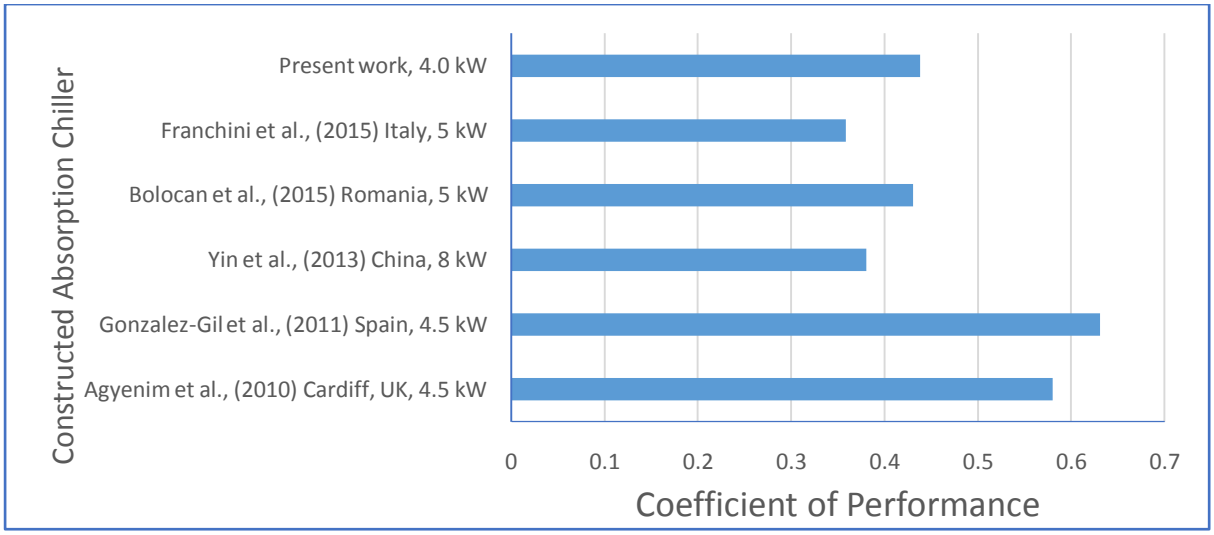


Fig. 4.173: Comparative COP of constructed absorption chillers

Figure 4.173 shows the coefficient of performance of similarly constructed single effect hot water fired absorption chillers, which fall within a close range of capacities. As seen from the figure, the average coefficient of performance of the present work at 0.438 falls within the range reported in literature. Bolocan *et al.*, (2015) reported a COP of 0.44 for a 5 kW capacity, Agyenim *et al.*, (2010) reported a COP of 0.58 for an 8 kW capacity, while Franchini *et al.*, (2015) reported a COP of 0.358 for a 5 kW capacity. This indicates that the "double tube" configuration introduced in the absorber and evaporator of the constructed absorption chiller prototype has performed satisfactorily.

4.6.2 Comparison of solar fraction (SF)

The solar fraction recorded within the days in which experiments were conducted in the present work ranged from 0.27 to 0.55. This falls within range of solar fraction reported in literature for similar works: Yin et al., (2013) reported a solar fraction of 0.19 to 0.43 in China, Ketjoy et al., (2013) reported a solar fraction of 0.38 to 0.55 in Thailand, Gonzalez – Gil et al., (2011) reported a solar fraction of 0.41 to 0.66 in Madrid, Spain.

4.6.3 Comparison of average space cooling temperatures

From the experiments conducted in all the experimental days in the present work, average room cooling temperatures between 24^{o}C to 27^{o}C were recorded. This compares favourably with room

cooling temperatures reported in similar works that used the LiBr/ H_2O pair: (Franchini et al, 2015 (24^oC – 26^oC), Yin et al, 2013 (24^oC – 27^oC), Gonzalez – Gil et al, 2011 (23^oC – 25^oC)).

4.6.4 Comparison of power consumption

Figure 4.174 compares the power consumption of constructed chiller to conventional chiller of varying EER.

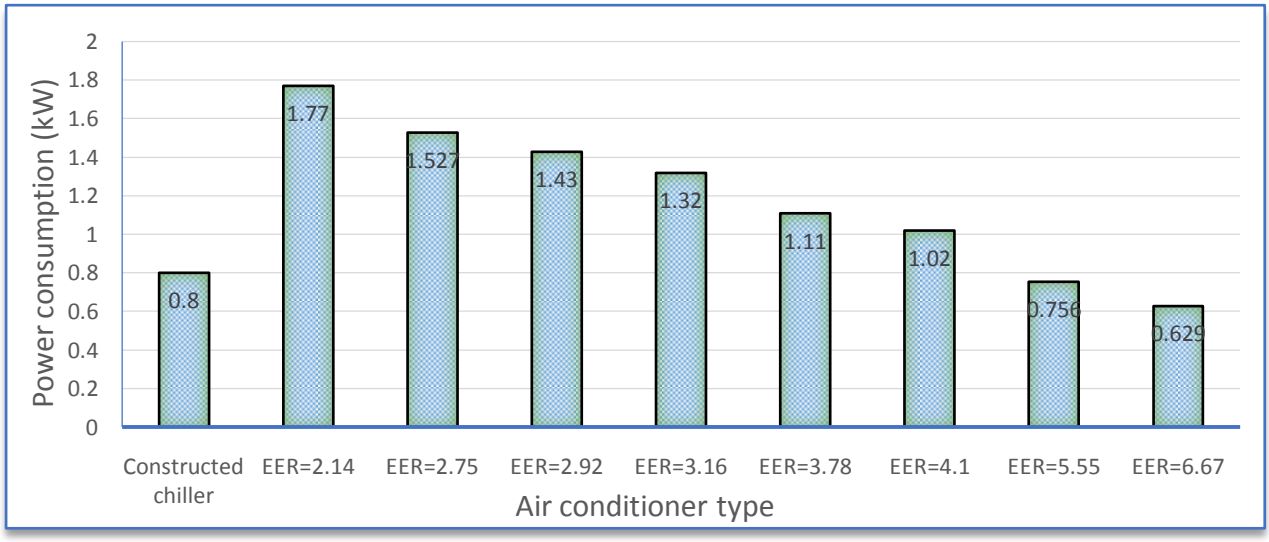


Fig. 4.174: Comparison of power consumption of constructed chiller with conventional chiller of varying EER

From figure 4.174, it is seen that the power consumption of the constructed chiller is lower than that of conventional air conditioners with EER in the range of minimum to average accepted standards. It is only a little higher than that of air conditioners with extreme maximum EER (5.55 and 6.67). This indicates that reduction in power consumption can be achieved with the absorption cooling system.

4.6.5 Comparison of cost per kWh of cooling

Figure 4.175 compares the cost per kWh of cooling of the constructed system to conventional chiller of varying EER.

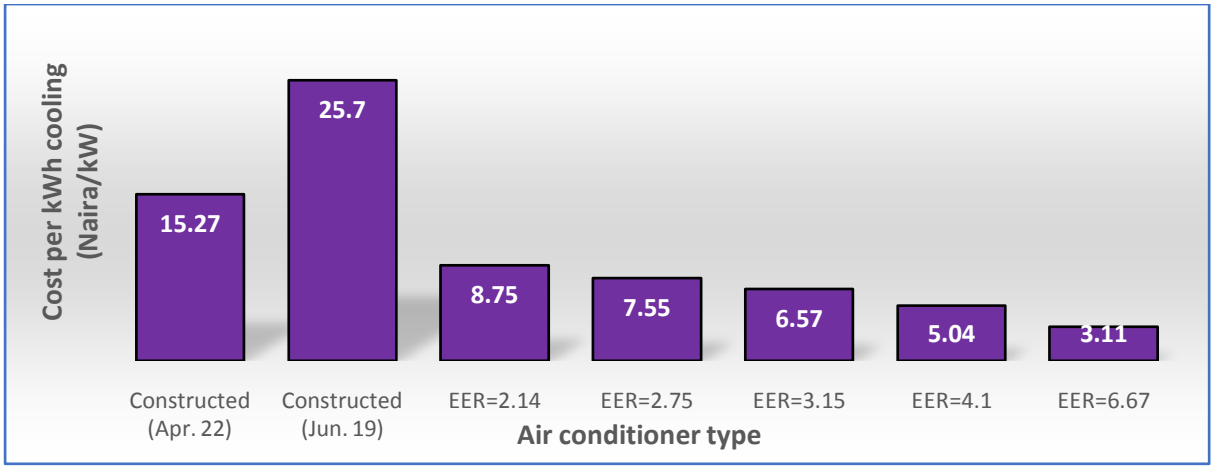


Fig. 4.175: Comparison of cost per kWh of cooling of constructed chiller with conventional chiller of varying EER

Fig. 4.175 shows the comparison of cost per kWh of cooling of the constructed plant on two experimental days (Apr. 22 and Jun. 19, 2017) to that of conventional air conditioners of varying EER. It is seen that the cost per kWh of cooling is higher for the constructed plant than the conventional air conditioners. This results due to the cost of gas used to produce the thermal energy for the constructed plant.

4.7 Results from Environmental Impact Assessment (CO_2 emission reduction and global warming potential)

This section presents results from the environmental impact assessment. Figure 4.176 Compares the CO_2 emitted to the atmosphere from constructed chiller to that emitted from conventional chiller of varying EER. Figure 4.177 compares the GWP of refrigerant used in the constructed chiller to those of commonly used refrigerants in conventional chillers.

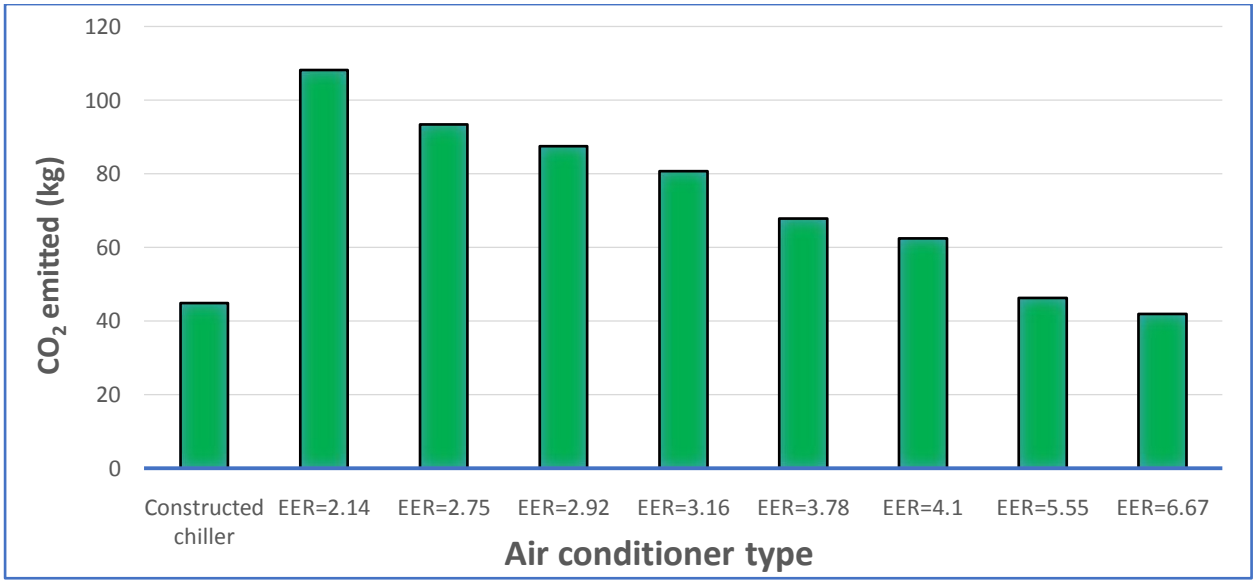


Fig. 4.176: Comparison of CO_2 emitted to the atmosphere from constructed chiller with conventional chiller of varying EER

From fig. 4.176, for the duration of the experiment, the constructed chiller has a much lower emission of CO_2 to the atmosphere compared to that from most of the conventional chillers. The reduction in CO_2 emission achieved is in the order of 2.7% to 58.4%, depending on the EER of the conventional chiller. The emission is however about the same with the chiller of extreme high EER (6.67).

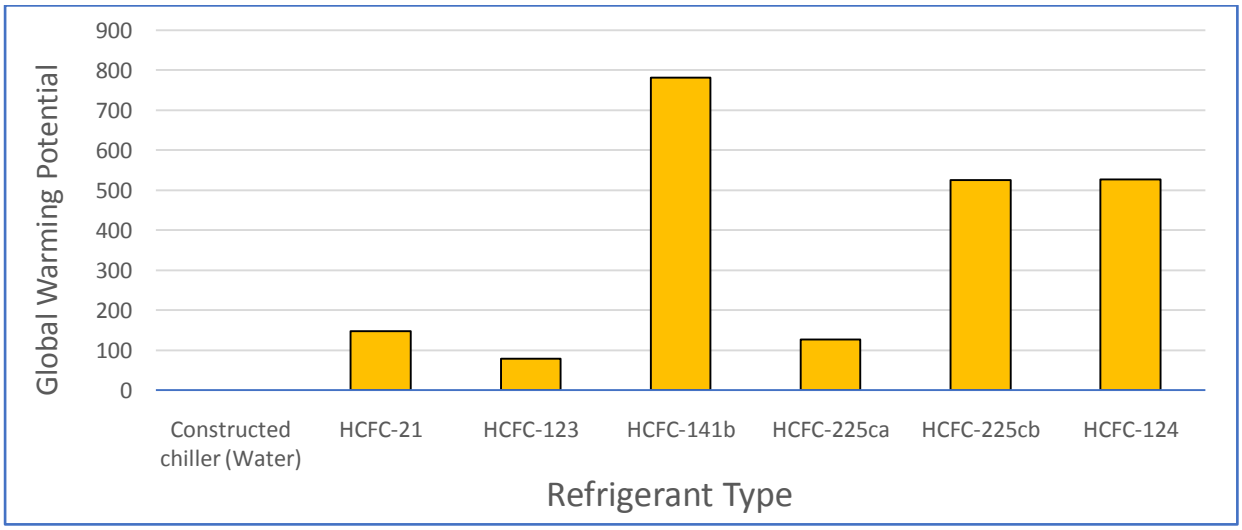


Fig. 4.177: Comparison of GWP of refrigerant in constructed chiller (water) with GWP of commonly used refrigerant in conventional chillers

From fig. 4.177, the constructed chiller with water as refrigerant has zero GWP to the environment, compared to refrigerants used in conventional chillers which have varying degrees of GWP to the environment.

CHAPTER FIVE

CONCLUSIONS& RECOMENDATIONS

The present work was conducted to study a solar/gas hybrid powered absorption air conditioning system for a Nigerian climate, specifically in Zaria. A TRNSYS model of the system was developed and used to obtain optimum system component sizes. Performance simulation of the system was done to ascertain its technical and economic feasibility in a Nigerian climate (Zaria). The system was designed and optimized. A reduced size version of the system which included a 4 kW absorption chiller prototype was successfully constructed. Experimental tests on the system was successfully performed. Economic viability simulation, economic evaluation of the

constructed system as well as environmental impact assessment (CO2 emission reduction and GWP) of the constructed system were done. With this, the objectives set out at the beginning of the study were achieved and the following conclusions can be drawn.

5.1 Conclusion

i. A TRNSYS model was developed and initial simulation was done which showed the solar absorption cooling system is feasible in the climate of study (Zaria). Optimum system component sizes for peak cooling load of 11.04 kW gave: absorption chiller: 12 kW, solar collector: 40 m^2, storage tank: 0.9 m^3.

ii. The gas assisted solar absorption air – conditioning system was successfully designed using program based design and calculation method in MATLAB.

iii. A reduced size version of the system was successfully constructed, this included a 4 kW absorption chiller prototype which operated with absorber and evaporator having a "double tube" configuration.

iv. Experiments were conducted on the constructed system. Space cooling between 24^oC – 27^oC was achieved. C.O.P. between 0.181 and 0.438 was achieved, while solar fraction ranged from 0.27 to 0.55.

v. Economic analysis showed cost per kWh cooling by the constructed system to be between N10/ kWh to N26/ kWh, depending on weather conditions. LCS analysis showed economic viability. LCS simulation showed energy savings of N2, 172,558 with 35m^2 collector area. LCS on the constructed system showed savings of N39, 991 with 1.74m^2 collector area.

vi. Environmental impact assessment (CO_2 emission reduction and GWP) conducted for the period of experiment showed CO_2 emission reduction between 2.7% and 58.4% by the constructed system compared to that from conventional chillers of varying EERs, as well as zero GWP to the environment.

5.2 Recommendations

i. In order to increase the water output temperatures from the collector, concentrating collectors such as evacuated tube collectors or parabolic trough collectors are recommended.

ii. In order to increase the duration in which the system can operate in solar power heating mode, the use of tracking system for the collector is recommended.

iii. In order to reduce the running cost associated with the use of liquefied petroleum gas, alternative fuel such as biogas can be combined with the solar mode.

iv. The absorber and condenser could be designed to be air cooled. This will eliminate the need for a cooling tower, which could reduce the system cost.

v. System design that would enable both solar heating mode and gas heating mode to operate simultaneously can be explored.

5.3 Contribution to Knowledge

i. A gas assisted solar powered absorption air – conditioning system has been successfully constructed, which includes a 4 kW absorption chiller prototype, the first in Nigeria (to the best of my knowledge). The system recorded a solar fraction of 0.55 in April for Zaria.

ii. The system performs satisfactorily in a Nigerian climate and it's economically viable. This has been shown by simulation and experiment, with LCS of N2, 172,558 and N39, 991 achieved in simulation and experiment respectively.

iii. The "Double tube" configuration adopted in the evaporator and the absorber of the absorption chiller was successful, this is shown in the COP achieved by the chiller (0.438) which compares favourably with those from reported works (Bolocan *et al.,* (2015) 0.44, Agyenim *et al.,* (2010) 0.58, Franchini *et al.,* (2015) 0.358).

iv. The system was able to achieve CO_2 emission reduction between 2.7% and 58.4% as compared to that from conventional chillers of varying Energy Efficiency ratios.

REFERENCES

Abdulateef, J., Sulaiman, M., Haw, L., Ali, B., Mat, S., Yahaya, M., Alghoul, M., Zaharim, A. and Sopian, K. (2009). An economic viability analysis and optimization of solar cooling system. Proceedings of the 4th IASME/ WSEAS International Conference on Energy and Environment, 24 – 26 February, 2009, Cambridge UK, pp. 425 – 430.

Abdullah, G., Saman, W., Whaley, D. and Belusko, M. (2015). Optimization of stand-alone solar heat fired absorption chiller for typical Australian homes. Proceedings of the International Conference on Solar Heating and Cooling for Buildings and Industry. 2nd – 4th December, 2015, Istanbul, Turkey. pp. 692 – 701.

Agrouaz, Y., Bouhal, T., Allouhi, A., Kousksan, T., Jamil, A. and Zeraouli, Y. (2017). Energy and parametric analysis of solar absorption cooling systems in various Moroccan climates. Case Studies in Thermal Engineering. Vol. 9 pp. 28 – 39.

Agyenim, F., Knight, I. and Rhodes, M. (2010). Design and experimental testing of the performance of an outdoor lithium bromide – water solar thermal absorption cooling system with a cold store.Solar Energy. Vol. 84pp 735 – 744.

Ahmed, M. H., Montagnino, F., Amir, A. M. and Hassan, R. (2016). Modelling of solar absorption cooling system under Egyptian climate using TRNSYS. Proceedings of the 12th International Conference on Energy, Environment, Ecosystems and Sustainable Development. 29th – 31st January, 2016, Venice, Italy. pp 258 – 264.

Ahmed, M. S., Ahmed, M. S. and Gilani, S. I. U. (2011). Steady state simulation of a double-effect steam absorption chiller. Journal of Applied Sciences. Vol. 11 (11), pp. 2018 – 2023.

Akhtar, S., Khan, T. S., Ilyas, S. and Alshehhi, M. S. (2015). Feasibility and basic design of solar absorption refrigeration for an industry. Energy Procedia. Vol. 5, pp. 508 – 513.

Al – Alili, A., Islam, M. D., Kubo, I., Hwang, Y. and Radermacher, R. (2012).Modelling of a solar powered absorption cycle for Abu – Dhabi.Applied Energy Vol. 93, pp. 160 – 167.

Albers, J. (2014). New absorption chiller and control strategy for the solar assisted cooling system at the German Federal Environment Agency. International Journal of Refrigeration. Vol. 39, pp. 48 – 56.

Ali, H. A., Noeres, P. and Pollerberg, C. (2008).Performance assessment of an integrated free cooling and solar powered single effect lithium bromide – water absorption chiller.Solar Energy. Vol. 82, pp. 1021 – 1030.

Anand, S., Gupta, A. and Tyagi, S. K. (2015). Solar cooling systems for climate change mitigation: a review. Renewable and Sustainable Energy Reviews. Vol. 41, pp. 143 – 161.

Arora, C.P. (2000). Refrigeration and air conditioning. 2nd edition Tata McGraw-Hill Publishing Company Limited, New Delhi.

Asim, M. Dewsbury, J. and Kanan, S. (2016). TRNSYS simulation of a solar cooling system for the hot climate of Pakistan. Energy Procedia. Vol. 91, pp. 702 – 706.

Assilzadeh, F., Kalogiron, S. A., Ali, Y. and Sopian, K. (2005). Simulation and optimization of a LiBr solar absorption cooling system with evacuated tube collectors.Renewable Energy. Vol. 30, pp. 1143 – 1159.

Atmaca, I. and Yigit, A. (2003). A simulation of solar powered absorption cooling system.Renewable Energy,Vol. 28(8). pp. 1277 – 93.

Ayadi, O. (2011). Solar cooling systems utilizing concentrating solar collectors: Design, experimental evaluation and optimization. Unpublished doctoral thesis, Energy cycle, Politecnico di Milano University, Italy.

Balamurugan, P. and Mani, A. (2013). Comparison of compact and tubular generators performance for R134a – DMF. Experimental Thermal and Fluid Science. Vol. 45, pp. 54 – 62.

Balghouthi, M., Chahbani, M. H. and Guizani, A. (2012).Investigation of a solar cooling installation in Tunisia. Applied Energy.Vol. 98, pp. 138 – 148.

Bansal, R. K. (2009). A text book of strength of materials. Laxmi publications, 113 golden house, Daryaganj, New Delhi, India.

Benhadid – Dib, S. and Benzaoui, A. (2012). Refrigerants and their environmental impact substitution of hydro chlorofluorocarbon HCFC and HFC hydro fluorocarbon. Search for an adequate refrigerant. Energy Procedia. Vol. 18, pp. 807 – 816.

Bolocan, S., Chiriac, F., Serban, A. and Dragomir, G. (2015). Development of a small capacity solar cooling absorption plant. Energy Procedia. Vol. 74, pp. 624 – 632.

Boudehenn, F., Demasles, H., Wyttenbach, J., Jobard, X., Cheze, D. and Papillon, P. (2012). Development of a 5 kW cooling capacity ammonia – water absorption chiller for solar cooling applications. Energy Procedia.Vol. 30, pp. 35 – 43.

Bujedo, L. A., Rodriguez, J. and Martinez, P. J (2011). Experimental results of different control strategies in a solar air conditioning system at part load. Solar Energy. Vol. 85, pp. 1302 – 1315.

Butterworth, D. (1996). Introduction to heat transfer. Oxford University Press, Oxford, United Kingdom. pp. 102 – 213.

Calise, F. (2012). High temperature solar heating and cooling systems for different Mediterranean climates: Dynamic simulation and economic assessment. Applied Thermal Engineering. Vol. 32, pp. 108 – 124.

Calise, F., Dentice d'Accadia, M. and Palombo, A. (2010). Transient analysis and energy optimization of solar heating and cooling systems in various configurations. Solar Energy. Vol. 84, pp. 432 – 449.

Chiriac, F., Serban, A., and Nastase, G. (2013). Heat exchanger with mini channels for absorption chillers with ammonia-water solution for small cooling powers. Proceedings of the 44th HVAC&R International Congress and Exhibition. 4th – 6th December, 2013.Belgrade, Serbia. pp. 865 – 871.

Choudhury, B., Saha, B. B., Chatterjee, P. K. and Sarka, J. P. (2013). An overview of developments in adsorption refrigeration systems towards a sustainable way of cooling. Applied Energy. Vol. 104, pp. 554 – 67.

Darkwa, J., Fraser, S. and Chow, D. H. C. (2012). Theoretical and practical analysis of an integrated solar hot water powered absorption cooling system. Energy Vol. 39, pp. 395 – 402.

Demirel, Y. (2012). Energy, green energy and technology. Springer – Verlag, London Ltd. Assessed from www.springer.com/cda/content on April 7, 2017.

Du, S., Wang, R. Z., Lin, P., Xu, Z. Z., Pan, Q. W. and Xu, S. C. (2012). Experimental studies on an air cooled two stage $NH_3 – H_2O$ solar air conditioning prototype. Energy. Vol. 45, pp. 581 – 587.

Duffie,J.A. and Beckman, W.A. (2013). Solar engineering of thermal processes. 4th Edition John Wiley and Sons Inc., 111 River Street Hoboken, New Jersey, U.S.A. pp.236 – 667.

Eicker, U., Pietruschka, D., Haag, M. and Schmitt, A. (2013). Energy and economic performance of solar cooling systems worldwide. Energy Procedia. Vol. 57, pp. 2581 – 2589.

Eicker, U. and Pietruschka, D. (2009). Design and performance of solar powered absorption cooling systems in office buildings. Energy and Buildings. Vol. 41, pp. 81 – 91.

Eke, A. B. (2011). Prediction of optimum angle of inclination for flat plate solar collector in Zaria. Agricultural Engineering International (CIGR Journal), 13(4): 1 – 7.

Estiot, E., Natzer, S. and Schweigler, C. (2007). Heat exchanger development for compact water/lithium bromide absorption systems. Proceedings of the 22nd International Congress of Refrigeration 21st – 26th August, 2007, Beijing, China B1 – 1253.

Evola, G., Le Pierres, N., Boudehenn, F. and Papillon, P. (2013). Proposal and validation of a model for the dynamic simulation of a solar assisted single stage LiBr/ water absorption chiller. International Journal of Refrigeration. Vol. 36, pp. 1015 – 1028.

Falahatkar, A. and Assadi, M. K. (2011). Analysis of solar lithium bromide – water absorption cooling system with heat pipe solar collector. Proceedings of the World Renewable Energy Congress: Solar Thermal Applications. 8th – 13th May, Linkoping, Sweden. pp. 3889 – 3896.

Femandes, M. S., Brites, G. J., Costa, J. J., Gaspar, A. R. and Costa, V. A. (2014). Review and future trends of solar adsorption refrigeration systems. Renewable and Sustainable Energy Reviews. Vol. 39, pp. 102 – 23.

Florides, G. A., Kalgirou, S. A. Tassou, S. A. and Worbel, L. C. (2002). Modeling and simulation of an absorption cooling system for Cyprus. Solar Energy; 72, 43-51.

Fraas, A. P. (1989). Heat exchanger design. Wiley Interscience, New York, pp. 114 – 265.

Franchini, G., Notarbartolo, E., Padovan, L., and Perdichizzi, A. (2015). Modelling, design and construction of a micro scale absorption chiller. Energy Procedia. Vol. 82, pp. 577 – 583.

Gebreslassie, B. H., Guillen-Gosalbez, G., Jimenez, L. and Boer, D. (2012). Solar assisted absorption cooling cycles for reduction of global warming: A multi-objective optimization approach. Solar energy. Vol. 86, pp. 2083 – 2094.

Ghafoor, A. and Munir, A. (2015). Worldwide overview of solar thermal cooling technologies. Renewable and Sustainable Energy Reviews. Vol. 43, pp. 763 – 774.

Gonzalez – Gil, A., Izquierdo, M., Marcos, J. D. and Palicios D. (2011). Experimental evaluation of a direct air cooled lithium bromide – water absorption prototype for solar air conditioning. Applied Thermal Engineering. Vol. 31, pp. 3358 – 3368.

Gugulothu, R., Somanchi, N. S., Banoth, H. B. and Banothu, K. (2015). A review on solar powered air conditioning system. Procedia Earth and Planetary Science. Vol. 11, pp. 361 – 367.

Hanson, S., Schwedler, M. and Bakkum, B. (2011). Chiller system design and control. Trane applications engineering manual. Assessed from www.trane.com on 17th October, 2016.

Hassan, H. Z. and Mohammad, A. A. (2012). A review on solar powered closed physisorption cooling systems. Renewable and Sustainable Energy Reviews. Vol. 16, pp. 2516 – 38.

Hassan, H. Z. and Mohammad, A. A. (2012). A review of solar cold production through absorption technology. Renewable and Sustainable Energy Reviews. Vol. 16, pp. 5331 – 5348.

Hasenohrl, T. (2011). Development of plate heat exchanger as main component of an absorption chiller. Unpublished M.Sc Thesis: Division of heat transfer, Department of Energy Sciences, Faculty of Engineering, LTH, Lund University, Sweden.

He, T., Zhang, X., Wang, C., Wang, M., Li, B., Xue, N., Shimizu, K., Takahashi, K. and Wu, Y. (2015). Application of solar thermal cooling system driven by low temperature heat source in China. Energy Procedia. Vol. 70, pp. 454 – 461.

Henning, H. (2007). Solar assisted air – conditioning of buildings, an overview. Applied Thermal Engineering. Vol. 27, pp. 1734 – 49.

Hensley, J. C. (2009). Cooling tower fundamentals, 2nd edition. SPX Cooling Technologies Inc. Overland park, Kansas, U.S.A.

Hidalgo, M. C., Aumente, P. R., Millan, M. I., Neumann, A. L. and Mangual, R. S. (2008). Energy and carbon emission savings in Spanish housing air conditioning using solar driven absorption system. Applied Thermal Engineering. Vol. 28, pp. 1734 – 1744.

Hottel, H. C., and Woertz, B. B. (1942). Evaluation of flat plate solar heat collector. Trans. ASME. Vol. 64, pp. 91 – 107.

Ibarra – Bahena, J., and Romero, R. J. (2014). Performance of different experimental absorber designs in absorption heat pump cycle technologies. A review. Energies. Vol. 7, pp. 751 – 766.

Incropera, J., Dewitt, A., Bergmann, P, and Lavine, C. (2004). Fundamentals of heat and mass transfer, 6th edition. John Wiley and Sons Inc., 111 River Street Hoboken, New Jersey, U.S.A. pp. 377 – 748.

Izquierdo, M., Marcos, J. D., Palacios, M. E. and Gonzalez – Gil, A. (2012). Experimental evaluation of a low power direct air cooled double effect LiBr – H_2O absorption prototype. Energy. Vol. 37, pp. 737 – 748.

Jeter, S.M., Lee, R.J., DiGuilio,R.M. and Tega, A.S. (1990). Properties of LiBr-water solutions at high temperature and concentration –II (Density and Viscosity). ASHARE Trans, Vol. 96, pp. 108 – 119.

Kalkan, N., Young, E. A. and Celiktas, A. (2012). Solar thermal air conditioning technology reducing the foot print of solar thermal air conditioning. Renewable and Sustainable Energy Reviews. Vol. 16, pp. 6352 – 83.

Kanan, S., Dewsbury, J. and Lane – Serff, G. (2015). Simulation of solar air conditioning system with salinity gradient solar pond. Proceedings of the international conference on alternative energy in developing countries and emerging economies. 28th – 29th May, 2015, Bangkok, Thailand. pp. 746 – 751.

Ketfi, O., Merzouk, M., Merzouk, N. K. and El Metenan, S. (2015). Performance of a single effect solar absorption cooling system (LiBr-H_2O). Energy Procedia. Vol. 74, pp. 130 – 138.

Ketjoy, N., Yongphayoon, R. and Mansiri, K. (2013). Performance evaluation of a 35 kW lithium bromide – water solar absorption cooling system in Thailand. Energy Procedia. Vol. 34, pp. 198 – 210.

Klein, S. A., Beckmann, W. A., Duffie, J. A., Mitchell, J. C., and Bradley, D. E. (2006). Transient system simulation (TRNSYS) program (manual). Solar Energy Laboratory, University of Wisconsin, Madison, U.S.A. available at www.sel.me.wisc.edu.trnsys

Lansing, F.L. (1984). Computer modelling of a single-stage LiBr/water absorption refrigeration unit. JPL Deep Space Network Progress Report 42:32. Accessed from http://ipnpr.jpl.nasa.gov on 30th November, 2016.

Li, Z. F. and Sumathy, K. (2000). Technology development in the solar absorption air conditioning systems. Renewable and Sustainable Energy Reviews. Vol. 4, pp. 267-293.

Lienhard, J.H. IV and Lienhard J.H. V. (2005) A heat transfer textbook 3rd Edition. Phlogiston Press, Cambridge Massachusetts, USA. pp. 78 – 256.

Lizarte, R., Izquierdo, M., Marcos, J. D. and Palacios, E. (2012). An innovative solar driven directly air cooled lithium bromide – water absorption chiller prototype for residential use. Energy and Building. Vol. 47, pp. 1 – 11.

Lostec, B., L., Galanis, N. and Millete, J. (2012). Experimental study of an ammonia – water absorption chiller. International Journal of Refrigeration. Vol. 35, pp. 2275 – 2286.

Mammoli, A., Vorobieff, P., Barsun, H., Burnett, R. and Fisher, D. (2011). Energetic, economic and environmental performance of a solar thermal assisted HVAC system. Energy and Buildings. Vol. 42, pp. 1524 – 1535.

Mayhew, Y. R. and Rogers, G. F. C. (1972). Thermodynamic and transport properties of fluids. Second edition. Oxford Basil Blackwell, England. pp. 2 – 10.

Mazloumi, M., Naghashzadegan, M. and Javaherdeh, K. (2008). Simulation of solar lithium bromide – water absorption cooling system with parabolic trough collector. Energy Conversion and Management. Vol. 49, pp. 2820 – 2832.

McAdams, W. H. (1954). Heat transmission, 3rd edition. McGraw Hill, New York.

Mendoza, C., Rousse, D. and Quesad, G. (2013). Modelling of a solar absorption cooling system for Guayaquil, Ecuador. Proceedings of the 2nd International Conference on Renewable Energy Research and Applications. 20th – 23rd October, 2013, Madrid Spain. pp. 978 – 981.

Mittal, V., Kasana, K. and Thakur, N. (2006). Modelling and simulation of solar absorption cooling system for India. Journal of Energy in Southern Africa, 17(3): 65 – 70.

Mugnier, D. and Jakob, U. (2012). Keeping cool with the sun. Sustainable Energy Reviews, 6(1): 28 – 30.

MYTO 2.1 report (2015). Accessed from http://www.nrecng.org on 15th of August, 2016.

Onyebuchi, E. I. (1989). Alternative energy strategies for the developing world's domestic use: A case study of Nigerian household's final use patterns and preferences. The Energy Journal, 10 (3): 121 – 138.

Otanicar, T., Taylor, R. A. and Phelan, P. E. (2012). Prospects for solar cooling: An economic and environmental assessment. Solar Energy. Vol. 86, pp. 1287 – 99.

Oyedepo, S. O. (2012). Energy and sustainable development in Nigeria: The way forward. Energy, Sustainability and Society. Springer Open Journal. pp. 1 – 17. Assessed from www.energsustainsoc.com/content/2/1/15 on 23rd June 2017.

Pachauri, R. K. and Reisinger, A. (2007). Climate change 2007, synthesis report. Assessed from www.ipcc.ch/pdf/assessment-repot on 15th March 2017.

Phadke, A., Abhyankar, N. and Shah, N. (2014). Avoiding 100 new power plants by increasing efficiency of room air conditioners in India. Opportunities and challenges. Lawrence Berkeley National Laboratory, Berkeley, U.S.A. Accessed from: www.cseindia.org on 25th September 2016.

Praene, J. P., Marco, O., Lucas, F. and Miranville, F. (2011). Simulation and experimental investigation of solar cooling system in Reunion Island.Applied Energy. Vol.88, pp. 831 – 839.

Prasartkaew, B. (2014). Performance test of a small size lithium bromide – water absorption chiller. Energy Procedia. Vol. 56, pp. 487 – 497.

Prasartkaew, B. and Kumar, S. (2010).A low carbon cooling system using renewable energy resources and technologies. Energy and Building, 42(9): 1453 – 82.

Pridasawas, W. (2006). Solar driven refrigeration systems with focus on the ejector cycle. Unpublished Doctoral Thesis, Royal Institute of Technology, KTH. Stockholm, Sweden.

Pongtorukulpanich, A., Thepa, S., Amornkitbamrung, M. and Butcher, C. (2008). Experience with a fully operational solar driven 10 ton LiBr/ H_2O single effect absorption cooling system in Thailand. Renewable Energy, 35(5): 943 – 9.

Qu, M., Yin, H. and Archer, D. H. (2010). A solar thermal cooling and heating system for a building: Experimental and model based performance analysis and design. Solar Energy. Vol. 84, pp. 166 – 182.

Rosiek, S. and Batlles, F. J. (2012). Shallow geothermal energy applied to a solar assisted air conditioning system in southern Spain: Two year experience. Applied Energy. Vol. 100,pp. 267 – 276.

Said, S. A. M., Spindler, K., El – Shaarawi, M. A. and Siddiqui, M. U. (2016). Design, construction and operation of a solar powered ammonia – water absorption refrigeration system in Saudi Arabia. International Journal of Refrigeration. Vol. 62, pp. 222 – 231.

Said, S. A. M., El – Shaarawi, M. A. I. and Siddiqui, M. U. (2015). Analysis of a solar powered absorption system. Energy Conversion and Management. Vol. 97, pp. 243 – 252.

Sarbu, I. and Sebarchievici, C. (2015). General review of solar powered close sorption refrigeration systems. Energy Conversion and Management. Vol. 105, pp. 403 – 442.

Schwerdt, P. and Ali, A. (2013). German/ Egyptian demonstration project on solar cooling in a hot arid climate. Proceedings of the International Conference on Solar Heating and Cooling for Buildings and Industry. 23rd – 25th September, 2013, Freiburg, Germany. pp.991 – 996.

Shaikh, T. A. and Morabiya, Y. J. (2013). Mathematical modelling and analysis of solar absorption refrigeration system. International Journal of Emerging Trends in Engineering and Development, 3(2): 45 – 57.

Shirazi, A., Taylor, R., White, S. and Morrison, G. (2015). Multi – effect absorption chillers powered by the sun: reality or reverie. Proceedings of the International Conference on Solar Heating and Cooling for Buildings and Industry. 2nd – 4th December, 2015, Istanbul, Turkey. pp. 844 – 856.

Ssembatya, M., Pokhrel, M. and Reddy, R. (2013). Simulation studies on performance of solar cooling system in UAE conditions. Proceedings of the International Conference on Solar Heating and Cooling for Buildings and Industry. 23rd – 25th September, 2013, Freiburg, Germany. pp. 1007 – 1016.

Stocker, T. F., Qin, D., Plattner, G. K., Tignor, M., Allen, S. K. and Boschung, J. (2014). Fifth assessment report of the Intergovernmental Panel on Climate Change (IPCC). Assessed from www.ipcc.ch/pdf/assessment-report/ar5 on 5th January, 2017.

Sun, H., Xu, Z. Y., Wang, H. and Wang, R. (2015). A solar/gas fired absorption system for cooling and heating in a commercial building. Energy Procedia. Vol. 70, pp. 518 – 528.

Tamasauskas, J., Kegel, M. and Sunye, R. (2013). An analysis of solar thermal technologies integrated into a Canadian office building. Proceedings of the International Conference on Solar Heating and Cooling for Buildings and Industry. 23rd – 25th September, 2013, Freiburg, Germany. pp. 1017 – 1026.

Thome, J. R. and Robinson, D. M. (2006). Prediction of local bundle boiling heat transfer coefficients: Pure refrigerant boiling on plain, low fin and turbo BII HP tube bundles. Heat Transfer Engineering, 27(10): 20 – 29.

Thome, J. R. (2016). Encyclopedia of two – phase heat transfer and flow I. Fundamentals and methods. World Scientific Publishing, 5 Toh Tuck link, Singapore. pp. 63 – 71.

Trot, A. R., and Welch, T. (2000). Refrigeration and Air – conditioning, 3rd edition. Butterworth – Heinemann publishers, Oxford, United Kingdom. pp. 58 – 234.

Tsoutsos, T., Aloumpi, E., Gkouskos, Z. and Karagiorgas, M (2010). Design of a solar absorption cooling system in a Greek hospital. Energy and Buildings. Vol. 42, pp. 265 – 272.

Ullah, K. R., Saidur, R., Ping, H. W., Akikur, R. K. and Shuvo, N. H. (2013). A review of solar thermal refrigeration and cooling methods. Renewable and Sustainable Energy Reviews. Vol. 24, pp. 490 – 513.

Wang, S. K. (2001). Hand book of air conditioning and refrigeration. Second edition. McGraw-Hill publishers, New York, U.S.A. pp. 35 – 398.

Welty, J. R., Rorrer, G. L., and Foster, D. G. (2014). Fundamentals of momentum, heat and mass transfer, 6th edition. Wiley and Sons Inc., New Jersey, U.S.A. pp. 75 – 341.

White, F. M. (2006). Fluid mechanics. McGraw-Hill publisher, NewYork, U.S.A. pp. 203 – 271.

Williamson, N. J. (2008). Numerical modelling of heat and mass transfer and optimization of a natural draft wet cooling tower. Unpublished PhD Thesis, School of Aerospace, Mechanical and Mechatronic Engineering, the University of Sydney, Australia.

Winston, R., Jiang, L., and Widyolar, B. (2014). Performance of a 23kW solar thermal cooling system employing a double effect absorption chiller and thermodynamically efficient non tracking concentrators. Energy Procedia. Vol. 48, pp. 1036 - 1046.

World Fact Book (2016). Central Bank of Nigeria discount rate. Accessed from http://www.indexmundi.com on 15th of August, 2016.

Yin, Y. L., Zhai, X. Q. and Wang, R. Z. (2013). Experimental investigation and performance analysis of a mini type solar absorption cooling system. Applied Thermal Energy. Vol. 59, pp. 267 – 277.

Yin, Y. L., Song, S. P., Li, Y., Wang, R. Z. and Zhai, X. Q. (2012). Experimental investigation of a mini type solar absorption cooling system under different cooling modes. Energy and Buildings. Vol. 47, pp. 131 – 138.

Zhai, X., Li, Y., Cheng, X. and Wang, R. (2015). Experimental investigation on a solar powered absorption radiant cooling system. Energy Procedia. Vol. 70, pp. 552 – 559.

Zheng, W. (2016). New generation of solar thermal cooling with yazaki. Solar heating and cooling task 53 report. Assessed from www.yazakienergy.com on 21st January, 2017.

APPENDIX A1

TRNSYS INPUT FILE FOR BUILDING COOLING LOAD SIMULATION
VERSION 16.1

```
**********************************************************************************
*** TRNSYS input file (deck) generated by TrnsysStudio
*** on Thursday, April 09, 2015 at 07:15
*** from TrnsysStudio project: D:\Documents and Settings\Talib\Desktop\TRNSYS simulations\building cooling load.tpf
***
*** If you edit this file, use the File/Import TRNSYS Input File function in
*** TrnsysStudio to update the project.
***
*** If you have problems, questions or suggestions please contact your local
*** TRNSYS distributor or mailto:software@cstb.fr
***
**********************************************************************************


**********************************************************************************
*** Units
**********************************************************************************

**********************************************************************************
*** Control cards
**********************************************************************************
* START, STOP and STEP
CONSTANTS 3
START=0
STOP=8760
STEP=1
* User defined CONSTANTS

SIMULATION          START       STOP  STEP ! Start time     End time        Time step
TOLERANCES 0.001 0.001                   ! Integration    Convergence
LIMITS 30 30 30                          ! Max iterations        Max warnings Trace limit
DFQ 1                                 ! TRNSYS numerical integration solver method
WIDTH 72                              ! TRNSYS output file width, number of characters
LIST                                  ! NOLIST statement
! MAP statement
SOLVER 0 1 1                             ! Solver statement     Minimum relaxation factor
       Maximum relaxation factor
NAN_CHECK 0                              ! Nan DEBUG statement
OVERWRITE_CHECK 0                        ! Overwrite DEBUG statement
TIME_REPORT 0                         ! disable time report
EQSOLVER 0                            ! EQUATION SOLVER statement

* EQUATIONS "Turn"
*
EQUATIONS 5
TURN = 12
AA_N = 180 + TURN
AA_S = TURN
AA_E = -90 + TURN
```

```
AA_W = 90 + TURN
*$UNIT_NAME Turn
*$LAYER Main
*$POSITION 49 61

*-------------------------------------------------------------------------


* EQUATIONS "Radiation"
*
EQUATIONS 18
AISZ = [109,10]
AISA = [109,11]
IT_H = Max([109,12],0)
IB_H = Max([109,13],0)
ID_H = [109,14]
AI_H = [109,16]
IT_N = [109,18]
AI_N = [109,22]
IB_N = [109,19] * LT(AI_N,90)
IT_S = [109,24]
IB_S = [109,25]
AI_S = [109,28]
IT_E = [109,30]
IB_E = [109,31]
AI_E = [109,34]
IT_W = [109,36]
IB_W = [109,37]
AI_W = [109,40]
*$UNIT_NAME Radiation
*$LAYER Main
*$POSITION 195 125

*-------------------------------------------------------------------------


* EQUATIONS "Shading+Light"
*
EQUATIONS 1
BRIGHT = [200,1]     !  27
*$UNIT_NAME Shading+Light
*$LAYER Controls
*$POSITION 664 722

*-------------------------------------------------------------------------


* EQUATIONS "Fixed Shading"
*
EQUATIONS 9
```

```
IT_N_SHD = [341,1]
IB_N_SHD = [341,2]
AI_N_SHD = AI_N
IT_S_SHD = [342,1]
IB_S_SHD = [342,2]
AI_S_SHD = AI_S
IT_H_SHD = IT_H
IB_H_SHD = IB_H
AI_H_SHD = AI_H
*$UNIT_NAME Fixed Shading
*$LAYER Main
*$POSITION 653 402

*-------------------------------------------------------------------------


* Model "Weather data" (Type 109)
*

UNIT 109 TYPE 109   Weather data
*$UNIT_NAME Weather data
*$MODEL .\Weather Data Reading and Processing\Standard Format\TMY2\Type109-TMY2.tmf
*$POSITION 95 200
*$LAYER Main #
PARAMETERS 4
2               ! 1 Data Reader Mode
30              ! 2 Logical unit
4               ! 3 Sky model for diffuse radiation
1               ! 4 Tracking mode
INPUTS 9
0,0             ! [unconnected] Ground reflectance
0,0             ! [unconnected] Slope of surface-1
0,0             ! [unconnected] Azimuth of surface-1
0,0             ! [unconnected] Slope of surface-2
0,0             ! [unconnected] Azimuth of surface-2
0,0             ! [unconnected] Slope of surface-3
0,0             ! [unconnected] Azimuth of surface-3
0,0             ! [unconnected] Slope of surface-4
0,0             ! [unconnected] Azimuth of surface-4
*** INITIAL INPUT VALUES
0.2 90 AA_N 90 AA_S 90 AA_E 90 AA_W
*** External files
ASSIGN                                                                  "D:\Program
Files\Trnsys16\Weather\Zaria_Nigeria_SPtMasterTable_472122_19790101_20100101_tmy2.tm2
" 30
*|? Weather data file |1000
*-------------------------------------------------------------------------

* Model "Psychrometrics" (Type 33)
*
```

```
UNIT 331 TYPE 33     Psychrometrics
*$UNIT_NAME Psychrometrics
*$MODEL .\Physical Phenomena\Thermodynamic Properties\Psychrometrics\Dry Bulb and Relative Humidity Known\Type33e.tmf
*$POSITION 204 325
*$LAYER Main #
PARAMETERS 3
2               ! 1 Psychrometrics mode
1               ! 2 Wet bulb mode
1               ! 3 Error mode
INPUTS 3
109,1           ! Weather data:Ambient temperature ->Dry bulb temp.
109,2           ! Weather data:relative humidity ->Percent relative humidity
0,0             ! [unconnected] Pressure
*** INITIAL INPUT VALUES
20 50 1
*------------------------------------------------------------------------------

* Model "Sky temp" (Type 69)
*

UNIT 69 TYPE 69      Sky temp
*$UNIT_NAME Sky temp
*$MODEL .\Physical Phenomena\Sky Temperature\calculate cloudiness factor\Type69b.tmf
*$POSITION 354 273
*$LAYER Main # #
PARAMETERS 2
0               ! 1 mode for cloudiness factor
0               ! 2 height over sea level
INPUTS 4
331,7           ! Psychrometrics:Dry bulb temperature ->Ambient temperature
331,8           ! Psychrometrics:Dew point temperature. ->Dew point temperature at ambient conditions
109,13              ! Weather data:beam radiation on horitonzal ->Beam radiation on the horizontal
109,14              ! Weather data:sky diffuse radiation on horizontal ->Diffuse radiation on the horizontal
*** INITIAL INPUT VALUES
0 0 0 0
*------------------------------------------------------------------------------

* EQUATIONS "Light Thresholds"
*
EQUATIONS 2
Toth_L_on = -3.6*120
Eoth_L_off = -3.6*200
*$UNIT_NAME Light Thresholds
*$LAYER Controls
*$POSITION 461 530
```

```
*--------------------------------------------------------------------------


* Model "Lights" (Type 2)
*

UNIT 200 TYPE 2      Lights
*$UNIT_NAME Lights
*$MODEL .\Controllers\Differential Controller w_ Hysteresis\generic\Solver 0 (Successive Substitution) Control Strategy\Type2d.tmf
*$POSITION 566 541
*$LAYER Controls #
*$# NOTE: This controller can only be used with Solver 0 (Successive substitution)
*$#
*$#
*$#
*$#
*$#
*$#
*$#
*$#
*$#
PARAMETERS 2
5               ! 1 No. of oscillations
40000           ! 2 High limit cut-out
INPUTS 6
0,0             ! [unconnected] Upper input value
IT_H            ! Radiation:IT_H ->Lower input value
0,0             ! [unconnected] Monitoring value
200,1           ! Lights:Output control function ->Input control function
Toth_L_on               ! Light Thresholds:Toth_L_on ->Upper dead band
Eoth_L_off              ! Light Thresholds:Eoth_L_off ->Lower dead band
*** INITIAL INPUT VALUES
0 0 0 0 0 0
*--------------------------------------------------------------------------

* Model "WingWall N" (Type 34)
*

UNIT 341 TYPE 34    WingWall N
*$UNIT_NAME WingWall N
*$MODEL .\Loads and Structures\Overhang and Wingwall Shading\Type34.tmf
*$POSITION 595 61
*$LAYER Main # #
PARAMETERS 16
0               ! 1 Upstream component mode
2.2             ! 2 Receiver height
2.45            ! 3 Receiver width
1.2             ! 4 Overhang projection
```

```
0.5             ! 5 Overhang gap
1.03            ! 6 Overhang left extension
1.03            ! 7 Overhang right extension
0               ! 8 Left wingwall projection
0               ! 9 Left wingwall gap
0               ! 10 Left wingwall top extension
0               ! 11 Left wingwall bottom extension
0               ! 12 Right wingwall projection
0               ! 13 Right wingwall gap
0               ! 14 Right wingwall top extension
0               ! 15 Right wingwall bottom extension
AA_N            ! 16 Receiver azimuth
INPUTS 7
AISZ            ! Radiation:AISZ ->Solar zenith angle
AISA            ! Radiation:AISA ->Solar azimuth angle
IT_H            ! Radiation:IT_H ->Total horizontal radiation
ID_H            ! Radiation:ID_H ->Horizontal diffuse radiation
IB_N            ! Radiation:IB_N ->Beam radiation on surface
0,0             ! [unconnected] Ground reflectance
AI_N            ! Radiation:AI_N ->Incidence angle of direct radiation
*** INITIAL INPUT VALUES
30 20 0 0 0 0.2 0
*------------------------------------------------------------------------------

* Model "WingWall S" (Type 34)
*

UNIT 342 TYPE 34    WingWall S
*$UNIT_NAME WingWall S
*$MODEL .\Loads and Structures\Overhang and Wingwall Shading\Type34.tmf
*$POSITION 606 264
*$LAYER Main # #
PARAMETERS 16
0               ! 1 Upstream component mode
2.2             ! 2 Receiver height
2.45            ! 3 Receiver width
1.5             ! 4 Overhang projection
0.5             ! 5 Overhang gap
1.02            ! 6 Overhang left extension
1.02            ! 7 Overhang right extension
0               ! 8 Left wingwall projection
0               ! 9 Left wingwall gap
0               ! 10 Left wingwall top extension
0               ! 11 Left wingwall bottom extension
0               ! 12 Right wingwall projection
0               ! 13 Right wingwall gap
0               ! 14 Right wingwall top extension
0               ! 15 Right wingwall bottom extension
AA_S            ! 16 Receiver azimuth
INPUTS 7
```

```
AISZ            ! Radiation:AISZ ->Solar zenith angle
AISA            ! Radiation:AISA ->Solar azimuth angle
IT_H            ! Radiation:IT_H ->Total horizontal radiation
ID_H            ! Radiation:ID_H ->Horizontal diffuse radiation
IB_S            ! Radiation:IB_S ->Beam radiation on surface
0,0             ! [unconnected] Ground reflectance
AI_S            ! Radiation:AI_S ->Incidence angle of direct radiation
*** INITIAL INPUT VALUES
30 20 0 0 0 0.2 0
*-------------------------------------------------------------------------------

* Model "Building" (Type 56)
*

UNIT 56 TYPE 56      Building
*$UNIT_NAME Building
*$MODEL .\Loads and Structures\Multi-Zone Building\With Standard Output Files\Type56a.tmf
*$POSITION 758 594
*$LAYER Main # #
*$#
PARAMETERS 6
31              ! 1 Logical unit for building description file (.bui)
1               ! 2 Star network calculation switch
0.5             ! 3 Weighting factor for operative temperature
32              ! 4 Logical unit for monthly summary
33              ! 5 Logical unit for hourly temperatures
34              ! 6 Logical unit for hourly loads
INPUTS 28
331,7           ! Psychrometrics:Dry bulb temperature -> 1- TAMB
331,6           ! Psychrometrics:Percent relative humidity  -> 2- RELHUMAMB
69,1            ! Sky temp:Fictive sky temperature -> 3- TSKY
IT_N            ! Radiation:IT_N -> 4- IT_NORTH
IT_S            ! Radiation:IT_S -> 5- IT_SOUTH
IT_E            ! Radiation:IT_E -> 6- IT_EAST
IT_W            ! Radiation:IT_W -> 7- IT_WEST
IT_H            ! Radiation:IT_H -> 8- IT_HORIZONTAL
IT_S_SHD                ! Fixed Shading:IT_S_SHD -> 9- IT_SHADSOUTH
IB_N            ! Radiation:IB_N -> 10- IB_NORTH
IB_S            ! Radiation:IB_S -> 11- IB_SOUTH
IB_E            ! Radiation:IB_E -> 12- IB_EAST
IB_W            ! Radiation:IB_W -> 13- IB_WEST
IB_H            ! Radiation:IB_H -> 14- IB_HORIZONTAL
IB_S_SHD                ! Fixed Shading:IB_S_SHD -> 15- IB_SHADSOUTH
AI_N            ! Radiation:AI_N -> 16- AI_NORTH
AI_S            ! Radiation:AI_S -> 17- AI_SOUTH
AI_E            ! Radiation:AI_E -> 18- AI_EAST
AI_W            ! Radiation:AI_W -> 19- AI_WEST
AI_H            ! Radiation:AI_H -> 20- AI_HORIZONTAL
AI_S_SHD                ! Fixed Shading:AI_S_SHD -> 21- AI_SHADSOUTH
BRIGHT                  ! Shading+Light:BRIGHT -> 22- BRIGHT
```

```
0,0             ! [unconnected]  23- CNAT_1
0,0             ! [unconnected]  24- CNAT_2
0,0             ! [unconnected]  25- CNAT_3
0,0             ! [unconnected]  26- CNAT_4
0,0             ! [unconnected]  27- CNAT_5
0,0             ! [unconnected]  28- CNAT_6
*** INITIAL INPUT VALUES
0 0 0 0 0 0 0 0 0 0 0 0 0 0 0 0 0 0 0 0 0 0 0 0 0 0 0 0
*** External files
ASSIGN "BuildingProject19.bui" 31
*|? Building description file (*.bui) |1000
ASSIGN "T56_std-Output.sum" 32
*|? Monthly Summary File |1000
ASSIGN "T56_std-temp.prn" 33
*|? Hourly Temperatures |1000
ASSIGN "T56_std-q.prn" 34
*|? Hourly Loads |1000
*--------------------------------------------------------------------------------

* Model "Temperature" (Type 65)
*

UNIT 25 TYPE 65      Temperature
*$UNIT_NAME Temperature
*$MODEL .\Output\Online Plotter\Online Plotter Without File\Type65d.tmf
*$POSITION 1057 594
*$LAYER Main # #
PARAMETERS 12
6               ! 1 Nb. of left-axis variables
0               ! 2 Nb. of right-axis variables
0               ! 3 Left axis minimum
50              ! 4 Left axis maximum
0.0             ! 5 Right axis minimum
50              ! 6 Right axis maximum
1               ! 7 Number of plots per simulation
12              ! 8 X-axis gridpoints
0               ! 9 Shut off Online w/o removing
-1              ! 10 Logical unit for output file
0               ! 11 Output file units
0               ! 12 Output file delimiter
INPUTS 6
56,1            ! Building: 1- TAIR_A1 ->Left axis variable-1
56,2            ! Building: 2- TAIR_B1 ->Left axis variable-2
56,3            ! Building: 3- TAIR_C1 ->Left axis variable-3
56,4            ! Building: 4- TAIR_A2 ->Left axis variable-4
56,5            ! Building: 5- TAIR_A3 ->Left axis variable-5
56,6            ! Building: 6- TAIR_B3 ->Left axis variable-6
*** INITIAL INPUT VALUES
Rm_B25 Rm_B23 Rm_B21 Passage Rm_B24 Rm_B22
LABELS  3
```

```
"Temperature   [C]"
"Temperature  [C]"
"Temperatures"
*-------------------------------------------------------------------------------

* Model "Type65c" (Type 65)
*

UNIT 15 TYPE 65      Type65c
*$UNIT_NAME Type65c
*$MODEL .\Output\Online Plotter\Online Plotter With File\No Units\Type65c.tmf
*$POSITION 876 637
*$LAYER Main #
PARAMETERS 12
6               ! 1 Nb. of left-axis variables
0               ! 2 Nb. of right-axis variables
0               ! 3 Left axis minimum
15000           ! 4 Left axis maximum
0.0             ! 5 Right axis minimum
15000           ! 6 Right axis maximum
1               ! 7 Number of plots per simulation
12              ! 8 X-axis gridpoints
0               ! 9 Shut off Online w/o removing
35              ! 10 Logical Unit for output file
0               ! 11 Output file units
0               ! 12 Output file delimiter
INPUTS 6
56,19           ! Building: 19- QCOOL_A1 ->Left axis variable-1
56,20           ! Building: 20- QCOOL_B1 ->Left axis variable-2
56,21           ! Building: 21- QCOOL_C1 ->Left axis variable-3
56,22           ! Building: 22- QCOOL_A2 ->Left axis variable-4
56,23           ! Building: 23- QCOOL_A3 ->Left axis variable-5
56,24           ! Building: 24- QCOOL_B3 ->Left axis variable-6
*** INITIAL INPUT VALUES
B25 B23 B21 Passage B24 B22
LABELS  3
"Cooling Load (J)"
"Cooling load (J)"
"cooling load"
*** External files
ASSIGN "***.plt" 35
*|? What file should the online print to? |1000
*-------------------------------------------------------------------------------

* Model "Type65c-2" (Type 65)
*

UNIT 16 TYPE 65      Type65c-2
*$UNIT_NAME Type65c-2
*$MODEL .\Output\Online Plotter\Online Plotter With File\No Units\Type65c.tmf
```

```
*$POSITION 907 532
*$LAYER Main #
PARAMETERS 12
6               ! 1 Nb. of left-axis variables
0               ! 2 Nb. of right-axis variables
0               ! 3 Left axis minimum
100             ! 4 Left axis maximum
0.0             ! 5 Right axis minimum
100             ! 6 Right axis maximum
1               ! 7 Number of plots per simulation
12              ! 8 X-axis gridpoints
0               ! 9 Shut off Online w/o removing
36              ! 10 Logical Unit for output file
0               ! 11 Output file units
0               ! 12 Output file delimiter
INPUTS 6
56,27           ! Building: 27- RELHUM_A1 ->Left axis variable-1
56,28           ! Building: 28- RELHUM_B1 ->Left axis variable-2
56,29           ! Building: 29- RELHUM_C1 ->Left axis variable-3
56,30           ! Building: 30- RELHUM_A2 ->Left axis variable-4
56,31           ! Building: 31- RELHUM_A3 ->Left axis variable-5
56,32           ! Building: 32- RELHUM_B3 ->Left axis variable-6
*** INITIAL INPUT VALUES
B25 B23 B21 Passage B24 B22
LABELS  3
"Relative humidity (%)"
"Relative humidity (%)"
"RH"
*** External files
ASSIGN "***.plt" 36
*|? What file should the online print to? |1000
*-------------------------------------------------------------------------------

END
```

APPENDIX A2

TRNSYS INPUT FILE FOR SOLAR ABSORPTION COOLING SYSTEM MODEL AND SIMULATION

```
VERSION 16.1
**********************************************************************************
*** TRNSYS input file (deck) generated by TrnsysStudio
*** on Thursday, April 09, 2015 at 07:25
*** from TrnsysStudio project: D:\Documents and Settings\Talib\Desktop\entropy\new4\BuildingProject17.tpf
***
*** If you edit this file, use the File/Import TRNSYS Input File function in
*** TrnsysStudio to update the project.
***
*** If you have problems, questions or suggestions please contact your local
*** TRNSYS distributor or mailto:software@cstb.fr
***
**********************************************************************************


**********************************************************************************
*** Units
**********************************************************************************

**********************************************************************************
*** Control cards
**********************************************************************************
* START, STOP and STEP
CONSTANTS 3
START=0
STOP=8760
STEP=1
* User defined CONSTANTS

SIMULATION START STOP STEP ! Start time End time Time step
TOLERANCES 1 1 ! Integration Convergence
LIMITS 30 200 30 ! Max iterations Max warnings Trace limit
DFQ 1 ! TRNSYS numerical integration solver method
WIDTH 72 ! TRNSYS output file width, number of characters
LIST ! NOLIST statement
! MAP statement
SOLVER 0 1 1 ! Solver statement Minimum relaxation factor Maximum relaxation factor
NAN_CHECK 0 ! Nan DEBUG statement
OVERWRITE_CHECK 0 ! Overwrite DEBUG statement
TIME_REPORT 0 ! disable time report
EQSOLVER 0 ! EQUATION SOLVER statement

* EQUATIONS "Turn"
*
EQUATIONS 5
TURN = 12
AA_N = 180 + TURN
AA_S = TURN
```

```
AA_E = -90 + TURN
AA_W = 90 + TURN
*$UNIT_NAME Turn
*$LAYER Main
*$POSITION 49 61

*------------------------------------------------------------------------


* EQUATIONS "Radiation"
*
EQUATIONS 18
AISZ = [109,10]
AISA = [109,11]
IT_H = Max([109,12],0)
IB_H = Max([109,13],0)
ID_H = [109,14]
AI_H = [109,16]
IT_N = [109,18]
AI_N = [109,22]
IB_N = [109,19] * LT(AI_N,90)
IT_S = [109,24]
IB_S = [109,25]
AI_S = [109,28]
IT_E = [109,30]
IB_E = [109,31]
AI_E = [109,34]
IT_W = [109,36]
IB_W = [109,37]
AI_W = [109,40]
*$UNIT_NAME Radiation
*$LAYER Main
*$POSITION 195 125

*------------------------------------------------------------------------


* EQUATIONS "Shading+Light"
*
EQUATIONS 1
BRIGHT = [200,1]     !  27
*$UNIT_NAME Shading+Light
*$LAYER Controls
*$POSITION 669 605

*------------------------------------------------------------------------


* EQUATIONS "Fixed Shading"
*
```

```
EQUATIONS 6
IT_S_SHD = [342,1]
IB_S_SHD = [342,2]
AI_S_SHD = AI_S
IT_H_SHD = IT_H
IB_H_SHD = IB_H
AI_H_SHD = AI_H
*$UNIT_NAME Fixed Shading
*$LAYER Main
*$POSITION 653 402

*-------------------------------------------------------------------------


* Model "Weather data" (Type 109)
*

UNIT 109 TYPE 109   Weather data
*$UNIT_NAME Weather data
*$MODEL .\Weather Data Reading and Processing\Standard Format\TMY2\Type109-TMY2.tmf
*$POSITION 99 200
*$LAYER Main #
PARAMETERS 4
2               ! 1 Data Reader Mode
30              ! 2 Logical unit
4               ! 3 Sky model for diffuse radiation
1               ! 4 Tracking mode
INPUTS 11
0,0             ! [unconnected] Ground reflectance
0,0             ! [unconnected] Slope of surface-1
0,0             ! [unconnected] Azimuth of surface-1
0,0             ! [unconnected] Slope of surface-2
0,0             ! [unconnected] Azimuth of surface-2
0,0             ! [unconnected] Slope of surface-3
0,0             ! [unconnected] Azimuth of surface-3
0,0             ! [unconnected] Slope of surface-4
0,0             ! [unconnected] Azimuth of surface-4
0,0             ! [unconnected] Slope of surface-5
0,0             ! [unconnected] Azimuth of surface-5
*** INITIAL INPUT VALUES
0.2 90 AA_N 90 AA_S 90 AA_E 90 AA_W 12 0
*** External files
ASSIGN                                                                  "D:\Program
Files\Trnsys16\Weather\Zaria_Nigeria_SPtMasterTable_472122_19790101_20100101_tmy2.tm2
" 30
*|? Weather data file |1000
*-------------------------------------------------------------------------

* Model "Psychrometrics" (Type 33)
*
```

```
UNIT 331 TYPE 33     Psychrometrics
*$UNIT_NAME Psychrometrics
*$MODEL .\Physical Phenomena\Thermodynamic Properties\Psychrometrics\Dry Bulb and Relative Humidity Known\Type33e.tmf
*$POSITION 204 325
*$LAYER Main #
PARAMETERS 3
2               ! 1 Psychrometrics mode
1               ! 2 Wet bulb mode
1               ! 3 Error mode
INPUTS 3
109,1           ! Weather data:Ambient temperature ->Dry bulb temp.
109,2           ! Weather data:relative humidity ->Percent relative humidity
0,0             ! [unconnected] Pressure
*** INITIAL INPUT VALUES
20 50 1
*------------------------------------------------------------------------------

* Model "Sky temp" (Type 69)
*

UNIT 69 TYPE 69      Sky temp
*$UNIT_NAME Sky temp
*$MODEL .\Physical Phenomena\Sky Temperature\calculate cloudiness factor\Type69b.tmf
*$POSITION 354 273
*$LAYER Main # #
PARAMETERS 2
0               ! 1 mode for cloudiness factor
0               ! 2 height over sea level
INPUTS 4
331,7           ! Psychrometrics:Dry bulb temperature ->Ambient temperature
331,8           ! Psychrometrics:Dew point temperature. ->Dew point temperature at ambient conditions
109,13              ! Weather data:beam radiation on horitonzal ->Beam radiation on the horizontal
109,14              ! Weather data:sky diffuse radiation on horizontal ->Diffuse radiation on the horizontal
*** INITIAL INPUT VALUES
0 0 0 0
*------------------------------------------------------------------------------

* EQUATIONS "Light Thresholds"
*
EQUATIONS 2
Toth_L_on = -3.6*120
Eoth_L_off = -3.6*200
*$UNIT_NAME Light Thresholds
*$LAYER Controls
*$POSITION 461 530
```

```
*-------------------------------------------------------------------------


* Model "Lights" (Type 2)
*

UNIT 200 TYPE 2      Lights
*$UNIT_NAME Lights
*$MODEL .\Controllers\Differential Controller w_ Hysteresis\generic\Solver 0 (Successive Substitution) Control Strategy\Type2d.tmf
*$POSITION 566 541
*$LAYER Controls #
*$# NOTE: This controller can only be used with Solver 0 (Successive substitution)
*$#
*$#
*$#
*$#
*$#
*$#
*$#
*$#
*$#
PARAMETERS 2
5               ! 1 No. of oscillations
40000           ! 2 High limit cut-out
INPUTS 6
0,0             ! [unconnected] Upper input value
IT_H            ! Radiation:IT_H ->Lower input value
0,0             ! [unconnected] Monitoring value
200,1           ! Lights:Output control function ->Input control function
Toth_L_on               ! Light Thresholds:Toth_L_on ->Upper dead band
Eoth_L_off              ! Light Thresholds:Eoth_L_off ->Lower dead band
*** INITIAL INPUT VALUES
0 0 0 0 0 0
*-------------------------------------------------------------------------

* Model "WingWall S" (Type 34)
*

UNIT 342 TYPE 34    WingWall S
*$UNIT_NAME WingWall S
*$MODEL .\Loads and Structures\Overhang and Wingwall Shading\Type34.tmf
*$POSITION 606 264
*$LAYER Main # #
PARAMETERS 16
0               ! 1 Upstream component mode
2.0             ! 2 Receiver height
2.7             ! 3 Receiver width
1.0             ! 4 Overhang projection
```

```
0.6             ! 5 Overhang gap
0.3             ! 6 Overhang left extension
0.3             ! 7 Overhang right extension
0               ! 8 Left wingwall projection
0               ! 9 Left wingwall gap
0               ! 10 Left wingwall top extension
0               ! 11 Left wingwall bottom extension
0               ! 12 Right wingwall projection
0               ! 13 Right wingwall gap
0               ! 14 Right wingwall top extension
0               ! 15 Right wingwall bottom extension
AA_S            ! 16 Receiver azimuth
INPUTS 7
AISZ            ! Radiation:AISZ ->Solar zenith angle
AISA            ! Radiation:AISA ->Solar azimuth angle
IT_H            ! Radiation:IT_H ->Total horizontal radiation
ID_H            ! Radiation:ID_H ->Horizontal diffuse radiation
IB_S            ! Radiation:IB_S ->Beam radiation on surface
0,0             ! [unconnected] Ground reflectance
AI_S            ! Radiation:AI_S ->Incidence angle of direct radiation
*** INITIAL INPUT VALUES
30 20 0 0 0 0.2 0
*------------------------------------------------------------------------------

* Model "Temperature" (Type 65)
*

UNIT 25 TYPE 65      Temperature
*$UNIT_NAME Temperature
*$MODEL .\Output\Online Plotter\Online Plotter Without File\Type65d.tmf
*$POSITION 1062 594
*$LAYER Main # #
PARAMETERS 12
6               ! 1 Nb. of left-axis variables
0               ! 2 Nb. of right-axis variables
0               ! 3 Left axis minimum
60              ! 4 Left axis maximum
0.0             ! 5 Right axis minimum
60              ! 6 Right axis maximum
1               ! 7 Number of plots per simulation
12              ! 8 X-axis gridpoints
0               ! 9 Shut off Online w/o removing
-1              ! 10 Logical unit for output file
0               ! 11 Output file units
0               ! 12 Output file delimiter
INPUTS 6
47,1            ! Building: 1- TAIR_A1 ->Left axis variable-1
47,2            ! Building: 2- TAIR_B1 ->Left axis variable-2
47,3            ! Building: 3- TAIR_C1 ->Left axis variable-3
47,4            ! Building: 4- TAIR_A2 ->Left axis variable-4
```

```
47,5            ! Building: 5- TAIR_A3 ->Left axis variable-5
47,6            ! Building: 6- TAIR_B3 ->Left axis variable-6
*** INITIAL INPUT VALUES
Rm_B25 Rm_B23 Rm_B21 Passage Rm_B24 Rm_B22
LABELS  3
"Temperature  [C]"
"Temperature  [C]"
"Temperatures"
*------------------------------------------------------------------------------

* Model "Type1b" (Type 1)
*

UNIT 16 TYPE 1       Type1b
*$UNIT_NAME Type1b
*$MODEL .\Solar Thermal Collectors\Quadratic Efficiency Collector\2nd-Order Incidence Angle Modifiers\Type1b.tmf
*$POSITION 67 498
*$LAYER Main #
PARAMETERS 11
1               ! 1 Number in series
30              ! 2 Collector area
4.190           ! 3 Fluid specific heat
1               ! 4 Efficiency mode
40.0            ! 5 Tested flow rate
0.80            ! 6 Intercept efficiency
13.0            ! 7 Efficiency slope
0.05            ! 8 Efficiency curvature
2               ! 9 Optical mode 2
0.2             ! 10 1st-order IAM
0.0             ! 11 2nd-order IAM
INPUTS 9
19,1            ! Type3b:Outlet fluid temperature ->Inlet temperature
19,2            ! Type3b:Outlet flow rate ->Inlet flowrate
109,1           ! Weather data:Ambient temperature ->Ambient temperature
109,42              ! Weather data:total radiation on tilted surface-5 ->Incident radiation
109,12              ! Weather data:total radiation on horizontal ->Total horizontal radiation
109,14              ! Weather data:sky diffuse radiation on horizontal ->Horizontal diffuse radiation
0,0             ! [unconnected] Ground reflectance
109,46              ! Weather data:angle of incidence for tilted surface -5 ->Incidence angle
109,47              ! Weather data:slope of tilted surface-5 ->Collector slope
*** INITIAL INPUT VALUES
20.0 324.000013 29 0. 0.0 0.0 0.2 45.0 12
*------------------------------------------------------------------------------

* Model "Type13" (Type 13)
*

UNIT 17 TYPE 13      Type13
```

```
*$UNIT_NAME Type13
*$MODEL .\Hydronics\Pressure Relief Valve\Type13.tmf
*$POSITION 169 509
*$LAYER Water Loop #
PARAMETERS 2
100.0       ! 1 Boiling point of fluid
4.19        ! 2 Specific heat of fluid
INPUTS 3
16,1        ! Type1b:Outlet temperature ->Inlet fluid temperature
16,2        ! Type1b:Outlet flowrate ->Inlet flow rate
0,0         ! [unconnected] Comparison temperature
*** INITIAL INPUT VALUES
20.0 100.0 100
*------------------------------------------------------------------------------

* Model "Type4c" (Type 4)
*

UNIT 18 TYPE 4      Type4c
*$UNIT_NAME Type4c
*$MODEL .\Thermal Storage\Stratified Storage Tank\Variable Inlets\Uniform Losses\Type4c.tmf
*$POSITION 248 530
*$LAYER Water Loop #
PARAMETERS 25
2           ! 1 Variable inlet positions
0.1         ! 2 Tank volume
4.190       ! 3 Fluid specific heat
1000.0      ! 4 Fluid density
2.5         ! 5 Tank loss coefficient
1.2         ! 6 Height of node-1
1.0         ! 7 Height of node-2
0.8         ! 8 Height of node-3
0.6         ! 9 Height of node-4
0.4         ! 10 Height of node-5
0.2         ! 11 Height of node-6
1           ! 12 Auxiliary heater mode
1           ! 13 Node containing heating element -1
1           ! 14 Node containing thermostat -1
60.0        ! 15 Set point temperature for element-1
5.0         ! 16 Deadband for heating element-1
0           ! 17 Maximum heating rate of element -1
1           ! 18 Node containing heating element -2
1           ! 19 Node containing thermostat -2
60.0        ! 20 Set point temperature for element-2
5.0         ! 21 Deadband for heating element-2
0           ! 22 Maximum heating rate of element -2
0.0         ! 23 Not used (Flue UA)
20.0        ! 24 Not used (Tflue)
100.0       ! 25 Boiling point
INPUTS 7
```

```
17,1            ! Type13:Outlet temperature ->Hot-side temperature
17,2            ! Type13:Outlet flow rate ->Hot-side flowrate
30,1            ! Type3b-4:Outlet fluid temperature ->Cold-side temperature
30,2            ! Type3b-4:Outlet flow rate ->Cold-side flowrate
0,0             ! [unconnected] Environment temperature
0,0             ! [unconnected] Control signal for element-1
0,0             ! [unconnected] Control signal for element-2
*** INITIAL INPUT VALUES
0 0 25 0 0 0.0 0.0
DERIVATIVES 6
25              ! 1 Initial temperature of node-1
23              ! 2 Initial temperature of node-2
21              ! 3 Initial temperature of node-3
19              ! 4 Initial temperature of node-4
17              ! 5 Initial temperature of node-5
15              ! 6 Initial temperature of node-6
*-------------------------------------------------------------------------------

* Model "Type3b" (Type 3)
*

UNIT 19 TYPE 3       Type3b
*$UNIT_NAME Type3b
*$MODEL .\Hydronics\Pumps\Single Speed\Type3b.tmf
*$POSITION 191 616
*$LAYER Water Loop #
PARAMETERS 5
324.000013              ! 1 Maximum flow rate
4.190           ! 2 Fluid specific heat
60.0            ! 3 Maximum power
0.05            ! 4 Conversion coefficient
0.5             ! 5 Power coefficient
INPUTS 3
18,1            ! Type4c:Temperature to heat source ->Inlet fluid temperature
18,2            ! Type4c:Flowrate to heat source ->Inlet mass flow rate
37,1            ! Type2b-3:Output control function ->Control signal
*** INITIAL INPUT VALUES
20.0 100.0 1.0
*-------------------------------------------------------------------------------

* Model "Type6" (Type 6)
*

UNIT 20 TYPE 6       Type6
*$UNIT_NAME Type6
*$MODEL .\HVAC\Auxiliary Heaters\Type6.tmf
*$POSITION 328 509
*$LAYER Water Loop #
PARAMETERS 4
4200.000182             ! 1 Maximum heating rate
```

```
4.19            ! 2 Specific heat of fluid
0.0             ! 3 Overall loss coefficient for heater during operation
1.0             ! 4 Efficiency of auxiliary heater
INPUTS 5
18,3            ! Type4c:Temperature to load ->Inlet fluid temperature
18,4            ! Type4c:Flowrate to load ->Fluid mass flow rate
0,0             ! [unconnected] Control Function
0,0             ! [unconnected] Set point temperature
0,0             ! [unconnected] Temperature of surroundings
*** INITIAL INPUT VALUES
0 1220.399952 1 90 29
*------------------------------------------------------------------------------

* Model "Type2b" (Type 2)
*

UNIT 21 TYPE 2       Type2b
*$UNIT_NAME Type2b
*$MODEL .\Controllers\Differential Controller w_ Hysteresis\for Temperatures\Solver 0 (Successive Substitution) Control Strategy\Type2b.tmf
*$POSITION 322 413
*$LAYER Controls #
*$# NOTE: This control strategy can only be used with solver 0 (Successive substitution)
*$#
PARAMETERS 2
5               ! 1 No. of oscillations
95              ! 2 High limit cut-out
INPUTS 6
18,12           ! Type4c:Average tank temperature ->Upper input temperature Th
0,0             ! [unconnected] Lower input temperature Tl
0,0             ! [unconnected] Monitoring temperature Tin
21,1            ! Type2b:Output control function ->Input control function
0,0             ! [unconnected] Upper dead band dT
0,0             ! [unconnected] Lower dead band dT
*** INITIAL INPUT VALUES
85 80 90 0 0 0
*------------------------------------------------------------------------------

* Model "Type107" (Type 107)
*

UNIT 24 TYPE 107    Type107
*$UNIT_NAME Type107
*$MODEL .\HVAC\Absorption Chiller (Hot-Water Fired, Single Effect)\Type107.tmf
*$POSITION 400 626
*$LAYER Main #
PARAMETERS 11
53999.998569        ! 1 Rated capacity
0.71            ! 2 Rated C.O.P.
39              ! 3 Logical unit for S1 data file
```

```
5               ! 4 Number of HW temperatures in S1 data file
3               ! 5 Number of CW steps in S1 data file
7               ! 6 Number of CHW set points in S1 data file
11              ! 7 Number of load fractions in S1 data file
4.190           ! 8 HW fluid specific heat
4.190           ! 9 CHW fluid specific heat
4.190           ! 10 CW fluid specific heat
1080            ! 11 Auxiliary electrical power
INPUTS 8
34,1            ! Type3b-5:Outlet fluid temperature ->Chilled water inlet temperature
34,2            ! Type3b-5:Outlet flow rate ->Chilled water flow rate
27,1            ! Type3b-2:Outlet fluid temperature ->Cooling water inlet temperature
27,2            ! Type3b-2:Outlet flow rate ->Cooling water flow rate
20,1            ! Type6:Outlet fluid temperature ->Hot water inlet temperature
20,2            ! Type6:Outlet fluid flow rate ->Hot water flow rate
0,0             ! [unconnected] CHW set point
0,0             ! [unconnected] Chiller control signal
*** INITIAL INPUT VALUES
17 21959.999657 30.0 2037.599945 90 1220.399952 11 1.0
*** External files
ASSIGN          "D:\Program          Files\Trnsys16_1\Examples\Data          Files\Type107-
HotWaterFiredAbsorptionChiller.dat" 39
*|? File with fraction of design energy input data |1000
*-------------------------------------------------------------------------------

* Model "Type3b-2" (Type 3)
*

UNIT 27 TYPE 3       Type3b-2
*$UNIT_NAME Type3b-2
*$MODEL .\Hydronics\Pumps\Single Speed\Type3b.tmf
*$POSITION 266 733
*$LAYER Water Loop #
PARAMETERS 5
2037.599945          ! 1 Maximum flow rate
4.190           ! 2 Fluid specific heat
60.0            ! 3 Maximum power
0.05            ! 4 Conversion coefficient
0.5             ! 5 Power coefficient
INPUTS 3
29,1            ! Type51b:Sump temperature ->Inlet fluid temperature
29,2            ! Type51b:Sump flow rate ->Inlet mass flow rate
0,0             ! [unconnected] Control signal
*** INITIAL INPUT VALUES
30 3200 1
*-------------------------------------------------------------------------------

* Model "Type51b" (Type 51)
*
```

```
UNIT 29 TYPE 51      Type51b
*$UNIT_NAME Type51b
*$MODEL .\HVAC\Cooling Towers\User-Supplied Coefficients\Type51b.tmf
*$POSITION 354 733
*$LAYER Water Loop #
PARAMETERS 11
1               ! 1 Calculation mode
1               ! 2 Flow geometry
1               ! 3 Number of tower cells
4000            ! 4 Maximum cell flow rate
1.0             ! 5 Fan power at maximum flow
10.0            ! 6 Minimum cell flow rate
1.0             ! 7 Sump volume
22              ! 8 Initial sump temperature
1.705           ! 9 Mass transfer constant
-0.4183                 ! 10 Mass transfer exponent
1               ! 11 Print performance results?
INPUTS 6
24,3            ! Type107:Cooling water temperature ->Water inlet temperature
24,4            ! Type107:Cooling water flow rate ->Inlet water flow rate
331,7           ! Psychrometrics:Dry bulb temperature ->Dry bulb temperature
331,2           ! Psychrometrics:Wet bulb temperature ->Wet bulb temperature
0,0             ! [unconnected] Sump make-up temperature
0,0             ! [unconnected] Relative fan speed for cell
*** INITIAL INPUT VALUES
36 2037.599945 34 24 21 0.85
*------------------------------------------------------------------------------

* Model "Type3b-4" (Type 3)
*

UNIT 30 TYPE 3       Type3b-4
*$UNIT_NAME Type3b-4
*$MODEL .\Hydronics\Pumps\Single Speed\Type3b.tmf
*$POSITION 308 605
*$LAYER Main #
PARAMETERS 5
58000           ! 1 Maximum flow rate
4.190           ! 2 Fluid specific heat
60.0            ! 3 Maximum power
0.05            ! 4 Conversion coefficient
0.5             ! 5 Power coefficient
INPUTS 3
24,5            ! Type107:Hot water outlet temperature ->Inlet fluid temperature
24,6            ! Type107:Hot water flow rate ->Inlet mass flow rate
21,1            ! Type2b:Output control function ->Control signal
*** INITIAL INPUT VALUES
20 1220.399952 1
*------------------------------------------------------------------------------
```

```
* Model "Type3b-5" (Type 3)
*

UNIT 34 TYPE 3       Type3b-5
*$UNIT_NAME Type3b-5
*$MODEL .\Hydronics\Pumps\Single Speed\Type3b.tmf
*$POSITION 707 733
*$LAYER Water Loop #
PARAMETERS 5
10000          ! 1 Maximum flow rate
4.190          ! 2 Fluid specific heat
60.0           ! 3 Maximum power
0.05           ! 4 Conversion coefficient
0.5            ! 5 Power coefficient
INPUTS 3
Toutfinal              ! Equa:Toutfinal ->Inlet fluid temperature
mflowout               ! Equa:mflowout ->Inlet mass flow rate
0,0            ! [unconnected] Control signal
*** INITIAL INPUT VALUES
17 23200 1.0
*-------------------------------------------------------------------------------

* Model "Type31" (Type 31)
*

UNIT 36 TYPE 31      Type31
*$UNIT_NAME Type31
*$MODEL .\Hydronics\Pipe_Duct\Type31.tmf
*$POSITION 747 829
*$LAYER Water Loop #
PARAMETERS 6
0.2            ! 1 Inside diameter
5              ! 2 Pipe length
3.0            ! 3 Loss coefficient
1000.0         ! 4 Fluid density
4.190          ! 5 Fluid specific heat
10.0           ! 6 Initial fluid temperature
INPUTS 3
24,1           ! Type107:Chilled water temperature ->Inlet temperature
24,2           ! Type107:Chilled water flow rate ->Inlet flow rate
0,0            ! [unconnected] Environment temperature
*** INITIAL INPUT VALUES
11 10000 25
*-------------------------------------------------------------------------------

* Model "Type2b-3" (Type 2)
*

UNIT 37 TYPE 2       Type2b-3
*$UNIT_NAME Type2b-3
```

```
*$MODEL .\Controllers\Differential Controller w_ Hysteresis\for Temperatures\Solver 0 (Successive Substitution) Control Strategy\Type2b.tmf
*$POSITION 31 648
*$LAYER Controls #
*$# NOTE: This control strategy can only be used with solver 0 (Successive substitution)
*$#
PARAMETERS 2
5               ! 1 No. of oscillations
95              ! 2 High limit cut-out
INPUTS 6
16,1            ! Type1b:Outlet temperature ->Upper input temperature Th
18,3            ! Type4c:Temperature to load ->Lower input temperature Tl
18,1            ! Type4c:Temperature to heat source ->Monitoring temperature Tin
37,1            ! Type2b-3:Output control function ->Input control function
0,0             ! [unconnected] Upper dead band dT
0,0             ! [unconnected] Lower dead band dT
*** INITIAL INPUT VALUES
20.0 10.0 95 0 10.0 2.0
*-------------------------------------------------------------------------------

* Model "Type65c-4" (Type 65)
*

UNIT 41 TYPE 65      Type65c-4
*$UNIT_NAME Type65c-4
*$MODEL .\Output\Online Plotter\Online Plotter With File\No Units\Type65c.tmf
*$POSITION 612 658
*$LAYER Main #
PARAMETERS 12
9               ! 1 Nb. of left-axis variables
0               ! 2 Nb. of right-axis variables
0.0             ! 3 Left axis minimum
60              ! 4 Left axis maximum
0.0             ! 5 Right axis minimum
1000.0          ! 6 Right axis maximum
1               ! 7 Number of plots per simulation
12              ! 8 X-axis gridpoints
0               ! 9 Shut off Online w/o removing
43              ! 10 Logical Unit for output file
0               ! 11 Output file units
0               ! 12 Output file delimiter
INPUTS 9
0,0             ! [unconnected] Left axis variable-1
0,0             ! [unconnected] Left axis variable-2
0,0             ! [unconnected] Left axis variable-3
0,0             ! [unconnected] Left axis variable-4
0,0             ! [unconnected] Left axis variable-5
0,0             ! [unconnected] Left axis variable-6
0,0             ! [unconnected] Left axis variable-7
0,0             ! [unconnected] Left axis variable-8
```

```
0,0                ! [unconnected] Left axis variable-9
*** INITIAL INPUT VALUES
cc1 cc2 cc3 cc4 cc5 cc6 cc7 cc8 cc9
LABELS  3
"Temperatures cc"
"Heat transfer rates"
"Graph cct"
*** External files
ASSIGN "***.plt" 43
*|? What file should the online print to? |1000
*------------------------------------------------------------------------------

* EQUATIONS "Equa"
*
EQUATIONS 2
mflowout = 7870
Toutfinal                                                                                =
(([47,33]*1858)+([47,34]*1214)+([47,35]*1380)+([47,36]*460)+([47,37]*1450)+([47,38]*1500))
/10000
*$UNIT_NAME Equa
*$LAYER Main
*$POSITION 799 722

*------------------------------------------------------------------------------


* EQUATIONS "Equa-2"
*
EQUATIONS 6
m1 = [36,2]*0.1858
m2 = [36,2]*0.1214
m3 = [36,2]*0.138
m4 = [36,2]*0.046
m5 = [36,2]*0.251
m6 = [36,2]*0.258
*$UNIT_NAME Equa-2
*$LAYER Main
*$POSITION 895 808

*------------------------------------------------------------------------------


* Model "Type24" (Type 24)
*

UNIT 42 TYPE 24      Type24
*$UNIT_NAME Type24
*$MODEL .\Utility\Integrators\Quantity Integrator\Type24.tmf
*$POSITION 97 389
*$LAYER Main #
```

```
PARAMETERS 2
24              ! 1 Integration period
0               ! 2 Relative or absolute start time
INPUTS 2
16,3            ! Type1b:Useful energy gain ->Input to be integrated-1
20,5            ! Type6:Rate of energy delivery to fluid stream ->Input to be integrated-2
*** INITIAL INPUT VALUES
0.0 0.0
*-------------------------------------------------------------------------------

* Model "Type25a" (Type 25)
*

UNIT 43 TYPE 25      Type25a
*$UNIT_NAME Type25a
*$MODEL .\Output\Printer\Unformatted\TRNSYS-Supplied Units\Type25a.tmf
*$POSITION 868 360
*$LAYER Outputs #
PARAMETERS 10
STEP            ! 1 Printing interval
START                   ! 2 Start time
STOP            ! 3 Stop time
46              ! 4 Logical unit
2               ! 5 Units printing mode
0               ! 6 Relative or absolute start time
-1              ! 7 Overwrite or Append
-1              ! 8 Print header
0               ! 9 Delimiter
1               ! 10 Print labels
INPUTS 25
0,0             ! [unconnected] Input to be printed-1
0,0             ! [unconnected] Input to be printed-2
0,0             ! [unconnected] Input to be printed-3
0,0             ! [unconnected] Input to be printed-4
0,0             ! [unconnected] Input to be printed-5
0,0             ! [unconnected] Input to be printed-6
0,0             ! [unconnected] Input to be printed-7
0,0             ! [unconnected] Input to be printed-8
0,0             ! [unconnected] Input to be printed-9
0,0             ! [unconnected] Input to be printed-10
Toutfinal               ! Equa:Toutfinal ->Input to be printed-11
16,1            ! Type1b:Outlet temperature ->Input to be printed-12
16,3            ! Type1b:Useful energy gain ->Input to be printed-13
18,3            ! Type4c:Temperature to load ->Input to be printed-14
18,1            ! Type4c:Temperature to heat source ->Input to be printed-15
30,1            ! Type3b-4:Outlet fluid temperature ->Input to be printed-16
20,1            ! Type6:Outlet fluid temperature ->Input to be printed-17
20,5            ! Type6:Rate of energy delivery to fluid stream ->Input to be printed-18
24,1            ! Type107:Chilled water temperature ->Input to be printed-19
109,1           ! Weather data:Ambient temperature ->Input to be printed-20
```

```
18,6            ! Type4c:Energy rate to load ->Input to be printed-21
18,11           ! Type4c:Energy rate from heat source ->Input to be printed-22
42,1            ! Type24:Result of integration-1 ->Input to be printed-23
42,2            ! Type24:Result of integration-2 ->Input to be printed-24
24,13           ! Type107:C.O.P ->Input to be printed-25
*** INITIAL INPUT VALUES
QCOOL_ZONE_A1 QCOOL_ZONE_B1 QCOOL_ZONE_C1 QCOOL_ZONE_A2 QCOOL_ZONE_B2
QCOOL_ZONE_C2 QCOOL_ZONE_A3 QCOOL_ZONE_B3 QCOOL_ZONE_C3 SQCool Toutfinal
Outlet Useful Temperature Temperature temperature Outlet Rate Chilled
Ambient Energy Energy Result Result C.O.P
*** External files
ASSIGN "Type25a.txt" 46
*|? Output File for printed results |1000
*-------------------------------------------------------------------------------

* EQUATIONS "Equa-3"
*
EQUATIONS 1
SF = ( ([42,1]+1e-6)/([42,2]+([42,1]+1e-6) ) )
*$UNIT_NAME Equa-3
*$LAYER Main
*$POSITION 21 424

*-------------------------------------------------------------------------------


* Model "Type25a-2" (Type 25)
*

UNIT 39 TYPE 25      Type25a-2
*$UNIT_NAME Type25a-2
*$MODEL .\Output\Printer\Unformatted\TRNSYS-Supplied Units\Type25a.tmf
*$POSITION 16 253
*$LAYER Outputs #
PARAMETERS 10
STEP            ! 1 Printing interval
START                   ! 2 Start time
STOP            ! 3 Stop time
48              ! 4 Logical unit
2               ! 5 Units printing mode
0               ! 6 Relative or absolute start time
-1              ! 7 Overwrite or Append
-1              ! 8 Print header
0               ! 9 Delimiter
1               ! 10 Print labels
INPUTS 1
0,0             ! [unconnected] Input to be printed
*** INITIAL INPUT VALUES
```

```
SF
*** External files
ASSIGN "Type25a.txt" 48
*|? Output File for printed results |1000
*-------------------------------------------------------------------------------

* Model "Type65c-3" (Type 65)
*

UNIT 40 TYPE 65      Type65c-3
*$UNIT_NAME Type65c-3
*$MODEL .\Output\Online Plotter\Online Plotter With File\No Units\Type65c.tmf
*$POSITION 16 157
*$LAYER Main #
PARAMETERS 12
1               ! 1 Nb. of left-axis variables
1               ! 2 Nb. of right-axis variables
0.0             ! 3 Left axis minimum
100             ! 4 Left axis maximum
0.0             ! 5 Right axis minimum
2               ! 6 Right axis maximum
1               ! 7 Number of plots per simulation
12              ! 8 X-axis gridpoints
0               ! 9 Shut off Online w/o removing
49              ! 10 Logical Unit for output file
0               ! 11 Output file units
0               ! 12 Output file delimiter
INPUTS 2
109,2           ! Weather data:relative humidity ->Left axis variable
SF              ! Equa-3:SF ->Right axis variable
*** INITIAL INPUT VALUES
RH SF
LABELS  3
"Relative Humidity (%)"
"Solar Fraction"
"sf"
*** External files
ASSIGN "***.plt" 49
*|? What file should the online print to? |1000
*-------------------------------------------------------------------------------

* Model "Type65c-5" (Type 65)
*

UNIT 44 TYPE 65      Type65c-5
*$UNIT_NAME Type65c-5
*$MODEL .\Output\Online Plotter\Online Plotter With File\No Units\Type65c.tmf
*$POSITION 234 829
*$LAYER Main #
PARAMETERS 12
```

```
2               ! 1 Nb. of left-axis variables
1               ! 2 Nb. of right-axis variables
0.0             ! 3 Left axis minimum
1.2             ! 4 Left axis maximum
0.0             ! 5 Right axis minimum
70000           ! 6 Right axis maximum
1               ! 7 Number of plots per simulation
12              ! 8 X-axis gridpoints
0               ! 9 Shut off Online w/o removing
50              ! 10 Logical Unit for output file
0               ! 11 Output file units
0               ! 12 Output file delimiter
INPUTS 3
24,13           ! Type107:C.O.P ->Left axis variable-1
scop            ! Equa-4:scop ->Left axis variable-2
24,7            ! Type107:Chilled water energy ->Right axis variable
*** INITIAL INPUT VALUES
cop scop coolingenergy
LABELS  3
"cop/scop"
"coolingenrgy"
"ce/scop"
*** External files
ASSIGN "***.plt" 50
*|? What file should the online print to? |1000
*-------------------------------------------------------------------------------

* EQUATIONS "Equa-4"
*
EQUATIONS 1
scop = ([24,7]+1e-6)/(([109,42]+1e-6)+([109,12]+1e-6)+([109,14]+1e-6))
*$UNIT_NAME Equa-4
*$LAYER Main
*$POSITION 95 744

*-------------------------------------------------------------------------------


* Model "Building" (Type 56)
*

UNIT 47 TYPE 56      Building
*$UNIT_NAME Building
*$MODEL .\Loads and Structures\Multi-Zone Building\With Standard Output Files\Type56a.tmf
*$POSITION 784 605
*$LAYER Main #
*$#
PARAMETERS 6
51              ! 1 Logical unit for building description file (.bui)
1               ! 2 Star network calculation switch
```

```
0.5             ! 3 Weighting factor for operative temperature
52              ! 4 Logical unit for monthly summary
53              ! 5 Logical unit for hourly temperatures
54              ! 6 Logical unit for hourly loads
INPUTS 46
331,7           ! Psychrometrics:Dry bulb temperature -> 1- TAMB
109,2           ! Weather data:relative humidity -> 2- RELHUMAMB
69,1            ! Sky temp:Fictive sky temperature -> 3- TSKY
IT_N            ! Radiation:IT_N -> 4- IT_NORTH
IT_S            ! Radiation:IT_S -> 5- IT_SOUTH
IT_E            ! Radiation:IT_E -> 6- IT_EAST
IT_W            ! Radiation:IT_W -> 7- IT_WEST
IT_H            ! Radiation:IT_H -> 8- IT_HORIZONTAL
IT_S_SHD            ! Fixed Shading:IT_S_SHD -> 9- IT_SHADSOUTH
IB_N            ! Radiation:IB_N -> 10- IB_NORTH
IB_S            ! Radiation:IB_S -> 11- IB_SOUTH
IB_E            ! Radiation:IB_E -> 12- IB_EAST
IB_W            ! Radiation:IB_W -> 13- IB_WEST
IB_H            ! Radiation:IB_H -> 14- IB_HORIZONTAL
IB_S_SHD            ! Fixed Shading:IB_S_SHD -> 15- IB_SHADSOUTH
AI_N            ! Radiation:AI_N -> 16- AI_NORTH
AI_S            ! Radiation:AI_S -> 17- AI_SOUTH
AI_E            ! Radiation:AI_E -> 18- AI_EAST
AI_W            ! Radiation:AI_W -> 19- AI_WEST
AI_H            ! Radiation:AI_H -> 20- AI_HORIZONTAL
AI_S_SHD            ! Fixed Shading:AI_S_SHD -> 21- AI_SHADSOUTH
0,0             ! [unconnected]  22- CNAT_2
0,0             ! [unconnected]  23- CNAT_3
0,0             ! [unconnected]  24- CNAT_4
0,0             ! [unconnected]  25- CNAT_5
0,0             ! [unconnected]  26- CNAT_6
0,0             ! [unconnected]  27- T_COOL_ON
0,0             ! [unconnected]  28- S_NORTH
0,0             ! [unconnected]  29- S_SOUTH
0,0             ! [unconnected]  30- S_EAST
0,0             ! [unconnected]  31- S_WEST
0,0             ! [unconnected]  32- 5800
0,0             ! [unconnected]  33- CNAT1
BRIGHT              ! Shading+Light:BRIGHT -> 34- BRIGHT
36,1            ! Type31:Outlet temperature -> 35- TIN1
m1              ! Equa-2:m1 -> 36- MFIN1
36,1            ! Type31:Outlet temperature -> 37- TIN2
m2              ! Equa-2:m2 -> 38- MFIN2
36,1            ! Type31:Outlet temperature -> 39- TIN3
m3              ! Equa-2:m3 -> 40- MFIN3
36,1            ! Type31:Outlet temperature -> 41- TIN4
m4              ! Equa-2:m4 -> 42- MFIN4
36,1            ! Type31:Outlet temperature -> 43- TIN5
m5              ! Equa-2:m5 -> 44- MFIN5
36,1            ! Type31:Outlet temperature -> 45- TIN6
```

```
m6               ! Equa-2:m6 -> 46- MFIN6
*** INITIAL INPUT VALUES
0 0 0 0 0 0 0 0 0 0 0 0 0 0 0 0 0 0 0 0 0 0 0 0 0 0 0 0 0 0 0 0 0 0 0 0 0 0 0 0 0 0 0 0 0 0
*** External files
ASSIGN "BuildingProject19.bui" 51
*|? Building description file (*.bui) |1000
ASSIGN "T56_std-Output.sum" 52
*|? Monthly Summary File |1000
ASSIGN "T56_std-temp.prn" 53
*|? Hourly Temperatures |1000
ASSIGN "T56_std-q.prn" 54
*|? Hourly Loads |1000
*------------------------------------------------------------------------------

* Model "Type65c-2" (Type 65)
*

UNIT 48 TYPE 65      Type65c-2
*$UNIT_NAME Type65c-2
*$MODEL .\Output\Online Plotter\Online Plotter With File\No Units\Type65c.tmf
*$POSITION 1045 701
*$LAYER Main #
PARAMETERS 12
6                ! 1 Nb. of left-axis variables
0                ! 2 Nb. of right-axis variables
0                ! 3 Left axis minimum
100              ! 4 Left axis maximum
0.0              ! 5 Right axis minimum
100              ! 6 Right axis maximum
1                ! 7 Number of plots per simulation
12               ! 8 X-axis gridpoints
0                ! 9 Shut off Online w/o removing
55               ! 10 Logical Unit for output file
0                ! 11 Output file units
0                ! 12 Output file delimiter
INPUTS 6
47,39            ! Building: 39- RELHUM_A1 ->Left axis variable-1
47,40            ! Building: 40- RELHUM_B1 ->Left axis variable-2
47,41            ! Building: 41- RELHUM_C1 ->Left axis variable-3
47,42            ! Building: 42- RELHUM_A2 ->Left axis variable-4
47,43            ! Building: 43- RELHUM_A3 ->Left axis variable-5
47,44            ! Building: 44- RELHUM_B3 ->Left axis variable-6
*** INITIAL INPUT VALUES
Rm_B25 Rm_B23 Rm_B21 Passage Rm_B24 Rm_B22
LABELS  3
"Relative Humidity (%)"
"Relative Humidity (%)"
"RH"
*** External files
ASSIGN "***.plt" 55
```

*|? What file should the online print to? |1000
*----------

END

APPENDIX B
MATLAB PROGRAM FOR FLAT PLATE SOLAR COLLECTOR DESIGN

% APPENDIX B

```
% PROGRAM FOR FLAT PLATE SOLAR COLLECTOR DESIGN
% Input constants
Cc=12000; %chiller capacity (W)
L=1.5; % desired length of single collector module (m)
W=1; % desired width of single collector module (m)
H=0.075; %collector thickness (m)
del=0.003; %plate thickness (m)
di=0.010; %inner dia of tube (m)
do=0.015; %outer dia of tube (m)
Eff=0.7; %collector efficiency
COPc=0.7; %chiller cop
tw=0.87; %transmittance
al=0.9; %absorptance
G=985; %solar radiation (w/m2)
Ta=302; %ambient temperature (K)
Ti=343; %temp. of fluid at inlet (K)
v= 1.13; %wind velocity (m/s)
Tpm=373; %mean plate temperature (K)
B=12; %collector tilt angle (deg)
Ep=0.95; %emmisivity of plate
Eg=0.88; %emmisivity of glass
Ng=1; %number of glass covers
sig=0.0000000567; %sigma
kb=0.6; %bond thermal conductivity
b=0.005; %bond thickness (m)
y=0.015; %bond width (m)
ki=0.045 ; %insulation thermalconductivity (w/mK)
kp=16; %plate thermal conductivity
li=0.05; %back insulation thickness (m)
xe=0.025; %edge insulation thickness (m)
df=991.1; %fluid density
yf=0.00065; %dynamic viscosity of fluid
kf=0.634; %thermal conductivity of fluid
Cp=4187; %specific heat capacity of fluid
mf=0.4841; %mass flow rate of fluid to collector array (Kg/sec)

% Calculate
Ac=1.1.*(Cc./(G.*Eff.*COPc)); % total area of collector array
Acm=L.*W; % area of collector module
Ncm=Ac./(L.*W); % number of collector modules
mfcm=mf./Ncm; % mass flow rate through each collector module (Kg/sec)
hw=5.7+(3.8.*v); %wind heat transfer coefficient
e=0.43.*(1-(100./Tpm));
c=520.*(1-(0.000051.*B^2));
f=(1+(0.089.*hw)-(0.1166.*hw.*Ep)).*(1+(0.07866.*Ng));
Ut=((Ng./((c./Tpm).*((Tpm-Ta)./(Ng+f))^e))+(1./hw))^(-
1)+((sig.*(Tpm+Ta).*(Tpm^2+Ta^2))./((1./(Ep+(0.00591.*Ng.*hw)))+(((2.*Ng)+f-
1+(0.133.*Ep))./Eg)-Ng));%top loss coefficient
Ub=ki./li; %bottom loss coefficient
Ue=(ki./xe).*((2.*(L+W).*H)./(L.*W)); %edge loss coefficient
```

```
UL=Ut+Ub+Ue; %total loss coefficient for single module
cb=(kb.*b)./y;
m=(UL./(kp.*del))^0.5;
Ts=((1.448./m)+do); %tube spacing
Nt=L./Ts; %number of tubes per collector module
Ax=(3.14.*di.^2)./4; %flow xsectional area for tube
Gt=mfcm./(Nt.*Ax); %mass flux in tubes per collector module
vt=Gt./df; %tube side velocity
Ret=(df.*vt.*di)./yf;%Reynolds number of flow in tube
fc=((1.82.*(log(Ret)./log(10)))-1.64).^(-2);%friction factor
Pr=(yf.*Cp)./kf; %Prandtl number
hfi=(kf./di).*(1.86.*Ret^0.33.*Pr^0.33.*(di./W)^0.33); %Heat Transfer Coefficient
F=tanh((m.*(Ts-do))./2)./((m.*(Ts-do))./2);
Fi=(1./UL)./(Ts.*((1./(UL.*(do+((Ts-do).*F)))+(1./(3.14.*di.*hfi)))));
FR=((mf.*Cp)./(Ac.*UL)).*(1-exp((-Ac.*UL.*Fi)./(mf.*Cp)));
Qu=Ncm.*Acm.*FR.*(G.*(tw.*al)-(UL.*(Ti-Ta))); %useful energy gain

disp('Qu:');
disp(Qu);
disp('mfcm:');
disp(mfcm);
disp('Acm');
disp(Acm);
disp('Ut:');
disp(Ut);
disp('Ub:');
disp(Ub);
disp('Ue:');
disp(Ue);
disp('UL:');
disp(UL);
disp('Ncm:');
disp(Ncm);
disp('Ts:');
disp(Ts);
disp('Nt:');
disp(Nt);
disp('Ac:');
disp(Ac);
```

APPENDIX C
MATLAB PROGRAM FOR GENERATOR DESIGN

```
% APPENDIX C
% PROGRAM FOR GENERATOR DESIGN
clc
```

```
clear all
%Input Design operating Parameters
%Generator
Tgh1=90; %Inlet hot water to generator
Tgh2=80; %Outlet hot water from generator
Tgs1=74; %Inlet solution tenp. to generator
Tgs2=81; %Outlet solution temperature from generator
%Absorber
Tacw1=32; %Inlet cooling water temp. to absorber
Tacw2=37; %outlet cooling water temp. from absorber
Tas1=55; %Inlet solution temp. to absorber
Tas2=40; %Outlet solution temp. from absorber
%Condenser
Tccw1=29; % Inlet cooling water temp. to condenser
Tccw2=32; %Outlet cooling water temp. from condenser
Tcrv1=90; %Refrigerant vapour inlet temp. to condenser
Tcr2=40; %refrigerant outlet temp. from condenser
%Evaporator
Qe=12000.0; %refrigerating capacity (W)
Techw1=15; %chilled water temp. into evaporator
Techw2=10; %chilled water temp. outfrom evaporator
Ter1=6; %Refrigerant inlet temp. to evaporator
Ter2=8; %Refrigerant outlet temp. from evaporator
COP=0.7; %Design coefficient of performance
%Pressure (Pa)
Ph=7340;
Pl=1200;
%Concentration
Xss=0.63; %strong solution concentration
Xws=0.55; %weak solution concentration
Xsw=(1-Xss); %strong solution concentration of water
Xww=(1-Xws); %weak solution concentration of water
f=(1-Xsw)./(Xww-Xsw); %specific circulation ratio
% Constants
g=9.81; % acceleration due to gravity
dv=0.0519; % density of vapour
y=0.000299; % dynamic viscosity
hfg=2406280; % enthalpy of evaporation
F1=0.00009; % fouling factor inside tube (m2oC/W)
F2=0.00009; % fouling factor outside tube (m2oC/W)
CTP=0.93; % clearance constant between shell and tube
CL=1.0; % tube layout constant
sig=0.058; % const
Csf=0.0128;
Tw=90; %wall temp
Tsat=40; %sat. temp
%Input Design Geometric Parameters
Lt=0.5; %tube length
d1=0.00925; %inner diameter of tubes
d2=0.01225; %outer diameter of tubes
```

```
Np=1;%umber of pass
Kt=383.2; %thermal conductivity of tubes (W/moC)
%Calculate flow crssectional area for a single tube(m2)
Ax=(3.14.*d1.^2)./4;
%Calculate surface area for a single tube
As=3.14.*d2.*Lt;
%Input Constants
%Density (Kg/m3)
dgw=972; %generator hot water side
daw=991.1; %absorber water side
dcr=963.97; %condenser refrigerant side
dcw=991.1; %condenser water side
dcv=0.0022.*Ph./Tgh1; %condenser vapour side
dech=999.0; %evaporator chilled water side
der=1000.0; %evaporator refrigerant side
dgs=1145.36+(470.48.*Xss)+(1374.79.*Xss^2)-(0.333393+(0.571749.*Xss)).*(273+Tgs2);
%gen. soln. side
das=1145.36+(470.48.*Xws)+(1374.79.*Xws^2)-(0.333393+(0.571749.*Xws)).*(273+Tas2);
%abs. soln. side
%Thermal conductivity (w/mk)
Kgw=0.677; %gen. hot water side
Kaw=0.634; %absorber water side
Kcw=0.634; %condenser water side
Kcr=0.677; %condenser refrigerant side
Kech=0.598; %evaporator chilled water side
Ker=0.582; %evaporator refrigerant side
Kgs=0.45; %gen. solution side
Kas=0.42; %absorber solution side;
%Specific heat capacity (J/KgK)
Cpgs=(1.01-(1.23.*Xss)+0.48).*4186; %gen. solution side
Cpas=(1.01-(1.23.*Xws)+0.48).*4186; %absorber solution side
Cpg=4187;
Cpa=4187;
Cpc=4187;
Cpe=4187;
%Latent heat
jg=2270; %aqueous LiBr solution
je=2270; %water
%Dynamic viscosity (Kg/m.s)
ygw=0.000355;
yaw=0.0008;
ycw=0.00065;
ycr=0.0008;
yech=0.00114;
yer=0.0015;
ygs=0.0031;
yas=0.0032;

%Calculate required loads (W)
Qg=Qe./COP; %generator heat load
```

```
%condenser cooling load (Qc)
hei=4.186.*Tcr2; %evaporator inlet enthalpy from condenser
heo=2501+(1.88.*Techw2); %enthalpy of chilled water exit from evaporator
qo=heo-hei; %refrigerating effect
D=(Qe.*60)/(qo.*1000); %water vapour distilled per ton of refrigeration
hci=2501+(1.88.*Tgh1); %enthalpy of refrigerant at inlet to condenser
hco=hei; %enthalpy of refrigerant at exit from condenser
Qc=((D./60).*(hci-hco)).*1000;
%Calculate absorber cooling load (Qa)
Qa=Qe+Qg-Qc;
%calculate flow rates (Kg/s)
hwv=2501.48+(1.78.*Ter2); %enthalpy of water vapour from evaporator
hw=4.2.*Tcr2; %enthalpy of water from condenser
hw2=4.2.*Ter1; %enthalpy of water from condenser after throttling
mref=Qe./(1000.*(hwv-hw)); %mass flow rate of refrigerant
mws=mref.*(Xss./(Xss-Xws)); %mass flow rate of weak solution
mss=mws-mref; %mass flow rate of strong solution
mgh=Qg./(Cpg.*(Tgh1-Tgh2)); %mass flow rate of hot water at generator
mgs=Qg./(Cpgs.*(Tgs2-Tgs1)); %mass flow rate of solution at generator
mac=Qa./(Cpa.*(Tacw2-Tacw1)); %mass flow rate of cooling water at absorber
mas=mgs; %mass flow rate of solution at absorber
mcc=Qc./(Cpc.*(Tccw2-Tccw1)); %mass flowrate of cooling water at condenser
mcr=Qc./(Cpc.*(Tcrv1-Tcr2)); %mass flow rate of refrigerant vapour at condenser
mech=Qe./(Cpe.*(Techw1-Techw2)); %mass flow rate of chilled water at evaporator
mer=Qe./(Cpe.*(Ter2-Ter1)); %mass flow rate of refrigerant at evaporator
%Calculate Logarithmic Mean Temperature Difference (LMTD)
%Generator
LMTDg=(((Tgh1-Tgs2)-(Tgh2-Tgs1))./log((Tgh1-Tgs2)./(Tgh2-Tgs1)));
%Calculate LMTD correction factor
Fg=0.93;
%Calculate corrected LMTD
LMTDgc=LMTDg.*Fg;
%Calculate provisional heat transfer area
%Assume overall heat transfer coefficient
Ug(1)=1300;
j=1;
for j = 1:25;

ApT=Qg./(Ug(j).*LMTDgc);
%Calculate number of tubes
Nt=ApT./As;
%Calculate tube pitch
pt=1.25.*d2;
%Calculate shell diameter
Ds=0.637.*((CL./CTP).^0.5).*(3.14.*((pt./d2).^2).*d2.^2.*Nt).^0.5;
%Calculate tube bundle cross flow area
Acf=((pt-d2).*Ds.*Lt)./pt;
%calculate shell side mass velocity
Gs=mgs./Acf;
%Calculate shell equivalent diameter
```

```
Dse=(1.27./d2).*(pt.^2-(0.785.*d2.^2));
% Calculate shell side Reynolds number
Res=Gs.*Dse./ygs;
% Calculate shell side Prandtl number
Pr=ygs.*Cpgs./Kgs;
% Calculate number of tubes per pass
Ntpp=Nt./Np;
%Calculate tube side mass velocity
Gt=mgh./(Ntpp.*Ax);
%Calculate tube side velocity
vt=Gt./dech;
%Calculate tube side reynolds number
Ret=(Gt.*d1)./ygw;
%Calculate friction factor
fc=((1.82.*(log(Ret)./log(10)))-1.64).^(-2);
%Calculate Heat Transfer Coefficients
hgw=0.023.*(Ret^0.8).*(Pr^0.3).*(Kgw./d1); % @ tube side
hgs=ygs.*hfg.*((g.*(dgs-dv))./sig)^0.5.*((Cpgs.*(Tw-Tsat))./(Csf.*hfg.*Pr))^3; %nucleate boiling
heat transfer coefficient
%Calculate Overall Heat Transfer Coefficient
%Generator
j=j+1;
Ug(j)=1./((d1./(d2.*hgs))+((d1./(2.*Kt)).*log(d2./d1))+(1./hgw));
Ncross5Matrix(j,1)=j;
Ncross5Matrix(j,2)=Ug(j)
Ncross5Matrix(j,3)=Nt
Ncross5Matrix(j,4)=ApT
Ncross5Matrix(j,5)=Ds


end
It=Ncross5Matrix(:,1:5);

VLiBr = 0.8*3.142*((It(:,5).^2)/4)*Lt;
ff=0.02;
d1p=0.005;
Ax2=(3.14.*d1p.^2)./4;
DelP=Ph-Pl;
Vf=mws./das; %volume flow rate
Vav=Vf./Ax2; % average velocity
Lg=(2.*DelP.*d1p)./(ff.*das.*(Vav)^2); % Length of strong solution pipe
```

APPENDIX D
MATLAB PROGRAM FOR CONDENSER DESIGN

```
% APPENDIX D
% PROGRAM FOR CONDENSER DESIGN
clc
```

```
clear all
%Input Design operating Parameters
%Generator
Tgh1=90; %Inlet hot water to generator
Tgh2=80; %Outlet hot water from generator
Tgs1=74; %Inlet solution tenp. to generator
Tgs2=81; %Outlet solution temperature from generator
%Absorber
Tacw1=32; %Inlet cooling water temp. to absorber
Tacw2=37; %outlet cooling water temp. from absorber
Tas1=55; %Inlet solution temp. to absorber
Tas2=40; %Outlet solution temp. from absorber
%Condenser
Tccw1=29; % Inlet cooling water temp. to condenser
Tccw2=32; %Outlet cooling water temp. from condenser
Tcrv1=90; %Refrigerant vapour inlet temp. to condenser
Tcr2=40; %refrigerant outlet temp. from condenser
%Evaporator
Qe=12000.0; %refrigerating capacity (W)
Techw1=15; %chilled water temp. into evaporator
Techw2=10; %chilled water temp. outfrom evaporator
Ter1=6; %Refrigerant inlet temp. to evaporator
Ter2=8; %Refrigerant outlet temp. from evaporator
COP=0.7; %Design coefficient of performance
%Pressure (Pa)
Ph=7340;
Pl=1200;
%Concentration
Xss=0.63; %strong solution concentration
Xws=0.55; %weak solution concentration
Xsw=(1-Xss); %strong solution concentration of water
Xww=(1-Xws); %weak solution concentration of water
f=(1-Xsw)./(Xww-Xsw); %specific circulation ratio
% Constants
g=9.81; % acceleration due to gravity
dv=0.03285; % density of vapour
y=0.000299; % dynamic viscosity
hfg=2431200; % enthalpy of evaporation
F1=0.00009; % fouling factor inside tube (m2oC/W)
F2=0.00009; % fouling factor outside tube (m2oC/W)
CTP=0.93; % clearance constant between shell and tube
CL=1.0; % tube layout constant
%Input Design Geometric Parameters
Lt=0.5; %tube length
d1=0.00825; %inner diameter of tubes
d2=0.0135; %outer diameter of tubes
Np=1;%number of pass
Kt=383.2; %thermal conductivity of tubes (W/moC)
%Calculate flow crssectional area for a single tube(m2)
Ax=(3.14.*d1.^2)./4;
```

```
%Calculate surface area for a single tube
As=3.14.*d2.*Lt;
%Input Constants
%Density (Kg/m3)
dgw=972; %generator hot water side
daw=991.1; %absorber water side
dcr=963.97; %condenser refrigerant side
dcw=991.1; %condenser water side
dcv=0.0022.*Ph./Tgh1; %condenser vapour side
dech=999.0; %evaporator chilled water side
der=1000.0; %evaporator refrigerant side
dgs=1145.36+(470.48.*Xss)+(1374.79.*Xss^2)-(0.333393+(0.571749.*Xss)).*(273+Tgs2);
%gen. soln. side
das=1145.36+(470.48.*Xws)+(1374.79.*Xws^2)-(0.333393+(0.571749.*Xws)).*(273+Tas2);
%abs. soln. side
%Thermal conductivity (w/mk)
Kgw=0.677; %gen. hot water side
Kaw=0.634; %absorber water side
Kcw=0.634; %condenser water side
Kcr=0.677; %condenser refrigerant side
Kech=0.598; %evaporator chilled water side
Ker=0.582; %evaporator refrigerant side
Kgs=0.45; %gen. solution side
Kas=0.42; %absorber solution side;
%Specific heat capacity (J/KgK)
Cpgs=(1.01-(1.23.*Xss)+0.48).*4186; %gen. solution side
Cpas=(1.01-(1.23.*Xws)+0.48).*4186; %absorber solution side
Cpg=4187;
Cpa=4187;
Cpc=4187;
Cpe=4187;
%Latent heat
jg=2270; %aqueous LiBr solution
je=2270; %water
%Dynamic viscosity (Kg/m.s)
ygw=0.000355;
yaw=0.0008;
ycw=0.00065;
ycr=0.0008;
yech=0.00114;
yer=0.0015;
ygs=0.0031;
yas=0.0032;

%Calculate required loads (W)
Qg=Qe./COP; %generator heat load
%condenser cooling load (Qc)
hei=4.186.*Tcr2; %evaporator inlet enthalpy from condenser
heo=2501+(1.88.*Techw2); %enthalpy of chilled water exit from evaporator
qo=heo-hei; %refrigerating effect
```

```
D=(Qe.*60)/(qo.*1000); %water vapour distilled per ton of refrigeration
hci=2501+(1.88.*Tgh1); %enthalpy of refrigerant at inlet to condenser
hco=hei; %enthalpy of refrigerant at exit from condenser
Qc=((D./60).*(hci-hco)).*1000;
%Calculate absorber cooling load (Qa)
Qa=Qe+Qg-Qc;
%calculate flow rates (Kg/s)
hwv=2501.48+(1.78.*Ter2); %enthalpy of water vapour from evaporator
hw=4.2.*Tcr2; %enthalpy of water from condenser
hw2=4.2.*Ter1; %enthalpy of water from condenser after throttling
mref=Qe./(1000.*(hwv-hw)); %mass flow rate of refrigerant
mws=mref.*(Xss./(Xss-Xws)); %mass flow rate of weak solution
mss=mws-mref; %mass flow rate of strong solution
mgh=Qg./(Cpg.*(Tgh1-Tgh2)); %mass flow rate of hot water at generator
mgs=Qg./(Cpgs.*(Tgs2-Tgs1)); %mass flow rate of solution at generator
mac=Qa./(Cpa.*(Tacw2-Tacw1)); %mass flow rate of cooling water at absorber
mas=mgs; %mass flow rate of solution at absorber
mcc=Qc./(Cpc.*(Tccw2-Tccw1)); %mass flowrate of cooling water at condenser
mcr=Qc./(Cpc.*(Tcrv1-Tcr2)); %mass flow rate of refrigerant vapour at condenser
mech=Qe./(Cpe.*(Techw1-Techw2)); %mass flow rate of chilled water at evaporator
mer=Qe./(Cpe.*(Ter2-Ter1)); %mass flow rate of refrigerant at evaporator
%Calculate Logarithmic Mean Temperature Difference (LMTD)
%Condenser
LMTDc=(((Tcr2-Tccw1)-(Tcr2-Tccw2))./log((Tcr2-Tccw1)./(Tcr2-Tccw2)));
%Calculate LMTD correction factor
Fc=0.99;
%Calculate corrected LMTD
LMTDcc=LMTDc.*Fc;
%Calculate provisional heat transfer area
%Assume overall heat transfer coefficient
Ua(1)=1300;
j=1;
for j = 1:25;

ApT=Qc./(Ua(j).*LMTDcc);
%Calculate number of tubes
Nt=ApT./As;
%Calculate tube pitch
pt=1.25.*d2;
%Calculate shell diameter
Ds=0.637.*((CL./CTP).^0.5).*(3.14.*((pt./d2).^2).*d2.^2.*Nt).^0.5;
%Calculate tube bundle cross flow area
Acf=((pt-d2).*Ds.*Lt)./pt;
%calculate shell side mass velocity
Gs=mcr./Acf;
%Calculate shell equivalent diameter
Dse=(1.27./d2).*(pt.^2-(0.785.*d2.^2));
% Calculate shell side Reynolds number
Res=Gs.*Dse./ycr;
% Calculate shell side Prandtl number
```

```
Pr=ycr.*Cpc./Kcr;
% Calculate number of tubes per pass
Ntpp=Nt./Np;
%Calculate tube side mass velocity
Gt=mcc./(Ntpp.*Ax);
%Calculate tube side velocity
vt=Gt./dcw;
%Calculate tube side reynolds number
Ret=(dcw.*vt.*d1)./ycw;
%Calculate friction factor
fc=((1.82.*(log(Ret)./log(10)))-1.64).^(-2);
%Calculate Heat Transfer Coefficients
hcw=(Kcw.*(fc./8).*Ret.*Pr)./(d1.*(1.07+(12.7.*(fc./8).^0.5.*((Pr.^0.667)-1)))); % @ water side
hcr=(0.725.*((dcr.*(dcr-dv).*g.*hfg.*Kcr.^3)./(y.*(Tcr2-Tccw1).*d2)).^0.25).*Nt.^0.25;%@
refrigerant side
%Calculate Overall Heat Transfer Coefficient
%Condenser
j=j+1;
Ua(j)=1./(((d2./d1).*(1./hcw))+((d2./d1).*F1)+((1./(2.*Kt)).*d2.*log(d2./d1))+F2+(1./hcr));
Ncross5Matrix(j,1)=j;
Ncross5Matrix(j,2)=Ua(j)
Ncross5Matrix(j,3)=Nt
Ncross5Matrix(j,4)=ApT
Ncross5Matrix(j,5)=Ds
%Compare Ua and Uc if difference is large, use value of Uc in Ua and calculate again until
successive values of Ua are close then
%then display Ua, Nt, ApT

end
It=Ncross5Matrix(:,1:5);

ff=0.02;
d1p=0.0025; % diameter of sucction pipe (m)
Ax2=(3.14.*d1p.^2)./4;
DelP=Ph-Pl;
Vf=mref./dcr; %volume flow rate
Vav=Vf./Ax2; % average velocity
Lc=(2.*DelP.*d1p)./(ff.*dcr.*(Vav)^2);
```

APPENDIX E
MATLAB PROGRAM FOR EVAPORATOR DESIGN

```
% APPENDIX E
% PROGRAM FOR EVAPORATOR DESIGN
clc
```

```
clear all
%Input Design operating Parameters
%Generator
Tgh1=90; %Inlet hot water to generator
Tgh2=80; %Outlet hot water from generator
Tgs1=74; %Inlet solution tenp. to generator
Tgs2=81; %Outlet solution temperature from generator
%Absorber
Tacw1=32; %Inlet cooling water temp. to absorber
Tacw2=37; %outlet cooling water temp. from absorber
Tas1=55; %Inlet solution temp. to absorber
Tas2=40; %Outlet solution temp. from absorber
%Condenser
Tccw1=29; % Inlet cooling water temp. to condenser
Tccw2=32; %Outlet cooling water temp. from condenser
Tcrv1=90; %Refrigerant vapour inlet temp. to condenser
Tcr2=40; %refrigerant outlet temp. from condenser
%Evaporator
Qe=12000.0; %refrigerating capacity (W)
Techw1=15; %chilled water temp. into evaporator
Techw2=10; %chilled water temp. outfrom evaporator
Ter1=6; %Refrigerant inlet temp. to evaporator
Ter2=8; %Refrigerant outlet temp. from evaporator
COP=0.7; %Design coefficient of performance
%Pressure (Pa)
Ph=7340;
Pl=1200;
%Concentration
Xss=0.63; %strong solution concentration
Xws=0.55; %weak solution concentration
Xsw=(1-Xss); %strong solution concentration of water
Xww=(1-Xws); %weak solution concentration of water
f=(1-Xsw)./(Xww-Xsw); %specific circulation ratio
% Constants
g=9.81; % acceleration due to gravity
dv=0.03285; % density of vapour
y=0.000299; % dynamic viscosity
hfg=2479600; % enthalpy of evaporation
F1=0.00009; % fouling factor inside tube (m2oC/W)
F2=0.00009; % fouling factor outside tube (m2oC/W)
CTP=0.93; % clearance constant between shell and tube
CL=1.0; % tube layout constant
sig=0.589; %s. Boltzmann const
Csf=0.013;
Tw=15; %wall temp
Tsat=9; %sat. temp
%Input Design Geometric Parameters
Lt=0.5; %tube length
d1=0.00825; %inner diameter of tubes
d2=0.01425; %outer diameter of tubes
```

```
Np=1;%number of pass
Kt=383.2; %thermal conductivity of tubes (W/moC)
%Calculate flow crssectional area for a single tube(m2)
Ax=(3.14.*d1.^2)./4;
%Calculate surface area for a single tube
As=3.14.*d2.*Lt;
%Input Constants
%Density (Kg/m3)
dgw=972; %generator hot water side
daw=991.1; %absorber water side
dcr=963.97; %condenser refrigerant side
dcw=991.1; %condenser water side
dcv=0.0022.*Ph./Tgh1; %condenser vapour side
dech=999.0; %evaporator chilled water side
der=1000.0; %evaporator refrigerant side
dgs=1145.36+(470.48.*Xss)+(1374.79.*Xss^2)-(0.333393+(0.571749.*Xss)).*(273+Tgs2);
%gen. soln. side
das=1145.36+(470.48.*Xws)+(1374.79.*Xws^2)-(0.333393+(0.571749.*Xws)).*(273+Tas2);
%abs. soln. side
%Thermal conductivity (w/mk)
Kgw=0.677; %gen. hot water side
Kaw=0.634; %absorber water side
Kcw=0.634; %condenser water side
Kcr=0.677; %condenser refrigerant side
Kech=0.598; %evaporator chilled water side
Ker=0.582; %evaporator refrigerant side
Kgs=0.45; %gen. solution side
Kas=0.42; %absorber solution side;
%Specific heat capacity (J/KgK)
Cpgs=(1.01-(1.23.*Xss)+0.48).*4186; %gen. solution side
Cpas=(1.01-(1.23.*Xws)+0.48).*4186; %absorber solution side
Cpg=4187;
Cpa=4187;
Cpc=4187;
Cpe=4187;
%Latent heat
jg=2270; %aqueous LiBr solution
je=2270; %water
%Dynamic viscosity (Kg/m.s)
ygw=0.000355;
yaw=0.0008;
ycw=0.00065;
ycr=0.0008;
yech=0.00114;
yer=0.0015;
ygs=0.0031;
yas=0.0032;

%Calculate required loads (W)
Qg=Qe./COP; %generator heat load
```

```
%condenser cooling load (Qc)
hei=4.186.*Tcr2; %evaporator inlet enthalpy from condenser
heo=2501+(1.88.*Techw2); %enthalpy of chilled water exit from evaporator
qo=heo-hei; %refrigerating effect
D=(Qe.*60)/(qo.*1000); %water vapour distilled per ton of refrigeration
hci=2501+(1.88.*Tgh1); %enthalpy of refrigerant at inlet to condenser
hco=hei; %enthalpy of refrigerant at exit from condenser
Qc=((D./60).*(hci-hco)).*1000;
%Calculate absorber cooling load (Qa)
Qa=Qe+Qg-Qc;
%calculate flow rates (Kg/s)
hwv=2501.48+(1.78.*Ter2); %enthalpy of water vapour from evaporator
hw=4.2.*Tcr2; %enthalpy of water from condenser
hw2=4.2.*Ter1; %enthalpy of water from condenser after throttling
mref=Qe./(1000.*(hwv-hw)); %mass flow rate of refrigerant
mws=mref.*(Xss./(Xss-Xws)); %mass flow rate of weak solution
mss=mws-mref; %mass flow rate of strong solution
mgh=Qg./(Cpg.*(Tgh1-Tgh2)); %mass flow rate of hot water at generator
mgs=Qg./(Cpgs.*(Tgs2-Tgs1)); %mass flow rate of solution at generator
mac=Qa./(Cpa.*(Tacw2-Tacw1)); %mass flow rate of cooling water at absorber
mas=mgs; %mass flow rate of solution at absorber
mcc=Qc./(Cpc.*(Tccw2-Tccw1)); %mass flowrate of cooling water at condenser
mcr=Qc./(Cpc.*(Tcrv1-Tcr2)); %mass flow rate of refrigerant vapour at condenser
mech=Qe./(Cpe.*(Techw1-Techw2)); %mass flow rate of chilled water at evaporator
mer=Qe./(Cpe.*(Ter2-Ter1)); %mass flow rate of refrigerant at evaporator
%Calculate Logarithmic Mean Temperature Difference (LMTD)
%Evaporator
LMTDe=(((Techw1-Ter2)-(Techw2-Ter1))./log((Techw1-Ter2)./(Techw2-Ter1)));
%Calculate LMTD correction factor
Fe=0.96;
%Calculate corrected LMTD
LMTDec=LMTDe.*Fe;
%Calculate provisional heat transfer area
%Assume overall heat transfer coefficient
Ue(1)=1300;
j=1;
for j = 1:25;

ApT=Qe./(Ue(j).*LMTDec);
%Calculate number of tubes
Nt=ApT./As;
%Calculate tube pitch
pt=1.25.*d2;
%Calculate shell diameter
Ds=0.637.*((CL./CTP).^0.5).*(3.14.*((pt./d2).^2).*d2.^2.*Nt).^0.5;
%Calculate tube bundle cross flow area
Acf=((pt-d2).*Ds.*Lt)./pt;
%calculate shell side mass velocity
Gs=mcr./Acf;
%Calculate shell equivalent diameter
```

```
Dse=(1.27./d2).*(pt.^2-(0.785.*d2.^2));
% Calculate shell side Reynolds number
Res=Gs.*Dse./ycr;
% Calculate shell side Prandtl number
Pr=ycr.*Cpc./Kcr;
% Calculate number of tubes per pass
Ntpp=Nt./Np;
%Calculate tube side mass velocity
Gt=mcc./(Ntpp.*Ax);
%Calculate tube side velocity
vt=Gt./dcw;
%Calculate tube side reynolds number
Ret=(dcw.*vt.*d1)./ycw;
%Calculate friction factor
fc=((1.82.*(log(Ret)./log(10)))-1.64).^(-2);
%Calculate Heat Transfer Coefficients
Ahex=pt^2;
Acfl=Ahex-(3.14.*d2./4);
ddel=(((4.*Acfl)./3.14)+(d2^2))^0.5;
del=(ddel-d2)./2;
her=yer.*hfg.*((g.*(der-dv))./sig)^0.5.*((Cpe.*(Tw-Tsat))./(Csf.*hfg.*Pr))^3;  %nucleate  boiling
heat transfer coefficient
hew=(Kech.*(fc./8).*Ret.*Pr)./(d1.*(1.07+(12.7.*(fc./8).^0.5.*((Pr.^0.667)-1)))); % @ water side
%Calculate Overall Heat Transfer Coefficient
%Evaporator
j=j+1;
Ue(j)=1./((d1./(d2.*her))+((d1./(2.*Kt)).*log(d2./d1))+(1./hew));
Ncross5Matrix(j,1)=j;
Ncross5Matrix(j,2)=Ue(j)
Ncross5Matrix(j,3)=Nt
Ncross5Matrix(j,4)=ApT
Ncross5Matrix(j,5)=Ds

end
It=Ncross5Matrix(:,1:5);
```

APPENDIX F
MATLAB PROGRAM FOR ABSORBER DESIGN

```
% APPENDIX F
% PROGRAM FOR ABSORBER DESIGN
clc
```

```
clear all
%Input Design operating Parameters
%Generator
Tgh1=90; %Inlet hot water to generator
Tgh2=80; %Outlet hot water from generator
Tgs1=74; %Inlet solution tenp. to generator
Tgs2=81; %Outlet solution temperature from generator
%Absorber
Tacw1=32; %Inlet cooling water temp. to absorber
Tacw2=37; %outlet cooling water temp. from absorber
Tas1=55; %Inlet solution temp. to absorber
Tas2=45; %Outlet solution temp. from absorber
%Condenser
Tccw1=29; % Inlet cooling water temp. to condenser
Tccw2=32; %Outlet cooling water temp. from condenser
Tcrv1=90; %Refrigerant vapour inlet temp. to condenser
Tcr2=40; %refrigerant outlet temp. from condenser
%Evaporator
Qe=12000.0; %refrigerating capacity (W)
Techw1=15; %chilled water temp. into evaporator
Techw2=10; %chilled water temp. outfrom evaporator
Ter1=6; %Refrigerant inlet temp. to evaporator
Ter2=8; %Refrigerant outlet temp. from evaporator
COP=0.7; %Design coefficient of performance
%Pressure (Pa)
Ph=7340;
Pl=1200;
%Concentration
Xss=0.63; %strong solution concentration
Xws=0.55; %weak solution concentration
Xsw=(1-Xss); %strong solution concentration of water
Xww=(1-Xws); %weak solution concentration of water
f=(1-Xsw)./(Xww-Xsw); %specific circulation ratio
% Constants
g=9.81; % acceleration due to gravity
dv=0.03285; % density of vapour
y=0.000299; % dynamic viscosity
hfg=2479600; % enthalpy of evaporation
F1=0.00009; % fouling factor inside tube (m2oC/W)
F2=0.00009; % fouling factor outside tube (m2oC/W)
CTP=0.93; % clearance constant between shell and tube
CL=1.0; % tube layout constant
sig=0.0115; %s. Boltzmann const
Csf=0.013;
Tw=15; %wall temp
Tsat=9; %sat. temp
%Input Design Geometric Parameters
Lt=0.5; %tube length
d1=0.00825; %inner diameter of tubes
d2=0.01225; %outer diameter of tubes
```

```
Np=1;%number of pass
Kt=383.2; %thermal conductivity of tubes (W/moC)
%Calculate flow crssectional area for a single tube(m2)
Ax=(3.14.*d1.^2)./4;
%Calculate surface area for a single tube
As=3.14.*d2.*Lt;
%Input Constants
%Density (Kg/m3)
dgw=972; %generator hot water side
daw=991.1; %absorber water side
dcr=963.97; %condenser refrigerant side
dcw=991.1; %condenser water side
dcv=0.0022.*Ph./Tgh1; %condenser vapour side
dech=999.0; %evaporator chilled water side
der=1000.0; %evaporator refrigerant side
dgs=1145.36+(470.48.*Xss)+(1374.79.*Xss^2)-(0.333393+(0.571749.*Xss)).*(273+Tgs2);
%gen. soln. side
das=1145.36+(470.48.*Xws)+(1374.79.*Xws^2)-(0.333393+(0.571749.*Xws)).*(273+Tas2);
%abs. soln. side
%Thermal conductivity (w/mk)
Kgw=0.677; %gen. hot water side
Kaw=0.634; %absorber water side
Kcw=0.634; %condenser water side
Kcr=0.677; %condenser refrigerant side
Kech=0.598; %evaporator chilled water side
Ker=0.582; %evaporator refrigerant side
Kgs=0.45; %gen. solution side
Kas=0.42; %absorber solution side;
%Specific heat capacity (J/KgK)
Cpgs=(1.01-(1.23.*Xss)+0.48).*4186; %gen. solution side
Cpas=(1.01-(1.23.*Xws)+0.48).*4186; %absorber solution side
Cpg=4187;
Cpa=4187;
Cpc=4187;
Cpe=4187;
%Latent heat
jg=2270; %aqueous LiBr solution
je=2270; %water
%Dynamic viscosity (Kg/m.s)
ygw=0.000355;
yaw=0.0008;
ycw=0.00065;
ycr=0.0008;
yech=0.00114;
yer=0.0015;
ygs=0.0031;
yas=0.0032;

%Calculate required loads (W)
Qg=Qe./COP; %generator heat load
```

```
%condenser cooling load (Qc)
hei=4.186.*Tcr2; %evaporator inlet enthalpy from condenser
heo=2501+(1.88.*Techw2); %enthalpy of chilled water exit from evaporator
qo=heo-hei; %refrigerating effect
D=(Qe.*60)/(qo.*1000); %water vapour distilled per ton of refrigeration
hci=2501+(1.88.*Tgh1); %enthalpy of refrigerant at inlet to condenser
hco=hei; %enthalpy of refrigerant at exit from condenser
Qc=((D./60).*(hci-hco)).*1000;
%Calculate absorber cooling load (Qa)
Qa=Qe+Qg-Qc;
%calculate flow rates (Kg/s)
hwv=2501.48+(1.78.*Ter2); %enthalpy of water vapour from evaporator
hw=4.2.*Tcr2; %enthalpy of water from condenser
hw2=4.2.*Ter1; %enthalpy of water from condenser after throttling
mref=Qe./(1000.*(hwv-hw)); %mass flow rate of refrigerant
mws=mref.*(Xss./(Xss-Xws)); %mass flow rate of weak solution
mss=mws-mref; %mass flow rate of strong solution
mgh=Qg./(Cpg.*(Tgh1-Tgh2)); %mass flow rate of hot water at generator
mgs=Qg./(Cpgs.*(Tgs2-Tgs1)); %mass flow rate of solution at generator
mac=Qa./(Cpa.*(Tacw2-Tacw1)); %mass flow rate of cooling water at absorber
mas=mgs; %mass flow rate of solution at absorber
mcc=Qc./(Cpc.*(Tccw2-Tccw1)); %mass flowrate of cooling water at condenser
mcr=Qc./(Cpc.*(Tcrv1-Tcr2)); %mass flow rate of refrigerant vapour at condenser
mech=Qe./(Cpe.*(Techw1-Techw2)); %mass flow rate of chilled water at evaporator
mer=Qe./(Cpe.*(Ter2-Ter1)); %mass flow rate of refrigerant at evaporator
%Calculate Logarithmic Mean Temperature Difference (LMTD)
%absorber
LMTDa=(((Tas1-Tacw2)-(Tas2-Tacw1))./log((Tas1-Tacw2)./(Tas2-Tacw1)));
%Calculate LMTD correction factor
Fa=0.98;
%Calculate corrected LMTD
LMTDac=LMTDa.*Fa;
%Calculate provisional heat transfer area
%Assume overall heat transfer coefficient
Ua(1)=1700;
j=1;
for j = 1:25;

ApT=Qa./(Ua(j).*LMTDac);
%Calculate number of tubes
Nt=ApT./As;
%Calculate tube pitch
pt=1.5.*d2;
%Calculate shell diameter
Ds=0.637.*((CL./CTP).^0.5).*(3.14.*((pt./d2).^2).*d2.^2.*Nt).^0.5;
%Calculate tube bundle cross flow area
Acf=((pt-d2).*Ds.*Lt)./pt;
%calculate shell side mass velocity
Gs=mas./Acf;
%Calculate shell equivalent diameter
```

```
Dse=(1.27./d2).*(pt.^2-(0.785.*d2.^2));
% calculate flow rate of falling film in shell (Kg/ms)
Ja=mas./Lt; %absorber falling film
% Calculate shell side Reynolds number
Reas=(4.*Ja)./yas; %Reynolds number absorber solution side;
% Calculate shell side Prandtl number
Pras=(Cpas.*yas)./Kas;
% Calculate tube side Prandtl number
Praw=(Cpa.*yaw)./Kaw;
% Calculate number of tubes per pass
Ntpp=Nt./Np;
%Calculate tube side mass velocity
Gt=mac./(Ntpp.*Ax);
%Calculate tube side velocity
vt=Gt./daw;
%Calculate tube side reynolds number
Ret=(Gt.*d1)./yaw;
%Calculate friction factor
fa=((1.82.*(log(Ret)./log(10)))-1.64).^(-2);
%Calculate Heat Transfer Coefficients
del=((3.*yas.*Ja)./(das.^2.*9.81)).^0.333;
haw=(Kaw.*(fa./8).*Ret.*Praw)./(d1.*(1.07+(12.7.*(fa./8).^0.5.*((Praw.^0.667)-1)))); % @ water
side
has=(Kas./del).*(0.029.*Reas.^0.53.*Pras.^0.344); % @ Solution side
%Calculate Overall Heat Transfer Coefficient
%Absorber
j=j+1;
Ua(j)=1./((d1./(d2.*has))+((d1./(2.*Kt)).*log(d2./d1))+(1./haw));
Ncross5Matrix(j,1)=j;
Ncross5Matrix(j,2)=Ua(j)
Ncross5Matrix(j,3)=Nt
Ncross5Matrix(j,4)=ApT
Ncross5Matrix(j,5)=Ds
end
It=Ncross5Matrix(:,1:5);

Vs = 0.5.*0.8*3.142*((It(:,5).^2)/4)*Lt;% Volume of absorber sump
```

APPENDIX G
MATLAB PROGRAM FOR SOLUTION HEAT EXCHANGER DESIGN

```
% APPENDIX G
% PROGRAM FOR SOLUTION HEAT EXCHANGER DESIGN
clc
```

```
clear all
%Input Design operating Parameters
%Generator
Tgh1=90; %Inlet hot water to generator
Tgh2=80; %Outlet hot water from generator
Tgs1=74; %Inlet solution tenp. to generator
Tgs2=81; %Outlet solution temperature from generator
%Absorber
Tacw1=32; %Inlet cooling water temp. to absorber
Tacw2=37; %outlet cooling water temp. from absorber
Tas1=55; %Inlet solution temp. to absorber
Tas2=45; %Outlet solution temp. from absorber
%Condenser
Tccw1=29; % Inlet cooling water temp. to condenser
Tccw2=32; %Outlet cooling water temp. from condenser
Tcrv1=90; %Refrigerant vapour inlet temp. to condenser
Tcr2=40; %refrigerant outlet temp. from condenser
%Evaporator
Qe=12000.0; %refrigerating capacity (W)
Techw1=15; %chilled water temp. into evaporator
Techw2=10; %chilled water temp. outfrom evaporator
Ter1=6; %Refrigerant inlet temp. to evaporator
Ter2=8; %Refrigerant outlet temp. from evaporator
COP=0.7; %Design coefficient of performance
%Pressure (Pa)
Ph=7340;
Pl=1200;
%Concentration
Xss=0.63; %strong solution concentration
Xws=0.55; %weak solution concentration
Xsw=(1-Xss); %strong solution concentration of water
Xww=(1-Xws); %weak solution concentration of water
f=(1-Xsw)./(Xww-Xsw); %specific circulation ratio
% Constants
g=9.81; % acceleration due to gravity
F1=0.00009; % fouling factor inside tube (m2oC/W)
F2=0.00009; % fouling factor outside tube (m2oC/W)
CTP=0.93; % clearance constant between shell and tube
CL=1.0; % tube layout constant
%Input Design Geometric Parameters
Lt=0.5; %tube length
d1=0.00925; %inner diameter of tubes
d2=0.01325; %outer diameter of tubes
Np=1;%number of pass
Kt=383.2; %thermal conductivity of tubes (W/moC)
%Calculate flow crssectional area for a single tube(m2)
Ax=(3.14.*d1.^2)./4;
%Calculate surface area for a single tube
As=3.14.*d2.*Lt;
%Input Constants
```

```
%Density (Kg/m3)
dgs=1145.36+(470.48.*Xss)+(1374.79.*Xss^2)-(0.333393+(0.571749.*Xss)).*(273+Tgs2);
%gen. soln. side
das=1145.36+(470.48.*Xws)+(1374.79.*Xws^2)-(0.333393+(0.571749.*Xws)).*(273+Tas2);
%abs. soln. side
%Thermal conductivity (w/mk)
Kgs=0.45; %gen. solution side
Kas=0.42; %absorber solution side;
%Specific heat capacity (J/KgK)
Cpgs=(1.01-(1.23.*Xss)+0.48).*4186; %gen. solution side
Cpas=(1.01-(1.23.*Xws)+0.48).*4186; %absorber solution side
%Dynamic viscosity (Kg/m.s)
ygs=0.0031;
yas=0.0032;
%Calculate required loads (W)
Qg=Qe./COP; %generator heat load
%condenser cooling load (Qc)
hei=4.186.*Tcr2; %evaporator inlet enthalpy from condenser
heo=2501+(1.88.*Techw2); %enthalpy of chilled water exit from evaporator
qo=heo-hei; %refrigerating effect
D=(Qe.*60)/(qo.*1000); %water vapour distilled per ton of refrigeration
hci=2501+(1.88.*Tgh1); %enthalpy of refrigerant at inlet to condenser
hco=hei; %enthalpy of refrigerant at exit from condenser
Qc=((D./60).*(hci-hco)).*1000;
%Calculate absorber cooling load (Qa)
Qa=Qe+Qg-Qc;
%calculate flow rates (Kg/s)
hwv=2501.48+(1.78.*Ter2); %enthalpy of water vapour from evaporator
hw=4.2.*Tcr2; %enthalpy of water from condenser
hw2=4.2.*Ter1; %enthalpy of water from condenser after throttling
mref=Qe./(1000.*(hwv-hw)); %mass flow rate of refrigerant
mws=mref.*(Xss./(Xss-Xws)); %mass flow rate of weak solution
mss=mws-mref; %mass flow rate of strong solution
mgs=Qg./(Cpgs.*(Tgs2-Tgs1)); %mass flow rate of solution at generator
mas=mgs; %mass flow rate of solution at absorber
%Solution Heat Exchanger
hgshx=(4180.*((42.81-(425.9.*Xss)+(404.67.*Xss^2))+(1.01-
(1.23.*Xss)+(0.48.*Xss^2)).*Tgs2)); %enthalpy from gen to shx
hshxa=(4180.*((42.81-(425.9.*Xss)+(404.67.*Xss^2))+(1.01-
(1.23.*Xss)+(0.48.*Xss^2)).*Tas1)); %enthalpy from shx to absorber
hshxg=(4180.*((42.81-(425.9.*Xws)+(404.67.*Xws^2))+(1.01-
(1.23.*Xws)+(0.48.*Xws^2)).*Tgs1)); %enthalpy from shx to gen
hashx=(4180.*((42.81-(425.9.*Xws)+(404.67.*Xws^2))+(1.01-
(1.23.*Xws)+(0.48.*Xws^2)).*Tas2)); %enthalpy from absorber to shx
%calculate solution heat exchanger load
Qshx=mws.*(hshxg-hashx);
%Calculate Logarithmic Mean Temperature Difference (LMTD)
%absorber
LMTDshx=(((Tgs2-Tgs1)-(Tas1-Tas2))./log((Tgs2-Tgs1)./(Tas1-Tas2)));
%Calculate LMTD correction factor
```

```
Fshx=0.98;
%Calculate corrected LMTD
LMTDshxc=LMTDshx.*Fshx;
%Calculate provisional heat transfer area
%Assume overall heat transfer coefficient
Ushx(1)=1700;
j=1;
for j = 1:25;

ApT=Qshx./(Ushx(j).*LMTDshxc);
%Calculate number of tubes
Nt=ApT./As;
%Calculate tube pitch
pt=1.5.*d2;
%Calculate shell diameter
Ds=0.637.*((CL./CTP).^0.5).*(3.14.*((pt./d2).^2).*d2.^2.*Nt).^0.5;
%Calculate tube bundle cross flow area
Acf=((pt-d2).*Ds.*Lt)./pt;
%calculate shell side mass velocity
Gs=mss./Acf;
%Calculate shell equivalent diameter
Dse=(1.27./d2).*(pt.^2-(0.785.*d2.^2));
% calculate flow rate of falling film in shell (Kg/ms)
Ja=mss./Lt; %absorber falling film
% Calculate shell side Reynolds number
Res=(4.*Ja)./ygs;
% Calculate shell side Prandtl number
Prs=(Cpgs.*ygs)./Kgs;
% Calculate tube side Prandtl number
Prt=(Cpas.*yas)./Kas;
% Calculate number of tubes per pass
Ntpp=Nt./Np;
%Calculate tube side mass velocity
Gt=mws./(Ntpp.*Ax);
%Calculate tube side velocity
vt=Gt./das;
%Calculate tube side reynolds number
Ret=(Gt.*d1)./yas;
%Calculate friction factor
fa=((1.82.*(log(Ret)./log(10)))-1.64).^(-2);
%Calculate Heat Transfer Coefficients
%Calculate Heat Transfer Coefficients
del=((3.*ygs.*Ja)./(dgs.^2.*9.81)).^0.333;
ht=(Kas.*(fa./8).*Ret.*Prt)./(d1.*(1.07+(12.7.*(fa./8).^0.5.*((Prt.^0.667)-1)))); % @ tube side
hs=(Kgs./del).*(0.029.*Res.^0.53.*Prs.^0.344); % @ Shell side
%Calculate Overall Heat Transfer Coefficient
%SHX
j=j+1;
Ushx(j)=1./((d1./(d2.*hs))+((d1./(2.*Kt)).*log(d2./d1))+(1./ht));
Ncross5Matrix(j,1)=j;
```

```
Ncross5Matrix(j,2)=Ushx(j)
Ncross5Matrix(j,3)=Nt
Ncross5Matrix(j,4)=ApT
Ncross5Matrix(j,5)=Ds
end
It=Ncross5Matrix(:,1:5);
```

APPENDIX H
MATLAB PROGRAM FOR PERFORMANCE SIMULATION OF ABSORPTION CHILLER

```
% APPENDIX H
%PROGRAM FOR PERFORMANCE SIMULATION OF ABSORPTION CHILLER
```

```
clc
clear all
% Generator
% Input constants
%Tgh1=90; %inlet hot water to gen
%Tgh1 = 1:1:90;

for Tgh1 = 75:90


  mref=(0.0000155.*Tgh1); %mass flow rate of refrigerant
  mws=0.0403; %mass flow rate of weak solution
  mss=0.0351; %mass flow rate of strong solution
  mgh=0.1024; %mass flow rate of gen hot water
  Cpg=4.209; %specific heat capacity gen
  Atg=1.0291; %area of tube bundle gen
  Ug=2.319; %overall heat transfer coefficient gen
  tc=45; %condenser temperature
% Calculate
  T8(1)=0.9.*Tgh1;
  j =1;
for j = 1:7;

    Xss=((49.04+(1.25.*T8(j))-tc)./(134.65+(0.47.*T8(j))));  %concentration  of
strong solution
    Xws=((mss.*Xss)./mref).*((mref./(mref+mss)));   %concentration   of   weak
solution
    A1=mref.*(2501.3+(1.87.*Tgh1));
    A2=(42.81-(425.92.*Xws)+(404.67.*Xws.^2));
    A3=(1.01-(1.23.*Xws)+(0.48.*Xws.^2));
    A4=(42.81-(425.92.*Xss)+(404.67.*Xss.^2));
    A5=(1.01-(1.23.*Xss)+(0.48.*Xss.^2));
    Z=(Ug.*Atg);
    A=[((4.2.*mgh)+(0.5.*Z)),-(0.5.*Z);-(4.2.*mgh),(4.19.*mws.*A3)];
    b=[((((4.2.*mgh)-(0.5.*Z)).*Tgh1)+(0.5.*Z.*T8(j)));(A1-(4.19.*mws.*A2)-
(4.2.*mgh.*Tgh1)+(mss.*(4.19.*(A4+(A5.*T8(j))))))];
    T=A\b;
    eo = T(1,1);
    eo1 = T(2,1);
    j = j+1;
    T8(j)=((((4.2.*mgh.*Tgh1)-(4.2.*mgh.*T(1,1))-
A1+(4.19.*mws.*A2)+(4.19.*mws.*A3.*T(2,1))./(mss.*4.19))-A4)./A5;
    Ncross4Matrix(j,1)=j;
    Ncross4Matrix(j,2)=T8(j);
    Ncross4Matrix(j,3)=eo;
    Ncross4Matrix(j,4)=eo1;
end
  It = Ncross4Matrix(:,1:4);
%Calculate condenser
  Tccw1=29; %inlet cooling water temp to condenser
  mcc=0.0953; %mass flow rate cooling water at condenser
  Apc=1.06;
  Uc=1.283;
  Z2=0.5.*Uc.*Atc;
  A6=mref.*(2501.3+(1.87.*Tgh1));
  B=[((4.2.*mcc)+Z2),-(2.*Z2);(4.2.*mcc),(4.2.*mref)];
  c=[((((4.2.*mcc)-Z2).*Tccw1));(A6+(4.2.*mcc.*Tccw1))];
  d=B\c;
%Calculate Evaporator
  Te=11; %evaporator temp
```

```
  Techw1=15; %chilled water inlet temp
  mech=0.1433; %mass flow rate of chilled water
  mer=0.3583; %mass flow rate of refrigerant at evaporator
  Cpe=4.2;
  Ue=1.627;
  Ate=1.003;
  Ter1=6;
  Z3=0.5.*Ue.*Ape;
  E=[(Z3),-((4.18.*mech)+Z3);-(1.87.*mref),-(4.19.*mech)];
  l=[(((Z3-(4.18.*mech)).*Techw1)-(Z3.*Ter1));((mref.*(2501.3-(4.19.*Ter1)))-
(4.19.*mech.*Techw1))];
  i=E\l;
  h7=4.19*(A4+(A5*T8));
  h8=4.19*(A2+(A3*T));
  h1=2501.3+(1.87*Tgh1);
  h4=2527.48;
  h3=167.6;
  Qg=mgh*Cpg*(Tgh1-T(1,1));
  Qe=mech.*Cpe.*(Te-i(1,1));
  COP=Qe./Qg;
  Ncross3Matrix(Tgh1,1) = COP;
  Ncross3Matrix(Tgh1,2) = Qg;
  Ncross3Matrix(Tgh1,3) = Qe;
end
COP = Ncross3Matrix(:,1:1);
Qg = Ncross3Matrix(:,1:2);
Qe = Ncross3Matrix(:,1:3);
for Tgh1 = 75:90
    x1 = Tgh1;
    Ncross2Matrix(Tgh1,2) = x1;
end

Tgh01 = Ncross2Matrix(:,1:2);
x = Tgh01(:,2);
y = Qg(:,2);
y2 = COP(:,1);
y3 = Qe(:,3);

%figure1
figure(1), plot(x,y2,'-bo','Markersize',8)
xlim([75 90]);
ylim([0.2 1.0]);
ylabel('Coefficient of performance')
xlabel('inlet temperature to generator (c)')

% Calculate Absorber
Tacw1=29; %cooling water inlet temp to absorber
macw=0.1222; %mass flow rate of absorber cooling water
Ua=1.682;
Apa=0.642;
EF=0.8;
Tas2=EF.*(T(2,1));
Tas1=EF.*T8;
Z4=Ua.*Apa;
A7=(4.2.*macw)+Z4;
A8=(((EF.*(0.9.*Tgh1))./2)+((EF.*(T(2,1)))./2)-(Tacw1./2));
A9=4.2.*macw.*Tacw1;
Tacw2=((Z4.*A8)+A9)./A7;
A10=(42.81-(425.92.*Xws)+(404.67.*Xws.^2));
A11=(1.01-(1.23.*Xws)+(0.48.*Xws.^2));
A12=(42.81-(425.92.*Xss)+(404.67.*Xss.^2));
```

```
A13=(1.01-(1.23.*Xss)+(0.48.*Xss.^2));
A14=macw.*4.2.*(Tacw1-Tacw2);
A15=((mws.*(4.19.*(A10+(A11.*(EF.*(T(2,1)))))))-
(mss.*(4.19.*(A12+(A13.*(EF.*T8))))));
Ter2=((mws.*(4.19.*(A10+(A11.*(EF.*(T(2,1)))))))-
(mss.*(4.19.*(A12+(A13.*(EF.*T8)))))-A14-(mer.*2501.3))./(1.87.*mer);
B1=1000.*((3.462033-(0.02679.*Xws)).*(EF.*(T(2,1)))+(0.5.*(0.001349-
(0.00000655.*Xws.^2)).*(T(2,1)).^2)+(162.81-(6.042.*Xws)-
0.000453.*Xws.^2+(0.0012.*Xws.^3)));
B2=1000.*((3.462033-(0.02679.*Xss)).*(EF.*0.9.*Tgh1)+(0.5.*(0.001349-
(0.00000655.*Xss.^2)).*((0.9.*Tgh1).^2))+(162.81-(6.042.*Xss)-
0.000453.*Xss.^2+(0.0012.*Xss.^3)));
Ter22=((mws.*B1)-(mss.*B2)-A14-(mer.*2501.3))./(mer.*1.87);
Ter23=((((mws.*B1)-(mss.*B2)-A14)./(1000.*mer))-2501.3)./1.87;A
```

APPENDIX I

MATLAB PROGRAM FOR COOLING TOWER DESIGN

```
% APPENDIX I
%PROGRAM FOR COOLING TOWER DESIGN
% Constants
```

```
A=0.786889159;
B=-0.001874457;
C=4.163042560;
D=-0.0000003334;
E=-0.007798602;
Cpw=4.18; %specific heat capacity of water (kJ/kgK)
Cpa=1.0005; %Specific heat capacity of air (kJ/kgK)
hfg=2500; %kJ/kg
P=101.325; %kPa
P1=101325; %Pa
Mb=29; % Molecular weight of air
Kga=0.0000001207;  %  volumetric  mass  transfer  coefficient  in  the  gas
(kgmol/s.m3.Pa)
% Parameters
Qct=30; % capacity of cooling tower
Rd=7; % design range
Tw1=45; %inlet temperature of water
Ta1=31; % Air inlet temp
Twb=(0.7555.*Ta1)-3.6281 ; % wet bulb temperature
rho=1000; %density of water (kg/m3)
y=0.1; % length of air inlet port (m)
a=200; % surface area per unit volume
d=0.5; %diameter of cooling tower (m)
uwo=0.001792; % dynamic viscosity coefficient of water at 0oC (kg/(m.s))
Cpsat=2.3516;
Be=0.803;
Bi=0.565;
% Calculations
L=linspace(0.1,1.5); % mass flow rate of water
uw=uwo./(1+(0.0337.*Tw1)+(0.000221.*Tw1.^2));
LoGopt=(Cpa./Cpw)+(hfg.*0.622.*exp(18.6-
(5206.9./(Tw1+273))).*5206.9.*P)./(Cpw.*((Tw1+273).^2).*(P-exp(18.6-
(5206.9./(Tw1+273)))).^2); %optimum ratio of water to air flow rate
G=L./LoGopt; %mass flow rate of air (Kg/s)
Ps=610.78.*exp((Ta1./(Ta1+238.3)).*17.2694);  %saturared  water  vapour  pressure
(Pa)
g=0.0000062.*Ps; %concentration of water vapour in air (kg/kgd.a.)
Cpv=(1360.5+(2.31334.*(Ta1+273.16))-
(0.000000000246784.*((Ta1+273.16).^5))+(0.000000000000591332.*((Ta1+273.16).^6)
))./1000; %specific heat capacity of vapour
ha1=(Cpa.*(Twb))+(g.*(2501.6+(Cpv.*(Twb))));  %enthalpy  of  air-water  vapour
mixture at inlet (KJ/Kg)
hw1=(A+(C.*Tw1)+(E.*((Tw1).^2))./(1+(B.*Tw1)+(D.*((Tw1).^2)));  %enthalpy  of
water at inlet
hw2=(A+(C.*Tw2)+(E.*((Tw2).^2))./(1+(B.*Tw2)+(D.*((Tw2).^2)));  %enthalpy  of
water at outlet
Tw2=Tw1-((Tw1-
Twb)./(((Cpw.*L)./(Be.*Cpsat.*G.^0.8))+((Cpw.*L.^0.2.*uw.^0.5)./(Bi))+((Cpw.*L)
./(2.*Cpsat.*G))+0.5)); % outlet temperature of water
Tm=(Tw1+Tw2)./2; % mean water temp
R=Tw1-Tw2; %range
Tap=Tw2-Twb; % Approach temp
hwm=(A+(C.*Tm)+(E.*((Tm).^2))./(1+(B.*Tm)+(D.*((Tm).^2)));  %enthalpy  of  water
at mean water temp
delh=1.25.*Cpw.*R; % total increase in enthalpy of air
ha2=ha1+delh; % enthalpy of air at outlet
delh2=hw1-ha2; % inlet enthalpy difference
delh1=hw2-ha1; % outlet enthalpy difference
dh=(hw1+hw2-(2.*hwm))./4; % enthalpy correction factor
delhm=(delh2-delh1)./(2.3.*(log10((delh2-dh)./(delh1-dh)))); %log mean enthalpy
difference
```

```
X=Cpw.*(R./delhm); %cooling tower characteristic
D=0.00010491143.*((Tw1.^1.774)./(P.*1000)); %diffusivity of water vapour in air
(m2/s)
K=(D.*rho)./y; % mass diffusivity
h1=X.*(G./Mb.*Kga.*P1); % height of packing
h=(4.*X.*L)./(3.14.*K.*a.*d^2); %cooling tower height
Eloss=0.00153.*R.*L; %evaporation loss (Kg/s)
Vw=36000.*Eloss;%volume of water used daily (litres)
Eff=((Tw1-Tw2)./(Tw1-Twb)); % efficiency
Eff2=1./((Cpw.*L).*((1./(Be.*Cpsat.*G.^0.8))+(uw.^0.5./(Bi.*L.^0.8))+(1./(2.*Cp
sat.*G))+(1./(2.*Cpw.*L))));
  figure (1), plot(L,Eff,'*-')
ylabel('height of tower')
xlabel('mass flow rate. ')
grid on
disp('X:');
disp(X);
disp('h:');
disp(h);
disp('LoGopt:');
disp(LoGopt);
disp('Vw:');
disp(Vw);
```

APPENDIX J
MATLAB PROGRAM FOR FAN COIL SIZING

```
% APPENDIX J
% PROGRAM FOR FAN COIL SIZING
% Enter constants
```

```
Q=2.0; % Cooling load (KW)
d1=0.014; % inner tube dia (m)
d2=0.0158; % outer tube dia (m)
SL=0.0381; % Longitudinalfin spacing (m)% tube spacing
ST=0.0432;% Transverse fin spacing (m) % row spacing
eff=0.92; % finned surface weigthed efficiency
Np=5;% No. of tube rows
Tw1=10; % Chilled water inlet temp (oC)
Tw2=15; % Chilled water outlet temp (oC)
Cpw=4.14; % Specific heat capacity of water KJ/(Kg.K)
dw=1000; % Density of water
Vw=0.735; % water inlet velocity (m/s)
Cpa=1.0057; % Specific heat capacity of air KJ/(Kg.K)
Vf=2.54; % Air face velocity (m/sec) % vel of coil
B=1060; % exchanger compactness (m2/m3)
Ta1=29; % Inlet air temp (oC)(dry bulb)
ha1=53.75; % enthalpy of air at inlet (KJ/Kg)
Wa1=0.0102; % Specific humidity of air at inlet (Kgv/Kga)
Ta2=16; % Outlet air temp (oC)
RH2=95; % Relative humidity at outlet (%)
ha2=40.5; % enthalpy at outlet (Kj/Kg)
da=1.205; % air density (Kg/m3)
ya=0.0000182; % air dynamic viscosity (Ns/m2)
Pra=0.71; % Prandtl no. air side
yw=0.00131; % dynamic viscosity of water (Ns/m)
kw=0.588; % thermal conductivity of water (W/mk)
Prw=9.12; % Prandtl no. water
ff=0.00009; % fouling factor (m2k/w)
AcAt=0.0321; %
Ac=0.5; %
FT=0.00023; % fin thickness (m)
FS=0.002; % fin spacing (m)
AtAi=10.567; % area ratio based on fin spacing
Fsf=14.21; % fin surface factor
% Calculate
ma=Q./(ha1-ha2); % mass flow rate of air
mw=Q./(Cpw.*(Tw2-Tw1)); % mass flow rate of water
DelTwm=((Ta1-Tw2)-(Ta2-Tw1))./(log((Ta1-Tw2)./(Ta2-Tw1))); %Mean temp. diff
Nct=(4.*Np.*mw)./(3.14.*dw.*(d1.^2).*Vw);% No. of coil tubes
Nctr=Nct./Np; %no. of tubes per row
Hc=ST.*Nctr; % Heigth of coil
Dc=Np.*SL; % Depth of coil
disp('ma:');
disp(ma);
disp('mw:');
```